IMPLICATIONS OF FERROPTOSIS-RELATED GENES TO THE GENETICS OF CANCER DEVELOPMENT

EDITED BY: Lian Xiang Luo, Lei Huang and Ying Li
PUBLISHED IN: Frontiers in Genetics and
Frontiers in Cell and Developmental Biology

frontiers Research Topics

frontiers

ISSN 1664-8714
ISBN 978-2-88976-834-9
DOI 10.3389/978-2-88976-834-9

About Frontiers

Frontiers is more than just an open-access publisher of scholarly articles: it is a pioneering approach to the world of academia, radically improving the way scholarly research is managed. The grand vision of Frontiers is a world where all people have an equal opportunity to seek, share and generate knowledge. Frontiers provides immediate and permanent online open access to all its publications, but this alone is not enough to realize our grand goals.

Frontiers Journal Series

The Frontiers Journal Series is a multi-tier and interdisciplinary set of open-access, online journals, promising a paradigm shift from the current review, selection and dissemination processes in academic publishing. All Frontiers journals are driven by researchers for researchers; therefore, they constitute a service to the scholarly community. At the same time, the Frontiers Journal Series operates on a revolutionary invention, the tiered publishing system, initially addressing specific communities of scholars, and gradually climbing up to broader public understanding, thus serving the interests of the lay society, too.

Dedication to Quality

Each Frontiers article is a landmark of the highest quality, thanks to genuinely collaborative interactions between authors and review editors, who include some of the world's best academicians. Research must be certified by peers before entering a stream of knowledge that may eventually reach the public - and shape society; therefore, Frontiers only applies the most rigorous and unbiased reviews.
Frontiers revolutionizes research publishing by freely delivering the most outstanding research, evaluated with no bias from both the academic and social point of view. By applying the most advanced information technologies, Frontiers is catapulting scholarly publishing into a new generation.

What are Frontiers Research Topics?

Frontiers Research Topics are very popular trademarks of the Frontiers Journals Series: they are collections of at least ten articles, all centered on a particular subject. With their unique mix of varied contributions from Original Research to Review Articles, Frontiers Research Topics unify the most influential researchers, the latest key findings and historical advances in a hot research area! Find out more on how to host your own Frontiers Research Topic or contribute to one as an author by contacting the Frontiers Editorial Office: frontiersin.org/about/contact

IMPLICATIONS OF FERROPTOSIS-RELATED GENES TO THE GENETICS OF CANCER DEVELOPMENT

Topic Editors:
Lian Xiang Luo, Guangdong Medical University, China
Lei Huang, University of Massachusetts Medical School, United States
Ying Li, The University of Texas Health Science Center at San Antonio, United States

Citation: Luo, L. X., Huang, L., Li, Y., eds. (2022). Implications of Ferroptosis-related Genes to the Genetics of Cancer Development. Lausanne: Frontiers Media SA. doi: 10.3389/978-2-88976-834-9

Table of Contents

frontiers | Frontiers in Genetics

EDITORIAL
published: 22 July 2022
doi: 10.3389/fgene.2022.952340

Editorial: Implications of Ferroptosis-Related Genes to the Genetics of Cancer Development

Manshan Li[1], *Lei Huang*[2], *Ying Li*[3] *and Lianxiang Luo*[4,5]*

[1]The First Clinical College, Guangdong Medical University, Zhanjiang, China, [2]Department of Molecular Cell and Cancer Biology University of Massachusetts Medical School, Worcester, MA, United States, [3]Department of Molecular Medicine, UT Health San Antonio, San Antonio, TX, United States, [4]The Marine Biomedical Research Institute, Guangdong Medical University, Zhanjiang, China, [5]The Marine Biomedical Research Institute of Guangdong Zhanjiang, Zhanjiang, China

Keywords: ferroptosis, cancer, lncRNAs, ferroptosis-related genes, traditional Chinese medicine

Editorial on the Research Topic

Implications of Ferroptosis-Related Genes for the Genetics of Cancer Development

Ferroptosis is a unique type of cell death, distinct from apoptosis, which refers to an iron-dependent cell death caused by the overload of lipid peroxides on cell membranes (Dixon et al., 2012). Current cancer treatment strategies selectively eliminate cancer cells without harming normal cells. Targeting ferroptosis may provide an alternative strategy for cancer therapy to inhibit tumor growth (Chen et al., 2021; Lei et al., 2022). Studies have shown that multiple cancer-related signaling pathways control ferroptosis in cancer cells, and ferroptosis is also involved in the activity of multiple tumor suppressors (Lei et al., 2022). In addition, some cancer cells rely on ferroptosis defense systems and oxidative stress conditions to survive, and disrupting these ferroptosis defenses can be fatal to cancer cells while leaving normal cells unharmed (Mao et al., 2021). At the same time, the unique metabolism of cancer cells, the high load of reactive oxygen species (ROS), and their specific mutations make cells inherently susceptible to ferroptosis, thus exposing the therapeutic vulnerability of some cancers (Wu et al., 2019). Furthermore, it has been found that oncogene-induced ferroptosis resistance can be mediated by downstream effectors, which can be targeted to reverse ferroptosis resistance and play a strong tumor inhibition effect (Yi et al., 2020). Recent research also suggests that EMT is thought to call into being cancer stem cells, leading to transfer diffusion (Yang et al., 2020), and EMT signaling can promote ferroptosis. Increased CD44-dependent iron endocytosis promotes iron-dependent demethylase activity, which promotes the expression of EMT signaling-related genes, thus making breast cancer cells sensitive to ferroptosis (Müller et al., 2020). Ferroptosis has a wide range of effects on cell metabolism and has many targets in cancer. In addition, various clinical drugs and herbal extracts can induce ferroptosis in cancer cells (Xu et al., 2021). Similarly, ferroptosis-related genes and lncRNA may become potential biomarkers that provide new anti-cancer treatment strategies. Our Research Topic included one review and fifteen original research articles related to Ferroptosis-related genes, lncRNA, and drugs, which may be potential targets for reversing cancer drug resistance and targeted therapy.

LncRNAs are considered to be major regulators of various cellular processes, and their dysregulation is implicated in all features of cancer (Balihodzic et al., 2021). More and more evidence confirmed the importance of lncRNA in regulating ferroptosis (Balihodzic et al., 2022). LncRNAs can regulate the expression of GPX4 and induce lipid peroxidation of the cell membrane through sponge miRNAs, resulting in the ferroptosis of cancer cells (Zuo et al., 2022). We included four ferroptosis-related long non-coding RNA articles. Jiang et al. explored the critical role of ferroptosis-related long non-coding RNAs in the prognosis of head and neck squamous cell carcinoma (HNSCC). They identified ferroptosis-related lncRNAs as independent risk factors for

OPEN ACCESS

Edited and reviewed by:
Jared C. Roach,
Institute for Systems Biology (ISB), United States

***Correspondence:**
Lianxiang Luo
luolianxiang321@gdmu.edu.cn

Specialty section:
This article was submitted to Human and Medical Genomics, a section of the journal Frontiers in Genetics

Received: *25 May 2022*
Accepted: *16 June 2022*
Published: *22 July 2022*

Citation:
Li M, Huang L, Li Y and Luo L (2022) Editorial: Implications of Ferroptosis-Related Genes to the Genetics of Cancer Development. Front. Genet. 13:952340. doi: 10.3389/fgene.2022.952340

predicting the overall survival outcome of HNSCC patients. In addition, the correlation between patient risk score and PD-1/PD-L1 also revealed the role of the prognosis-related FElncRNA signature (PFLS) in immunotherapy. Zhou et al. also provided ferroptosis-related long non-coding RNA (FRlncRNA) signature to improve the prognostic prediction of ccRCC, suggesting that FRlncRNAs may be a molecular biomarker and therapeutic target of ccRCC. The combination of immunotherapy and targeted therapy can effectively prolong the survival rate of hepatocellular carcinoma (HCC). The FRlncRNAs identified by Zhang et al. have reasonable specificity and sensitivity, which is conducive to immunotherapy and targeted therapy for HCC patients. Li et al. constructed a prognostic model based on 8 FRlncRNAs to provide prognostic assessment for OSCC patients and analyzed differences in immune cells, function, immune checkpoint, and m6A expression between high-risk and low-risk groups. These FRlncRNAs may become novel biomarkers for the treatment of OSCC.

Inducing ferroptosis is a promising strategy for cancer treatment. Finding novel biomarkers of ferroptosis with the good predictive ability and therapeutic targets will effectively reverse drug resistance in cancer. Wang et al. found that a ferroptosis-related gene signature predicts the prognosis of lung adenocarcinoma. Patients in the low-risk group with a better prognosis benefit from enhanced anti-tumor immunity, and this prognostic feature may be a reliable tool for risk stratification in lung adenocarcinoma patients. Similarly, Guan et al. also developed and tested a risk assessment model of genes associated with ferroptosis in sarcomas, in which SLC7A11, FANCD2, CISD1, and ATP3MC3 will be used as new markers to identify patients who are likely to receive adequate ferroptosis induction therapy or combined immunotherapy. A prognostic model based on nine prognostic FRGS was established. Yan et al. established a ferroptosis-related prognostic model to screen patients with low-grade glioma (LGG) for sensitivity to chemotherapy and immunotherapy. The prognostic model is closely related to autophagy and hypoxia. Moreover, this model is helpful for diagnosis, treatment, and prognosis prediction. Cai et al. established ferroptosis-related genes prognostic index (FRGPI) based on HMOX1, TFRC, JUN, and SOCS1, which may help distinguish immune and molecular characteristics and accurately distinguish immune and molecular characteristics predict clinical outcomes, temozolomide resistance, and ICI response in gliomas. In addition, fifteen potential small-molecule compounds were predicted based on FRGPI, which provides a reference for finding effective drugs for treating glioma. Such a systematic assessment of FRGPI in glioma patients may contribute to anti-cancer therapies based on ferroptosis. The study of Zhu et al. also found 14 FRGS, including HMOX1, PEBP1, KEAP1, and LPCAT3. They reveal ferroptosis's vital role in metastatic tumors by exploring the relationship between ferroptosis and BCBM expression, prognosis, immune response, and drug sensitivity. Interestingly, both pyroptosis and ferroptosis affect the progression and treatment of pancreatic cancer. Yu et al. established a pyroptosis-ferroptosis scoring system based on cell death profiles for pancreatic adenocarcinoma (PAAD) patients. Moreover, the P-F score can predict the outcome and response of chemotherapy drugs or immunotherapy in patients with PAAD. Han et al. found that novel characterization of ferroptosis-related genes driven by CNV can be used to predict the survival of AML. Additionally, CNV-driven DE-FRG may be related to cell cycle disorders and inflammatory immune responses during the disease process. This prognostic model provides potential targets and is helpful for clinical analysis and diagnosis of the AML. ACSL4 is associated with amino acids, lipid synthesis, and lipid peroxide-dependent ferroptosis. Yu et al. explored the expression and prognosis of ACSL4 in pan-cancer and found that ACSL4 plays an essential role in the recruitment and regulation of immune-infiltrating cells in cancer. In addition, the mechanism of ACSL4 in cancer may be closely related to the IGF signaling pathway. IGF-1 receptor (IGF-1R) inhibitors can prevent the binding of IGF-1 to IGF1R, inhibit the PI3K/Akt pathway, and exert anti-tumor activity. ACSL4 may be a potential prognostic immunotherapy biomarker and a potential target for cancer therapy. The study of Ke et al. comprehensively analyzed the potential mechanism and prognostic role of ferroptosis-related genes in hepatocellular carcinoma and found that FTL is a crucial regulator of ferroptosis in HCC. The high expression level of FTL is a poor predictor of survival, and FTL plays a role as an independent prognostic and diagnostic factor for HCC. Finally, Guang et al. analyzed the multiple omics differences among cancer cell lines with high and low ferroptosis scores and constructed a ferroptosis-related model, providing insights into the treatment of various malignancies and targets for cancer drugs.

Ferroptosis can be triggered by small external molecules or drugs (Liang et al., 2019). We have included an article about small molecules in Traditional Chinese medicine to introduce the relevant content. Feng et al. found that Nobiletin can induce ferroptosis in melanoma cells and play an anti-tumor role. Their results showed that Nobiletin induces ferroptosis by modulating the GSK3β -mediated Keap1/Nrf2/HO-1 signaling pathway in melanoma cells, confirming that Nobiletin is a promising therapeutic target for melanoma. In addition, a review article by Zhao et al. summarized the mechanism of ferroptosis in hepatocellular carcinoma and described recent advances in the treatment of drug resistance, demonstrating that multiple genes or compounds can sensitize sorafenib. Moreover, the preparation of nanoparticles such as MMSN and LDL-DHA in the tumor microenvironment and exosomes with ferroptosis induction can induce ferroptosis in HCC, thus effectively treating patients.

In conclusion, ferroptosis is associated with various pathophysiological processes and diseases, including cancer. Cancer cells require more iron than normal non-cancer cells, indicating that cancer cells are more susceptible to iron-dependent cell death. Therefore, inducing ferroptosis is a promising cancer treatment strategy that can effectively overcome resistance to conventional cancer treatments. This study provides evidence for the important role of ferroptosis in cancer treatment and suggests that many ferroptosis-related genes and molecules can be used as potential biomarkers for treatment and prognosis. Although ferroptosis has great

advantages in cancer treatment, accurately determining clinical biomarkers related to ferroptosis, how to simply and accurately predict *in vivo* biomarkers of patients, and screening suitable ferroptosis inducer treatment are all problems that we need to solve in the future. In addition, cancer cells and immune cells have different internal mechanisms for ferroptosis, and we need to understand how they contribute to vulnerability to ferroptosis. More importantly, a subset of GPX4 inhibitors has shown adverse effects in animal models, which need to be addressed in ferroptosis targeted cancer therapies.

AUTHOR CONTRIBUTIONS

All authors listed have made a substantial, direct, and intellectual contribution to the work, and approved it for publication.

ACKNOWLEDGMENTS

We thank all the authors, reviewers and editors who contributed to this Research Topic.

REFERENCES

Balihodzic, A., Barth, D. A., Prinz, F., and Pichler, M. (2021). Involvement of long non-coding RNAs in glucose metabolism in cancer. *Cancers (Basel)* 13 (5), 977. doi:10.3390/cancers13050977

Balihodzic, A., Prinz, F., Dengler, M. A., Calin, G. A., Jost, P. J., Pichler, M., et al. (2022). Non-coding RNAs and ferroptosis: Potential implications for cancer therapy. *Cell Death Differ.* 29, 1094–1106. doi:10.1038/s41418-022-00998-x

Chen, X., Kang, R., Kroemer, G., and Tang, D. (2021). Broadening horizons: The role of ferroptosis in cancer. *Nat. Rev. Clin. Oncol.* 18 (5), 280–296. doi:10.1038/s41571-020-00462-0

Dixon, S. J., Lemberg, K. M., Lamprecht, M. R., Skouta, R., Zaitsev, E. M., Gleason, C. E., et al. (2012). Ferroptosis: An iron-dependent form of nonapoptotic cell death. *Cell* 149 (5), 1060–1072. doi:10.1016/j.cell.2012.03.042

Lei, G., Zhuang, L., and Gan, B. (2022). Targeting ferroptosis as a vulnerability in cancer. *Nat. Rev. Cancer* 22, 381–396. doi:10.1038/s41568-022-00459-0

Liang, C., Zhang, X., Yang, M., and Dong, X. (2019). Recent progress in ferroptosis inducers for cancer therapy. *Adv. Mat.* 31 (51), e1904197. doi:10.1002/adma.201904197

Mao, C., Liu, X., Zhang, Y., Lei, G., Yan, Y., Lee, H., et al. (2021). DHODH-mediated ferroptosis defence is a targetable vulnerability in cancer. *Nature* 593 (7860), 586–590. doi:10.1038/s41586-021-03539-7

Müller, S., Sindikubwabo, F., Cañeque, T., Lafon, A., Versini, A., Lombard, B., et al. (2020). CD44 regulates epigenetic plasticity by mediating iron endocytosis. *Nat. Chem.* 12 (10), 929–938. doi:10.1038/s41557-020-0513-5

Wu, J., Minikes, A. M., Gao, M., Bian, H., Li, Y., Stockwell, B. R., et al. (2019). Intercellular interaction dictates cancer cell ferroptosis via NF2-YAP signalling. *Nature* 572 (7769), 402–406. doi:10.1038/s41586-019-1426-6

Xu, G., Wang, H., Li, X., Huang, R., and Luo, L. (2021). Recent progress on targeting ferroptosis for cancer therapy. *Biochem. Pharmacol.* 190, 114584. doi:10.1016/j.bcp.2021.114584

Yang, J., Antin, P., Berx, G., Blanpain, C., Brabletz, T., Bronner, M., et al. (2020). Guidelines and definitions for research on epithelial-mesenchymal transition. *Nat. Rev. Mol. Cell Biol.* 21 (6), 341–352. doi:10.1038/s41580-020-0237-9

Yi, J., Zhu, J., Wu, J., Thompson, C. B., and Jiang, X. (2020). Oncogenic activation of PI3K-AKT-mTOR signaling suppresses ferroptosis via SREBP-mediated lipogenesis. *Proc. Natl. Acad. Sci. U. S. A.* 117 (49), 31189–31197. doi:10.1073/pnas.2017152117

Zuo, Y. B., Zhang, Y. F., Zhang, R., Tian, J. W., Lv, X. B., Li, R., et al. (2022). Ferroptosis in cancer progression: Role of noncoding RNAs. *Int. J. Biol. Sci.* 18 (5), 1829–1843. doi:10.7150/ijbs.66917

Conflict of Interest: The authors declare that the research was conducted in the absence of any commercial or financial relationships that could be construed as a potential conflict of interest.

Publisher's Note: All claims expressed in this article are solely those of the authors and do not necessarily represent those of their affiliated organizations, or those of the publisher, the editors and the reviewers. Any product that may be evaluated in this article, or claim that may be made by its manufacturer, is not guaranteed or endorsed by the publisher.

frontiers in Cell and Developmental Biology

ORIGINAL RESEARCH
published: 06 December 2021
doi: 10.3389/fcell.2021.794475

Multi-Omics Analysis of Cancer Cell Lines with High/Low Ferroptosis Scores and Development of a Ferroptosis-Related Model for Multiple Cancer Types

Guangyao Shan†, Huan Zhang†, Guoshu Bi†, Yunyi Bian, Jiaqi Liang, Besskaya Valeria, Dejun Zeng, Guangyu Yao, Cheng Zhan and Hong Fan**

Department of Thoracic Surgery, Zhongshan Hospital, Fudan University, Shanghai, China

OPEN ACCESS

Edited by:
Lian Xiang Luo, Guangdong Medical University, China

Reviewed by:
Bufu Tang, Zhejiang University, China
Qinyu Zhao, Australian National University, Australia

***Correspondence:**
Cheng Zhan
czhan10@fudan.edu.cn
Hong Fan
fan.hong@zs-hospital.sh.cn

†These authors have contributed equally to this work

Specialty section:
This article was submitted to Cell Death and Survival, a section of the journal Frontiers in Cell and Developmental Biology

Received: *13 October 2021*
Accepted: *12 November 2021*
Published: *06 December 2021*

Citation:
Shan G, Zhang H, Bi G, Bian Y, Liang J, Valeria B, Zeng D, Yao G, Zhan C and Fan H (2021) Multi-Omics Analysis of Cancer Cell Lines with High/Low Ferroptosis Scores and Development of a Ferroptosis-Related Model for Multiple Cancer Types. Front. Cell Dev. Biol. 9:794475. doi: 10.3389/fcell.2021.794475

Background: Ferroptosis is a newly identified regulated cell death characterized by iron-dependent lipid peroxidation and subsequent membrane oxidative damage, which has been implicated in multiple types of cancers. The multi-omics differences between cancer cell lines with high/low ferroptosis scores remain to be elucidated.

Methods and Materials: We used RNA-seq gene expression, gene mutation, miRNA expression, metabolites, copy number variation, and drug sensitivity data of cancer cell lines from DEPMAP to detect multi-omics differences associated with ferroptosis. Based on the gene expression data of cancer cell lines, we performed LASSO-Logistic regression analysis to build a ferroptosis-related model. Lung adenocarcinoma (LUAD), lung squamous cell carcinoma (LUSC), esophageal cancer (ESCA), bladder cancer (BLCA), cervical cancer (CESC), and head and neck cancer (HNSC) patients from the TCGA database were used as validation cohorts to test the efficacy of this model.

Results: After stratifying the cancer cell lines into high score (HS) and low score (LS) groups according to the median of ferroptosis scores generated by gene set variation analysis, we found that IC50 of 66 agents such as oxaliplatin ($p < 0.001$) were significantly different, among which 65 were higher in the HS group. 851 genes such as KEAP1 and NRAS were differentially muted between the two groups. Differentially expressed genes, miRNAs and metabolites were also detected—multiple items such as IL17F (logFC = 6.58, $p < 0.001$) differed between the two groups. Unlike the TCGA data generated by bulk RNA-seq, the gene expression data in DEPMAP are from pure cancer cells, so it could better reflect the traits of tumors in cancer patients. Thus, we built a 15-signature model (AUC = 0.878) based on the gene expression data of cancer cell lines. The validation cohorts demonstrated a higher mutational rate of NFE2L2 and higher expression levels of 12 ferroptosis-related genes in HS groups.

Conclusion: This article systemically analyzed multi-omics differences between cancer cell lines with high/low ferroptosis scores and a ferroptosis-related model was developed

for multiple cancer types. Our findings could improve our understanding of the role of ferroptosis in cancer and provide new insight into treatment for malignant tumors.

Keywords: ferroptosis, cell line, drug resisitance, multi-omics, pan-cancers

INTRODUCTION

Ferroptosis is a newly identified regulated cell death (RCD) characterized by iron-dependent lipid peroxidation and subsequent membrane oxidative damage (Stockwell et al., 2017). Another type of RCD, apoptosis, has been perceived as the only form of RCD suitable for developing anti-tumor therapies for a long time (Liang et al., 2019). While the effect of agents targeted apoptosis is not as good as expected owing to the multiple mechanisms cancer cells have developed to resist cell death. Distinct from apoptosis, ferroptosis has its unique molecular mechanisms. Ferroptosis can be induced *via* extrinsic or intrinsic pathways. The extrinsic pathway is initiated by the blockage of cell membrane transporters such as the cystine/glutamate transporter (also known as system xc^-) or by activation of the iron transporters serotransferrin and lactotransferrin. The intrinsic pathway is triggered by inhibiting intracellular antioxidant systems such as glutathione-glutathione peroxidase 4 (GSH-GPX4) (Lu et al., 2017).

Compared with normal cells, the growth of cancer cells (especially cancer stem cells) strongly depends on iron. The pretreatment of erastin, an inducer of ferroptosis, could synergize with cisplatin (a GSH inhibitor and interfering agent of DNA replication) to magnify its anti-tumor effects (Sato et al., 2018). Likewise, multiple ferroptosis inducers, such as Sorafenib and Altretamine, could serve as radiosensitizers *via* inhibiting SLC7A11 (a protein controlling the transport of cystine and glutamate) or GPX4 activities (Lei et al., 2021). It could be concluded that ferroptosis provides new strategies to kill tumor cells alone or in combination with other conventional therapies. Given the promising potential of ferroptosis in cancer treatment, it's imperative to elucidate the multi-omics differences influenced by this pathway.

In this article, we systemically analyzed the multi-omics differences between the cancer cell lines from the Dependency Map (DEPMAP) with high/low ferroptosis scores generated by gene set variation analysis (GSVA). Unlike the bulk RNA-seq data from the cancer genome atlas (TCGA), the gene expression data in DEPMAP are only from cancer cells, which could better reflect the traits of tumors in cancer patients. Therefore, we built a Least absolute shrinkage and selection operator (LASSO)-Logistic model based on the gene expression data of cancer cell lines to classify the cancer patients into HS and LS groups. Finally, we validated this model in bladder cancer (BLCA), cervical cancer (CESC), esophageal cancer (ESCA), head and neck cancer (HNSC), lung adenocarcinoma (LUAD), and lung squamous cell carcinoma (LUSC) patients from TCGA. We hope our study could improve our understanding of the role of ferroptosis in cancer, thus shedding new light on the development of new regimens.

MATERIALS AND METHODS

Data Collection and Processing

Data of cancer cell lines, including sample information, RNA-seq gene expression, gene mutation, miRNA expression, metabolites, copy number variation (CNV), and drug sensitivity IC50 (Sanger GDSC2), were obtained from DEPMAP (*https://depmap.org/portal/*). After matching the gene expression, gene mutation, miRNA expression, and CNV data with sample information, 1376 gene expression, 940 miRNA, 911 metabolites, 1295 gene mutation, 1356 CNV, and 595 drug sensitivity data were included for further analysis.

For the 33 kinds of cancer types in TCGA (*https://portal.gdc.cancer.gov/*), ones that complied with the following two standards were used as validation cohorts for the ferroptosis-based classification model: 1) The RNA-seq gene expression data, somatic mutation data, and survival information of the patients were intact. 2) The number of patients in the HS or LS group was greater than 10, respectively. 400 BLCA (23 HS *vs.* 377 LS), 283 CESC (11 HS *vs.* 272 LS), 151 ESCA (40 HS *vs.* 111 LS), 494 HNSC (50 HS *vs.* 444 LS), 497 LUAD (45 HS *vs.* 452 LS), and 489 LUSC (162 HS *vs.* 372 LS) patients were included in this study.

GSVA and Drug Sensitivity

108 driver genes that promote ferroptosis and 69 suppressor genes preventing ferroptosis were obtained from the FerrDb (Zhou and Bao, 2020) (*http://www.zhounan.org/ferrdb/*). After removing the duplicated ones, 173 ferroptosis-related genes were recruited for further analysis. Besides ferroptosis, multiple biological processes (**Supplementary file S1**) were also detected. By integrating the collective expression of the given gene sets above, the enrichment scores of 76 biological pathways for 1376 cancer cell lines were obtained *via* an unsupervised gene set enrichment method in the R *GSVA* package. Instead of ssGSEA, the GSVA method is preferred in our study because GSVA includes the normalization of gene expression to reduce the noise of the data and has been shown to outperform ssGSEA when measuring the signal-to-noise ratio in differential gene expression and differential pathway activity identification analyses (Bi et al., 2020). According to the median value of the GSVA score of ferroptosis, the cancer cell lines were stratified into the high score group (HS) and low score group (LS). To further explore the relationship between drug sensitivity and ferroptosis, we compared the IC50 of 169 agents between the two groups.

Differentially Muted Genes

Gene mutation data of cancer cell lines were separated into HS and LS groups. Next, the R package *ComplexHeatmap* was used to visualize the different mutation patterns of the two groups. The two-sided Fisher exact test was used to determine the DMGs between the two groups, and $p < 0.05$ was considered significant. Besides, mutational load and CNV were calculated for every cancer cell line and subsequently compared between the two groups.

Differentially Expressed Genes, miRNAs, Metabolites, and Enrichment Analysis

Based on the RNA-seq gene expression data of cancer cell lines, DEGs were investigated by the R *edgeR* package. The absolute value of $Log_2FoldChange$ (|Log FC |) >1 and *p*-value <0.05 were considered as significantly different. Subsequently, Gene Ontology (GO) and Kyoto Encyclopedia of Genes and Genomes (KEGG) enrichment analyses were performed using R *org.Hs.eg.db* and *Clusterprofiler* packages. Similarly, different miRNA and metabolite expression patterns were also explored between the two groups. |Log FC | >0.5 and *p*-value <0.05 were considered as significantly different for miRNAs. The criteria for defining differentially expressed metabolites were set as follows: | Log FC| >1 and *p*-value <0.05.

Protein-To-Protein Interaction Network

To further investigate the inner correlation of the DEGs, we mapped the top 100 most significantly upregulated and downregulated DEGs in STRING (*version 11.0b, https://www.string-db.org/*) to make a PPI network. Next, the Molecular Complex Detection (MCODE) plugin (Bader and Hogue, 2003) in Cytoscape (*version 3.8.2*) was used to detect modules of the PPI network (degree cutoff = 2, node score cutoff = 0.2, k-score = 2, and max depth = 100).

Construction of the Ferroptosis-Related Model

Compared to the gene expression data from TCGA generated by bulk RNA-seq, data in DEAPMAP are pure cancer cells, which could better reflect the traits of tumor cells in cancer patients. Therefore, they are more appropriate to build the ferroptosis-related classification model. Based on the gene expression data in DEPMAP, we developed a ferroptosis-related model to stratify the cancer cell lines into HS and LS groups. Firstly, we take the intersection of 173 ferroptosis-related genes and DEGs, and 22 genes were recognized as ferroptosis-related DEGs. Based on the 22 candidate genes, we performed LASSO and binary Logistic regression analysis to construct the model. LASSO is a penalized method to select data with high dimensions and reduce the impact of overfitting (Vasquez et al., 2016). Ten-fold cross-validation was adopted using the R *glmnet* package to determine the optimal parameter λ and corresponding genes. Fifteen genes were enrolled by LASSO regression analysis, and their coefficients were decided by binary logistic regression analysis. Harrell's concordance index (C-index) was used to evaluate the accuracy of the classification model.

Validation of the Ferroptosis-Related Model

The BLCA, CESC, ESCA, HNSC, LUAD, and LUSC patients from TCGA were stratified into HS and LS groups according to the cutoff value of the classification model. Ferroptosis-associated DMGs, ferroptosis-related gene expression patterns, and Kaplan–Meier (K-M) survival analysis were investigated between the two groups.

Statistical Analyses

All statistical analyses were carried out in R software (Version 4.1.1, see in Data Availability Statement). The comparison of the baseline characteristics of cancer cell lines from different groups was conducted, of which categorical variables were compared by Chi-square test or Fisher exact test when appropriate and continuous variables were compared by Student's t-test. The Student's t-test was also used to compare continuous variables such as the CNV, mutation load, IC50 of agents. K-M survival curves were visualized by the R *ggplot2* package, and the log-rank test was used to compare the overall survival between the two groups. All the *p* values were two-sided, and the significance threshold for *p*-value in all tests was 0.05.

RESULT

GSVA and Drug Sensitivity

The whole design of this study is shown in **Figure 1A**. The cancer cell lines (**Figure 1B**) were divided into the HS ($n = 688$) and LS ($n = 688$) groups according to the median of the ferroptosis score generated by GSVA. Beside ferroptosis, the two groups differed in multiple biological ways, such as epithelial-mesenchymal transition and cell cycle activated (**Figure 1C**).

After comparing the IC50 of 169 drugs between the two groups, we found 66 of them were significantly different (**Figures 1D–F**). Among them, oxaliplatin (460.3 HS *vs.* 333.2 LS, μM/L, $p < 0.001$) is the most significantly different drug, and vincristine (21.3 HS *vs.* 2.8 LS, μM/L, $p < 0.05$) is the agent with the greatest fold change. Except for RO-3306 (60.8 HS *vs.* 201.2 LS, μM/L, $p < 0.05$), all agents with a significant difference have a higher IC50 in the HS group, indicating patients with a high ferroptosis score may be less likely to benefit from these chemotherapeutic and targeted drugs. For example, the IC50 of cisplatin (477.0 HS *vs.* 211.4 LS, μM/L, $p < 0.01$), afatinib (35.3 HS *vs.* 15.8 LS, μM/L, $p < 0.01$), and crizotinib (124.8 HS *vs.* 73.1 LS, μM/L, $p < 0.01$) were lower in the LS group; thus lung cancer patients with a low ferroptosis score may be more likely to acquire better clinical outcomes when administrated these agents.

DMGs

Different mutational patterns of the two groups are shown in **Figures 2A,B**. Among the 18,725 genes analyzed, 851 were recognized as DMGs, and nine of them such as KEAP1(37% HS *vs.* 17% LS, $p < 0.01$), NRAS (18% HS *vs.* 43% LS, $p < 0.001$), and PROM2 (23% HS *vs.* 14% LS, $p < 0.05$) were related to

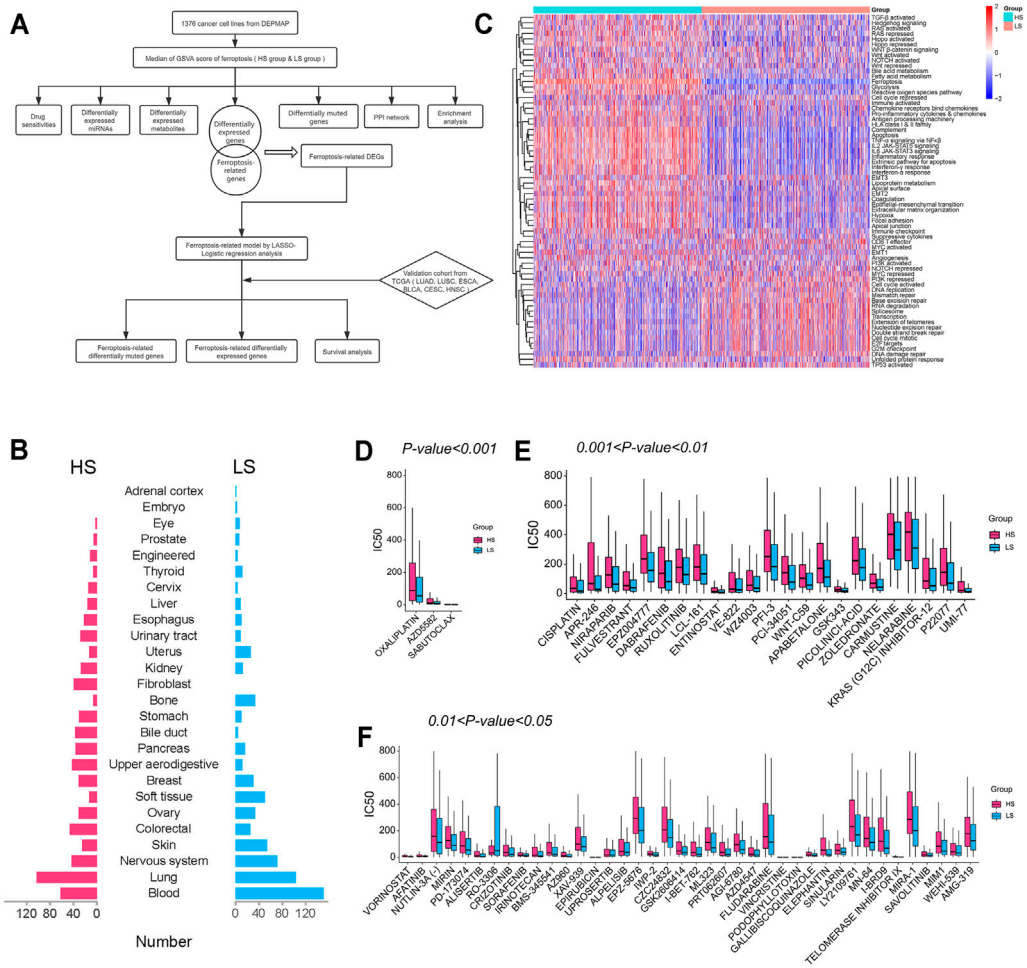

FIGURE 1 | (A) Flow diagram of the whole design. **(B)** Tissue source of cancer cell lines included in this study. **(C)** Heatmap of gene set variation analysis (GSVA) of cancer cell lines. **(D–F)** IC50 of agents with different thresholds of significance between the HS and LS groups.

ferroptosis. Next, we detected the CNV and mutational load (**Figures 2C,D**) between the two groups. The result suggested the LS group had a higher level of CNV ($p < 0.01$), while the difference of mutational load was not significant.

DEGs, miRNAs, Metabolites, and Enrichment Analysis

Among the 16,383 genes analyzed, 868 were upregulated, and 1628 were downregulated in the HS group (**Figure 3A**). NEUROD6 (logFC = -9.70, $p < 0.001$), PHOX2B (logFC = −9.50, $p < 0.001$), and FSHB (logFC = −8.90, $p < 0.001$) were the most significantly downregulated genes. CRP (logFC = 6.68, $p < 0.001$), IL17F (logFC = 6.58, $p < 0.001$), and PGC (logFC = 6.35, $p < 0.001$) were the most significantly upregulated genes. The expression levels of 12 genes related to ROS detoxification, GSH, and iron metabolism in ferroptosis are shown in **Figure 3B**; most of them were observed with higher expression levels in the HS group. For miRNAs, 22 were upregulated, and 15 were downregulated among 940 miRNAs (**Supplementary Figure S1A**). Besides, we also compared metabolites between the two groups, among which 56 were upregulated, and 55 were downregulated in the HS group (**Supplementary Figure S1B**). Methylnicotinamide (logFC = 19.83, $p < 0.001$) and lactose (logFC = 7.91, $p < 0.001$) were the most significantly upregulated metabolites. Deoxycytidine (logFC = −10.67, $p < 0.001$) and cytidine (logFC = −9.11, $p < 0.001$) were the most significantly downregulated ones.

Next, we used the DEGs to perform GO and KEGG analysis (**Figures 3C,D**). The GO analysis showed these DEGs were closely related to biological pathways such as regulation of membrane potential and extracellular structure organization.

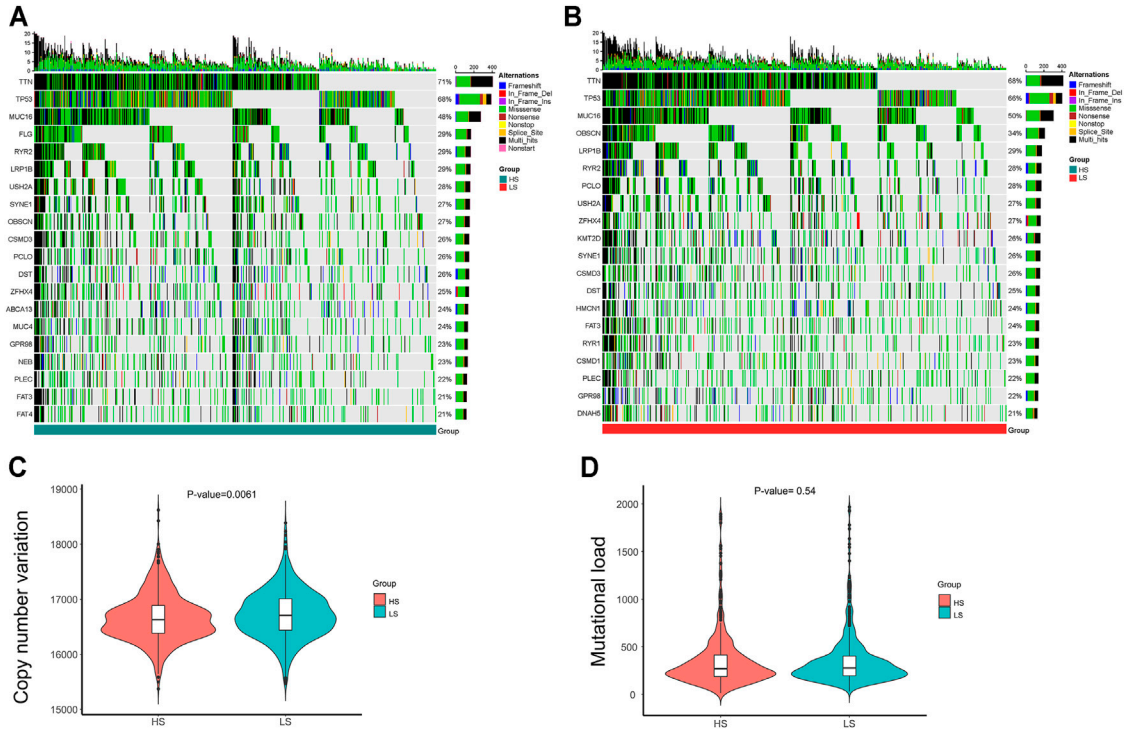

FIGURE 2 | (A–B) Top 20 muted genes in the HS and LS groups, separately. **(C–D)** Copy number variation (CNV) and mutational load between the HS and LS groups.

KEGG enrichment analysis indicated items such as neuroactive ligand-receptor interaction, cytokine-cytokine receptor interaction, and calcium signaling pathway differed between the two groups.

Finally, the expression level of the common co-stimulators and immune checkpoint inhibitors (Bian et al., 2021) were compared between the two groups (**Figures 3E,F**). Most of them were positively correlated (**Figure 3G**) and differentially expressed. The HS group has a higher expression level of CD274 ($p < 0.0001$), suggesting cancer patients with a high ferroptosis score may be more likely to benefit from PD-L1 inhibitors.

PPI Network

Based on the 200 DEGs, a PPI network was made to elucidate their inner interactions (**Figure 4A**). The cluster with the highest clustering score (Score = 16.632, Nodes = 20, Edges = 158) demonstrated that 20 genes, including AMBN, SERPIND1, TF, SERPINA4, IGFBP1, F2, ALB, ITIH2, APOB, AFP, AHSG, AMBP, VTN, KNG1, APOA2, APOH, SERPINA7, CRP, GC, and TTR play an important role in the PPI network (**Figure 4B**). The *Pearson* correlation test showed most of them were positively correlated with significant differences (**Figure 4C**). KEGG enrichment analysis showed these 20 genes were relevant to complement and coagulation cascades and cholesterol metabolism (**Figure 4D**).

Construction of the Ferroptosis-Related Model

In LASSO analysis, the optimal parameter λ was set as lambda.min criteria, which means the minimum binomial deviance (**Supplementary Figures S2A,B**). Fifteen genes were included in the model, including NOX1, CD44, TP63, NOX3, EPAS1, MYB, CDO1, DUOX2, EGFR, SLC7A11, AKR1C2, PROM2, SQSTM1, CYBB, FTH1 (**Supplementary Figure S2C**). NOX1, NOX3, EPAS1, MYB, CDO1, DUOX2, EGFR, and CYBB were ferroptosis promoters, and the remaining ones were ferroptosis suppressors. Based on these candidate genes, the model built by binary logistic regression analysis is as follows: score= (*0.3025*expression level of NOX1*) + (*0.1184* expression level of CD44*) + (*0.0898* expression level of TP63*) + (*0.2861* expression level of NOX3*) + (*0.2285* expression level of EPAS1*) + (*0.2573* expression level of MYB*) + (*0.1948* expression level of CD O 1*) + (*0.0747* expression level of DUOX2*) + (*0.1221* expression level of EGFR*) + (*0.4443* expression level of SLC7A11*) + (*0.1399* expression level of AKR1C2*) + (*0.0520* expression level of PROM2*) + (*0.4473* expression level of SQSTM1*) + (*0.1503* expression level of CYBB*) + (*0.3022* expression level of FTH1*). The calibration curve showed the bias-corrected curve and the ideal line almost overlapped, indicating this model has a satisfying classification power (**Supplementary Figure S2D**). The receiver operating curve (ROC) showed the area under the curve (AUC) was 0.878, and the cutoff value was −0.072 (**Supplementary**

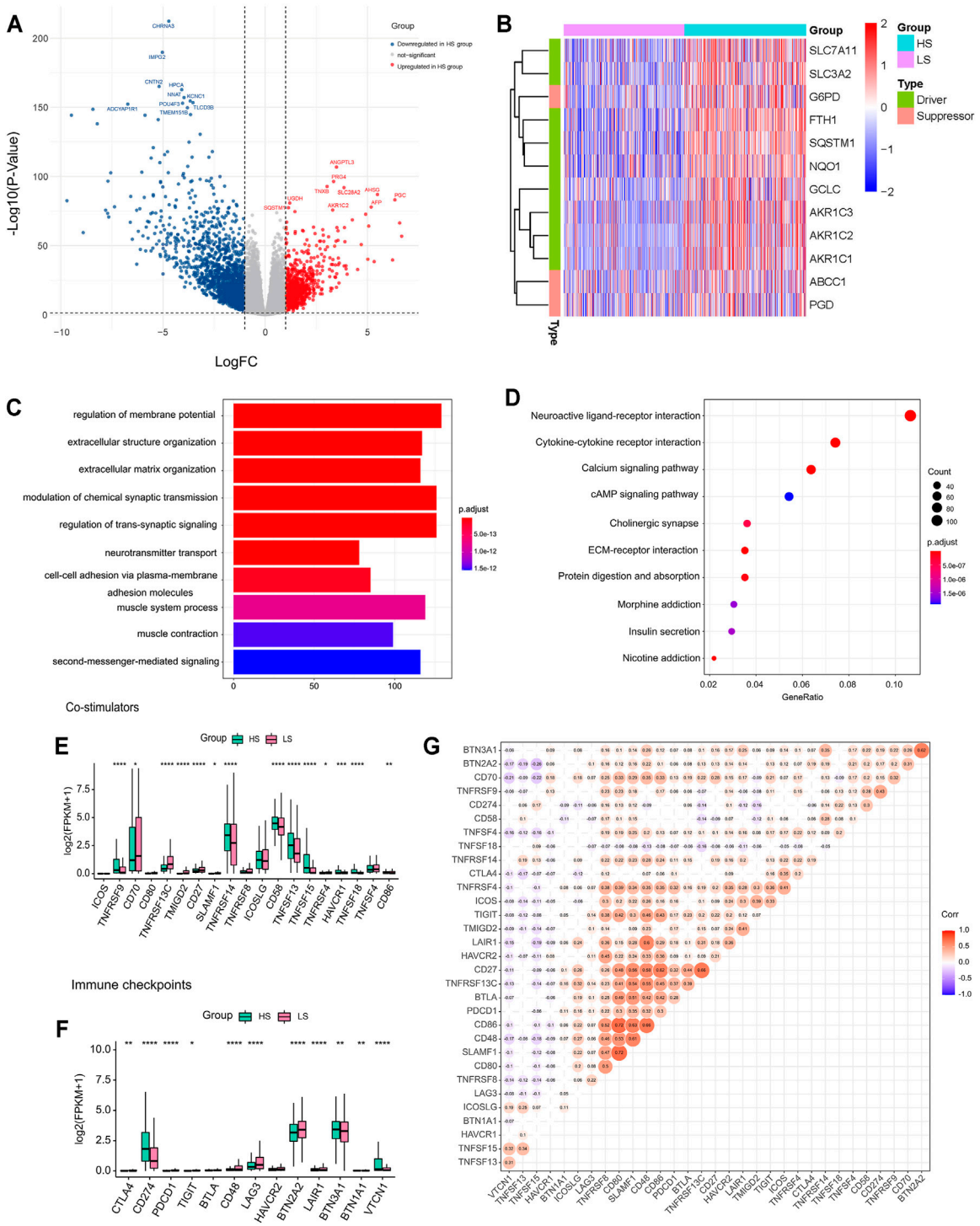

FIGURE 3 | (A) Differentially expressed genes (DEGs) between the HS and LS groups. **(B)** Heatmap of 12 ferroptosis-related genes between the HS and LS groups. **(C)** Gene Ontology (GO) enrichment analysis of the biological process of the DEGs. **(D)** Kyoto Encyclopedia of Genes and Genomes (KEGG) enrichment analysis of the DEGs. **(E,F)** Comparison of the expression levels of immune checkpoints and co-stimulators between the HS and LS groups. **(G)** Correlation analysis of the immune checkpoints and co-stimulators. Labels in the circles indicated the correlation coefficients of the corresponding variables. Correlation coefficients without significant levels were hidden. *, $p < 0.05$; **, $p < 0.01$; ***, $p < 0.001$; ****, $p < 0.0001$.

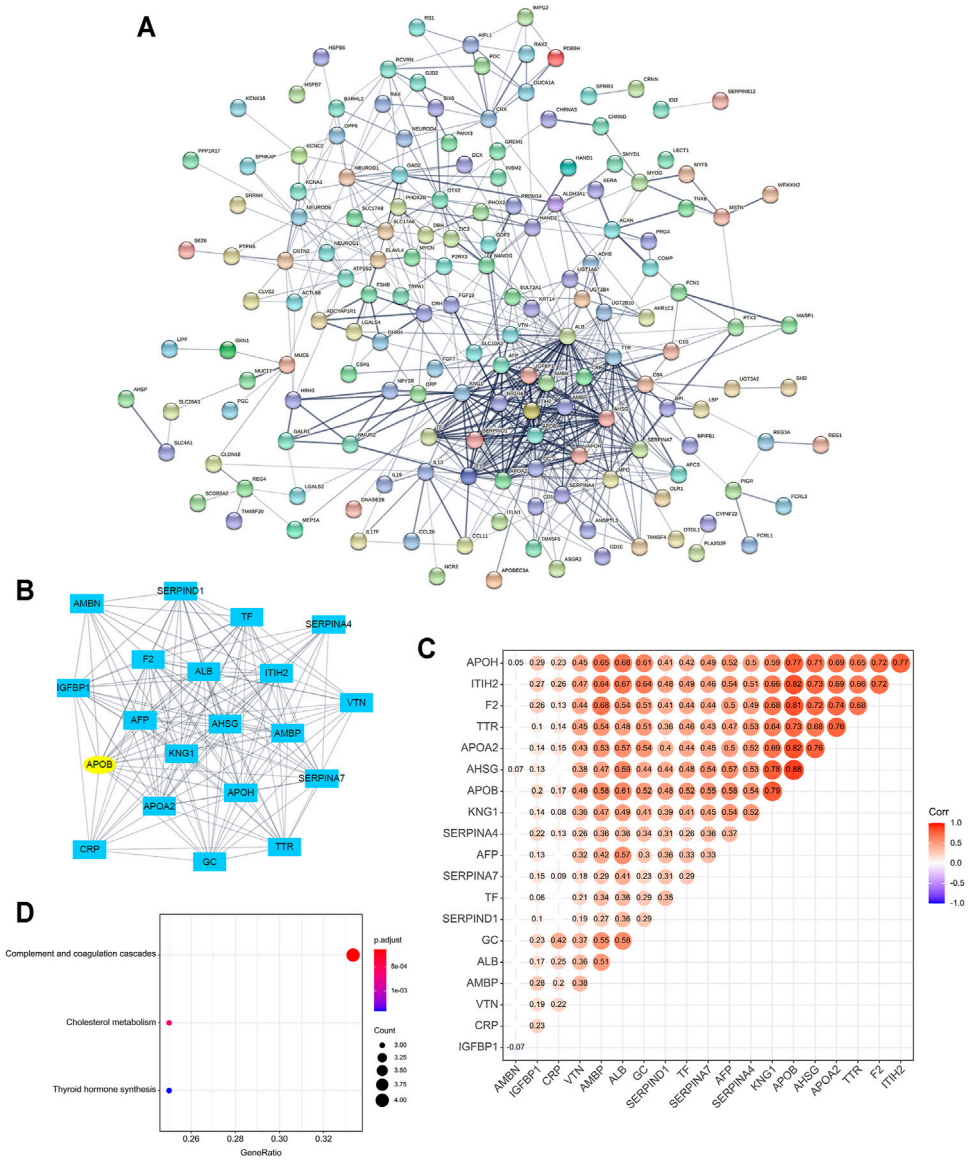

FIGURE 4 | (A) Protein-to-protein interaction (PPI) network of the top 200 most significantly upregulated and downregulated genes. The minimum required interaction score is set as 0.400 (medium confidence). Line thickness indicates the strength of data support. **(B)** The cluster of genes with the highest clustering score in the PPI network. **(C,D)** Correlation and KEGG enrichment analysis of the genes with the highest clustering score.

Figure S2E). If the score is greater than this value, it will be stratified as the HS group; otherwise, the LS group.

Validation of the Ferroptosis-Related Model

After dividing the LUAD, LUSC, ESCA, BLCA, CESC, and HNSC patients into HS and LS groups according to the classification model, we explored the ferroptosis-related DMGs between the two groups (**Figures 5A–F**). NFE2L2, which is associated with response to oxidative stress, was observed with a higher mutational rate in HS groups of all validation cohorts (BLCA, 48% HS *vs* 4% LS, $p < 0.0001$; CESC, 56% HS *vs* 4% LS, $p < 0.0001$; ESCA, 32% HS *vs* 4% LS, $p < 0.0001$; HNSC, 28% HS *vs* 3% LS, $p < 0.0001$; LUAD, 11% HS *vs* 2% LS, $p < 0.01$; LUSC, 40% HS *vs* 3% LS, $p < 0.0001$).

Next, the expression levels of 12 ferroptosis-related genes (GCLC, AKR1C3, AKR1C2, AKR1C1, SLC7A11, SLC3A2, G6PD, FTH1, SQSTM1, NQO1, ABCC1, and PGD) were detected between the two groups. Roughly in accordance with the distribution in cancer cell lines, the HS groups in all validation cohorts had a higher expression level of these ferroptosis-related genes than the LS groups (**Figures 5G–L**).

Finally, we explored the relationship between the ferroptosis score and survival (**Figure 6**). K-M survival analysis showed that the HS groups in BLCA, CESC, ESCA, HNSC, and LUAD had

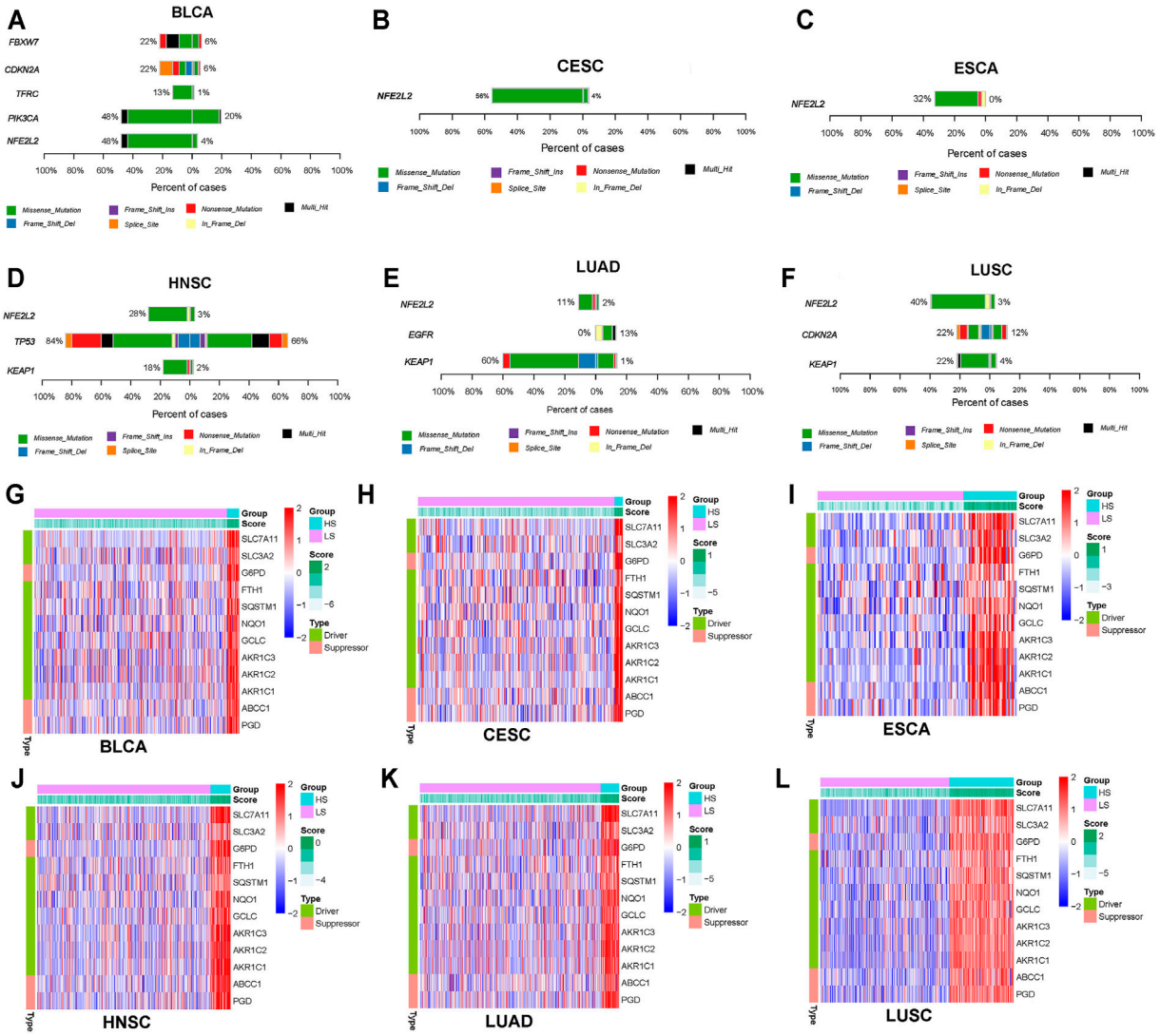

FIGURE 5 | (A–F) Ferroptosis-related differentially muted genes between the HS and LS groups in bladder cancer (BLCA), cervical cancer (CESC), esophageal cancer (ESCA), head and neck cancer (HNSC), lung adenocarcinoma (LUAD), and lung squamous cell carcinoma (LUSC) patients. The left side of each figure indicated the HS group; the right side of each figure indicated the LS group. **(G–L)** Heatmap of the fifteen ferroptosis-related genes between the HS and LS groups in BLCA, CESC, ESCA, HNSC, LUAD, and LUSC. Driver indicates gene that promotes ferroptosis; suppressor indicates gene that inhibits ferroptosis.

poorer survival than the LS groups; however, the difference was not significant except for BLCA.

DISCUSSION

This study systematically analyzed the multi-omics differences between the cancer cell lines with high/low ferroptosis scores. Multiple biological pathways such as epithelial-mesenchymal transition and drug sensitivities were significantly different between the HS and LS groups. Among 18725 genes analyzed, 851 were defined as DMGs, indicating they may play an important role in the ferroptosis pathway. Compared to the LS group, 868 protein-coding genes such as CRP and IL17F were upregulated in the HS group. In the PPI network, 20 genes, including APOB were recognized as hub genes. Based on the gene expression data of the cancer cell lines, we subsequently built a ferroptosis-related model which could predict the ferroptosis-related gene mutation and expression levels of specific ferroptosis-related genes.

As is shown in **Figure 1B**, multiple pathways such as epithelial-mesenchymal transition and cell cycle activated differed between the HS and LS groups, suggesting the ferroptosis pathway may have a significant influence on quite

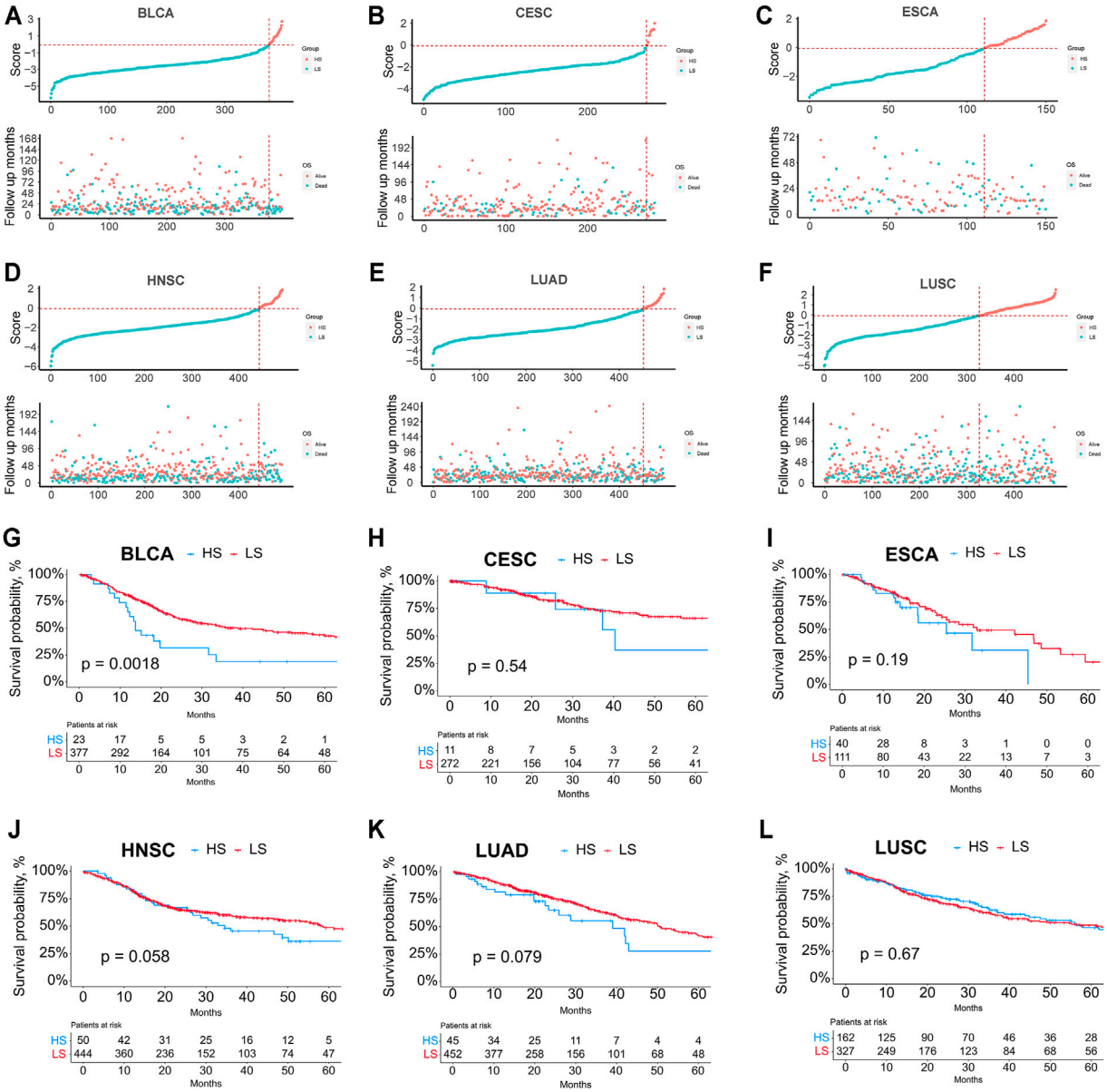

FIGURE 6 | (A–F) Relationship between the risk score rank and survival time/survival status in BLCA, CESC, ESCA, HNSC, LUAD, and LUSC. **(G–L)** Kaplan-Meier survival analysis between the HS and LS groups in BLCA, CESC, ESCA, HNSC, LUAD, and LUSC.

a few biological processes. Subsequently, the IC50 of 169 agents was investigated, 66 of which were found significantly different between the two groups. Except for RO-3306 (60.8 HS *vs.* 201.2 LS, μM/L, $p < 0.05$), the IC50 of the remaining 65 agents was higher in the HS group. Oxaliplatin (460.3 HS *vs.* 333.2 LS, μM/L, $p < 0.001$), the most significantly different agent, is a third-generation platinum drug widely used in the treatment of colorectal cancer (CRC). However, less than 40% patients with advanced CRC could benefit from oxaliplatin due to the development of drug resistance (Hsu et al., 2018). A recent study has shown that congenital or acquired oxaliplatin resistance in CRC cell lines could be reversed by the treatment of RSL3 (a ferroptosis inducer) (Yang et al., 2021). Another broad-spectrum anti-cancer drug, vincristine (21.3 HS *vs.* 2.8 LS, μM/L, $p < 0.05$), also inevitably falls into the dilemma of drug resistance after a period of usage (Xia et al., 2018). It has been elucidated that vincristine could significantly increase the expression of LINC00618, which could promote ferroptosis *via*

inhibiting SLC7A11 (Wang et al., 2021). Besides, it's notable that the HS group has a higher expression level of CD274 ($p < 0.0001$), indicating cancer patients with a high ferroptosis score may be more likely to benefit from PD-L1 inhibitors. In general, ferroptosis plays a critical part in the effect and resistance acquisition of multiple anti-cancer drugs. The combination use with ferroptosis inducers may improve the clinical benefit of chemotherapeutic and targeted agents for cancer patients. The role of ferroptosis in drug resistance sheds new light on the development of new regimens, but it still needs further investigation in experiment and clinical trials.

C-reactive protein, which is encoded by the CRP gene, is well-known in the acute-phase inflammatory response. Identified as a hallmark of cancer, tumor-promoting inflammation is proven to lead to multiple hallmark capabilities acquisition, such as sustaining proliferative signals by providing some bioactive substance into the tumor microenvironment (Hanahan and Weinberg, 2011). As an indicator of inflammatory levels, patients who harbor a high level of CRP postoperatively are more likely to suffer from more complications and increased mortality (Jones et al., 2006; Lopez-Pastorini et al., 2017). The DEG analysis has shown the CRP is upregulated (logFC = 6.68, $p < 0.001$) in the HS group, suggesting patients with a high ferroptosis score may have a higher level of inflammation and poorer survival.

In the PPI network, 20 genes were recognized as hub genes, which were closely related to the cholesterol metabolism by KEGG analysis. Studies in both cell and animal levels revealed that cholesterol synthesis induced by the AKT/mTORC1/SREBP pathway could lead to cell growth and promoted cancer aggressiveness and bone metastases. Besides, numerous cholesterol metabolites such as steroids were found to favor tumor growth and metastasis (Deng et al., 2020). APOB (logFC = 3.41, $p < 0.001$) functions as the seed gene in the hub cluster of genes. Apolipoprotein B (ApoB) is an amphipathic glycoprotein that plays a central role in human lipoprotein metabolism, the mutation of which could either cause hypercholesterolemia or hypobetalipoproteinemia (Whitfield et al., 2004). Since ferroptosis is characterized by excessive lipid peroxidation, this process may be indirectly influenced by ApoB. Few pieces of research focused on the effect of APOB in ferroptosis; thus, its role in ferroptosis still needs further investigation.

Typically, GSVA is more suitable for a rather large group of subjects to classify them into different groups. For a single patient or a small group of patients, GSVA may not be appropriate. Therefore, we developed a LASSO-Logistic model to identify the ferroptosis status of a single patient or a small group of patients by employing just 15 ferroptosis-related genes. Unlike the TCGA data generated by bulk RNA-seq, the gene expression data in DEPMAP are only from cancer cells, so this model could better reflect the traits of tumors in cancer patients. Since the model was generated from pure cancer cells, it may be more suitable for the analysis of cancer cells. However, it is not easy to get pure cancer cells in clinical settings. Through analysis, we found this model could also be used in the bulk RNA-seq data of entire tumor samples like TCGA.

Compared to the LS groups, the HS groups of all validation cohorts harbored a significantly higher mutational rate of NFE2L2, which is a ferroptosis suppressor that can protect cells from oxidative damage (Kuang et al., 2020). As a critical transcription factor in ferroptosis, multiple genes were regulated by NFE2L2. GSS, GCLC SLC7A11, and GPX4, which are NFE2L2-dependent genes, play an important role in the synthesis and function of GSH-GPX4 antioxidation system (Dai et al., 2020; Tang et al., 2021). What's more, iron metabolism-associated genes such as FTH1, FTL, and SLC40A1 also have a close relationship with NFE2L2. Among them, FTH1-FTL complex is responsible for iron storage and could prevent Fe^{2+} from being oxidated; SLC40A1 is in charge of iron export from cells (Chen et al., 2021). Recent studies suggested that aldo-keto reductases (AKRs), a superfamily of NADPH-linked oxidoreductases, including AKR1C1, AKR1C2, and AKR1C3, are potential NFE2L2 target genes responsible for ferroptosis resistance via inhibiting lipid peroxidation in melanoma cells (Dai et al., 2020). Given the key role of NFE2L2 in ferroptosis, it may be a promising target for drug development for treating malignant tumors.

The HS groups of all the five cancer types tested had a higher expression level of the 12 ferroptosis-related genes (GCLC, AKR1C3, AKR1C2, AKR1C1, SLC7A11, SLC3A2, G6PD, FTH1, SQSTM1, NQO1, ABCC1, and PGD). Notably, about half of them could be regulated by NFE2L2. GO enrichment analysis suggested these genes were related to response to oxidative stress *(adjusted p-value < 0.001)* and glutathione metabolism (*adjusted p-value < 0.001*), both of which are critical biological processes in ferroptosis. It could be concluded from the distribution of these ferroptosis-associated genes that the model had a superior discrimination power.

The relationship between the groups stratified by the model and prognosis was vague, partially attributed to the insufficient number of patients in the HS group. Although the significant difference in survival analysis could only be seen in BLCA, the HNSC and LUAD cohorts also demonstrated a better prognosis in the LS groups with *p*-values slightly greater than 0.05. The correlation between the classification model and prognosis may be further clarified in a larger number of cohorts. It's likely that a panel consisting of the 15 ferroptosis-related genes may be developed for clinical use to test the ferroptosis status of cancer patients in the future. And we hope the efficacy of this model and the relationship with radiotherapy, chemotherapy, and immunotherapy can be further investigated at that moment.

There are also some limitations of our study. The ferroptosis-related geneset provided by the FerrDb website may not be accurate enough due to insufficient studies about the role of ferroptosis in tumors up to now. Therefore, some important ferroptosis-related genes may be neglected. Besides, the reaction and mechanisms of ferroptosis vary with cancer types. Although we used 1376 cell lines from more than 20 cancer types to build this model and tried to validate it in 33 kinds of cancer types to reach a general conclusion, the efficacy and universality of this ferroptosis-related classification model still needs to be further evaluated a larger outer data and prospective studies. What's more, as single-cell sequencing may be more widely used in the future, it is promising that obtaining the RNA-seq data of pure tumor cells from a tumor tissue will be easier. We hope this model can be further investigated at single-cell level at that time.

CONCLUSION

In a word, we systemically analyzed the multi-omics differences between the cancer cell lines with high or low ferroptosis scores. Based on the gene expression data of multiple cancer cell lines, the LASSO-binary Logistic regression analysis was performed to build a 15-signature model which could predict the expression levels of specific ferroptosis-related genes and ferroptosis-related gene mutation. We hope our research could improve our understanding of the ferroptosis pathway in cancer and provide new insight into treating patients with malignant tumors.

DATA AVAILABILITY STATEMENT

The original contributions presented in the study are included in the article/**Supplementary Material**. The working sheets and code used to analyze the data in our study could be obtained by clicking the link (https://www.jianguoyun.com/p/DUk4IxEQituHChjT2p0E), further inquiries can be directed to the corresponding authors.

AUTHOR CONTRIBUTIONS

Conceptualization was contributed by CZ and HF; Data collection and curation were contributed by JL, DZ and GB; Data analysis and interpretation were contributed by GS, HZ, GB, YB, JL, BV, and GY; Draft of the manuscript was contributed by GS and HZ; Critical revision of the manuscript was contributed by CZ and HF. Final approval of manuscript and submission were contributed by all authors.

FUNDING

This research was funded by the Training Programme for the Talents of Zhongshan Hospital, Fudan University (Grant No. 2021ZSYQ24).

SUPPLEMENTARY MATERIAL

The Supplementary Material for this article can be found online at: https://www.frontiersin.org/articles/10.3389/fcell.2021.794475/full#supplementary-material

REFERENCES

Bader, G. D., and Hogue, C. W. (2003). An Automated Method for Finding Molecular Complexes in Large Protein Interaction Networks. *BMC Bioinformatics* 4, 2. doi:10.1186/1471-2105-4-2

Bi, G., Chen, Z., Yang, X., Liang, J., Hu, Z., Bian, Y., et al. (2020). Identification and Validation of Tumor Environment Phenotypes in Lung Adenocarcinoma by Integrative Genome-Scale Analysis. *Cancer Immunol. Immunother.* 69, 1293–1305. doi:10.1007/s00262-020-02546-3

Bian, Y., Bi, G., Wei, T., Yao, G., Chen, Z., Zhan, C., et al. (2021). Integrative Genome-Scale Analysis of Immune Infiltration in Esophageal Carcinoma. *Int. Immunopharmacology* 93, 107371. doi:10.1016/j.intimp.2021.107371

Chen, X., Kang, R., Kroemer, G., and Tang, D. (2021). Broadening Horizons: the Role of Ferroptosis in Cancer. *Nat. Rev. Clin. Oncol.* 18, 280–296. doi:10.1038/s41571-020-00462-0

Dai, C., Chen, X., Li, J., Comish, P., Kang, R., and Tang, D. (2020). Transcription Factors in Ferroptotic Cell Death. *Cancer Gene Ther.* 27, 645–656. doi:10.1038/s41417-020-0170-2

Deng, W., Liu, H., Luo, S., Clarke, J., Glass, C., Su, L., et al. (2020). APOB Genotypes and CDH13 Haplotypes in the Cholesterol-Related Pathway Genes Predict Non-small Cell Lung Cancer Survival. *Cancer Epidemiol. Biomarkers Prev.* 29, 1204–1213. doi:10.1158/1055-9965.epi-19-1262

Hanahan, D., and Weinberg, R. A. (2011). Hallmarks of Cancer: the Next Generation. *Cell* 144, 646–674. doi:10.1016/j.cell.2011.02.013

Hsu, H. H., Chen, M. C., Baskaran, R., Lin, Y. M., Day, C. H., Lin, Y. J., et al. (2018). Oxaliplatin Resistance in Colorectal Cancer Cells Is Mediated via Activation of ABCG2 to Alleviate ER Stress Induced Apoptosis. *J. Cel Physiol* 233, 5458–5467. doi:10.1002/jcp.26406

Jones, J. M., McGonigle, N. C., McAnespie, M., Cran, G. W., and Graham, A. N. (2006). Plasma Fibrinogen and Serum C-Reactive Protein Are Associated with Non-small Cell Lung Cancer. *Lung Cancer* 53, 97–101. doi:10.1016/j.lungcan.2006.03.012

Kuang, F., Liu, J., Tang, D., and Kang, R. (2020). Oxidative Damage and Antioxidant Defense in Ferroptosis. *Front. Cel Dev. Biol.* 8, 586578. doi:10.3389/fcell.2020.586578

Lei, G., Mao, C., Yan, Y., Zhuang, L., and Gan, B. (2021). *Ferroptosis, Radiotherapy, and Combination Therapeutic Strategies*. Berlin, Germany: Protein Cell.

Liang, C., Zhang, X., Yang, M., and Dong, X. (2019). Recent Progress in Ferroptosis Inducers for Cancer Therapy. *Adv. Mater.* 31, e1904197. doi:10.1002/adma.201904197

Lopez-Pastorini, A., Riedel, R., Koryllos, A., Beckers, F., Ludwig, C., and Stoelben, E. (2017). The Impact of Preoperative Elevated Serum C-Reactive Protein on Postoperative Morbidity and Mortality after Anatomic Resection for Lung Cancer. *Lung Cancer* 109, 68–73. doi:10.1016/j.lungcan.2017.05.003

Lu, B., Chen, X. B., Ying, M. D., He, Q. J., Cao, J., and Yang, B. (2017). The Role of Ferroptosis in Cancer Development and Treatment Response. *Front. Pharmacol.* 8, 992. doi:10.3389/fphar.2017.00992

Sato, M., Kusumi, R., Hamashima, S., Kobayashi, S., Sasaki, S., Komiyama, Y., et al. (2018). The Ferroptosis Inducer Erastin Irreversibly Inhibits System Xc− and Synergizes with Cisplatin to Increase Cisplatin's Cytotoxicity in Cancer Cells. *Sci. Rep.* 8, 968. doi:10.1038/s41598-018-19213-4

Stockwell, B. R., Friedmann Angeli, J. P., Bayir, H., Bush, A. I., Conrad, M., Dixon, S. J., et al. (2017). Ferroptosis: A Regulated Cell Death Nexus Linking Metabolism, Redox Biology, and Disease. *Cell* 171, 273–285. doi:10.1016/j.cell.2017.09.021

Tang, D., Chen, X., Kang, R., and Kroemer, G. (2021). Ferroptosis: Molecular Mechanisms and Health Implications. *Cell Res* 31, 107–125. doi:10.1038/s41422-020-00441-1

Vasquez, M. M., Hu, C., Roe, D. J., Chen, Z., Halonen, M., and Guerra, S. (2016). Least Absolute Shrinkage and Selection Operator Type Methods for the Identification of Serum Biomarkers of Overweight and Obesity: Simulation and Application. *BMC Med. Res. Methodol.* 16, 154. doi:10.1186/s12874-016-0254-8

Wang, Z., Chen, X., Liu, N., Shi, Y., Liu, Y., Ouyang, L., et al. (2021). A Nuclear Long Non-coding RNA LINC00618 Accelerates Ferroptosis in a Manner Dependent upon Apoptosis. *Mol. Ther.* 29, 263–274. doi:10.1016/j.ymthe.2020.09.024

Whitfield, A. J., Barrett, P. H. R., van Bockxmeer, F. M., and Burnett, J. R. (2004). Lipid Disorders and Mutations in the APOB Gene. *Clin. Chem.* 50, 1725–1732. doi:10.1373/clinchem.2004.038026

Xia, H., Qu, X. L., Liu, L. Y., Qian, D. H., and Jing, H. Y. (2018). LncRNA MEG3 Promotes the Sensitivity of Vincristine by Inhibiting Autophagy in Lung

Cancer Chemotherapy. *Eur. Rev. Med. Pharmacol. Sci.* 22, 1020–1027. doi:10.26355/eurrev_201802_14384

Yang, C., Zhang, Y., Lin, S., Liu, Y., and Li, W. (2021). Suppressing the KIF20A/NUAK1/Nrf2/GPX4 Signaling Pathway Induces Ferroptosis and Enhances the Sensitivity of Colorectal Cancer to Oxaliplatin. *Aging* 13, 13515–13534. doi:10.18632/aging.202774

Zhou, N., and Bao, J. (2020). *FerrDb: A Manually Curated Resource for Regulators and Markers of Ferroptosis and Ferroptosis-Disease Associations*. Oxford, England: Database Oxford, 2020.

Conflict of Interest: The authors declare that the research was conducted in the absence of any commercial or financial relationships that could be construed as a potential conflict of interest.

Publisher's Note: All claims expressed in this article are solely those of the authors and do not necessarily represent those of their affiliated organizations, or those of the publisher, the editors and the reviewers. Any product that may be evaluated in this article, or claim that may be made by its manufacturer, is not guaranteed or endorsed by the publisher.

frontiers in Genetics

ORIGINAL RESEARCH
published: 17 December 2021
doi: 10.3389/fgene.2021.785839

Ferroptosis-Related Long Non-Coding RNA Signature Contributes to the Prediction of Prognosis Outcomes in Head and Neck Squamous Cell Carcinomas

Wenru Jiang[1]†, Yingtao Song[1†], Zhaowei Zhong[1], Jili Gao[1] and Xiaofei Meng[2]*

[1]*Department of Implant and Prosthodontics, The First Affiliated Hospital of Harbin Medical University, Harbin, China,* [2]*Donglai Road Stomatological Clinic, Laizhou, China*

Background: Head and neck squamous cell carcinoma (HNSCC) is a malignant tumor, which makes the prognosis prediction challenging. Ferroptosis is an iron-dependent form of non-apoptotic regulated cell death, which could affect cancer development. However, the prognostic value of ferroptosis-related long non-coding RNA (lncRNA) in HNSCC is still limited.

Methods: In the current study, we employed the DESeq2 method to characterize the differentially expressed ferroptosis-related genes (FEGs) between cancer and normal samples. Next, the FEG-related lncRNAs (FElncRNAs) were identified using Spearman's correlation analysis and multiple permutation hypotheses. Subsequently, LASSO and stepwise multivariate Cox regression analyses were undertaken to recognize the prognosis-related FElncRNA signature (PFLS) and risk scores.

Results: Herein, we first identified 60 dysregulated FEGs and their co-expressed FElncRNAs in HNSCC. Then, we recognized a set of six FElncRNAs PFLS (*SLCO4A1-AS1*, *C1RL-AS1*, *PCED1B-AS1*, *HOXB-AS3*, *MIR9-3HG*, and *SFTA1P*) for predicting patients' prognostic risks and survival outcomes. We also assessed the efficiency of PFLS in the test set and an external validation cohort. Further parsing of the tumor immune microenvironment showed the PFLS was closely associated with immune cell infiltration abundances. Notably, the low-risk group of the PFLS showed a higher MHC score and cytolytic activity (CYT) score than the high-risk group, implying the low-risk group may have greater tumor surveillance and killing ability. In addition, we observed that the expression levels of two immune checkpoints (ICPs), i.e., programmed cell death protein 1 (*PD-1*) and programmed cell death 1 ligand 1 (*PD-L1*), showed significant associations with patients' risk score, prompting the role of the PFLS in ICP blockade therapy. Finally, we also constructed a drug–PFLS network to reinforce the clinical utilities of the PFLS.

OPEN ACCESS

Edited by:
Ying Li,
The University of Texas Health Science Center at San Antonio, United States

Reviewed by:
Yuying Xie,
Michigan State University, United States
Qiuji Wu,
Wuhan University, China

****Correspondence:***
Wenru Jiang
wjdingy@163.com

†These authors have contributed equally to this work

Specialty section:
This article was submitted to Human and Medical Genomics, a section of the journal Frontiers in Genetics

Received: *29 September 2021*
Accepted: *03 December 2021*
Published: *17 December 2021*

Citation:
Jiang W, Song Y, Zhong Z, Gao J and Meng X (2021) Ferroptosis-Related Long Non-Coding RNA Signature Contributes to the Prediction of Prognosis Outcomes in Head and Neck Squamous Cell Carcinomas. Front. Genet. 12:785839. doi: 10.3389/fgene.2021.785839

Abbreviations: AUC, area under the ROC curve; DEG, differentially expressed gene; FEG, ferroptosis-related gene; FElncRNA, FEG-related lncRNA; HNSCC, head and neck squamous cell carcinoma; ICP, immune checkpoint; LncRNA, long non-coding RNA; OS, overall survival; PFLS, prognosis-related FElncRNA signature; ROC, receiver operating characteristic curve; TCGA, the cancer genome atlas

Conclusion: In summary, our study indicated that FElncRNAs played an important role in HNSCC survival prediction. Identification of PFLS will contribute to the development of novel anticancer therapeutic strategies.

Keywords: head and neck squamous cell carcinoma, lncRNA, prognosis prediction, tumor immune microenvironment, immune checkpoint blockade therapy

INTRODUCTION

Head and neck squamous cell carcinoma (HNSCC) is the sixth most common type of malignant tumor among adults with a 5-year survival rate of less than 70% (Pulte and Brenner, 2010; Johnson et al., 2020). As an epithelial tumor, HNSCC frequently appears in linings of the oral cavity, the pharynx, or the larynx (Tumino and Vicario, 2004). These tumors affect over 800,000 individuals worldwide (Johnson et al., 2020). Although novel clinical therapeutic methods have been utilized, the survival rate has not improved significantly over the recent decades (Pfister et al., 2011). Therefore, the identification of a novel signature for predicting the prognosis risk is urgently demanded.

Ferroptosis is a type of programmed cell death, which is driven by the iron-dependent peroxidation of lipids and is distinct from apoptosis, cell necrosis, and autophagy (Dixon et al., 2012; Stockwell et al., 2017; Jiang et al., 2021). Long non-coding RNAs (lncRNAs) are defined as transcripts with more than 200 nucleotides without a detectable coding potential (Wilusz et al., 2009; Ulitsky, 2016). Previous studies have demonstrated that lncRNAs showed a promising potential for indicating the tumor development risk. For example, *LINC01215* was characterized as an immune regulator and prognostic biomarker in multiple human cancers (Li et al., 2021); ferroptosis-related lncRNA *LINC00336* is highly expressed in lung cancer and acts as a competitive endogenous RNA to affect carcinogenesis (Wang et al., 2019a). However, characterization of the ferroptosis-related lncRNA signature for improving survival prediction in HNSCC is still limited.

Herein, we systemically portrayed the dysregulated FEGs between HNSCC tumors and adjacent normal tissues, including 44 up-regulated and 16 down-regulated. Next, we identified their co-expressed FElncRNAs and recognized a set of six prognosis-related FElncRNA signature (PFLS, *SLCO4A1-AS1*, *C1RL-AS1*, *PCED1B-AS1*, *HOXB-AS3*, *MIR9-3HG*, and *SFTA1P*) for predicting patients' prognostic risks and survival outcomes (**Supplementary Figure S1**). Notably, the PFLS showed close associations with the tumor immune microenvironment and some immune checkpoint (ICP) expression. This highlighted the important role of PFLS in ICP blockade therapy. Finally, a drug–PFLS network was employed to identify more potential clinical utilities of PFLS.

MATERIALS AND METHODS

Data Collection

The RNA-seq profiles and clinical information of head and neck squamous cell carcinomas (HNSCCs) were collected from The Cancer Genome Atlas (TCGA) database (https://portal.gdc.cancer.gov/). Ferroptosis-related genes (FEGs) were from the FerrDb database (http://www.zhounan.org/ferrdb/), including 111 genes that indicate the occurrence of ferroptosis, 108 genes that promote ferroptosis, and 69 genes that prevent ferroptosis (**Supplementary Table S1**) (Zhou and Bao, 2020). Besides, an independent HNSCC cohort GSE65858 (Wichmann et al., 2015) was obtained from Gene Expression Omnibus (GEO). The TCGA HNSCC cohort was utilized as the training cohort, while the GSE65858 dataset was employed for the external validation cohort. GSE65858 is a 270-sample HNSCC dataset yielded by the Illumina HumanHT-12 V4.0 expression beadchip (GPL10558). We employed the R package "illuminaHumanv4" to perform the probe reannotation (https://bioconductor.org/packages/release/data/annotation/html/illuminaHumanv4.db.html). For lncRNA/gene with multiple probes, the average probe intensity was used to indicate the expression level of the lncRNA/gene.

Differential Expression Analysis of Ferroptosis-Related Genes

We identified the differentially expressed FEGs between cancer and normal samples using DESeq2 (Love et al., 2014). FEGs with adjusted p-values < 0.01 and $|\log_2 FC| > 1$ were considered as the differentially expressed FEGs (DE-FEGs) (**Supplementary Table S2**).

Identification of Ferroptosis-Related Long Non-Coding RNAs

To identify the ferroptosis-related lncRNAs (FElncRNAs), we performed Spearman's correlation test between the expression levels of FEGs and lncRNAs in the TCGA cohort. Spearman's correlation p-values (P_r) were adjusted by multiple hypotheses based on a permutation method (Yao et al., 2015). For each lncRNA, the expression value was held consistent, and in total, 10,000 random FEGs were used to perform the same Spearman's correlation test, generating a set of 10,000 permutation p-values (P_p). Finally, an empirical p-value (P_e) was corrected as $P_e = [num(P_p \le P_r) + 1]/10001$. P_e was adjusted by the BH method (q_e). LncRNAs with $q_e < 0.001$ and an absolute value of correlation coefficient > 0.3 were identified as the FElncRNAs (**Supplementary Table S3**).

Construction of the Prognosis Prediction Model

We first divided the TCGA-HNSCC dataset into three parts, with two as the training set and one as the test set. In the training, the

univariate Cox regression model adjusted by gender, age, and tumor stage was constructed based on the expression levels of FElncRNAs. FElncRNAs with p-values < 0.05 were identified as the candidate prognosis-related FElncRNAs. Next, we employed the LASSO (least absolute shrinkage and selection operator) regression model to further screen the prognosis-related FElncRNAs and prevent the model overfitting (**Supplementary Figure S2**). Subsequently, we applied the bi-directional stepwise multivariate Cox regression based on the AIC (Akaike information criterion) value on the potential FElncRNAs to select the ones that minimize the AIC to attain the best model fit. A six-FElncRNA signature was identified as the prognosis-related FElncRNA signature (PFLS) which showed a significant correlation with HNSCC tumor samples' overall survival (OS) probability. Specifically, the risk score for each patient was calculated according to the linear combination of expression values weighted by the coefficient from the multivariate Cox regression analysis:

$$Risk\ score = \sum_{k=1}^{n} coef\,(FElncRNA_k) * Expression(FElncRNA_k)$$

We subgrouped the samples into high-risk and low-risk groups based on the median value. of PFLS risk scores. Kaplan–Meier (KM) analysis with the log-rank test was applied to compare the survival difference between patients' risk groups using the R package "survival". Alternatively, the risk score was examined through the time-dependent receiver operating characteristic (ROC) curve for one-, three-, and 5-year survival, respectively. The ROC analysis was conducted using the R package "survivalROC".

Nomogram Analysis

We also performed the nomogram analysis to predict the one-, three-, and 5-year survival for the patients with HNSCC using the R package rms. Calibration curves were further used to assess the discrimination between actual and nomogram predicted OS probability. Besides, we adjusted other clinical features in independent prognostic analysis in order to confirm whether the PFLS was an independent indicator to predict the prognosis of patients with HNSCC.

Tumor Immune Microenvironment Analysis

To evaluate the antitumor activity, we calculated the MHC score (Lauss et al., 2017) and cytolytic activity (CYT) score (Rooney et al., 2015). The MHC score represents the capability of antigen presentation by T cells and subsequent T cell-mediated tumor killing, which could be expressed as the average gene expression levels of the "core" MHC-I set (including genes *HLA-A*, *HLA-B*, *HLA-C*, *TAP1*, *TAP2*, *NLRC5*, *PSMB9*, *PSMB8,* and *B2M*) (Lauss et al., 2017). The CYT score indicates the cytolytic activity used by immune cells to kill tumor cells, computed as the geometric mean of the genes *GZMA* and *PRF1* (Rooney et al., 2015). We estimated the immune cell landscape using the ESTIMATE (Yoshihara et al., 2013), TIMER (Li et al., 2017), CIBERSORT (Newman et al., 2015), EPIC (Racle et al., 2017), FARDEEP (Hao et al., 2019), and MuSiC (Wang et al., 2019b; Avila Cobos et al., 2020), respectively. Next, we calculated Spearman's correlation between the immune cell abundance and the PFLS risk score. The p-value was adjusted by the BH method. We also compared the immune cell abundance between high- and low-risk groups using the Mann–Whitney U test. The p-value was adjusted by the BH method. In addition, we performed the enrichment analysis between the risk groups and four pre-defined HNSCC microenvironment subtypes (immune-enriched, fibrotic [IE/F]; immune-enriched, non-fibrotic [IE]; fibrotic [F]; and immune-depleted [D]) by Bagaev et al. using accumulative hypergeometric distribution (Bagaev et al., 2021). The p-value was adjusted by the BH method.

Immune Checkpoints Analysis

We manually curated 150 potential immune checkpoints (ICPs) from previous studies. And, we performed Spearman's correlation analysis between the expression levels of these ICPs and the PFLS risk score. The p-value was adjusted by the BH method. Additionally, we also compared the expression levels of common immune checkpoint genes, including CD274 and PDCD1 (Waldman et al., 2020) between the high- and low-risk groups using the Mann–Whitney U test (**Supplementary Table S4**).

Functional Enrichment Analysis of the Prognosis-related FElncRNA Signature

We first identified the differentially expressed genes (DEGs) between cancer and normal samples using the Mann–Whitney U test (q-value < 0.01, $|\log_2 FC| > 1$). Next, the corresponding co-expressed genes of each FElncRNA (FELGs) in the PFLS were recognized from DEGs using the permutation method mentioned above ($q_e < 0.01$, $|Rho| > 0.3$). For each given FELG list, the pathway and process enrichment analysis have been carried out with the following ontology sources: KEGG Pathway, GO Biological Processes, Reactome Gene Sets, Canonical Pathways, and WikiPathways. All genes in the genome have been used as the enrichment background. Terms with adjusted p-values < 0.01, a minimum count of 3, and an enrichment factor > 1.5 are collected and grouped into clusters based on their membership similarities. More specifically, p-values are calculated based on the accumulative hypergeometric distribution, and q-values are calculated using the BH method to account for multiple testing. The functional enrichment analysis was conducted by Metascape (Zhou et al., 2019).

Construction of the Drug Sensitivity Network

We obtained the FElncRNA-related drugs from the D-lnc database (Jiang et al., 2019). D-lnc included the experimentally validated and the computationally predicted modification of drugs on the lncRNA expression. And, the drug sensitivity network was constructed by Cytoscape (Shannon et al., 2003).

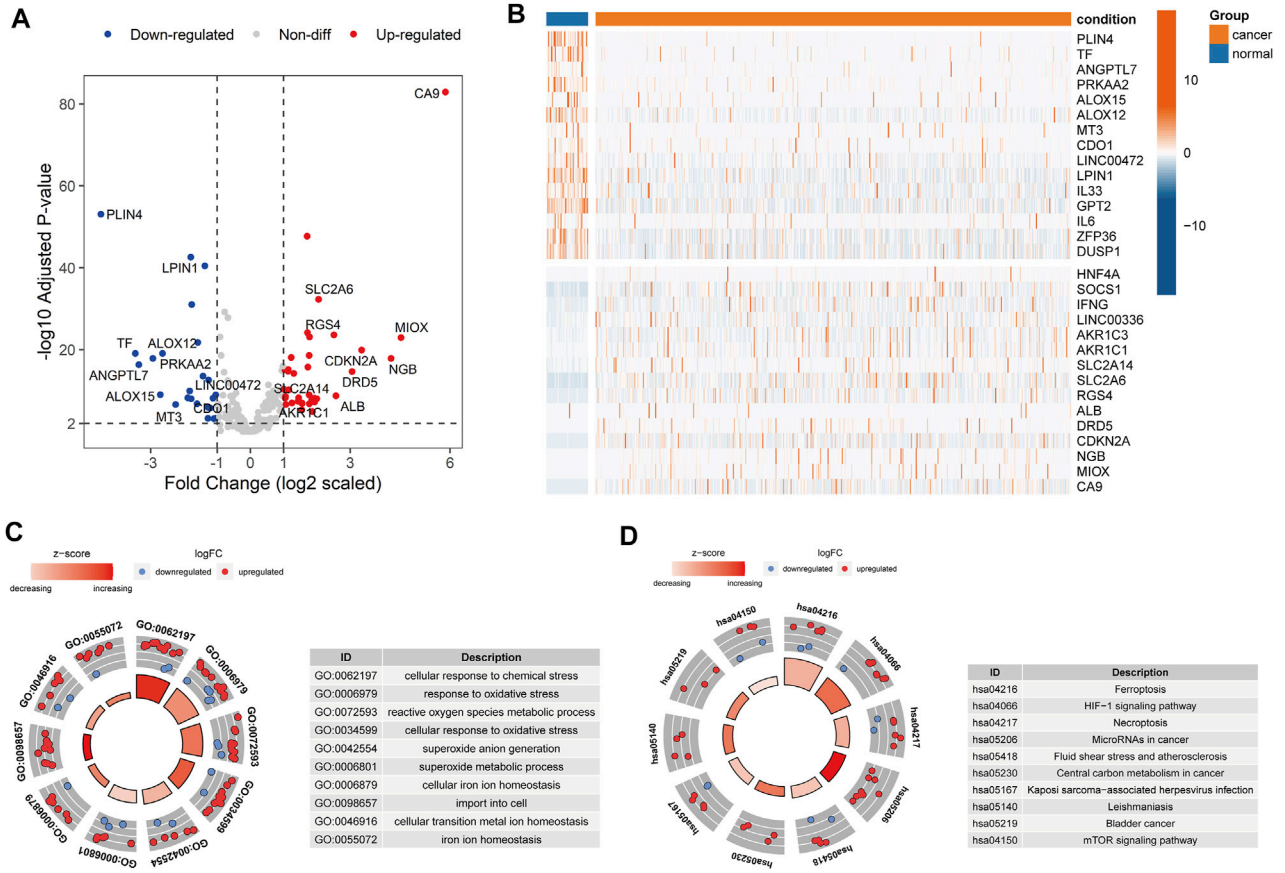

ID	Description
GO:0062197	cellular response to chemical stress
GO:0006979	response to oxidative stress
GO:0072593	reactive oxygen species metabolic process
GO:0034599	cellular response to oxidative stress
GO:0042554	superoxide anion generation
GO:0006801	superoxide metabolic process
GO:0006879	cellular iron ion homeostasis
GO:0098657	import into cell
GO:0046916	cellular transition metal ion homeostasis
GO:0055072	iron ion homeostasis

ID	Description
hsa04216	Ferroptosis
hsa04066	HIF−1 signaling pathway
hsa04217	Necroptosis
hsa05206	MicroRNAs in cancer
hsa05418	Fluid shear stress and atherosclerosis
hsa05230	Central carbon metabolism in cancer
hsa05167	Kaposi sarcoma−associated herpesvirus infection
hsa05140	Leishmaniasis
hsa05219	Bladder cancer
hsa04150	mTOR signaling pathway

FIGURE 1 | Dysregulated ferroptosis-related genes in HNSCC. **(A)** Volcano plot showing the differentially expressed FEGs between cancer and normal samples. Red and blue dots represent the up and downregulated FEGs, respectively. **(B)** Heatmap showing the top 15 up and downregulated FEGs between cancer and normal samples. C-D. Circle plot showing the z-score of significantly enriched **(C)** GO terms and **(D)** KEGG pathways. Red dots indicated upregulation, while the blue indicated downregulation. The Z-score was calculated by the R package "GOplot". The significantly enriched GO terms and KEGG pathways are listed on the left.

RESULTS

Dysregulated Ferroptosis-Related Genes Were Associated With Metabolic Processes and Cancer-Related Pathways

To explore the expression levels of 259 ferroptosis-related genes (FEGs), we performed the differential expression analysis between cancer and normal samples in HNSCC (*Materials and Methods*). A total of 36 upregulated and 24 downregulated FEGs were identified (**Figures 1A,B**, **Supplementary Table S2**). Furthermore, we annotated their biological functions and observed that these FEGs mainly participated in multiple metabolic processes and cancer-related pathways (**Figures 1C,D**), such as cellular response to chemical stress (GO:0062197), reactive oxygen species metabolic process (GO:0072593), cellular response to oxidative stress (GO:0034599), microRNAs in cancer (hsa05206), and central carbon metabolism in cancer (hsa05230), etc. These results indicated that dysregulated FERGs were associated with metabolic processes and might play an important role in HNSCC.

A Six-Ferroptosis-Related Long Non-Coding RNA Signature Contributes to the Survival Outcome Prediction

Long non-coding RNA (lncRNA) is emerging as a promising biomarker and shows prognostic values in multiple cancer types (Bolha et al., 2017; Xu et al., 2019; Yang et al., 2017). Hence, we systemically identified the ferroptosis-related lncRNAs (FElncRNAs) in HNSCC (Materials and methods). A total of 926 lncRNAs were recognized as FElncRNAs. To explore the prognosis values of these FElncRNAs, we constructed the prognostic risk model (*Materials and Methods*) and recognized a six-FElncRNA prognosis signature (PFLS). The PFLS consisted of six FElncRNAs, including two risk factors: *HOXB-AS3* and *SFTA1P*, and four protective factors: *SLCO4A1-AS1*, *C1RL-AS1*, *PCED1B-AS1*, and *MIR9-3HG*, which showed correlations with the HNSCC tumor samples' overall survival (OS) probability

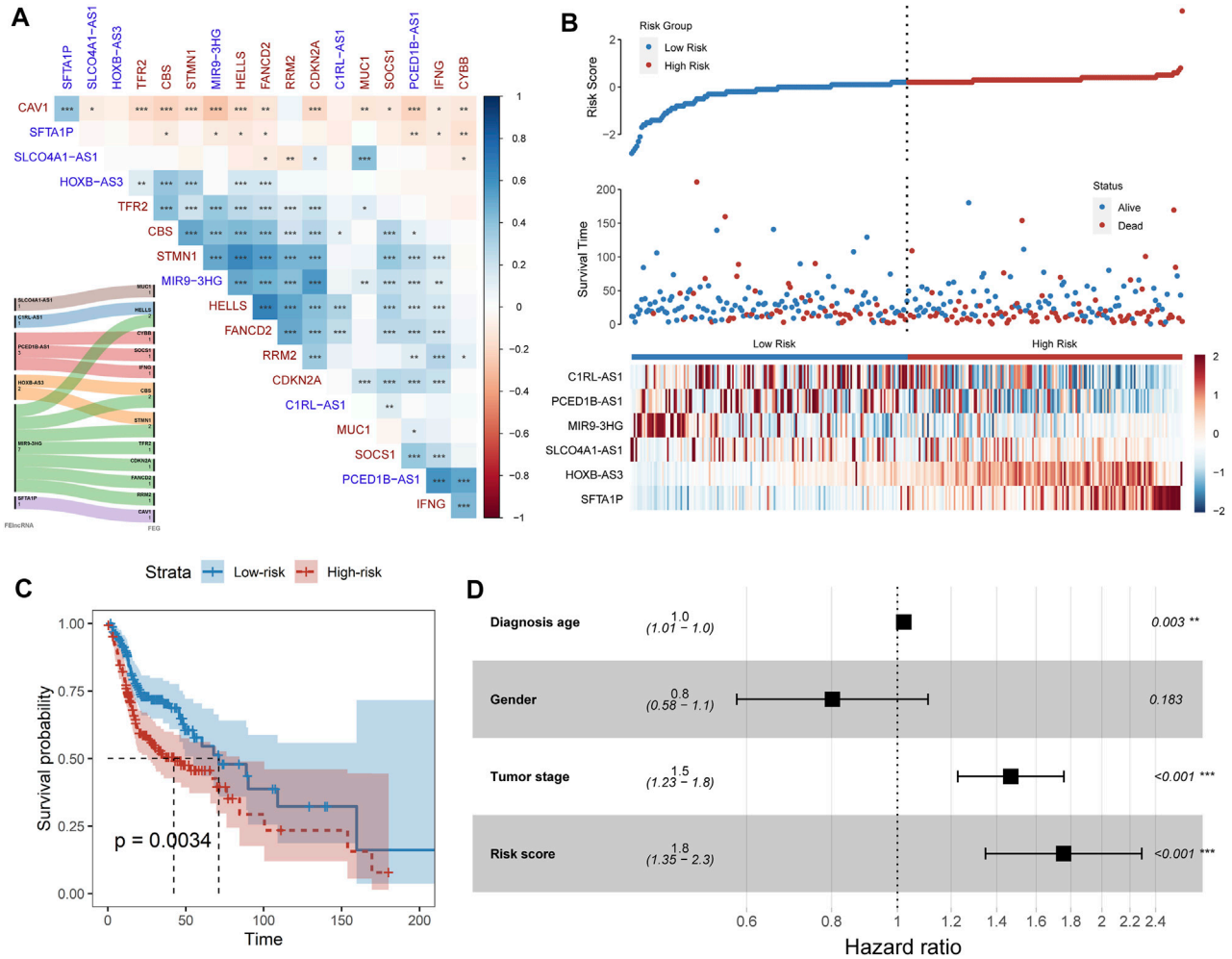

FIGURE 2 | FElncRNAs indicated the prognosis values in HNSCC. **(A)** Heatmap showing the Spearman's correlation between FElncRNAs and FEGs. **(B)** Risk score distribution, survival status, and lncRNA expression patterns for patients in high- and low-risk groups by the PFLS. **(C)** Kaplan–Meier curve of HNSCC cancer samples stratified by the risk group with the log-rank test *p*-value provided. **(D)** Forest plot showing the result of multivariate Cox regression analysis for correlation between the PFLS and clinical features and the overall survival in the TCGA cohort.

(**Supplementary Figure S3**). We further explored the associations between the PFLS, FElncRNAs, and FEGs (**Figure 2A**). *MIR9-3HG* showed a broad correlation with multiple FEGs, such as *STMN1*, *CBS*, and *HELLS*. Previous studies also further supported that *MIR9-3HG* was a prognosis-related biomarker in HNSCC (Hu et al., 2020; Guo et al., 2021).

Prognosis-Related FElncRNA Signature Reveals the Potential Prognostic Risk in Head and Neck Squamous Cell Carcinomas

We next calculated the risk score of the PFLS to characterize the prognosis risk of TCGA HNSCC. The PFLS risk score could be expressed as: (−0.423**SLCO4A1-AS1*) + (−0.393**C1RL-AS1*) + (−0.207**PCED1B-AS1*) + (0.159**HOXB-AS3*) + (−0.231**MIR9-3HG*) + (0.036**SFTA1P*) (**Figure 2B**). We then subgrouped the patients into high- and low-risk groups based on the median values of the risk score. The PFLS risk group was able to indicate patients' survival outcomes (**Figure 2C**). Notably, the multivariate Cox regression model adjusted by age, gender, and tumor stage also suggested that the PFLS risk score was an independent risk factor for predicting the overall survival outcomes of HNSCC patients (HR = 1.8, $p < 0.001$) (**Figure 2D**). These results suggested that the PFLS was a promising biomarker for indicating the prognosis risk of HNSCC.

Prognosis-Related FElncRNA Signature as an Independent Factor Prompts Prognostic Risk

Further parsing of the nomogram, PFLS was the most significant contribution to OS of one-, three-, and 5-year of HNSCC (**Figure 3A**). The calibration also supported that the PFLS was a

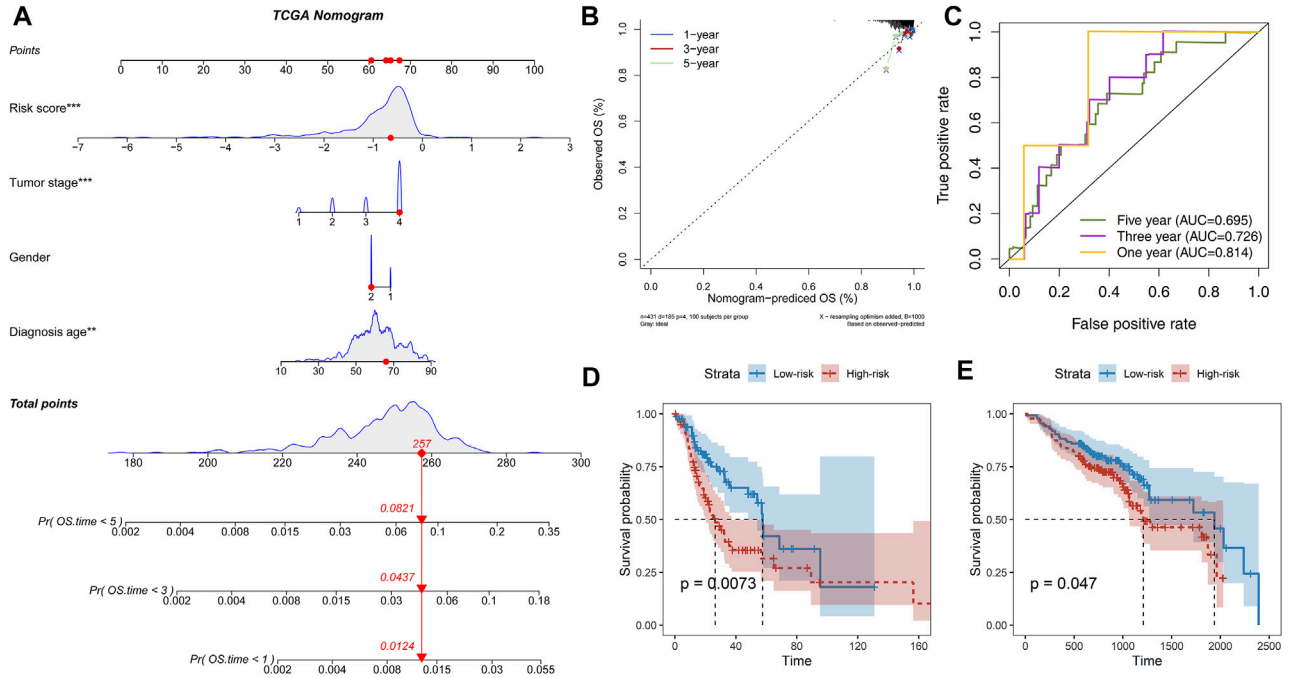

FIGURE 3 | PFLS was an independent prognosis factor in HNSCC. **(A)** Nomogram composed of age, gender, stage, and risk score for the prediction of 1-, 3-, and 5-years OS probability. **(B)** Calibration for assessing the consistency between the predicted and the actual OS at 1, 3, and 5 years. **(C)** ROC curves at one, three, and five years were applied to verify the prognostic performance of the PFLS in the TCGA training set. D-E. The Kaplan–Meier curve of HNSCC cancer samples stratified by the risk group with the log-rank test *p*-value provided in **(D)** TCGA test set and **(E)** GSE65858.

promising prognostic biomarker with high accuracy (**Figure 3B**). In addition, the time-dependent ROC curve was constructed for one-, three-, and 5-year, and the area under the curve (AUC) was calculated to estimate the prognostic competence of the PFLS risk score (**Figure 3C**). The AUC of the risk score was >0.695, indicating the PFLS has powerful predictive prognostic capacity. To further confirm the PFLS is a robust biomarker in HNSCC, we employed the risk scoring model in the TCGA test set an independent HNSCC dataset GSE65858 (Wichmann et al., 2015) (n = 270). The PFLS risk score was identified as a poor prognosis marker (**Figures 3D,E**). These demonstrated the potential for PFLS risk scores to improve the prognosis of HNSCC as a complement to epidemiological features.

Prognosis-Related FElncRNA Signature Suggests the Risk of Tumor Progression and Radiotherapy Benefits

We next explored the relationship between the PFLS and progression-free survival. By constructing the Cox proportional hazards model, we found patients in the high-risk group were more likely to experience the tumor progression than those in the low-risk group (HR = 1.5, p = 0.014) (**Figure 4A**). Furthermore, we investigated the clinical implication of the PFLS. In the patients who received radiation therapy, we found that the high-risk group of PFLS showed the association with poor OS probability (HR = 1.91, p = 0.007) (**Figure 4B**). These results also highlighted the potential clinical implications of the PFLS for predicting tumor progression and radiotherapy benefits.

Prognosis-Related FElncRNA Signature-Risk Group Shows Association With the Tumor Immune Microenvironment and Prompts Potential Immunotherapy Values

To explore the potential mechanism of the PFLS in patients' survival outcomes, we performed the gene set function enrichment based on the ferroptosis pathway (WP4313) between high- and low-risk groups. We observed the ferroptosis pathway significantly enriched in the low-risk group (**Supplementary Figure S4A**). Additionally, we also found that the tumor purity of the low-risk group is significantly lower than that of the high-risk group, in which the tumor immune score showed a significant difference between the two risk groups (**Supplementary Figure S4B**). Besides, we characterized the antitumor activity by calculating the MHC score and CYT score (*Materials and Methods*). We found that patients in the low-risk group showed higher MHC and CYT scores than those in the high-risk group (**Supplementary Figures S4C,D**), implying the low-risk group typically exhibited stronger tumor monitor and killing ability. Hence, we characterized the tumor immune microenvironment between the high- and low-risk groups based on multiple cell-type deconvolution algorithms

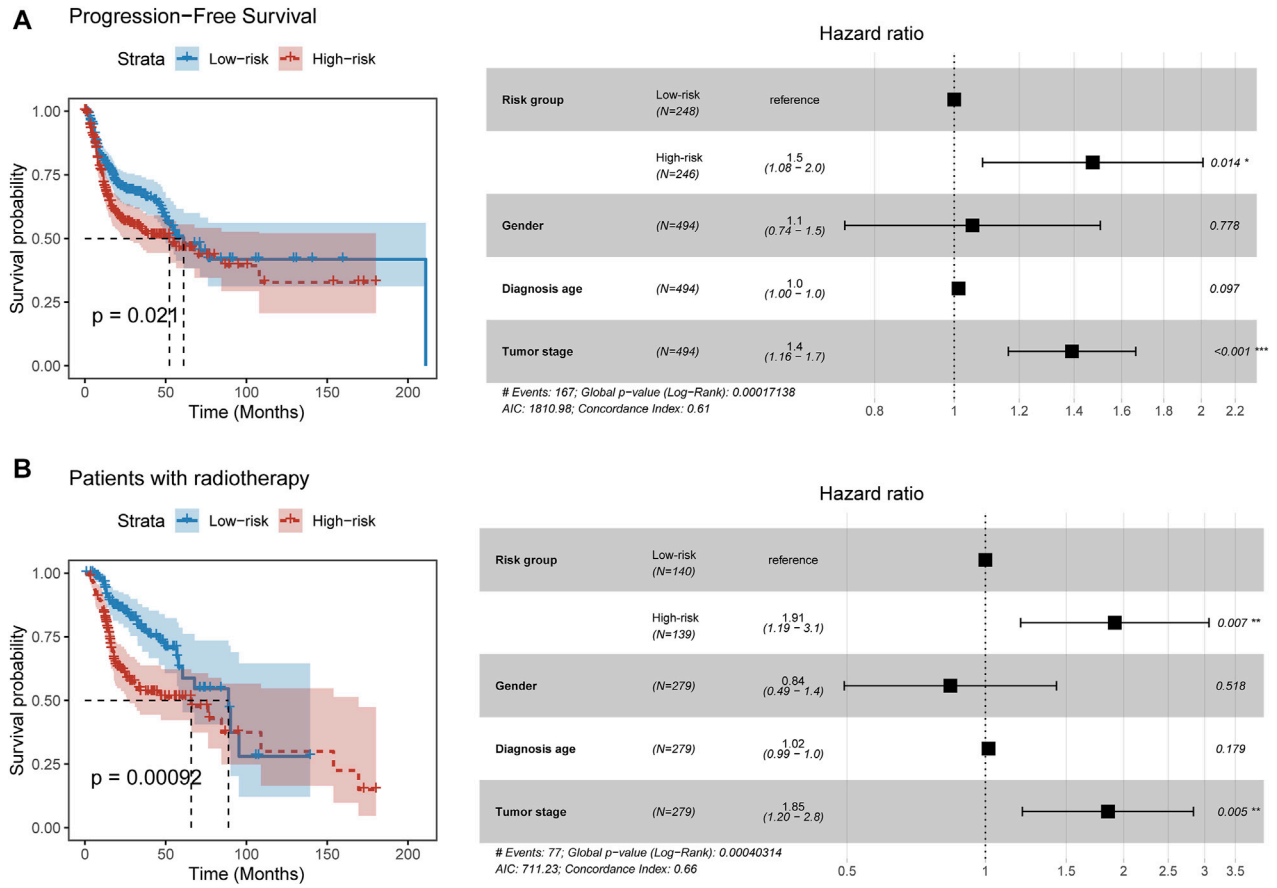

FIGURE 4 | PFLS contributes to tumor progression and radiotherapy benefits. **(A,B)** On the left of each panel, the Kaplan–Meier curve of HNSCC cancer samples was stratified by the risk group with the log-rank test *p*-value provided. Forest plot showing the result of multivariate Cox regression analysis for correlation between the PFLS and clinical features and the **(A)** progression-free or **(B)** overall survival was plotted on the right.

(Avila Cobos et al., 2020). There were generally higher immune cell infiltration levels in the low-risk group than in the high-risk group (**Figure 5A** and **Supplementary Figure S5**), further highlighting the antitumor activity of the low-risk group.

Besides, we enriched our risk groups to four pre-defined HNSCC microenvironment subtypes (immune-enriched, fibrotic [IE/F]; immune-enriched, non-fibrotic [IE]; fibrotic [F]; and immune-depleted [D]) using accumulative hypergeometric distribution (Bagaev et al., 2021). The result showed that there were significant enrichments between the low-risk group and two immune-enriched subtypes (IE/F and IE) (**Figure 5B**), which could be a reasonable explanation for the better survival outcome in the low-risk group. Notably, the IE/F and IE subtypes were also characterized as the responsive factors for immune checkpoint (ICP) blockade therapy (Bagaev et al., 2021). Hence, we manually curated 150 potential ICPs from previous studies and performed Spearman's correlation analysis between the expression levels of these ICPs and the PFLS risk score (Materials and methods). There were 109 ICPs that showed significant correlations with the PFLS risk score (**Supplementary Table S4**). Interestingly, we found two well-known ICPs, i.e., programmed cell death protein 1 (PD-1, *PDCD1*) and programmed cell death 1 ligand 1 (PD-L1, *CD274*), that showed obvious correlations with the PFLS risk score, which also implied the PFLS might play an important role in anti-PD-1/PD-L1 immunotherapy (**Figure 5D**). These results indicated that the PFLS also showed the immunological correlation and prompts the potential immunotherapy benefits.

Biological Function Annotations for the Prognosis-Related FElncRNA Signature With Identification of Potential Clinical Implications

To explore the potential biological functions of the PFLS, we first identified the corresponding co-expressed genes of each FElncRNA (FELGs) in the PFLS (Materials and Methods). There was obvious co-expression crosstalk among *SFTA1P*, *C1RL-AS1*, and *MIR9-3HG* (**Figure 6A**), implying they could share similar biological functions in HNSCC. Furthermore, based on the functional enrichment analysis, we found that PFLS could be engaged in the cell cycle , DNA replication , and immune-related biological processes (**Figures 6B,C**). Finally, we also constructed a PFLS drug sensitivity network to identify the

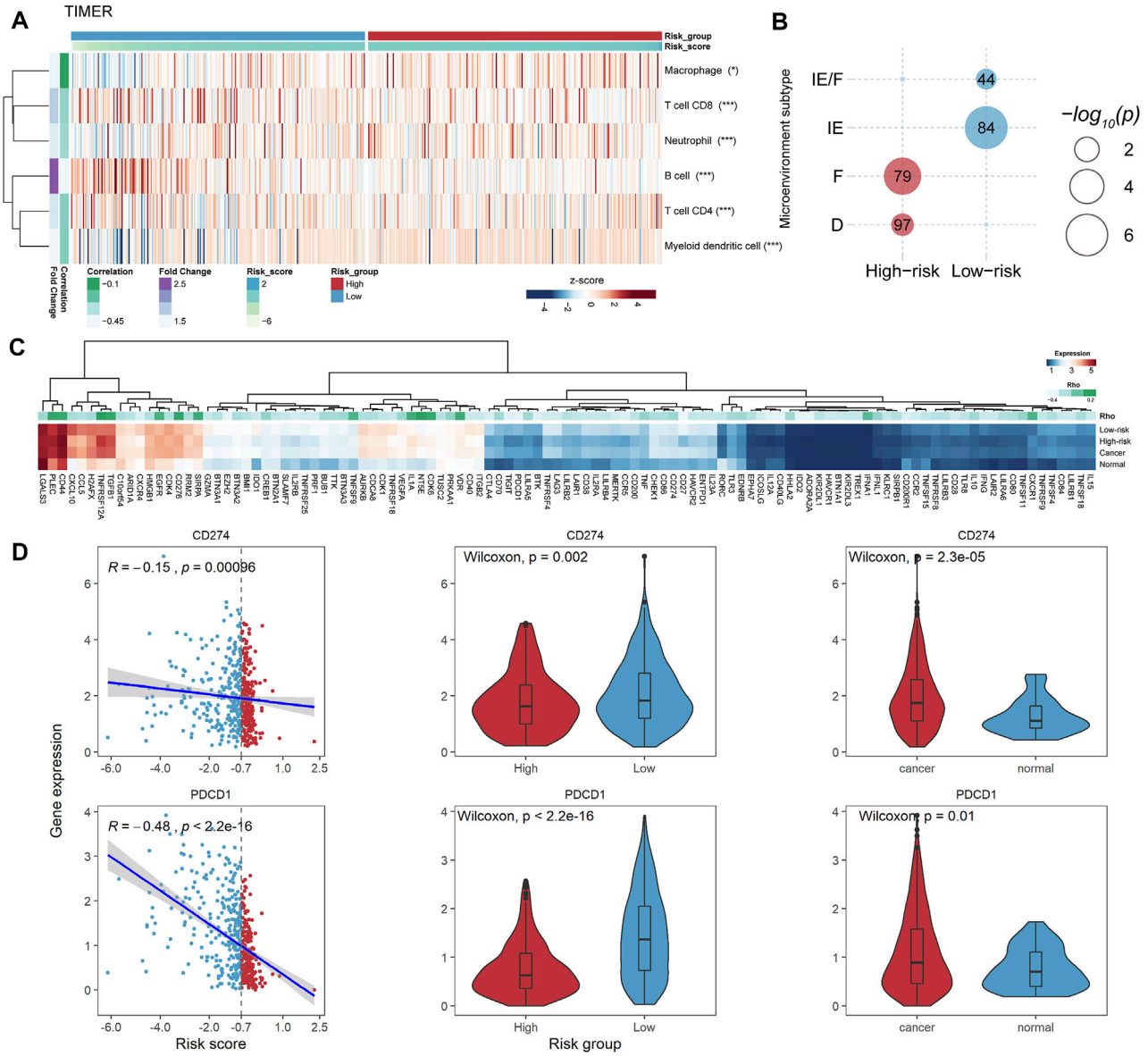

FIGURE 5 | PFLS-risk groups were associated with the tumor immune microenvironment. **(A)** Heatmap showing the tumor immune cell infiltration levels assessed by TIMER. The Spearman's correlation significance between cell abundance and the risk score was also computed for each cell shown on the right (*$p < 0.05$, **$p < 0.001$, and ***$p < 0.0001$). **(B)** Bubble plot showing the significant enrichment between HNSCC microenvironment subtypes and risk groups. **(C)** Heatmap showing the expression levels of PFLS-related ICPs. D. CD274 and PDCD1 were closely associated with the PFLS risk score. *$p < 0.05$, **$p < 0.001$, and ***$p < 0.0001$ as calculated using the **(B)** accumulative hypergeometric distribution, **(C)** Spearman's correlation test.

potential clinical uses of the PFLS based on the drug–gene interactome data from the D-lnc database (Jiang et al., 2019). Some known anticancer drugs, such as foretinib and paclitaxel, were also contained in the network (**Figure 6D** and **Supplementary Table S5**).

DISCUSSION

Growing evidence has indicated that ferroptosis-related lncRNAs played an important role in tumor prognostic prediction (Lu et al., 2021; Zhu et al., 2021). However, the prognostic value of ferroptosis-related lncRNAs in HNSCC remains unknown. Hence, in this study, we explored the potential prognostic values of FElncRNAs. We first characterized the differentially expressed FEGs, which showed the biological functions manifested in multiple metabolic processes and cancer-related pathways. The result also demonstrated that ferroptosis might play an important role in HNSCC cancer development.

Next, to investigate the role of FElncRNAs in patients' survival, we employed the stepwise multivariate Cox regression model to identify a six-FElncRNA signature named the PFLS. The

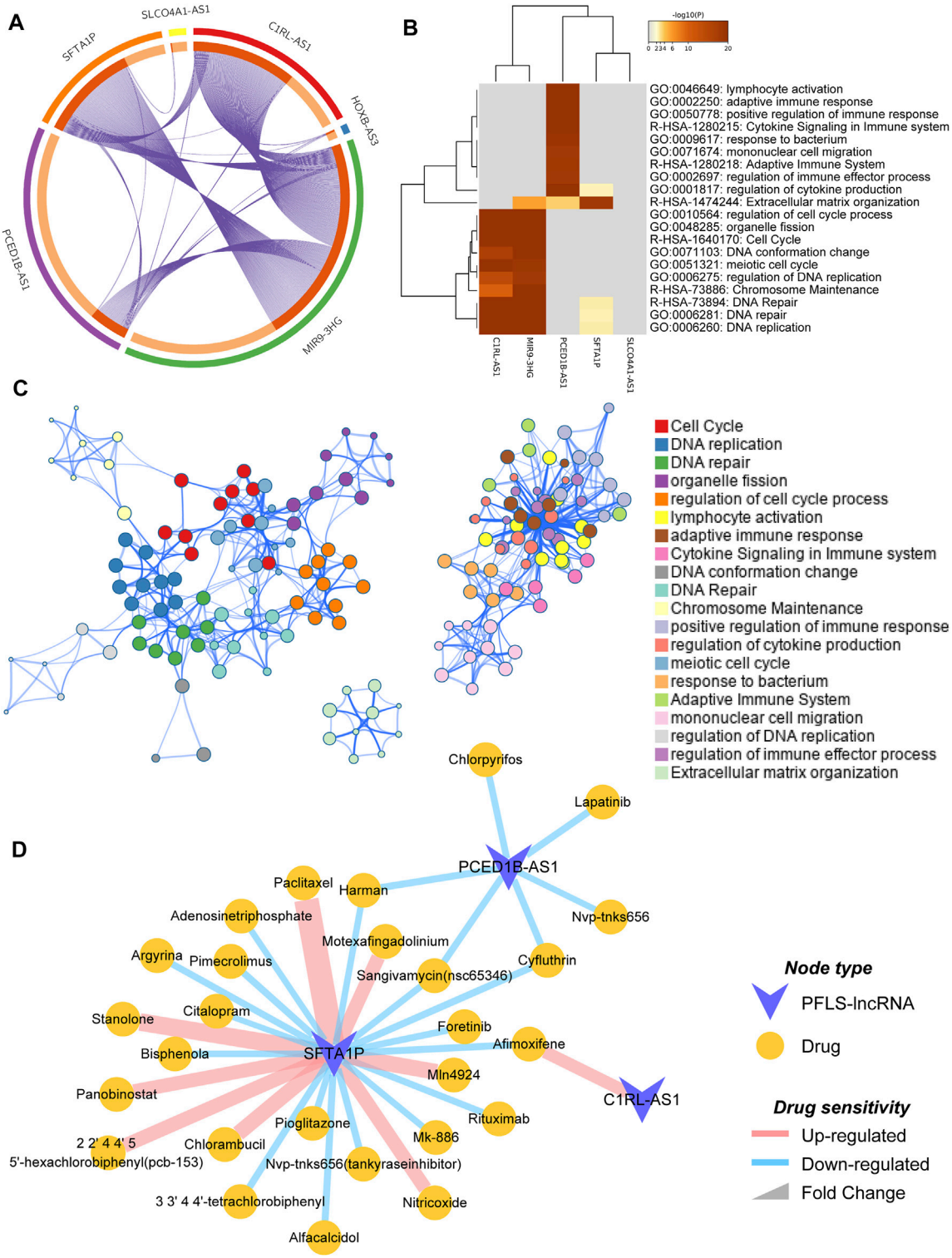

FIGURE 6 | Functional enrichment analysis and potential clinical utilities of PFLS. **(A)** Circosplot showing the overlap among PFLS co-expressed genes. Purple curves link identical genes. The inner circle represents gene lists, where hits are arranged along the arc. Genes that hit multiple lists are colored in dark orange, and genes unique to a list are shown in light orange. **(B)** Network of enriched terms colored by functional clusters, where nodes that share the same functional cluster are typically close to each other. **(C)** Heatmap of enriched terms across PFLS co-expressed genes, colored by *p*-values. **(D)** PFLS-related drug sensitivity network.

PFLS showed a good performance for predicting the prognostic risk and survival outcomes in both the TCGA training set, testing, and external validation sets. Additionally, by calculating the PFLS risk score for each cancer patient, we observed that the high-PFLS risk score was a poor prognosis biomarker for the overall survival probability. These results highlighted that the PFLS was a promising biomarker with a potential prognostic value. However, compared to the wide range of HNSCC patients, our study has only covered a small proportion. Therefore, as sequencing technology becomes more widely available, we will also continue to deepen our examination of the predictive power of the PFLS for survival.

Alternatively, the PFLS also showed immunological correlations. By linking the microenvironment subtypes identified by Bagaev et al., we found that the patients in the low-risk group were significantly enriched in the two immunotherapy responsive subtypes (IE/F and IE). And, we also observed that the programmed cell death protein 1 (PD-1, *PDCD1*) and programmed cell death 1 ligand 1 (PD-L1, *CD274*) showed the significant correlation with the PFLS risk score. Anti-PD-1/PD-L1 immunotherapy has emerged as an effective weapon for fighting against multiple cancer types (Waldman et al., 2020). Therefore, the correlations between PD-1/PD-L1 and PFLS risk scores could also imply the clinical immunotherapy benefits. Exploring the role of ferroptosis-related lncRNAs in the immunotherapy response will also provide new insights into the development of novel antitumor treatment strategies. In addition, by identifying the co-expressed genes and subsequent functional enrichment analysis, we observed that the PFLS mainly participated in the cell cycle, DNA repair, and immune-related biological processes. Notably, a recent study by Lin et al. showed that dihydroartemisinin (DHA) could induce ferroptosis and cause cell cycle arrest in head and neck carcinoma cells (Lin et al., 2016), which also highlighted the role of ferroptosis in HNSCC. Finally, we also constructed a drug–PFLS network to reinforce the clinical utilities of the PFLS. Some known and potential anticancer drugs were also included. Although these results are currently limited to the computational level, they provide a guide for our subsequent research.

In summary, our study provided a novel insight on understanding the ferroptosis-related lncRNAs in HNSCC. These FElncRNAs also showed associations with prognostic prediction, immunological associations, and potential clinical utilities.

DATA AVAILABILITY STATEMENT

Publicly available datasets were analyzed in this study. The source code and datasets could be accessed at https://github.com/HNSCC/PFLS.

AUTHOR CONTRIBUTIONS

WJ and YS designed the study and wrote the manuscript. ZZ and JG performed analysis. XM collected the dataset. All authors read and approved the final manuscript.

ACKNOWLEDGMENTS

The authors gratefully thank the TCGA and GEO for providing data for this work.

SUPPLEMENTARY MATERIAL

The Supplementary Material for this article can be found online at: https://www.frontiersin.org/articles/10.3389/fgene.2021.785839/full#supplementary-material

REFERENCES

Avila Cobos, F., Alquicira-Hernandez, J., Powell, J. E., Mestdagh, P., and De Preter, K. (2020). Benchmarking of Cell Type Deconvolution Pipelines for Transcriptomics Data. *Nat. Commun.* 11, 5650. doi:10.1038/s41467-020-19015-1

Bagaev, A., Kotlov, N., Nomie, K., Svekolkin, V., Gafurov, A., Isaeva, O., et al. (2021). Conserved Pan-Cancer Microenvironment Subtypes Predict Response to Immunotherapy. *Cancer Cell* 39, 845–865. e7. doi:10.1016/j.ccell.2021.04.014

Bolha, L., Ravnik-Glavač, M., and Glavač, D. (2017). Long Noncoding RNAs as Biomarkers in Cancer. *Dis. Markers* 2017, 7243968. doi:10.1155/2017/7243968

Dixon, S. J., Lemberg, K. M., Lamprecht, M. R., Skouta, R., Zaitsev, E. M., Gleason, C. E., et al. (2012). Ferroptosis: an Iron-dependent Form of Nonapoptotic Cell Death. *Cell* 149, 1060–1072. doi:10.1016/j.cell.2012.03.042

Guo, Q., Zhang, X., Shen, T., and Wang, X. (2021). Identification of Autophagy- and Ferroptosis-Related lncRNAs Functioned through Immune-Related Pathways in Head and Neck Squamous Carcinoma. *Life (Basel, Switzerland)* 11, 835. doi:10.3390/life11080835

Hao, Y., Yan, M., Heath, B. R., Lei, Y. L., and Xie, Y. (2019). Fast and Robust Deconvolution of Tumor Infiltrating Lymphocyte from Expression Profiles Using Least Trimmed Squares. *Plos Comput. Biol.* 15, e1006976. doi:10.1371/journal.pcbi.1006976

Hu, Y., Guo, G., Li, J., Chen, J., and Tan, P. (2020). Screening Key lncRNAs with Diagnostic and Prognostic Value for Head and Neck Squamous Cell Carcinoma Based on Machine Learning and mRNA-lncRNA Co-expression Network Analysis. *Cbm* 27, 195–206. doi:10.3233/cbm-190694

Jiang, W., Qu, Y., Yang, Q., Ma, X., Meng, Q., Xu, J., et al. (2019). D-lnc: a Comprehensive Database and Analytical Platform to Dissect the Modification of Drugs on lncRNA Expression. *RNA Biol.* 16, 1586–1591. doi:10.1080/15476286.2019.1649584

Jiang, X., Stockwell, B. R., and Conrad, M. (2021). Ferroptosis: Mechanisms, Biology and Role in Disease. *Nat. Rev. Mol. Cel Biol* 22, 266–282. doi:10.1038/s41580-020-00324-8

Johnson, D. E., Burtness, B., Leemans, C. R., Lui, V. W. Y., Bauman, J. E., and Grandis, J. R. (2020). Head and Neck Squamous Cell Carcinoma. *Nat. Rev. Dis. Primers* 6, 92. doi:10.1038/s41572-020-00224-3

Lauss, M., Donia, M., Harbst, K., Andersen, R., Mitra, S., Rosengren, F., et al. (2017). Mutational and Putative Neoantigen Load Predict Clinical Benefit of Adoptive T Cell Therapy in Melanoma. *Nat. Commun.* 8, 1738. doi:10.1038/s41467-017-01460-0

Li, T., Fan, J., Wang, B., Traugh, N., Chen, Q., Liu, J. S., et al. (2017). TIMER: A Web Server for Comprehensive Analysis of Tumor-Infiltrating Immune Cells. *Cancer Res.* 77, e108–e110. doi:10.1158/0008-5472.can-17-0307

Li, X., Pan, X., Zhou, H., Wang, P., Gao, Y., Shang, S., et al. (2021). Comprehensive Characterization Genetic Regulation and Chromatin Landscape of Enhancer-

Associated Long Non-coding RNAs and Their Implication in Human Cancer. *Brief. Bioinform.* 1, bbab401. doi:10.1093/bib/bbab401

Lin, R., Zhang, Z., Chen, L., Zhou, Y., Zou, P., Feng, C., et al. (2016). Dihydroartemisinin (DHA) Induces Ferroptosis and Causes Cell Cycle Arrest in Head and Neck Carcinoma Cells. *Cancer Lett.* 381, 165–175. doi:10.1016/j.canlet.2016.07.033

Love, M. I., Huber, W., and Anders, S. (2014). Moderated Estimation of Fold Change and Dispersion for RNA-Seq Data with DESeq2. *Genome Biol.* 15, 550. doi:10.1186/s13059-014-0550-8

Lu, L., Liu, L.-P., Zhao, Q.-Q., Gui, R., and Zhao, Q.-Y. (2021). Identification of a Ferroptosis-Related LncRNA Signature as a Novel Prognosis Model for Lung Adenocarcinoma. *Front. Oncol.* 11, 2443. doi:10.3389/fonc.2021.675545

Newman, A. M., Liu, C. L., Green, M. R., Gentles, A. J., Feng, W., Xu, Y., et al. (2015). Robust Enumeration of Cell Subsets from Tissue Expression Profiles. *Nat. Methods* 12, 453–457. doi:10.1038/nmeth.3337

Pfister, D. G., Ang, K.-K., Brizel, D. M., Burtness, B. A., Cmelak, A. J., Colevas, A. D., et al. (2011). Head and Neck Cancers. *J. Natl. Compr. Canc Netw.* 9, 596–650. doi:10.6004/jnccn.2011.0053

Pulte, D., and Brenner, H. (2010). Changes in Survival in Head and Neck Cancers in the Late 20th and Early 21st century: a Period Analysis. *The Oncologist* 15, 994–1001. doi:10.1634/theoncologist.2009-0289

Racle, J., de Jonge, K., Baumgaertner, P., Speiser, D. E., and Gfeller, D. (2017). Simultaneous Enumeration of Cancer and Immune Cell Types from Bulk Tumor Gene Expression Data. *Elife* 6, 1. doi:10.7554/eLife.26476

Rooney, M. S., Shukla, S. A., Wu, C. J., Getz, G., and Hacohen, N. (2015). Molecular and Genetic Properties of Tumors Associated with Local Immune Cytolytic Activity. *Cell* 160, 48–61. doi:10.1016/j.cell.2014.12.033

Shannon, P., Markiel, A., Ozier, O., Baliga, N. S., Wang, J. T., Ramage, D., et al. (2003). Cytoscape: a Software Environment for Integrated Models of Biomolecular Interaction Networks. *Genome Res.* 13, 2498–2504. doi:10.1101/gr.1239303

Stockwell, B. R., Friedmann Angeli, J. P., Bayir, H., Bush, A. I., Conrad, M., Dixon, S. J., et al. (2017). Ferroptosis: A Regulated Cell Death Nexus Linking Metabolism, Redox Biology, and Disease. *Cell* 171, 273–285. doi:10.1016/j.cell.2017.09.021

Tumino, R., and Vicario, G. (2004). Head and Neck Cancers: Oral Cavity, Pharynx, and Larynx. *Epidemiol. Prev.* 28, 28–33.

Ulitsky, I. (2016). Evolution to the rescue: Using Comparative Genomics to Understand Long Non-coding RNAs. *Nat. Rev. Genet.* 17, 601–614. doi:10.1038/nrg.2016.85

Waldman, A. D., Fritz, J. M., and Lenardo, M. J. (2020). A Guide to Cancer Immunotherapy: from T Cell Basic Science to Clinical Practice. *Nat. Rev. Immunol.* 20, 651–668. doi:10.1038/s41577-020-0306-5

Wang, M., Mao, C., Ouyang, L., Liu, Y., Lai, W., Liu, N., et al. (2019). Long Noncoding RNA LINC00336 Inhibits Ferroptosis in Lung Cancer by Functioning as a Competing Endogenous RNA. *Cell Death Differ* 26, 2329–2343. doi:10.1038/s41418-019-0304-y

Wang, X., Park, J., Susztak, K., Zhang, N. R., and Li, M. (2019). Bulk Tissue Cell Type Deconvolution with Multi-Subject Single-Cell Expression Reference. *Nat. Commun.* 10, 380. doi:10.1038/s41467-018-08023-x

Wichmann, G., Rosolowski, M., Krohn, K., Kreuz, M., Boehm, A., Reiche, A., et al. (2015). The Role of HPV RNA Transcription, Immune Response-Related Gene Expression and disruptiveTP53mutations in Diagnostic and Prognostic Profiling of Head and Neck Cancer. *Int. J. Cancer* 137, 2846–2857. doi:10.1002/ijc.29649

Wilusz, J. E., Sunwoo, H., and Spector, D. L. (2009). Long Noncoding RNAs: Functional Surprises from the RNA World. *Genes Dev.* 23, 1494–1504. doi:10.1101/gad.1800909

Xu, M., Xu, X., Pan, B., Chen, X., Lin, K., Zeng, K., et al. (2019). LncRNA SATB2-AS1 Inhibits Tumor Metastasis and Affects the Tumor Immune Cell Microenvironment in Colorectal Cancer by Regulating SATB2. *Mol. Cancer* 18, 135–216. doi:10.1186/s12943-019-1063-6

Yang, H., Han, Y., Wu, L., and Wu, C. (2017). Long Non-coding RNA Expression Signature Hallmarks Promising Efficacy in Identification of Human Non-small Cell Lung Cancer: a Meta-Analysis Study. *Clin. Lab.* 63, 1447–1456. doi:10.7754/Clin.Lab.2017.170325

Yao, L., Shen, H., Laird, P. W., Farnham, P. J., and Berman, B. P. (2015). Inferring Regulatory Element Landscapes and Transcription Factor Networks from Cancer Methylomes. *Genome Biol.* 16, 105. doi:10.1186/s13059-015-0668-3

Yoshihara, K., Shahmoradgoli, M., Martínez, E., Vegesna, R., Kim, H., Torres-Garcia, W., et al. (2013). Inferring Tumour Purity and Stromal and Immune Cell Admixture from Expression Data. *Nat. Commun.* 4, 2612. doi:10.1038/ncomms3612

Zhou, N., and Bao, J. (2020). FerrDb: a Manually Curated Resource for Regulators and Markers of Ferroptosis and Ferroptosis-Disease Associations. *Database (Oxford)* 2020, baaa021. doi:10.1093/database/baaa021

Zhou, Y., Zhou, B., Pache, L., Chang, M., Khodabakhshi, A. H., Tanaseichuk, O., et al. (2019). Metascape Provides a Biologist-Oriented Resource for the Analysis of Systems-Level Datasets. *Nat. Commun.* 10, 1523. doi:10.1038/s41467-019-09234-6

Zhu, L., Tian, Q., Jiang, S., Gao, H., Yu, S., Zhou, Y., et al. (2021). A Novel Ferroptosis-Related Gene Signature for Overall Survival Prediction in Patients with Breast Cancer. *Front. Cel Developmental Biol.* 9, 1471. doi:10.3389/fcell.2021.670184

Conflict of Interest: The authors declare that the research was conducted in the absence of any commercial or financial relationships that could be construed as a potential conflict of interest.

Publisher's Note: All claims expressed in this article are solely those of the authors and do not necessarily represent those of their affiliated organizations, or those of the publisher, the editors, and the reviewers. Any product that may be evaluated in this article, or claim that may be made by its manufacturer, is not guaranteed or endorsed by the publisher.

frontiers in Genetics

ORIGINAL RESEARCH
published: 14 January 2022
doi: 10.3389/fgene.2021.793636

Establishment and Validation of a Ferroptosis-Related Gene Signature to Predict Overall Survival in Lung Adenocarcinoma

Su Wang[1], *Zhen Xie*[2] *and Zenghong Wu*[3]*

[1]Department of Emergency Medicine, Union Hospital, Tongji Medical College, Huazhong University of Science and Technology, Wuhan, China, [2]Department of Otorhinolaryngology, Union Hospital, Tongji Medical College, Huazhong University of Science and Technology, Wuhan, China, [3]Department of Infectious Diseases, Union Hospital, Tongji Medical College, Huazhong University of Science and Technology, Wuhan, China

OPEN ACCESS

Edited by:
Lei Huang,
University of Massachusetts Medical School, United States

Reviewed by:
Jeremy W. Chambers,
Florida International University, United States
Can Cui,
Yale University, United States

***Correspondence:**
Zenghong Wu
D201981596@hust.edu.cn

Specialty section:
This article was submitted to Human and Medical Genomics, a section of the journal Frontiers in Genetics

Received: 12 October 2021
Accepted: 01 December 2021
Published: 14 January 2022

Citation:
Wang S, Xie Z and Wu Z (2022) Establishment and Validation of a Ferroptosis-Related Gene Signature to Predict Overall Survival in Lung Adenocarcinoma. Front. Genet. 12:793636. doi: 10.3389/fgene.2021.793636

Background: Lung adenocarcinoma (LUAD) is the most common and lethal subtype of lung cancer. Ferroptosis, an iron-dependent form of regulated cell death, has emerged as a target in cancer therapy. However, the prognostic value of ferroptosis-related genes (FRGs)x in LUAD remains to be explored.

Methods: In this study, we used RNA sequencing data and relevant clinical data from The Cancer Genome Atlas (TCGA) dataset and Gene Expression Omnibus (GEO) dataset to construct and validate a prognostic FRG signature for overall survival (OS) in LUAD patients and defined potential biomarkers for ferroptosis-related tumor therapy.

Results: A total of 86 differentially expressed FRGs were identified from LUAD tumor tissues versus normal tissues, of which 15 FRGs were significantly associated with OS in the survival analysis. Through the LASSO Cox regression analysis, a prognostic signature including 11 FRGs was established to predict OS in the TCGA tumor cohort. Based on the median value of risk scores calculated according to the signature, patients were divided into high-risk and low-risk groups. Kaplan–Meier analysis indicated that the high-risk group had a poorer OS than the low-risk group. The area under the curve of this signature was 0.74 in the TCGA tumor set, showing good discrimination. In the GEO validation set, the prognostic signature also had good predictive performance. Functional enrichment analysis showed that some immune-associated gene sets were significantly differently enriched in two risk groups.

Conclusion: Our study unearthed a novel ferroptosis-related gene signature for predicting the prognosis of LUAD, and the signature may provide useful prognostic biomarkers and potential treatment targets.

Keywords: Lung Adenocarcinoma, ferroptosis, genes, immune infiltration, data mining

INTRODUCTION

Lung cancer is the leading cause of cancer-related lethality around the world, with almost 1.6 million deaths per year, and the 5-year survival rate still lags at below 20% (Uras et al., 2020). Lung adenocarcinoma (LUAD) represents the most common subtype of lung cancer, accounting for ~50% of all cases (Chen et al., 2020). Some risk factors such as smoking, family history of lung cancer, aging, and virus infection have been implicated in the initiation and progression of LUAD (Nakhaie et al., 2020), and molecules and pathways mediating the occurrence and development of LUAD have been continuously investigated (Wang et al., 2020; Zhou et al., 2020). Unfortunately, more than 70% of cases are with advanced disease at diagnosis (Domagala-Kulawik and Trojnar, 2020). Moreover, despite neoplasm of the lowest stage, there is still a high risk of metastatic relapse after excision (Liljedahl et al., 2020). Over the last decades, the survival rate of patients with LUAD has been improved very little, although progress has been made in treatment (Ma et al., 2020). Therefore, it is vital to explore reliable and promising prognostic biomarkers for LUAD and identify valuable therapeutic targets. At present, several drugs have been reported to possess remarkable antitumor effects on LUAD *via* inducing autophagy and apoptosis (Liu et al., 2016; Cao et al., 2019). In addition, dynamic BH3 profiling is used to measure changes in chemotherapeutics-induced apoptotic signaling, and using BH3 mimetic drugs which increase mitochondrial apoptotic priming may enforce the apoptotic fate of LUAD cells (Montero et al., 2015; Sánchez-Rivera et al., 2021). However, the exploration of other forms of cell death to uncover new biomarkers and targets for LUAD is also urgently required.

Ferroptosis is a novel type of regulated cell death driven by the lethal levels of iron-dependent lipid hydroperoxide accumulation and has attracted much interest in recent years (Stockwell et al., 2017). Oxidative stress caused by excess iron is correlated with carcinogenesis which is considered a process of ferroptosis resistance as well as iron addiction, and both of them also occur in tumor cells (Toyokuni, 2016; Toyokuni et al., 2017). Due to the strong demand for iron to support rapid proliferation, tumor cells are vulnerable to the overload of iron and accumulation of reactive oxygen species (ROS), which in turn enables the ferroptosis-mediated cancer therapy (Liang et al., 2019). Moreover, ferroptosis might enhance the antitumor effect of apoptosis inducer cisplatin, indicating that ferroptosis inducers may help overcome the resistance of cancer cells to traditional anticancer drugs (Roh et al., 2017; Wu et al., 2020). Increasing studies have explored the role of ferroptosis-related genes in lung cancer. Lai et al. found that overexpression of glutathione peroxidase 4 (*GPX4*) in lung cancer cells promoted proliferation but attenuated abnormalities specific to ferroptosis (Lai et al., 2019). The sensitivity of non-small cell lung cancer (NSCLC) cells to cysteine deprivation-induced ferroptosis could be regulated by nuclear factor-erythroid 2-like 2 (*NRF2*) *via* the FOCAD-FAK signaling pathway (Liu et al., 2020). Erastin-induced ROS promoted the upregulation and activation of *p53*, which contributed to the cytostatic and cytotoxic effects in lung cancer cells (Huang et al., 2018). Moreover, Ji et al. showed that highly expressed cystine-glutamate transporter (*SLC7A11*) mediated metabolic requirements during NSCLC progression and predicted a worse 5-year survival (Ji et al., 2018). A few previous studies have studied prognostic models related to ferroptosis (Jin et al., 2021; Wang et al., 2021). However, the role of a large number of ferroptosis-related genes in LUAD patients remains unclear and to systematically evaluate ferroptosis-related gene signature and its relationship with overall survival (OS) in LUAD is still needed. In this study, we used data extracted from The Cancer Genome Atlas (TCGA) database and Gene Expression Omnibus (GEO) database to construct and validate a prognostic signature of ferroptosis-related genes and assess their importance as biomarkers for ferroptosis-mediated cancer therapy.

MATERIALS AND METHODS

Data Collection

We obtained RNA-seq data of 54 normal samples and 497 LUAD samples, along with related clinical data, from the TCGA database (https://tcgadata.nci.nih.gov/tcga/, October 2020). The expression profiles and relevant clinical data of 462 tumor samples (GSE68465) were gained from the GEO portal (https://www.ncbi.nlm.nih.gov/geo/). A list of 259 (108 drivers; 69 suppressors; 111 markers) ferroptosis-related genes (FRGs) was gained from FerrDb (Zhou and Bao, 2020) and is shown in **Supplementary Table S1**.

Identification of Prognosis-Related Differentially Expressed FRGs

The R package "limma" was used for screening out FRGs in the TCGA transcriptome data. To facilitate subsequent validation, we identified the shared FRGs between the TCGA and GEO datasets through intersecting the selected FRGs with gene expression profiles of GSE68465 *via* R package "limma" and "sva." The shared FRGs and their expression with correction and standardization were extracted from the TCGA dataset and GEO dataset, respectively. In the TCGA cohort, among all shared FRGs, differentially expressed FRGs (DEFRGs) were identified between LUAD samples and normal samples, based on the cutoff threshold as $|\log2 \text{ fold change (FC)}| > 0.5$ and adjusted p-value < 0.05. A volcano map was conducted to visualize the DEFRGs. We explored the biological functions of the identified DEFRGs using Gene Ontology (GO) function and Kyoto Encyclopedia of Genes and Genomes (KEGG) analyses *via* the R language "ggplot2" package. Last, univariate Cox regression analysis was used to screen out the prognostic DEFRGs (PDEFRGs) that were significantly related to OS of patients in the TCGA LUAD dataset.

Establishment and Validation of a Prognostic FRGs Signature

Based on the PDEFRG expression and survival data, a prognostic gene signature was established through the least absolute shrinkage and selection operator (LASSO) Cox regression

analysis with R package called "glmnet." FRGs with independent prognostic values were included in the signature, and the risk score of this signature was calculated as follows: score = sum (each gene's expression × corresponding regression coefficient). According to the signature, the risk score for each LUAD patient was calculated. Based on the median value of all patients' risk scores in the TCGA LUAD cohort, all patients were separated into a high-risk group and a low-risk group. The signature and identified median value were subsequently applied to the GEO cohort for validation, and all LUAD patients in the GEO dataset were also divided into two risk groups. A heatmap was used to visualize the distribution of clinicopathological features in the high-risk and low-risk groups. The correlation analysis with R package "ggpubr" and "limma" was used to explain the correlation between the risk scores and subgroups of clinicopathological characteristics. The survivals of the two groups of patients were analyzed through Kaplan–Meier (K–M) curve analysis with R packages "survival" and "survminer." Univariate and multivariate Cox regression analysis were used to evaluate the association between risk score and prognosis. In addition, a nomogram was built to predict OS for clinical application, based on the results of the multivariate Cox analysis. The time-dependent receiver operating characteristic (ROC) curve was plotted to assess the predictive ability of the prognostic signature for 1-, 3-, and 5-year survival using R packages "timeROC" and "survival."

Enrichment analysis

Gene set enrichment analysis (GSEA) was performed according to the GSEA software (version 4.1.0) to explore the molecular mechanism and critical signaling pathways difference between the low-risk and high-risk groups. False discovery rate (FDR) < 0.25 and nominal p value < 0.05 were considered noteworthy. Moreover, we used the single-sample GSEA (ssGSEA) and R package "GSVA" to quantify activities of tumor-infiltrating immune cells between risk groups using 29 immune signatures and find different immune responses and functions.

Online Database Analysis

Online databases were used to study different types of gene alterations in tumors and provide distinct prognostic values in LUAD patients. We utilized the cBioPortal (http://cbioportal.org) (Wu et al., 2019), an open-access site providing download, analysis, and visualization of large-scale cancer genomics

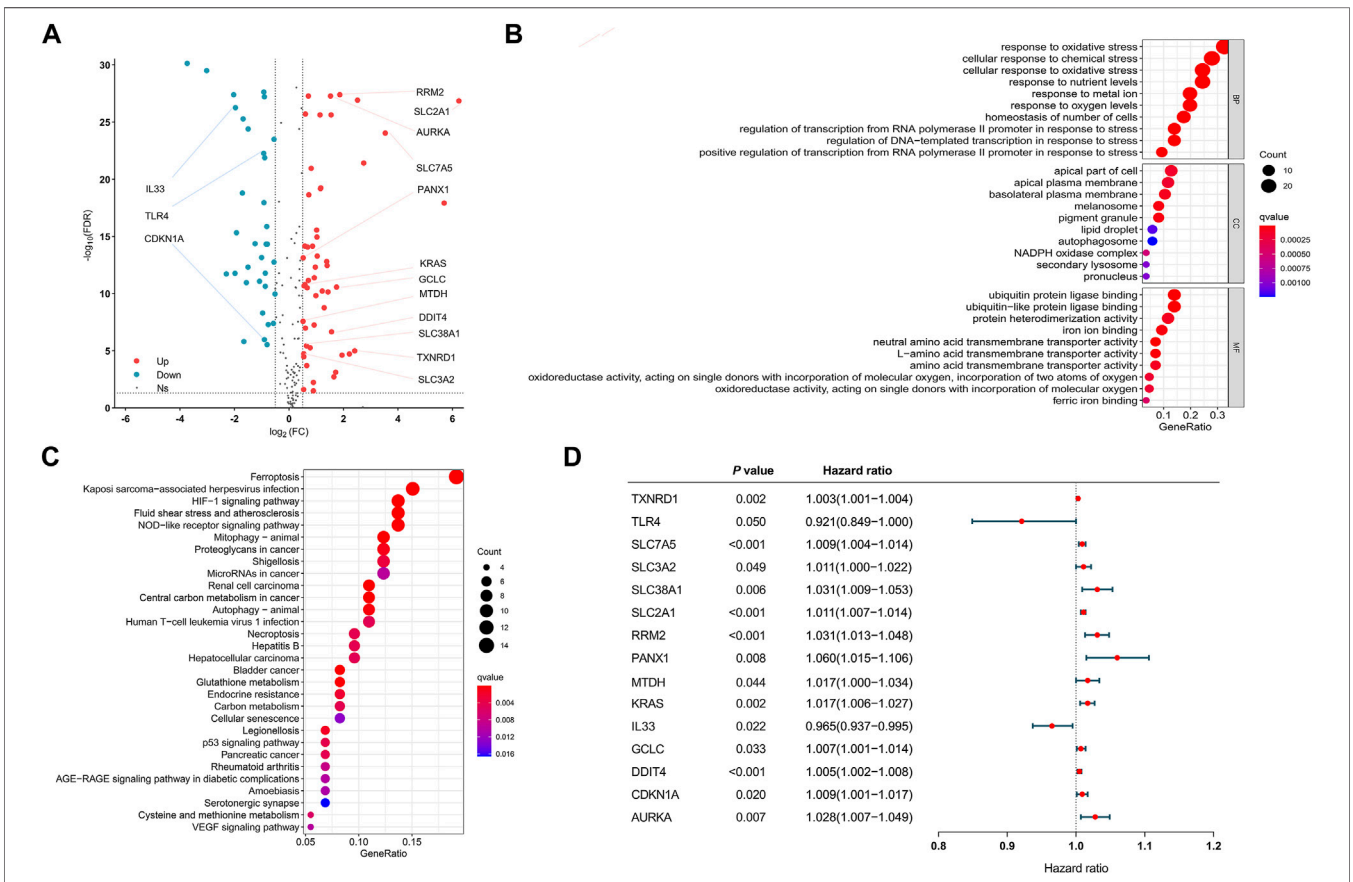

FIGURE 1 | Visualization of differential ferroptosis-related genes. **(A)** Volcano map showing FRGs between normal and tumor tissues. **(B)** GO results of differentially expressed FRGs. **(C)** KEGG results of differentially expressed FRGs. **(D)** Forest plots showing the results of the univariate Cox regression analysis between DFRG expression and overall survival. GO: gene ontology. KEGG: Kyoto Encyclopedia of Genes and Genomes. FRGs: ferroptosis-related genes. DFRGs: differentially expressed ferroptosis-related genes.

datasets, to analyze the mutations of FRGs in the prognostic model. The kmplot (https://kmplot.com) online tool was performed to assess the impact of genes expression on survival of lung cancer.

Statistical Analysis

R software (version 4.0.3) and SPSS (version 23.0) were used for all statistical analyses, and Strawberry Perl (version 5.32.0.1) was applied to data matrix and data processing. The unpaired Student's t-test and the Wilcoxon test or Mann–Whitney *U*-test were performed to evaluate the normal distribution variables and the non-normal distribution variables, respectively. Categorical variables were tested with a chi-square or Fisher's exact test. Univariate Cox, multivariate Cox, and LASSO Cox analyses were used to identify significant prognostic variables. The OS was analyzed by K–M analysis using a log-rank test. p value < 0.05 meant statistical significance.

RESULTS

Identification of Prognosis-Related DEFRGs in LUAD Patients

After all genes were searched in sequence, 245 FRGs were identified to be expressed in the TCGA cohort. Next, we identified 210 FRGs shared between the TCGA samples and the GEO samples. Among these shared genes, 86 FRGs (52 upregulated genes and 34 downregulated genes) were differentially expressed between normal and tumor tissues and were used to model the prognostic signature for LUAD patients (**Figure 1A** and **Supplementary Table S2**). Biological processes (BP) of 86 DEFRGs were mainly enriched in response to oxidative stress and cellular response to chemical stress (**Figure 1B**). Cellular components (CC) were mainly enriched in the apical part of the cell and apical plasma membrane. Molecular functions (MF) were mainly enriched in iron ion binding and ubiquitin protein ligase binding. Ferroptosis, HIF-1 signaling pathway, and NOD-like receptor signaling pathway were significantly enriched in the KEGG pathway analysis (**Figure 1C**). Through the univariate Cox analysis, 15 DEFRGs (13 risk factors and two protective factors) were significantly associated with OS in the TCGA tumor cohort (**Figure 1D**).

Development of the Prognostic FRG Signature

The 15 prognosis-related DEFRGs mentioned above were further analyzed by LASSO Cox regression analysis, and 11 FRGs were filtered to construct a prognostic model, including *CDKN1A*, *DDIT4*, *IL33*, *KRAS*, *MTDH*, *PANX1*, *RRM2*, *SLC2A1*, *SLC7A5*, *TLR4*, and *TXNRD1*. Finally, we established an 11-FRG signature to predict OS in the LUAD patients. The risk score formula was as follows: Risk score = $(0.0049 \times \text{expression}_{CDKN1A}) + (0.0037 \times \text{expression}_{DDIT4}) - (0.0121 \times \text{expression}_{IL33}) + (0.0057 \times$

TABLE 1 | Characteristics of two risk group patients in TCGA LUAD cohort.

Characteristics	TCGA-LUAD cohort		
	High risk (n = 227)	Low risk (n = 227)	p-value
Age, years	63.7 (38-88)	66.1 (33-87)	0.023
Gender	—	—	0.059
Male	112 (49.3)	92 (40.5)	—
Female	115 (50.7)	135 (59.5)	—
Stage			
I	95 (41.9)	149 (65.6)	0.000
II	65 (28.6)	40 (17.6)	0.005
III	48 (21.1)	25 (11.0)	0.003
IV	16 (7.0)	8 (3.5)	0.093
T			
T1	57 (25.1)	100 (44.1)	0.000
T2	132 (58.1)	105 (46.3)	0.011
T3	28 (12.3)	11 (4.8)	0.004
T4	9 (4.0)	9 (4.0)	1.000
M			
M0	149 (65.6)	153 (67.4)	0.691
M1	16 (7.0)	7 (3.1)	0.054
N			
N0	129 (56.8)	165 (72.7)	0.000
N1	52 (22.9)	32 (14.1)	0.016
N2	43 (18.9)	20 (8.8)	0.002
N3	1 (0.4)	1 (0.4)	1.000
Fustat	—	—	0.000
Dead	99 (43.6)	57 (25.1)	—
Alive	128 (56.4)	170 (74.9)	—
Futime, years	2 (0.0-18.7)	2.2 (0.0-18.4)	0.006

Data were expressed as mean (min, max) or n (%).

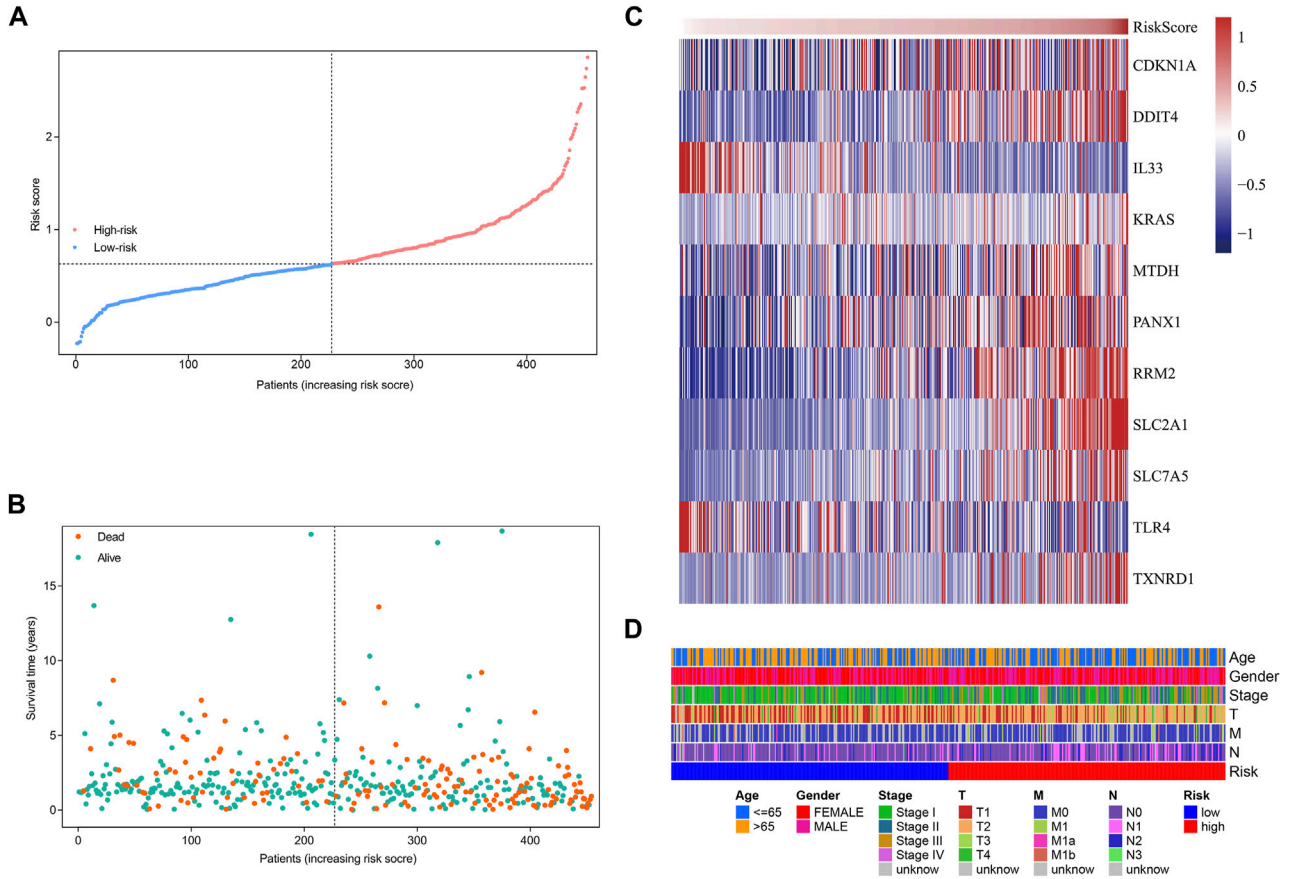

FIGURE 2 | Characteristics of risk scores and ferroptosis-related gene signature in the TCGA tumor cohort. **(A)** The distribution and median value of the risk scores. **(B)** The distributions of survival status, survival time, and risk score. **(C)** Heatmap showing the expression of model genes in two risk groups. **(D)** Heatmap showing the distribution of clinicopathological features in two risk groups.

expression_{KRAS}) + (0.0089 × expression_{MTDH}) + (0.0169 × $\text{expression}_{PANX1}$) + (0.0060 × expression_{RRM2}) + (0.0057 × $\text{expression}_{SLC2A1}$) + (0.0041 × $\text{expression}_{SLC7A5}$) - (0.0380 × expression_{TLR4}) + (0.0003 × $\text{expression}_{TXNRD1}$).

Survival Results and Multivariate Examination

Based on the formula, we calculated the risk scores of LUAD patients in the TCGA dataset. According to the median risk score, the TCGA tumor cohort was divided into high-risk and low-risk groups, and each group was assigned 227 LUAD patients (**Table 1**). The impact of risk scores on risk level and survival, the expression of eleven prognostic-associated FRGs based on the risk scores, and the clinicopathological features in two risk groups are presented in **Figures 2A–D**. Comparisons of the risk scores among subgroups according to clinicopathological characteristics are shown in **Supplementary Figures S1A–D**, and there existed a significant correlation between risk scores and age, tumor stage, tumor size stage, and lymph node stage. To identify the prognostic difference between the risk groups, we performed a KM survival analysis and the results showed that the high-risk group had a significantly poorer outcome compared with the low-risk group (**Figure 3A**, $p < 0.0001$). The further performed multivariate Cox analysis demonstrated that the risk model was a significant prognostic predictor, independent of other clinical factors (**Supplementary Table S3** and **Figure 3B,** $p < 0.001$). Moreover, the area under the ROC curve (AUC) of the risk score model was 0.737, which was higher than that of other clinical indices, showing a better prognostic prediction efficacy (**Figure 3C**). We also plotted the ROC curves to assess the efficiency of risk scores in predicting 1-, 3-, and 5-year survival, and the AUC was 0.74, 0.66, and 0.62, respectively (**Figure 3D**). In addition, the nomogram was constructed in combination of clinicopathological parameters and an 11-FRG signature (**Figure 3E**). Based on the score of each item in the nomogram, the total score could be calculated to predict the 1-, 3-, and 5-year survival rates of LUAD patients.

The Validation in the GEO Cohort

The data of GEO samples were used to verify the prediction ability of the model. The patients were stratified into a high-risk group ($n = 214$) and a low-risk group ($n = 228$), based on the median value of risk scores of the TCGA tumor cohort. The

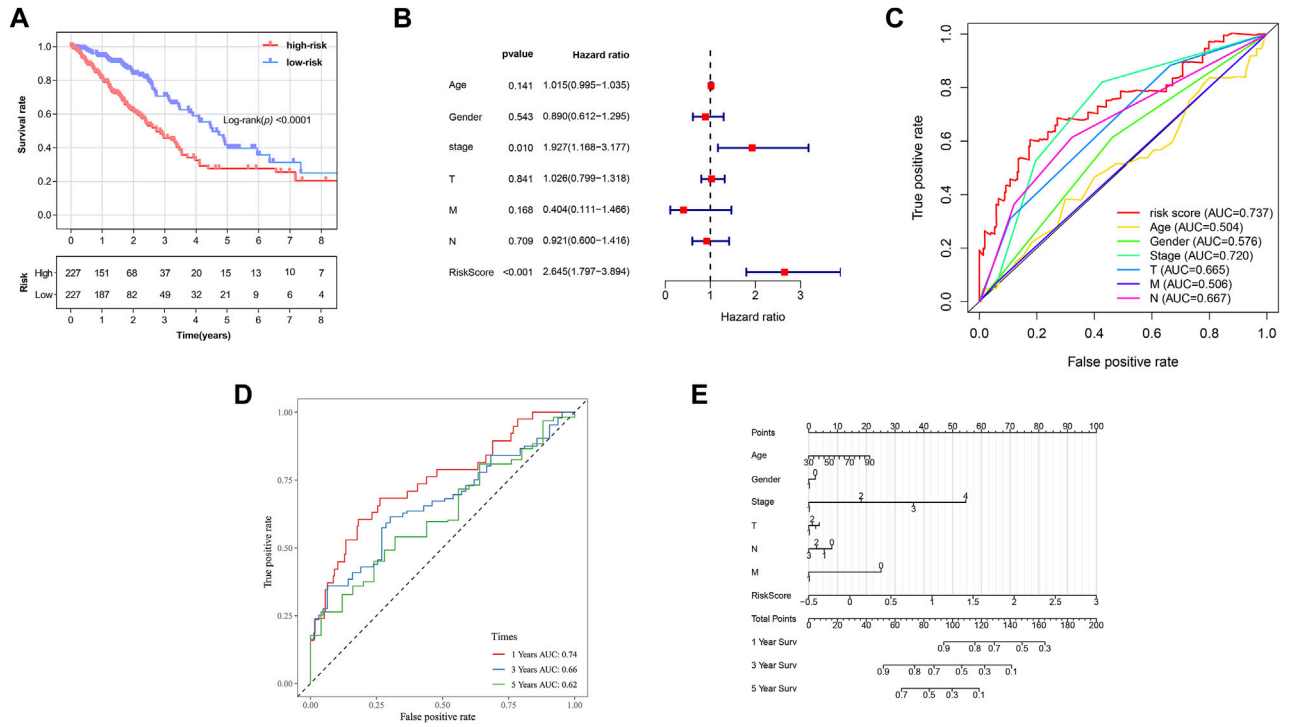

FIGURE 3 | Prognostic analysis of ferroptosis-related gene signature in the TCGA tumor cohort. **(A)** Kaplan–Meier survival curve of the high- and low-risk groups. **(B)** Multivariate Cox regression analysis on overall survival. **(C)** ROC curves for predicting the overall survival of clinical factors and risk score. **(D)** ROC curves for predicting the 1-, 3-, and 5-year survival of risk score. **(E)** Nomogram for predicting overall survival. Gender: 1, male; 0, female. Surv: survival. ROC: receiver operating characteristic curve. AUC: area under the curve.

clinical features of patients in the GSE68465 dataset, such as age, smoking history, chemoradiotherapy, and pathological differentiation, are shown in **Table 2**. Obviously, risk with survival and gene expression trends were similar to those of the TCGA LUAD cohort (**Figure 4A**). The heatmap showed the distributions of clinicopathological features in two risk groups (**Figure 4B**). The significant differences were observed in risk scores within various subgroups classified by clinicopathological features including tumor size stage and lymph node stage (**Supplementary Figure S1E–K**). Patients with poorer tumor grade or receiving chemotherapy/radiotherapy had significantly higher risk scores. As expected, patients in the high-risk group had a poorer prognosis (**Figure 4C**, p = 0.0004). The results of multivariate Cox regression analysis also verified the independent effective prognostic value of the model (**Figure 4D** and **Supplementary Table S3**). Moreover, the AUC value of risk score in the validation cohort was the highest, in line with the result of the training cohort (**Figure 4E**). In the GEO dataset, the AUC values at 1, 3, and 5 years, respectively, were 0.72, 0.71, and 0.61 (**Figure 4F**). Taken together, these data indicated that the constructed prognostic tool possessed good performance in predicting survival outcomes.

GSEA Enrichment Analysis

We used GSEA to distinguish the potential functional differences between the two risk groups in the TCGA LUAD cohort. Increased activations of the cell cycle were markedly enriched in the high-risk group, including pyrimidine metabolism, homologous recombination, and nucleotide excision repair (**Figure 5** and **Table 3**). Inflammation and immune-related pathways such as the Fc epsilon RI-mediated signaling pathway and B cell receptor signaling pathway were enriched in the low-risk group. The further ssGSEA was performed to score the samples from the high- and low-risk groups in the TCGA tumor cohort, and the differences in immune cells and functions between the groups were detected. The scores of dendritic cells (DCs), B lymphocytes, and T helper cells were significantly higher in the low-risk group, as well as type II IFN response and HLA (**Figure 6,** $p < 0.001$), which indicated that the low-risk group had greater immune cell infiltration and antitumor immune activities.

Online Database Analysis

Based on cBioPortal, we explored the frequency and types of mutation in 11 FRGs in LUAD. These genes were altered in 57% of LUAD patients in the online database. KRAS was modified the most, and missense mutations were common (**Figure 7**). Through the kmplot online tool, KM survival analyses demonstrated that *DDIT4*, *IL33*, *KRAS*, *MTDH*, *RRM2*, *SLC2A1*, *SLC7A5*, *TLR4*, and *TXNRD1* overexpression was markedly related to OS ($p < 0.05$) in lung cancer. The overexpression of *DDIT4*, *RRM2*, *SLC2A1*, *SLC7A5*, *TLR4*, and

TABLE 2 | Characteristics of two risk group patients in GEO LUAD cohort.

Characteristics	GEO-LUAD cohort		
	High-risk (*n* = 214)	Low-risk (*n* = 228)	*p* value
Age, years	63.7 (33-86)	65.0 (35-87)	0.236
Gender	—	—	0.002
Male	124 (57.9)	99 (43.4)	—
Female	90 (42.1)	129 (56.6)	—
Smoking history			
Yes	152 (71.0)	148 (64.9)	0.169
No	22 (10.3)	35 (15.4)	0.112
Chemotherapy			
Yes	49 (22.9)	40 (17.5)	0.161
No	155 (72.4)	185 (81.1)	0.030
Radiotherapy			
Yes	39 (18.2)	26 (11.4)	0.043
No	165 (77.1)	198 (86.8)	0.008
Differentiation			
Well	11 (5.1)	49 (21.5)	0.000
Moderate	81 (37.9)	128 (56.1)	0.000
Poorly	118 (55.1)	48 (21.1)	0.000
T			
T1	48 (22.4)	102 (44.7)	0.000
T2	140 (65.4)	111 (48.7)	0.000
T3	22 (10.3)	6 (2.6)	0.001
T4	3 (1.4)	8 (3.5)	0.223
N			
N0	135 (63.1)	164 (71.9)	0.047
N1	49 (22.9)	38 (16.7)	0.100
N2	29 (13.6)	24 (10.5)	0.328
Fustat	—	—	0.000
Dead	134 (62.6)	102 (44.7)	—
Alive	80 (37.4)	126 (55.3)	—
Futime, years	4.1 (0.0-17)	4.6 (0.0-13.6)	0.003

Data are expressed as mean (min, max) or n (%).

TXNRD1 were risk factors for poor prognosis, while *IL33*, *KRAS*, and *MTDH* were the opposite (**Figure 8**).

DISCUSSION

LUAD as a highly lethal cancer has a large number of patients worldwide, and only 15% of LUAD patients achieved 5-year survival, despite advances in treatment (Ma et al., 2020). Due to the high heterogeneity and complexity of LUAD, it is still challenging to effectively predict the prognosis of LUAD patients (Song et al., 2019), emphasizing the search for novel biomarkers with good predictive power as well as new treatment targets. Tumor cells can go through several forms of regulated cell death during the cancer development. Ferroptosis has been found participating in the process of cancer cell death, and stimulation of ferroptosis is a hopeful strategy for cancer therapy. Targeted exosome-encapsulated erastin has been demonstrated to efficiently induce ferroptosis in tumor cells (Yu et al., 2019). In our current study, an effective and novel ferroptosis-related prognostic gene signature in LUAD patients was constructed based on the TCGA dataset and was validated in the GEO dataset. Our signature had a good prognostic value and could be used as underlying biomarker and therapeutic target in the ferroptosis regulation pathways.

In this study, we first screened out 86 differentially expressed FRGs and explored their potential functions. The univariate Cox model selected 15 survival-related DFRGs. Then, we constructed a prognostic 11-FRG signature to predict OS in LUAD patients through LASSO Cox regression analysis. According to our results, *KRAS*, *SL2A1*, *RRM2*, and *TXNRD1* were significantly upregulated genes in LUAD samples. Ribonucleoside-diphosphate reductase subunit M2 (*RRM2*) could promote proliferation and chemotherapy resistance of NSCLC cells *via* upregulating epidermal growth factor receptor expression and AKT phosphorylation (Huang et al., 2019). Recent studies have shown that *RRM2* facilitated tumor immune infiltration through inhibiting ferroptotic death in LUAD patients (Tang et al., 2021). *KRAS* was the most commonly mutated oncogene in lung, pancreatic, and colorectal carcinomas and enabled an improved rate of glutathione regeneration and ferroptosis protection by elevating nicotinamide adenine dinucleotide phosphate hydrogen levels through metabolic reprogramming (Pylayeva-Gupta et al., 2011; Bebber et al., 2020). Solute carrier family two member 1 (*SLC2A1*/*GLUT1*) was an important regulator of the glycolysis pathway and was found to have an increased expression in premalignant lesions and neoplasms of

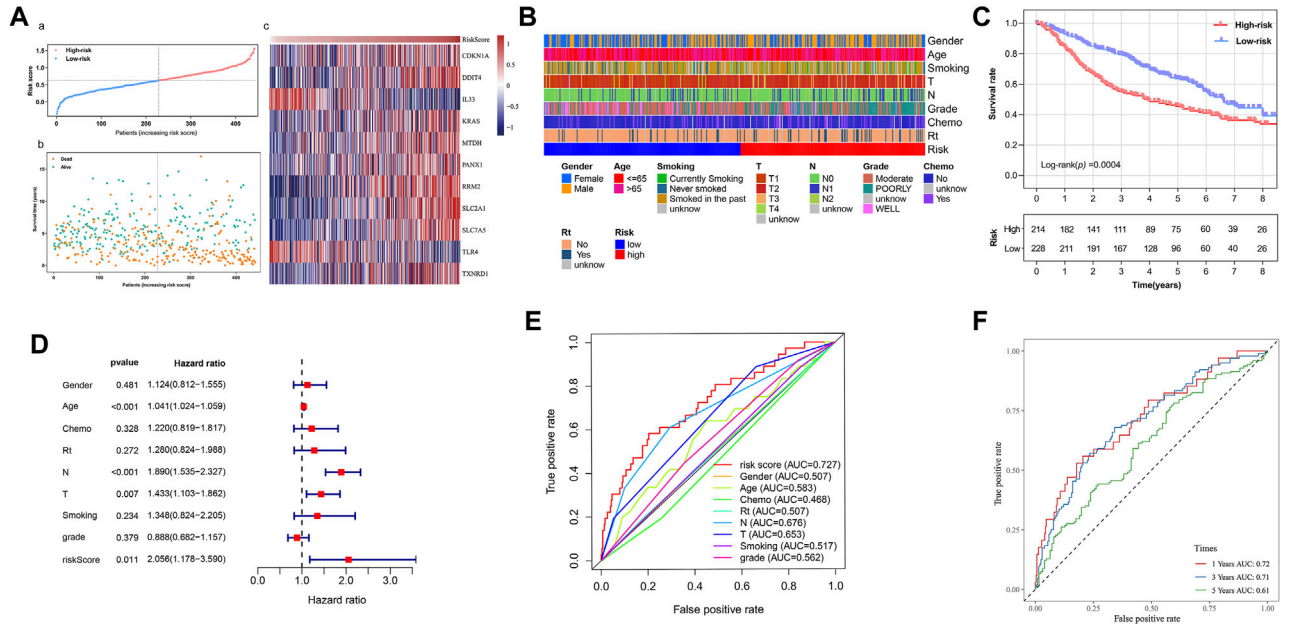

FIGURE 4 | The validation of prognostic signature in the GEO tumor cohort. **(A)** The distribution of survival status, survival time, and risk score and the expression of model genes in two risk groups. **(B)** Heatmap of clinicopathological feature distribution in two risk groups. **(C)** Kaplan–Meier survival curve of high- and low-risk groups. **(D)** Multivariate Cox regression analyses on overall survival. **(E)** ROC curves for predicting overall survival of clinical factors and risk score. **(F)** ROC curves for predicting the 1-, 3-, and 5-year survival of risk score. ROC: receiver operating characteristic curve. AUC: area under the curve. Chemo: chemotherapy. Rt: radiotherapy.

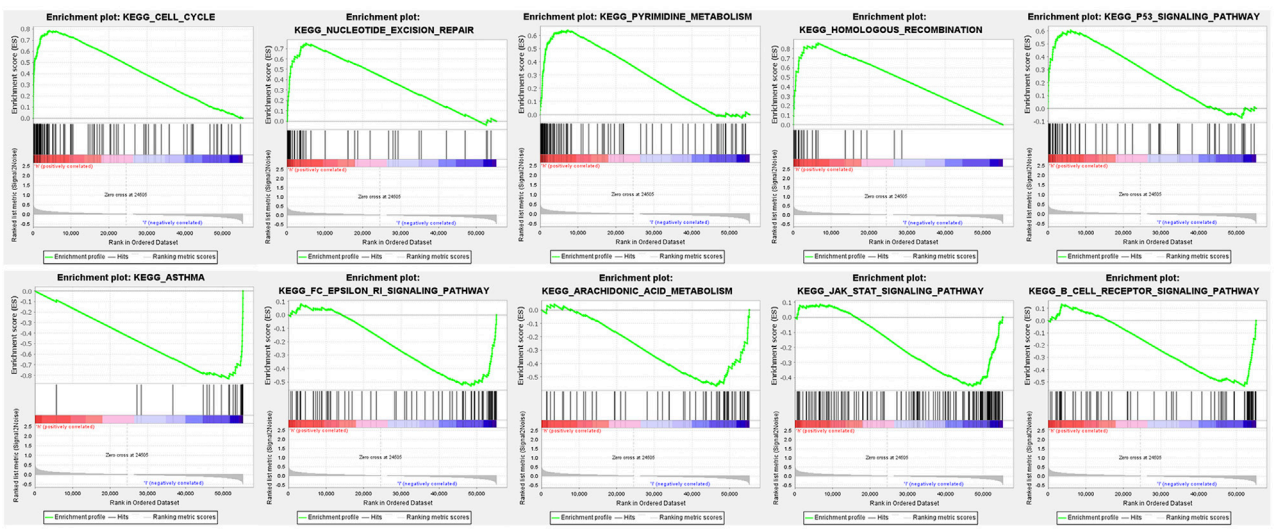

FIGURE 5 | Functional enrichment analysis of genes between high-risk and low-risk groups based on the TCGA tumor dataset.

lung cancer patients due to tumors' high demand of glucose (Ooi and Gomperts, 2015). Jiang et al. indicated that *SLC2A1* inhibited the accumulation of intracellular iron and lipid ROS which were required for ferroptosis (Jiang et al., 2017). Thioredoxin reductase 1 (*TXNRD1*) modulating the cellular redox balance through reducing oxidized thioredoxin (TXN) protected cells against oxidative stress, and direct knockdown of *TNXRD1* increased the basal ROS level and sensitized radiation-resistant lung tumor cells to radiation (Hao et al., 2017). Moreover, the *TXNRD* inhibitor enhanced lysine oxidase (LO)-induced necroptosis and ferroptosis *via* a ROS-dependent mechanism (Chepikova et al., 2020). These aforementioned genes appear to suppress ferroptosis, which may potentially explain the correlation between their high expression and poor prognosis in LUAD patients.

DNA damage-inducible transcript 4 (*DDIT4/REDD1*) was a stress response gene, and its expression increased cellular

TABLE 3 | Gene functional enrichment in high- and low-risk groups.

Gene set name	Size	NES	NOM *p*-value
KEGG_CELL_CYCLE	125	2.44	0.000
KEGG_PYRIMIDINE_METABOLISM	98	2.27	0.000
KEGG_P53_SIGNALING_PATHWAY	68	2.25	0.000
KEGG_NUCLEOTIDE_EXCISION_REPAIR	44	2.25	0.000
KEGG_HOMOLOGOUS_RECOMBINATION	28	2.18	0.000
KEGG_ASTHMA	28	−2.14	0.002
KEGG_FC_EPSILON_RI_SIGNALING_PATHWAY	79	−2.04	0.002
KEGG_ARACHIDONIC_ACID_METABOLISM	58	−2.01	0.000
KEGG_JAK_STAT_SIGNALING_PATHWAY	155	−1.85	0.010
KEGG_B_CELL_RECEPTOR_SIGNALING_PATHWAY	75	−1.84	0.017

NES, normalized enrichment score; NOM, nominal; Gene sets with NOM p-value <0.05 are considered as significant.

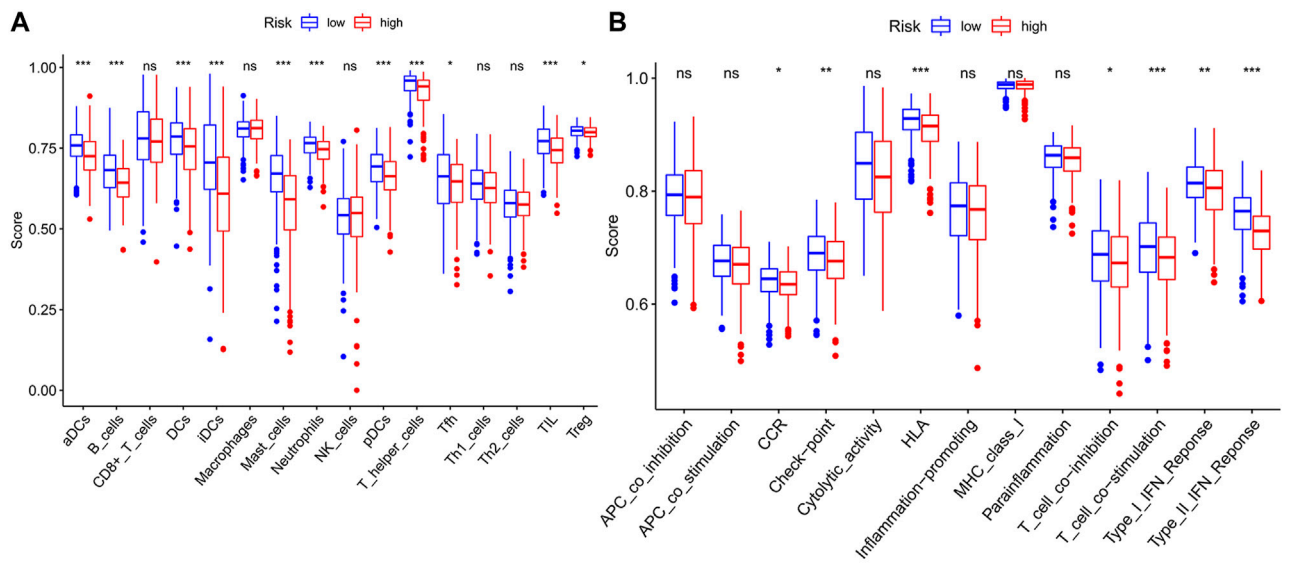

FIGURE 6 | The ssGSEA scores between two risk groups in the TCGA tumor cohort. The scores of 16 immune cells **(A)** and 13 immune-related functions **(B)** are displayed in boxplots. ssGSEA: single-sample gene set enrichment analysis. CCR: cytokine–cytokine receptor. ns, not significant; **p* < 0.05; ***p* < 0.01; ****p* < 0.001.

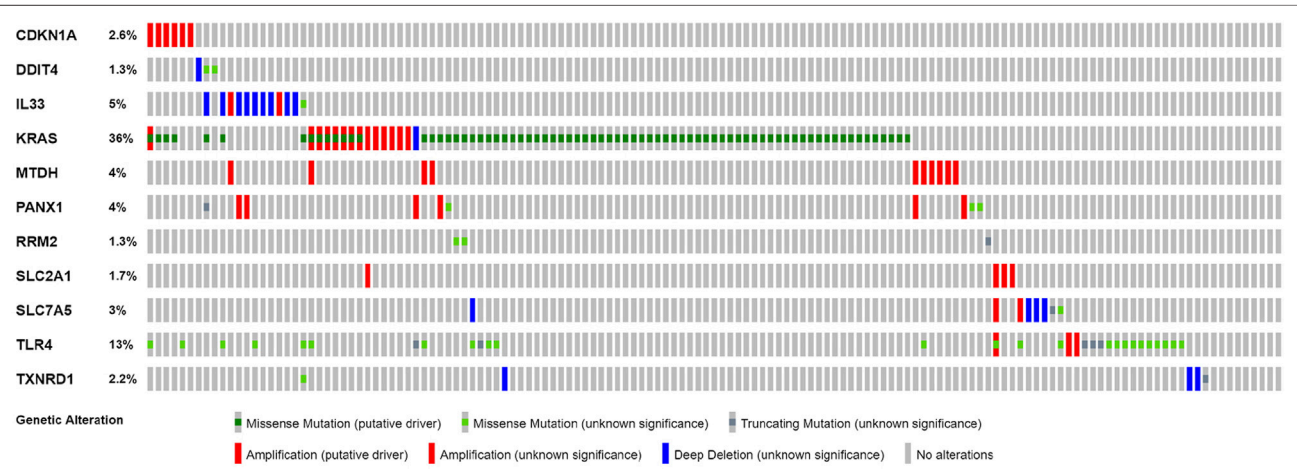

FIGURE 7 | Online database analysis of prognosis ferroptosis-related genes. The total variation frequency of 11 ferroptosis-related genes in LUAD patients.

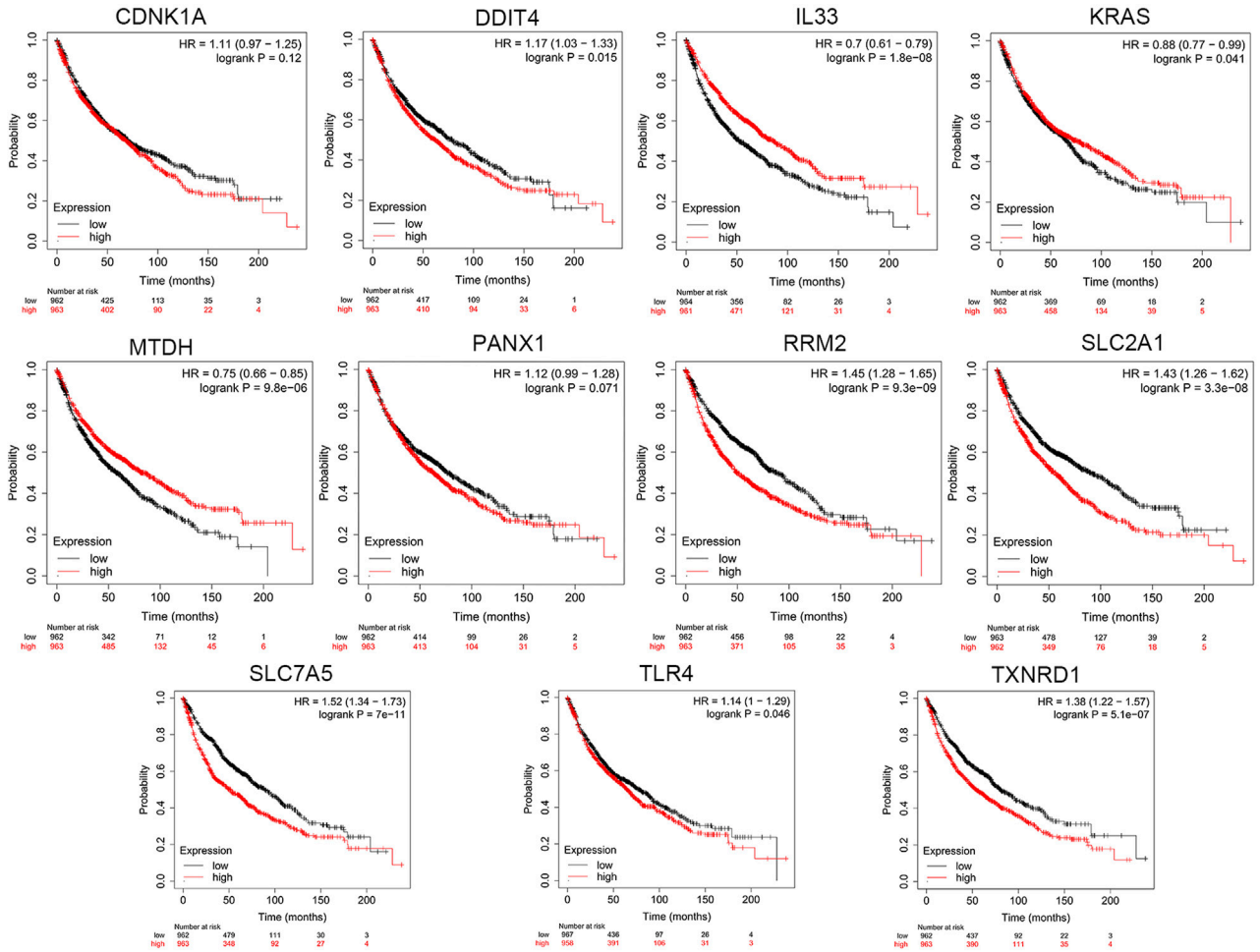

FIGURE 8 | The KM survival analysis between the high and low expressions of 11 ferroptosis-related genes in lung cancer in the online database.

sensitivity to lethal oxidative stress (Ellisen et al., 2002). The transient elevation of *DDIT4* expression might reduce tumor growth, while high and constitutive expression was linked with poor prognosis in diverse hematologic and solid tumors (Britto et al., 2020). Overexpression of pannexin 1 (*PANX1*) promoted the invasion and migration of hepatocellular carcinoma cells *via* modulation of EMT depending on AKT signaling (Shi et al., 2019). Su et al. indicated that *PANX1* deletion inhibited ferroptinophagy through the MAPK/ERK pathway (Su et al., 2019). Solute carrier family seven member 5 (*SLC7A5*) as an amino acid transporter was overexpressed in multiple cancers including NSCLC, and its expression level was related to cancer progression and aggressiveness (Li et al., 2018). The increased expression of *SLC7A5* facilitated by sublethal concentrations of ferroptosis inducers could facilitate cells better coping with oxidative stress (Alborzinia et al., 2018). Metadherin (*MTDH*) facilitated transcription by regulating transcription factors such as HIF1A and TWIST1 to control cancer cell migration, invasion, and angiogenesis, which was correlated with poor OS in many types of cancers, but it enhanced the vulnerability of tumor cells to ferroptosis through inhibiting *GPX4* and *SLC3A2* (Lu et al., 2018; Bi et al., 2019). It is obvious that these four genes can promote ferroptosis. However, their high expression occurs in many types of tumors and contributes to cancer progression and poor prognosis. Similarly, our study confirmed that these genes were upregulated in LUAD samples and were associated with worse outcomes.

There were also three genes that were significantly downregulated in LUAD tumor tissues. Among them, the expressions of *IL33* and *TLR4* were negatively correlated with poor OS. Interleukin 33 (*IL33*) was an alarmin connected to necroptosis, and its upregulation could be prevented by ferrostatin-1, an inhibitor of ferroptosis (Martin-Sanchez et al., 2017). Kim et al. observed that plasma *IL-33* levels were elevated at the early stage of lung cancer but decreased with advanced stages (Kim et al., 2015). Toll-like receptor 4 (*TLR4*) knockdown could significantly inhibit the ferroptosis through the NADPH oxidase 4 (NOX4) pathway, while *TLR4* signaling activation in LUAD cells activated downstream p65 nucleus translocation and finally promoted proliferation and migration (Zhou et al., 2018; Chen et al., 2019). In addition, *CDKN1A*, cyclin-dependent kinase inhibitor 1A (*CDKN1A*/*p21*), was found to be

oncogenic in lung cancer by promoting anti-apoptosis and cell proliferation (Su et al., 2018). Tarangelo et al. reported that *CDKN1A* expression mediated by p53 delayed the onset of ferroptosis induced by cystine deprivation in human cancer cells (Tarangelo et al., 2018). Interestingly, the higher the expression of *CDKN1A*, the higher the risk of poor prognosis, but it was significantly downregulated in tumor tissues. Overall, we think that tumor cells under persistent oxidative stress can make an exquisite balance between the expression of ferroptosis driver genes and suppressor genes, thereby escaping ferroptosis, eventually facilitating proliferation and infiltration. Therefore, understanding the mechanism of these genes acting in ferroptosis may shed new light on treating cancers. Our work explored the effect of these 11 FRGs on tumors, which may provide indispensable sight into future further in-depth research.

In our study, the risk score was calculated based on the eleven meaningful FRGs. We observed a higher risk score related to the clinicopathological characteristics of LUAD patients, such as current smoking history and poor differentiation. Cigarette smoke extract could induce lipid peroxidation and intracellular GSH depletion which are key features of ferroptosis, and ferroptosis played a key role in the toxicity caused by cigarette smoke (Sampilvanjil et al., 2020; Sepand et al., 2021). Tumor progression and resistance to treatment are usually accompanied by the polarization of malignant cells toward a poorly differentiated state, and this transition generates an accumulated vulnerability to the induction of ferroptosis, which may pave the way to novel therapeutic strategies (Chen and Galluzzi, 2018). Here, we also analyzed the potential functional differences after classifying tumor patients into two risk groups according to the risk score. GSEA revealed that tumor-related pathways were most active in the high-risk group, such as the p53 signaling pathway. Tumor suppressor p53 (*TP53*) was frequently mutated in lung cancer, and multiple signaling pathways to induce oncogenicity could be activated by R273H-mutated p53 (Hao et al., 2019). *TP53* was reported to limit ferroptosis by blocking dipeptidyl peptidase-4 activity, although it has been demonstrated to promote ferroptosis, which meant that *TP53* played pleiotropic functions in regulating ferroptosis (Xie et al., 2017). The signal transduction pathway of p53 mediators also had a regulation relationship with our prognostic-related genes *CDKN1A* and *RRM2* (Tarangelo et al., 2018; Jin et al., 2020). In the low-risk group, functional enrichments were mainly linked with immune-related pathways and the significantly upregulated immune infiltrates including DCs and TILs were also observed. Dendritic cells (DCs) promoting the cross-presentation of tumor-associated antigens were considered paramount in antitumor immunity, and the effector activity of $CD8^+$ T cells which were main effectors of anticancer immunity was dependent on DC-derived cytokines (Wculek et al., 2020). Previous studies have suggested that high densities of TILs were correlated with improved OS in multiple tumor types (Liu et al., 2018), and our results reconfirmed this association. Immune-related molecules may play a key role in tumor therapy and may become therapeutic targets. We speculate that the low-risk group patients with a better prognosis benefit from enhanced antitumor immunity. Overall, our prognostic signature may be a reliable tool for risk stratification in LUAD patients.

Ferroptosis as a different form of cell death from autophagy and apoptosis provides tumor treatment with a new therapeutic direction. Nevertheless, cancer cells can exhibit an adaptative response to ferroptosis, and the sensitivity of different tumor cells to ferroptosis may vary greatly. Hence, unveiling the mechanism of ferroptosis resistance versus sensitivity promotion is key to the development of personalized antitumor strategies, and the connection between ferroptosis and host immunogenicity also needs to be explored. In our study, we integrated some ferroptosis biomarkers to predict OS among LUAD patients, which may promote the development of precision medicine in LUAD. Moreover, compared with previous studies and established FRG-related prognostic models (Cai et al., 2021; Wang et al., 2021), our model could provide better predictive performance, and we emphasized the analysis of differentially expressed FRGs and their relationship with OS. However, our study was subject to several limitations. First, all our data were from public databases and our results lacked clinical sample validation. Our signature needs to be proved in independent cohort studies and further experiments of ferroptosis function study in the future. Second, this study failed to explore the underlying link mechanism between ferroptosis and the stages on LUAD development, radiotherapy, and chemotherapy. Third, our research was limited by the comparatively small sample size.

CONCLUSION

We defined a novel 11-FRG signature for predicting OS in LUAD patients based on online databases. Our findings may provide useful biomarkers for prognosis prediction and new insights into searching novel molecules or targets for cancer treatment.

DATA AVAILABILITY STATEMENT

The original contributions presented in the study are included in the article/**Supplementary Material**; further inquiries can be directed to the corresponding author.

AUTHOR CONTRIBUTIONS

SW, ZW, and ZX conceived and designed the study. SW analyzed the data. SW and ZW wrote the manuscript. ZX and ZW revised the manuscript.

SUPPLEMENTARY MATERIAL

The Supplementary Material for this article can be found online at: https://www.frontiersin.org/articles/10.3389/fgene.2021.793636/full#supplementary-material

REFERENCES

Alborzinia, H., Ignashkova, T. I., Dejure, F. R., Gendarme, M., Theobald, J., Wölfl, S., et al. (2018). Golgi Stress Mediates Redox Imbalance and Ferroptosis in Human Cells. *Commun. Biol.* 1, 210. doi:10.1038/s42003-018-0212-6

Bebber, C. M., Müller, F., Prieto Clemente, L., Weber, J., and von Karstedt, S. (2020). Ferroptosis in Cancer Cell Biology. *Cancers (Basel)* 12 (1). doi:10.3390/cancers12010164

Bi, J., Yang, S., Li, L., Dai, Q., Borcherding, N., Wagner, B. A., et al. (2019). Metadherin Enhances Vulnerability of Cancer Cells to Ferroptosis. *Cell Death Dis* 10 (10), 682. doi:10.1038/s41419-019-1897-2

Britto, F. A., Dumas, K., Giorgetti-Peraldi, S., Ollendorff, V., and Favier, F. B. (2020). Is REDD1 a Metabolic Double Agent? Lessons from Physiology and Pathology. *Am. J. Physiology-Cell Physiol.* 319 (5), C807–C824. doi:10.1152/ajpcell.00340.2020

Cai, J., Li, C., Li, H., Wang, X., and Zhou, Y. (2021). Establishment of a Ferroptosis-Related Gene Signature for Prognosis in Lung Adenocarcinoma Patients. *PeerJ* 9, e11931. doi:10.7717/peerj.11931

Cao, P., Liu, B., Du, F., Li, D., Wang, Y., Yan, X., et al. (2019). Scutellarin Suppresses Proliferation and Promotes Apoptosis in A549 Lung Adenocarcinoma Cells via AKT/mTOR/4EBP1 and STAT3 Pathways. *Thorac. Cancer* 10 (3), 492–500. doi:10.1111/1759-7714.12962

Chen, D., Mao, Y., Ding, Q., Wang, W., Zhu, F., Chen, C., et al. (2020). Prognostic Implications of Programmed Death Ligand 1 Expression in Resected Lung Adenocarcinoma: a Systematic Review and Meta-Analysis. *Eur. J. Cardio-Thoracic Surg.* 58 (5), 888–898. doi:10.1093/ejcts/ezaa172

Chen, J. J., and Galluzzi, L. (2018). Fighting Resilient Cancers with Iron. *Trends Cell Biology* 28 (2), 77–78. doi:10.1016/j.tcb.2017.11.007

Chen, X., Xu, S., Zhao, C., and Liu, B. (2019). Role of TLR4/NADPH Oxidase 4 Pathway in Promoting Cell Death through Autophagy and Ferroptosis during Heart Failure. *Biochem. Biophysical Res. Commun.* 516 (1), 37–43. doi:10.1016/j.bbrc.2019.06.015

Chepikova, O. E., Malin, D., Strekalova, E., Lukasheva, E. V., Zamyatnin, A. A., Jr., and Cryns, V. L. (2020). Lysine Oxidase Exposes a Dependency on the Thioredoxin Antioxidant Pathway in Triple-Negative Breast Cancer Cells. *Breast Cancer Res. Treat.* 183 (3), 549–564. doi:10.1007/s10549-020-05801-4

Domagala-Kulawik, J., and Trojnar, A. (2020). Lung Cancer in Women in 21th century. *J. Thorac. Dis.* 12 (8), 4398–4410. doi:10.21037/jtd-20-287

Ellisen, L. W., Ramsayer, K. D., Johannessen, C. M., Yang, A., Beppu, H., Minda, K., et al. (2002). REDD1, a Developmentally Regulated Transcriptional Target of P63 and P53, Links P63 to Regulation of Reactive Oxygen Species. *Mol. Cel* 10 (5), 995–1005. doi:10.1016/s1097-2765(02)00706-2

Hao, C., Xu, X., Ma, J., Xia, J., Dai, B., Liu, L., et al. (2017). MicroRNA-124 Regulates the Radiosensitivity of Non-small Cell Lung Cancer Cells by Targeting TXNRD1. *Oncol. Lett.* 13 (4), 2071–2078. doi:10.3892/ol.2017.5701

Hao, X.-l., Han, F., Zhang, N., Chen, H.-q., Jiang, X., Yin, L., et al. (2019). TC2N, a Novel Oncogene, Accelerates Tumor Progression by Suppressing P53 Signaling Pathway in Lung Cancer. *Cell Death Differ* 26 (7), 1235–1250. doi:10.1038/s41418-018-0202-8

Huang, C., Yang, M., Deng, J., Li, P., Su, W., and Jiang, R. (2018). Upregulation and Activation of P53 by Erastin-induced R-eactive O-xygen S-pecies C-ontribute to C-ytotoxic and C-ytostatic E-ffects in A549 L-ung C-ancer C-ells. *Oncol. Rep.* 40 (4), 2363–2370. doi:10.3892/or.2018.6585

Huang, N., Guo, W., Ren, K., Li, W., Jiang, Y., Sun, J., et al. (2019). LncRNA AFAP1-AS1 Supresses miR-139-5p and Promotes Cell Proliferation and Chemotherapy Resistance of Non-small Cell Lung Cancer by Competitively Upregulating RRM2. *Front. Oncol.* 9, 1103. doi:10.3389/fonc.2019.01103

Ji, X., Qian, J., Rahman, S. M. J., Siska, P. J., Zou, Y., Harris, B. K., et al. (2018). xCT (SLC7A11)-Mediated Metabolic Reprogramming Promotes Non-small Cell Lung Cancer Progression. *Oncogene* 37 (36), 5007–5019. doi:10.1038/s41388-018-0307-z

Jiang, Y., Mao, C., Yang, R., Yan, B., Shi, Y., Liu, X., et al. (2017). EGLN1/c-Myc Induced Lymphoid-specific Helicase Inhibits Ferroptosis through Lipid Metabolic Gene Expression Changes. *Theranostics* 7 (13), 3293–3305. doi:10.7150/thno.19988

Jin, C.-Y., Du, L., Nuerlan, A.-H., Wang, X.-L., Yang, Y.-W., and Guo, R. (2020). High Expression of RRM2 as an Independent Predictive Factor of Poor Prognosis in Patients with Lung Adenocarcinoma. *Aging* 13 (3), 3518–3535. doi:10.18632/aging.202292

Jin, J., Liu, C., Yu, S., Cai, L., Sitrakiniaina, A., Gu, R., et al. (2021). A Novel Ferroptosis-Related Gene Signature for Prognostic Prediction of Patients with Lung Adenocarcinoma. *Aging* 13 (12), 16144–16164. doi:10.18632/aging.203140

Kim, M. S., Kim, E., Heo, J.-S., Bae, D.-J., Lee, J.-U. W., Lee, T.-H., et al. (2015). Circulating IL-33 Level Is Associated with the Progression of Lung Cancer. *Lung Cancer* 90 (2), 346–351. doi:10.1016/j.lungcan.2015.08.011

Lai, Y., Zhang, Z., Li, J., Li, W., Huang, Z., Zhang, C., et al. (2019). STYK1/NOK Correlates with Ferroptosis in Non-small Cell Lung Carcinoma. *Biochem. Biophysical Res. Commun.* 519 (4), 659–666. doi:10.1016/j.bbrc.2019.09.032

Li, H., Chen, S., Liu, J., Guo, X., Xiang, X., Dong, T., et al. (2018). Long Non-coding RNA PVT1-5 Promotes Cell Proliferation by Regulating miR-126/SLC7A5 axis in Lung Cancer. *Biochem. Biophysical Res. Commun.* 495 (3), 2350–2355. doi:10.1016/j.bbrc.2017.12.114

Liang, C., Zhang, X., Yang, M., and Dong, X. (2019). Recent Progress in Ferroptosis Inducers for Cancer Therapy. *Adv. Mater.* 31 (51), e1904197. doi:10.1002/adma.201904197

Liljedahl, H., Karlsson, A., Oskarsdottir, G. N., Salomonsson, A., Brunnstrom, H., Erlingsdottir, G., et al. (2020). A Gene Expression-Based Single Sample Predictor of Lung Adenocarcinoma Molecular Subtype and Prognosis. *Int. J. Cancer* 148 (1), 238–251. doi:10.1002/ijc.33242

Liu, K., Guo, J., Liu, K., Fan, P., Zeng, Y., Xu, C., et al. (2018). Integrative Analysis Reveals Distinct Subtypes with Therapeutic Implications in KRAS-Mutant Lung Adenocarcinoma. *EBioMedicine* 36, 196–208. doi:10.1016/j.ebiom.2018.09.034

Liu, P., Wu, D., Duan, J., Xiao, H., Zhou, Y., Zhao, L., et al. (2020). NRF2 Regulates the Sensitivity of Human NSCLC Cells to Cystine Deprivation-Induced Ferroptosis via FOCAD-FAK Signaling Pathway. *Redox Biol.* 37, 101702. doi:10.1016/j.redox.2020.101702

Liu, T., Wu, L., Wang, D., Wang, H., Chen, J., Yang, C., et al. (2016). Role of Reactive Oxygen Species-Mediated MAPK and NF-Kb Activation Inpolygonatum Cyrtonemalectin-Induced Apoptosis and Autophagy in Human Lung Adenocarcinoma A549 Cells. *J. Biochem.* 160 (6), 315–324. doi:10.1093/jb/mvw040

Lu, Q., Shan, S., Li, Y., Zhu, D., Jin, W., and Ren, T. (2018). Long Noncoding RNASNHG1promotes Non-small Cell Lung Cancer Progression by up-regulatingMTDH Viasponging miR-145-5p. *FASEB j.* 32 (7), 3957–3967. doi:10.1096/fj.201701237rr

Ma, B., Geng, Y., Meng, F., Yan, G., and Song, F. (2020). Identification of a Sixteen-Gene Prognostic Biomarker for Lung Adenocarcinoma Using a Machine Learning Method. *J. Cancer* 11 (5), 1288–1298. doi:10.7150/jca.34585

Martin-Sanchez, D., Ruiz-Andres, O., Poveda, J., Carrasco, S., Cannata-Ortiz, P., Sanchez-Niño, M. D., et al. (2017). Ferroptosis, but Not Necroptosis, Is Important in Nephrotoxic Folic Acid-Induced AKI. *Jasn* 28 (1), 218–229. doi:10.1681/asn.2015121376

Montero, J., Sarosiek, K. A., DeAngelo, J. D., Maertens, O., Ryan, J., Ercan, D., et al. (2015). Drug-induced Death Signaling Strategy Rapidly Predicts Cancer Response to Chemotherapy. *Cell* 160 (5), 977–989. doi:10.1016/j.cell.2015.01.042

Nakhaie, M., Charostad, J., Kaydani, G. A., and Faghihloo, E. (2020). The Role of Viruses in Adenocarcinoma Development. *Infect. Genet. Evol.* 86, 104603. doi:10.1016/j.meegid.2020.104603

Ooi, A. T., and Gomperts, B. N. (2015). Molecular Pathways: Targeting Cellular Energy Metabolism in Cancer via Inhibition of SLC2A1 and LDHA. *Clin. Cancer Res.* 21 (11), 2440–2444. doi:10.1158/1078-0432.ccr-14-1209

Pylayeva-Gupta, Y., Grabocka, E., and Bar-Sagi, D. (2011). RAS Oncogenes: Weaving a Tumorigenic Web. *Nat. Rev. Cancer* 11 (11), 761–774. doi:10.1038/nrc3106

Roh, J.-L., Kim, E. H., Jang, H., and Shin, D. (2017). Nrf2 Inhibition Reverses the Resistance of Cisplatin-Resistant Head and Neck Cancer Cells to Artesunate-Induced Ferroptosis. *Redox Biol.* 11, 254–262. doi:10.1016/j.redox.2016.12.010

Sampilvanjil, A., Karasawa, T., Yamada, N., Komada, T., Higashi, T., Baatarjav, C., et al. (2020). Cigarette Smoke Extract Induces Ferroptosis in Vascular Smooth

Muscle Cells. *Am. J. Physiology-Heart Circulatory Physiol.* 318 (3), H508–H518. doi:10.1152/ajpheart.00559.2019

Sánchez-Rivera, F. J., Ryan, J., Soto-Feliciano, Y. M., Clare Beytagh, M., Xuan, L., Feldser, D. M., et al. (2021). Mitochondrial Apoptotic Priming Is a Key Determinant of Cell Fate upon P53 Restoration. *Proc. Natl. Acad. Sci. U S A.* 118 (23), e2019740118. doi:10.1073/pnas.2019740118

Sepand, M. R., Maghsoudi, A. S., Shadboorestan, A., Mirnia, K., Aghsami, M., and Raoufi, M. (2021). Cigarette Smoke-Induced Toxicity Consequences of Intracellular Iron Dysregulation and Ferroptosis. *Life Sci.* 281, 119799. doi:10.1016/j.lfs.2021.119799

Shi, G., Liu, C., Yang, Y., Song, L., Liu, X., Wang, C., et al. (2019). Panx1 Promotes Invasion-Metastasis cascade in Hepatocellular Carcinoma. *J. Cancer* 10 (23), 5681–5688. doi:10.7150/jca.32986

Song, Y., Chen, D., Zhang, X., Luo, Y., and Li, S. (2019). Integrating Genetic Mutations and Expression Profiles for Survival Prediction of Lung Adenocarcinoma. *Thorac. Cancer* 10 (5), 1220–1228. doi:10.1111/1759-7714.13072

Stockwell, B. R., Friedmann Angeli, J. P., Bayir, H., Bush, A. I., Conrad, M., Dixon, S. J., et al. (2017). Ferroptosis: A Regulated Cell Death Nexus Linking Metabolism, Redox Biology, and Disease. *Cell* 171 (2), 273–285. doi:10.1016/j.cell.2017.09.021

Su, L., Jiang, X., Yang, C., Zhang, J., Chen, B., Li, Y., et al. (2019). Pannexin 1 Mediates Ferroptosis that Contributes to Renal Ischemia/reperfusion Injury. *J. Biol. Chem.* 294 (50), 19395–19404. doi:10.1074/jbc.ra119.010949

Su, W., Feng, S., Chen, X., Yang, X., Mao, R., Guo, C., et al. (2018). Silencing of Long Noncoding RNA MIR22HG Triggers Cell Survival/Death Signaling via Oncogenes YBX1, MET, and P21 in Lung Cancer. *Cancer Res.* 78 (12), 3207–3219. doi:10.1158/0008-5472.can-18-0222

Tang, B., Xu, W., Wang, Y., Zhu, J., Wang, H., Tu, J., et al. (2021). Identification of Critical Ferroptosis Regulators in Lung Adenocarcinoma that RRM2 Facilitates Tumor Immune Infiltration by Inhibiting Ferroptotic Death. *Clin. Immunol.* 232, 108872. doi:10.1016/j.clim.2021.108872

Tarangelo, A., Magtanong, L., Bieging-Rolett, K. T., Li, Y., Ye, J., Attardi, L. D., et al. (2018). p53 Suppresses Metabolic Stress-Induced Ferroptosis in Cancer Cells. *Cel Rep.* 22 (3), 569–575. doi:10.1016/j.celrep.2017.12.077

Toyokuni, S., Ito, F., Yamashita, K., Okazaki, Y., and Akatsuka, S. (2017). Iron and Thiol Redox Signaling in Cancer: An Exquisite Balance to Escape Ferroptosis. *Free Radic. Biol. Med.* 108, 610–626. doi:10.1016/j.freeradbiomed.2017.04.024

Toyokuni, S. (2016). The Origin and Future of Oxidative Stress Pathology: From the Recognition of Carcinogenesis as an Iron Addiction with Ferroptosis-Resistance to Non-thermal Plasma Therapy. *Pathol. Int.* 66 (5), 245–259. doi:10.1111/pin.12396

Uras, I. Z., Moll, H. P., and Casanova, E. (2020). Targeting KRAS Mutant Non-small-cell Lung Cancer: Past, Present and Future. *Int. J. Mol. Sci.* 21 (12). doi:10.3390/ijms21124325

Wang, X., Shi, B., Zhao, Y., Lu, Q., Fei, X., Lu, C., et al. (2020). HKDC1 Promotes the Tumorigenesis and Glycolysis in Lung Adenocarcinoma via Regulating AMPK/mTOR Signaling Pathway. *Cancer Cel Int* 20, 450. doi:10.1186/s12935-020-01539-7

Wang, Y., Chen, W., Zhu, M., and Xian, L. (2021). Ferroptosis-Related Gene Signature and Patterns of Immune Infiltration Predict the Overall Survival in Patients With Lung Adenocarcinoma. *Front. Mol. Biosci.* 8, 692530. doi:10.3389/fmolb.2021.692530

Wculek, S. K., Cueto, F. J., Mujal, A. M., Melero, I., Krummel, M. F., and Sancho, D. (2020). Dendritic Cells in Cancer Immunology and Immunotherapy. *Nat. Rev. Immunol.* 20 (1), 7–24. doi:10.1038/s41577-019-0210-z

Wu, P., Heins, Z. J., Muller, J. T., Katsnelson, L., de Bruijn, I., Abeshouse, A. A., et al. (2019). Integration and Analysis of CPTAC Proteomics Data in the Context of Cancer Genomics in the cBioPortal. *Mol. Cell Proteomics* 18 (9), 1893–1898. doi:10.1074/mcp.tir119.001673

Wu, Y., Zhang, S., Gong, X., Tam, S., Xiao, D., Liu, S., et al. (2020). The Epigenetic Regulators and Metabolic Changes in Ferroptosis-Associated Cancer Progression. *Mol. Cancer* 19 (1), 39. doi:10.1186/s12943-020-01157-x

Xie, Y., Zhu, S., Song, X., Sun, X., Fan, Y., Liu, J., et al. (2017). The Tumor Suppressor P53 Limits Ferroptosis by Blocking DPP4 Activity. *Cel Rep.* 20 (7), 1692–1704. doi:10.1016/j.celrep.2017.07.055

Yu, M., Gai, C., Li, Z., Ding, D., Zheng, J., Zhang, W., et al. (2019). Targeted Exosome-encapsulated Erastin Induced Ferroptosis in Triple Negative Breast Cancer Cells. *Cancer Sci.* 110 (10), 3173–3182. doi:10.1111/cas.14181

Zhou, N., and Bao, J. (2020). *A Manually Curated Resource for Regulators and Markers of Ferroptosis and Ferroptosis-Disease Associations*. Oxford: Database.

Zhou, W., Chen, X., Hu, Q., Chen, X., Chen, Y., and Huang, L. (2018). Galectin-3 Activates TLR4/NF-Kb Signaling to Promote Lung Adenocarcinoma Cell Proliferation through Activating lncRNA-NEAT1 Expression. *BMC Cancer* 18 (1), 580. doi:10.1186/s12885-018-4461-z

Zhou, W., Liu, Y., Gao, Y., Cheng, Y., Chang, R., Li, X., et al. (2020). MICAL2 Is a Novel Nucleocytoplasmic Shuttling Protein Promoting Cancer Invasion and Growth of Lung Adenocarcinoma. *Cancer Lett.* 483, 75–86. doi:10.1016/j.canlet.2020.04.019

Conflict of Interest: The authors declare that the research was conducted in the absence of any commercial or financial relationships that could be construed as a potential conflict of interest.

Publisher's Note: All claims expressed in this article are solely those of the authors and do not necessarily represent those of their affiliated organizations, or those of the publisher, the editors, and the reviewers. Any product that may be evaluated in this article, or claim that may be made by its manufacturer, is not guaranteed or endorsed by the publisher.

frontiers in Genetics

ORIGINAL RESEARCH
published: 20 January 2022
doi: 10.3389/fgene.2022.812674

Genetic Alteration, Prognostic and Immunological Role of Acyl-CoA Synthetase Long-Chain Family Member 4 in a Pan-Cancer Analysis

Yongsheng Yu[1†], *Xuepu Sun*[2†], *Fei Chen*[3] *and Miao Liu*[4*]

[1]Department of General Surgery, The Fourth Affiliated Hospital of Harbin Medical University, Harbin, China, [2]Department of General Surgery, The First Affiliated Hospital of Harbin Medical University, Harbin, China, [3]Department of General Surgery, Linyi Traditional Chinese Medicine Hospital, Linyi, China, [4]Department of Pathology, Beidahuang Industry Group General Hospital, Harbin, China

OPEN ACCESS

Edited by:
Ying Li,
The University of Texas Health Science Center at San Antonio, United States

Reviewed by:
Chih-Yang Wang,
Taipei Medical University, Taiwan
Miaowei Wu,
Zhejiang University, China

***Correspondence:**
Miao Liu
lm3000_2001@163.com

[†]*These authors have contributed equally to this work and share first authorship*

Specialty section:
This article was submitted to Human and Medical Genomics, a section of the journal Frontiers in Genetics

Received: *10 November 2021*
Accepted: *03 January 2022*
Published: *20 January 2022*

Citation:
Yu Y, Sun X, Chen F and Liu M (2022) Genetic Alteration, Prognostic and Immunological Role of Acyl-CoA Synthetase Long-Chain Family Member 4 in a Pan-Cancer Analysis. Front. Genet. 13:812674. doi: 10.3389/fgene.2022.812674

Acyl-CoA Synthetase long-chain family member 4 (ACSL4) is a member of acyl-CoA synthetase protein long-chain family, which is associated with amino acid synthesis, lipid synthesis and lipid peroxidation dependent iron death. However, the role of ACSL4 in generalized carcinoma remains unclear. We aim to analyze the expression and prognostic value of ACSL4 in pan-cancer, and further explore the correlation between ACSL4 and immune infiltration. Through ONCOMINE, TIMER (Tumor Immune Estimation Resource), GEPIA (Gene expression Profiling Interactive), UALCAN and HPA, ACSL4 expression patterns of in pan-cancer were analyzed. The prognostic value of ACSL4 was analyzed using PrognoScan and Kaplan-Meier Plotter databases. Furthermore, gene variation and epigenetic modification of ACSL4 were analyzed by cBioPortal and GSCA databases. Meanwhile, GEPIA and TIMER databases applied to evaluate the relationship between ACSL4 expression and immune infiltration. These results indicate that ACSL4 expression is down-regulated and associated with prognosis in most tumors. In general, lower ACSL4 expression shows more beneficial prognosis. The most common genetic alteration of ACSL4 is point mutation. ACSL4 is negatively correlated with DNA methylation levels in most cancers. ACSL4 mutations or hypomethylation are associated with poor prognosis. In addition, ACSL4 is positively correlated with immune infiltration in cancers. ACSL4 and immune infiltration are strongly associated with prognosis in BRCA (Breast invasive carcinoma) and SKCM (Skin Cutaneous Melanoma). ACSL4 mutation caused significant changes of immune infiltration in UCEC (Uterine Corpus Endometrial Carcinoma) and SARC (Sarcoma). ACSL4 may be a promising prognostic biomarker for pan-cancer and is closely associated with immune infiltration in the tumor microenvironment.

Keywords: ACSL4, Pan-cancer analysis, prognosis, immunological, genetic alteration

INTRODUCTION

Cancer relies on metabolic reprogramming to drive malignant transformation (Boroughs and DeBerardinis, 2015). More and more tumor metabolic phenotypes have been identified and validated and are becoming biomarkers for the disease (Chen et al., 2019; Qin et al., 2020). Alterations in glucose and lipid metabolic pathways are one of the most striking metabolic features present in many different types of cancer. Changes in lipid metabolism of cancer cells showed increased proliferation, progression and metastasis (Cheng et al., 2018; Snaebjornsson et al., 2020). Activation of fatty acids catalyzed by acyl-coA synthase (ACS) is essential for the metabolism of both extracellular derived and *de novo* synthesized fatty acids. There are five members of the ACSL family, namely ACSL1, ACSL3, ACSL4, ACSL5 and ACSL6. Previous studies have shown that almost all ACSL members are deregulated in clinical cancers, which is conducive to excessive lipid biosynthesis and deposition, and ultimately makes the body susceptible to metabolic disorders and carcinogenesis (Tang et al., 2018). ACSL1 and ACSL4 are overexpressed in most cancer types and may have synergistic effects to promote unregulated cell growth, promote tumor invasion and evade programmed cell death (Sánchez-Martínez et al., 2017; Yen et al., 2017). While ACSL5 showed the opposite effect and was associated with a good prognosis in breast cancer patients. In addition, each with unique substrate of the ACSL family preferences and enzyme activity at different cellular sites, which depended on the chain length and saturation status of fatty acids (Grevengoed et al., 2014). ACSL4 is mainly present in peroxisome, mitochondria and endoplasmic reticulum. In contrast, ACSL4 prefers longer polyunsaturated fatty acids (PUFA) as substrates, such as arachidonic acid. It catalyzes the conversion of free arachidonic acid to arachidonic acid-coA ester, which is then esterified by interaction with membrane phospholipids and leads to ferroptosis (Küch et al., 2014; Kagan et al., 2017; Sánchez-Martínez et al., 2017). Recent studies have linked ferroptosis to a variety of cancers. Ferroptosis is a new iron-dependent form of regulated cell death,which characterized by iron-dependent accumulation of lipid-ROS and subsequent depletion of polyunsaturated fatty acid phospholipids (PUFA-PLS) (Hirschhorn and Stockwell, 2019). ACSL4 has been shown to be overexpressed in several cancer types, including colon cancer, breast cancer, liver and prostate cancer (Sánchez-Martínez et al., 2017; Wang J. et al., 2020; Chen et al., 2020; Ma et al., 2021; Sha et al., 2021), but often down-regulated in gastric cancer and lung cancer (Ye et al., 2016; Zhang et al., 2021).

As a percentage of genome length, the level of Copy number variation (CNV) in the tumor genome reflects the degree of tumor genome change (Hieronymus et al., 2018). The level of genomic copy number alteration is associated with prognosis in many cancers (Cao et al., 2019; Su et al., 2019; Lu et al., 2020; Woo et al., 2021). Recent analyses have linked cancer genomic characteristics, including TMB and CNA, to anti-tumor immunity. Studies suggest that high mutation load and low aneuploidy may be associated with increased T cell response (Budczies et al., 2018). The tumor microenvironment (TME) is composed of cellular components and non-cellular extracellular matrix. Cellular components include stromal fibroblasts, infiltrating immune cells, blood and lymphatic networks. TME is usually characterized by nutritional competition, low PH, hypoxia, and metabolite accumulation. This environment results in immunosuppression or a tolerant phenotype of immune cells and promotes metabolism that relies more on oxidative phosphorylation and fatty acid oxidation to meet energy requirements (Bader et al., 2020). The role of metabolic reprogramming in the activation and differentiation of immune cells has also attracted increasing attention (Biswas, 2015). As an important part of tumor environment, immune cell infiltration has been extensively studied for its role and prognostic value in various malignant tumors. With the development of immunotherapy, potential targets have been gradually discovered. But only a small percentage of patients with specific cancer types respond well to current immunotherapies. Therefore, it is necessary to explore the characteristics of various immune cells and their relationship with tumor interaction.

In this study, we analyzed the expression pattern and prognostic value of ACSL4 in various cancers using data from multiple public databases and discovered the impact of genetic changes of ACSL4 on prognosis. In addition, the potential relationship between ACSL4 expression and immune infiltration level was discussed. The results suggest that ACSL4 can affect the prognosis of cancer patients through its interaction with invasive immune cells.

MATERIALS AND METHODS

Differential Gene Expression Analysis of ACSL4

We used Oncomine (www.oncomine.org), The TIMER (Tumor Immune Estimation Resource, https://cistrome.shinyapps.io/timer/) and GEPIA (Gene Expression Profiling Interactive Analysis, http://gepia.cancer-pku.cn/) to analyze ACSL4 expression in pan-cancer (Rhodes et al., 2004; Li et al., 2017; Tang et al., 2017). Specifically, the Oncomine Gene Expression Array Dataset is an online oncogene microarray database and data mining platform containing 65 gene expression datasets, including nearly 48 million gene expression measurements from more than 4,700 microarray experiments.Thresholds was determined based on the following values: $p = 0.001$, folding change 1.5, and gene ranking of all. TIMER is a visual and interactive site for comprehensive research on tumor immune interactions. It precalculated the levels of six tumor osmotic immune subsets for 10,897 tumors from 32 cancer types to explore associations between immune osmosis and various factors, including gene expression, clinical outcomes, somatic mutations, and somatic copy number changes. GEPIA is an interactive web-based application for gene expression analysis of 9736 tumors and 8587 normal samples based on TCGA and GTEx databases. It can carry out differential expression analysis, Survival analysis, Correlation analysis and similar gene detection analysis. The method for differential analysis is one-way ANOVA, $|\log2FC| = 1$ and $p = 0.01$ is used as the cut-off

standard. The Cancer Cell Line Encyclopedia (CCLE) (https://sites.broadinstitute.org/ccle/) is an effort to generate large-scale profiling data sets across nearly 1,000 cell lines from diverse tissue lineages. (Nusinow et al., 2020). DepMap Portal can be used for CCLE Data Visualization and Analysis. ACSL4 expression in cancer cell lines was validated by DepMap Portal.

The types of cancer acronyms analyzed in this study are as follows: ACC (adrenocortical carcinoma); BLCA (bladder urothelial carcinoma); BRCA (breast invasive carcinoma); CESC (cervical squamous cell carcinoma); CHOL (cholangiocarcinoma); COAD (colon adenocarcinoma); DLBC (lymphoid neoplasm diffuse large B cell lymphoma); ESCA (esophageal carcinoma); GBM (glioblastoma multiforme); HNSC (head and neck squamous cell carcinoma); KICH (kidney chromophobe); KIRC (kidney renal clear cell carcinoma); KIRP (kidney renal papillary cell carcinoma); LAML (lacute myeloid leukemia); LGG (brain lower grade glioma); LIHC (liver hepatocellular carcinoma); LUAD (lung adenocarcinoma); LUSC (lung squamous cell carcinoma); MESO (mesothelioma); OV (ovarian serous cystadenocarcinoma); PAAD (pancreatic adenocarcinoma); PCPG (pheochromocytoma and paraganglioma); PRAD (prostate adenocarcinoma); READ (rectum adenocarcinoma); SARC (sarcoma); SKCM (skin cutaneous melanoma); STAD (stomach adenocarcinoma); TGCT (testicular germ cell tumors); THCA (thyroid carcinoma); THYM (thymoma); UCEC (uterine corpus endometrial carcinoma); UCS (uterine carcinosarcoma); and UVM (uveal melanoma).

Differentially Expressed at ACSL4 Protein Level

UALCAN (http://ualcan.path.uab.edu/analysis-prot.html) is used to analyze the cancer Omics data interactive Web resources (Chandrashekar et al., 2017). It analyzed protein expression using TCGA level 3 RNA-SEQ and clinical data from 31 cancer types. In this study, protein expression of ACSL4 between different cancer tissues and normal tissues was analyzed according to CPTAC workflow. $p < 0.05$ was considered to be significant. The HPA (Human Protein Atlas, www.proteinatlas.org) is a valuable tool for studying protein localization and expression in human tissues and cells, combining antibody-based approaches with transcriptional data. It has more than 10 million images showing patterns of protein expression at the single-cell level (Thul and Lindskog, 2018). In this study, immunohistochemical images of ACSL4 protein expression between normal and cancer tissues were observed by HPA.

Analysis of ACSL4 Gene Variation

We used the cBio Cancer Genomics Portal (http://cbioportal.org) and GSCA (http://bioinfo.life.hust.edu.cn/GSCA/#/) to analyze variations in ACSL4 in different cancers, including mutations and copy number abnormalities (Cerami et al., 2012; Liu et al., 2018). UALCAN and MethSurv were used to analyze ACSL4 methylation and its correlation with survival prognosis in different cancers (Modhukur et al., 2018). Specifically, cBioPortal is an open platform for cancer genomics, providing data from more than 5,000 tumor samples from 20 cancer studies. The portal also includes copy number changes, changes in mRNA expression based on microarray and RNA sequencing, DNA methylation values, and protein and phosphoprotein levels. GSCA is provide a series of services to perform gene set genomic (Expression, SNV, CNV and methylation) and immunogenomic (24 immune cells) analyses. MethSurv is a survival analysis network tool based on CpG methylation pattern. It includes 7358 methylomes from 25 different human Bombs. Survival analysis of patient methylation levels at any CpG site (probe) was performed using the Cox proportional hazard model. Hazard ratio (HR) with 95% CI is derived from Cox fitting.

Survival Prognosis Analysis of ACSL4

We use PrognoScan (http://www.abren.net/PrognoScan/), Kaplan-Meier (https://kmplot.com/analysis/) to analyzed the correlation between ACSL4 expression and survival was found in different carcinoma (Mizuno et al., 2009; Yuan et al., 2019). PrognoScan is a clinically annotated and extensive publicly available cancer microarray dataset for assessing the biological relationship between gene expression and prognosis. A univariate Cox $p < 0.05$ was defined as statistically significant. Kaplan-Meier is a powerful online tool that can be used to assess the effect of 54,000 genes on survival in 21 cancer types. We analyzed the relationship of ACSL4 expression with overall survival (OS) and relapse-free survival (RFS) in different cancer, Hazard ratios (HR) with 95% confidence intervals (CI) and log-rank P-values were calculated.

Analysis of ACSL4 Expression and Immune Cell Infiltration Level

We used TIMER database to analyze the correlation between ACSL4 expression and the level of immune cell infiltration, including $CD4^+$ T cells, $CD8^+$ T cells, macrophages, neutrophils, monocytes, NK, DC, cancer-associated fibroblast (CAF) and Myeloid derived suppressor cell (MDSC). We used GSCA to analyze the correlation between single nucleotide variation (SNV), CNV levels in ACSL4 and immune cell infiltration levels in different cancers. Meanwhile, TIMER and GEPIA were used to analyze the correlation between ACSL4 and immune cell markers. Correlation analysis was determined by Spearman. $p < 0.05$ was considered statistically significant.

ACSL4 Related Drugs Discovery in CMap

The Connectivity Map (https://clue.io/cmap), or CMap, is an open database that can be used to identify connections among small molecules which sharing a mechanism of chemicals, physiological processes and action, and then predict potential drugs in silicon (Wang C. Y. et al., 2020). The Touchstone module can be used to explore connectivities between signatures from ~3,000 drugs and genetic loss/gain of function of ~2,000 genes. Sets of compound perturbagens with enrichment scores above 90 (similar) and below -90 (opposing). We used CMap analysis tools to identify the association between ACSL4 and drugs.

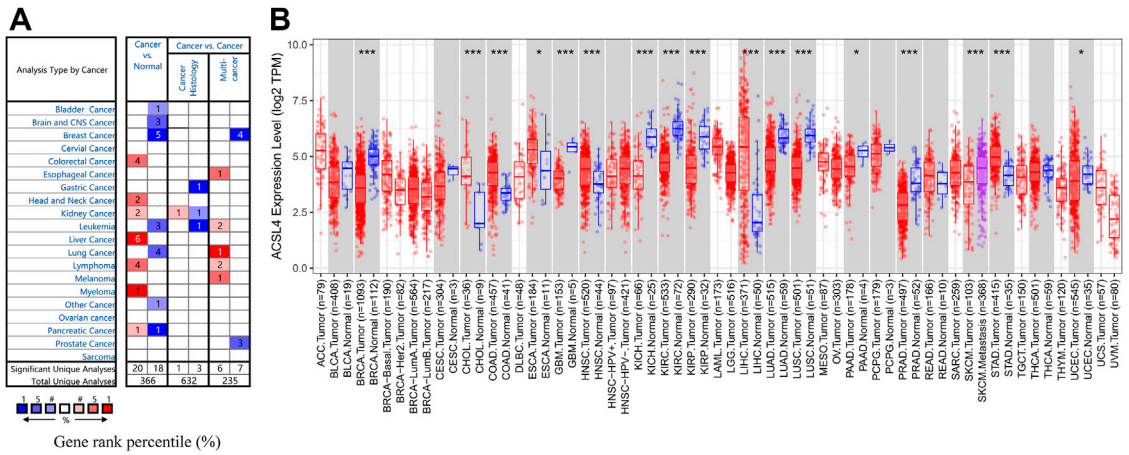

FIGURE 1 | mRNA Expression Levels of ACSL4 in different Cancers. **(A)**. High or low expression of ACSL4 in different human cancer tissues compared with normal tissues in Oncomine database. The number in each cell present the amount of datasets. **(B)**. ACSL4 expression level in different cancers or specific cancer subtypes with corresponding normal tissues from the TCGA database in TIMER (*$p < 0.05$, **$p < 0.01$, ***$p < 0.001$).

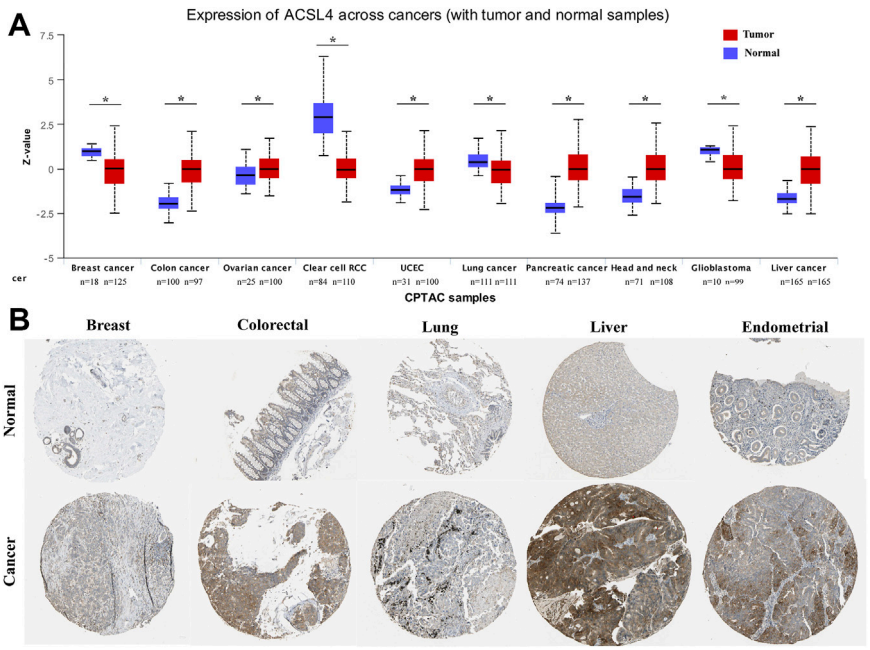

FIGURE 2 | Protein expression levels of ACSL4 in different Cancers. **(A)**. The protein expression of ACSL4 in six cancers and normal tissues from the UALCAN database (*$p < 0.05$). Z-values represent standard deviations from the median across samples for the given cancer type. Log2 Spectral count ratio values from CPTAC were first normalized within each sample profile, then normalized across samples. UCEC (uterine corpus endometrial carcinoma). **(B)**. the protein expression of ACSL4 in tumors and normal tissues were obtained from the Human Protein Atlas.

RESULTS

Differential Expression Analysis ACSL4 Between Tumor and Normal Samples

To evaluate ACSL4 mRNA expression patterns in different cancers, we analyzed ACSL4 expression between normal tissues and tumors using Oncomine database (**Figure 1A**). The results showed that compared with normal tissues, ACSL4 expression was higher in colorectal cancer, head and neck cancer, kidney cancer, liver cancer, lymphoma, myeloma, and pancreatic cancer, but decreased in bladder cancer, brain and CNS cancer, breast cancer, leukemia, lung cancer, and pancreatic cancer. Notably, in the pancreatic cancer data set, one went up and the other went down. Further using the TIMER database to verify the differences between ACSL4 in different tumors and normal tissues (**Figure 1B**). The results showed that ACSL4 was

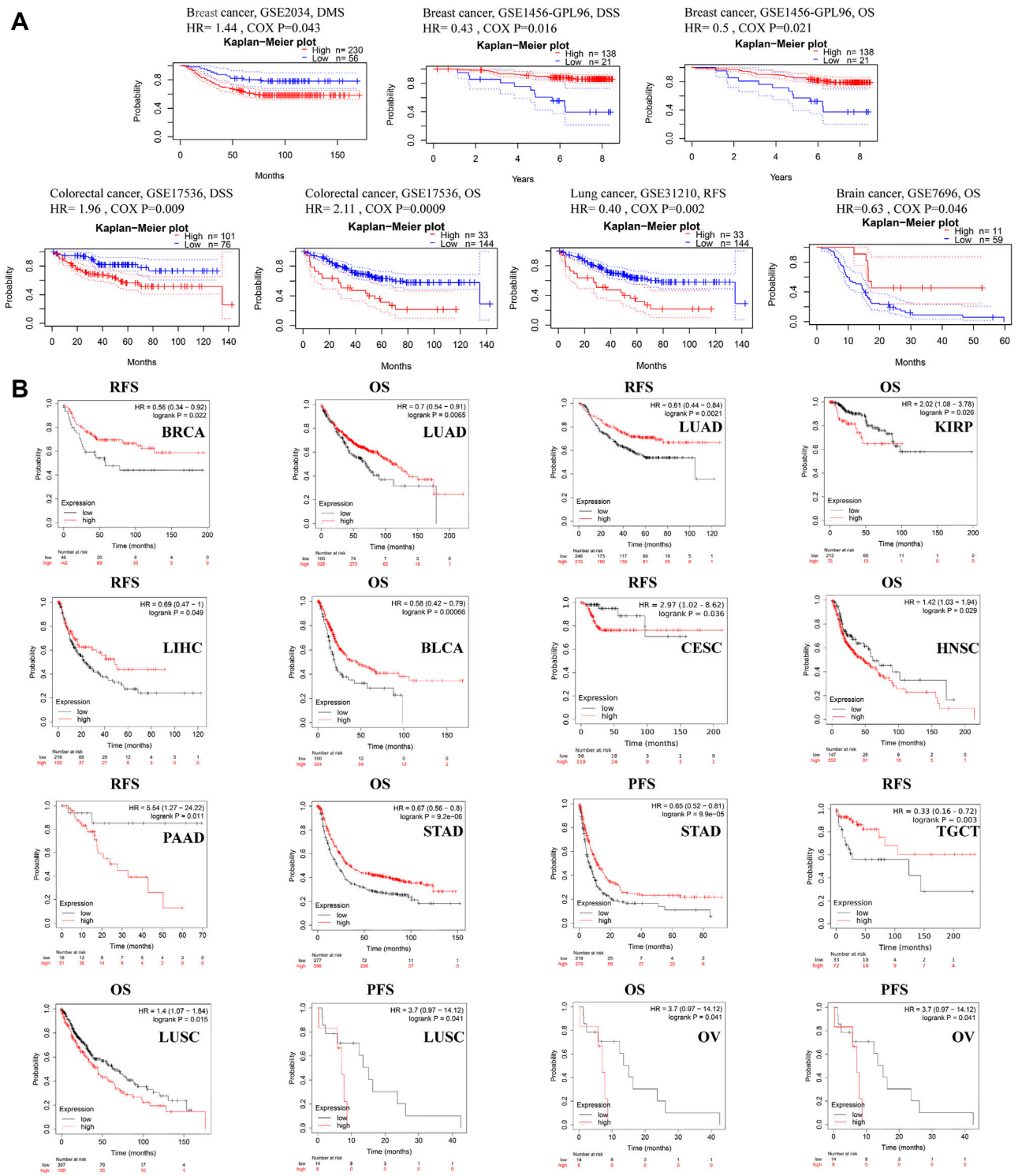

FIGURE 3 | Survival data evaluating the prognostic value of ACSL4. **(A)**. Correlation between ACSL4 and prognosis of various types of cancer in the PrognoScan. DMFS (*n* = 286) in breast cancer cohort GSE 2034. DSS (n = 159) in breast cancer cohort GSE1456-GPL96. OS (*n* = 159) in breast cancer cohort GSE1456-GPL96. DSS (*n* = 177) in colorectal cancer cohort GSE17536. OS (*n* = 177) in colorectal cancer cohort GSE17536. RFS (*n* = 204) in lung cancer (Adenocarcinoma) cohort GSE31210. OS (*n* = 70) in brain cancer (Glioblastoma) cohort GSE7696. DMFS, distant metastasis-free survival; OS, overall survival; DSS, disease-specific survival;

(*Continued*)

FIGURE 3 | RFS, relapse-free survival. **(B)**. Correlation between ACSL4 and prognosis of various types of cancer in the Kaplan-Meier plotter database. RFS of BRCA (breast invasive carcinoma), OS and RFS of LUAD (lung adenocarcinoma); OS of KIRP (kidney renal papillary cell carcinoma); RSF of LIHC (liver hepatocellular carcinoma); OS of BLAC (bladder urothelial carcinoma); RFS of CESC (cervical squamous cell carcinoma); OS of HNSC (head and neck squamous cell carcinoma); RFS of PAAD (pancreatic adenocarcinoma); OS and PFS of STAD (stomach adenocarcinoma); RFS of TGCT (testicular germ cell tumors); OS and PFS of LUSC (lung squamous cell carcinoma); OS and PFS of OV (ovarian serous cystadenocarcinoma). Red curve represents patients with high expression of ACSL4. OS, overall survival; PFS, Progression-free survival; RFS, recurrence-free survival.

significantly increased in CHOL, COAD, ESCA, LIHC, STAD and HNSC ($p < 0.05$). In addition, ACSL4 was Significantly decreased in BRCA Breast invasive carcinoma, KICH, KIRP, GBM, PAAD, SKCM, KIRC, PRAD and UCEC ($p < 0.05$). We also performed analysis using GEPIA and obtained consistent results (**Supplementary Figure S1**). By assembling the Cancer Cell Line Encyclopedia (CCLE), we further analyzed the expression of ACSL4 in cancer cell lines. The results showed that ACSL4 was highly dependent on leukemia, bladder cancer, lymphoma and lung cancer cell lines. The expression of ACSL was low in breast Cancer and prostate cancer cell lines, but high in liver cancer, thyroid cancer and skin cancer cell lines, which was consistent with the previous results (**Supplementary Table S1**).

In order to determine the protein expression of ACSL4 in various cancers, the UALCAN database was used to analyze the ACSL4 protein expression. The results showed that compared with normal tissues, ACSL4 expression was higher in COAD, OV and UCEC tissues ($p < 0.05$), but lower in BRAC and KIRC tissues ($p < 0.05$, **Figure 2A**). This was consistent with ACSL4 mRNA expression in TIMER and GEPIA databases. Meanwhile, compared with normal tissues, ACSL4 was strongly positive in endometrial cancer and liver cancer, and low in breast, lung, and renal cell carcinoma tissues in the human protein atlas (**Figure 2B**).

Prognostic Analysis of ACSL4 in Patients with Different Cancers

The relationship between ACSL4 expression and prognosis in patients with various cancers was analyzed using the PrognoScan database (**Figure 3A**). We found that ACSL4 was associated with prognosis of four cancer types. The patients with high expression of ACSL4 have poor prognosis in colorectal cancer (OS: total number, 177; 95% CI, 1.36–3.28, HR, 2.11; Cox *P*, 0.000896,433; DSS: total number, 177; 95% CI, 1.19–3.25, HR, 1.96; Cox *P*, 0.00877,945). While low expression of ACSL4 has poor prognosis in lung cancer (RFS: total number, 204; 95% CI, 0.22–0.71, HR, 0.40; Cox *P*, 0.008784533), brain cancer (OS: total number, 70; 95% CI, 0.41–0.99, HR, 0.63.11; Cox *P*, 0.0457,155) and breast cancer (DSS: total number, 159; 95% CI, 0.22–0.85, HR, 0.43; Cox *P*, 0.0158,694; OS: total number, 159; 95% CI, 0.28–0.90, HR, 0.50; Cox *P*, 0.0205,638). However, another data set of breast cancer showed high expression of ACSL4 and poor prognosis (DMFS: total number, 286; 95% CI, 1.01–2.05, HR, 1.44; Cox *P*, 0.0432,055). The same analysis was performed on the Kaplan-Meier mapping database and ACSL4 expression was associated with prognosis for 14 cancer types (**Figure 3B**). Brain cancer was not analyzed in kaplan-Meie database. Compared with PrognoScan database, low ACSL4 expression was associated with poorer prognosis in LUAD (OS: HR = 0.7; 95% CI, 0.54–0.91; Cox p = 0.0065; RFS: HR = 0.61; 95% CI, 0.44–0.84; logrank p = 0.0021), BRCA (RFS: HR = 0.56; 95% CI, 0.34–0.92; logrank p = 0.022). There was no significant association in rectal adenocarcinoma (OS: HR = 1.91; 95% CI, 0.8–0.455; logrank p = 0.14; RFS: HR = 3.4; 95% CI, 0.39–29.73; logrank p = 0.24). In addition, high ACSL4 expression in KIRP and LIHC has a poor prognosis. Low ACSL4 expression was associated with poor prognosis in six other cancers, including BLCA, CESC, HNSC, PAAD, STAD and TGCT. The prognostic analysis of ACSL4 in OV (OS: HR = 1.16; 95% CI, 1.01–1.33; logrank p = 0.03; RFS: HR = 0.83; 95% CI,0.7–0.98; logrank p = 0.031) and LUSC (OS: HR = 1.4; 95% CI, 1.07–1.84; logrank p = 0.015; RFS: HR = 3.7; 95% CI, 0.97–14.12; logrank p = 0.041) showed opposite trends. Further use of the GEPIA database to assess the correlation between ACSL4 expression and patient outcome was consistent with the PrognoScan and Kaplan-Meier results. Patients with high ACSL4 expression in CHOL, LIHC and LUAD had poor prognosis; patients with low ACSL4 expression in KIRC, ACC, LGG, PCPG and SKCM had poor prognosis (**Supplementary Figure S2**). In summary, the combined analysis of the three databases shows that ACSL4 has prognostic value in certain cancers, which may be beneficial or harmful. In general, low ACSL4 expression has shown a beneficial role in pan-cancer.

Genetic Alterations of ACSL4 in Different Cancers

Using the cBioPortal database, we explored the genetic changes of ACSL4 in various cancers and their correlation with patients' OS and PFS in TCGA-Pan cancer panel. In 10,953 patients with ACSL4 mutation information from the TCGA dataset, the percentage of ACSL4 mutation was 1.6% (**Figure 4A**). The most common mutations are point mutations, which are mainly found in endometrial cancer, melanoma, cervical squamore cell carcinoma, pleural mesothelioma and Glioblastoma. All cases of Melanoma have point mutations. "Amplification" exists in all cases of Renal clear cell carcinoma, Hepatocellular carcinoma and well-differentiated thyroid cancer. The types and mutation sites of ACSL4 gene are shown in the figure (**Figure 4B**). Among mutations, missense mutation has the highest frequency. Critical to changes in ACSL4 function are mutations in AMP-biding containing the active site of ACSL4. The most common site was X60-splice/R60C, which was found in 3 cases of endometrial carcinoma and 1 case of cutaneous melanoma. We explored the potential relationship between genetic changes in ACSL4 and clinical outcomes in patients with different types of cancer. The results showed that the OS (p = 0.034), DFS (p = 0.0278) and PFS (p = 0.005) of

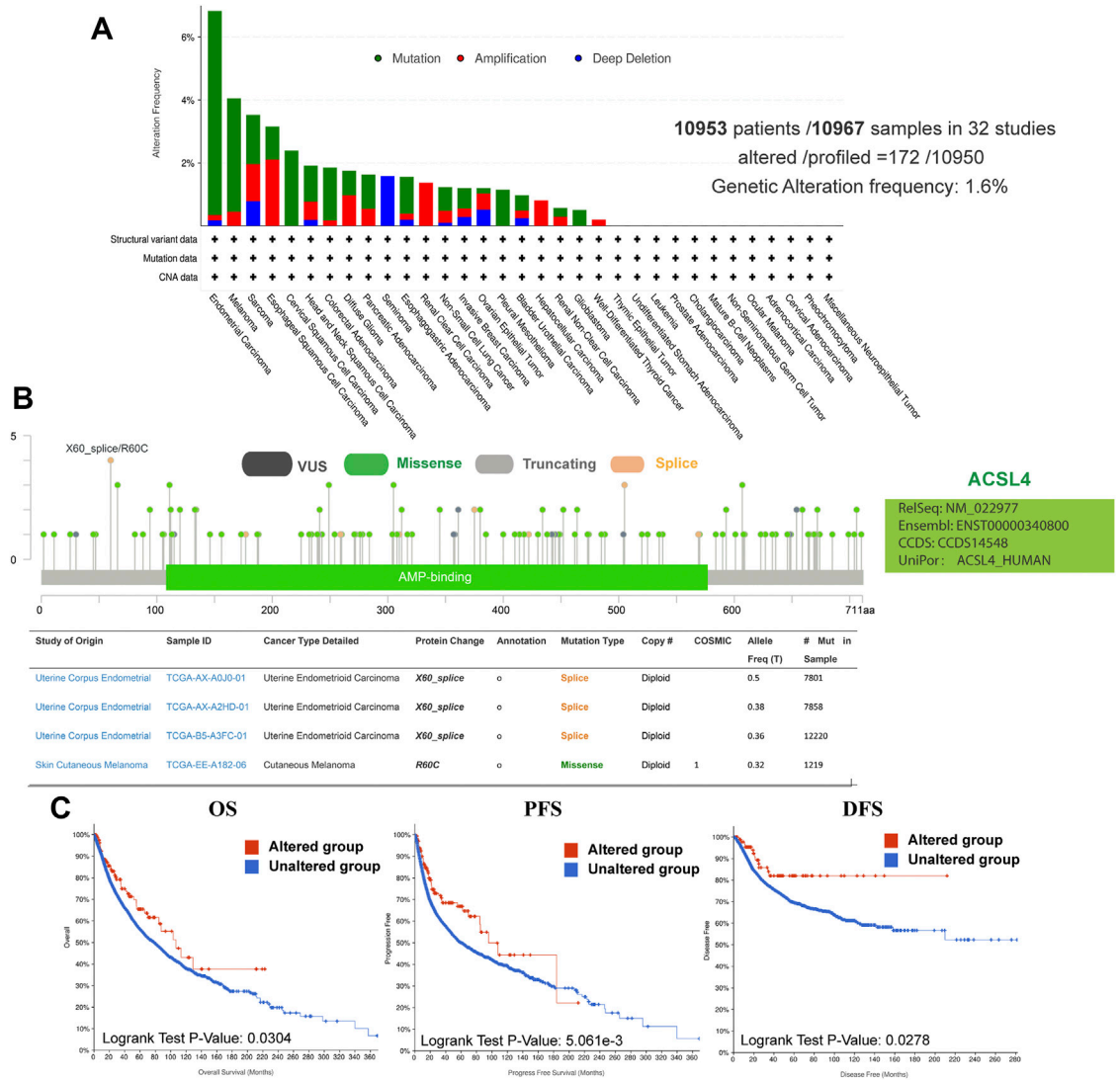

FIGURE 4 | Genetic alterations of ACSL4 in different cancers from the cBioPortal database. **(A)**. Genetic aberration of ACSL4 in tumors using cBioPortal-TCGA pan-cancer panel. This data includes 10953 patients/10967 samples in 32 studies. The global genetic alteration frequency is 1.6%. **(B)**. The types and mutation sites of ACSL4 gene. **(C)**. Correlation between ACSL4 altered and prognosis of various types of cancer. OS of pan-cancer in 32 studies (n = 10803); PFS of pan-cancer (n = 10613) in 32 studies; DFS of pan-cancer (n = 5383) in 32 studies. OS, overall survival; PFS, Progression-free survival; DFS, Disease-free survival.

patients with ACSL4 mutation were significantly higher than those without ACSL4 mutation (**Figure 4C**). In short, genetic alterations in ACSL4 can significantly affect patient outcomes. Analysis of CCLE database showed that "copy number amplification" occurred frequently in cervical cancer, fibroblast, ovarian cancer, breast cancer and endometrial/uterine cancer. The most frequently mutated entity is lymphoma, followed by Leukemia. In addition, endometrial/uterine cancer and lung cancer mutation frequency is high, which is consistent with cBioPortal results (**Supplementary Table S1**).

Meanwhile, GSCA database was used to analyze the SNV of ACSL4, and SNV was found in 19 kinds of cancer (**Figure 5A**). Consistent with cBioPortal, mutations were most common in UCEC and SKCM. Moreover, patients with ACSL4 mutations had a shorter overall survival time than those with wild-type in SKCM (HR, 2.76, Cox p = 0.01), while had a longer PFS than those with wild-type in UCEC (HR, 0.29, Cox p = 0.01) (**Figure 5B**). CNA is a common genetic alteration associated with the occurrence and progression of cancer by regulating the expression of tumor-related genes (Davoli et al., 2017). We analyzed the CNV of ACSL4 and the correlation between CNV and mRNA expression through GSCA database (**Figure 5C**). The results showed that ACSL4 CNV was positively correlated with mRNA expression in 10 cancers, including BLCA, BRCA, ESCA, HNSC, LUAD, LUSC, PAAD, PRAD, SARC and STAD. Only in KIRP, ACSL4 CNV was negatively correlated with mRNA expression. Similarly, we

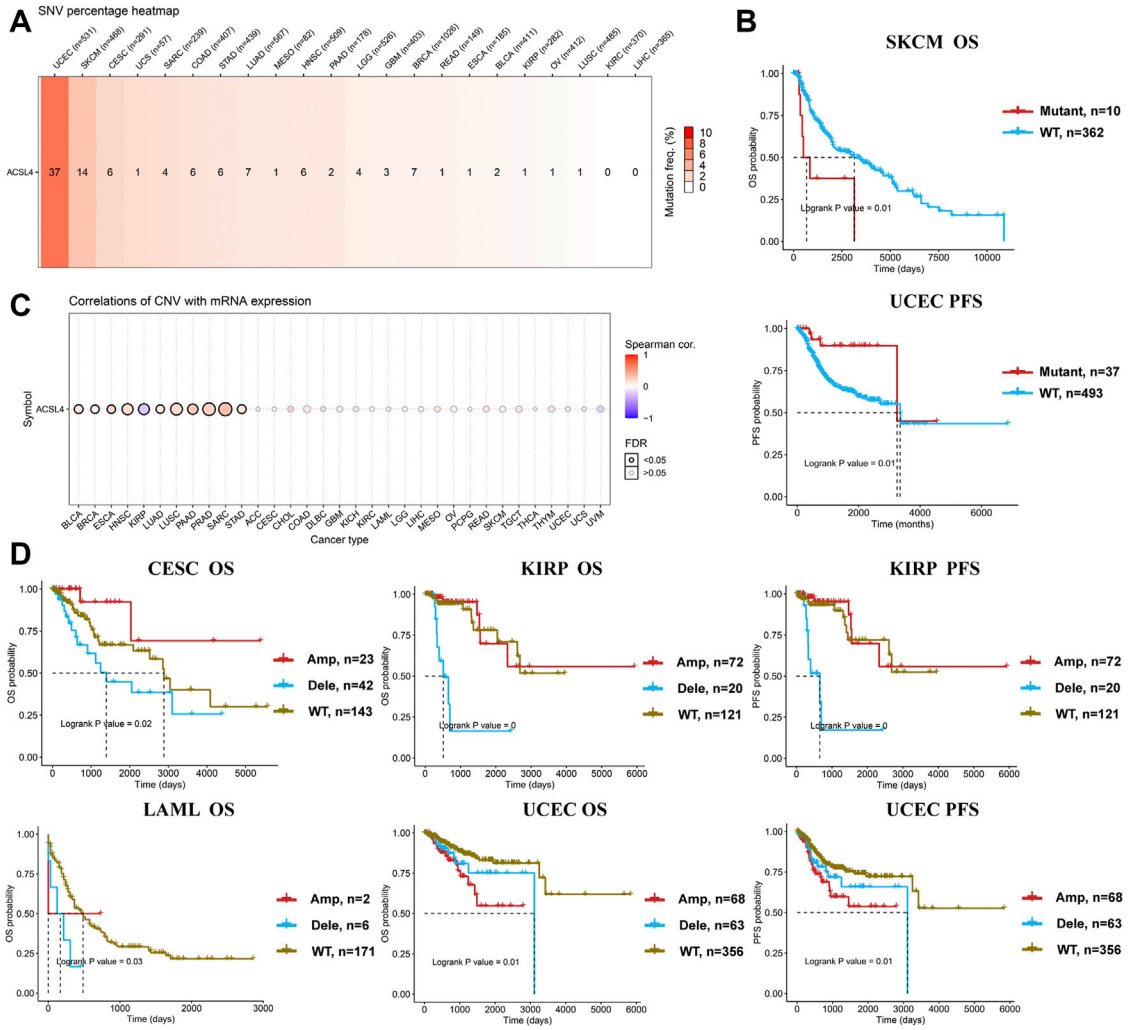

FIGURE 5 | Genetic alterations of ACSL4 in different cancers from the GSCA database. **(A)**. SNV percentage heatmap of ACSL4 in different cancers. **(B)**. Correlation between ACSL4 mutant and prognosis in SKCM and UCEC. OS of SKCM (skin cutaneous melanoma); PFS of UCEC ((uterine corpus endometrial carcinoma). OS, overall survival; PFS, Progression-free survival. **(C)**. Correlation of CNV with mRNA expression in different cancers. **(D)**. Correlation between ACSL4 CNV and prognosis in different cancers. OS of CESC (cervical squamous cell carcinoma); OS and PFS of KIRP (kidney renal papillary cell carcinoma); OS of LAML (lacute myeloid leukemia); OS and PFS of UCEC (uterine corpus endometrial carcinoma). OS, overall survival; PFS, Progression-free survival.

assessed the effect of ACSL4 CNV on prognosis in patients with various cancers. In CSEC, KIRP, and LAML, patients with copy number deletion had a worse prognosis, while patients with copy number amplification had a worse prognosis in UCEC (**Figure 5D**).

DNA methylation regulates gene expression and closure and is closely related to human development and tumorigenesis. Subsequently, ACSL4 methylation in different cancers was analyzed using the UALCAN database (**Figure 6A**). The results showed that ACSL4 was hypomethylated in BLCA, BRCA, LIHC, STAD and TCGT. We found that lowly ACSL4 express tumors presented with decreased DNA methylation level of ACSL4, including BLCA and BRCA. In addition, DNA methylation of ACSL4 had higher levels in PRAD and UCEC. Similar results were obtained in GSCA database. ACSL4 was hypomethylated in LIHC and THCA, while it was hypermethylated in PRAD (**Supplementary Figure S3A**). Contrary to the UALCAN database results, ACSL4 was hypomethylated in UCEC. We further analyzed the correlation between ACSL4 methylation level and mRNA expression. The results showed that ACSL4 methylation was inversely correlated with mRNA in most cancers, including BRCA, CESC, COAD, ESCA, GBM, HNSC, KIRP, KIRC, LAML, LIHC, PCPG, PRAD, PEAD, SARC, SKCM, STAD, TGCT, THCA and UCEC. In BRCA, LIHC, LUSC, and ESCA (**Supplementary Figure S3B**). ACSL4 methylation levels were associated with poor prognosis (**Figure 6B**). The DNA methylation level of ACSL4 and the prognostic value of each single CpG were analyzed by MethSurv database (**Supplementary Figure S3C**). Compared with patients with ACSL4 hypermethylation, Hypomethylation was associated with poorer prognosis in 11 cancers, including BRCA, CESC, COAD, ESCA, GBM, KIRP, LGG, LIHC, STAD, SKCM and

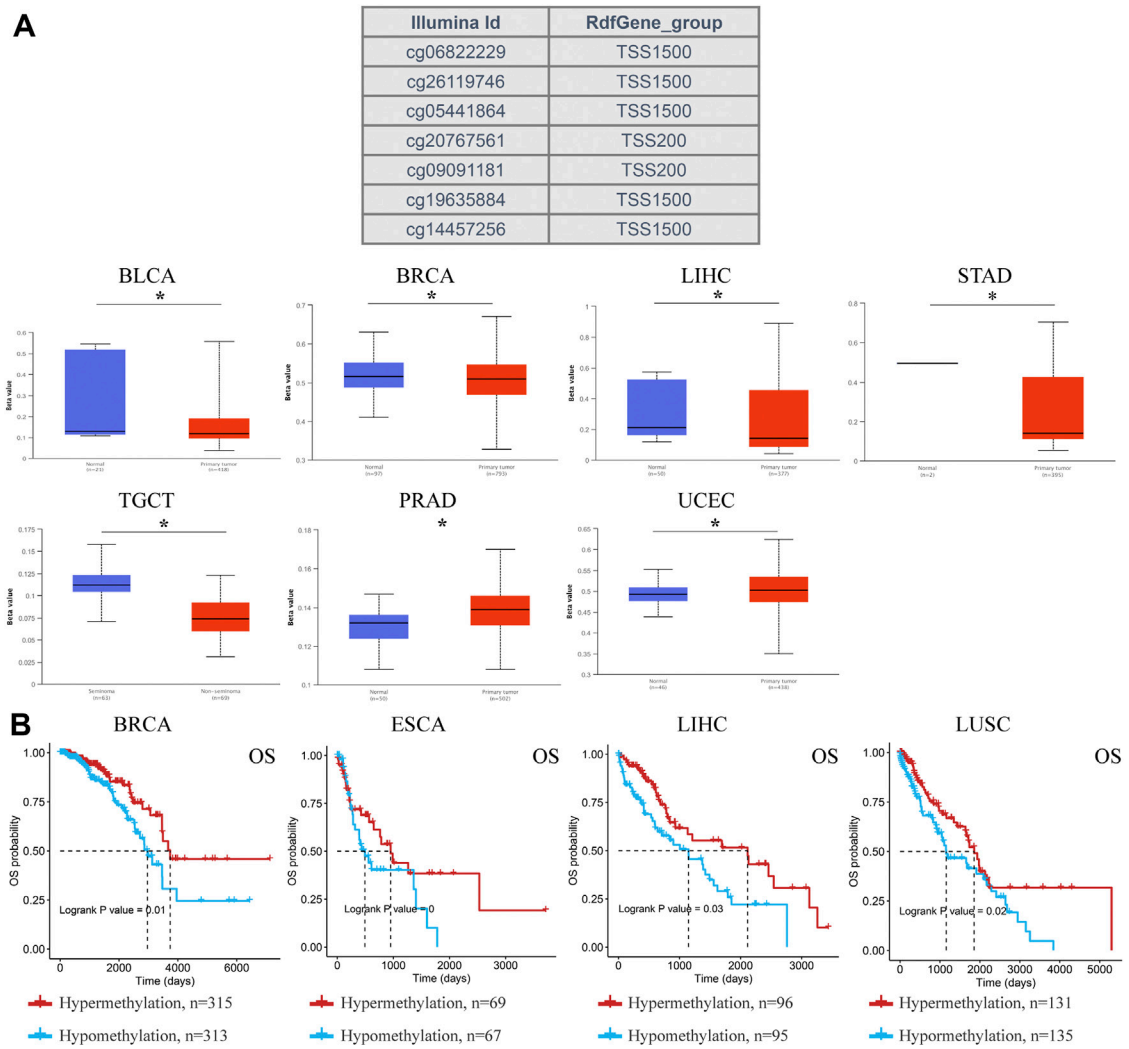

FIGURE 6 | DNA methylation aberration of ACSL4 in different cancers from the UACLAN and GSCA database. **(A)**. Probes for detecting DNA methylation of ACSL4 promoter and ACSL4 promoter methylation profile in different cancers. ACSL4 hypomethylated in BLCA, BRCA, LIHC, STAD and TCGT, while higher methylation levels in PRAD and UCEC from UACLAN database (*$p < 0.05$). The Beta value indicates level of DNA methylation ranging from 0 (unmethylated) to 1 (fully methylated). Different beta value cut-off has been considered to indicate hyper-methylation (Beta value: 0.7–0.5) or hypo-methylation (Beta-value: 0.3–0.25). BLCA (bladder urothelial carcinoma); BRCA (breast invasive carcinoma); LIHC (liver hepatocellular carcinoma); STAD (stomach adenocarcinoma); TGCT (testicular germ cell tumors); PRAD (prostate adenocarcinoma); UCEC (uterine corpus endometrial carcinoma). **(B)**. Correlation between ACSL4 DNA hypomethylation and prognosis in different cancers from GSCA database. OS of BRCA (breast invasive carcinoma), ESCA (esophageal carcinoma), LIHC (liver hepatocellular carcinoma) and LUSC (lung squamous cell carcinoma). OS, overall survival.

UCEC. Which is located in the CPG island site prognosis is poorer, including cg0544164, cg06822229, cg10721440 (**Supplementary Figure S4**). Patients with ACSL4 hypermethylation had poorer prognosis and survival in other cancers: ACC, HNSC, KIRC, LUSC, PAAD and UCS.

Analysis of Immune Infiltration of ACSL4 in Different Cancers

Studies have shown that tumor-infiltrating lymphocytes are associated with cancer survival. The correlation between ACSL4 expression and TIL level was analyzed by TISIDB database. The heat map showed that ACSL4 was positively correlated with most immune cells (**Supplementary Figure S5**). We also evaluated the association between ACSL4 expression and tumor-infiltrating immune cells in the TIMER database (**Figure 7A**). The results showed that ACSL4 expression was significantly associated with NK, B cells, macrophages, DC, $CD4^+$ T cells, $CD8^+$ T cells, monocytes and neutrophil infiltration in 13, 16, 19, 24, 25, 26, 28 and 31 cancer types. ACSL4 was positively correlated with neutrophils, $CD4^+$ T cells and monocyte infiltration. There was no correlation between ACSL4 expression and immune cell infiltration in UCS. In addition, we also found that the cancer with high ACSL4

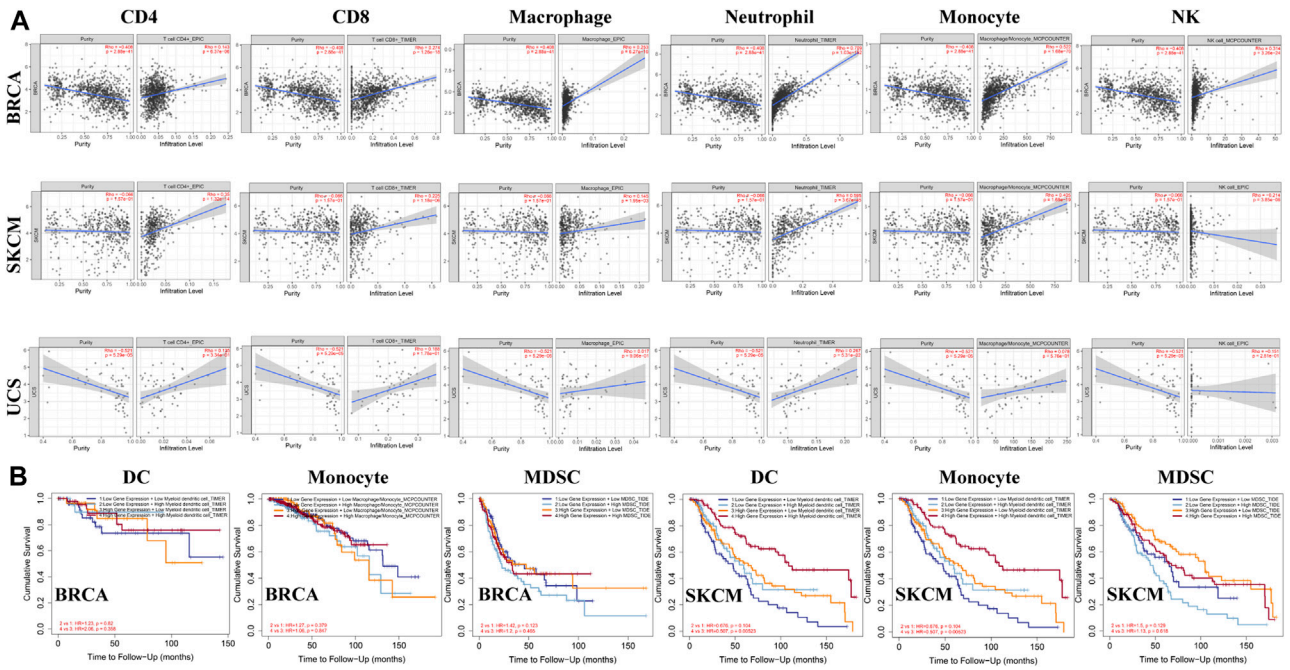

FIGURE 7 | Analysis of immune infiltration of ACSL4 in different cancers from the TIMER database. **(A)**. ACSL4 expression has significantly negatively correlated with tumor purity and significantly positively correlated with the infiltration levels of CD4+T cell, CD8+T cell, macrophage, neutrophil, monocyte and NK in BRCA (breast invasive carcinoma). ACSL4 expression has no relation with tumor purity and significantly negatively correlated with NK, and significantly positively correlated with the infiltration levels of CD4+T cell, CD8+T cell, macrophage, neutrophil, monocyte and in SKCM (skin cutaneous melanoma). ACSL4 expression has significantly negatively correlated with tumor purity and NK, and no relation with infiltrating levels of CD4+T cell, CD8+T cell, macrophage, neutrophil, monocyte in UCS (uterine carcinosarcoma). $p < 0.05$ is considered as significant. **(B)**. Correlation between ACSL4 mRNA expression, with infiltrating levels of DC, monocyte, MDSC (Myeloid derived suppressor cell) and prognosis in BRCA (breast invasive carcinoma) and SKCM (skin cutaneous melanoma).

expression was positively correlated with the infiltration level of MDSC, including COAD, LIHC and STAD, whereas the cancer with low ACSL4 expression was negatively correlated with the infiltration level of MDSC, including BRCA, KIRC, LUSC, GBM and SKCM.

We further analyzed the effects of ACSL4 and immune cell infiltration levels on survival outcomes. The results showed that MDSC infiltration level was correlated with the prognosis of 16 types of Cancer patients, while neutrophils, cancer-associated fibroblast (CAF) and DC were correlated with the prognosis of 10, nine and nine types of Cancer patients, respectively. And in BRCA and SKCM, ACSL4 and the level of immune cell infiltration are closely related to survival prognosis (**Figure 7B**). These results indicate that ACSL4 plays an important role in regulating the immune cells infiltration in BRCA and SKCM, especially monocytes, DC and MDSC.

In addition, we analyzed the effect of ACSL4 mutation on immune cell levels in various cancers by Mutation module. The results showed that ACSL4 mutation caused significant changes in the levels of various immune cells, especially in UCEC and SARC. Compared with ACSL4 wild type, ACSL4 mutation caused significant changes in $CD4^+$ T cells, DC, macrophages and CAF, and showed opposite trends in both types of cancer (**Supplementary Figure S6A**). Similarly, the SCAN module was used to analyze the influence of ACSL4 on the level of immune cell invasion in High Amplification or Deep Deletion. The results showed that abnormality of ACSL4 at different copy numbers mainly caused changes in CAF levels, including HNSC, LGG, OV and BRCA (**Supplementary Figure S6B**). In addition, it can also cause changes in neutrophils, $CD8^+$ T cells, DC, NK and Tfh infiltration levels.

Analysis of Immunoinfiltrating Cell Markers of ACSL4 in Various Cancers

Next, we analyzed the correlation between ACSL4 and immunoinfiltrating cell markers through TIMER and GEPIA databases respectively. We selected cancer types, mainly BRCA and SKCM, that express poor prognosis in cancers and are related to the level of immune cell infiltration and affect prognosis. UCS as a control. Immune cells include B cells, T cells (general), $CD8^+$ T cells, Tfh, Treg, Exhaust T cells, TAM, M1 and M2 macrophages, monocytes, NK, neutrophils, DC, CAF and MDSC. After adjusting for tumor purity, ACSL4 expression was strongly associated with 57 of 58 BRCA immune cell markers, 41 of SKCM, and 24 of LIHC. In contrast, only three markers in UCS were significantly associated with ACSL4 (**Table 1**). Markers of $CD8^+$ T cells, TAM, M2 macrophages, monocytes, DC, CAF and MDSC were most closely correlated with ACSL4 expression in BRCA and SKCM, while no correlation was found in USC. ACSL4 was significantly correlated with CCL2, CD68, IL10 of TAM, CD113, MS4A4A, VSIG4 of M2

TABLE 1 | Correlations between ACSL4 and gene markers of immune cells in TIMER.

Cell type	Gene markers	BRCA				SKCM				UCS			
		None		Purity		None		Purity		None		Purity	
		Cor	*p*	Cor	*p*	Cor	p	Cor	*p*	Cor	*p*	Cor	*p*
B	CD19	0.275	***	0.096	*	0.122	*	0.093	0.047	0.148	0.271	−0.046	0.746
	CD79A	0.324	***	0.138	***	0.087	0.087	0.05	0.282	−0.03	0.826	−0.179	0.2
T	CD2	0.457	***	0.314	***	0.23	***	0.23	***	0.134	0.322	−0.136	0.331
	CD3D	0.404	***	0.241	***	0.161	**	0.138	*	0.003	0.982	−0.259	0.061
	CD3E	0.436	***	0.278	***	0.131	*	0.097	0.039	−0.081	0.55	−0.274	0.047
$CD8^+$ T cell	CD8A	0.444	***	0.314	***	0.214	***	0.204	***	0.196	0.144	0.029	0.838
	CD8B	0.405	***	0.28	***	0.157	**	0.132	*	0.069	0.612	0.043	0.759
Tfh	BCL6	0.259	***	0.244	***	0.388	***	0.378	***	0.241	0.071	0.136	0.333
	CXCR5	0.331	***	0.155	***	0.12	*	0.091	0.053	−0.051	0.709	−0.264	0.056
	ICOS	0.483	***	0.377	***	0.327	***	0.333	***	0.299	0.024	0.194	0.164
Treg	CCR8	0.5	***	0.444	***	0.358	***	0.445	***	0.35	*	0.191	0.172
	FOXP3	0.443	***	0.34	***	0.082	0.115	0.096	0.041	0.317	0.016	0.193	0.165
	IL2RA	0.583	***	0.507	***	0.231	***	0.435	***	0.438	**	0.299	0.029
	IL7R	0.673	***	0.6	***	0.354	***	0.51	***	0.502	***	0.388	*
Exhaust T	CTLA4	0.432	***	0.313	***	0.336	***	0.276	***	0.083	0.54	−0.065	0.644
	GZMB	0.41	***	0.295	***	−0.05	0.115	0.107	0.023	0.147	0.275	−0.103	0.461
	HAVCR2	0.578	***	0.509	***	0.208	***	0.334	***	0.326	0.013	0.142	0.309
	LAG3	0.246	***	0.155	***	0.118	0.023	0.122	*	−0.154	0.253	−0.391	*
	PDCD1	0.333	***	0.176	***	0.319	***	0.097	0.039	0.034	0.805	−0.244	0.079
TAM	CCL2	0.514	***	0.422	***	0.091	0.079	0.244	***	0.122	0.368	−0.001	0.996
	CD68	0.529	***	0.462	***	0.189	**	0.17	**	0.372	*	0.145	0.3
	IL10	0.543	***	0.459	***	0.167	*	0.387	***	0.158	0.24	−0.006	0.967
M1	IRF5	0.265	***	0.208	***	0.177	**	0.176	**	0.289	0.029	0.259	0.062
	NOS2	0.284	***	0.28	***	-0.058	0.264	-0.08	0.087	−0.178	0.185	0.018	0.901
	PTGS2	0.578	***	0.51	***	0.199	**	0.267	***	0.179	0.183	0.164	0.242
M2	CD163	0.557	***	0.5	***	0.03	0.567	0.433	***	0.329	0.013	0.216	0.12
	MS4A4A	0.572	***	0.492	***	0.091	0.082	0.373	***	0.286	0.031	0.137	0.328
	VSIG4	0.462	***	0.385	***	0.049	0.346	0.311	***	0.302	0.023	0.169	0.226
monocyte	CD86	0.595	***	0.525	***	0.179	**	0.406	***	0.358	*	0.157	0.261
	CSF1R	0.566	***	0.47	***	0.11	0.035	0.338	***	0.306	0.02	0.11	0.431
NK	NCAM1	0.445	***	0.359	***	0.043	0.414	0.153	*	−0.162	0.228	−0.03	0.834
	KIR2DL1	0.266	***	0.186	***	-0.092	0.075	0.041	0.381	−0.023	0.864	−0.008	0.954
	KIR2DL3	0.252	***	0.165	***	-0.018	0.726	0.021	0.658	0.203	0.13	0.073	0.604
	KIR2DL4	0.301	***	0.222	***	-0.062	0.237	0.086	0.068	0.052	0.7	−0.135	0.335
	KIR2DS4	0.237	***	0.237	***	-0.072	0.168	0.034	0.463	−0.006	0.962	−0.006	0.962
	KIR3DL1	0.334	***	0.334	***	-0.101	0.052	0.052	0.258	0.221	0.099	0.221	0.099
	KIR3DL2	0.296	***	0.296	***	0.085	0.101	0.1	0.031	0.105	0.438	0.105	0.438
	KIR3DL3	0.176	***	0.176	***	0.072	0.168	-0.039	0.394	0.138	0.306	0.138	0.306
	KLRD1	0.581	***	0.49	***	-0.051	0.327	0.328	***	0.39	*	0.187	0.179
	KLRK1	0.424	***	0.275	***	0.134	*	0.288	***	0.115	0.392	−0.086	0.541
Neutrophil	CCR7	0.365	***	0.199	***	0.313	***	0.123	*	0.17	0.205	0.009	0.947
	CEACAM8	0.042	0.166	0.075	0.018	0.034	0.514	0.063	0.178	−0.023	0.868	−0.021	0.88
	FUT4	0.654	***	0.586	***	0.308	***	0.42	***	0.217	0.105	0.209	0.133
	ITGAM	0.446	***	0.357	***	0.064	0.221	0.352	***	0.292	0.028	0.15	0.282
	MPO	0.356	***	0.286	***	0.066	0.206	0.056	0.228	−0.097	0.471	−0.04	0.778
DC	ITGAX	0.496	***	0.4	***	0.275	***	0.213	***	0.355	*	0.183	0.191
	CD1C	0.386	***	0.232	***	0.281	***	0.154	**	0.14	0.298	0.062	0.661
	HLA-DPA1	0.504	***	0.387	***	0.127	0.014	0.216	***	0.252	0.059	0.033	0.814
	HLA-DPB1	0.395	***	0.225	***	0.108	0.038	0.2	***	0.265	0.046	0.061	0.666
	HLA-DQB1	0.334	***	0.197	***	0.305	***	0.156	**	0.317	0.016	0.123	0.379
	HLA-DRA	0.534	***	0.425	***	0.118	0.023	0.304	***	0.398	*	0.173	0.215
	NRP1	0.656	***	0.603	***	0.031	0.551	0.485	***	0.45	**	0.302	0.028
CAF	HGF	0.536	***	0.456	***	0.193	**	0.431	***	−0.201	0.133	−0.206	0.14
	PDGFRB	0.478	***	0.39	***	0.35	***	0.122	*	0.01	0.94	−0.03	0.832
	TGFB1	0.343	***	0.206	***	0.289	***	0.191	***	0.378	0.004	0.221	0.112
	THBS1	0.465	***	0.454	***	0.314	***	0.392	***	0.457	**	0.406	*
MDSC	CD14	0.368	***	0.265	***	-0.029	0.581	0.186	***	0.229	0.086	0.088	0.529
	CD33	0.503	***	0.404	***	0.134	*	0.324	***	0.212	0.113	0.092	0.512

BRCA, breast invasive carcinoma; SKCM, skin cutaneous melanoma; UCS, uterine carcinosarcoma.

CAF, cancer-associated fibroblast; DC, dendritic cell; MDSC, myeloid derived suppressor cell; NK, natural killer cell; Tfh, follicular helper T cell; Th, T helper cell; Treg, regulatory T cell; TAM, tumor-associated- macrophage.

None, correlation without adjustment; Purity, correlation adjusted for tumor purity; Cor, R value of Spearman's correlation. *p < *0.01;* **p < *0.001;* ***p < *0.0001.*

TABLE 2 | Correlations between ACSL4 and Gene Markers of CD8$^+$ T cell, TAM, M2, Neutrophil, CAF in GEPIA.

Cell type	Gene markers	BRCA		SKCM		UCS	
		R	*p*	R	*p*	R	*p*
CD8+T cell	CD8A	0.21	***	0.16	***	0.024	0.86
	CD8B	0.15	***	0.13	*	–0.022	0.87
TAM	CCL2	0.48	***	0.14	*	0.012	0.93
	IL10	0.45	***	0.25	***	0.068	0.61
	CD68	0.39	***	0.14	*	0.31	0.02
M2	CD163	0.34	***	0.31	***	0.089	0.51
	VSIG4	0.33	***	0.25	***	0.2	0.13
	MS4A4A	0.43	***	0.32	***	0.7	0.21
Neutrophil	CD86	0.44	***	0.33	***	0.21	0.12
	CSF1R	0.43	***	0.3	***	0.2	0.14
CAF	HGF	0.25	***	0.13	*	0.043	0.75
	PDGFRB	0.25	***	0.16	**	–0.05	0.71
	TGFB1	0.15	***	0.27	***	0.24	0.074
	THBS1	0.28	***	0.21	***	0.18	0.19
CAF	CD14	0.18	***	0.21	***	0.17	0.2
	CD33	0.33	***	0.22	***	0.15	0.26
DC	CD1C	0.22	***	0.025	0.59	0.062	0.65
	HLA-DPB1	0.23	***	0.19	***	0.1	0.45
	HLA-DQB1	0.13	***	0.078	0.095	0.15	0.28
	HLA-DRA	0.33	***	0.25	***	0.16	0.22
	HLA-DPA1	0.33	***	0.19	***	0.098	0.47
	NRP1	0.51	***	0.39	***	0.3	0.022
	ITGAX	0.31	***	0.21	***	0.23	0.082

*BRCA, breast invasive carcinoma; SKCM, skin cutaneous melanoma; UCS, uterine carcinosarcoma. Cor, R value of Spearman's correlation. *p < 0.01; **p < 0.001; ***p < 0.0001.*

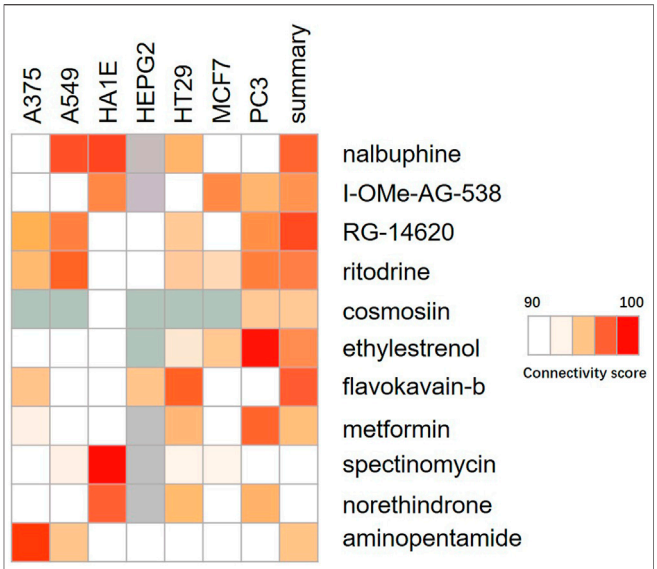

FIGURE 8 | Heat map of compounds interacting with ACSL4. The connectivity score was calculated using kolmogorov-Smirnov two-sided statistics implemented in CMap.

macrophages, and CD86 and CSF1R of monocytes in BCRC and SKCM.

In BRCA and SKCM, DC markers (CD1C, GAX, HLA-DPA1, HLA-DPB1, HLA-DPB2, HLA-DRA and NRP1) were significantly correlated with ACSL4 expression levels (**Table 1**). This supports that ACSL4 expression is closely related to DC infiltration, thus affecting the prognosis and survival of patients. Similarly, CAF markers (HGF, PDGFRB, FGB1, THBS1) and MDSC markers (CD14, CD33) were positively correlated with ACSL4 expression in BRCA and SKCM. These results suggest that ACSL4 plays a role in the immunosuppressive state of cancer. In order to verify the results of TIMER analysis, GEPIA database was further used to analyze the correlation between ACSL4 expression and immune cell markers (**Table 2**). The results were consistent with the TIMER database. In BRCA and SKCM, ACSL4 expression was significantly correlated with CD8$^+$ T cells, TAM, M2 macrophages, monocytes, CAF and MDSC markers. There was no correlation between ACSL4 and DC markers CD1C and HLA-DQB1 in SKCM. Other markers were correlated with both cancers.

Identification of ACSL4 Related Compounds

The Connectivity Map was used as a first step in the drug discovery process. By comparing the queried and existing gene signatures, links can be found between gene knockout/overexpression or small molecules with similar or opposite effects (Lamb, 2007). Their related transcriptional effects suggest they confer related physiological effects on the cell. Genes with positive and negative scores have similar and opposite gene characteristics to ACSL4 expression, respectively. Connections were viewed as a heat map ranked by the summary connectivity score. Heat map showed that compounds with high similarity to ACSL4 included inhibitor of Insulin Growth factor 1 receptor protein Tyrosine kinase, nalbuphine opioid receptor agonist, opioid receptor antagonist, EGFR inhibitor, Cytochrome P450 inhibitor and carcinoma cell growth inhibitor. (**Figure 8**).

DISCUSSION

Metabolic reprogramming is one of the hallmarks of cancer (Hanahan and Weinberg, 2011). Alterations in lipid metabolism, including catabolism and anabolism, are part of metabolic reprogramming that occurs in tumor cells to promote gene mutations, loss of tumor suppressors, and epigenetic modifications (Currie et al., 2013). Free fatty acids are converted into fatty acyl-coA synthase in an ATP-dependent manner, which causes membrane phospholipid biosynthesis, energy utilization and storage, lipid signaling and other physiological and metabolic processes (Coleman et al., 2000). Dysregulation of fatty acid metabolism leads to excessive lipid biosynthesis and deposition, which promotes the occurrence and development of cancer (Tang et al., 2018). ACSL4 is a key factor involved in metabolism-related diseases. Recent studies have shown that ACSL4 promotes arachidonic acid (AA) and

epinephrine lipid peroxidation, participating in ferroptosis-related processes, and overexpression of ACSL4 promotes ferroptosis (Kagan et al., 2017; Cheng et al., 2020). Different from apoptosis, necrosis and autophagy, iron death is an iron-dependent, lipid peroxidation mediated form of cell death (Dixon et al., 2012). Wang W. et al. found that $CD8^+$ T cells activated by immunotherapy enhanced the occurrence of lipid peroxidation in tumor cells, which then initiated ferroptosis, further enhancing the anti-tumor effect of immunotherapy (Wang et al., 2019). It suggests that the ferroptosis is involved in T cell mediated cancer immunity. There is a lack of research on the correlation between ferroptosis and immune response.

More and more evidence highlights the important role of ACSL4 in regulating the proliferation and apoptosis of cancer cells. Sung et al. found that ACSL4 was overexpressed in HCC tissues and cells (Sung et al., 2007). Arachidonic acid drives ACSL4 ubiquitination through substrate-induced post-translational regulatory mechanisms (Kan et al., 2014). Recent studies have shown that ACSL4 also increased GLUT1-mediated O-Glcnacylation promotes hepatocellular carcinoma cell growth and survival. In addition, ACSL4 acts as an activator of mTOR signaling, increasing HCC cell growth and inhibiting apoptosis (Wang J. et al., 2020). In breast cancer, ACSL4 promotes breast cancer cell proliferation, invasion and migration through the same mechanism (Orlando et al., 2015). Overexpression of ACSL4 is associated with the development of colon cancer. Apatinib promotes the ferroptosis in CRC cells by targeting ELOVL6 and subsequently regulating ACSL4 expression (Tian et al., 2021). Studies in human glioma have found that ACSL4 expression is down-regulated and iron death is also reduced. Therefore, ACSL4 is proposed to protect glioma cells and play an anti-proliferative role by activating the ferroptosis pathway, and highlights the key role of ACSL4 in regulating ferroptosis in the protection of glioma (Cheng et al., 2020). To analyze ACSL4 expression levels in different cancers, this study analyzed ACSL4 mRNA differential expression in 32 cancer types from Oncomine database and TIMER database compared with normal tissues. The two data sets were consistent: high expression of ACSL4 in colorectal cancer and liver cancer, low expression in breast cancer and central nervous tumor. It's both elevated and decreased in pancreatic cancer. In addition, the expression was inconsistent in renal cell carcinoma, with high expression in Oncomine and down expression in TIMER, which may be due to differences in data sources and standardized methods of different databases. We also added the analysis results of GEPIA and found that ACSL4 expression was low in BRCA. In addition, the protein expression pattern of ACSL4 was analyzed by UALCAN database, and it was found that ACSL4 was highly expressed in colorectal cancer and low in breast cancer. Further, the prognostic value of ACSL4 in different cancers was evaluated in these databases, and we found that the prognosis of ACSL4 in breast cancer and lung cancer was consistently poor. To be specific, the GEO dataset analyzed by PrognoScan indicates that high expression of ACSL4 is associated with poor prognosis in Colorectal cancer and Brain cancer, and low expression of ACSL4 is associated with poor prognosis in Lung and Breast cancer. Similarly, low expression of ACSL4 in BRCA, LUAD, BLCA, CESC, HNSC, PAAD, STAD and TGCT showed poor prognosis in Kaplan-Meier database. GEPIA explored the poorer prognosis of ACSL4 low expression in ACC, KIRC, LGG, PCPG, and SKCM. These results suggest that ACSL4 has potential prognostic value in breast cancer, lung cancer, skin malignant melanoma and other cancers, and can be used as a biomarker reflecting the prognosis.

Genetic structural variation in the human genome can exist in many forms (Redon et al., 2006). Single nucleotide polymorphism (SNP) is considered to be the main form of structural variation, and CNV is also widely existed, which is associated with the occurrence and development of various cancers (Zhou et al., 2019; Wu et al., 2020; Zhong et al., 2020). There are few studies on the relationship between ACSL4 gene alteration and cancer. In this study, mixed-cancer panel found that ACSL4 had different degrees of genetic changes in 21 cancers, among which ACSL4 was most prone to genetic changes in Endometrial carcinoma, Melanoma and Sarcoma. In the cervical Squamous cell carcinoma, pleural Mesothelioma and Glioblastoma, all the cases were mutation. In Renal Clear cell carcinoma, Hepatocellular carcinoma and well-differentiated Thyroid cancer, Amplification occurred in all cases. Deep deletion occurred only in Seminoma in all cases. In addition, we found that patients with ACSL4 mutations had poor OS and PFS.

In recent years, more and more attention has been paid to the molecular classification of endometrium, which was mainly divided into four subtypes, which were believed to be caused by driver changes, i.e. POLE EDM, TP53 mutation or MMR defect, with significantly different prognosis (León-Castillo et al., 2020). Oxidative stress (OS) played an important role in melanoma metastasis through excessive production of reactive oxygen species (ROS). Other studies have shown that ionizing radiation (IR) not only induced the production of ROS in tumor cells, but also induced ACSL4 expression. ACSL4 preferentially utilized arachidonic acid as a substrate, resulting in increased lipid peroxidation and ferroptosis, thus exerting antitumor activity (Lei G. et al., 2020). This is also consistent with the poor prognosis of the low expression of ACSL4 in melanoma in this study. We further analyzed ACSL4 single nucleotide variation (SNV) using GSCA. The results showed that the most variation was found in UCEC and SKCM, and the prognosis of ACSL4 mutant was worse in SKCM. CNV analysis showed that ACSL4 CNV was positively correlated with ACSL4 expression in 10 cancers, which was consistent with cBioPortal results. The prognosis was worse in patients with copy number deletion in KIPR, CESC, and LAML, and worse in patients with copy number amplification in UCEC. DNA methylation is a common epigenetic modification by linking methyl groups to the C5 site of cytosine (5mC) in the CpG environment (Cao et al., 2019). Hypomethylation has been shown to be widespread in cancer progression (Muhammad et al., 2021; Sugiura et al., 2021). Hypomethylation of ACSL4 in BRCA, BLCA, LIHC, STAD and TCGT was found in the UALCAN database. In GSCA. we found that ACSL4 expression was negatively correlated with methylation levels in 19 cancers. Interestingly, in LIHC, ACSL4 overexpression may be associated with hypomethylation of ACSL4 and a worse prognosis. This is consistent with the correlation between

ASLC4 mRNA expression and prognosis in LIHC, that is, high expression of ACSL4 leads to worse prognosis. A previous study also found that hypomethylated CpG sites of ACSL4 were associated with an increased risk of non-alcoholic fatty liver disease (NAFLD) (Zhang et al., 2018). These results suggest that hypomethylation of ACSL4 may be one of the epigenetic regulatory mechanisms in many cancers.

Immune evasion is an important marker of cancer and has long been considered as a basic process of tumor formation and progression (Chen and Mellman, 2017; Lei X. et al., 2020). The prognostic value of immune-infiltrating cells has been extensively studied in various malignancies, but ACSL4 has not been well studied in immuno-oncology (Ge et al., 2021; Yu et al., 2021). A major finding in this study was that ACSL4 expression was associated with levels of immune invasion across multiple cancer types. We found that ACSL4 expression was positively correlated with neutrophils, monocytes and CD4+T cells. As expected, ACSL4 was not consistently associated with levels of infiltration of CD8 T cells, Tfh, Treg, B cells, macrophages, NK, and DC across different cancers. In BRCA and SKCM, ACSL4 was more closely related to the level of immune cell infiltration. In SKCM, ACSL4 expression level was not correlated with tumor purity, suggesting that there was no significant difference in ACSL4 expression level between tumor cells and tumor microenvironment. However, in BRCA, ACSL4 expression levels were significantly negatively correlated with tumor purity, suggesting sustained enrichment of ACSL4 in tumor cells. After adjusting for tumor purity, ACSL4 was significantly positively correlated with the level of immune cell infiltration in SKCM and BRCA. These findings suggest that ACSL4 plays an important role in the recruitment and regulation of immune-infiltrating cells in cancer. Patricia P. Yee et al. found in glioma studies that neutrophils play an anti-tumor role by inducing iron death in tumor cells through myeloperoxidase (MPO) and ACSL4 (Yee et al., 2020). CD4+T cells secrete a variety of cytokines, which directly or indirectly activate other immune cells (such as B cells and CD8 +T cells) and enhance the anti-tumor activity of CTL. The original theory postulated that higher expression of immune cells in the early stages of carcinogenesis contributed to anti-tumor activity (Bindea et al., 2013). Our data analysis confirmed that ACSL4 and higher levels of immune cell infiltration were associated with better survival outcomes in BRCA and SKCM. As cancer progresses, the immune microenvironment may promote cancer cell growth while mediating immunosuppression. Myeloid suppressor cells are immature myeloid cells that also have immunosuppressive effects in the tumor microenvironment. In this study, it was found that cancers with high ACSL4 expression (LICH, COAD, STAD) had high levels of MDSC infiltration, while cancers with low ACSL4 expression (BRCA, KIRC, LUSC, SKCM) had high levels of MDSC infiltration, and had poor prognosis and survival in BRCA and SKCM. The prognosis was consistent with ACSL4 mRNA. Another study analyzed the possible association between tumor mutation load (TMB) prognosis and immune cell infiltration in SKCM. Studies have shown that SNPS are more frequent than insertions or deletions in SKCM, and patients with characteristic mutants in the high TMB group have poor survival outcomes and inhibit immune infiltration levels (Cao et al., 2019).These results suggest that ACSL4 may influence the level of tumor immune cell infiltration and ultimately affect patient survival, providing a reference for immunotherapy.

Considering that ACSL4 is genetically altered in a variety of cancers, we further analyzed whether there is a correlation between ACSL4 gene alteration or epigenetic modification and tumor immune cell infiltration level by using TIMER database. In this study, ACSL4 mutation was significantly positively correlated with CD4+T cells, CD4+T cells, B, DC, macrophages and CAFS infiltration levels in UCEC, while significantly negatively correlated with immune cell infiltration levels in SARC. In UCEC, Mutation mainly occurred, the level of immune cell invasion increased, and the prognosis and survival became worse. In SARC, Amplification and deep deletion mainly occurred, and the level of immune cell invasion decreased. When ACSL4 copy number is abnormal, the infiltration level of CAFs in BRCA and OV is reduced, and the prognosis of ACSL4 mRNA is poor. Although changes in the ACSL4 gene in our data affect immune cell infiltration levels in only a few cancer types, it also suggests that ACSL4 mutations or copy number abnormalities are closely associated with immune cell infiltration and affect prognosis in UCEC, SARC, BRCA and OV. It may be a potential immune and prognostic biomarker. This has not been suggested in previous studies.

In addition, this study further analyzed the association between ACSL4 and immune cell biomarkers in different cancers. It was found that ACSL4 had significant positive correlation with biomarkers of CD4+T cells, TAM, M2 macrophages, monocytes, DC, CAFs and MDSC in BRAC and SKCM. Notably, ACSL4 mRNA expression was low in both cancers and the prognosis was poor. This suggests that ACSL4 may affect prognosis by regulating immune cell recruitment and activation. In addition, ACSL4 was positively correlated with the markers of Exhaust T cells (CTLA4, HAVCR2, LAG3, PDCD1) and Treg cells (CCR8, IL2RA, IL7R). There is increasing evidence that exhaust cells play an inhibitory role in the tumor microenvironment by changing signal cascade and epigenetic metabolism, attenuating effector cytotoxicity, reducing cytokine production, and regulating various inhibitory molecular receptors (Franco et al., 2020; Zeng et al., 2020). Increased infiltration of Exhaust T cells was found in many tumors, and patients with high expression of PD-L1 had better anti-PD1 treatment (Zheng et al., 2017; Guo et al., 2018). These results suggest that ACSL4 may affect the efficacy of immunotherapy and may become a potential predictive biomarker of immunotherapy.

By searching the CMap database, it was found that the compound with high similarity to ACSL4 was mainly inhibitor of Insulin growth factor 1 receptor protein tyrosine kinase. EGFR inhibitor etc. The insulin-like growth factor (IGF) signaling system plays a crucial role in human cancer. IGF-1 receptor (IGF-1R) inhibitors prevent binding of IGF-1 to IGF1R and subsequently inhibit down stream signaling, including PI3K/Akt pathway, exerting antitumor activity and being potential targets for cancer treatment (Pollard and Daniel, 2019). In this study, we speculate that the

mechanism of ACSL4 in cancer is closely related to the IGF signaling pathway. These highly similar compounds may contribute to the treatment of cancers with elevated ACSL4 expression, including colorectal cancer and liver cancer. However, CMap model is based on microarray data, and the accuracy of prediction may be limited. A large number of experimental studies are still needed to develop and verify the efficacy of the drug.

In this study, the expression and prognostic value of ACSL4 in different cancers were analyzed using multiple online public databases. Individual cancer results may be inconsistent due to differences in data collection and standardization across different databases. Therefore, further *in vivo* and *in vitro* experiments are needed to realize the mechanisms of ACSL4 in different cancer types at the cellular and molecular level. This is what the Bioinformatics Research Institute lacks. Although ACSL4 expression was found to be associated with immune cell infiltration and patient survival, it has not been demonstrated that ACSL4 affects patient survival through immune infiltration. ACSL4 is not only a sensitive monitor of ferroptosis, but also an important contributor of ferroptosis. The relationship between acSL4-mediated ferroptosis and immune infiltration and the clinical response to immunotherapy are also important topics for future research.

CONCLUSION

This study analyzed the expression of ACSL4 in generalized carcinoma, and for the first time analyzed the genetic and epigenetic changes of ACSL4 in different cancers, as well as its impact on survival and prognosis. In addition, ACSL4 mediates the level of immune cell infiltration in BRCA and SKCM, providing new ideas for personalized cancer immunotherapy. ACSL4 is expected to be a potential prognostic and prognostic immunotherapy biomarker.

DATA AVAILABILITY STATEMENT

The datasets presented in this study can be found in online repositories. The names of the repository/repositories and accession number(s) can be found in the article/ **Supplementary Material**.

AUTHOR CONTRIBUTIONS

ML and YY conceived the project. ML and XS extracted the information from the databases. XS conducted clinical data collection and analysis. YY and FC participated in data analysis. YY, XS and FC participated in discussion and language editing. ML wrote the manuscript. All authors have read and approved the final manuscript.

ACKNOWLEDGMENTS

We sincerely thank the public databases, including Oncomine, GEPIA, CCLE, UALCAN, HPA, cBioPortal, PrognoScan, Kaplan-Meier Plotter, TIMER, GSCA, and CMap for providing open access.

SUPPLEMENTARY MATERIAL

The Supplementary Material for this article can be found online at: https://www.frontiersin.org/articles/10.3389/fgene.2022.812674/full#supplementary-material

REFERENCES

Bader, J. E., Voss, K., and Rathmell, J. C. (2020). Targeting Metabolism to Improve the Tumor Microenvironment for Cancer Immunotherapy. *Mol. Cel.* 78, 1019–1033. doi:10.1016/j.molcel.2020.05.034

Bindea, G., Mlecnik, B., Tosolini, M., Kirilovsky, A., Waldner, M., Obenauf, A. C., et al. (2013). Spatiotemporal Dynamics of Intratumoral Immune Cells Reveal the Immune Landscape in Human Cancer. *Immunity* 39, 782–795. doi:10.1016/j.immuni.2013.10.003

Biswas, S. K. (2015). Metabolic Reprogramming of Immune Cells in Cancer Progression. *Immunity* 43, 435–449. doi:10.1016/j.immuni.2015.09.001

Boroughs, L. K., and DeBerardinis, R. J. (2015). Metabolic Pathways Promoting Cancer Cell Survival and Growth. *Nat. Cel Biol* 17, 351–359. doi:10.1038/ncb3124

Budczies, J., Seidel, A., Christopoulos, P., Endris, V., Kloor, M., Győrffy, B., et al. (2018). Integrated Analysis of the Immunological and Genetic Status in and across Cancer Types: Impact of Mutational Signatures beyond Tumor Mutational burden. *Oncoimmunology* 7, e1526613. doi:10.1080/2162402x.2018.1526613

Cao, T., Pan, W., Sun, X., and Shen, H. (2019). Increased Expression of TET3 Predicts Unfavorable Prognosis in Patients with Ovarian Cancer-A Bioinformatics Integrative Analysis. *J. ovarian Res.* 12, 101. doi:10.1186/s13048-019-0575-4

Cerami, E., Gao, J., Dogrusoz, U., Gross, B. E., Sumer, S. O., Aksoy, B. A., et al. (2012). The cBio Cancer Genomics portal: an Open Platform for Exploring Multidimensional Cancer Genomics Data. *Cancer Discov.* 2, 401–404. doi:10.1158/2159-8290.cd-12-0095

Chandrashekar, D. S., Bashel, B., Balasubramanya, S. A. H., Creighton, C. J., Ponce-Rodriguez, I., Chakravarthi, B., et al. (2017). UALCAN: A Portal for Facilitating Tumor Subgroup Gene Expression and Survival Analyses. *Neoplasia (New York, N.Y.).* 19, 649–658. doi:10.1016/j.neo.2017.05.002

Chen, D. S., and Mellman, I. (2017). Elements of Cancer Immunity and the Cancer-Immune Set point. *Nature* 541, 321–330. doi:10.1038/nature21349

Chen, P. H., Cai, L., Huffman, K., Yang, C., Kim, J., Faubert, B., et al. (2019). Metabolic Diversity in Human Non-small Cell Lung Cancer Cells. *Mol. Cel.* 76, 838–851.e5. doi:10.1016/j.molcel.2019.08.028

Chen, J., Ding, C., Chen, Y., Hu, W., Lu, Y., Wu, W., et al. (2020). ACSL4 Promotes Hepatocellular Carcinoma Progression via C-Myc Stability Mediated by ERK/FBW7/c-Myc axis. *Oncogenesis* 9, 42. doi:10.1038/s41389-020-0226-z

Cheng, C., Geng, F., Cheng, X., and Guo, D. (2018). Lipid Metabolism Reprogramming and its Potential Targets in Cancer. *Cancer Commun. (London, England)* 38, 27. doi:10.1186/s40880-018-0301-4

Cheng, J., Fan, Y. Q., Liu, B. H., Zhou, H., Wang, J. M., and Chen, Q. X. (2020). ACSL4 Suppresses Glioma Cells Proliferation via Activating Ferroptosis. *Oncol. Rep.* 43, 147–158. doi:10.3892/or.2019.7419

Coleman, R. A., Lewin, T. M., and Muoio, D. M. (2000). Physiological and Nutritional Regulation of Enzymes of Triacylglycerol Synthesis. *Annu. Rev. Nutr.* 20, 77–103. doi:10.1146/annurev.nutr.20.1.77

Currie, E., Schulze, A., Zechner, R., Walther, T. C., and Farese, R. V., Jr. (2013). Cellular Fatty Acid Metabolism and Cancer. *Cel Metab.* 18, 153–161. doi:10.1016/j.cmet.2013.05.017

Davoli, T., Uno, H., Wooten, E. C., and Elledge, S. J. (2017). *Tumor Aneuploidy Correlates with Markers of Immune Evasion and with Reduced Response to Immunotherapy*. New York, N.Y.: Science, 355.

Dixon, S. J., Lemberg, K. M., Lamprecht, M. R., Skouta, R., Zaitsev, E. M., Gleason, C. E., et al. (2012). Ferroptosis: an Iron-dependent Form of Nonapoptotic Cell Death. *Cell* 149, 1060–1072. doi:10.1016/j.cell.2012.03.042

Franco, F., Jaccard, A., Romero, P., Yu, Y. R., and Ho, P. C. (2020). Metabolic and Epigenetic Regulation of T-Cell Exhaustion. *Nat. Metab.* 2, 1001–1012. doi:10.1038/s42255-020-00280-9

Ge, Q., Li, G., Chen, J., Song, J., Cai, G., He, Y., et al. (2021). Immunological Role and Prognostic Value of APBB1IP in Pan-Cancer Analysis. *J. Cancer* 12, 595–610. doi:10.7150/jca.50785

Grevengoed, T. J., Klett, E. L., and Coleman, R. A. (2014). Acyl-CoA Metabolism and Partitioning. *Annu. Rev. Nutr.* 34, 1–30. doi:10.1146/annurev-nutr-071813-105541

Guo, X., Zhang, Y., Zheng, L., Zheng, C., Song, J., Zhang, Q., et al. (2018). Global Characterization of T Cells in Non-small-cell Lung Cancer by Single-Cell Sequencing. *Nat. Med.* 24, 978–985. doi:10.1038/s41591-018-0045-3

Hanahan, D., and Weinberg, R. A. (2011). Hallmarks of Cancer: the Next Generation. *Cell* 144, 646–674. doi:10.1016/j.cell.2011.02.013

Hieronymus, H., Murali, R., Tin, A., Yadav, K., Abida, W., Moller, H., et al. (2018). Tumor Copy Number Alteration burden Is a Pan-Cancer Prognostic Factor Associated with Recurrence and Death. *eLife* 7, e37294. doi:10.7554/eLife.37294

Hirschhorn, T., and Stockwell, B. R. (2019). The Development of the Concept of Ferroptosis. *Free Radic. Biol. Med.* 133, 130–143. doi:10.1016/j.freeradbiomed.2018.09.043

Kagan, V. E., Mao, G., Qu, F., Angeli, J. P., Doll, S., Croix, C. S., et al. (2017). Oxidized Arachidonic and Adrenic PEs Navigate Cells to Ferroptosis. *Nat. Chem. Biol.* 13, 81–90. doi:10.1038/nchembio.2238

Kan, C. F., Singh, A. B., Stafforini, D. M., Azhar, S., and Liu, J. (2014). Arachidonic Acid Downregulates Acyl-CoA Synthetase 4 Expression by Promoting its Ubiquitination and Proteasomal Degradation. *J. lipid Res.* 55, 1657–1667. doi:10.1194/jlr.m045971

Küch, E. M., Vellaramkalayil, R., Zhang, I., Lehnen, D., Brügger, B., Sreemmel, W., et al. (2014). Differentially Localized Acyl-CoA Synthetase 4 Isoenzymes Mediate the Metabolic Channeling of Fatty Acids towards Phosphatidylinositol. *Biochim. Biophys. Acta* 1841, 227–239. doi:10.1016/j.bbalip.2013.10.018

Lamb, J. (2007). The Connectivity Map: a New Tool for Biomedical Research. *Nat. Rev. Cancer* 7, 54–60. doi:10.1038/nrc2044

Lei, G., Zhang, Y., Koppula, P., Liu, X., Zhang, J., Lin, S. H., et al. (2020a). The Role of Ferroptosis in Ionizing Radiation-Induced Cell Death and Tumor Suppression. *Cel Res.* 30, 146–162. doi:10.1038/s41422-019-0263-3

Lei, X., Lei, Y., Li, J. K., Du, W. X., Li, R. G., Yang, J., et al. (2020b). Immune Cells within the Tumor Microenvironment: Biological Functions and Roles in Cancer Immunotherapy. *Cancer Lett.* 470, 126–133. doi:10.1016/j.canlet.2019.11.009

León-Castillo, A., Gilvazquez, E., Nout, R., Smit, V. T., McAlpine, J. N., McConechy, M., et al. (2020). Clinicopathological and Molecular Characterisation of 'multiple-Classifier' Endometrial Carcinomas. *J. Pathol.* 250, 312–322. doi:10.1002/path.5373

Li, T., Fan, J., Wang, B., Traugh, N., Chen, Q., Liu, J. S., et al. (2017). TIMER: A Web Server for Comprehensive Analysis of Tumor-Infiltrating Immune Cells. *Cancer Res.* 77, e108–e110. doi:10.1158/0008-5472.can-17-0307

Liu, C. J., Hu, F. F., Xia, M. X., Han, L., Zhang, Q., and Guo, A. Y. (2018). GSCALite: a Web Server for Gene Set Cancer Analysis. *Bioinformatics (Oxford, England)* 34, 3771–3772. doi:10.1093/bioinformatics/bty411

Lu, Z., Chen, H., Li, S., Gong, J., Li, J., Zou, J., et al. (2020). Tumor Copy-Number Alterations Predict Response to Immune-Checkpoint-Blockade in Gastrointestinal Cancer. *J. Immunother. Cancer* 8, e000374. doi:10.1136/jitc-2019-000374

Ma, Y., Zhang, X., Alsaidan, O. A., Yang, X., Sulejmani, E., Zha, J., et al. (2021). Long-Chain Acyl-CoA Synthetase 4-Mediated Fatty Acid Metabolism Sustains Androgen Receptor Pathway-independent Prostate Cancer. *Mol. Cancer Res. : MCR* 19, 124–135. doi:10.1158/1541-7786.mcr-20-0379

Mizuno, H., Kitada, K., Nakai, K., and Sarai, A. (2009). PrognoScan: a New Database for Meta-Analysis of the Prognostic Value of Genes. *BMC Med. genomics* 2, 18. doi:10.1186/1755-8794-2-18

Modhukur, V., Iljasenko, T., Metsalu, T., Lokk, K., Laisk-Podar, T., and Vilo, J. (2018). MethSurv: a Web Tool to Perform Multivariable Survival Analysis Using DNA Methylation Data. *Epigenomics* 10, 277–288. doi:10.2217/epi-2017-0118

Muhammad, J. S., Guimei, M., Jayakumar, M. N., Shafarin, J., Janeeh, A. S., AbuJabal, R., et al. (2021). Estrogen-induced Hypomethylation and Overexpression of YAP1 Facilitate Breast Cancer Cell Growth and Survival. *Neoplasia (New York, N.Y.).* 23, 68–79. doi:10.1016/j.neo.2020.11.002

Nusinow, D. P., Szpyt, J., Ghandi, M., Rose, C. M., McDonald, E. R., 3rd, Kalocsay, M., et al. (2020). Quantitative Proteomics of the Cancer Cell Line Encyclopedia. *Cell* 180, 387–402.e16. doi:10.1016/j.cell.2019.12.023

Orlando, U. D., Castillo, A. F., Dattilo, M. A., Solano, A. R., Maloberti, P. M., and Podesta, E. J. (2015). Acyl-CoA Synthetase-4, a New Regulator of mTOR and a Potential Therapeutic Target for Enhanced Estrogen Receptor Function in Receptor-Positive and -negative Breast Cancer. *Oncotarget* 6, 42632–42650. doi:10.18632/oncotarget.5822

Pollard, K. J., and Daniel, J. M. (2019). Nuclear Estrogen Receptor Activation by Insulin-like Growth Factor-1 in Neuro-2A Neuroblastoma Cells Requires Endogenous Estrogen Synthesis and Is Mediated by Mutually Repressive MAPK and PI3K Cascades. *Mol. Cell. Endocrinol.* 490, 68–79. doi:10.1016/j.mce.2019.04.007

Qin, C., Yang, G., Yang, J., Ren, B., Wang, H., Chen, G., et al. (2020). Metabolism of Pancreatic Cancer: Paving the Way to Better Anticancer Strategies. *Mol. Cancer* 19, 50. doi:10.1186/s12943-020-01169-7

Redon, R., Ishikawa, S., Fitch, K. R., Feuk, L., Perry, G. H., Andrews, T. D., et al. (2006). Global Variation in Copy Number in the Human Genome. *Nature* 444, 444–454. doi:10.1038/nature05329

Rhodes, D. R., Yu, J., Shanker, K., Deshpande, N., Varambally, R., Ghosh, D., et al. (2004). ONCOMINE: a Cancer Microarray Database and Integrated Data-Mining Platform. *Neoplasia (New York, N.Y.).* 6, 1–6. doi:10.1016/s1476-5586(04)80047-2

Sánchez-Martínez, R., Cruz-Gil, S., García-Álvarez, M. S., Reglero, G., and Ramírez de Molina, A. (2017). Complementary ACSL Isoforms Contribute to a Non-warburg Advantageous Energetic Status Characterizing Invasive colon Cancer Cells. *Scientific Rep.* 7, 11143. doi:10.1038/s41598-017-11612-3

Sha, R., Xu, Y., Yuan, C., Sheng, X., Wu, Z., Peng, J., et al. (2021). Predictive and Prognostic Impact of Ferroptosis-Related Genes ACSL4 and GPX4 on Breast Cancer Treated with Neoadjuvant Chemotherapy. *EBioMedicine* 71, 103560. doi:10.1016/j.ebiom.2021.103560

Snaebjornsson, M. T., Janaki-Raman, S., and Schulze, A. (2020). Greasing the Wheels of the Cancer Machine: The Role of Lipid Metabolism in Cancer. *Cel Metab.* 31, 62–76. doi:10.1016/j.cmet.2019.11.010

Su, Z., Wang, Z., Ni, X., Duan, J., Gao, Y., Zhuo, M., et al. (2019). Inferring the Evolution and Progression of Small-Cell Lung Cancer by Single-Cell Sequencing of Circulating Tumor Cells. *Clin. Cancer Res. : official J. Am. Assoc. Cancer Res.* 25, 5049–5060. doi:10.1158/1078-0432.ccr-18-3571

Sugiura, M., Sato, H., Kanesaka, M., Imamura, Y., Sakamoto, S., Ichikawa, T., et al. (2021). Epigenetic Modifications in Prostate Cancer. *Int. J. Urol. : official J. Jpn. Urol. Assoc.* 28, 140–149. doi:10.1111/iju.14406

Sung, Y. K., Park, M. K., Hong, S. H., Hwang, S. Y., Kwack, M. H., Kim, J. C., et al. (2007). Regulation of Cell Growth by Fatty Acid-CoA Ligase 4 in Human Hepatocellular Carcinoma Cells. *Exp. Mol. Med.* 39, 477–482. doi:10.1038/emm.2007.52

Tang, Z., Li, C., Kang, B., Gao, G., Li, C., and Zhang, Z. (2017). GEPIA: a Web Server for Cancer and normal Gene Expression Profiling and Interactive Analyses. *Nucleic Acids Res.* 45, W98–W102. doi:10.1093/nar/gkx247

Tang, Y., Zhou, J., Hooi, S. C., Jiang, Y. M., and Lu, G. D. (2018). Fatty Acid Activation in Carcinogenesis and Cancer Development: Essential Roles of Long-Chain Acyl-CoA Synthetases. *Oncol. Lett.* 16, 1390–1396. doi:10.3892/ol.2018.8843

Thul, P. J., and Lindskog, C. (2018). The Human Protein Atlas: A Spatial Map of the Human Proteome. *Protein Sci.* 27, 233–244. doi:10.1002/pro.3307

Tian, X., Li, S., and Ge, G. (2021). Apatinib Promotes Ferroptosis in Colorectal Cancer Cells by Targeting ELOVL6/ACSL4 Signaling. *Cancer Manag. Res.* 13, 1333–1342. doi:10.2147/cmar.s274631

Wang, W., Green, M., Choi, J. E., Gijón, M., Kennedy, P. D., Johnson, J. K., et al. (2019). CD8(+) T Cells Regulate Tumour Ferroptosis during Cancer Immunotherapy. *Nature* 569, 270–274. doi:10.1038/s41586-019-1170-y

Wang, J., Wang, Z., Yuan, J., Wang, J., and Shen, X. (2020a). The Positive Feedback between ACSL4 Expression and O-GlcNAcylation Contributes to the Growth and Survival of Hepatocellular Carcinoma. *Aging* 12, 7786–7800. doi:10.18632/aging.103092

Wang, C. Y., Chiao, C. C., Phan, N. N., Li, C. Y., Sun, Z. D., Jiang, J. Z., et al. (2020b). Gene Signatures and Potential Therapeutic Targets of Amino Acid Metabolism in Estrogen Receptor-Positive Breast Cancer. *Am. J. Cancer Res.* 10, 95–113.

Woo, X. Y., Giordano, J., Srivastava, A., Zhao, Z. M., Lloyd, M. W., de Bruijn, R., et al. (2021). Conservation of Copy Number Profiles during Engraftment and Passaging of Patient-Derived Cancer Xenografts. *Nat. Genet.* 53, 86–99. doi:10.1038/s41588-020-00750-6

Wu, B., Lu, X., Shen, H., Yuan, X., Wang, X., Yin, N., et al. (2020). Intratumoral Heterogeneity and Genetic Characteristics of Prostate Cancer. *Int. J. Cancer* 146, 3369–3378. doi:10.1002/ijc.32961

Ye, X., Zhang, Y., Wang, X., Li, Y., and Gao, Y. (2016). Tumor-suppressive Functions of Long-Chain Acyl-CoA Synthetase 4 in Gastric Cancer. *IUBMB life* 68, 320–327. doi:10.1002/iub.1486

Yee, P. P., Wei, Y., Kim, S. Y., Lu, T., Chih, S. Y., Lawson, C., et al. (2020). Neutrophil-induced Ferroptosis Promotes Tumor Necrosis in Glioblastoma Progression. *Nat. Commun.* 11, 5424. doi:10.1038/s41467-020-19193-y

Yen, M. C., Kan, J. Y., Hsieh, C. J., Kuo, P. L., Hou, M. F., and Hsu, Y. L. (2017). Association of Long-Chain Acyl-Coenzyme A Synthetase 5 Expression in Human Breast Cancer by Estrogen Receptor Status and its Clinical Significance. *Oncol. Rep.* 37, 3253–3260. doi:10.3892/or.2017.5610

Yu, Y., Wang, Z., Zheng, Q., and Li, J. (2021). GREB1L Overexpression Correlates with Prognosis and Immune Cell Infiltration in Lung Adenocarcinoma. *Scientific Rep.* 11, 13281. doi:10.1038/s41598-021-92695-x

Yuan, Q., Sun, N., Zheng, J., Wang, Y., Yan, X., Mai, W., et al. (2019). Prognostic and Immunological Role of FUN14 Domain Containing 1 in Pan-Cancer: Friend or Foe? *Front. Oncol.* 9, 1502. doi:10.3389/fonc.2019.01502

Zeng, Z., Wei, F., and Ren, X. (2020). Exhausted T Cells and Epigenetic Status. *Cancer Biol. Med.* 17, 923–936. doi:10.20892/j.issn.2095-3941.2020.0338

Zhang, R. N., Pan, Q., Zheng, R. D., Mi, Y. Q., Shen, F., Zhou, D., et al. (2018). Genome-wide Analysis of DNA Methylation in Human Peripheral Leukocytes Identifies Potential Biomarkers of Nonalcoholic Fatty Liver Disease. *Int. J. Mol. Med.* 42, 443–452. doi:10.3892/ijmm.2018.3583

Zhang, Y., Li, S., Li, F., Lv, C., and Yang, Q. K. (2021). High-fat Diet Impairs Ferroptosis and Promotes Cancer Invasiveness via Downregulating Tumor Suppressor ACSL4 in Lung Adenocarcinoma. *Biol. direct* 16, 10. doi:10.1186/s13062-021-00294-7

Zheng, C., Zheng, L., Yoo, J. K., Guo, H., Zhang, Y., Guo, X., et al. (2017). Landscape of Infiltrating T Cells in Liver Cancer Revealed by Single-Cell Sequencing. *Cell* 169, 1342–1356.e16. doi:10.1016/j.cell.2017.05.035

Zhong, Q., Fan, J., Chu, H., Pang, M., Li, J., Fan, Y., et al. (2020). Integrative Analysis of Genomic and Epigenetic Regulation of Endometrial Cancer. *Aging* 12, 9260–9274. doi:10.18632/aging.103202

Zhou, J., Wang, J., Hong, B., Ma, K., Xie, H., Li, L., et al. (2019). Gene Signatures and Prognostic Values of m6A Regulators in clear Cell Renal Cell Carcinoma - a Retrospective Study Using TCGA Database. *Aging* 11, 1633–1647. doi:10.18632/aging.101856

Conflict of Interest: The authors declare that the research was conducted in the absence of any commercial or financial relationships that could be construed as a potential conflict of interest.

Publisher's Note: All claims expressed in this article are solely those of the authors and do not necessarily represent those of their affiliated organizations, or those of the publisher, the editors and the reviewers. Any product that may be evaluated in this article, or claim that may be made by its manufacturer, is not guaranteed or endorsed by the publisher.

frontiers in Genetics

ORIGINAL RESEARCH
published: 25 January 2022
doi: 10.3389/fgene.2021.819632

Genomic Analysis Uncovers Immune Microenvironment Characteristics and Drug Sensitivity of Ferroptosis in Breast Cancer Brain Metastasis

Lei Zhu[1,2†], Mu Chen[1†], Bingsong Huang[1†], Tao Zhang[1†], Kui Chen[1], Hao Lian[1], Min Liu[1], Kaijun Zhao[1], Ying Pang[1], Jing Zhang[1,3]*, Qinchuan Li[2]* and Chunlong Zhong[1]**

[1]Department of Neurosurgery, Shanghai East Hospital, School of Medicine, Tongji University, Shanghai, China, [2]Department of Thoracic Surgery, Shanghai East Hospital, School of Medicine, Tongji University, Shanghai, China, [3]Institute for Advanced Study, Tongji University, Shanghai, China

Background: The role of ferroptosis in breast cancer brain metastasis (BCBM) is unclear. This study aimed to explore the ferroptosis-related genes (FRG) relations with the tumor microenvironment, as well as evaluate their values in predicting survival and drug sensitivity in patients with BCBM.

Materials and Methods: Genes expression and clinical data were downloaded from Gene Expression Omnibus (GEO). Univariate and multivariate Cox regression analyses were performed to explore the independent prognostic factors. Consensus cluster principal component analysis (PCA) was used to establish the ferroptosis score. Immunological signatures were analyzed by the single-sample gene set enrichment analysis (ssGSEA). Drug sensitivity was evaluated through the estimated half-maximal inhibitory concentration (IC50). Finally, results were validated in external cohorts.

Results: Fourteen significantly different FRG were identified between breast cancer (BC) and BCBM tissues. Survival analysis demonstrated HMOX1, PEBP1, KEAP1, and LPCAT3 were significantly associated with overall survival (OS) and relapse-free survival (RFS) (all $p < 0.05$). High ferroptosis score was correlated with iron ion homeostasis, iron metabolism, higher stromal cells and immune cells scores. Patients with high- and low-ferroptosis scores were characterized by different drug sensitivities. Following external validations, the ferroptosis had distinct expression profiles between the BC and BCBM, and could serve as biomarkers for OS and drug response.

Conclusion: Our findings suggested that ferroptosis may be involved in the process of BCBM, and ferroptosis could serve as prognostic biomarkers. Evaluation of ferroptosis may deepen our understanding about the tumor microenvironment, and could help clinicians to make individualized therapy.

Keywords: ferroptosis, breast cancer, brain metastasis, prognosis, drug sensitivity

OPEN ACCESS

Edited by:
Lian Xiang Luo,
Guangdong Medical University, China

Reviewed by:
Mingxiao Feng,
Johns Hopkins University, United States
Kun Xiang,
Duke University, United States
Yixuan Guo,
the University of Utah, United States

***Correspondence:**
Ying Pang
1931195@tongji.edu.cn
Jing Zhang
zhangjingwt@tongji.edu.cn
Qinchuan Li
qinchuanli@tongji.edu.cn
Chunlong Zhong
drchunlongzhong@tongji.edu.cn

†These authors have contributed equally to this work

Specialty section:
This article was submitted to Human and Medical Genomics, a section of the journal Frontiers in Genetics

Received: *22 November 2021*
Accepted: *24 December 2021*
Published: *25 January 2022*

Citation:
Zhu L, Chen M, Huang B, Zhang T, Chen K, Lian H, Liu M, Zhao K, Pang Y, Zhang J, Li Q and Zhong C (2022) Genomic Analysis Uncovers Immune Microenvironment Characteristics and Drug Sensitivity of Ferroptosis in Breast Cancer Brain Metastasis. Front. Genet. 12:819632. doi: 10.3389/fgene.2021.819632

INTRODUCTION

Breast cancer (BC) is the most prevalent tumor in women worldwide, ranking the third most common malignancy followed by lung and colon cancer. It's reported that approximately 1,700,000 new cases and almost 500,000 deaths per year globally (Ferlay et al., 2015; Torre et al., 2015). Breast cancer brain metastasis (BCBM) becomes a major limitation of life expectancy and remains a substantial contributor to overall mortality. Nearly 5–20% breast cancer will develop brain metastasis, and it is the second common primary tumor associated with brain metastasis after lung cancer (Achrol et al., 2019). Breast cancer patients with basal-like (25–27%) and HER2-enriched cancer (11–20%) have higher propensities to metastasize to the brain, compared with those in luminal A (8–15%) and luminal B (11%) subtypes (Kennecke et al., 2010). Since no clinically approved biomarkers of brain metastasis is available, and the presences or absences of estrogen receptor (ER), progesterone receptor (PgR), HER2 and Ki67 status are not sufficient to accurately prognosticate metastasis due to heterogeneity between primary and metastatic sites (Harbeck and Gnant, 2017). Hence, BCBM is often diagnosed late and represents dismal survival.

Diverse underlying mechanisms such as gene alterations, immune dysregulation, as well as estrogen and progesterone imbalance have resulted in the poor prognosis (Shiovitz and Korde, 2015; Bates et al., 2018; Vaz-Luis and Partridge, 2018; Terry et al., 2019). It's estimated that the 1-year survival rate of patients with BCBM is merely 20%, although the tremendous progress has been made in the multidisciplinary treatment, including surgery, chemoradiotherapy and endocrine therapy (Arslan et al., 2010). Considering the therapeutic resistance, several targeted agents such as lapatinib, pazopanib have been tested in patients with BCBM. However, the clinical trial failed to demonstrate improved survival, except for a small subset of patients (Seligmann et al., 2020). Therefore, it's imperative to identify biomarkers that could optimize the implementation of precision targeted therapy.

A thorough understanding of molecular mechanisms that drive BCBM should aid in the discovery of novel strategies to improve clinical management. The extensive applications of high-throughput sequencing technologies in cancer biology, such as cell death analysis, have revealed the relations between thousands of aberrant gene expressions associated with BCBM patients. There is increasing evidence showing that ferroptosis, an iron-catalyzed form of regulated necrosis, plays important role in various cancers, including breast tumors, brain tumors and breast cancer metastasis (Ma et al., 2016; Nagpal et al., 2019; Weiland et al., 2019).

Ferroptosis can be induced by iron accumulation, glutathione (GSH) depletion, glutathione peroxidase 4 (GPX4) inactivation, and is characterized by lipid peroxidation products and toxic reactive oxygen species (ROS) derived from iron metabolism (Stockwell et al., 2017; Bersuker et al., 2019). Several studies have shown that ferroptosis could be triggered in BC (Ma et al., 2016; Yu et al., 2019a). The activities of ferroptosis are regulated precisely by ferroptosis-related genes (FRG), and its dysfunction links with many kinds of diseases (Stockwell et al., 2017; Bersuker et al., 2019; Weiland et al., 2019). In addition, the activation of ferroptosis has tumor suppression efficacy and exerts great potential as a salient anti-cancer target. However, the role of ferroptosis in BCBM is unclear, and few studies explored the relationship between ferroptosis and survival in patients with BC. In this study, we aimed to investigate and validate the FRG signatures that correlate with BCBM, as well as evaluate the FRG values in predicting prognosis and drug sensitivity.

MATERIALS AND METHODS

Data Collection and Extraction

Gene expression data and clinical information of patients with BCBM were downloaded from Gene Expression Omnibus (GEO) database (https://www.ncbi.nlm.nih.gov/gds/). Two datasets (GSE10893 and GSE43837) were used in our study. Both experiment types were expression profiling by array, and both of them contained primary breast cancer and breast cancer brain metastatic tissues. The raw data of gene expressions were selected by "GEO2R" online tool and normalized using the "limma" package in R software (version 4.0.3). The 60 FRG were retrieved from previously published literatures and were available in the **Supplementary Table S1** (Stockwell et al., 2017; Bersuker et al., 2019; Hassannia et al., 2019).

Identification of Significantly Different Genes and Enrichment Analysis

The significantly different genes (SDG) among the FRG were identified using "GEO2R" and the "limma" package with the Wilcoxon test. The cut-off value was determined with $p < 0.05$. SDG interactions were performed through "igraph" "corrplot" packages in R software. To get more reliable data, the overlapping FRG between GSE10893 and GSE43837 were identified and were used for further analysis.

Gene Ontology (GO), including the biological process (BP), cellular component (CC) and molecular function (MF), was performed by "clusterProfiler" package in R software. The Kyoto Encyclopedia of Genes and Genomes (KEGG) was also done using the same tool.

Functional similarity refers to semantic correlation and biological resemblance, which could be used for the purpose of assessing the intimacy and relationship between each gene and its partners by evaluating function and location. Functional similarity was performed by the "GOSemSim" R package (Wang et al., 2007).

Prognostic Survival Analysis

GSE10893 contained gene expression data and corresponding clinical information, and thus was used to perform survival analysis. Univariate and multivariate Cox regressions were used to assess the relationships between the SDG and the patients' overall survival (OS) and relapse-free survival (RFS). In order to explore the independent risk factors of OS and RFS,

we combined the FRG with clinical information using the univariate Cox regression. Significant prognostic factors ($p < 0.05$) were then enrolled into multivariate Cox regression. Independent prognostic genes were used to calculate the risk score following formula: risk score = $\sum_{n=1}^{j} Coef\,j * X\,j$, with Coef j representing the coefficient and Xj representing the relative expression levels of each SDG standardized by z-score. Patients were divided into high- and low-risk groups according to the median of the risk score. Furthermore, we analyzed the correlations between the SDG and clinical features using the *t*-test or Kruskal-Wallis test.

Single-Sample Gene Set Enrichment Analysis

The infiltrating score of 16 immune cells and the activity of 13 immune-related pathways were calculated with single-sample gene set enrichment analysis (ssGSEA) by the "gsva" package in R (Rooney et al., 2015). The effects of FRG on immune cells were assessed using linear regression. The annotated gene set file is provided in **Supplementary Table S2**.

Establishment of Ferroptosis Gene Signature

The unsupervised clustering was executed by the "ConsensuClusterPlus" R package, and the classification was confirmed by 1000 times permutations. Principal component analysis (PCA) was implemented to classify the patients with BC into groups A and B. Then, the ferroptosis score was defined according to the similar method by a previous study: ferroptosis score = $\sum$ group A-$\sum$ group B (Zhang et al., 2020). Where the group A represented the first component in the PCA, and group B presented the second component in the PCA.

Tumor Microenvironment and Drug Sensitivity Analysis

To explore the effects of ferroptosis on stromal and immune cells in TME, we calculated the stromal cells and immune cells score by applying the Estimation of STromal and Immune cells in MAlignant Tumour tissues using Expression data (ESTIMATE) algorithm (Yoshihara et al., 2013). We compared the stromal cells, immune cells and tumor purity differences between the high- and low-ferroptosis score groups.

Genomics of Drug Sensitivity in Cancer (GSDC) is the largest public resource for cancer cell drug sensitivity and drug response molecular marker, containing 1000 human cancer cell lines and 100s of compounds (https://www.cancerrxgene.org/). On this website, you will find drug response data and genomic markers of sensitivity. To identify the molecular characteristics related to drug sensitivity and resistance, we applied the database to predict the targeted and chemotherapeutic responses by estimating the half-maximal inhibitory concentration (IC50) (Yang et al., 2013). The IC50 of each patient was estimated by the pRRophetic R package (Geeleher et al., 2014). Lastly, the IC50 differences were calculated between the high- and low-ferroptosis score groups.

Potential Small Molecular Compounds Prediction

To screen potential drugs that could target BC, we conducted the small molecular compounds analysis in the Connectivity map (CMap; http://portals.broadinstitute.org/cmap/) database. Firstly, we compared the SDG between high- and low-ferroptosis score groups. Then, we investigated the SDG functions through GO and KEGG enrichment analyses. Lastly, the up- and down-regulated genes were uploaded into the CMap website, and potential drugs and mechanisms were predicted.

External Validation

We used another dataset from GEO (GSE125989) to verify the FRG, which contained 16 primary BC and 16 matched BCBM tissues. The primary goal was to verify the expression profiles of FRG between BC and BCBM tissues, and explore the ferroptosis-related cluster patterns and relations with TME. The second goal was to investigate the prognostic values of ferroptosis in BC patients with and without metastasis. The prognostic values of ferroptosis were validated in The Cancer Genome Atlas (TCGA) dataset by performing Kaplan-Meier survival analysis. In addition, the drug sensitivity was also assessed in patients from TCGA. The gene expression data in GSE125989 were provided in **Supplementary Table S3**, and TCGA data can be obtained online (https://portal.gdc.cancer.gov/). The overall design of this study was seen in **Figure 1**.

Statistical Analysis

Wilcoxon test was used to compare gene expression differences between BC and BCBM tissues. Univariate and multivariate Cox regression analyses were used to evaluate the correlation between the genes and OS, RFS. Log-rank test was used to compare the survival differences, and Kaplan-Meier curves were implemented to visualize the survival. Mann-Whitney test with *p* values adjusted by the BH method was used to compare the ssGSEA scores of immune cells or pathways between the two groups. Spearman correlation analysis was used to evaluate the interactions. All the statistical analyses were done using the R software (version 4.0.3). $p < 0.05$ was set as statistically significant.

RESULTS

GSE10893 contained 275 samples from primary breast cancer tissues and 35 metastatic tissues measured by microarray, and they were sequenced on different platforms. To reduce the heterogeneity and we selected the samples on the GPL1390 ($n = 185$). We exclude eight normal samples, and 49 samples without clinical information. A total of 128 samples with gene expression profiles and clinical information were downloaded from the GSE10893, including 6 BCBM samples and 122 BC

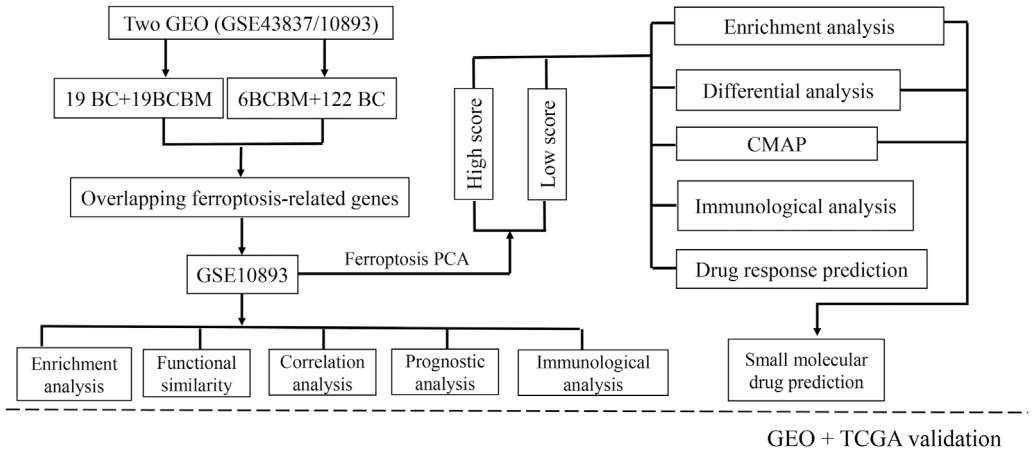

FIGURE 1 | Flowchart of the study design. BCBM: breast cancer brain metastasis; BC: breast cancer; GO: Gene Ontology; KEGG: Kyoto Encyclopedia of Genes and Genomes; PPI: protein-protein interaction; CMAP: Connectivity Map; GEO: Gene Expression Omnibus; TCGA: the Cancer Genome Atlas.

TABLE 1 | Significantly differentially expressed FRG in BC and BCBM tissues.

Gene	logFC	t	B	FDR	*p* Value
DPP4	−1.824	−3.753	0.317	0.039	0.000
HMOX1	−1.130	−2.251	−3.608	0.330	0.026
GLS2	−0.911	−3.063	−1.696	0.208	0.003
CD44	−0.677	−2.276	−3.558	0.324	0.025
ACO1	−0.663	−2.384	−3.331	0.295	0.019
ALOX5	−0.658	−2.293	−3.521	0.320	0.023
KEAP1	−0.476	−2.495	−3.089	0.257	0.014
LPCAT3	0.371	2.220	−3.666	0.301	0.020
G6PD	0.437	2.091	−3.922	0.386	0.038
CS	0.459	2.759	−2.473	0.189	0.007
PEBP1	0.509	2.303	−3.501	0.317	0.023
FDFT1	0.638	2.406	−3.282	0.288	0.018
HSBP1	0.742	2.715	−2.579	0.200	0.008
TFRC	0.977	2.545	−2.976	0.191	0.007

BC: breast cancer; BCBM: breast cancer brain metastasis; LogFC: log fold change; FDR: false discovery rate; t: t-test statistics; B: regression coefficient.

samples. GSE43837 contained 19 BC and matched 19 BCBM tissues, and 57 FRG were obtained from this dataset (**Supplementary Table S4**). A total of 14 overlapping FRG were identified. Among them, 7 genes were significantly upregulated in the BCBM compared with BC tissues, and 7 genes were significantly downregulated (**Table 1**).

Gene Interaction Network and Enrichment Analysis

We firstly investigated the 14 FRG interactions through the "corrplot" R package (**Figure 2A**). The results showed ALOX5 and DDP4 had the strongest positive correlation (r = 0.53), implying they were synergetic contributors to the genetic architecture of ferroptosis, and resulted in the susceptibility of breast cancer. While the HMOX1 and PEBP1 had the strongest negative correlation (r = −0.45), implying they exerted the opposite effects on the ferroptosis (**Figure 2B**).

Then, we performed the GO enrichment analysis using the 1660 SDG, which showed the SDG were enriched in the iron homeostasis and iron-related transition pathways. In the BP process, they were strongly associated with iron ion homeostasis. In the CC and MF processes, the SDG were enriched in the lamellipodium membrane and virus receptor activity (**Figure 2C**). KEGG enrichment analysis showed that these SDG were significantly enriched in the ferroptosis and metabolic activities (**Figure 2D**).

Based on the GO analysis and semantic similarities, we ranked the FRG by average functional similarities between every gene and their partners, with the cut-off value of 0.75. The box plots and raincloud plots were demonstrated in **Figures 2E,F**. The results implied the HMOX1 and ACO1 had significant similarities, suggesting they functioned consistently.

Prognostic FRG for OS and RFS

To investigate the prognostic values of FRG, we performed survival analysis. We found that HMOX1 and PEBP1 were significantly associated with OS (p = 0.035, 0.017 respectively). However, they were not significantly statistical in the multivariate Cox regression analysis (p > 0.05). For RFS, the KEAP1 and LPCAT3 had significant prognostic values in the multivariate cox regression (p = 0.002, 0.008 respectively) (**Table 2**).

According the median of the risk score (risk score = $\sum_{n=1}^{j} Coef\,j * Xj$, risk score for OS = 0.581 * expression level of HMOX1 + −0.650 * expression level of PEBP1; risk score for RFS = −0.295 * expression level of KEAP1 + 0.930 * expression level of LPCAT3), patients were stratified into high- and low-risk groups respectively. Then, we combined the clinical information with gene expression levels to explore the independent risk factors. In the univariate cox analysis, we found that lymph node number, tumor grade, tumor size and risk score were significantly associated with OS (all p < 0.05) (**Figure 3A**). Moreover, the multivariate cox regression showed the tumor size was the only independent risk factor for OS (HR = 2.588, p = 0.005) (**Figure 3B**). For RFS, the ER, PgR status, lymph node

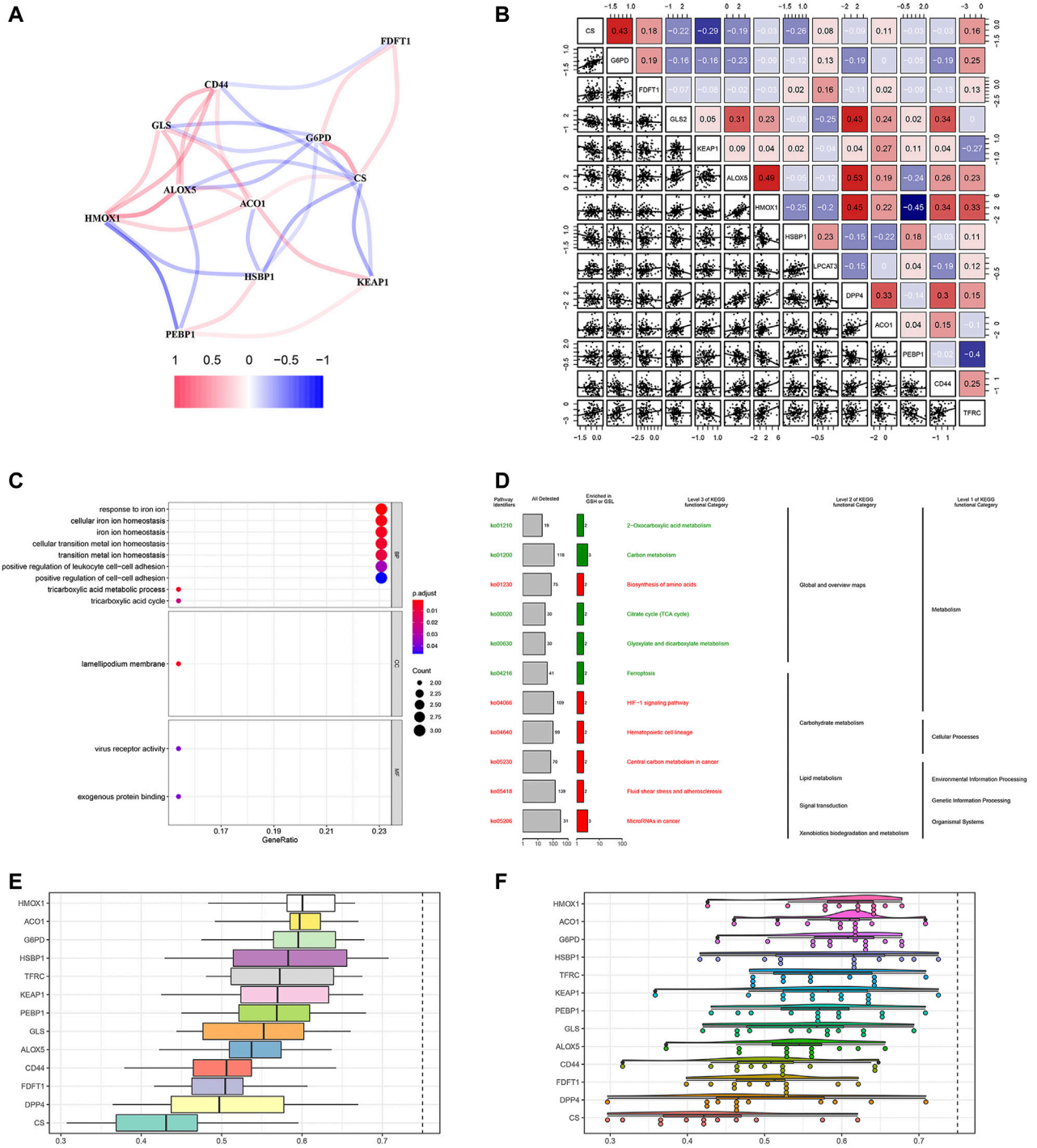

FIGURE 2 | Gene correlation network and enrichment analysis. **(A)** The correlation network of FRG. The correlation coefficients are represented by different colors, in which red lines represent positive correlation, while negative in blue. **(B)** Gene interaction analysis. The correlations were represented in the data. **(C)** GO analysis results showed FRG were enriched in the iron homeostasis and ferroptosis-related pathways. **(D)** KEGG enrichment demonstrated metabolic activities and ferroptosis. **(E)** Summary of FRG similarities. The boxes indicated the middle 50% of the similarities; and the upper and lower boundaries show the 75th and 25th percentile. **(F)** Raincloud plots of OGG. Data were shown as the mean and standard error. Each dot represented a single gene. The dashed line represents the cutoff value (0.75).

number, tumor grade, tumor size and risk score were significantly associated with RFS (all $p < 0.05$) (**Figure 3C**). And the multivariate cox regression results showed that tumor size and risk score were independent risk factors for RFS in breast cancer patients (HR = 2.209, $p = 0.007$; HR = 1.251, $p < 0.001$ respectively) (**Figure 3D**).

TABLE 2 | cox regression analysis of OS and RFS in breast cancer patients.

Gene	Univariate cox regression			Multivariate cox regression		
	HR	95%CI	P	HR	95%CI	*P*
HMOX1[a]	2.100	1.054–4.186 0.035	1.788	0.906–3.526	0.094	—
PEBP1[a]	0.421	0.207–0.858	0.017	0.522	0.241–1.130	0.100
KEAP1[b]	0.722	0.595–0.875	<0.001	0.745	0.616–0.900	0.002
LPCAT3[b]	2.152	1.106–4.187	0.024	2.536	1.281–5.018	0.008

HR: hazard ratio; CI: confidence interval.
[a]*Genes related OS.*
[b]*Genes related RFS.*

Next, we examined the predictive abilities using the risk score. By evaluating the area under curves (AUC), we found that risk score had excellent ability to discriminate the OS between the high- and low-risk groups (p = 0.015). Similarly, we found that risk score also demonstrated good predictive abilities to predict RFS. However, the difference was not statistical (p = 0.167). The results are visualized in **Figures 3E,F**.

Prognostic Hazard Curves in High- and Low-Risk Patients

Ninety-one primary breast cancer patients were divided into high- and low-risk patients (n = 46, 45, respectively) according to the median of the risk score (Thirty-six patients' information were incomplete and one brain metastasis patient was excluded). The

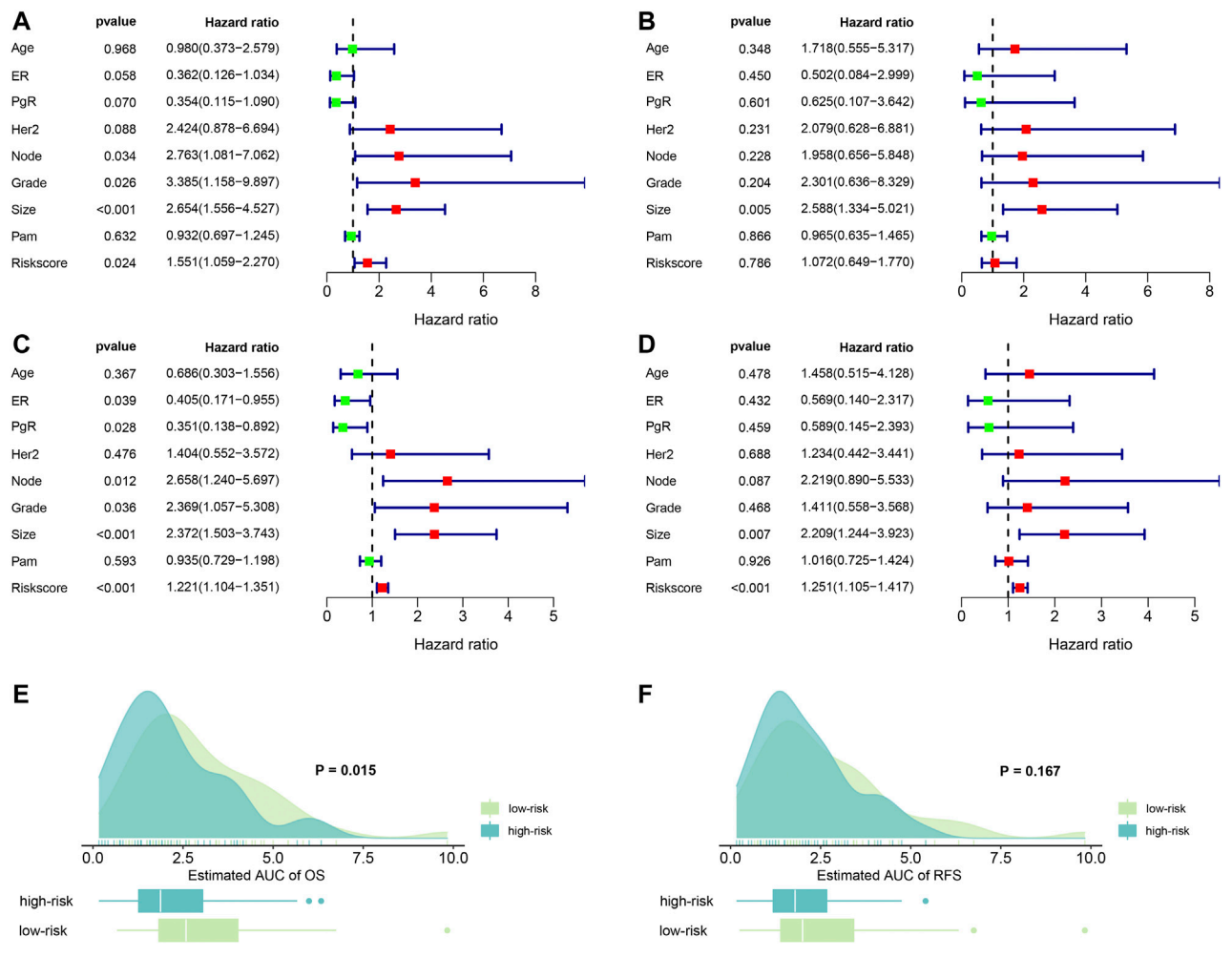

FIGURE 3 | Forest plots of independent risk factors and survival prediction. **(A)** univariate Cox regression analysis for OS. **(B)** Multivariate Cox regression analysis for OS. **(C)** Univariate Cox regression analysis for RFS. **(D)** multivariate Cox regression analysis for RFS. **(E)** OS prediction of the estimated AUC using the risk score. **(F)** RFS prediction of the estimated AUC using the risk score. ER: estrogen receptor; PgR: progesterone receptor; node: lymph node number; Grade: tumor grade; size: tumor size; PAM: a classification method.

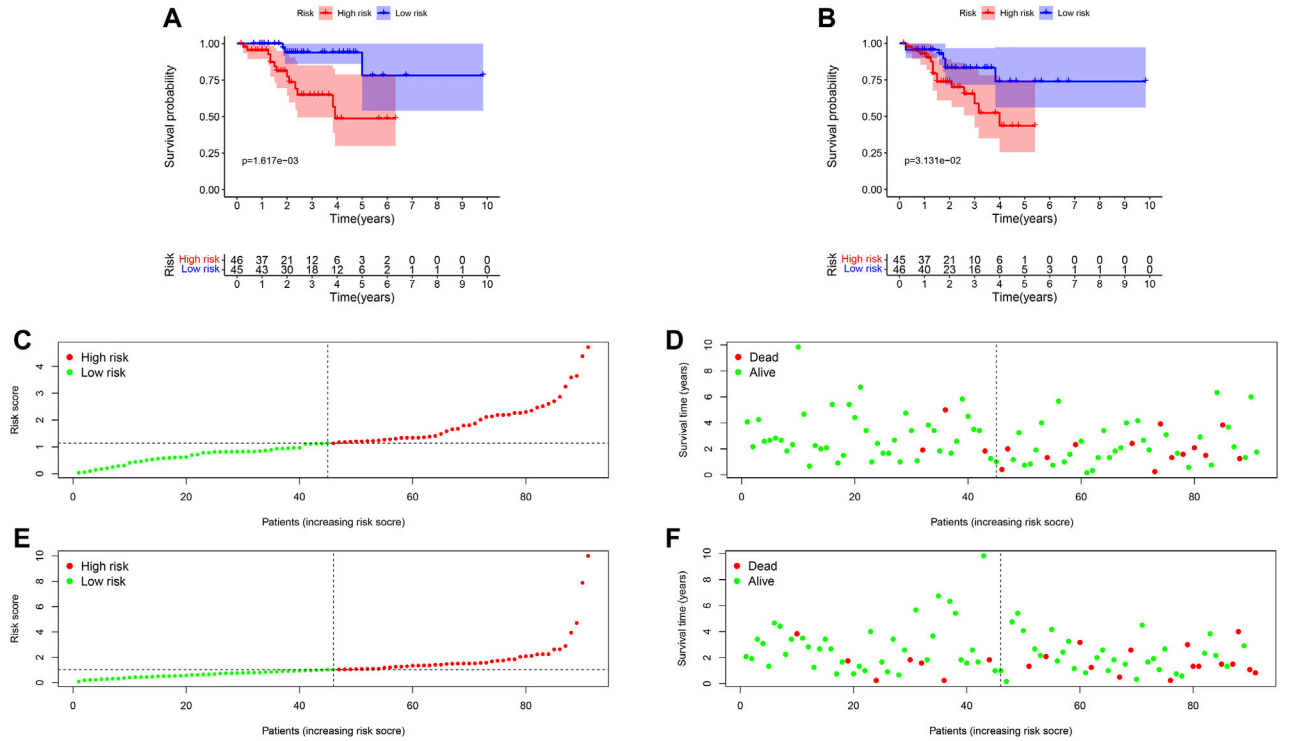

FIGURE 4 | Survival comparison and risk score hazard analyses of high- and low-risk groups in breast cancer patients. **(A)** K-M curve for OS; The result showed the survival status is significantly different between the two groups (p = 0.004). **(B)** K-M curve for RFS; High-risk groups patients had worse RFS than that in the low-risk group (p = 0.021). **(C)** Risk score hazard curve for OS. The dotted line indicated the individual inflection point of the risk score curve, by which the patients were categorized into low- and high-risk groups. Red represented high-risk and green represented low-risk. **(D)** Risk score scatters plot of OS in high and low-risk groups. Red dots represented the dead patients and green represented the alive. With the increase of risk scores, more patients died. **(E)** Risk score hazard curve for RFS. **(F)** Scatter plot of patients for RFS.

Kaplan-Meier (K-M) curve showed that patients with high-risk score had a significant higher death probability than those with low-risk (median time = 1.333 vs. 3.417 years, p = 0.002) for OS (**Figure 4A**). Similarly, patients in high-risk score group had worse RFS than those with low-risk scores (median time = 1.250 vs. 3.083 years, p = 0.031) (**Figure 4B**). In addition, we performed prognostic hazard analysis between high- and low-risk score groups. The results showed that as the risk score increased, the patients' death risk increased, and the survival time decreased (**Figures 4C–F**).

Ferroptosis Is Correlated With Clinical Characteristics

In order to assess whether ferroptosis was correlated with patients' clinical information, we calculated statistical differences between the 14 FRG and clinical features using the t-test or Kruskal-Wallis test. The results demonstrated that ACO1, DPP4, HMOX1, and TFRC were significantly associated with breast cancer grades (all $p < 0.05$). As the tumor grade increased, DPP4, HMOX1, and TFRC expression levels also increased. The results suggested these genes may be significant contributors to tumor grade, and inhibiting their expressions may control the increase of tumor grade. While, the ACO1 was the opposite. The result suggested ACO1 was a negative contributor of tumor grade, and increasing the ACO1 expression may play the protective role of tumor grade. The ACO1, FDFT1, DPP4, HMOX1, and TFRC were closely associated with patients' ER and PgR status (all $p < 0.05$). Moreover, we also found CD44 and PEBP1 were significantly correlated with Her2 status in patients with BC (all $p < 0.05$). The details were shown in **Figures 5A–O**.

Effects of Ferroptosis on Breast Cancer Subtypes

To further evaluate the effects of ferroptosis on breast cancer subtypes, we systematically investigated the relations between breast cancer subtypes and ferroptosis, and compared the FRG expression profiles differences. According to the Her2, ER, and PgR expressions, we divided patients into HER2-enriched, triple-negative breast cancer (TNBC) and other subtypes (n = 8, 28, 55, respectively). The FRG expression levels of the three subtypes were shown in **Supplementary Figure S1**. Next, we investigated the prognostic values of FRG in the TNBC and other subtypes (HER2-enriched subtype was not performed survival analysis due to the small sample number.). The results showed that ACACA (HR = 7.917, p = 0.041) and DPP4 (HR = 0.535, p = 0.040) were independent prognostic factors for OS in patients with HER2-enriched subtype. GSS (HR = 0.541, p = 0.046) and HMOX1 (HR = 2.184, p = 0.031) were independent prognostic factors for OS in patients with other subtypes (**Supplementary Figure S2**).

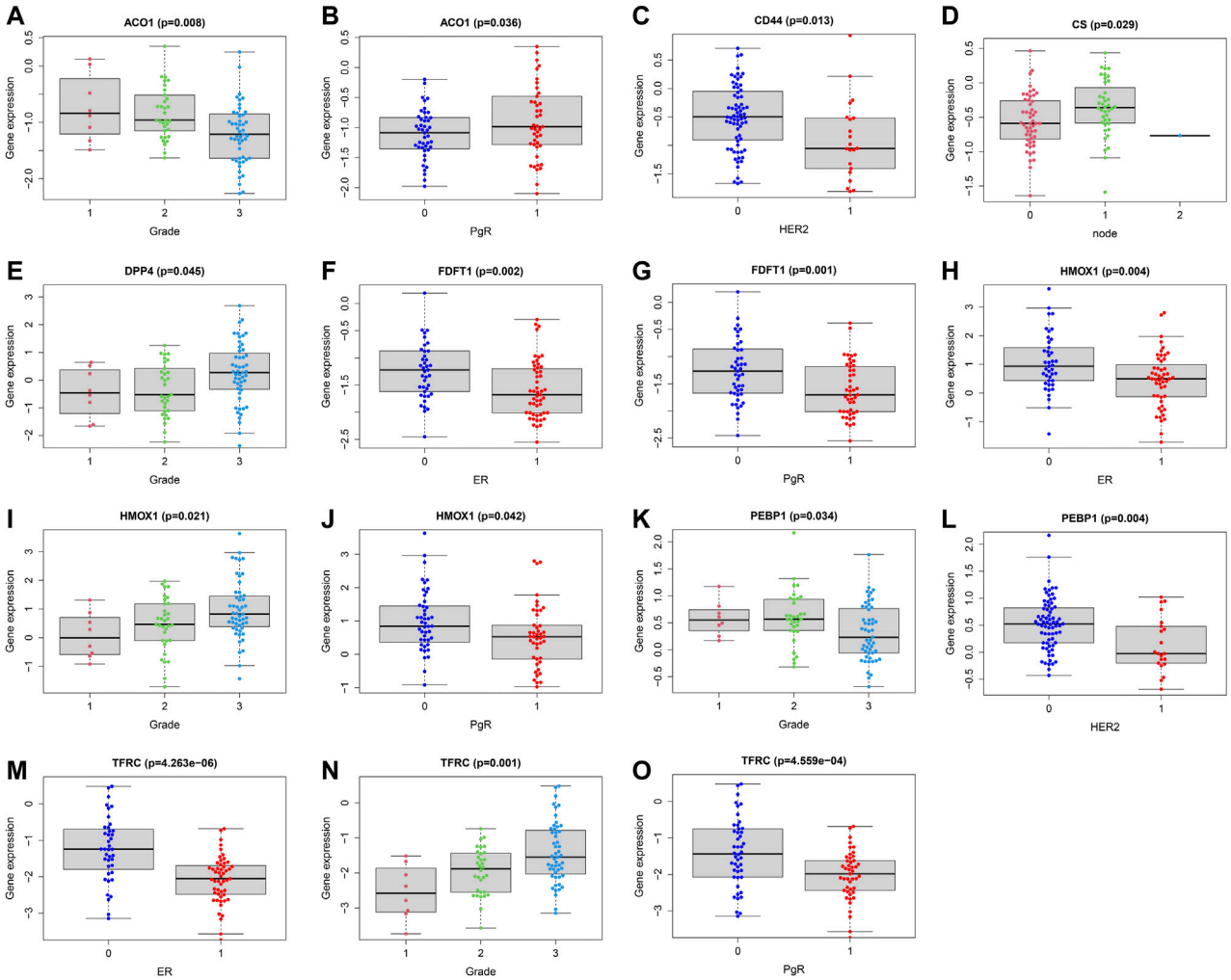

FIGURE 5 | Correlations analysis between FRG and patients' clinical characteristics. Correlations between ACO1 and tumor grade **(A)** and PgR **(B)**. Correlations between CD44 and HER2 **(C)**. Correlations between CS and lymph nodes **(D)**. Correlations between DPP4 and tumor grade **(E)**. Correlations between FDFT1 and ER **(F)** and PgR **(G)**. Correlations between HMOX1 and ER **(H)**, tumor grade **(I)** and PgR **(J)**. Correlations between PEBP1 and tumor grade **(K)** and HER2 **(L)**. Correlations between TFRC and ER **(M)**, tumor grade **(N)** and PgR **(O)**. ER (1 = positive; 0 = negative); PgR (1 = positive; 0 = negative); HER2 (1 = positive; 0 = negative); node status (1 = positive; 1 = 2 or more nodes+; 0 = negative); size (1 = ≤2 cm; 2 = 2-5 cm; 3 = >5 cm; 4 = any size with direct extension to chest wall or skin).

Then, we calculated the correlations between FRG and clinical features in patients with the three subtypes. For HER2-enriched subtype, KEAP1 was significantly associated with breast cancer grade and lymph node metastasis (all $p < 0.05$) (**Supplementary Figure S3**). For TNBC, CD44, FDFT1, G6PD, and GLS2 were significantly associated with breast cancer grade (all $p < 0.05$). G6PD was significantly associated with breast cancer grade lymph node metastasis ($p = 0.021$) (**Supplementary Figure S4**). For other subtypes, CS and PEBP1 were significantly associated with breast cancer size (all $p < 0.05$). GLS2 and PEBP1 were significantly associated with breast cancer grade (all $p < 0.05$) (**Supplementary Figure S5**).

Ferroptosis and Immune Status

To explore the relationships between FRG and immune cells and immune functions, we quantified the 16 immune cell subtypes and 13 immune functions by "ssGSEA" package in R software. We found the FRG had significant effects on the content of immune cells and immunological functions, especially the aDCs, B cells, iDCs, neutrophils, Tfh, Th2, TIL (all $p < 0.05$) (**Figure 6A**). Additionally, the antigen presentation process, including APC co-inhibition, APC co-stimulation, HLA, IFN response were significantly influenced by different FRG (all $p < 0.05$).

The tumor microenvironments (including immune cells) are responsible for tumor metastasis and patients' survival (Arslan et al., 2010; Bates et al., 2018). To fully explore relationships between FRG and immune, we selected the four prognostic genes (HMOX1, PEBP1, KEAP1, LPCAT3) and performed the Spearman correlation analysis by "limma" package. The results showed the HMOX1 was strongly associated with Th2 cells, and chemokine receptors (CCR) (all $p < 0.05$) (**Figure 6B**). KEAP1 had a close relationship

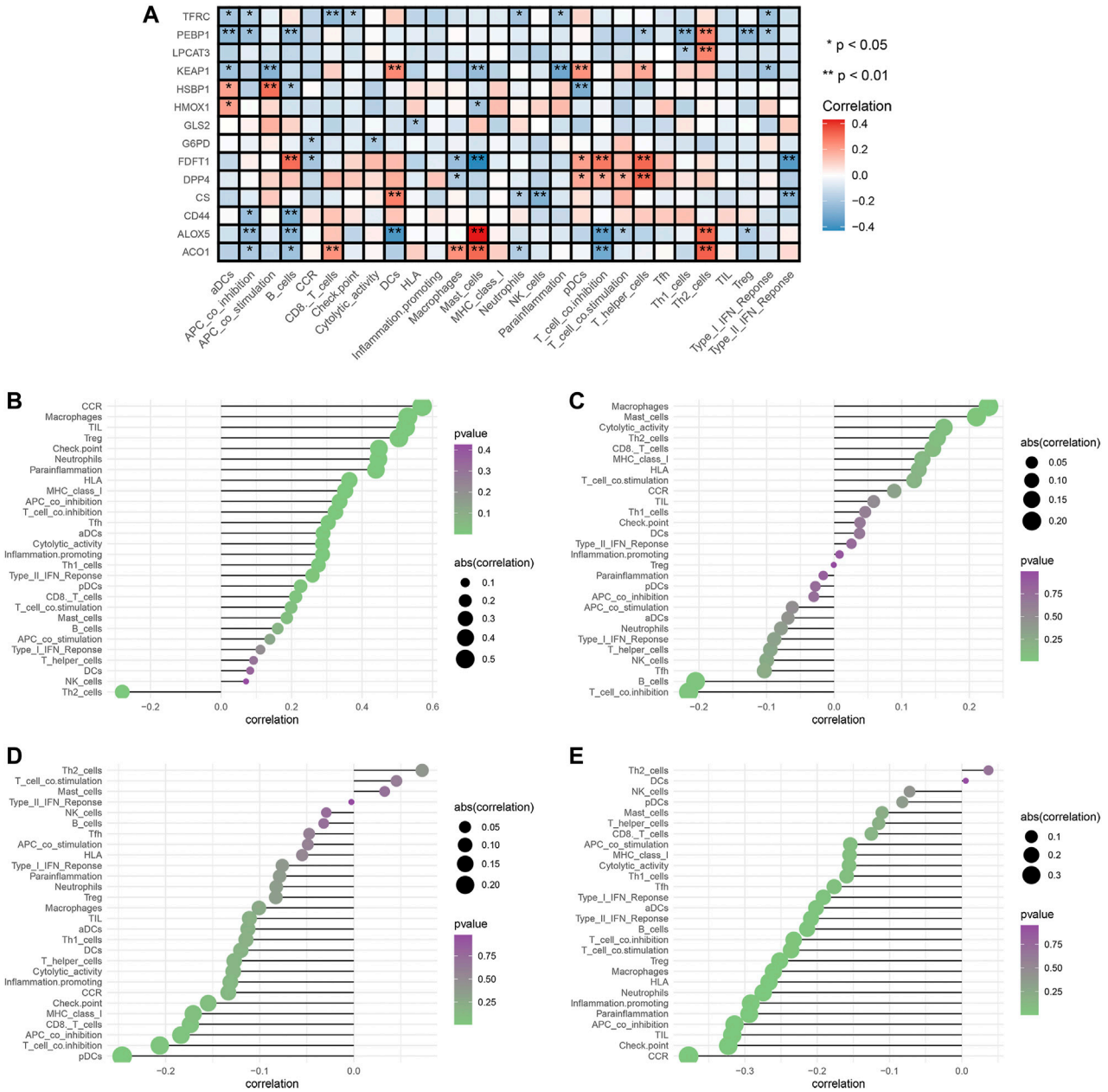

FIGURE 6 | Analysis of ferroptosis-related genes effects on immune signatures. **(A)** Heatmap was demonstrating the correlation between 14 genes and the ssGSEA scores of 29 immune signatures. **(B)** HMOX1 and immune signatures. **(C)** KEAP1 and immune signatures. **(D)** LPCAT3 and immune signatures. **(E)** PEBP1 and immune signatures. Spearman correlation analysis was used to evaluate the relations with $p < 0.05$. *$p < 0.05$; **$p < 0.01$. DCs: dendritic cells, iDCs: immature DCs, pDCs: plasmacytoid dendritic cells, TIL: tumor infiltrating lymphocyte, CCR: cytokine-cytokine receptor, APC: antigen presenting cells.

with macrophages and T cell co-inhibition (all $p < 0.05$) (**Figure 6C**). LPCAT3 showed close relationships with Th2 cells and pDCs (all $p < 0.05$) (**Figure 6D**). PEBP1 exhibited significant associations with Th2 cells and chemokine receptors (CCR) (all $p < 0.05$) (**Figure 6E**). Collectively, these findings suggested that FRG were accompanied by changes in immune cell contents and immunological functions.

Ferroptosis-Related Cluster Patterns and Relations With TME

We identified two different clusters through the consensus cluster analysis in patients with BC (cluster 1: $n = 45$; cluster 2: $n = 77$), and patients in clusters 1 and cluster 2 had different consensus matrices (**Figure 7A**). To obtain quantitative indicators of cluster 1 and 2, we further probed into the ferroptosis implications by the

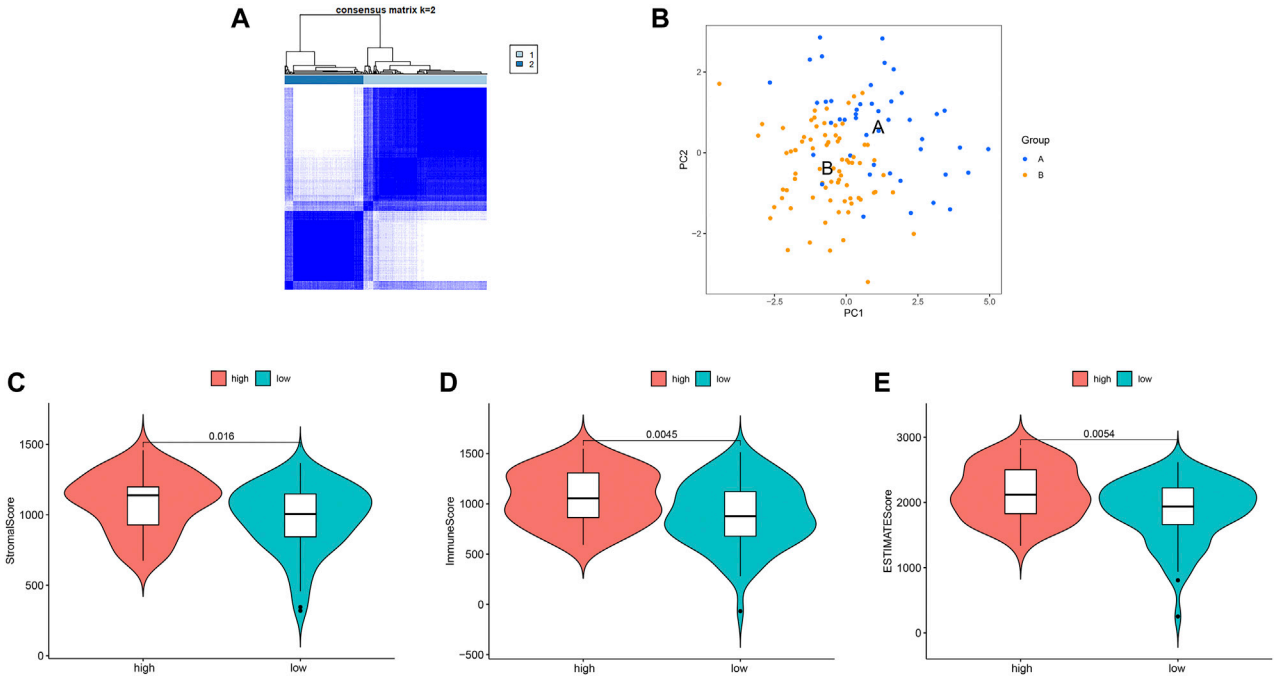

FIGURE 7 | Ferroptosis clusters and correlations with the tumor microenvironment. **(A)** Results obtained from consensus clustering identified two different clusters, namely cluster 1, and 2. **(B)** Two-dimensional plots of two groups with the top two principal components, in which blue dots represented group A, and orange dots represented group B. **(C)** Patients in high-ferroptosis had higher stromal score, immune score and ESTIMATE score, as shown in **(C–E)** respectively.

PCA, and patients were classified into group A and group B (n = 45, n = 77 respectively) (**Figure 7B**). Each patient in group A and group B was computed as the sum of individual relevant individual scores. Next, the ferroptosis score was defined as group A subtracts group B. Patients were stratified into high- or low-ferroptosis according to the median of ferroptosis score. Our data showed that patients with high-ferroptosis scores had significantly higher stromal score, immune score and ESTIMATE score compared with those in group B (**Figures 7C–E**, respectively), indicating the ferroptosis had dramatic influences on TME features.

Drug Sensitivity Analysis

We compared the IC50 differences of 12 targeted and chemotherapeutic agents, including the Cisplatin (**Figure 8A**), Dasatinib (**Figure 8B**), Etoposide (**Figure 8C**), Gefitinib (**Figure 8D**), Lapatinib (**Figure 8E**), Pazopanib (**Figure 8F**), Sorafenib (**Figure 8G**), Sunitinib (**Figure 8H**), Vorinostat (**Figure 8I**), Docetaxel (**Figure 8J**), Vinorelbine (**Figure 8K**), and Doxorubicin (**Figure 8L**). Our results demonstrated that the IC50 levels of Cisplatin, Dasatinib, Etoposide, Gefitinib, Lapatinib, Pazopanib, Sunitinib, Docetaxel, and Vinorelbine were higher in the low-ferroptosis score group, indicating patients with high-ferroptosis scores were more sensitive to these drugs. Oppositely, the IC50 of Sorafenib, Vorinostat and Doxorubicin was higher in the high-ferroptosis score group, indicating that patients in the low-ferroptosis group were more sensitive to the three drugs.

Potential Small Molecular Compounds

To screen the potential small molecular compounds that may target patients with BC, we further analyzed the SDG between high- and low-ferroptosis groups. There were 1183 SDG with the FDR <0.05, including the 522 up-regulated and 661 down-regulated genes. The volcano plot and heatmap were visualized in **Figures 9A,B**. GO enrichment analysis showed the SDG were significantly associated with ion transmembrane transport, potassium and cation transmembrane transport pathways (**Figure 9C**). KEGG results showed the SDG were strongly associated with MAPK, Ras, and Rap1 signal pathways (**Figure 9D**). Then, the up- and down-regulated genes were uploaded into the CMap database. A total of 29 small molecular compounds and 30 mechanisms were identified (**Figures 9E,F**, respectively). The details of the small molecular compounds were provided in **Supplementary Table S5**.

Ferroptosis and Other Metastatic Sites in Patients With Breast Cancer

To explore whether ferroptosis has any effects on other metastatic sites of breast cancer, we analyzed the FRG expression profiles in lung metastasis and lymph nodes metastasis in GSE10893. There are four lung metastasis samples, nine lymph nodes samples and 67 breast cancer samples in GPL887 in GSE10893. The results demonstrated that MT1G, SQLE, NQO1, and GOT1 were significantly differently expressed between BC and lung metastasis (all $p < 0.05$). In addition, HSBP1, FTH1, and ACSF2 expression levels were significantly different in lymph nodes metastasis sites compared to BC (all $p < 0.05$). The details can be seen in

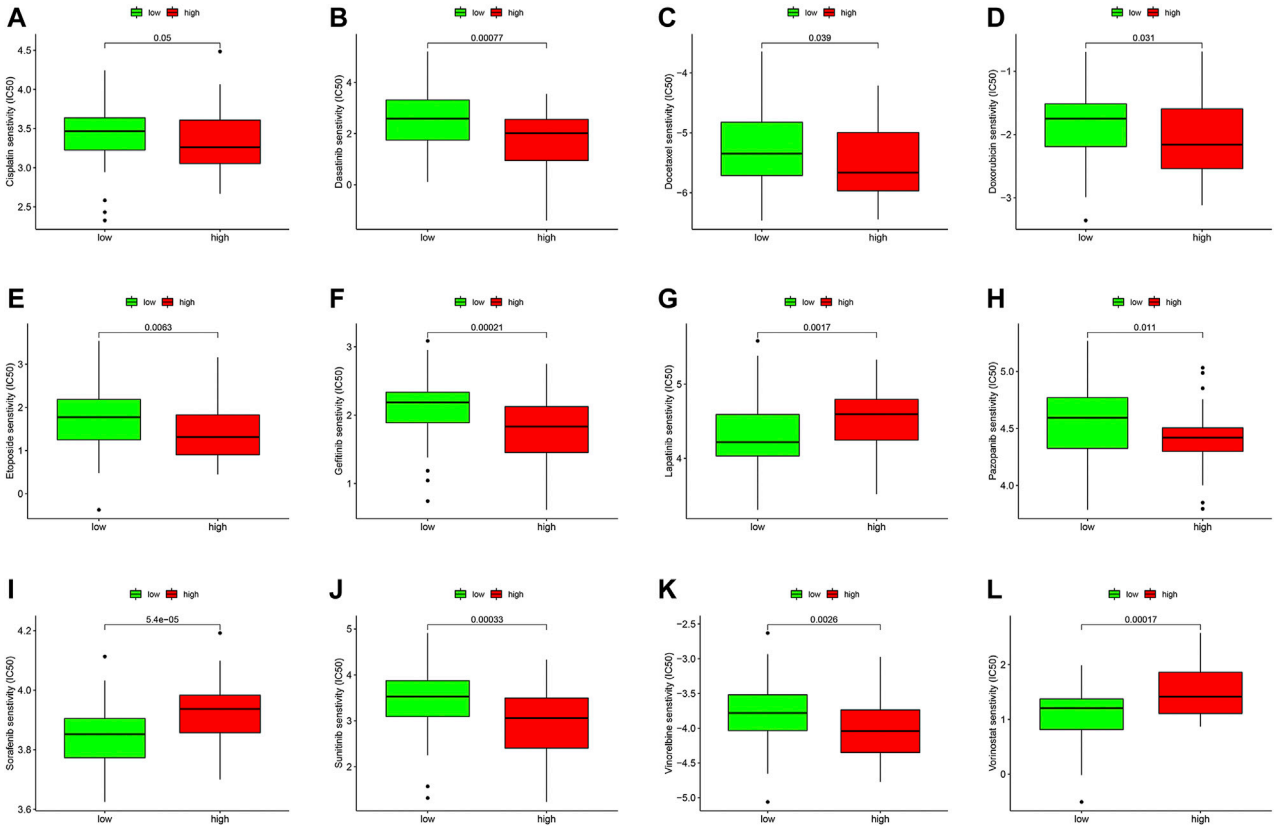

FIGURE 8 | Drug sensitivity analysis between the high- and low-ferroptosis groups. Box plots demonstrated the differences of IC50 in Cisplatin **(A)**, Dasatinib **(B)**, Etoposide **(C)**, Gefitinib **(D)**, Lapatinib **(E)**, Pazopanib **(F)**, Sorafenib **(G)**, Sunitinib **(H)**, Vorinostat **(I)**, Docetaxel **(J)**, Vinorelbine **(K)**, and Doxorubicin **(L)**. The lower the IC50, the more sensitive the drug is.

Supplementary Table S6. These finding suggested that the occurrences of lung metastasis and lymph nodes metastasis are companied by a small amount of aberrant FRG expressions.

External Validation of FRG and Survival Analysis

We verified the ferroptosis-related genes using another dataset (GSE125989) from GEO, which contained 16 primary BC and 16 matched BCBM tissues. A total of 55 FRG were obtained, and 14 intersection genes were overlapped among the three datasets (GSE10893, GSE43837, and GSE125989) (**Figure 10A**). Then, to further validate the discriminative abilities of ferroptosis for BC stratification, we performed the PCA analysis and explored the ferroptosis-related cluster patterns and relations with TME. Consistent with the above results, PCA exhibited good ability to classify BCBM patients based on the ferroptosis-related genes expressions (**Figure 10B**). In addition, **Figure 10C** demonstrated that patients with high-ferroptosis scores had significantly higher stromal score, immune score and ESTIMATE score in TME, and these results were in line with the above results from GSE10893.

Furthermore, the practicability of the ferroptosis score was validated in TCGA database. Firstly, we classified breast cancer patients into metastasis group and non-metastasis group ($n = 22$, $n = 906$, respectively). Next, we calculated the ferroptosis score for each patient by the method described above, and compared the survival differences between high- and low-ferroptosis score groups. In the metastasis group, the K-M plot showed that patients in the low-ferroptosis group had higher survival probabilities compared to those in high-ferroptosis group ($p < 0.001$) (**Figure 10D**). Similarly, in the non-metastasis group, patients in the low-ferroptosis score group had better survival than those in the high-ferroptosis score group ($p < 0.001$) (**Figure 10E**).

In addition, the drug sensitivity was also evaluated in patients from TCGA. In line with the results from GEO, the data demonstrated that patients in the high-ferroptosis score group had lower IC50 of Cisplatin (**Figure 10F**), Gefitinib (**Figure 10G**) and Sunitinib (**Figure 10H**). However, patients in the low-ferroptosis score group had lower IC50 of Lapatinib (**Figure 10I**), indicating these patients were more sensitive to Lapatinib.

DISCUSSION

Cell death is of vital importance for normal development, physiological homeostasis and excessive proliferation, such as tumors. Tumor cells exhibit more iron demand than normal cells. Ferroptosis is a newly recognized, iron-dependent form of cell death

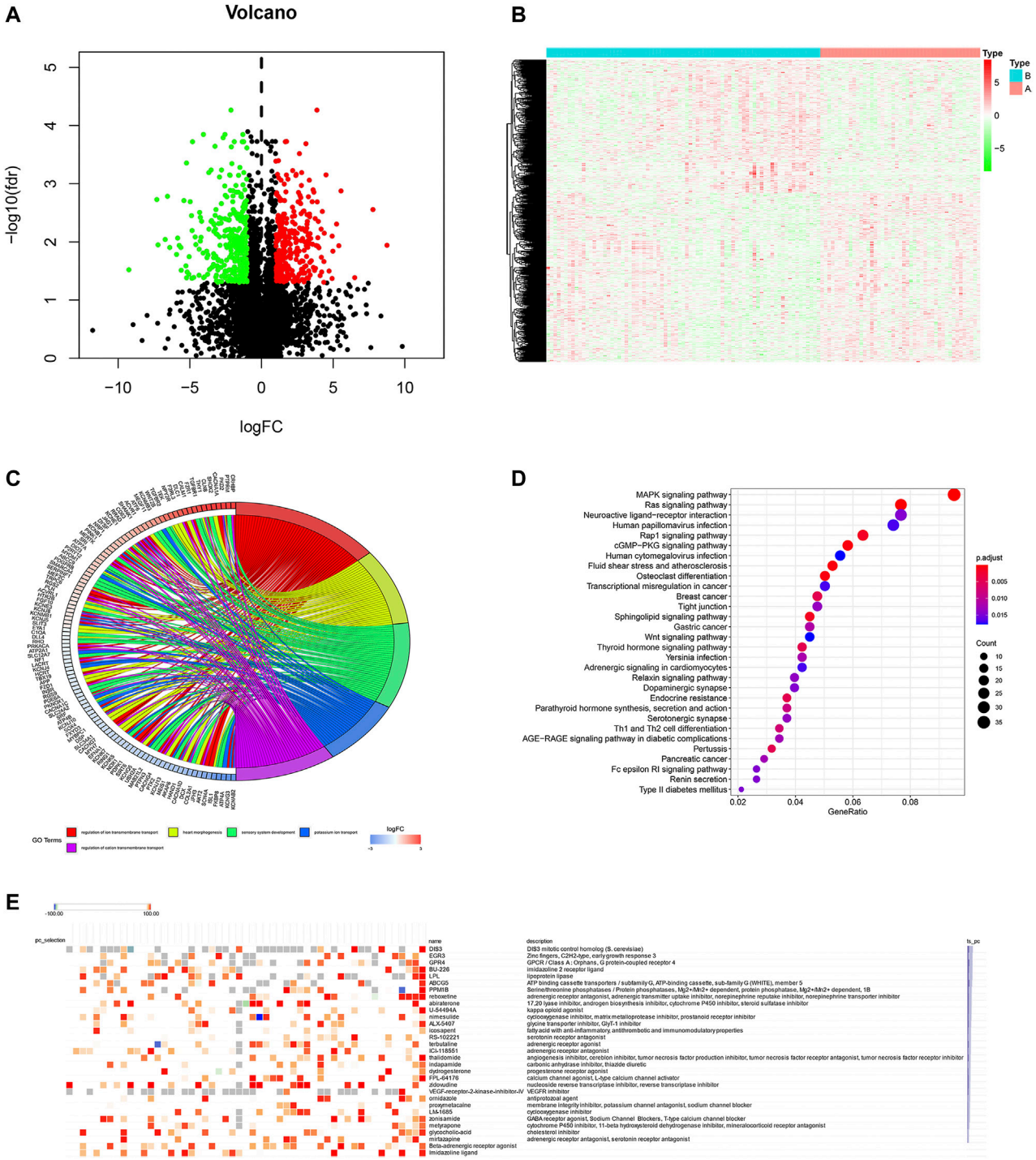

FIGURE 9 | Potential small molecule compounds based on the ferroptosis. **(A)** The volcano plot demonstrated the up-regulated genes (red dots) and down-regulated genes (green dots). **(B)** Heatmap showed the SDG expression profiles between high- and low-ferroptosis score groups. **(C)** GO circle plot showed the enrichment analysis results ranked by logFC and FDR. **(D)** KEGG enrichment analysis revealed the possible pathways and mechanisms. **(E)** Small molecular compounds and possible mechanisms. The results were downloaded from the CMap website.

by Dixon and colleagues in 2012, which shares none of the characteristics of morphology, biochemistry and functions associated with necrosis, apoptosis and autophagy (Dixon et al., 2012). It's increasingly evident that ferroptosis has been linked to various cancers, especially cancers from iron-rich tissues such as the brain (Zille et al., 2019; Zhang et al., 2021). Studies have demonstrated that altered iron metabolism is correlated closely with the prognosis of breast cancer patients (Shen et al., 2018; Yu et al., 2019a; Nagpal et al.,

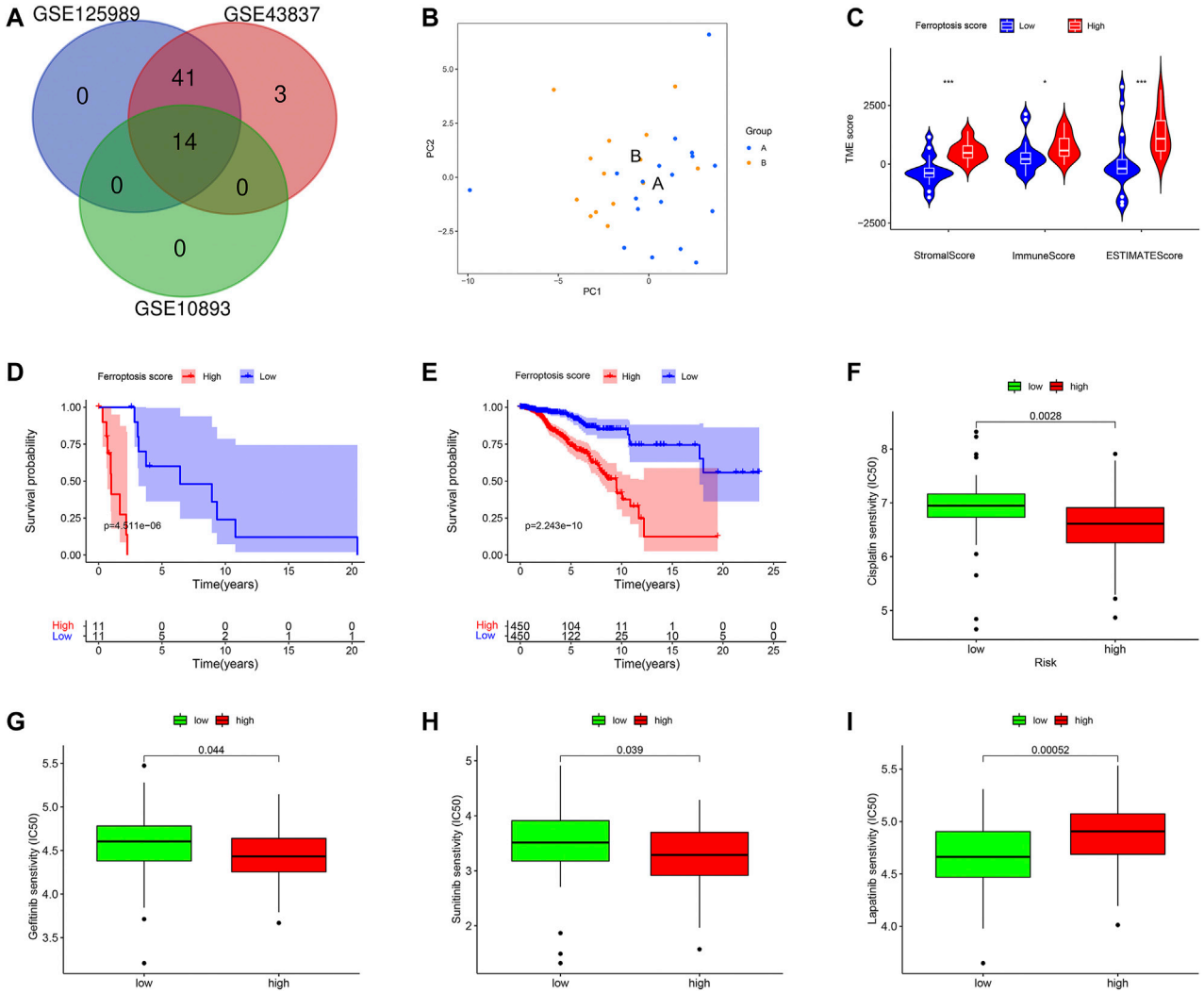

FIGURE 10 | External validations based on ferroptosis. **(A)** The venn graph demonstrated there were 14 intersection FRG among the three datasets. **(B)** Principal component analysis to classify patients with BCBM according to the ferroptosis. **(C)** Patients in high-ferroptosis had higher stromal score, immune score and ESTIMATE score. **(D)** K-M survival plot for patients with high- and low-ferroptosis scores in metastatic group. **(E)** K-M survival plot for patients with high- and low-ferroptosis scores in non-metastatic group. Drug sensitivity analysis of Cisplatin **(F)**, Gefitinib **(G)**, Sunitinib **(H)**, and Lapatinib **(I)**.

2019). In addition, ferroptosis could promote tumor metastasis in some cancers (Boult et al., 2008; Ferroptosis Is Inhibited, 2020). Considering the evidence above, it's reasonable to hypothesize that ferroptosis may be involved in the process of BCBM through an unknown mechanism. Therefore, we explored the roles of ferroptosis in BCBM using large public database by bioinformatics analysis. In this study, we found 14 differently expressed ferroptosis-related genes between the BC and BCBM tissues. Functional enrichment analysis showed these genes were closely associated with the iron ion homeostasis and ferroptosis-related activities. Moreover, TME analysis implied that ferroptosis had intimate crosstalk with immunity and drug sensitivity. Further, survival analysis suggested ferroptosis had prognostic values in predicting patients' survival.

Despite several studies have investigated the roles of ferroptosis in BC, the underlying mechanisms between ferroptosis and BC cells remain elusive, and the FRG expression profiles of BCBM is never explored (Ma et al., 2016; Yu et al., 2019a; Nagpal et al., 2019). Functional enrichment analysis in this study has demonstrated that ferroptosis may be involved in BCBM through disrupting the iron ion homeostasis. Iron metabolism is tightly associated with iron uptake, utilization, storage and export. High iron level gives rise to reactive oxygen species (ROS) and determines the sensitivity of cells to ferroptosis (Brown et al., 2020; Chen et al., 2020). Subsequently, iron-induced oxidative stress could promote the metastasis initiation possibly through the following mechanisms: 1) modifying the genome, epigenome, leading to the tumor heterogeneity and metastatic abilities; 2) remodeling the extracellular matrix (ECM), which increases the matrix metalloproteinases (MMPs) expression, such as matrix metalloproteinases-9 (MMP-9) that facilitates the metastasis; 3) modulating the tumor microenvironment by restraining the

immune response and stimulating the angiogenesis to enable the cancer cell mobility and invasion; 4) changing the metabolic plasticity of cancer cells to compete for and utilize more energy for surviving longer and metastasis; 5) interacting with the secondary site by releasing some signals, such as exosomes to establish a pre-metastatic niche (Kaomongkolgit et al., 2008; Akatsuka et al., 2012; Torti and Torti, 2013a; Torti and Torti, 2013b; Brown et al., 2020). In fact, cancer cells which are prone to metastasis are often highly susceptible to ferroptosis (Hangauer et al., 2017). Consistent with previous findings, our enrichment analysis also showed the iron homeostasis played vital role in the development of breast cancer cells metastasize to the brain. The result highlights the significance of ferroptosis in BCBM and represents a potential approach to prevent metastatic disease.

The FRG signatures proposed in the present study was composed of 14 genes, which could be generally classified into 4 categories, including iron metabolism (ACO1, HMOX1, TFRC), lipid metabolism (ALOX5, CS, LPCAT3, GPX4, PEBP1, FDFT1, PEBP1), (anti)oxidant metabolism (KEAP1, HMOX1) and energy metabolism (GLS2, G6PD) (Stockwell et al., 2017; Hassannia et al., 2019). The correlation network showed the HMOX1 and TFRC were hub genes regulating ferroptosis. HMOX1, also known as HO-1 (heme oxygenase 1), could catalyze the degradation of heme to biliverdin and Fe^{2+}. The study showed that HMOX1 knockout could enhance ferroptosis (Adedoyin et al., 2018). The expression of HO-1 is significantly associated with distant metastasis, and predicts an unfavorable OS in patients with BC (Noh et al., 2013). Moreover, clinical correlation analysis showed the HO-1 expression is significant with histologic grade, which was in line with our result (Noh et al., 2013). In contrast to the evidence that the HO-1 expression promotes the ferroptosis (Noh et al., 2013), Li Q et al. demonstrated HO-1 could inhibit mammary tumor metastasis mediated by Notch1 pathway (Li et al., 2019). Hence, the elucidation of HMOX1 in breast cancer metastasis needs to be further investigated. TFRC refers to the transferrin receptor, which promotes ferroptosis by importing iron into cells and sparks ferroptotic cascade reaction ultimately. Notably, TFRC modulates the ROS generation and silencing of TFRC significantly inhibits ferroptosis (Stockwell et al., 2017; Hassannia et al., 2019). Consistent with the previous study, our result also showed the TFRC expression was lower in ER+ BC tissues than that in ER-tissues (Yu et al., 2019b). Therefore, it's conceivable that the activation degree of ferroptosis is different in ER+ and ER-tissues and this can partly explain why different subtypes of breast cancer have different abilities to metastasize to the brain.

The prognostic model constructed in our study identified KEAP1 and LPCAT3 were independent genes for RFS. Breast cancer patients in high- and low-risk groups exhibit significantly different prognoses ($p < 0.05$), implying risk score based on the FRG signatures has excellent ability to predict survival. Studies about molecular mechanisms revealed KEAP1 could bind to and regulate NRF2 (another ferroptosis-related gene), and its knockdown confers cells' resistance to ferroptosis (Hassannia et al., 2019). Cumulative evidence demonstrated KEAP1 is associated with worse prognoses in patients with BC, which is concordant with our results (Hartikainen et al., 2015; Almeida et al., 2019). In addition to predicting survival, KEAP1 could also render BC metastasis by interacting with other molecules, for instance, the TrkB and HBXIP (Kim et al., 2016; Zhou et al., 2019). LPCAT3 is a member of the lipid metabolism family, which incorporates acylated fatty acids into membranes and is involved in the biosynthesis of phospholipids (Stockwell et al., 2017; Hassannia et al., 2019). The LPCAT3 knockdown will suppress the ferroptosis (Stockwell et al., 2017). However, the role of LPCAT3 in BC is still in its early stages and much less has been uncovered. So, experimental models *in vitro* and *in vivo* need to be developed to assess the roles of LPCAT3 in BCBM.

Mounting studies from preclinical assays have linked ferroptosis to the immune cells and functions relevant to tumors (Friedmann Angeli et al., 2019; Wang et al., 2019; Tang et al., 2020). Ferroptosis cells will release chemotactic signals, such as lipid mediators to attract antigen-presenting cells (APC) and other immune cells to degrade these aberrant cells (Almeida et al., 2019). It should be stressed that GPX4, an anti-ferroptosis agent, could reduce phospholipid hydroperoxide and repress lipoxygenase-mediated lipid peroxidation (Zhou et al., 2020). Further evidence demonstrated that $CD4^+$ and $CD8^+$ T cells lacking GPX4 failed to expand and could not prevent immunity to infection (Matsushita et al., 2015). Besides, GPX4 is key factors involved in ferroptosis and lipid metabolism that regulate tumor metastasis (Li and Li, 2020). Similarly, our study also showed that the level of the antigen presentation process and the contents of immune cells were significantly different between high- and low-risk score groups. These studies enforce the notion that ferroptosis will affect immunity and may open up new possibilities to efficiently improve cancer treatment. Several lines of evidence have confirmed that ferroptosis enhanced the tumor suppression mediating by interferon-gamma (INF-γ) secreted by $CD8^+$ T cells in response to immune checkpoint blockade (Stockwell and Jiang, 2019; Wang et al., 2019). In turn, immunotherapy-activated T cells also enhance ferroptosis-specific lipid peroxidation in tumor cells (Wang et al., 2019). Immune checkpoint inhibitors have revolutionized the treatment of brain metastasis and breast cancer patients in recent years (Solinas et al., 2017; Lauko et al., 2018). It's thus tempting to speculate that, if sufficient details between ferroptosis and immunity have been uncovered, patients with BC may benefit more and a shift from anti-tumor to immunosuppressive responses might take place.

There is an increasing trend of clinical trials recruiting patients with BCBM to explore the efficacy of targeted agents. However, the therapeutic response rate is still low, ranging from 6% for alone to 49% for in combination (Pedrosa et al., 2018). Our data suggested that patients in the high-ferroptosis group were more sensitive to Cisplatin, Dasatinib etc., and low-ferroptosis patients were more sensitive to Lapatinib and Sorafenib. This finding could assist the clinicians in selecting suitable patients who may reap survival benefits. In addition, given the limited efficacy of traditional chemotherapy, there is an urgent necessity to exploit new agents that target BC. In this study, we identified 29 molecular compounds, involving the possible mechanisms. Evaluation of the small molecular drugs is crucial to the development of BCBM treatment. A more pronounced understanding of the possible mechanisms through the basic

experiments will lead a substantial shift to tailed therapeutic applications (Waks and Winer, 2019).

The strength of our study is that we performed a systematic analysis of FRG signatures in breast cancer patients from national database and validated using external databases, which provided robust statistical support. To our best known, it's the first time to explore the relationships between ferroptosis and BCBM, which shed light on the significance of ferroptosis in metastatic tumors. It's also the first time to construct FRG signatures to predict patients' survival and therapeutic response, which may be useful to assist clinicians in making individualized strategy for patients with BCBM. Meanwhile, there are some limitations in our study. Firstly, this is a retrospective study with data from public repositories. A large-scale and multicenter real-world analysis is warranted to verify these results. Secondly, the mechanisms of how ferroptosis modulates BCBM precisely are still unclear, and metastatic animal models are essential to understand the specific roles of ferroptosis. Lastly, it should be emphasized that the links between breast cancer ferroptosis and immune cells are not fully understood and needs to be validated experimentally. Notwithstanding its limitations, this study does provide a comprehensive overview of FRG profiles in BCBM and these limitations can be solved if there are enough data in the future.

In conclusion, we identified ferroptosis expression profiles that may be involved in the process of BCBM, and the ferroptosis patterns have values in predicting survival and drug sensitivity. New efforts targeting BCBM should incorporate the idea that ferroptosis could influence the breast cancer microenvironment.

DATA AVAILABILITY STATEMENT

The original contributions presented in the study are included in the article/**Supplementary Material**, further inquiries can be directed to the corresponding authors.

AUTHOR CONTRIBUTIONS

LZ, MC, BH, and TZ contributed to conception, design, data acquisition of the work. KC and HL contributed to interpretation and data analysis. ML and KZ contributed to data collection and interpreted the results. YP revised and remodified the manuscript. JZ and QL conceived and designed the study protocol. CZ reviewed and approved the final version of the manuscript. All authors contributed to the article and approved the submitted version.

FUNDING

This research was supported by grants from the Outstanding Leaders Training Program of Pudong Health Bureau of Shanghai (PWR12018-07), the Outstanding Clinical Discipline Project of Shanghai Pudong (PWYgy 2021-07) and the Key Discipline Construction Project of Pudong Health Bureau of Shanghai (PWZxk 2017-23).

ACKNOWLEDGMENTS

We acknowledge TCGA and GEO database for providing their platforms and contributors for uploading their meaningful datasets, and would like to thank all the authors listed for their contribution to the present study.

SUPPLEMENTARY MATERIAL

The Supplementary Material for this article can be found online at: https://www.frontiersin.org/articles/10.3389/fgene.2021.819632/full#supplementary-material

REFERENCES

Achrol, A. S., Rennert, R. C., Anders, C., Soffietti, R., Ahluwalia, M. S., Nayak, L., et al. (2019). Brain Metastases. *Nat. Rev. Dis. Primers* 5 (1), 5. doi:10.1038/s41572-018-0055-y

Adedoyin, O., Boddu, R., Traylor, A., Lever, J. M., Bolisetty, S., George, J. F., et al. (2018). Heme Oxygenase-1 Mitigates Ferroptosis in Renal Proximal Tubule Cells. *Am. J. Physiology-Renal Physiol.* 314 (5), F702–F714. doi:10.1152/ajprenal.00044.2017

Akatsuka, S., Yamashita, Y., Ohara, H., Liu, Y.-T., Izumiya, M., Abe, K., et al. (2012). Fenton Reaction Induced Cancer in Wild Type Rats Recapitulates Genomic Alterations Observed in Human Cancer. *PLoS One* 7 (8), e43403. doi:10.1371/journal.pone.0043403

Almeida, M., Soares, M., Ramalhinho, A. C., Moutinho, J. F., and Breitenfeld, L. (2019). Prognosis of Hormone-dependent Breast Cancer Seems to Be Influenced by KEAP1, NRF2 and GSTM1 Genetic Polymorphisms. *Mol. Biol. Rep.* 46 (3), 3213–3224. doi:10.1007/s11033-019-04778-8

Arslan, C., Dizdar, O., and Altundag, K. (2010). Systemic Treatment in Breast-Cancer Patients with Brain Metastasis. *Expert Opin. Pharmacother.* 11 (7), 1089–1100. doi:10.1517/14656561003702412

Bates, J. P., Derakhshandeh, R., Jones, L., and Webb, T. J. (2018). Mechanisms of Immune Evasion in Breast Cancer. *BMC Cancer* 18 (1), 556. doi:10.1186/s12885-018-4441-3

Bersuker, K., Hendricks, J. M., Li, Z., Magtanong, L., Ford, B., Tang, P. H., et al. (2019). The CoQ Oxidoreductase FSP1 Acts Parallel to GPX4 to Inhibit Ferroptosis. *Nature* 575 (7784), 688–692. doi:10.1038/s41586-019-1705-2

Boult, J., Roberts, K., Brookes, M. J., Hughes, S., Bury, J. P., Cross, S. S., et al. (2008). Overexpression of Cellular Iron Import Proteins Is Associated with Malignant Progression of Esophageal Adenocarcinoma. *Clin. Cancer Res.* 14 (2), 379–387. doi:10.1158/1078-0432.CCR-07-1054

Brown, R. A. M., Richardson, K. L., Kabir, T. D., Trinder, D., Ganss, R., and Leedman, P. J. (2020). Altered Iron Metabolism and Impact in Cancer Biology, Metastasis, and Immunology. *Front. Oncol.* 10, 476. doi:10.3389/fonc.2020.00476

Chen, X., Yu, C., Kang, R., and Tang, D. (2020). Iron Metabolism in Ferroptosis. *Front. Cel Dev. Biol.* 8, 590226. doi:10.3389/fcell.2020.590226

Dixon, S. J., Lemberg, K. M., Lamprecht, M. R., Skouta, R., Zaitsev, E. M., Gleason, C. E., et al. (2012). Ferroptosis: an Iron-dependent Form of Nonapoptotic Cell Death. *Cell* 149 (5), 1060–1072. doi:10.1016/j.cell.2012.03.042

Ferlay, J., Soerjomataram, I., Dikshit, R., Eser, S., Mathers, C., Rebelo, M., et al. (2015). Cancer Incidence and Mortality Worldwide: Sources, Methods and Major Patterns in GLOBOCAN 2012. *Int. J. Cancer* 136 (5), E359–E386. doi:10.1002/ijc.29210

Ferroptosis Is Inhibited in Lymph (2020). Ferroptosis Is Inhibited in Lymph, Promoting Metastasis of Melanoma. *Cancer Discov.* 10 (11), 1621. doi:10.1158/2159-8290.CD-RW2020-128

Friedmann Angeli, J. P., Krysko, D. V., and Conrad, M. (2019). Ferroptosis at the Crossroads of Cancer-Acquired Drug Resistance and Immune Evasion. *Nat. Rev. Cancer* 19 (7), 405–414. doi:10.1038/s41568-019-0149-1

Geeleher, P., Cox, N., and Huang, R. S. (2014). pRRophetic: an R Package for Prediction of Clinical Chemotherapeutic Response from Tumor Gene Expression Levels. *PLoS One* 9 (9), e107468. doi:10.1371/journal.pone.0107468

Hangauer, M. J., Viswanathan, V. S., Ryan, M. J., Bole, D., Eaton, J. K., Matov, A., et al. (2017). Drug-tolerant Persister Cancer Cells Are Vulnerable to GPX4 Inhibition. *Nature* 551 (7679), 247–250. doi:10.1038/nature24297

Harbeck, N., and Gnant, M. (2017). Breast Cancer. *The Lancet* 389 (10074), 1134–1150. doi:10.1016/S0140-6736(16)31891-8

Hartikainen, J. M., Tengström, M., Winqvist, R., Jukkola-Vuorinen, A., Pylkäs, K., Kosma, V.-M., et al. (2015). KEAP1 Genetic Polymorphisms Associate with Breast Cancer Risk and Survival Outcomes. *Clin. Cancer Res.* 21 (7), 1591–1601. doi:10.1158/1078-0432.CCR-14-1887

Hassannia, B., Vandenabeele, P., and Vanden Berghe, T. (2019). Targeting Ferroptosis to Iron Out Cancer. *Cancer Cell* 35 (6), 830–849. doi:10.1016/j.ccell.2019.04.002

Kaomongkolgit, R., Cheepsunthorn, P., Pavasant, P., and Sanchavanakit, N. (2008). Iron Increases MMP-9 Expression through Activation of AP-1 via ERK/Akt Pathway in Human Head and Neck Squamous Carcinoma Cells. *Oral Oncol.* 44 (6), 587–594. doi:10.1016/j.oraloncology.2007.08.005

Kennecke, H., Yerushalmi, R., Woods, R., Cheang, M. C. U., Voduc, D., Speers, C. H., et al. (2010). Metastatic Behavior of Breast Cancer Subtypes. *Jco* 28 (20), 3271–3277. doi:10.1200/JCO.2009.25.9820

Kim, M. S., Lee, W. S., and Jin, W. (2016). TrkB Promotes Breast Cancer Metastasis via Suppression of Runx3 and Keap1 Expression. *Mol. Cell* 39 (3), 258–265. doi:10.14348/molcells.2016.2310

Lauko, A., Thapa, B., Venur, V. A., and Ahluwalia, M. S. (2018). Management of Brain Metastases in the New Era of Checkpoint Inhibition. *Curr. Neurol. Neurosci. Rep.* 18 (10), 70. doi:10.1007/s11910-018-0877-8

Li, D., and Li, Y. (2020). The Interaction between Ferroptosis and Lipid Metabolism in Cancer. *Sig Transduct Target. Ther.* 5 (1), 108. doi:10.1038/s41392-020-00216-5

Li, Q., Liu, Q., Cheng, W., Wei, H., Jiang, W., Fang, E, et al. (2019). Heme Oxygenase-1 Inhibits Tumor Metastasis Mediated by Notch1 Pathway in Murine Mammary Carcinoma. *Oncol. Res.* 27 (6), 643–651. doi:10.3727/096504018X15415906335771

Ma, S., Henson, E. S., Chen, Y., and Gibson, S. B. (2016). Ferroptosis Is Induced Following Siramesine and Lapatinib Treatment of Breast Cancer Cells. *Cell Death Dis* 7, e2307. doi:10.1038/cddis.2016.208

Matsushita, M., Freigang, S., Schneider, C., Conrad, M., Bornkamm, G. W., and Kopf, M. (2015). T Cell Lipid Peroxidation Induces Ferroptosis and Prevents Immunity to Infection. *J. Exp. Med.* 212 (4), 555–568. doi:10.1084/jem.20140857

Nagpal, A., Redvers, R. P., Ling, X., Ayton, S., Fuentes, M., Tavancheh, E., et al. (2019). Neoadjuvant Neratinib Promotes Ferroptosis and Inhibits Brain Metastasis in a Novel Syngeneic Model of Spontaneous HER2+ve Breast Cancer Metastasis. *Breast Cancer Res.* 21 (1), 94. doi:10.1186/s13058-019-1177-1

Noh, S. J., Bae, J. S., Jamiyandorj, U., Park, H. S., Kwon, K. S., Jung, S. H., et al. (2013). Expression of Nerve Growth Factor and Heme Oxygenase-1 Predict Poor Survival of Breast Carcinoma Patients. *BMC Cancer* 13, 516. doi:10.1186/1471-2407-13-516

Pedrosa, R. M. S. M., Mustafa, D. A., Soffietti, R., and Kros, J. M. (2018). Breast Cancer Brain Metastasis: Molecular Mechanisms and Directions for Treatment. *Neuro Oncol.* 20 (11), 1439–1449. doi:10.1093/neuonc/noy044

Rooney, M. S., Shukla, S. A., Wu, C. J., Getz, G., and Hacohen, N. (2015). Molecular and Genetic Properties of Tumors Associated with Local Immune Cytolytic Activity. *Cell* 160 (1-2), 48–61. doi:10.1016/j.cell.2014.12.033

Seligmann, J. F., Wright-Hughes, A., Pottinger, A., Velikova, G., Oughton, J. B., Murden, G., et al. (2020). Lapatinib Plus Capecitabine versus Trastuzumab Plus Capecitabine in the Treatment of Human Epidermal Growth Factor Receptor 2-positive Metastatic Breast Cancer with Central Nervous System Metastases for Patients Currently or Previously Treated with Trastuzumab (LANTERN): a Phase II Randomised Trial. *Clin. Oncol.* 32 (10), 656–664. doi:10.1016/j.clon.2020.06.003

Shen, Y., Li, X., Dong, D., Zhang, B., Xue, Y., and Shang, P. (2018). Transferrin Receptor 1 in Cancer: a New Sight for Cancer Therapy. *Am. J. Cancer Res.* 8 (6), 916–931.

Shiovitz, S., and Korde, L. A. (2015). Genetics of Breast Cancer: a Topic in Evolution. *Ann. Oncol.* 26 (7), 1291–1299. doi:10.1093/annonc/mdv022

Solinas, C., Gombos, A., Latifyan, S., Piccart-Gebhart, M., Kok, M., and Buisseret, L. (2017). Targeting Immune Checkpoints in Breast Cancer: an Update of Early Results. *ESMO Open* 2 (5), e000255. doi:10.1136/esmoopen-2017-000255

Stockwell, B. R., Friedmann Angeli, J. P., Bayir, H., Bush, A. I., Conrad, M., Dixon, S. J., et al. (2017). Ferroptosis: A Regulated Cell Death Nexus Linking Metabolism, Redox Biology, and Disease. *Cell* 171 (2), 273–285. doi:10.1016/j.cell.2017.09.021

Stockwell, B. R., and Jiang, X. (2019). A Physiological Function for Ferroptosis in Tumor Suppression by the Immune System. *Cel Metab.* 30 (1), 14–15. doi:10.1016/j.cmet.2019.06.012

Tang, B., Zhu, J., Li, J., Fan, K., Gao, Y., Cheng, S., et al. (2020). The Ferroptosis and Iron-Metabolism Signature Robustly Predicts Clinical Diagnosis, Prognosis and Immune Microenvironment for Hepatocellular Carcinoma. *Cell Commun Signal* 18 (1), 174. doi:10.1186/s12964-020-00663-1

Terry, M. B., Michels, K. B., Michels, K. B., Brody, J. G., Byrne, C., Chen, S., et al. (2019). Environmental Exposures during Windows of Susceptibility for Breast Cancer: a Framework for Prevention Research. *Breast Cancer Res.* 21 (1), 96. doi:10.1186/s13058-019-1168-2

Torre, L. A., Bray, F., Siegel, R. L., Ferlay, J., Lortet-Tieulent, J., and Jemal, A. (2015). Global Cancer Statistics, 2012. *CA: A Cancer J. Clinicians* 65 (2), 87–108. doi:10.3322/caac.21262

Torti, S. V., and Torti, F. M. (2013). Iron and Cancer: More Ore to Be Mined. *Nat. Rev. Cancer* 13 (5), 342–355. doi:10.1038/nrc3495

Torti, S. V., and Torti, F. M. (2013). Iron and Cancer: More Ore to Be Mined. *Nat. Rev. Cancer* 13 (5), 342–355. doi:10.1038/nrc3495

Vaz-Luis, I., and Partridge, A. H. (2018). Exogenous Reproductive Hormone Use in Breast Cancer Survivors and Previvors. *Nat. Rev. Clin. Oncol.* 15 (4), 249–261. doi:10.1038/nrclinonc.2017.207

Waks, A. G., and Winer, E. P. (2019). Breast Cancer Treatment: A Review. *JAMA* 321 (3), 288–300. doi:10.1001/jama.2018.19323

Wang, J. Z., Du, Z., Payattakool, R., Yu, P. S., and Chen, C.-F. (2007). A New Method to Measure the Semantic Similarity of GO Terms. *Bioinformatics* 23 (10), 1274–1281. doi:10.1093/bioinformatics/btm087

Wang, W., Green, M., Choi, J. E., Gijón, M., Kennedy, P. D., Johnson, J. K., et al. (2019). CD8+ T Cells Regulate Tumour Ferroptosis during Cancer Immunotherapy. *Nature* 569 (7755), 270–274. doi:10.1038/s41586-019-1170-y

Weiland, A., Wang, Y., Wu, W., Lan, X., Han, X., Li, Q., et al. (2019). Ferroptosis and its Role in Diverse Brain Diseases. *Mol. Neurobiol.* 56 (7), 4880–4893. doi:10.1007/s12035-018-1403-3

Yang, W., Soares, J., Greninger, P., Edelman, E. J., Lightfoot, H., Forbes, S., et al. (2013). Genomics of Drug Sensitivity in Cancer (GDSC): a Resource for Therapeutic Biomarker Discovery in Cancer Cells. *Nucleic Acids Res.* 41 (Database issue), D955–D961. doi:10.1093/nar/gks1111

Yoshihara, K., Shahmoradgoli, M., Martínez, E., Vegesna, R., Kim, H., Torres-Garcia, W., et al. (2013). Inferring Tumour Purity and Stromal and Immune Cell Admixture from Expression Data. *Nat. Commun.* 4, 2612. doi:10.1038/ncomms3612

Yu, H., Yang, C., Jian, L., Guo, S., Chen, R., Li, K., et al. (2019). Sulfasalazine-induced F-erroptosis in B-reast C-ancer C-ells I-s R-educed by the I-nhibitory E-ffect of E-strogen R-eceptor on the T-ransferrin R-eceptor. *Oncol. Rep.* 42 (2), 826–838. doi:10.3892/or.2019.7189

Yu, M., Gai, C., Li, Z., Ding, D., Zheng, J., Zhang, W., et al. (2019). Targeted Exosome-encapsulated Erastin Induced Ferroptosis in Triple Negative Breast Cancer Cells. *Cancer Sci.* 110 (10), 3173–3182. doi:10.1111/cas.14181

Zhang, J., Yang, J., Zuo, T., Ma, S., Xokrat, N., Hu, Z., et al. (2021). Heparanase-driven Sequential Released Nanoparticles for Ferroptosis and Tumor Microenvironment Modulations Synergism in Breast Cancer Therapy. *Biomaterials* 266, 120429. doi:10.1016/j.biomaterials.2020.120429

Zhang, X., Shi, M., Chen, T., and Zhang, B. (2020). Characterization of the Immune Cell Infiltration Landscape in Head and Neck Squamous Cell Carcinoma to Aid Immunotherapy. *Mol. Ther. - Nucleic Acids* 22, 298–309. doi:10.1016/j.omtn.2020.08.030

Zhou, B., Liu, J., Kang, R., Klionsky, D. J., Kroemer, G., and Tang, D. (2020). Ferroptosis Is a Type of Autophagy-dependent Cell Death. *Semin. Cancer Biol.* 66, 89–100. doi:10.1016/j.semcancer.2019.03.002

Zhou, X.-L., Zhu, C.-Y., Wu, Z.-G., Guo, X., and Zou, W. (2019). The Oncoprotein HBXIP Competitively Binds KEAP1 to Activate NRF2 and Enhance Breast Cancer Cell Growth and Metastasis. *Oncogene* 38 (21), 4028–4046. doi:10.1038/s41388-019-0698-5

Zille, M., Kumar, A., Kundu, N., Bourassa, M. W., Wong, V. S. C., Willis, D., et al. (2019). Ferroptosis in Neurons and Cancer Cells Is Similar but Differentially Regulated by Histone Deacetylase Inhibitors. *eNeuro* 6, 0263–318. doi:10.1523/ENEURO.0263-18.2019

Conflict of Interest: The authors declare that the research was conducted in the absence of any commercial or financial relationships that could be construed as a potential conflict of interest.

Publisher's Note: All claims expressed in this article are solely those of the authors and do not necessarily represent those of their affiliated organizations, or those of the publisher, the editors and the reviewers. Any product that may be evaluated in this article, or claim that may be made by its manufacturer, is not guaranteed or endorsed by the publisher.

GLOSSARY

APC antigen-presenting cells

AUC area under curves

BC breast cancer

BCBM breast cancer brain metastasis

BP biological process

CC cellular component

CI confidence interval

ECM extracellular matrix

ER estrogen receptor

FRG ferroptosis-related genes

GEO Gene Expression Omnibus

GO Gene Ontology

GPX4 glutathione peroxidase 4;

GSDC Genomics of Drug Sensitivity in Cancer

GSH glutathione

HO-1 heme oxygenase 1

HR hazard ratio

INF-γ interferon gamma

KEGG Kyoto Encyclopedia of Genes and Genomes

K-M Kaplan-Meier

MF molecular function

MMPs matrix metalloproteinases

MMP-9 matrix metalloproteinases-9

OS overall survival

PCA principal component analysis

PgR progesterone receptor

RFS relapse-free survival

ROC receiver operating curves

ROS reactive oxygen species

SDG significantly different genes

ssGSEA single-sample gene set enrichment analysis

TCGA The Cancer Genome Atlas

TME tumor microenvironment

TNBC triple-negative breast cancer.

frontiers in Cell and Developmental Biology

ORIGINAL RESEARCH
published: 31 January 2022
doi: 10.3389/fcell.2021.812422

A Ferroptosis-Related Gene Prognostic Index to Predict Temozolomide Sensitivity and Immune Checkpoint Inhibitor Response for Glioma

Yonghua Cai[1†], Xianqiu Liang[1†], Zhengming Zhan[1†], Yu Zeng[1], Jie Lin[1], Anqi Xu[1], Shuaishuai Xue[1], Wei Xu[1], Peng Chai[1], Yangqi Mao[1], Zibin Song[1], Lei Han[1], Jianqi Xiao[2], Ye Song[1,3]* and Xian Zhang[1]**

[1]Department of Neurosurgery, Nanfang Hospital, Southern Medical University, Guangzhou, China, [2]Department of Neurosurgery, The First Hospital of Qiqihar City, Qiqihar, China, [3]Department of Neurosurgery, Ganzhou People's Hospital, Ganzhou, China

Background: Gliomas are highly lethal brain tumors. Despite multimodality therapy with surgery, radiotherapy, chemotherapy, and immunotherapy, glioma prognosis remains poor. Ferroptosis is a crucial tumor suppressor mechanism that has been proven to be effective in anticancer therapy. However, the implications of ferroptosis on the clinical prognosis, chemotherapy, and immune checkpoint inhibitor (ICI) therapy for patients with glioma still need elucidation.

Methods: Consensus clustering revealed two distinct ferroptosis-related subtypes based on the Cancer Genome Atlas (TCGA) glioma dataset (*n* = 663). Subsequently, the ferroptosis-related gene prognostic index (FRGPI) was constructed by weighted gene co-expression network analysis (WGCNA) and "stepAIC" algorithms and validated with the Chinese Glioma Genome Atlas (CGGA) dataset (*n* = 404). Subsequently, the correlation among clinical, molecular, and immune features and FRGPI was analyzed. Next, the temozolomide sensitivity and ICI response for glioma were predicted using the "pRRophetic" and "TIDE" algorithms, respectively. Finally, candidate small molecular drugs were defined using the connectivity map database based on FRGPI.

Results: The FRGPI was established based on the *HMOX1*, *TFRC*, *JUN*, and *SOCS1* genes. The distribution of FRGPI varied significantly among the different ferroptosis-related subtypes. Patients with high FRGPI had a worse overall prognosis than patients with low FRGPI, consistent with the results in the CGGA dataset. The final results showed that high FRGPI was characterized by more aggressive phenotypes, high *PD-L1* expression, high tumor mutational burden score, and enhanced temozolomide sensitivity; low FRGPI was associated with less aggressive phenotypes, high microsatellite instability score, and stronger response to immune checkpoint blockade. In addition, the infiltration of memory resting $CD4^+$ T cells, regulatory T cells, M1 macrophages, M2 macrophages, and neutrophils was positively correlated with FRGPI. In contrast, plasma B cells and naïve

OPEN ACCESS

Edited by:
Lian Xiang Luo, Guangdong Medical University, China

Reviewed by:
Wenchao Gu, Gunma University, Japan
Ling Li, University of North Dakota, United States
Xi Lou, University of Alabama at Birmingham, United States

***Correspondence:**
Xian Zhang
zxa@smu.edu.cn
Ye Song
songye@smu.edu.cn
Jianqi Xiao
xjiqi@126.com

†These authors have contributed equally to this work

Specialty section:
This article was submitted to Cell Death and Survival, a section of the journal Frontiers in Cell and Developmental Biology

Received: *10 November 2021*
Accepted: *30 December 2021*
Published: *31 January 2022*

Citation:
Cai Y, Liang X, Zhan Z, Zeng Y, Lin J, Xu A, Xue S, Xu W, Chai P, Mao Y, Song Z, Han L, Xiao J, Song Y and Zhang X (2022) A Ferroptosis-Related Gene Prognostic Index to Predict Temozolomide Sensitivity and Immune Checkpoint Inhibitor Response for Glioma. Front. Cell Dev. Biol. 9:812422. doi: 10.3389/fcell.2021.812422

$CD4^+$ T cells were negatively correlated. A total of 15 potential small molecule compounds (such as depactin, physostigmine, and phenacetin) were identified.

Conclusion: FRGPI is a promising gene panel for predicting the prognosis, immune characteristics, temozolomide sensitivity, and ICI response in patients with glioma.

Keywords: ferroptosis, glioma, temozolomide, immune checkpoint inhibitor, tumor microenvironment, ferroptosis-based anticancer therapy, immunotherapy

INTRODUCTION

Gliomas, including low grade (LGG, World Health Organization grades I–II) and high grade (HGG, World Health Organization grades III–IV), are the most common and lethal solid tumors of all brain cancers (Louis et al., 2016; Aldape et al., 2019). The annual incidence of gliomas is approximately six out of 100,000 individuals worldwide (Weller et al., 2021). Current glioma multimodal therapy includes surgery, radiotherapy, chemotherapy, and immunotherapy. Studies have identified IDH1 mutations, 1p19q chromosome deletions, and O-6-Methylguanine-DNA Methyltransferase (MGMT) epigenetic alterations as specific targets for enhancing treatment response, improving survival, and personalizing anticancer therapeutics (Nagashima et al., 2016). However, the overall prognosis remains poor, especially for glioblastomas, the most fatal of gliomas, which have 14.6 months of median survival (Tan et al., 2020). Additionally, there is 2- to 4-fold longer median survival in patients with IDH1 mutant glioma compared to those with IDH1 wild-type glioma (Yan et al., 2009; Nagashima et al., 2016).

Immune checkpoint inhibitors (ICI) have transformed the cancer treatment landscape, significantly improving survival (Brahmer et al., 2015; Larkin et al., 2015; Motzer et al., 2015; Bellmunt et al., 2017). Several studies have been conducted on immune-based therapy for gliomas, specifically for glioblastomas (Khasraw et al., 2020; Maire et al., 2020). Research has shown that standard therapies, including surgery, radiotherapy, and chemotherapy, may have immunosuppressive effects, further emphasizing opportunities to target the immune response for novel therapies (Lim et al., 2018). However, the initial results for trials of ICI, predominantly anti-*PD-1*/*PD-L1* and anti-*CTLA-4*, have been disappointing, and a phase III trial of nivolumab versus bevacizumab for recurrent glioblastoma did not demonstrate any meaningful benefits (Lim et al., 2018; Jackson et al., 2019; McGranahan et al., 2019; Reardon et al., 2020). Temozolomide, an imidazotetrazine prodrug alkylating agent, is an oral chemotherapeutic drug that crosses the blood–brain barrier and is widely used in patients with glioma (Friedman et al., 2000). Although temozolomide is traditionally considered to have a direct antitumor effect, many studies have confirmed its immunomodulatory properties (Karachi et al., 2018). However, approximately 55% of the patients with glioblastoma present with temozolomide resistance because of high MGMT expression (Hegi et al., 2005; Donson et al., 2007; van Nifterik et al., 2010). The evasion of apoptosis is, to a large extent, one of the main obstacles leading to poor therapeutic effects in malignant glioma. Thus, bypassing apoptosis resistance is a promising approach to overcome this problem (Gong et al., 2019; Tang et al., 2021).

Ferroptosis is a non-apoptotic cell death mechanism defined as iron-dependent regulated necrosis induced by membrane rupture mediated by excessive lipid peroxidation (Chen et al., 2021; Jiang et al., 2021). Ferroptosis has been proven to be a crucial tumor suppressor mechanism and may influence chemotherapy effects by triggering immune responses (Angeli et al., 2019). Many studies have shown that the expression of ferroptosis-related genes (including *GPX4, SLC7A11, and ACSL4*) is associated with sensitivity to temozolomide in glioma cells (Hu et al., 2020). In addition, T cells and interferon-gamma (IFN-γ) sensitize cancer cells to ferroptosis. Subsequently, the damage-associated molecular patterns (such as high mobility group box 1, *HMGB1*) released by cancer cells undergoing ferroptosis may induce cancer cell immunogenicity. This suggests that the role of ferroptosis in cancer therapy has synergistic potential with immunotherapy (Angeli et al., 2019; Liang et al., 2019; Llabani et al., 2019; Stockwell and Jiang, 2019; Wen et al., 2019; Tang et al., 2020). Ferroptosis-resistant cancer cells do not respond to *PD-L1* inhibitors, and the suppression of ferroptosis prevents gaining benefits from *PD-L1* inhibitors (Wang et al., 2019). Direct evidence of the link between ferroptosis and antitumor immunity was not evident until Wang et al. demonstrated that immunotherapy-activated $CD8^+$ T cells suppressed tumor growth by sensitizing tumors to ferroptosis via IFN-γ (Wang et al., 2019; Tang et al., 2020). *In vitro* culture with low cystine and *in vivo* data showed that ferroptosis was involved in T-cell-mediated cancer immunity (Wang et al., 2019). Moreover, Liu et al. developed the ferroptosis potential index (FPI) to explore the functional roles of ferroptosis in various cancers, revealing that ferroptosis was associated with survival, the immune system, and chemotherapy resistance (Liu et al., 2020). Unfortunately, there is no ferroptosis-related potential prognostic marker that can simultaneously predict immune characteristics, temozolomide sensitivity, and the response of glioma to ICI.

In this study, we focused on the effects of ferroptosis on the immune characteristics of glioma and aimed to find markers that can accurately predict survival and ICI response of all patients with glioma. We screened hub ferroptosis-related genes (FRGs) by consistency analysis, WGCNA, and "stepAIC" algorithms to construct a ferroptosis-related gene prognostic index (FRGPI). We examined the prognostic predictive ability of FRGPI and characterized its molecular and immune profiles. We then predicted the sensitivity of patients with different FRGPI to temozolomide via the Genomics of Drug Sensitivity in Cancer (GDSC) database and the "pRRophetic" algorithms. Furthermore, we explored the relationship between the FRGPI and ICI responses through "TIDE" algorithms and verified it in an ICI therapy cohort.

MATERIALS AND METHODS

Collection of Glioma Datasets, Ferroptosis-Related Genes (FRGs) and Immune-Related Gene (IRGs)

RNA sequencing (RNA-seq) and the corresponding complete clinical information for patients with glioma were retrieved from The Cancer Genome Atlas (TCGA) dataset (Version: 28.0, https://portal.gdc.cancer.gov/) and the Chinese Glioma Genome Atlas (CGGA) dataset (2021 Feb, http://www.cgga.org.cn/index.jsp) (Zhao et al., 2021). The main study was conducted using TCGA dataset (n = 663, including 248 LGG, 414 HGG, 1 unknown), and the CGGA dataset (n = 404, including 130 LGG and 274 HGG) was used for validation of the FRGPI for prognosis. The data of normal tissue samples were obtained from TCGA (n = 5), CGGA (n = 20), and GTEx (n = 2,642) (Version: 8.0, https://gtexportal.org/home/datasets). The gene-level transcription values were normalized to fragments per kilobase million (FPKM) and further transformed to log2 (FPKM+1) for downstream analysis. In addition, we used the "ComBat" function in the "sva" R package for the batcheffect within TCGA and GTEx datasets. Both somatic mutation data and copy number alteration data were obtained from TCGA database. The baseline clinical characteristics of glioma patients are shown in **Supplementary Table 1**. Twenty-four FRGs (**Supplementary Table 2**) were identified according to previously published literature (Liu et al., 2020). A total of 173 FRGs (**Supplementary Table 3**) were acquired from FerrDb (Version:1.0, http://www.zhounan.org/ferrdb/) (Zhou and Bao, 2020). A total of 1,793 IRGs (**Supplementary Table 4**) were obtained from ImmPort (https://www.immport.org/home) (Bhattacharya et al., 2018).

Cell Culture

Human glioma cell lines U87-MG (HTB-14) and T98G (CRL-1690) were purchased from American Type Culture Collection (ATCC, Manassas, VA, United States). Human glioma cell lines were cultured in Dulbecco's modified Eagle's medium (DMEM; 06-1055-57-1A, Biological Industries) supplemented with 10% fetal bovine serum (FBS; 04-001-1A, Biological Industries) at 37°C with 5% CO_2. The sources of all the cell lines were identified and verified by STR profiling. No *mycoplasma* contamination was detected in any of the cell lines by MycoSEQ™ *Mycoplasma* Real-Time PCR Detection Kit (ThermoFisher, 4460623).

CCK-8 Assay

We used a CCK-8 kit (Beyotime, C0039) to measure the proliferation of U87-MG and T98G cells. First, we measured the IC_{50} of erastin, a ferroptosis activator. A total of 1×10^3 cells (100 μl per well) were cultured in four replicate wells of a 96-well plate in a medium containing 10% FBS for 24 h. Then, erastin at different concentrations (0, 5, 10, 20, and 40 μmol/L) was added to a 96-well plate and divided into five groups (with an equal volume of DMSO added to the blank control group). Finally, the CCK-8 reagent (10 μl) was added to 90 μl DMEM to generate a working solution, of which 100 μl was added per well and incubated for 2 h. We performed this assay for 24 and 48 h after adding erastin. In U87-MG group, IC50 of erastin is 14.49 uM while 16.57 uM in T98 group. We then identified the influence of erastin on the proliferation ability of two glioma cell lines by adding different concentrations of temozolomide. All operations are roughly the same as the previous steps. The cells seeded in 96-well plates and were allowed to grow for 24 h. Then gradient concentrations of temozolomide and IC_{50} concentrations of erastin were added together in a 96-well plate. The drug concentrations of erastin (IC_{50} of U87 and T98G) at 24 h were too high, and this meant more DMSO had to be added, which had large impact on cell viability and proliferation both in the experimental and control groups and affected the accuracy of the experiment. Therefore, we chose 48 h as a reasonable drug treatment time. After 48 h, a 1:9 CCK reagent to DMEM was made and 100 μl of this solution was added to each well and incubated for 2 h.

Immunofluorescence and Immunohistochemistry Staining

The subcellular distribution of proteins encoded by *GPX4*, *FSP1*, *GCH1*, and *DHODH* in human cell lines and their protein expression levels were investigated by confocal microscopy immunofluorescence (ICC-IF) and immunohistochemistry staining using the Human Protein Atlas database (Version: 21.0, https://www.proteinatlas.org/).

Consensus Clustering for Patients With Glioma

The number of unsupervised classes in TCGA-Glioma dataset was estimated and validated based on the mRNA expression profiles of 24 FRGs (**Supplementary Table 2**) and 94 ferroptosis suppressors (**Supplementary Table 5**) using the consensus clustering method by the "ConsesusClusterPlus" R package.

Somatic Mutation Landscape, stromalScore, immuneScore, and Immune Cell Infiltration in Distinct Ferroptosis-Related Subtypes

Mutation data were downloaded and visualized using the "maftools" R package to identify the somatic mutation landscape of patients with gliomas from TCGA database in distinct ferroptosis-related subtypes (Mayakonda et al., 2018). The immuneScore, stromalScore, and ESTIMATE score for each patient were calculated via the "estimate" R package (Yoshihara et al., 2013) and patients were divided into high and low immuneScore and stromalScore groups (based on the score above and below the median value, respectively). To make reliable immune infiltration estimations, we utilized the "immunedeconv" R package, which integrates six state-of-the-art algorithms, including TIMER, xCell, MCP-counter, CIBERSORT, EPIC, and quanTIseq (Sturm et al., 2019).

Gene Set Enrichment Analysis and Gene Set Variation Analysis

Gene set enrichment analysis (GSEA) was conducted using the hallmark gene set "h.all.v7.2.symbols.gmt" between two

ferroptosis-related subtypes using the "GSEA" R package. Gene set variation analysis (GSVA) was performed with the "GSVA" R package to compute a ssGSEA score of each functional pathway in each patient with glioma. The pathways with nominal p-value < 0.05, and false discovery rate (FDR) < 0.05, were considered significantly enriched.

The Construction of FRGPI and Nomogram Model

Differentially expressed genes (DEGs) with FDR < 0.05 and |Fold Change (FC)| ≥ 1 were identified among different clusters and groups using the "limma" R package and visualized using volcano plots and heatmaps. Weighted gene co-expression network analysis (WGCNA) (Langfelder and Horvath, 2008) was performed using the "WGCNA" R package (networkType = "unsigned", minModuleSize = 30) to identify modules associated with ferroptosis (correlation coefficient > 0.50 and p-value < 0.05 were set as the inclusion criterion). Protein–protein interaction (PPI) analysis was performed using STRING database (https://string-db.org/). The FRGPI was established using the "stepAIC" algorithm in the "MASS" R package, and the model with the lowest Akaike Information Criterion (AIC) value was then chosen as the best model to yield the FRGPI equation with the coefficient multiplied by mRNA expression. According to this equation, the FRGPI of each patient was calculated separately for the training and validation cohorts. Subsequently, the patients were divided into high and low FRGPI groups, and the median value of the FRGPI score was set as the cut-off point. Principal component analysis (PCA) was performed using these signature genes. Univariate and multivariate Cox regression analyses were performed to identify the appropriate terms to build the nomogram. A forest plot was used to show the p-value, hazard ratio (HR), and 95% confidence interval (CI) of each variable through the "forestplot" R package. The nomogram was built based on the multivariate cox proportional hazards analysis ("p-value < 0.05" was set as the inclusion criterion) through the "rms" R package to predict the 1-, 3-, and 5-year overall survival (OS).

Estimation of Ferroptosis Potential Index, Tumor Mutational Burden, Microsatellite Instability, and Stemness Index

The FPI, which can be used to represent the potential level of ferroptosis based on transcriptome data, was computed for each sample according to previously published literature (Liu et al., 2020). Tumor mutational burden (TMB) score, microsatellite instability (MSI) score, and two independent stemness indices (mRNA expression-based stemness index, mRNAsi, and DNA methylation-based stemness index, mDNAsi) were calculated according to previously defined methods (Bonneville et al., 2017; Chalmers et al., 2017; Malta et al., 2018).

Correlation of FRGPI With Temozolomide Sensitivity and ICI Response

The sensitivity of each patient to temozolomide was estimated using the GDSC database (https://www.cancerrxgene.org/). The estimated half-maximal inhibitory concentration (IC_{50}) was quantified via the "pRRophetic" R package. The potential ICI response was predicted using the TIDE algorithm (Jiang et al., 2018). Furthermore, one immunotherapy cohort (metastatic urothelial cancer treated with atezolizumab, IMvigor210 cohort) (Mariathasan et al., 2018) was included to validate the tumor response to *PD-L1* blockade.

Predicting Candidate Small Molecules Based on FRGPI

The DEGs (**Supplementary Table 9**) with FDR < 0.05 and |FC| ≥ 1 were identified as high- and low-FRGPI groups by the "limma" R package, and the function enrichment terms of DEGs were acquired from the STRING database (https://string-db.org/). Based on these DEGs, candidate small molecular drugs and mechanisms of action were defined using the connectivity map database (CMap, http://portals.broadinstitute.org/cmap/) (Lamb et al., 2006) and CMap mode-of-action analysis.

Statistical Analysis

All statistical analyses were conducted using R software (version 4.0.2). The normality of the variables was tested using the Shapiro-Wilk normality test. For comparisons of two normally distributed groups, statistical analysis was performed using unpaired t-tests, and for non-normally distributed variables, statistical analysis was performed using the Wilcoxon rank-sum test. For comparisons of three or more groups, Kruskal-Wallis tests or one-way ANOVA were used as nonparametric or parametric methods, respectively. Correlations between normally distributed variables were assessed using Pearson's correlation test, while correlations between non-normally distributed variables were assessed using Spearman's correlation test. A p-value < 0.05, and |correlation coefficient |(R)| > 0.30 were considered as statistically significant. Kaplan–Meier curves for OS were presented between different subgroups, and OS comparisons were performed using the log-rank test. The receiver operating characteristic (ROC) curve was used to assess the prognosis classification performance of the FRGPI model, and the area under the curve (AUC) was calculated using the "timeROC" R package. All statistical p values were two-sided, with $p < 0.05$ considered statistically significant.

RESULTS

Ferroptosis Plays a Potential Functional Role in the Progression and Treatment of Glioma

GPX4, *FSP1*, *GCH1*, and *DHODH* are key genes involved in cell ferroptosis defense (Zheng and Conrad, 2020; Mao et al., 2021). Immunofluorescence and confocal microscopy showed that *GPX4* was mainly located in nucleoplasm and mitochondria, *DHODH* was located in the mitochondria, *GCH1* was located in nucleoplasm and cytosol, and *FSP1* was located in cytosol (**Figures 1A–D**). The analysis of mRNA expression profiles of

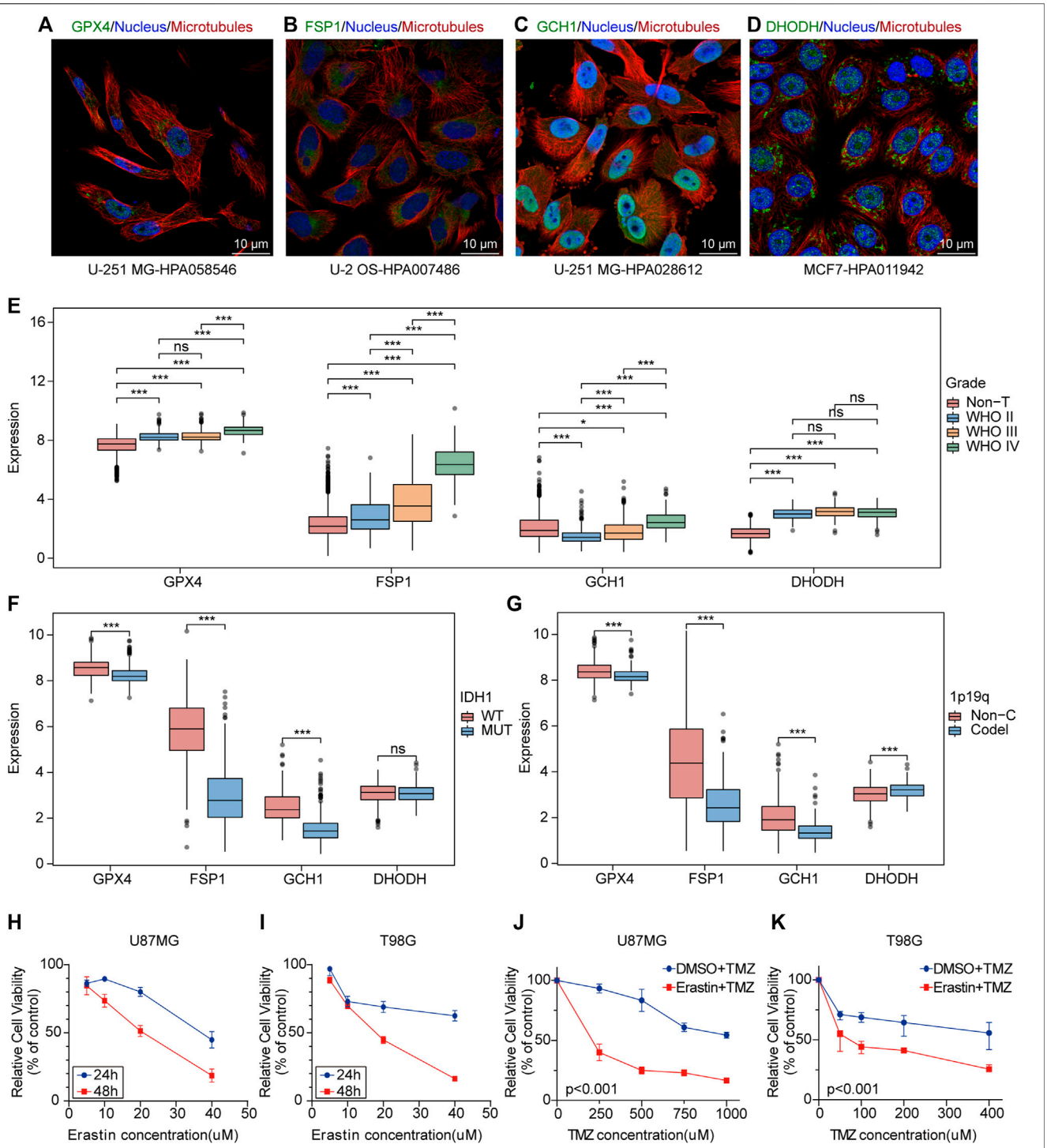

FIGURE 1 | Ferroptosis plays an potential biological role in the progression and treatment of glioma. **(A–D)** Confocal immunofluorescence staining for *GPX4*, *DHODH*, *GCH1*, *FSP1* in cell lines from HPA database. Green, antibody; blue, nucleus; red, microtubules. **(E–G)** Boxplots of *GPX4*, *GCH1*, *FSP*1 and *DHODH* expression in different grade, IDH1-status and 1p19q-codeletion-status glioma samples from TCGA database. ns, no significance; **p* < 0.05; ***p* < 0.01; ****p* < 0.001. **(H,I)** The cell viability of U87MG and T98G cells transfected with erastin was evaluated by the CCK-8 assays in 24 and 48 h. Five technical repeats were performed for two biological repeats. **(G,K)** The cell viability of U87MG and T98G cells transfected with erastin and temozolomide was evaluated by the CCK8 assays in 48 h. Five technical repeats were performed for two biological repeats.

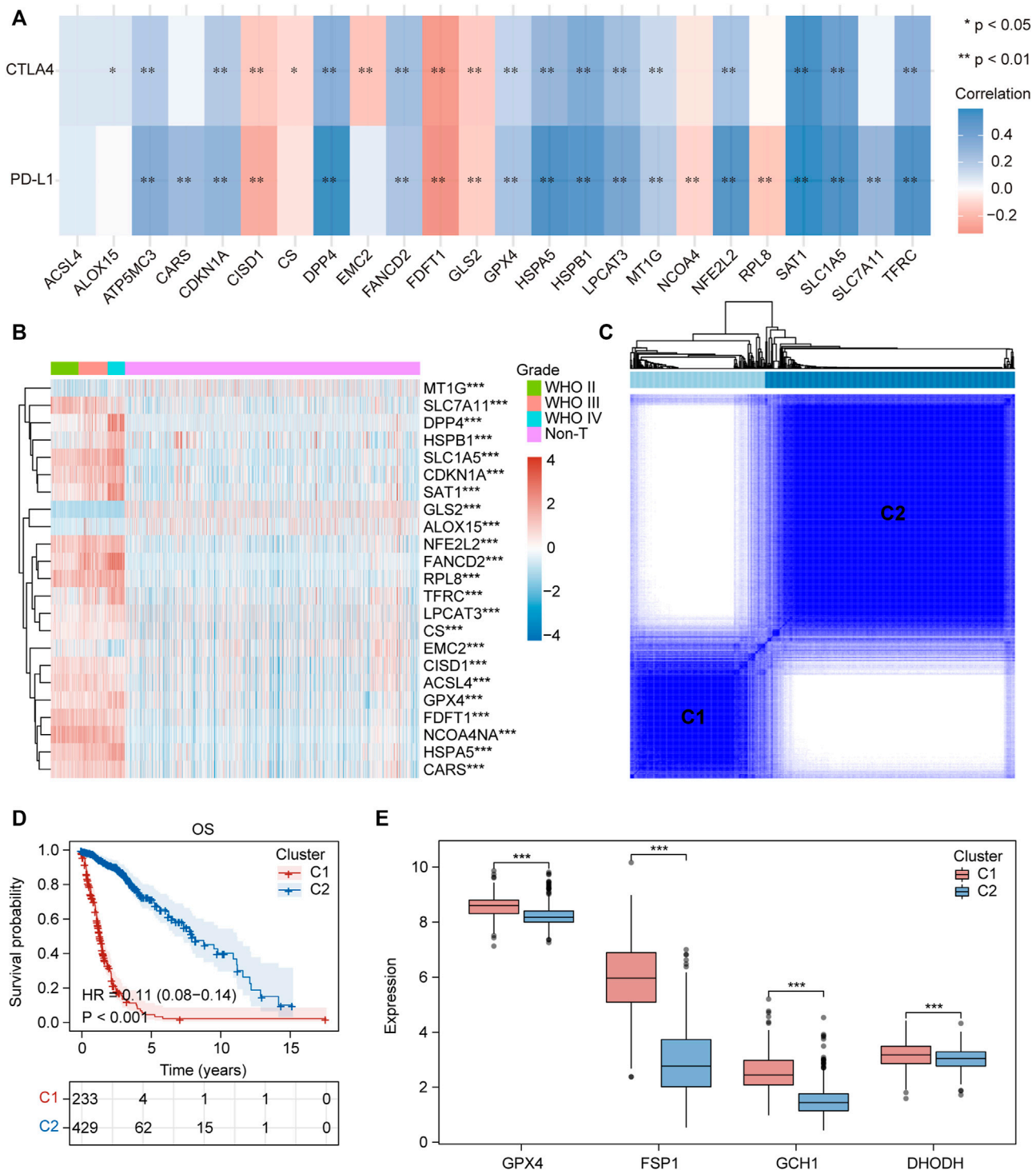

FIGURE 2 | Two ferroptosis-related subtypes were identified based on the expression profile of FRGs. **(A)** Correlation heatmap between 24 FRGs expression and *PDL-L1/CTAL4*. Blue, positive correlation; red, negative correlation. *$p < 0.05$, **$p < 0.01$. **(B)** Heatmap depicted the FRGs expression profile landscape in gliomas of TCGA database. Red, high expression, blue, low expression. **(C)** Consensus clustering matrix for k = 2. **(D)** Kaplan–Meier analysis of patients in the two different ferroptosis-related subtypes. **(E)** Boxplots of *GPX4*, *GCH1*, *FSP1* and *DHODH* expression level in the two different ferroptosis-related subtypes. ns, no significance; *$p < 0.05$; **$p < 0.01$; ***$p < 0.001$.

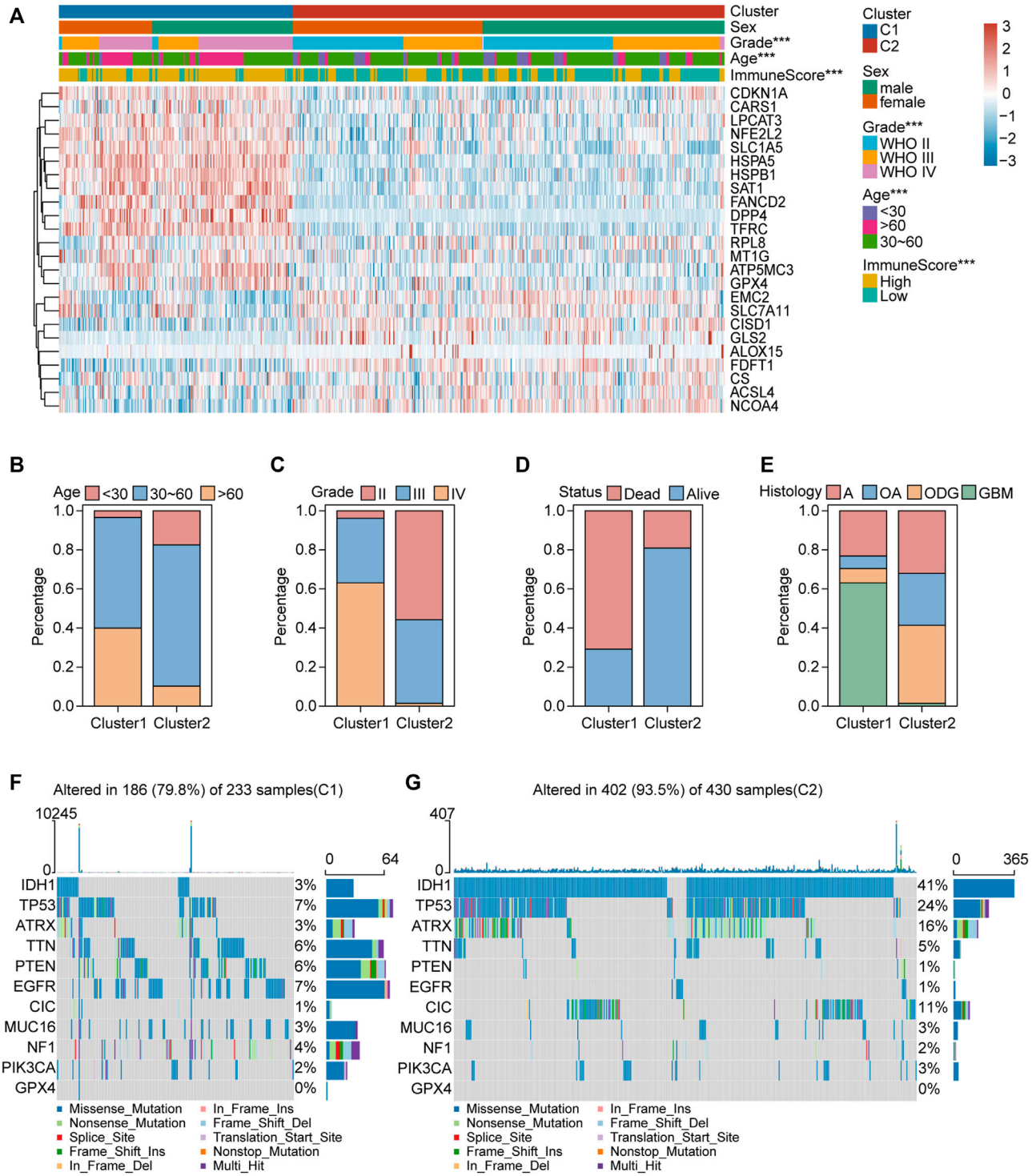

FIGURE 3 | Clinical features and somatic landscapes of two ferroptosis-related subtypes. **(A)** Heatmap visualized the distribution of sex, age, grade, immuneScore between the two ferroptosis-related subtypes. *$p < 0.05$; **$p < 0.01$; ***$p < 0.001$. **(B–E)** Histograms depicted the differences of age, grade, status and histology between two ferroptosis-related subtypes. **(F,G)** Oncoplot displaying the somatic landscape of glioma cohort of two ferroptosis-related subtypes. Genes are ordered by their mutation frequency, and samples are ordered according to disease histology as indicated by the annotation bar (bottom). Side bar plot shows log10 transformed Q-values estimated by MutSigCV. Landscape of mutation profiles in OC samples. Mutation information of each gene in each sample was shown in the waterfall plot, where different colors with specific annotations at the bottom meant the various mutation types. The bar plot above the legend exhibited the number of mutation burden.

glioma samples and non-tumor brain tissues provided evidence that *GPX4*, *FSP1*, and *DHODH* were highly expressed in tumoral tissue compared to that in non-tumor brain tissues (**Figure 1E** and **Supplementary Figures 1A,B**). Additionally, the expression of *GCH1* and *FSP1* increased with increasing malignancy of the tumor (**Figure 1E**); *GPX4*, *FSP1*, and *GCH1* were highly expressed in patients with glioma and wild-type *IDH1* compared to mutant *IDH1* (**Figure 1F**). *GPX4*, *FSP1*, and *GCH1* were highly expressed, while *DHODH* expression was low in patients with gliomas with a 1p19q non-codeletion compared to those with a 1p19q codeletion (**Figure 1G**). Immunohistochemistry (IHC) demonstrated that the four genes were highly expressed at the protein level in gliomas compared to non-tumor brain tissues (**Supplementary Figures 1C,D**). The CCK-8 assay results showed that ferroptosis induction by erastin inhibited proliferation and enhanced the sensitivity of U87MG and T98G cells to temozolomide (**Figures 1H–K**). These data indicate that ferroptosis played an important role in the maintenance, progression, and treatment of gliomas.

Clinical Features, Somatic Landscapes, and Immune Infiltration of Different Ferroptosis-Related Subtypes in Glioma

We collected 24 FRGs according to Liu et al. (2020). Spearman correlation analysis indicated a significant correlation between the mRNA expression of FRGs and *PDL-L1/CTAL4* (**Figure 2A**). Most FRGs were highly expressed in glioma tissues compared to non-tumor brain tissues, as shown in **Figure 2B**. The patients with glioma were divided into two ferroptosis-related subtypes (C1 and C2) by performing consistency analysis based on FRGs mRNA expression profiles (**Figure 2C**). The OS for patients in C1 was shorter than that for patients in C2 (**Figure 2D**). *GPX4*, *GCH1*, *FSP1*, and *DHODH* were expressed at higher levels in patients in C1 than in C2 (**Figure 2E**). The expression of FRGs and clinical features of the two subtypes were then compared (**Figure 3A**). The C1 group mainly contained patients with glioma over 60 years of age, preferentially associated with a high WHO grade and glioblastoma (**Figures 3B–E**). The oncoplot displaying the somatic landscape showed that *IDH1*, *TP53*, *ATRX*, and *CIC* mutation frequencies in C2 were higher than in C1, but *PTEN* and *EGFR* in C1 were higher than in C2 (**Figures 3F,G**). A total of 22 immune cell infiltration scores of each sample were estimated using the CIBERSORT algorithm. The scores of resting and activated memory $CD4^+$ T cells, $CD8^+$ T cells, regulatory T cells (Tregs), neutrophils, memory B cells, M0 macrophages, M1 macrophages, M2 macrophages, activated myeloid dendritic cells, and activated mast cells in the samples of C1 were higher than those of C2. However, the activated NK cell, resting mast cell, monocyte, naïve B cell, plasma B cell, and naïve $CD4^+$ T cell scores in the samples of C1 were lower than in those in C2 (**Figure 4A**). The percentage of tumor-infiltrating immune cells in each sample is shown in **Figure 4B**. The ESTIMATE algorithm showed that the immuneScore and stromalScore in the samples of C1 were higher than those of C2 (**Figures 4C,D**). To elucidate the underlying regulatory mechanisms leading to the difference between the two ferroptosis subtypes in glioma, GSEA was performed. Our data indicated that PI3K_AKT_MTOR_SIGNALING, MTORC1_SIGNALING, GLYCOLYSIS, HYPOXIA, and APOPTOSIS were mainly enriched in the C1 group but were not enriched in the C2 group (**Figure 4E**). These results suggest that distinct differences in the clinical, genomic, and immune infiltration characteristics of ferroptosis-related subtypes were divided by the expression of 24 FRGs.

To verify this hypothesis, consistency analysis was performed based on 94 ferroptosis suppressors that have been verified in humans and dividing the sample into ferroptosis subgroups (including G1 and G2; **Supplementary Figure 2A**). Survival analysis revealed that patients in G2 had longer OS than those in G1 (**Supplementary Figure 2B**). The differences in immuneScore, stromalScore, and tumor-infiltrating immune cell scores between G1 and G2 were similar to the differences between C1 and C2 (**Supplementary Figures 2C–E**).

FRGPI Was Developed to Reveal the Functional Roles of Ferroptosis in Glioma Based on FRGs

Differential expression gene analysis was performed between C1 and C2 or G1 and G2, and the DEGs (**Supplementary Tables S6, S7**) expression heatmap is shown in **Figure 5A** and **Supplementary Figure 3A**. WGCNA was performed to divide all protein-coding genes into 10 modules (**Supplementary Figure 3B**), of which the one most related to ferroptosis-related subtypes and tumor immunity was the blue module (**Figure 5B**). Then, 173 FRGs were acquired from the FerrDb database, and 1,793 IRGs were obtained from the ImmPort database. Furthermore, FRGs, IRGs, DEGs, and genes in the blue module (**Supplementary Table 8**) were intersected, and seven hub genes (*JUN, TNFAIP3, NOX4, HMOX1, SOCS1, CYBB,* and *TFRC*), related to both ferroptosis and tumor immunity, were obtained (**Figure 5C**). The protein-protein interaction network of the seven hub genes is shown in **Supplementary Figure 3C**. The seven hub genes were used to develop the FRGPI model in TCGA training set using the stepAIC algorithm. The optimal model equation was yielded using four factors (*HMOX1, TFRC, JUN,* and *SOCS1*) with the lowest AIC (**Figure 5D**):

$$\begin{aligned} FRGPI = {} & (0.279 \times HMOX1\,expression\,level) + (0.558 \\ & \times TFRC\,expression\,level) + (0.107 \\ & \times JUN\,expression\,level) + (0.469 \\ & \times SOCS1\,expression\,level) \end{aligned}$$

The model was verified in the CGGA validation set (**Supplementary Figure 4A**). PCA verified that patients with glioma in TCGA training set or the CGGA validation set could be divided into high and low FRGPI groups, respectively (**Figure 5E**; **Supplementary Figure 3D**). Compared with low FRGPI, patients with glioma and a high FRGPI had a worse OS (**Figure 5F**; **Supplementary Figure 4B**), with a high predictive accuracy of FRGPI for OS (TCGA training set: 1 year AUC: 0.86, 3 years AUC: 0.88, 5 years AUC: 0.84; CGGA validation set: 1 year AUC: 0.60, 3 years AUC: 0.70, 5 years AUC: 0.70) (**Figure 5G** and **Supplementary Figure 4C**). Univariate and multivariate Cox regression analyses indicated that FRGPI was a variable

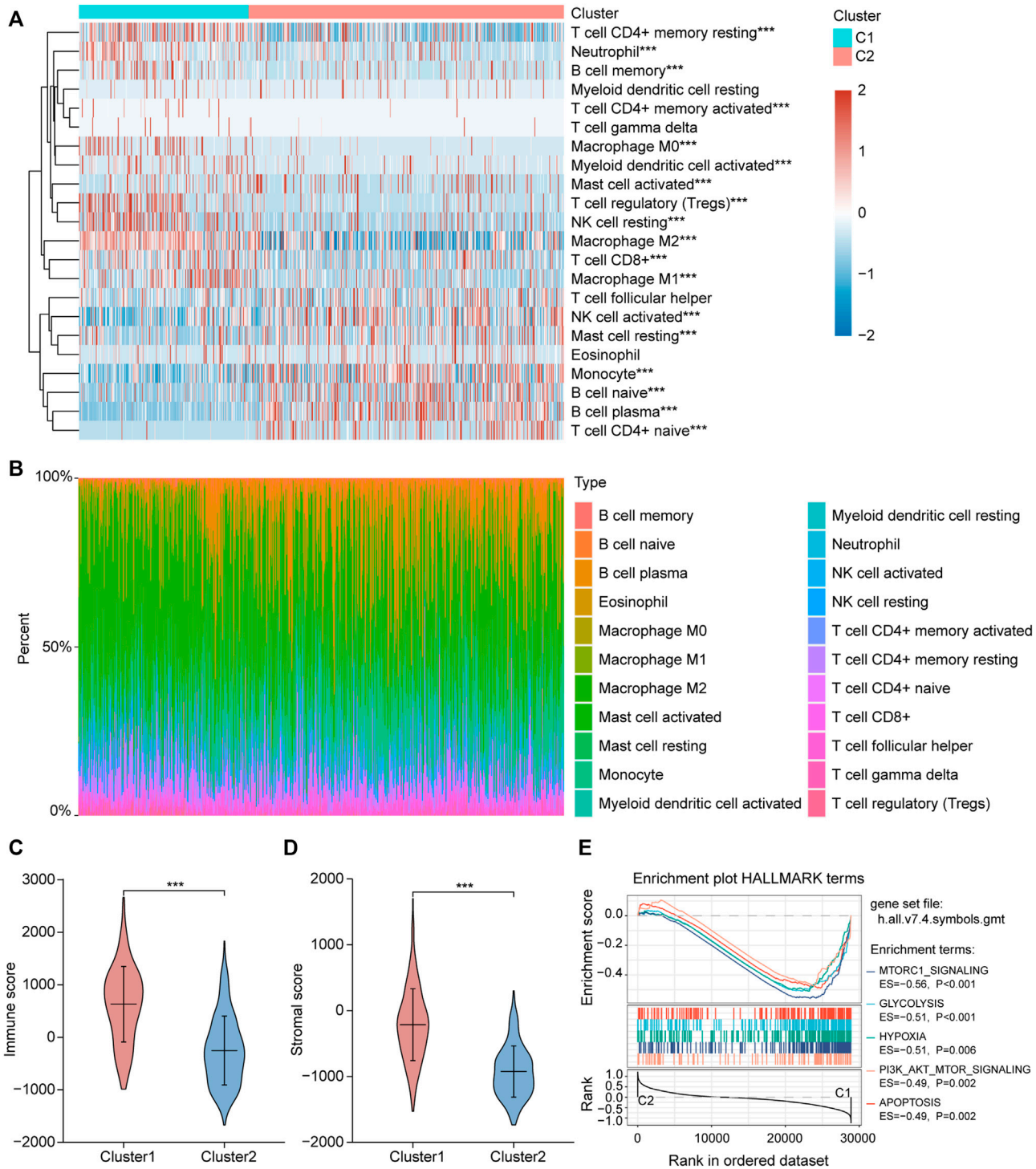

FIGURE 4 | Different immune cell infiltration between two ferroptosis-related subtypes. **(A)** Immune cell score heat map, where different colors represent the expression trend in each sample between two ferroptosis-related subtypes. *$p < 0.05$, **$p < 0.01$, ***$p < 0.001$. **(B)** The percentage abundance of tumor infiltrating immune cells in each sample, with different colors and different types of immune cells. The abscissa represents the sample, and the ordinate represents the percentage of immune cell content in a single sample. **(C,D)** Violin plots of the immuneScore and stromalScore between the two ferroptosis-related subtypes. *$p < 0.05$, **$p < 0.01$, ***$p < 0.001$. **(E)** The enrichment plots of representative Gene Set Enrichment Analysis (GSEA) results. ES, enrichment score.

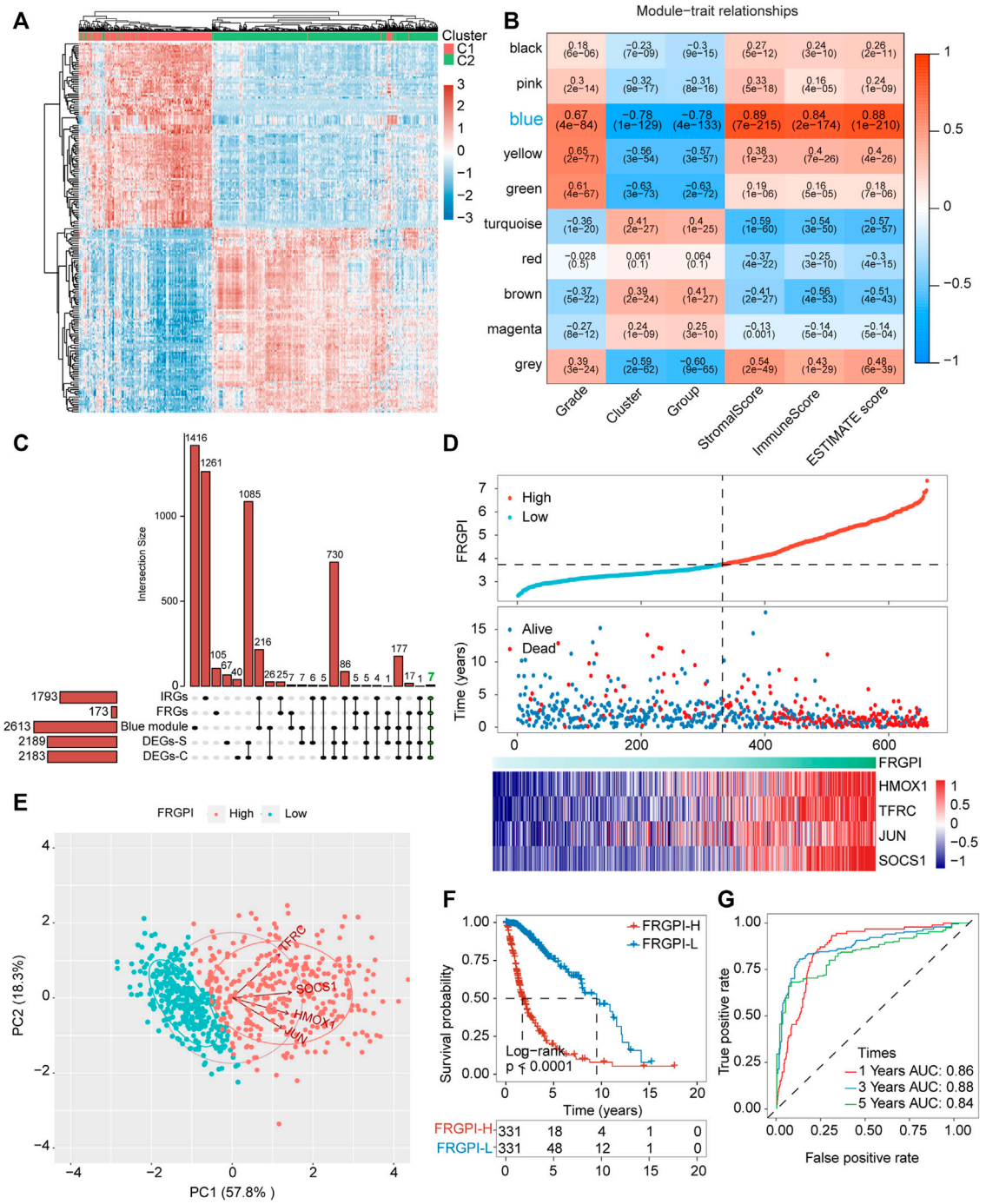

FIGURE 5 | FRGPI was developed based on FRGs for glioma. **(A)** Differential gene expression heat map, where different colors represent expression trends in different tissues. Due to the large number of differential genes, the 50 up-regulated genes and 50 down-regulated genes with the largest differential changes are shown here. **(B)** Correlation of weighted gene correlation network analysis (WGCNA) modules with ferroptosis-related subtypes and immuneScore. **(C)** Upset plot for DEGs between the two ferroptosis-related subtypes, DEGs between the two ferroptosis-related subgroups, FRGs, IRGs and genes in blue module. IRGs, immune-related genes. **(D)** FRGPI, survival outcome and *HMOX1*, *TFRC*, *JUN* and *SOCS1* expression profiles of each sample are shown. **(E)** Principal component analysis (PCA) plot of glioma samples based on *HMOX1*, *TFRC*, *JUN* and *SOCS1* expression profiles. **(F)** Kaplan–Meier analysis of glioma patients with low or high FRGPI. **(G)** ROC curves predicted prognostic value of FRGPI in glioma patients.

independent of other clinical factors, including age, grade, *IDH1* status, and 1p19q codeletion status (**Figures 6A,B**). Additionally, the prediction accuracy of FRGPI was highly stable in different clinical character groups, including <45 and >45-year age group, LGG (grade I–II gliomas are classified as LGG in the TCGA database) and GBM (grade IV gliomas) groups, IDH1-WT and

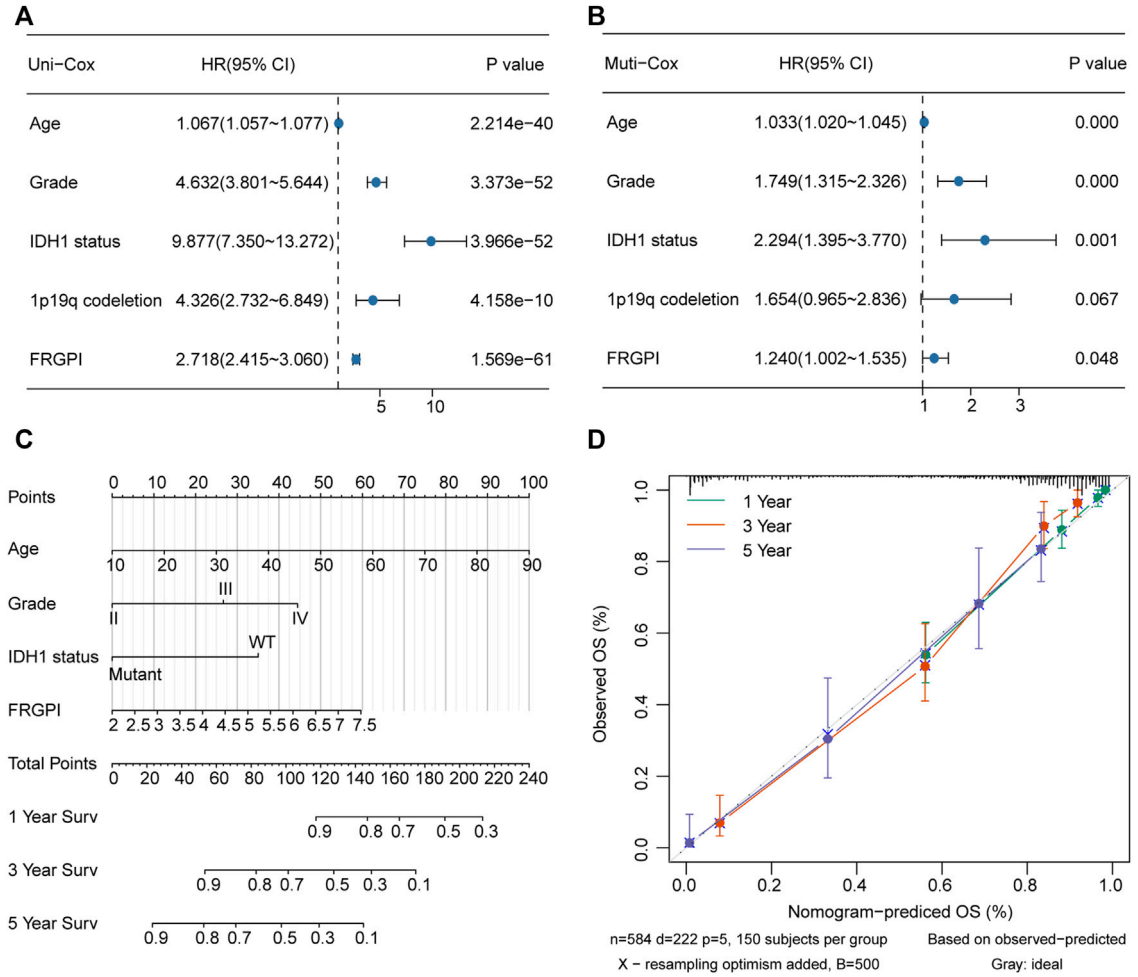

FIGURE 6 | Nomogram was constructed to calculated prognostic risk score for individual. **(A,B)** Hazard ratio and *p*-value of constituents involved in univariate and multivariate Cox regression for FRGPI, age, grade, IDH1 status and 1p19q codeletion in TCGA glioma samples. **(C)** Nomogram to predict the 1-, 3- and 5-year OS of glioma patients. **(D)** Calibration curve indicated that predicted 1-, 3- and 5-year survival rates were close to the actual survival rates. The gray dashed diagonal line represents the ideal nomogram, and the green line, red line and blue line represent the 1-, 3- and 5-y observed nomograms.

IDH1-Mut groups, 1p19q non-codel group, except in 1p19q codel group, in TCGA training set (**Supplementary Figures 5A–H**), and these results were verified again in the CGGA validation set (**Supplementary Figures 5I–P**). A nomogram was developed based on the multivariate Cox proportional hazards analysis results to precisely calculate the prognostic total risk points for an individual (**Figure 6C**). The calibration curve showed that the predicted 1-, 3-, and 5-year survival probabilities by the nomogram were close to the actual survival probability (**Figure 6D**).

FRGPI Is Associated With Clinicopathologic Features, Immunity, and Intrinsic Immune Escape in Glioma

The expression of *TFRC*, *JUN*, *HMOX1*, and *SOCS1* and the clinicopathologic features between the two FRGPI groups were compared. *TFRC*, *JUN*, *HMOX1*, and *SOCS1* were highly expressed in the high FRGPI group. Most of the patients with glioma in C1, with high WHO grade or high immuneScore, were distributed in the high FRGPI group (**Figure 7A**). The Sankey diagram fully summarized the association between FRGPI, ferroptosis-related subtypes, clinical characteristics, and prognostic signature (**Figure 7B**). In addition, GSVA was conducted to assess potential changes in pathway activity, and the results showed that most of the pathways associated with cancer progression were activated in patients with glioma with high FRGPI (**Figure 7C**). The FPI was established to model ferroptosis levels by Liu et al. We found that FRGPI was positively correlated with FPI (**Figure 8A**), which implied that FRGPI could also be associated with antitumor immunity and intrinsic immune escape in glioma. Spearman correlation test was conducted between FRGPI and stromalScore, immuneScore, the expression of PD-L1, TMB score, and MSI score (**Figures 8B–F**). FRGPI positively correlated with the stromalScore (Spearman: r = 0.670, $p < 0.001$), immuneScore (Spearman: r

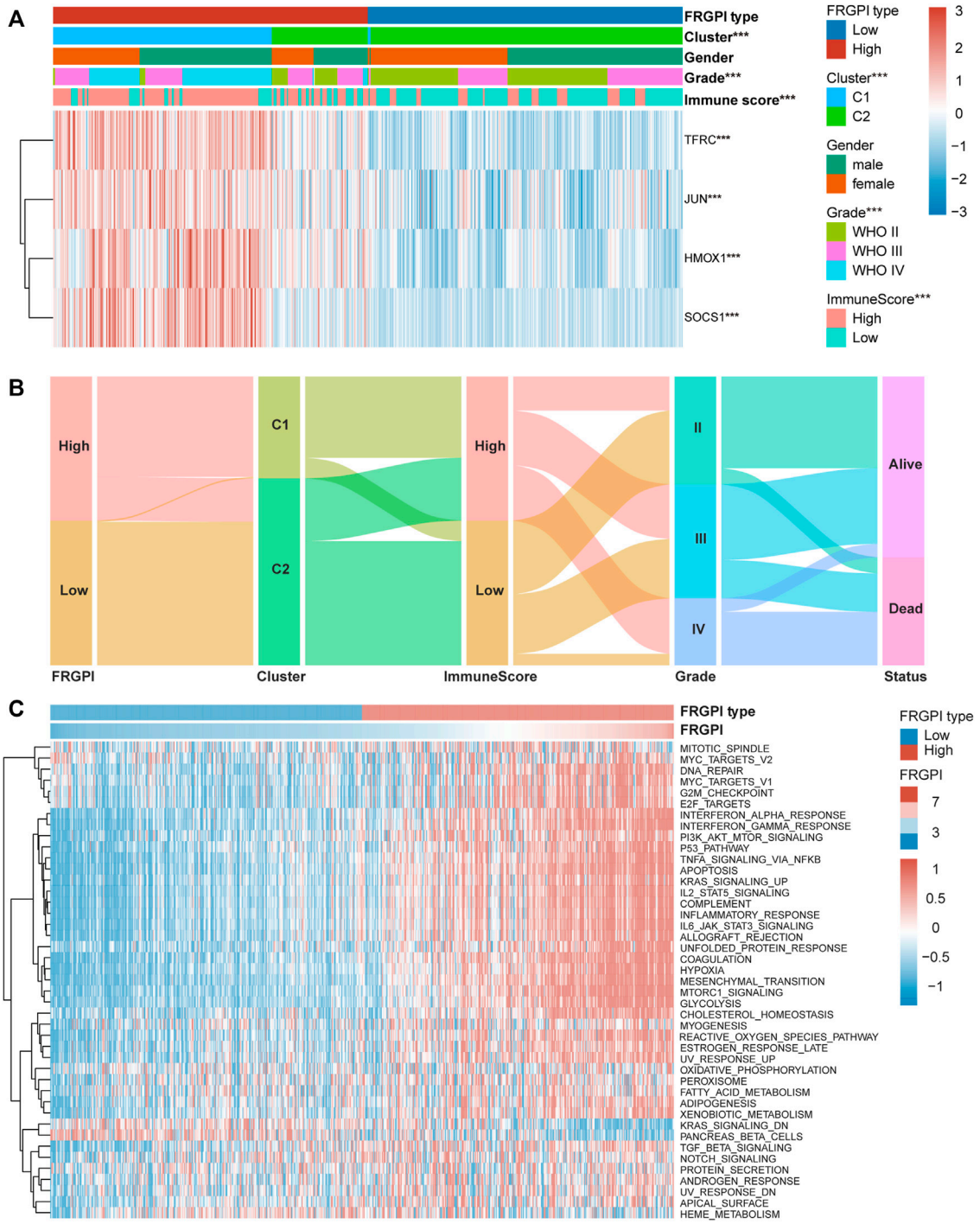

FIGURE 7 | High FRGPI is associated with glioma progression. **(A)** Heatmap showed that ferroptosis-related subtypes, grade and immuneScore were significantly associated with FRGPI. *$p < 0.05$; **$p < 0.01$; ***$p < 0.001$. **(B)** The relationship between FRGPI, ferroptosis-related subtypes, immuneScore, grade and survival status in glioma patients was illustrated by the Sankey diagram. **(C)** Heatmap of Gene set variation analysis (GSVA) results between High and Low FRGPI groups.

= 0.670, $p < 0.001$), PD-L1 expression (Spearman: r = 0.650, $p < 0.001$), and TMB score (Spearman: r = 0.440, $p < 0.001$), but negatively correlated with MSI score (Spearman: r = –0.410, $p < 0.001$). Previous research has indicated potential associations between the tumor immune microenvironment and cancer cell stemness (Saygin et al., 2019). We calculated stemness indices (mRNAsi and mDNAsi) for each glioma sample according to Malta et al. (2018), and found that FRGPI was negatively correlated with the mRNAsi score (Spearman: r = –0.520, $p < 0.001$, **Figure 8G**), but positively correlated with the mDNAsi

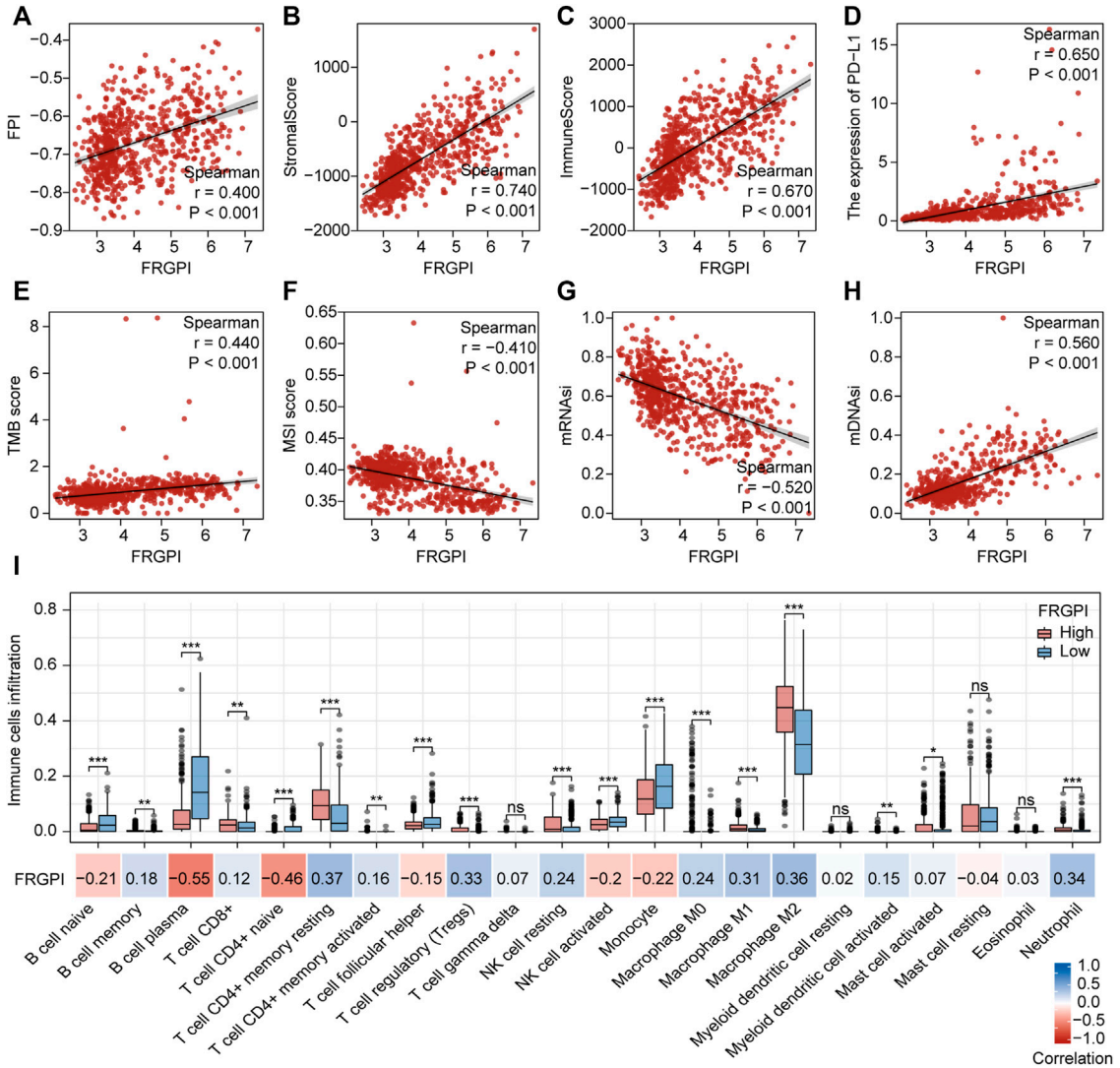

FIGURE 8 | Anti-tumor immunity and intrinsic immune escape associated with FRGPI. Spearman correlation coefficients and associated *p*-value of FRGPI with **(A)** FPI, **(B)** stromalScore, **(C)** immuneScore, **(D)** the expression of *PD-L1*, **(E)** TMB score, **(F)** MSI score, **(G)** mRNAsi, **(H)** mDNAsi are shown. r, Spearman coefficient; ns, no significance; **p* < 0.05; ***p* < 0.01; ****p* < 0.001. **(I)** Different immune cell infiltration between high and low FRGPI group, and the correlation between FRGPI and immune cells infiltration. ns, no significance; **p* < 0.05; ***p* < 0.01; ****p* < 0.001; blue, positive correlation; red, negative correlation.

score (Spearman: r = 0.560, $p < 0.001$, **Figure 8H**). Twenty-two immune cell infiltration scores of the different FRGPI groups were compared, and the correlation between FRGPI and each immune infiltrating cell score was calculated using the Spearman correlation test (**Figure 8I**). The scores of resting memory T cells $CD4^+$ (Spearman: r = 0.37, $p < 0.001$), regulatory T cells (Spearman: r = 0.33, $p < 0.001$), M1 macrophages (Spearman: r = 0.31, $p < 0.001$), M2 macrophages (Spearman: r = 0.36, $p < 0.001$), and neutrophils (Spearman: r = 0.34, $p < 0.001$) were positively correlated with FRGPI, while the scores of plasma B cell (Spearman: r = −0.55, $p < 0.001$), and naïve T cell $CD4^+$ (Spearman: r = −0.46, $p < 0.001$) were negatively correlated with FRGPI. These results indicate that FRGPI was associated with antitumor immunity and intrinsic immune escape in glioma. The GSVA results (**Supplementary Figures 3E,F**) showed FRGPI was highly correlated with PI3K_AKT_MTOR_SIGNALING (Spearman: r = 0.660, $p < 0.001$) and MTORC1_SIGNALING (Spearman: r = 0.810, $p < 0.001$).

A High FRGPI Is More Sensitive to Temozolomide, but a Low FRGPI Is More Sensitive to ICI Therapy

Next, we explored the role of FRGPI in the treatment of glioma. We investigated if FRGPI predicts the sensitivity of gliomas to temozolomide chemotherapy. Our data suggested that the estimated IC_{50} of temozolomide in the high FRGPI group was significantly lower than that in the low FRGPI group (**Figure 9A**), and FRGPI was negatively correlated with the IC_{50} of temozolomide (Spearman: r = −0.180, $p < 0.001$; **Figure 9B**),

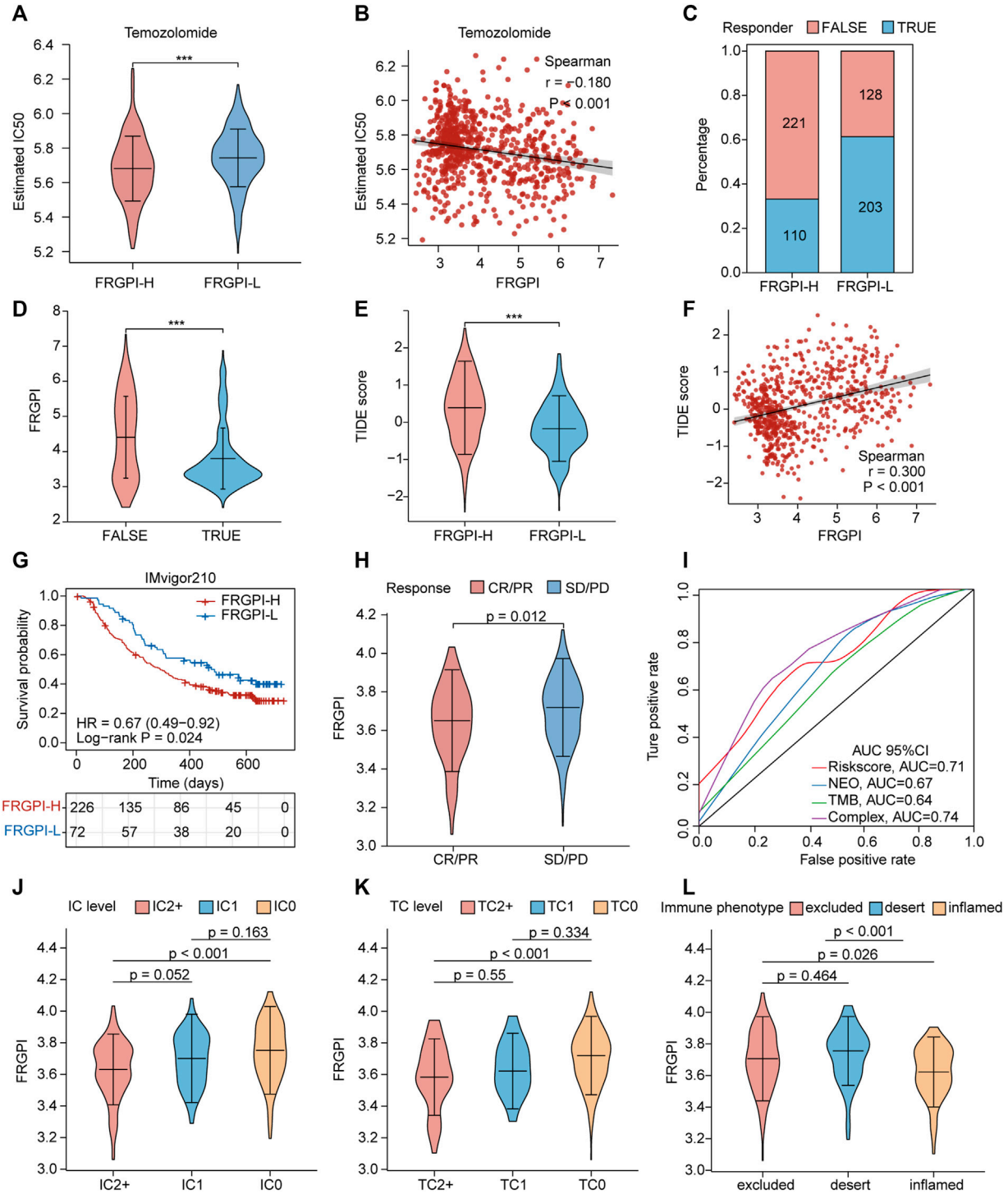

FIGURE 9 | FRGPI is predictive of temozolomide sensitivity and ICI response in glioma. **(A)** Different estimated temozolomide IC_{50} between high and low FRGPI group. **(B)** The spearman correlation between FRGPI and estimated temozolomide IC_{50}. The ICI response of each patient in high and low FRGPI group was predicted by TIDE algorithm, **(C)** stacked histogram showed the distribution of "TURE" or "FALSE" responder in high and low FRGPI group; **(D,E)** Violin plots showed the FRGPI level of "TURE"- and "FALSE"-responder group, and the different TIDE score between high- and low-FRGPI group. **(F)** The spearman correlation between FRGPI and TIDE score. **(G)** Kaplan–Meier curves showing overall survival in patients with low or high FRGPI in the anti-*PD-L1* cohort. **(H)** The distribution of FRGPI in distinct anti-*PD-L1* clinical response groups. **(I)** Roc curves showing predicting value of FRGPI, neoantigen (NEO), TMB and complex (FRGPI combined with NEO and TMB) group for anti-*PD-L1* therapy response. CR, complete response; PD, disease progression, PR, partial response; SD, stable disease. **(J–L)** Distribution of the FRGPI in distinct IC-level, TC-level and immune-phenotype group respectively in the anti-*PD-L1* cohort. IC-level, *PD-L1* expression level on immune cells; TC-level, *PD-L1* expression level on tumor cells.

suggesting that patients with glioma and high FRGPI were more sensitive to temozolomide therapy. Then, the correlation between FRGPI and the sensitivity of immunotherapy for glioma was explored. The potential ICI response was predicted using the TIDE algorithm. Our data suggested that the proportion of people responding to ICI therapy in the low FRGPI group was greater than that of the high FRGPI group (**Figure 9C**), and the "TURE-responder" group had significantly lower FRGPI than the "FALSE-responder" group (**Figure 9D**). The low FRGPI group had significantly lower TIDE scores than the high FRGPI group (**Figure 9E**), and FRGPI was positively correlated with the TIDE score (Spearman: r = 0.300, $p < 0.001$; **Figure 9F**), indicating that patients with low FRGPI had better response and efficacy to ICI therapy. In addition, we verified the reliability of FRGPI in predicting the benefit of immunotherapy in patients with urothelial cancer who received anti-*PD-L1* immunotherapy in IMvigor210 cohorts. The low FRGPI group had a longer survival time after anti-*PD-L1* therapy than the high FRGPI group (**Figure 9G**), and the complete response (CR)/partial response (PR) group had lower FRGPI than the stable disease (SD)/ progressive disease (PD) group (**Figure 9H**). The ROC curve suggested that FRGPI combined with neoantigen and TMB could predict the benefit of anti-*PD-L1* therapy more accurately (complex, AUC = 0.74; **Figure 9I**). The IC2+ level group, TC2+ level group, and inflamed phenotypes had the lowest FRGPI in terms of *PD-L1* expression level in immune cells (IC level), *PD-L1* expression level in tumor cells (TC level), and immune phenotype, respectively (**Figures 9J–L**). The above results indicate that patients with glioma and low FRGPI could be more sensitive to ICI therapy, especially anti-*PD-1* therapy.

Potential Small Molecule Compounds Based on FRGPI

The DEGs between the high and low FRGPI groups were further analyzed to identify potential small molecule compounds for glioma treatment. Consequently, 263 DEGs (**Supplementary Table 9**) were identified, including 184 upregulated and 79 downregulated genes (**Supplementary Figure 3G**). Functional enrichment analysis revealed that the DEGs were mainly enriched in response to cytokines, cytokine-mediated signaling pathways, cytokine signaling in the immune system, innate immune system, and phagosomes (**Figure 10A**; **Supplementary Table 10**). The DEGs were uploaded to the CMap database, and the underlying mechanisms of drug action were analyzed. As shown in **Figure 10B**, a total of 15 potential small molecule compounds (such as depactin, physostigmine, and phenacetin) and 15 drug action mechanisms (such as HDAC inhibitor, acetylcholinesterase inhibitor, cyclooxygenase inhibitor) were identified, which provide a reference to search for potential drugs for the treatment of glioma.

DISCUSSION

In this study, we successfully developed a ferroptosis-related gene prognostic index (FRGPI) to predict the sensitivity to temozolomide and the response to ICI therapy in patients with glioma. We comprehensively analyzed the role of FRGPI to identify different clinicopathological, molecular, and immune characteristics of patients with glioma that could improve treatment selection. From a new perspective of ferroptosis and glioma immune microenvironment regulation, our study can be used for more effective chemotherapy, immunotherapy, and targeted therapy plans for glioma.

Studies identified at least three major ferroptosis defense mechanisms have been identified in cells. Glutathione peroxidase 4 (GPX4) protects cells from ferroptosis by specifically catalyzing lipid peroxides in a glutathione-dependent manner (Seibt et al., 2019). Ferroptosis suppressor protein 1 (FSP1), locating on the cell membrane, prevents lipid peroxidation on the cell membrane and thus inhibiting ferroptosis by reducing ubiquinone (CoQ) to dihydroubiquinone (CoQH2) (Bersuker et al., 2019; Doll et al., 2019). Guanosine triphosphate cyclic hydrolase (GCH1), a rate-limiting enzyme for the synthesis of tetrahydrobiopterin (BH_4), counteracts ferroptosis in a GPX4-independent manner (Kraft et al., 2020; Soula et al., 2020). Until Mao et al. discovered a new inhibitor of ferroptosis, dihydrowhey dehydrogenase (DHODH), which is independent of the classical GPX4 signaling pathway, and discovered the way of ferroptosis based on mitochondrial lipid peroxidation for the first time (Mao et al., 2021). Mao et al. proposed that there are at least three different subcellular localization of ferroptosis defense systems in cells: GPX4 in cytoplasm and mitochondria, FSP1 in plasma membrane, and DHODH in mitochondria, among which DHODH and GPX4 are the two main suppressors to defense against ferroptosis in mitochondrial (Mao et al., 2021). Tran et al. have demosrated GCH1 has an obvious ascending trend with grade increase, and plays a role in promoting progression in GBM (Tran et al., 2018), suggesting that GCH1 may play a more important role in high-grade glioma, while its role in low-grade glioma needs further discussion in the future. Our analysis showed that *GPX4*, *FSP1*, *GCH1*, and *DHODH* were more highly expressed in tumor tissue than in non-tumor brain tissue, especially in high-grade, IDH1 wild type, 1p19q non-codeletion gliomas, suggesting that glioma cells had a strong potential to resist ferroptosis. Identifying markers that could affect tumor immunity and ferroptosis status for the construction of FRGPI is pivotal. First, based on the expression profiles of FRGs, patients in TCGA cohort with glioma were divided into two ferroptosis-related subtypes (C1 and C2) with distinct differences in molecular and immune characteristics. *GPX4*, *FSP1*, *GCH1*, and *DHODH* were significantly upregulated in the patients of C1, implying that C1 represented a ferroptosis-suppressive status. Some genetic aberrations in glioma have been known for years, such as IDH1, TP53, MGMT, EGFR, ATRX, PTEN, AND CIC (Siegal, 2015; Weissmann et al., 2018; Ghosh et al., 2019). Our results showed that *IDH1*, *TP53*, *ATRX*, and *CIC* mutation frequencies in C2 were higher than in C1, but *PTEN* and *EGFR* in C1 were higher than in C2, suggesting that mutation frequencies of those genes may lead to different ferroptosis status. The patients in C1 had a worse overall prognosis than those in C2, indicating that identifying subtypes with different ferroptosis statuses had

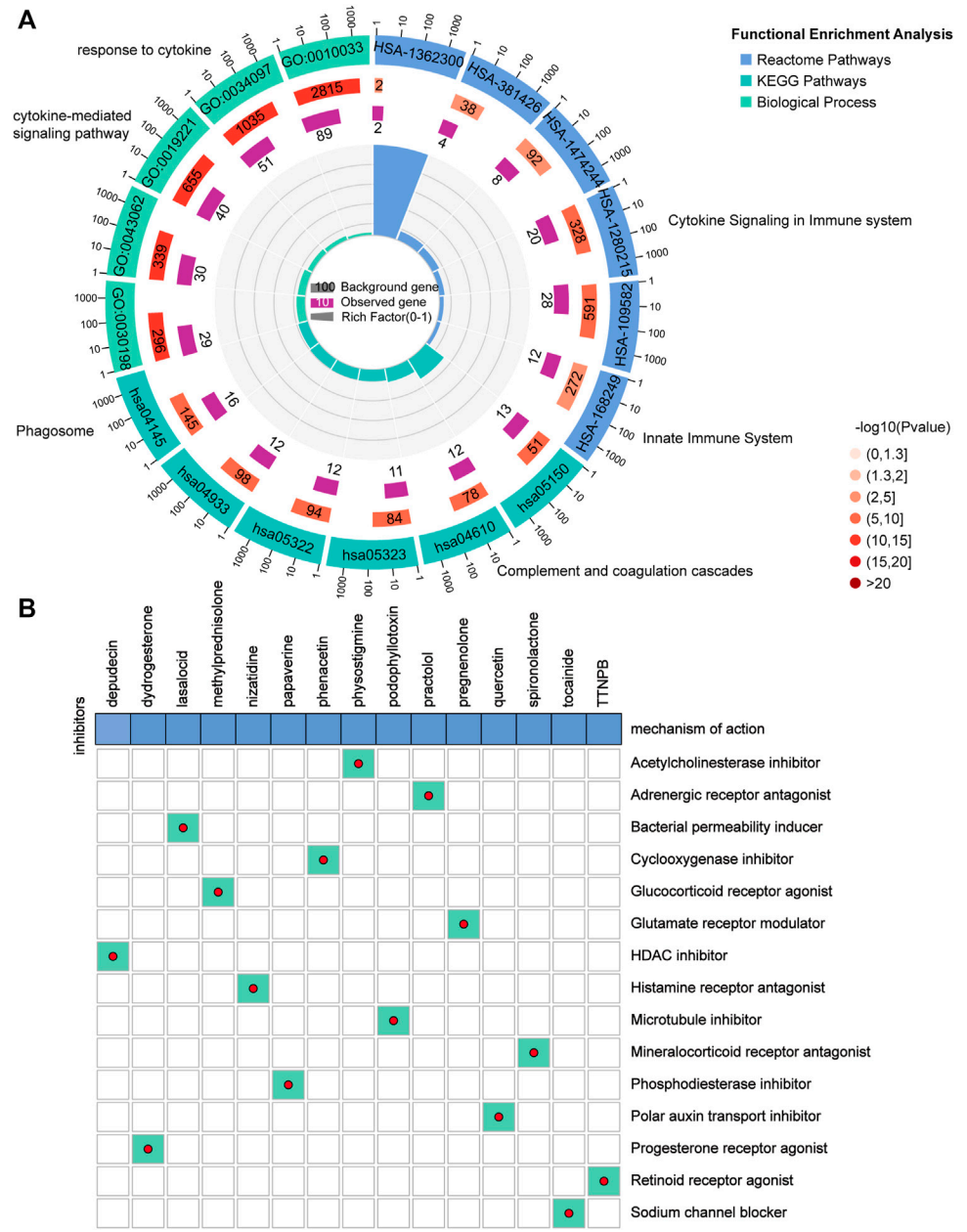

FIGURE 10 | Potential small molecule compounds based on PRGPI. **(A)** Function enrichment analysis results of 263 DEGs between the high and low FRGPI groups. **(B)** Candidate small molecular drugs and mechanisms of action were discovered based on FRGPI. The abscissa represents the drugs, and the ordinate represents drug mechanisms of action.

clinical prognostic implications. We then utilized WGCNA to identify candidate genes related to ferroptosis status and immunity. Afterward, we applied the "stepAIC" algorithm to construct the FRGPI based on four genes (*HMOX1*, *TFRC*, *JUN*, and *SOCS1*). The FRGPI proved to be an independent ferroptosis-related prognostic biomarker for glioma, with better survival in patients with FRGPI-low and worse survival in patients with FRGPI-high in both TCGA and CGGA cohorts.

FRGPI comprises four genes, *HMOX1*, *TFRC*, *JUN*, and *SOCS1*. Heme oxygenase 1 (*HMOX1*), a membrane-bound enzyme that cleaves the heme ring at the alpha-methene bridge to produce biliverdin, iron, and carbon monoxide, catalyzes the degradation of heme. Chang et al. discovered that *HMOX1* was a key mediator of BAY 11-7085 -induced ferroptosis that operated through cellular redox regulation and iron accumulation (Chang et al., 2018). Lu et al. (2019) discovered that the overexpression of HMOX1 enhanced both erastin- and RSL-3-triggered lipid reactive oxygen species to enhance ferroptosis. Arnold et al. (2014) observed that macrophages overexpressing *HMOX1* led to tumor immune suppression in

pancreatic ductal adenocarcinoma. In addition, *HMOX1* was also observed to be related to immune suppression in neuroblastoma (Fest et al., 2016). The transferrin receptor (*TFRC*) encodes a cell surface receptor necessary for cellular iron uptake by receptor-mediated endocytosis. Wu et al. (2019) indicated that upregulation of *TFRC* promoted ferroptosis. Crepin et al. (2010) defined a novel class of fully human anti-*TFRC* antibodies suitable for immunotherapy against tumors whose proliferation depended on high levels of *TFRC* and iron uptake, such as myeloid leukemia and acute lymphoid. Jun proto-oncogene, AP-1 transcription factor subunit (*JUN*, also known as c-Jun) encodes a protein that is highly similar to the viral protein and interacts directly with specific target DNA sequences to regulate gene expression. A study observed that erastin could inhibit O-GlcNAcylation of *c-Jun* to suppress the malignant phenotypes of liver cancer cells (Chen et al., 2019). *C-Jun* has been shown to be related to T-cell proliferation and *PD-L1* expression (Jiang et al., 2013; Zdanov et al., 2016). The suppressor of cytokine signaling 1 (*SOCS1*) encodes a member of the *STAT*-induced *STAT* inhibitor, which functions downstream of cytokine receptors and takes part in a negative feedback loop to attenuate cytokine signaling. Saint-Germain et al. (2017) revealed that exogenous *SOCS1* was sufficient to regulate the sensitivity of cells to ferroptosis by reducing the expression of the cystine transporter *SLC7A11* and the level of glutathione. Saudemont et al. (2007) demonstrated that *SOCS1* expression restored via demethylation contributed to the resistance of tumor cells to $CD8^+$ CTL-mediated killing. In the FRGPI calculation formula, the coefficients of *HMOX1*, *TFRC*, *JUN*, and *SOCS1* were positive. Therefore, there was a positive relationship between FRGPI, *HMOX1*, *TFRC*, *JUN*, and *SOCS1*, and they were promising therapeutic targets for glioma. Liu et al. (2020) established the ferroptosis potential index (FPI) based on 24 FRGs to explore the functional roles of ferroptosis and revealed that ferroptosis was associated with clinical features and the immune microenvironment in cancers. FRGPI was positively correlated with FPI, implying that FRGPI was a simpler and more convenient ferroptosis potential indicator in gliomas. In summary, FRGPI has been found to be a prognostic biomarker associated with cell sensitivity to ferroptosis and tumor immunity.

Screening patients with glioma who are good candidates for temozolomide chemotherapy and ICI therapy was a vital function of the FRGPI. Our data showed that patients with a high FRGPI were more sensitive to temozolomide treatment than those with a low FRGPI. Additionally, the low FRGPI group had a stronger response to ICI and better efficacy from ICI therapy than the group with a high FRGPI. Stemness, defined as the potential for self-renewal and differentiation from the cell of origin, is highly associated with tumor progression and chemoresistance (Shibue and Weinberg, 2017; Su et al., 2018; Cooper and Giancotti, 2019). Malta et al. (2018) developed stemness indexes (including mRNAsi and mDNAsi) to reveal intra-tumor molecular heterogeneity and indicated a strong relationship between immune microenvironment content and stemness. Our results showed that patients with a high FRGPI had lower mRNAsi but higher mDNAsi than those with a low FRGPI, indicating that FRGPI could affect chemoresistance and ICI response by altering tumor cell stemness. We also explored the correlation between the FRGPI and *PD-L1*, TMB, and MSI, which are well-known predictive biomarkers for immunotherapy. In general, *PD-L1*-positive cancers tended to respond to anti-*PD-1*/*PD-L1* therapies compared to *PD-L1*-negative cancers (Hansen and Siu, 2016). However, our results showed that the FRGPI had a negative ICI response but was positively related to the expression of *PD-L1*. *PD-L1* expression within the tumor microenvironment has predictive value for assessing response to anti-*PD-1*/*PD-L1* in many studies in melanoma (Weber et al., 2017), non-small-cell lung cancer (Fehrenbacher et al., 2016), and bladder cancer (Rosenberg et al., 2016) but this was not a consistent finding (Rosenberg et al., 2016; Sharma et al., 2017). Noticeably, tumors with negative *PD-L1* that escaped immune elimination were still sensitive to antibody-mediated *PD-L1* inhibitors (Noguchi et al., 2017). We hypothesized that the subcellular distribution of *PD-L1* in glioma tissues was more valuable than the *PD-L1* expression level measured by transcriptome data. Therefore, further studies are necessary to clarify the relationship between the subcellular distribution of *PD-L1* and the FRGPI. TMB and MSI have been recently evaluated as potential biomarkers for predicting ICI response in many cancer types (Bonneville et al., 2017; Yarchoan et al., 2017). Here, we found that the FRGPI had a significant correlation with TMB and MSI scores, which implied that TMB and MSI could explain why the FRGPI affected the response of patients with glioma to ICI, although there are other possible mechanisms involved in it.

The tumor immune microenvironment (TIME) is closely related to the progression, chemoresistance, and immunotherapy response (Cao and Yan, 2020; Hegde and Chen, 2020). Understanding the landscape of the TIME could help find new treatments for glioma or alter the TIME to improve the efficacy of immunotherapy. The infiltration of immune cells was distinct between the two subgroups. $CD8^+$ T cells, resting and activated memory $CD4^+$ T cells, regulatory T cells, resting NK cells, M0, M1, and M2 macrophages, activated myeloid dendritic cells, activated mast cells, memory B cells, and neutrophils were mainly enriched in the FRGPI-high subgroup with a worse prognosis, while naive $CD4^+$ T cells, follicular helper T cells, activated NK cells, plasma B cells, naïve B cells, and monocytes were more common in the FRGPI-low subgroup with a better prognosis. Numerous studies have shown that dense infiltration of cytotoxic $CD8^+$ T cells indicates a favorable prognosis (Bindea et al., 2013; Gentles et al., 2015; Fridman et al., 2017). M2 macrophages have been proven to be related to tumor growth, the development of an invasive phenotype, and are associated with a poor prognosis in breast, gastric, bladder, ovarian, and prostate cancers (Ruffell and Coussens, 2015). Conversely, M1 macrophages could signal a favorable prognosis in non-small-cell lung cancer, hepatocellular carcinoma, and ovarian and gastric cancers (Ruffell and Coussens, 2015). Our research results do not fully support these conclusions. Yin et al. found that high infiltrating levels of $CD4^+$ T cells, B cells, $CD8^+$ T cells, neutrophils, macrophages, and dendritic cells were all negatively correlated with the OS of lower-grade gliomas (Yin et al., 2020), which supports our study results. Considering that

we did not use multiple algorithms to compare the immune cell infiltration landscape of glioma, we will further explore the relationship between the FRGPI and immune infiltration in future studies. Most importantly, the FRGPI could be of great significance for future researchers to develop an algorithm that specifically predicts the immune infiltration of glioma cells.

In addition, 184 upregulated and 79 downregulated genes were identified between the high and low FRGPI groups to explore the mechanism of action and potential small molecule compounds related to FRGPI. Functional enrichment analysis revealed that the FRGPI was significantly associated with immune-related pathways, including responses to cytokines, cytokine-mediated signaling pathways, cytokine signaling in the immune system, innate immune system, and phagosomes, which further indicated that tumor cell ferroptosis had a potential regulatory effect on tumor immunity. Finally, 15 potential small molecule compounds, such as depactin, physostigmine, and phenacetin, were predicted based on the FRGPI, which provided a reference for us to search for effective drugs to treat glioma.

Potential limitations of the present study are as follows. Firstly, a major limitation is that we use a public database rather than our own samples, so we will focus on collecting our own glioma samples to further verify the reliability of the research results. Secondly, the number of immunotherapy cohorts is limited, and it is extremely important to collect more ICI cohorts, especially for glioma, in the future. Finally, we did not explore the specific action mechanism of the FRGPI members, which will be an important direction of our future research.

CONCLUSION

In conclusion, the FRGPI is a promising ferroptosis-related prognostic biomarker. It may help in distinguishing immune and molecular characteristics and accurately predicting the clinical outcome, possible temozolomide resistance, and ICI response in glioma. Hence, it is essential to systematically evaluate the FRGPI for each patient with glioma, which might assist oncologists to make decisions to administer ferroptosis-based anticancer therapy.

DATA AVAILABILITY STATEMENT

The datasets presented in this study can be found in online repositories. The names of the repository/repositories and accession number(s) can be found in the article/ **Supplementary Material**.

ETHICS STATEMENT

Studies involving human participants were reviewed and approved by Ethics Committees of Nanfang Hospital. The patients/participants provided written informed consent to participate in the study.

AUTHOR CONTRIBUTIONS

Research design: XZ, YS, JX. Data analysis: YC, XL, ZZ, YZ, JL, AX. Experiments: YC, XL, WX. Manuscript writing: YC, XL. Manuscript revision: XZ, YS, YC, YZ, XL, JL, WX, PC, YM, SX, ZS, LH. All authors have read and approved the final manuscript.

FUNDING

Science and Technology Program of Guangzhou, China (NO. 201903010048); National Nature Science Fund of China (No. 81872064); the Natural Science Fund of Guangdong Province, China (No. 2020A1515010122 and 2021A1515012465); Natural Science Fund of Heilongjiang, China (Grant NO. LH2019H124). The funders had no role in study design, data collection, data analysis, decision to publish, or preparation of the manuscript.

ACKNOWLEDGMENTS

We acknowledge TCGA database and CGGA database for providing their platform and contributors for uploading their meaningful datasets. We would like to thank Editage (www.editage.cn) for English language editing of this manuscript.

SUPPLEMENTARY MATERIAL

The Supplementary Material for this article can be found online at: https://www.frontiersin.org/articles/10.3389/fcell.2021.812422/full#supplementary-material

Supplementary Figure 1 | Aberrant expression of GPX4, GCH1, FSP1 and DHODH in glioma. **(A,B)** Boxplots of GPX4, FSP1, GCH1 and DHODH expression in different grade glioma samples in CGGA cohort. ns, no significance; $^{*}p < 0.05$; $^{**}p < 0.01$; $^{***}p < 0.001$. **(C–F)** Immunohistochemistry (IHC) staining for GPX4, FSP1, GCH1 and DHODH, respectively, in glioma and non-tumor brain tissue.

Supplementary Figure 2 | Consensus clustering based on based on the expression of 94 ferroptosis suppressors. **(A)** CGGA validation set were divided into two different ferroptosis-related subgroups (G1 and G2) by consensus clustering based on based on 94 ferroptosis suppressors. **(B)** Kaplan–Meier analysis of patients in the two different ferroptosis-related subgroups. **(C)** Boxplots of the immuneScore and stromalScore between the two ferroptosis-related subtypes. $^{*}p < 0.05$, $^{**}p < 0.01$, $^{***}p < 0.001$. **(D)** Immune cell score heat map, where different colors represent the expression trend in each sample between two ferroptosis-related subgroups. $^{*}p < 0.05$, $^{**}p < 0.01$, $^{***}p < 0.001$. **(E)** The percentage abundance of tumor infiltrating immune cells in each sample, with different colors and different types of immune cells. The abscissa represents the sample, and the ordinate represents the percentage of immune cell content in a single sample.

Supplementary Figure 3 | Screening and verification of the hub gene used to construct FRGPI. **(A)** Differential gene expression heatmap, where different colors represent expression trends in different tissues. Due to the large number of differential genes, the 50 up-regulated genes and 50 down-regulated genes with the largest differential changes are shown here. Red, up-regulated; blue, down-regulated. **(B)** Correlation of weighted gene correlation network analysis (WGCNA) divided all protein-coding genes into 10 modules. **(C)** The protein-protein interaction network of the 7 hub genes related both ferroptosis and tumor immunity. **(D)** Principal component analysis (PCA) plot of glioma samples based on HMOX1, TFRC, JUN and SOCS1 expression profiles in CGGA validation set. **(E,F)** GSVA

analysis results of the relationship between FRGPI and PI3K_AKT_MTOR_SIGNALING (Spearman r = 0.660, $p < 0.001$) and MTORC1_SIGNALING (Spearman r = 0.810, $p < 0.001$).

Supplementary Figure 4 | The validation of the prognosis predicting value of FRGPI in CGGA validation set. **(A)** FRGPI, survival status and HMOX1, TFRC, JUN and SOCS1 expression profiles of each sample are shown. **(B)** Kaplan–Meier analysis of glioma patients with low or high FRGPI. **(C)** ROC curves validate the prognostic value of FRGPI in glioma patients (1 year AUC: 0.86, 3 years AUC: 0.88, 5 years AUC: 0.84).

Supplementary Figure 5 | The prediction accuracy of FRGPI in different clinical character groups. (**A–H)** The prediction accuracy of FRGPI in <45- and >45- year old group, LGG and GBM group, IDH1-WT and IDH1-Mut group, 1p19q codel and 1p19q non-codel group in TCGA training set. (**I–P)** The prediction accuracy of FRGPI in <45- and >45- years group, LGG and GBM group, IDH1-WT and IDH1-Mut group, 1p19q codel and 1p19q non-codel group in in CGGA validation set.

Supplementary Table 1 | The baseline clinical characteristics of glioma patients.

Supplementary Table 2 | 24 ferroptosis-related genes for consensus clustering.

Supplementary Table 3 | 173 ferroptosis-related genes list.

Supplementary Table 4 | 1793 immune-related genes list.

Supplementary Table 5 | 94 ferroptosis suppressors list.

Supplementary Table 6 | 2183 DEGs list between C1 and C2.

Supplementary Table 7 | 2189 DEGs list between G1 and G2.

Supplementary Table 8 | 2613 genes list in blue module.

Supplementary Table 9 | 263 DEGs between the high and low FRGPI groups.

Supplementary Table 10 | Function enrichment analysis results for 263 DEGs.

REFERENCES

Aldape, K., Brindle, K. M., Chesler, L., Chopra, R., Gajjar, A., Gilbert, M. R., et al. (2019). Challenges to Curing Primary Brain Tumours. *Nat. Rev. Clin. Oncol.* 16, 509–520. doi:10.1038/s41571-019-0177-5

Angeli, J. P. F., Krysko, D. V., and Conrad, M. (2019). Ferroptosis at the Crossroads of Cancer-Acquired Drug Resistance and Immune Evasion. *Nat. Rev. Cancer* 19, 405–414. doi:10.1038/s41568-019-0149-1

Arnold, J. N., Magiera, L., Kraman, M., and Fearon, D. T. (2014). Tumoral Immune Suppression by Macrophages Expressing Fibroblast Activation Protein-α and Heme Oxygenase-1. *Cancer Immunol. Res.* 2, 121–126. doi:10.1158/2326-6066.cir-13-0150

Bellmunt, J., De Wit, R., Vaughn, D. J., Fradet, Y., Lee, J.-L., Fong, L., et al. (2017). Pembrolizumab as Second-Line Therapy for Advanced Urothelial Carcinoma. *N. Engl. J. Med.* 376, 1015–1026. doi:10.1056/nejmoa1613683

Bersuker, K., Hendricks, J. M., Li, Z., Magtanong, L., Ford, B., Tang, P. H., et al. (2019). The CoQ Oxidoreductase FSP1 Acts Parallel to GPX4 to Inhibit Ferroptosis. *Nature* 575, 688–692. doi:10.1038/s41586-019-1705-2

Bhattacharya, S., Dunn, P., Thomas, C. G., Smith, B., Schaefer, H., Chen, J., et al. (2018). ImmPort, toward Repurposing of Open Access Immunological Assay Data for Translational and Clinical Research. *Sci. Data* 5, 180015. doi:10.1038/sdata.2018.15

Bindea, G., Mlecnik, B., Tosolini, M., Kirilovsky, A., Waldner, M., Obenauf, A. C., et al. (2013). Spatiotemporal Dynamics of Intratumoral Immune Cells Reveal the Immune Landscape in Human Cancer. *Immunity* 39, 782–795. doi:10.1016/j.immuni.2013.10.003

Bonneville, R., Krook, M. A., Kautto, E. A., Miya, J., Wing, M. R., Chen, H. Z., et al. (2017). Landscape of Microsatellite Instability across 39 Cancer Types. *JCO Precis Oncol.* 1, 1–15. doi:10.1200/po.17.00073

Brahmer, J., Reckamp, K. L., Baas, P., Crinò, L., Eberhardt, W. E. E., Poddubskaya, E., et al. (2015). Nivolumab versus Docetaxel in Advanced Squamous-Cell Non-small-cell Lung Cancer. *N. Engl. J. Med.* 373, 123–135. doi:10.1056/nejmoa1504627

Cao, J., and Yan, Q. (2020). Cancer Epigenetics, Tumor Immunity, and Immunotherapy. *Trends Cancer* 6, 580–592. doi:10.1016/j.trecan.2020.02.003

Chalmers, Z. R., Connelly, C. F., Fabrizio, D., Gay, L., Ali, S. M., Ennis, R., et al. (2017). Analysis of 100,000 Human Cancer Genomes Reveals the Landscape of Tumor Mutational burden. *Genome Med.* 9, 34. doi:10.1186/s13073-017-0424-2

Chang, L.-C., Chiang, S.-K., Chen, S.-E., Yu, Y.-L., Chou, R.-H., and Chang, W.-C. (2018). Heme Oxygenase-1 Mediates BAY 11-7085 Induced Ferroptosis. *Cancer Lett.* 416, 124–137. doi:10.1016/j.canlet.2017.12.025

Chen, X., Kang, R., Kroemer, G., and Tang, D. (2021). Broadening Horizons: the Role of Ferroptosis in Cancer. *Nat. Rev. Clin. Oncol.* 18, 280–296. doi:10.1038/s41571-020-00462-0

Chen, Y., Zhu, G., Liu, Y., Wu, Q., Zhang, X., Bian, Z., et al. (2019). O-GlcNAcylated C-Jun Antagonizes Ferroptosis via Inhibiting GSH Synthesis in Liver Cancer. *Cell Signal.* 63, 109384. doi:10.1016/j.cellsig.2019.109384

Cooper, J., and Giancotti, F. G. (2019). Integrin Signaling in Cancer: Mechanotransduction, Stemness, Epithelial Plasticity, and Therapeutic Resistance. *Cancer Cell* 35, 347–367. doi:10.1016/j.ccell.2019.01.007

Crepin, R., Goenaga, A.-L., Jullienne, B., Bougherara, H., Legay, C., Benihoud, K., et al. (2010). Development of Human Single-Chain Antibodies to the Transferrin Receptor that Effectively Antagonize the Growth of Leukemias and Lymphomas. *Cancer Res.* 70, 5497–5506. doi:10.1158/0008-5472.can-10-0938

Doll, S., Freitas, F. P., Shah, R., Aldrovandi, M., Da Silva, M. C., Ingold, I., et al. (2019). FSP1 Is a Glutathione-independent Ferroptosis Suppressor. *Nature* 575, 693–698. doi:10.1038/s41586-019-1707-0

Donson, A. M., Addo-Yobo, S. O., Handler, M. H., Gore, L., and Foreman, N. K. (2007). MGMT Promoter Methylation Correlates with Survival Benefit and Sensitivity to Temozolomide in Pediatric Glioblastoma. *Pediatr. Blood Cancer* 48, 403–407. doi:10.1002/pbc.20803

Fehrenbacher, L., Spira, A., Ballinger, M., Kowanetz, M., Vansteenkiste, J., Mazieres, J., et al. (2016). Atezolizumab versus Docetaxel for Patients with Previously Treated Non-small-cell Lung Cancer (POPLAR): a Multicentre, Open-Label, Phase 2 Randomised Controlled Trial. *The Lancet* 387, 1837–1846. doi:10.1016/s0140-6736(16)00587-0

Fest, S., Soldati, R., Christiansen, N. M., Zenclussen, M. L., Kilz, J., Berger, E., et al. (2016). Targeting of Heme Oxygenase-1 as a Novel Immune Regulator of Neuroblastoma. *Int. J. Cancer* 138, 2030–2042. doi:10.1002/ijc.29933

Fridman, W. H., Zitvogel, L., Sautès–Fridman, C., and Kroemer, G. (2017). The Immune Contexture in Cancer Prognosis and Treatment. *Nat. Rev. Clin. Oncol.* 14, 717–734. doi:10.1038/nrclinonc.2017.101

Friedman, H. S., Kerby, T., and Calvert, H. (2000). Temozolomide and Treatment of Malignant Glioma. *Clin. Cancer Res.* 6, 2585–2597.

Gentles, A. J., Newman, A. M., Liu, C. L., Bratman, S. V., Feng, W., Kim, D., et al. (2015). The Prognostic Landscape of Genes and Infiltrating Immune Cells across Human Cancers. *Nat. Med.* 21, 938–945. doi:10.1038/nm.3909

Ghosh, M. K., Chakraborty, D., Sarkar, S., Bhowmik, A., and Basu, M. (2019). The Interrelationship between Cerebral Ischemic Stroke and Glioma: a Comprehensive Study of Recent Reports. *Sig Transduct Target. Ther.* 4, 42. doi:10.1038/s41392-019-0075-4

Gong, Y., Fan, Z., Luo, G., Yang, C., Huang, Q., Fan, K., et al. (2019). The Role of Necroptosis in Cancer Biology and Therapy. *Mol. Cancer* 18, 100. doi:10.1186/s12943-019-1029-8

Hansen, A. R., and Siu, L. L. (2016). PD-L1 Testing in Cancer: Challenges in Companion Diagnostic Development. *JAMA Oncol.* 2, 15–16. doi:10.1001/jamaoncol.2015.4685

Hegde, P. S., and Chen, D. S. (2020). Top 10 Challenges in Cancer Immunotherapy. *Immunity* 52, 17–35. doi:10.1016/j.immuni.2019.12.011

Hegi, M. E., Diserens, A.-C., Gorlia, T., Hamou, M.-F., De Tribolet, N., Weller, M., et al. (2005). MGMTGene Silencing and Benefit from Temozolomide in Glioblastoma. *N. Engl. J. Med.* 352, 997–1003. doi:10.1056/nejmoa043331

Hu, Z., Mi, Y., Qian, H., Guo, N., Yan, A., Zhang, Y., et al. (2020). A Potential Mechanism of Temozolomide Resistance in Glioma-Ferroptosis. *Front. Oncol.* 10, 897. doi:10.3389/fonc.2020.00897

Jackson, C. M., Choi, J., and Lim, M. (2019). Mechanisms of Immunotherapy Resistance: Lessons from Glioblastoma. *Nat. Immunol.* 20, 1100–1109. doi:10.1038/s41590-019-0433-y

Jiang, P., Gu, S., Pan, D., Fu, J., Sahu, A., Hu, X., et al. (2018). Signatures of T Cell Dysfunction and Exclusion Predict Cancer Immunotherapy Response. *Nat. Med.* 24, 1550–1558. doi:10.1038/s41591-018-0136-1

Jiang, X., Stockwell, B. R., and Conrad, M. (2021). Ferroptosis: Mechanisms, Biology and Role in Disease. *Nat. Rev. Mol. Cell Biol* 22, 266–282. doi:10.1038/s41580-020-00324-8

Jiang, X., Zhou, J., Giobbie-Hurder, A., Wargo, J., and Hodi, F. S. (2013). The Activation of MAPK in Melanoma Cells Resistant to BRAF Inhibition Promotes PD-L1 Expression that Is Reversible by MEK and PI3K Inhibition. *Clin. Cancer Res.* 19, 598–609. doi:10.1158/1078-0432.ccr-12-2731

Karachi, A., Dastmalchi, F., Mitchell, D. A., and Rahman, M. (2018). Temozolomide for Immunomodulation in the Treatment of Glioblastoma. *Neuro Oncol.* 20, 1566–1572. doi:10.1093/neuonc/noy072

Khasraw, M., Reardon, D. A., Weller, M., and Sampson, J. H. (2020). PD-1 Inhibitors: Do They Have a Future in the Treatment of Glioblastoma? *Clin. Cancer Res.* 26, 5287–5296. doi:10.1158/1078-0432.ccr-20-1135

Kraft, V. A. N., Bezjian, C. T., Pfeiffer, S., Ringelstetter, L., Müller, C., Zandkarimi, F., et al. (2020). GTP Cyclohydrolase 1/Tetrahydrobiopterin Counteract Ferroptosis through Lipid Remodeling. *ACS Cent. Sci.* 6, 41–53. doi:10.1021/acscentsci.9b01063

Lamb, J., Crawford, E. D., Peck, D., Modell, J. W., Blat, I. C., Wrobel, M. J., et al. (2006). The Connectivity Map: Using Gene-Expression Signatures to Connect Small Molecules, Genes, and Disease. *Science* 313, 1929–1935. doi:10.1126/science.1132939

Langfelder, P., and Horvath, S. (2008). WGCNA: an R Package for Weighted Correlation Network Analysis. *BMC Bioinformatics* 9, 559. doi:10.1186/1471-2105-9-559

Larkin, J., Chiarion-Sileni, V., Gonzalez, R., Grob, J. J., Cowey, C. L., Lao, C. D., et al. (2015). Combined Nivolumab and Ipilimumab or Monotherapy in Untreated Melanoma. *N. Engl. J. Med.* 373, 23–34. doi:10.1056/nejmoa1504030

Liang, C., Zhang, X., Yang, M., and Dong, X. (2019). Recent Progress in Ferroptosis Inducers for Cancer Therapy. *Adv. Mater.* 31, e1904197. doi:10.1002/adma.201904197

Lim, M., Xia, Y., Bettegowda, C., and Weller, M. (2018). Current State of Immunotherapy for Glioblastoma. *Nat. Rev. Clin. Oncol.* 15, 422–442. doi:10.1038/s41571-018-0003-5

Liu, Z., Zhao, Q., Zuo, Z.-X., Yuan, S.-Q., Yu, K., Zhang, Q., et al. (2020). Systematic Analysis of the Aberrances and Functional Implications of Ferroptosis in Cancer. *iScience* 23, 101302. doi:10.1016/j.isci.2020.101302

Llabani, E., Hicklin, R. W., Lee, H. Y., Motika, S. E., Crawford, L. A., Weerapana, E., et al. (2019). Diverse Compounds from Pleuromutilin lead to a Thioredoxin Inhibitor and Inducer of Ferroptosis. *Nat. Chem.* 11, 521–532. doi:10.1038/s41557-019-0261-6

Louis, D. N., Perry, A., Reifenberger, G., Von Deimling, A., Figarella-Branger, D., Cavenee, W. K., et al. (2016). The 2016 World Health Organization Classification of Tumors of the Central Nervous System: a Summary. *Acta Neuropathol.* 131, 803–820. doi:10.1007/s00401-016-1545-1

Lu, B., Chen, X.-b., Hong, Y.-c., Zhu, H., He, Q.-j., Yang, B., et al. (2019). Identification of PRDX6 as a Regulator of Ferroptosis. *Acta Pharmacol. Sin* 40, 1334–1342. doi:10.1038/s41401-019-0233-9

Maire, C. L., Mohme, M., Bockmayr, M., Fita, K. D., Riecken, K., Börnigen, D., et al. (2020). Glioma Escape Signature and Clonal Development under Immune Pressure. *J. Clin. Invest.* 130, 5257–5271. doi:10.1172/jci138760

Malta, T. M., Sokolov, A., Gentles, A. J., Burzykowski, T., Poisson, L., Weinstein, J. N., et al. (2018). Machine Learning Identifies Stemness Features Associated with Oncogenic Dedifferentiation. *Cell* 173, 338–354.e15. doi:10.1016/j.cell.2018.03.034

Mao, C., Liu, X., Zhang, Y., Lei, G., Yan, Y., Lee, H., et al. (2021). DHODH-mediated Ferroptosis Defence Is a Targetable Vulnerability in Cancer. *Nature* 593, 586–590. doi:10.1038/s41586-021-03539-7

Mariathasan, S., Turley, S. J., Nickles, D., Castiglioni, A., Yuen, K., Wang, Y., et al. (2018). TGFβ Attenuates Tumour Response to PD-L1 Blockade by Contributing to Exclusion of T Cells. *Nature* 554, 544–548. doi:10.1038/nature25501

Mayakonda, A., Lin, D.-C., Assenov, Y., Plass, C., and Koeffler, H. P. (2018). Maftools: Efficient and Comprehensive Analysis of Somatic Variants in Cancer. *Genome Res.* 28, 1747–1756. doi:10.1101/gr.239244.118

McGranahan, T., Therkelsen, K. E., Ahmad, S., and Nagpal, S. (2019). Current State of Immunotherapy for Treatment of Glioblastoma. *Curr. Treat. Options. Oncol.* 20, 24. doi:10.1007/s11864-019-0619-4

Motzer, R. J., Escudier, B., Mcdermott, D. F., George, S., Hammers, H. J., Srinivas, S., et al. (2015). Nivolumab versus Everolimus in Advanced Renal-Cell Carcinoma. *N. Engl. J. Med.* 373, 1803–1813. doi:10.1056/nejmoa1510665

Nagashima, H., Tanaka, K., Sasayama, T., Irino, Y., Sato, N., Takeuchi, Y., et al. (2016). Diagnostic Value of Glutamate with 2-hydroxyglutarate in Magnetic Resonance Spectroscopy for IDH1 Mutant Glioma. *Neuro Oncol.* 18, 1559–1568. doi:10.1093/neuonc/now090

Noguchi, T., Ward, J. P., Gubin, M. M., Arthur, C. D., Lee, S. H., Hundal, J., et al. (2017). Temporally Distinct PD-L1 Expression by Tumor and Host Cells Contributes to Immune Escape. *Cancer Immunol. Res.* 5, 106–117. doi:10.1158/2326-6066.cir-16-0391

Reardon, D. A., Brandes, A. A., Omuro, A., Mulholland, P., Lim, M., Wick, A., et al. (2020). Effect of Nivolumab vs Bevacizumab in Patients with Recurrent Glioblastoma: The CheckMate 143 Phase 3 Randomized Clinical Trial. *JAMA Oncol.* 6, 1003–1010. doi:10.1001/jamaoncol.2020.1024

Rosenberg, J. E., Hoffman-Censits, J., Powles, T., Van Der Heijden, M. S., Balar, A. V., Necchi, A., et al. (2016). Atezolizumab in Patients with Locally Advanced and Metastatic Urothelial Carcinoma Who Have Progressed Following Treatment with Platinum-Based Chemotherapy: a Single-Arm, Multicentre, Phase 2 Trial. *The Lancet* 387, 1909–1920. doi:10.1016/s0140-6736(16)00561-4

Ruffell, B., and Coussens, L. M. (2015). Macrophages and Therapeutic Resistance in Cancer. *Cancer Cell* 27, 462–472. doi:10.1016/j.ccell.2015.02.015

Saint-Germain, E., Mignacca, L., Vernier, M., Bobbala, D., Ilangumaran, S., and Ferbeyre, G. (2017). SOCS1 Regulates Senescence and Ferroptosis by Modulating the Expression of P53 Target Genes. *Aging* 9, 2137–2162. doi:10.18632/aging.101306

Saudemont, A., Hamrouni, A., Marchetti, P., Liu, J., Jouy, N., Hetuin, D., et al. (2007). Dormant Tumor Cells Develop Cross-Resistance to Apoptosis Induced by CTLs or Imatinib Mesylate via Methylation of Suppressor of Cytokine Signaling 1. *Cancer Res.* 67, 4491–4498. doi:10.1158/0008-5472.can-06-1627

Saygin, C., Matei, D., Majeti, R., Reizes, O., and Lathia, J. D. (2019). Targeting Cancer Stemness in the Clinic: From Hype to Hope. *Cell Stem Cell* 24, 25–40. doi:10.1016/j.stem.2018.11.017

Seibt, T. M., Proneth, B., and Conrad, M. (2019). Role of GPX4 in Ferroptosis and its Pharmacological Implication. *Free Radic. Biol. Med.* 133, 144–152. doi:10.1016/j.freeradbiomed.2018.09.014

Sharma, P., Retz, M., Siefker-Radtke, A., Baron, A., Necchi, A., Bedke, J., et al. (2017). Nivolumab in Metastatic Urothelial Carcinoma after Platinum Therapy (CheckMate 275): a Multicentre, Single-Arm, Phase 2 Trial. *Lancet Oncol.* 18, 312–322. doi:10.1016/s1470-2045(17)30065-7

Shibue, T., and Weinberg, R. A. (2017). EMT, CSCs, and Drug Resistance: the Mechanistic Link and Clinical Implications. *Nat. Rev. Clin. Oncol.* 14, 611–629. doi:10.1038/nrclinonc.2017.44

Siegal, T. (2015). Clinical Impact of Molecular Biomarkers in Gliomas. *J. Clin. Neurosci.* 22, 437–444. doi:10.1016/j.jocn.2014.10.004

Soula, M., Weber, R. A., Zilka, O., Alwaseem, H., La, K., Yen, F., et al. (2020). Metabolic Determinants of Cancer Cell Sensitivity to Canonical Ferroptosis Inducers. *Nat. Chem. Biol.* 16, 1351–1360. doi:10.1038/s41589-020-0613-y

Stockwell, B. R., and Jiang, X. (2019). A Physiological Function for Ferroptosis in Tumor Suppression by the Immune System. *Cell Metab.* 30, 14–15. doi:10.1016/j.cmet.2019.06.012

Sturm, G., Finotello, F., Petitprez, F., Zhang, J. D., Baumbach, J., Fridman, W. H., et al. (2019). Comprehensive Evaluation of Transcriptome-Based Cell-type Quantification Methods for Immuno-Oncology. *Bioinformatics* 35, i436–i445. doi:10.1093/bioinformatics/btz363

Su, S., Chen, J., Yao, H., Liu, J., Yu, S., Lao, L., et al. (2018). CD10+GPR77+ Cancer-Associated Fibroblasts Promote Cancer Formation and Chemoresistance by Sustaining Cancer Stemness. *Cell* 172, 841–856. doi:10.1016/j.cell.2018.01.009

Tan, A. C., Ashley, D. M., López, G. Y., Malinzak, M., Friedman, H. S., and Khasraw, M. (2020). Management of Glioblastoma: State of the Art and Future Directions. *CA A. Cancer J. Clin.* 70, 299–312. doi:10.3322/caac.21613

Tang, D., Chen, X., Kang, R., and Kroemer, G. (2021). Ferroptosis: Molecular Mechanisms and Health Implications. *Cell Res* 31, 107–125. doi:10.1038/s41422-020-00441-1

Tang, R., Xu, J., Zhang, B., Liu, J., Liang, C., Hua, J., et al. (2020). Ferroptosis, Necroptosis, and Pyroptosis in Anticancer Immunity. *J. Hematol. Oncol.* 13, 110. doi:10.1186/s13045-020-00946-7

Tran, A. N., Walker, K., Harrison, D. G., Chen, W., Mobley, J., Hocevar, L., et al. (2018). Reactive Species Balance via GTP Cyclohydrolase I Regulates Glioblastoma Growth and Tumor Initiating Cell Maintenance. *Neuro Oncol.* 20, 1055–1067. doi:10.1093/neuonc/noy012

van Nifterik, K. A., Van Den Berg, J., Van Der Meide, W. F., Ameziane, N., Wedekind, L. E., Steenbergen, R. D. M., et al. (2010). Absence of the MGMT Protein as Well as Methylation of the MGMT Promoter Predict the Sensitivity for Temozolomide. *Br. J. Cancer* 103, 29–35. doi:10.1038/sj.bjc.6605712

Wang, W., Green, M., Choi, J. E., Gijón, M., Kennedy, P. D., Johnson, J. K., et al. (2019). CD8+ T Cells Regulate Tumour Ferroptosis during Cancer Immunotherapy. *Nature* 569, 270–274. doi:10.1038/s41586-019-1170-y

Weber, J., Mandala, M., Del Vecchio, M., Gogas, H. J., Arance, A. M., Cowey, C. L., et al. (2017). Adjuvant Nivolumab versus Ipilimumab in Resected Stage III or IV Melanoma. *N. Engl. J. Med.* 377, 1824–1835. doi:10.1056/nejmoa1709030

Weissmann, S., Cloos, P. A., Sidoli, S., Jensen, O. N., Pollard, S., and Helin, K. (2018). The Tumor Suppressor CIC Directly Regulates MAPK Pathway Genes via Histone Deacetylation. *Cancer Res.* 78, 4114–4125. doi:10.1158/0008-5472.can-18-0342

Weller, M., Van Den Bent, M., Preusser, M., Le Rhun, E., Tonn, J. C., Minniti, G., et al. (2021). EANO Guidelines on the Diagnosis and Treatment of Diffuse Gliomas of Adulthood. *Nat. Rev. Clin. Oncol.* 18, 170–186. doi:10.1038/s41571-020-00447-z

Wen, Q., Liu, J., Kang, R., Zhou, B., and Tang, D. (2019). The Release and Activity of HMGB1 in Ferroptosis. *Biochem. Biophysical Res. Commun.* 510, 278–283. doi:10.1016/j.bbrc.2019.01.090

Wu, J., Minikes, A. M., Gao, M., Bian, H., Li, Y., Stockwell, B. R., et al. (2019). Intercellular Interaction Dictates Cancer Cell Ferroptosis via NF2-YAP Signalling. *Nature* 572, 402–406. doi:10.1038/s41586-019-1426-6

Yan, H., Parsons, D. W., Jin, G., Mclendon, R., Rasheed, B. A., Yuan, W., et al. (2009). IDH1andIDH2Mutations in Gliomas. *N. Engl. J. Med.* 360, 765–773. doi:10.1056/nejmoa0808710

Yarchoan, M., Hopkins, A., and Jaffee, E. M. (2017). Tumor Mutational Burden and Response Rate to PD-1 Inhibition. *N. Engl. J. Med.* 377, 2500–2501. doi:10.1056/nejmc1713444

Yin, W., Jiang, X., Tan, J., Xin, Z., Zhou, Q., Zhan, C., et al. (2020). Development and Validation of a Tumor Mutation Burden-Related Immune Prognostic Model for Lower-Grade Glioma. *Front. Oncol.* 10, 1409. doi:10.3389/fonc.2020.01409

Yoshihara, K., Shahmoradgoli, M., Martínez, E., Vegesna, R., Kim, H., Torres-Garcia, W., et al. (2013). Inferring Tumour Purity and Stromal and Immune Cell Admixture from Expression Data. *Nat. Commun.* 4, 2612. doi:10.1038/ncomms3612

Zdanov, S., Mandapathil, M., Abu Eid, R., Adamson-Fadeyi, S., Wilson, W., Qian, J., et al. (2016). Mutant KRAS Conversion of Conventional T Cells into Regulatory T Cells. *Cancer Immunol. Res.* 4, 354–365. doi:10.1158/2326-6066.cir-15-0241

Zhao, Z., Zhang, K. N., Wang, Q., Li, G., Zeng, F., Zhang, Y., et al. (2021). Chinese Glioma Genome Atlas (CGGA): A Comprehensive Resource with Functional Genomic Data from Chinese Gliomas. *Genomics Proteomics Bioinformatics* 19, 1–12. doi:10.1016/j.gpb.2020.10.005

Zheng, J., and Conrad, M. (2020). The Metabolic Underpinnings of Ferroptosis. *Cell Metab.* 32, 920–937. doi:10.1016/j.cmet.2020.10.011

Zhou, N., and Bao, J. (2020). *FerrDb: A Manually Curated Resource for Regulators and Markers of Ferroptosis and Ferroptosis-Disease Associations*. Oxford: Database.

Conflict of Interest: The authors declare that the research was conducted in the absence of any commercial or financial relationships that could be construed as a potential conflict of interest.

Publisher's Note: All claims expressed in this article are solely those of the authors and do not necessarily represent those of their affiliated organizations, or those of the publisher, the editors and the reviewers. Any product that may be evaluated in this article, or claim that may be made by its manufacturer, is not guaranteed or endorsed by the publisher.

frontiers in Cell and Developmental Biology

ORIGINAL RESEARCH
published: 15 February 2022
doi: 10.3389/fcell.2022.826879

Integratively Genomic Analysis Reveals the Prognostic and Immunological Characteristics of Pyroptosis and Ferroptosis in Pancreatic Cancer for Precision Immunotherapy

*Ting Yu[1,2], Huaicheng Tan[1], Chunhua Liu[1], Wen Nie[1], Yang Wang[1], Kexun Zhou[1] and Huashan Shi[1]**

[1]*Department of Biotherapy, Cancer Center, West China Hospital, Sichuan University, Chengdu, China,* [2]*Department of Pathology and Laboratory of Pathology, State Key Laboratory of Biotherapy, West China Hospital, West China School of Medicine, Sichuan University, Chengdu, China*

OPEN ACCESS

Edited by:
Lian Xiang Luo, Guangdong Medical University, China

Reviewed by:
Mingxiao Feng, Johns Hopkins University, United States
Lei Zhou, Yale University, United States
Bowen Xing, Children's Hospital of Philadelphia, United States

***Correspondence:**
Huashan Shi
shihuashan@scu.edu.cn

Specialty section:
This article was submitted to Cell Death and Survival, a section of the journal Frontiers in Cell and Developmental Biology

Received: *01 December 2021*
Accepted: *05 January 2022*
Published: *15 February 2022*

Citation:
Yu T, Tan H, Liu C, Nie W, Wang Y, Zhou K and Shi H (2022) Integratively Genomic Analysis Reveals the Prognostic and Immunological Characteristics of Pyroptosis and Ferroptosis in Pancreatic Cancer for Precision Immunotherapy. Front. Cell Dev. Biol. 10:826879. doi: 10.3389/fcell.2022.826879

The non-apoptotic cell death processes including pyroptosis and ferroptosis have been implicated in the progression and therapeutic responses of pancreatic adenocarcinoma (PAAD). However, the extent to which pyroptosis and ferroptosis influence tumor biology remains ambiguous, especially in PAAD, which is characterized with "cold" immunity. Considering the heterogeneity among different patients, it was more practical to quantify distinct cell death profiles in an individual tumor sample. Herein, we developed a pyroptosis-ferroptosis (P-F) score for PAAD patients in The Cancer Genome Atlas (TCGA) database. A high P-F score was associated with active immune phenotype, decreased genomic alterations, and significantly longer survival. Good accuracy of the P-F score in predicting overall survival (OS) was further confirmed in the TCGA-PAAD, ICGC-PACA-CA, and E-MTAB-6134 cohorts. Besides, one immunotherapy cohort (IMvigor210 dataset) has verified that patients with high P-F scores exhibited significant advantages in therapeutic responses and clinical benefits. The sensitivity to chemotherapeutics was analyzed through the Genomics of Drug Sensitivity in Cancer (GDSC), and patients with low P-F score might be more sensitive to paclitaxel and 5-fluorouracil. Collectively, the P-F score based on the systematic evaluation of cell death profiles could serve as an effective biomarker in predicting the outcomes and responses of PAAD patients to treatments with chemotherapeutic agents or immunotherapies.

Keywords: pyroptosis, ferroptosis, pancreatic cancer, P-F score, immunity

INTRODUCTION

As a lethal malignancy, pancreatic adenocarcinoma (PAAD) is characterized with a highly annual mortality rate that is close to the incidence rate (Gordon-Dseagu et al., 2018). Many challenges remain in the diagnosis and treatment of PAAD, with approximately 10% surviving 5 years after diagnosis (Siegel et al., 2020). During the past few decades, great progresses have been achieved in detection approaches and systemic treatment modality of PAAD, while only modest progress is made

in patient prognosis. Even as the cornerstone of treatment for advanced PAAD, systemic chemotherapy still fails to control this disease (Sultana et al., 2007). Although brilliant clinical benefits have been observed with immunotherapy in multiple cancer types, PAAD that featured with "cold" immunity has proven to be insensitive to this approach (Brahmer et al., 2012; Neoptolemos et al., 2018). Therefore, classification of specific molecular subtypes of PAAD might provide assistance for precise and individual therapy to improve the outcomes of patients.

Current clinical challenges about PAAD mainly focus on the late diagnosis and resistance to the treatment-induced apoptosis (Tang et al., 2021). Therefore, targeting non-apoptotic cell death processes might develop promising strategies to conquer drug resistance and suppress tumor progression. Particularly, non-apoptotic cell death processes including pyroptosis and ferroptosis have been recently implicated in the progression and therapeutic responses of PAAD. As a lytic and inflammatory process, pyroptosis is a gasermins (GSDM)-mediated programmed necrosis, characterized with the activation of pro-inflammatory caspases and release of interleukin (IL) 1 family members (e.g., IL1β and IL18) (Cookson and Brennan, 2001). Some studies have reported the protumorigenic role of pyroptosis. Inflammatory mediators like IL1β released during the activation of pyroptosis might promote cancer stemness and progression (Vidal-Vanaclocha et al., 2000; Li et al., 2012). As key effectors of pyroptosis, gasdermin C and gasdermin D were found to be overexpressed in some cancers, which were associated with tumor progression and poor prognosis of patients (Miguchi et al., 2016; Gao et al., 2018). However, two recently published studies have shown the tumor-suppressive effect of pyroptosis through activating tumor immune microenvironment (TIME) (Wang et al., 2020; Zhang et al., 2020). Gasdermin E could facilitate the phagocytosis of tumor cells by macrophages and increase the number and efficiency of $CD8^+$ T cells and natural killer (NK) cells, thereby inducing the pyroptosis of tumor cells and forming a positive feedback loop (Zhang et al., 2020). Moreover, ferroptosis, referred to as an iron-mediated accumulation of lipid peroxidation to lethal levels, was found to exhibit dual effects in the progression and suppression of PAAD (Tang et al., 2021). Immunotherapy-activated $CD8^+$ T cells could suppress the tumor growth by enhancing ferroptosis-mediated lipid peroxidation in tumor cells (Wang et al., 2019). However, the ferroptosis induced by high-iron diets or Gpx4 (ferroptosis suppressor) depletion has been reported to activate the TMEM173/STING-dependent DNA sensor pathway and increase tumor-infiltrating macrophages, thereby promoting the *KRAS*-driven pancreatic tumorigenesis (Dai et al., 2020).

The crosstalk among pyroptosis, ferroptosis, and TIME is extremely complicated. Tumor cells undergoing pyroptosis could release gasdermin E and inflammatory factors to boost the infiltration of both tumor-suppressed immune cells such as $CD8^+$ T cells and NK cells as well as tumor-promoting cells like myeloid-derived suppressor cells (MDSCs) (Zhang et al., 2020; Tan et al., 2021). In addition, interferon-gamma (INF-γ) released from activated $CD8^+$ T cells could promote lipid peroxidation, resulting in the ferroptosis of tumor cells (Wang et al., 2019). Besides, ferroptotic tumor cells further inhibit the tumor-suppressing function of cytotoxic T cells and NK cells through releasing prostaglandin E2 (PGE2) (Yang et al., 2014; Johnson et al., 2020; Xu et al., 2021). Moreover, n-3 PUFA docosahexaenoic acid (DHA), which was reported to cause ferroptosis of tumor cells, could also induce the pyroptosis in tumor cells, suggesting that lipid metabolism might well be the junction point between ferroptosis and pyroptosis (Ou et al., 2017; Pizato et al., 2018; Du et al., 2019). Considering that the process of impaired plasma membrane occurred in both cell death types, underlying connections between ferroptosis and pyroptosis remain intriguing for investigation. Though recently published study has explored the role of ferroptosis-related genes in prognosis and immune activity of PAAD, the lack of analyzing pyroptosis-related gene is insufficient to reflect the crosstalk between cell death subtypes and tumor biology (Tang et al., 2020a). Currently, the extent to which pyroptosis and ferroptosis influences the tumor biology remains ambiguous, especially in PAAD that characterized with "cold" immunity. Developing translational strategies against PAAD depends on better understanding about the complicated roles and related signaling pathways of pyroptosis and ferroptosis.

In this study, four robust cell death subtypes of PAAD were identified based on consensus clustering of pyroptosis- and ferroptosis-related gene expression profiles, which were associated with distinct survival, mutational, and immune signatures. Furthermore, the pyroptosis-ferroptosis (P-F) score was developed, with superior capacity in predicting the outcomes and responses of patients to chemotherapeutic agents and immune checkpoint blockades (ICBs) (**Supplementary Figure S1**).

MATERIALS AND METHODS

Data Extraction and Data Processing

The RNA-sequence (RNA-Seq) data with matched clinical information of all available PAAD patients were extracted from The Cancer Genome Atlas (TCGA) (https://www.cancer.gov/tcga) (TCGA-PAAD, n = 176) and the International Cancer Genome Consortium (ICGC) (https://daco.icgc.org/) (ICGC-PACA-CA, n = 165) databases. For subsequent analyses, fragments per kilobase million (FPKM) values were converted to transcripts per kilobase millions (TPMs)-normalized. Additionally, the E-MTAB-6134 dataset with complete clinical information of 288 PAAD patients and datasets without detailed clinical information including GSE57495 based on platform GPL15048, GSE21501 based on platform GPL4133, and GSE85916 based on platform GPL13667 were all extracted from the Array Express database (https://www.ebi.ac.uk/arrayexpress). The raw data of the gene expression in E-MTAB-6134, GSE57495, GSE21501, and GSE85916 datasets were normalized by using the "limma" R package. The TCGA-PAAD dataset was utilized as training cohort, and the other datasets were set as validation cohorts. Based on the Creative Commons 3.0 license that was downloaded from http://research-pub.gene.com/IMvigor210CoreBiologie, the IMvigor210 dataset was extracted

from a freely available data package. The IMvigor210 dataset containing 298 patients of urothelial cancer who had received immunotherapy was performed to validate the prediction value of the P-F score. The corresponding information of somatic mutations in TCGA-PAAD patients was extracted from UCSC Xena (https://xena.ucsc.edu/). Somatic mutations were analyzed and visualized through the "maftool" R package (Mayakonda et al., 2018). Furthermore, the copy number variations (CNVs) of TCGA-PAAD patients were visualized and presented by using the "RCircos" package.

Cell Death Subgrouping

Through referring to previously published reviews and relevant bioinformatic study, we extracted 33 pyroptosis-related genes (Man and Kanneganti, 2015; Wang and Yin, 2017; Kambara et al., 2018; Kang et al., 2018; Karki and Kanneganti, 2019; Xia et al., 2019; Li et al., 2021; Wang et al., 2021). Considering that some bioinformatic studies and basic studies have identified extra pyroptosis-related genes, we verified the function of these genes in the HUMAN GENE database (https://www.genecards.org/) and further extracted another 6 pyroptosis-related genes (Zhu et al., 2017; Dong et al., 2021; Ju et al., 2021; Zhang et al., 2021). By taking the union, a total of 39 pyroptosis-related genes were extracted and listed in **Supplementary Table S1**. Moreover, 113 ferroptosis-related genes were also identified mainly based on previously published reviews and relevant bioinformatic studies (**Supplementary Table S2**) (Stockwell et al., 2017; Bersuker et al., 2019; Doll et al., 2019; Hassannia et al., 2019; Liang et al., 2020; Liu et al., 2020; Zhuo et al., 2020). Then, consensus clustering was carried out based on pyroptosis- and ferroptosis-related genes through the "ConsensusClusterPlus" R package, with the repeats of 1,000, pItem of 0.8, and pFeature of 1 to guarantee the stability of classification. With max k = 5, the Ward. D2 and Pearson correlations were separately served as the clustering algorithm and distance metric. Next, each sample was assigned into the quiescent (pyroptosis ≤0, ferroptosis ≤0), pyroptosis (pyroptosis >0, ferroptosis ≤0), ferroptosis (pyroptosis ≤0, ferroptosis >0), and mixed (pyroptosis >0, ferroptosis >0) subtypes according to the median expression levels of co-expressed pyroptosis- and ferroptosis-related genes.

Collection of Immune-Related Data

Based on evaluating the LM22 signature, the immune cell infiltration in each sample of the TCGA-PAAD cohort was analyzed using the "CIBERSORT" R package (Newman et al., 2015). Besides, the ESTIMATE algorithm was applied to calculate the ESTMATE, immune, and stromal scores in each PAAD sample (Yoshihara et al., 2013).

Dimension Reduction and Construction of the P-F Score

According to the expression levels of identified genes associated with cell death patterns, the PAAD patients were assigned into corresponding subtypes. Then, the differentially expressed genes (DEGs) across these subtypes were screened by using the "limma" R package, setting the cutoff values as $|\log_2$ fold change (FC)$| > 1$ and $p < 0.05$ (adjusted). The R package of "clusterProfiler" was performed for Gene Ontology (GO) enrichment analysis. Next, unsupervised clustering analysis was performed to stratify the patients of the TCGA-PAAD cohort into distinct gene clusters according to their DEG values. The DEGs that positively correlated to the cluster signature were referred to as P-F gene signature A, while the residual DEGs were referred to as P-F gene signature B. To get rid of the noise or redundant genes, the dimension reduction of the P-F gene signatures A and B was further conducted by using the Boruta algorithm (Kursa and Rudnicki, 2010). Moreover, the principal component analysis (PCA) algorithm was used for extracting principal component 1 as the signature score. Finally, referring to the gene expression grade index, the P-F score of each sample was calculated according to the following equation: P-F score = $\sum PC1_A$ - $\sum PC1_B$ $PC1_A$ stands for the first component of signature A, and $PC1_B$ stands for the first component of signature B.

Prediction of Therapeutic Benefits in Patients With Distinct P-F Scores

To better predict the response to ICBs in cancer patients, the Tumor Immune Dysfunction and Exclusion (TIDE) algorithm was developed as a computational method to model the primary mechanisms of tumor immune escape (Jiang et al., 2018). Therefore, the TIDE web application (http://tide.dfci.harvard.edu) was utilized to evaluate the utility of the P-F score in predicting the therapeutic response to ICBs for PAAD patients. Subsequently, the subclass mapping algorithm (https://cloud.genepattern.org/gp/) was implemented to visualize the therapeutic responses to anti-PD-1 and anti-CTLA4 therapeutics between distinct subgroups based on previously reported 47 melanoma patients with detailed immunotherapy records (Roh et al., 2017). Furthermore, sensitivity to chemotherapeutic agents including gemcitabine, cisplatin, paclitaxel, and 5-fluorouracil was estimated by using the R package of "pRRophetic," which was based on the Genomics of Drug Sensitivity in Cancer (GDSC). To compare the drug sensitivity between the high and low P-F score groups, the estimated half-maximal inhibitory concentration (IC50) of each sample was computed with the ridge regression, and tenfold cross-validation was employed to evaluate the accuracy of this prediction (Geeleher et al., 2014).

Connectivity MAP Analysis

As a public online tool, the Connectivity MAP database (CMap, https://portals.broadinstitute.org/cmap/) enables the user to predict small molecules that could target cancer-related genes based on gene expression profiles (Lamb et al., 2006). To predict potential small molecular drugs for PAAD, the DEGs between the high and low P-F score groups were identified and input into the CMap database. Besides, the CMap mode-of-action (MoA) analysis was performed in order to reveal the underlying mechanism of drug actions (Subramanian et al., 2017).

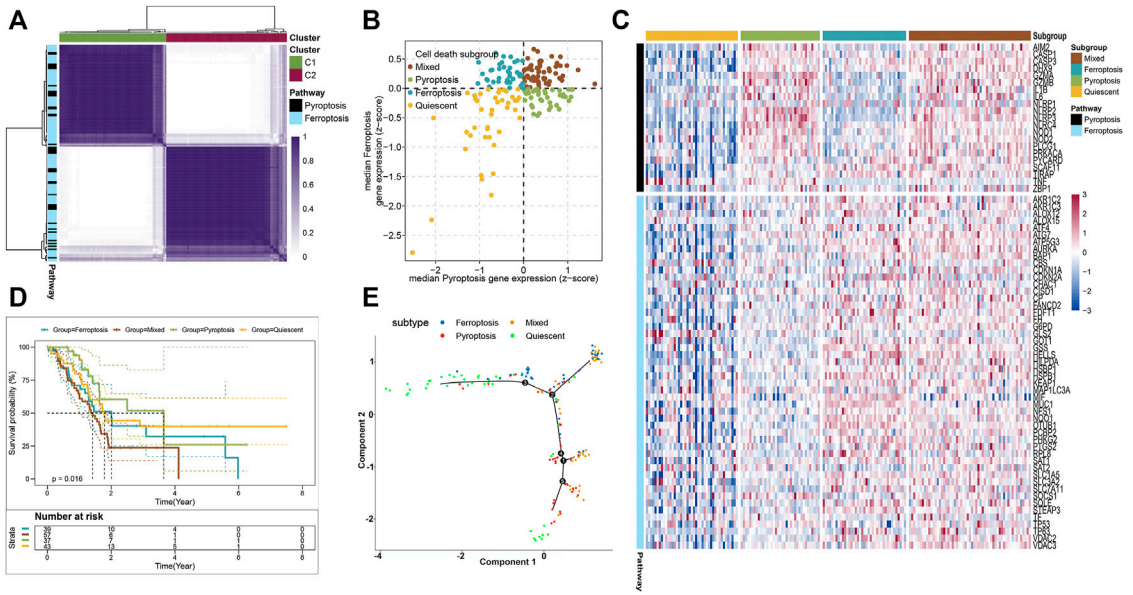

FIGURE 1 | Stratifying the cell death subgroups of PAAD according to the expression profile of pyroptosis- and ferroptosis-related genes. **(A)** Clustering heatmap of the pyroptosis- and ferroptosis-related genes in the TCGA-PAAD cohort (n = 176). **(B)** As shown in the scatter plot, the PAAD patients were stratified into 4 cell death subtypes based on the median expression levels of coexpressed pyroptosis- (*x*-axis) and ferroptosis-related genes (*y*-axis). **(C)** Heatmap demonstrated the expression status of the pyroptosis- and ferroptosis-related genes among each subtype. **(D)** Survival analysis of the PAAD patients with different cell death subtypes (log-rank $p = 0.016$). **(E)** The distributions of the four subtypes using dimensionality reduction analysis. Each point represented a patient, with the color corresponding to the previously defined cell death subtypes.

Statistical Analysis

All statistical analyses in this study were conducted using the R software (version 4.0.4). Comparisons between two groups or more than two groups were conducted through the Wilcoxon test or Kruskal–Wallis test, respectively. Chi-square test was used for analyzing the correlations between categorical variables. The correlation coefficient was calculated through Spearman analysis. Survival analysis for each dataset was conducted using the Kaplan–Meier plotter, where the statistical difference was evaluated through the log rank test. To estimate the predictive efficacy of the variate, time-dependent analysis of the receiver operating characteristic (ROC) curve was performed to calculate the area under the curves (AUCs) through the R package "survivalROC." The R package "survival" was used for univariate and multivariate Cox regression analyses. Unless stated otherwise above, the statistical significance was considered with a two-tailed $p < 0.05$.

RESULTS

Stratify the Cell Death Subtypes of PAAD Based on Dual Analysis of Pyroptosis- and Ferroptosis-Related Genes

To stratify the cell death subtypes of PAAD, the RNA-sequence data from the TCGA-PAAD cohort were analyzed with their expression levels of pyroptosis and ferroptosis pathway genes. As shown in **Figure 1A**, the consensus cluster plus was applied to identify the groups that mainly coexpressed pyroptosis and ferroptosis pathway genes for cell death subgrouping. The median expression levels of coexpressed pyroptosis- and ferroptosis-related genes in each PAAD sample were computed. The PAAD samples were then assigned into the cell death subtypes particularly corresponding to these two pathways: quiescent, pyroptosis, ferroptosis, and mixed (**Figure 1B**). The heatmap displayed the expression profiles of the pyroptosis- and ferroptosis-related genes across these four subtypes (**Figure 1C** and **Supplementary Figure S2**). The patients in the mixed subtype were significantly relevant to the worst survival, while a relatively better survival was found in patients of the pyroptosis subtype (**Figure 1D**). To better visualize the distribution of individual patients, dimensionality reduction analysis was utilized through analyzing pyroptosis- and ferroptosis-related gene expression profiles. The locations of individual patients were assigned into the tree structure, which indicated the differences among the four subtypes (**Figure 1E**). Collectively, these findings demonstrated four distinct cell death subtypes associated with the pyroptosis–ferroptosis pathway in PAAD, in which the tumors that coexpressed with higher levels of pyroptosis- and ferroptosis-related genes were associated with worse prognosis. We further investigated the correlations between the cell death subtypes and TIME. The pyroptosis subtype exhibited significantly higher infiltrations of activated $CD4^+$ memory T cells and $CD8^+$ T cells, while the mixed subtype showed the lowest infiltration of activated NK cells (**Supplementary Figure S3A**). Besides, the expression levels of immune checkpoints (ICPs)-related genes and immunogenic cell

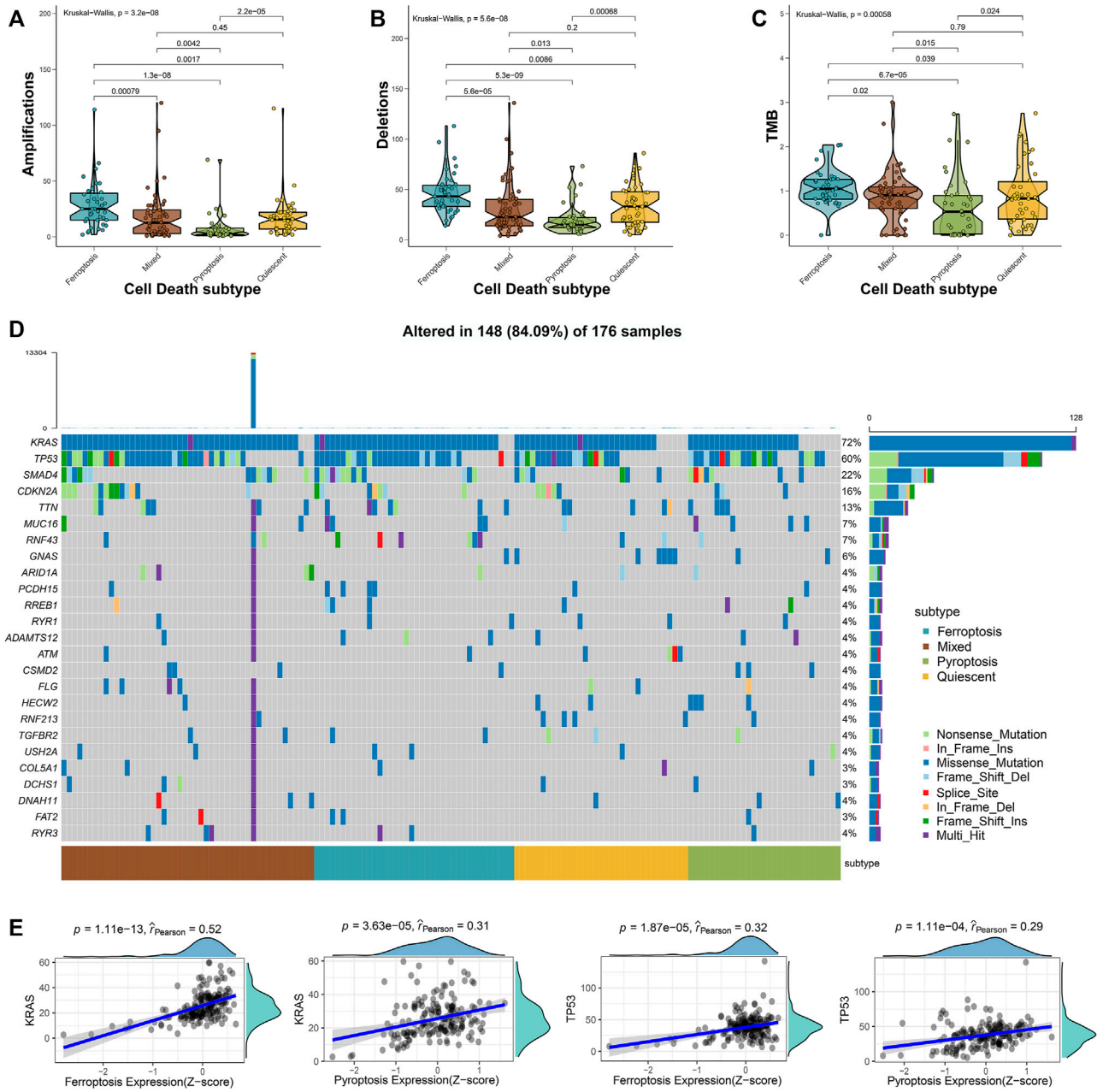

FIGURE 2 | Mutational landscape across the cell death subtypes in PAAD samples. The amplications **(A)**, deletions **(B)**, and TMB **(C)** were evaluated across the 4 cell death subtypes. **(D)** The oncoplot depicted the top 25 most frequently mutated genes across the subgroups of PAAD samples. **(E)** The correlations between the expression of ferroptosis- or pyroptosis-related genes and *KRAS* and *TP53* expressions.

death (ICD)-related genes also showed distinct differences across the four subtypes (**Supplementary Figures S3B, C**). Given that the "limma" R package could only compare two groups at a time, the DEGs across the four subtypes were the summation of DEGs identified between two subtypes by using the "limma" R package, setting the cutoff values as $|\log_2 FC| > 1$ and $p < 0.05$ (adjusted). A total of 6,164 DEGs across the four subtypes were then identified (**Supplementary Table S3**), and the GO functional enrichment of these DEGs was mainly enriched in the biological process (BP) involved in the T-cell activation, positive regulation of cell adhesion, and leukocyte cell–cell adhesion (**Supplementary Figure S3D** and **Supplementary Table S4**).

Approximately 95% of the PAAD patients have gene alterations, including mutations, amplifications, deletions, or inversions (Escobar-Hoyos et al., 2020). Therefore, the mutational landscape was investigated among the 4 cell death subtypes. The ferroptosis subtype exhibited significantly highest gene alterations involved in amplifications,

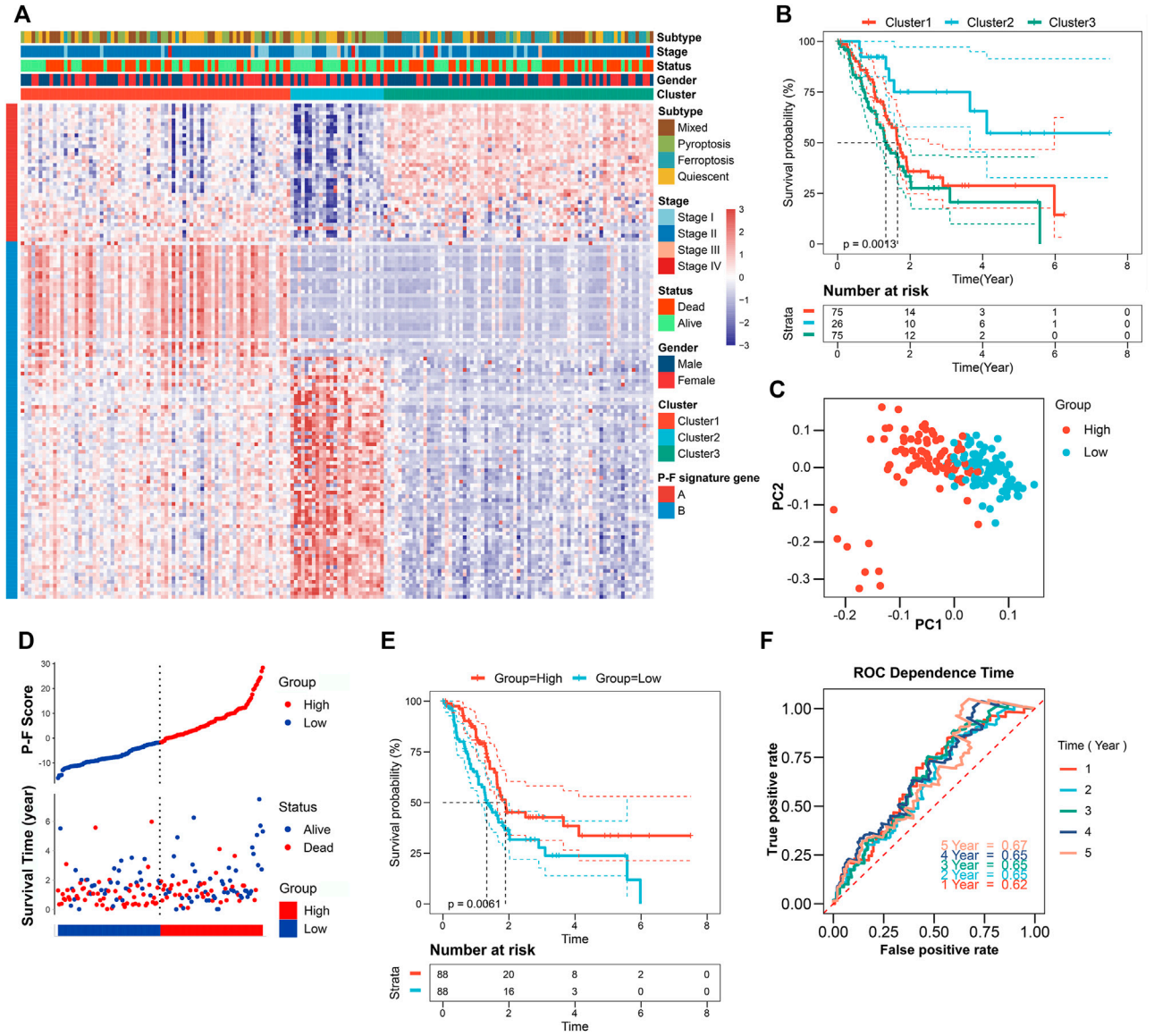

FIGURE 3 | Identification of the P-F score in the TCGA-PAAD training dataset. **(A)** Unsupervised clustering of the DEGs among the 4 cell death subtypes to further stratify PAAD patients into three gene clusters. **(B)** Survival analysis of the PAAD patients in three gene clusters (log-rank p = 0.0013). **(C)** Principal components analysis (PCA) of the PAAD patients with high or low P-F scores. **(D)** Distribution of the P-F score and survival status of PAAD patients. **(E)** Survival analysis of the PAAD patients in high and low P-F score groups (log-rank p = 0.0061). **(F)** ROC curves for the 1-, 2-, 3-, 4-, and 5-year survival times based on the P-F score.

deletions, and tumor mutation burden (TMB) (**Figures 2A–C**). Besides, the mutational landscape of the top 25 most frequently mutated genes was evaluated in PAAD, which demonstrated obviously maximum mutations in the mixed subtype (**Figure 2D**). We further observed a strong correlation between the expressions of ferroptosis-related genes with *KRAS* (Spearman coefficient R = 0.52, p = 1.11e-13) and a moderate correlation with *TP53* (Spearman coefficient R = 0.32, p = 1.87e-5), while the expression of pyroptosis-related genes showed a moderate correlation with the *KRAS* expression (Spearman coefficient R = 0.31, p = 3.63e-5) and a weak correlation with the *TP53* expression (Spearman coefficient R = 0.29, p = 1.11e-4) (**Figure 2E**). The relatively worse survival of patients in ferroptosis and mixed subtypes was compatible with the notion that the higher mutation accumulation in cancer has negative correlation with the overall survival (OS) of patients (Pleasance et al., 2020). These results implied that ferroptosis and pyroptosis might cooperate to promote the progression of PAAD, even when accounting the better survival in patients of the pyroptosis subtype. Thus, a comprehensive classification about distinct cell death profiles was needful for better stratifying the PAAD patients.

Identification of the P-F Score in TCGA-PAAD Training Dataset

To reveal the underlying biological behaviors of these cell death subtypes, differential expression analysis was performed. Based on the 6,164 DEGs identified from previous differential analysis, the unsupervised clustering stratified the TCGA-PAAD cohort into three genomic clusters, named clusters 1–3 (**Supplementary Figure S4**). The 2,602 DEGs that have positive correlations with the gene cluster were referred to as P-F gene signature A, and the residual DEGs were referred to as P-F gene signature B (**Supplementary Table S5**). To get rid of the noise or redundant genes, the dimension reduction of the P-F gene signatures A and B was further conducted through the Boruta algorithm (Kursa and Rudnicki, 2010). The transcriptomic profile of the 133 most abundant DEGs identified among the genomic clusters was displayed by the heatmap (**Figure 3A** and **Supplementary Table S6**). When compared with other genomic clusters, the patients in cluster 2 exhibited the significantly longest OS, while the patients in clusters 1 and 3 had relatively poorer prognosis (**Figure 3B**). Concurrently, for the purpose of achieving a quantitative indicator of the P-F landscape in PAAD patients, PCA was used to calculate the integrated scores, including $PC1_A$ from P-F gene signature A (n = 37) and $PC1_B$ from P-F gene signature B (n = 96). The individual score of each patient was calculated from the integration of corresponding $PC1_A$ and $PC1_B$. Finally, the obtained signature score was defined as the P-F score. Thereafter, the patients in the TCGA-PAAD cohort were divided into high and low P-F score groups based on the corresponding median value of P-F scores. Furthermore, PCA of individual patients has shown a fine distinction between the high and low P-F score groups, which further confirmed that our P-F scoring system could distinguish the PAAD patients well (**Figure 3C**). The prognostic value of the P-F score was evaluated. The survival status of individual patients was depicted by the scatter plot (**Figure 3D**). The patients in the high score group showed a significantly longer OS (log-rank p = 0.0061; **Figure 3E**). The AUCs were 0.62, 0.65, 0.65, 0.65, and 0.67 for 1-, 2-, 3-, 4-, and 5-year survival times, respectively, indicating the reliability of the P-F score for predicting the outcomes of PAAD patients (**Figure 3F**). Moreover, the prognostic efficiency of the P-F score was also validated in the ICGC-PACA-CA cohort (**Supplementary Figure S5**), the E-MTAB-6134 cohort (**Supplementary Figure S6**), GSE57495, GSE21501, and GSE85916 (**Supplementary Figure S7**), which have shown similar results.

Prognostic Value of the P-F Score for PAAD Patients

The prognostic value of the P-F score was further explored in depth. The constitution of clinical features and cell death subtypes in high and low P-F score groups from the TCGA-PAAD cohort is depicted in **Figure 4A**. No significant difference in stage, gender, and age was found between the high and low score groups, while the low score group showed a significantly worse survival status (p = 0.01). Besides, the distribution of cell death subtypes showed a significant difference, with the pyroptosis subtype mainly distributed in the high score group and the ferroptosis subtype mainly in the low score groups (p = 1.7e-14). Both in the training cohort (TCGA-PAAD) and the validation cohort (ICGC-PACA-CA and E-MTAB-6134) the P-F score was identified as an independent protective factor for PAAD, based on the univariate and multivariate Cox regression analyses (**Figures 4B,C**). According to time-dependent AUC values, the P-F score displayed a well predictive power for OS in comparison with that of age, gender, or stage in the TCGA-PAAD cohort (**Figure 4D**). The excellent predictive ability of the P-F score for OS was also explored in ICGC-PACA-CA and E-MTAB-6134 cohorts (**Figure 4E**). Furthermore, stratified analysis has also shown a significant difference in the OS between the high and low score groups with distinct stage, gender, and age (**Supplementary Figure S8**). Taken together, these results suggested that the P-F score could serve as an independent protective factor for PAAD patients.

The Correlation Between the P-F Score and TIME

To further illuminate intrinsic biological diversities that contributed to the distinct survival status, the correlation between the P-F score and the infiltration of immune components was investigated. The correlation analyses indicated that the P-F score was significantly and positively related to the immune score (Spearman coefficient R = 0.282, p = 0.001) (**Figures 5A,B**). Meanwhile, the high P-F score group demonstrated significantly higher levels of ESTIMATE score, immune score, and stromal score, while the higher tumor purity was found in the low P-F score group (**Figure 5C**). Furthermore, the relation between tumor immunological status and the P-F score was evaluated. The high P-F score group exhibited significantly escalated infiltration of activated $CD4^+$ memory T cells, $CD8^+$ T cells, and gamma-delta (γδ) T cells, which was characterized with the active immune phenotype. The low P-F score group was associated with significantly higher infiltration of immunosuppressive regulatory T cells (Tregs) (**Figure 5D**). The active immune phenotype characterized with abundant T-cell infiltration and enhanced cytolytic activity was correlated with better outcomes, just as we have observed in the high P-F score group (Chen et al., 2019). Moreover, the expression levels of the ICPs- and ICDs-related genes also showed significant differences between the two groups. Among the 28 differentially expressed ICPs-related genes, a total of 18 (18/28, 64.2%) genes were significantly upregulated in the high P-F score group than the low P-F score group (**Figure 5E**). The low P-F score group exhibited significantly higher expression levels of the ICDs-related genes (9/12, 75%) (**Figure 5F**). Therefore, we speculated from these results that the high P-F score group with higher expressions of ICPs-related genes might benefit more from the ICBs therapy, while the low P-F score group with higher expressions of ICDs-related genes might benefit more from the ICDs-based cancer vaccines (Jin and Wang, 2021). The consistency between the immune phenotype and prognosis status in these two P-F score subgroups further

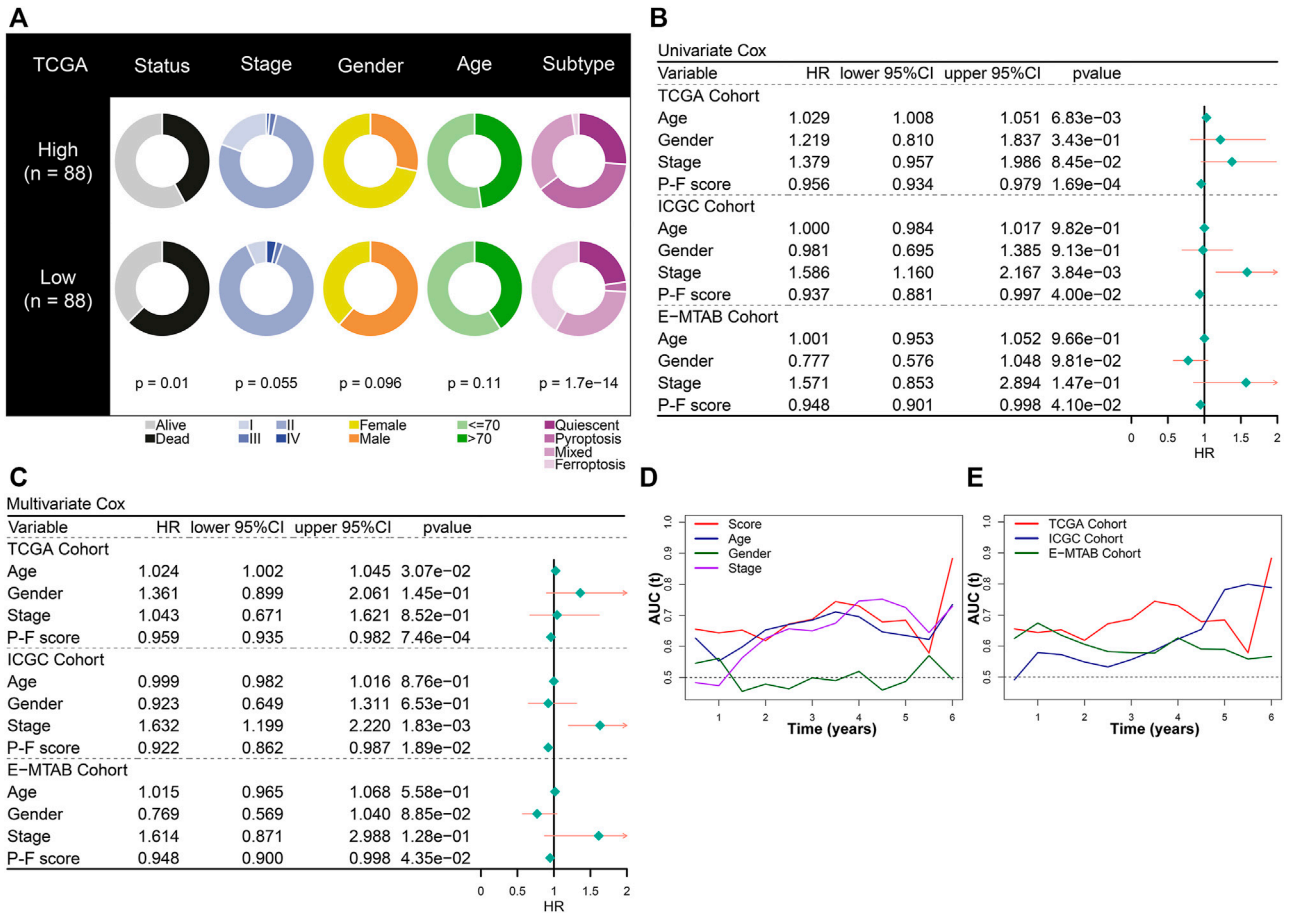

FIGURE 4 | The prognostic value of the P-F score in PAAD. **(A)** Constitution of the clinical features and cell death subtypes in the high and low P-F score groups. Both univariate **(B)** and multivariate **(C)** Cox regression analyses suggested that the P-F score was a significant prognostic factor for OS in the training (TCGA-PAAD) and validation (ICGC-PACA-CA and E-MTAB-6134) cohorts. **(D)** The time-dependent AUC values of P-F score, age, gender, and stage for the OS prediction in the training cohort (TCGA-PAAD). **(E)** The time-dependent AUC values of the P-F score for the OS prediction in the training and validation cohorts.

demonstrated the scientificity and reliability of our classification strategy.

Functional Enrichment Analysis of the DEGs in the P-F Score Groups

Additionally, functional enrichment analysis was performed to elucidate the bioinformatic functions of the DEGs between the P-F score groups. Compared with the low P-F score group, the upregulated DEGs in the high P-F score group were mainly enriched in the activation and proliferation of immune cells, inflammatory response, chemokine, and positive regulation of immune effector process, while the downregulated DEGs were mainly enriched in the mitotic nuclear division, nuclear division, and ERBB signaling pathway (**Figures 6A,B** and **Supplementary Tables S7, S8**). Moreover, Gene Set Enrichment Analysis (GSEA) revealed that the chemokine signaling pathway, cytokine–cytokine receptor interaction, and T-cell receptor signaling pathway were significantly enriched in the high P-F score group, whereas the p53 signaling pathway was enriched in the low P-F score group (**Figures 6C,D** and **Supplementary Tables S9, S10**). Consistently with the immune profiles, the high P-F score was mainly relevant to the active immune phenotype and better outcome, while the low P-F score group was relevant to the phenotype of more active cell proliferation and worse outcome.

Correlations Between the P-F Score and Somatic Mutations

Given the significant value of genomic alterations in regulating tumor immunity, analyses about the somatic mutation and CNVs were performed to investigate the genomic alterations between the P-F score subgroups (Rooney et al., 2015). As demonstrated in **Figure 7A**, the P-F score was significantly and negatively associated with all mutation counts (Spearman coefficient R = 0.5, p = 7.2e-12). Compared with the patients in the high P-F score group, the patients in the low P-F score group have shown significantly elevated somatic mutations, including the non-synonymous and synonymous mutations (**Figures 7B,C**). Besides, CNV analysis has exhibited significantly improved

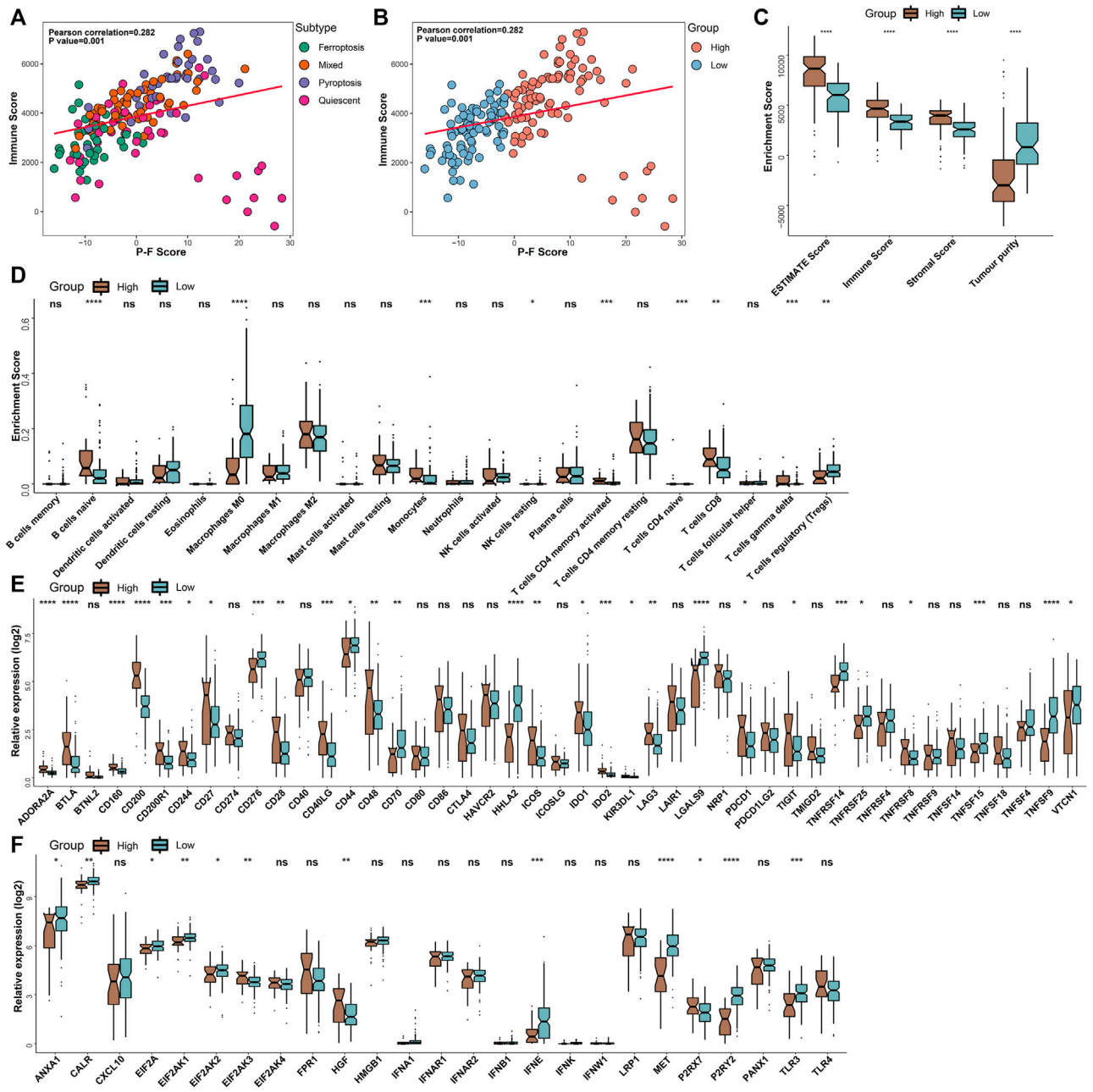

FIGURE 5 | Tumor immunological analyses in the P-F score subgroups. The scatter plots depicted the correlation between the immune score and the P-F score of tumor samples corresponding to 4 cell death subtypes **(A)** and P-F score groups **(B)** in the TCGA-PAAD cohort. **(C)** Enrichment scores of the ESTIMATE score, immune score, stromal score, and tumor purity in the high and low P-F score groups. **(D)** Box plots demonstrated the infiltration levels of multiple immune cells between the distinct P-F score groups. Evaluating the expression levels of the ICPs-relevant genes **(E)** and ICDs-relevant genes **(F)** between the distinct P-F score groups (ns, not significant; *$p < 0.05$; **$p < 0.01$; ***$p < 0.001$; and ****$p < 0.0001$).

copy number amplifications and deletions in the low P-F score group than those in the high P-F score group (**Figures 7D–F**). Additionally, the top 24 genes with the most frequently genomic alteration in PAAD were analyzed between the high and low P-F score groups. The patients in the low P-F score group have showed more frequently genomic alterations than those in the high P-F score group (**Figures 7G,H**). As the most frequently oncogenic mutation in PAAD, the proportion *KRAS* mutations in the low P-F score group (92%) was remarkably higher than that in the high P-F score group (62%). Meanwhile, the alterations of *TP53*, *SMAD4*, *USP8*, and *RNF43* also were significantly distinct between the high and low P-F score groups (**Figure 7I**). Among these mutated genes, the *KRAS*, *TP53*, *SMAD4*, and *RNF43* exhibited significant co-occurrence (**Figure 7J**). Taken

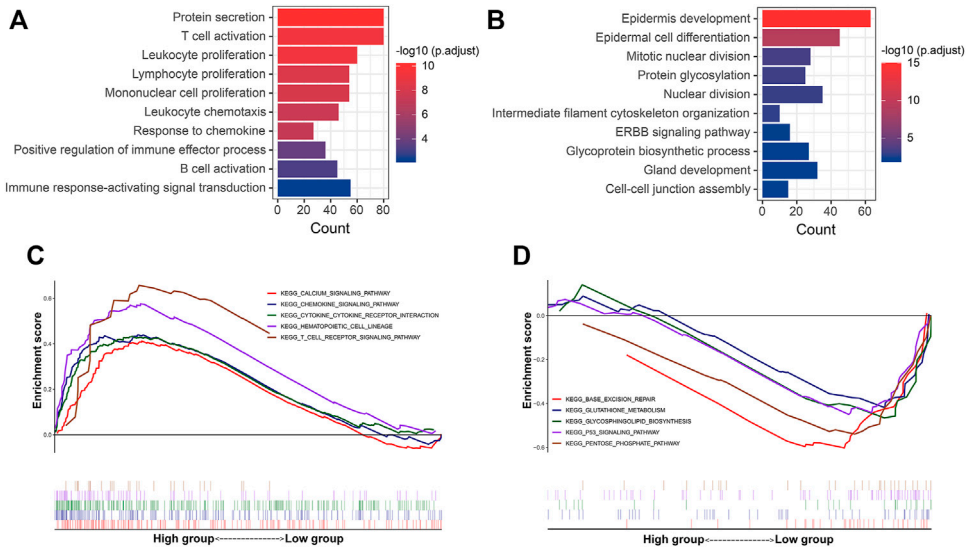

FIGURE 6 | Functional enrichment analyses of the DEGs between the high and low P-F score groups. The GO enrichment analysis of the upregulated **(A)** and downregulated **(B)** DEGs in the high P-F score group when compared with the low group. GSEA showing the pathways enriched in the high **(C)** and **(D)** low P-F score groups.

together, these results revealed the relationships of the P-F score and genomic alteration in PAAD, in which the patients in the low P-F score group manifested with remarkably more alterations.

Role of the P-F Scores in Predicting Therapeutic Benefits

A myriad of studies has validated the great potential of ICB therapy in various cancer types (Sharma and Allison, 2015). However, given the complexity of the TIME, not all cancer patients could respond to ICB therapy (Brahmer et al., 2012; Powles et al., 2014). Therefore, we next explored the availability of the P-F score in predicting the benefits from immunotherapy. First, cancer patients from the IMvigor210 cohort who have received anti-PD-L1 immunotherapy were allocated into the high or low P-F score group based on P-F scoring. As shown in the Kaplan–Meier curve, the patients in the high P-F score group exhibited a significantly better survival when compared with the patients in the low P-F score group (**Figure 8A**). Notably, it was a phenomenon in which significantly more responders after anti-PD-L1 treatment were observed in the high P-F score group (**Figure 8B**). Additionally, the high P-F score group has shown a complete response/partial response (CR/PR) rate of 28% to anti-PD-L1 immunotherapy in the IMvigor210 cohort, which was remarkably higher than that in the low P-F score group (17%) (**Figure 8C**). Encouraged by the abundant T lymphocytes infiltration in the high P-F score group, we next speculated the response to ICBs through the TIDE algorithm. As expected, the patients in the high P-F score group had a significantly higher response rate to the ICBs than the low P-F score group in the TCGA-PAAD cohort (Fisher's test $p = 0.022$) (**Figure 8D**). Furthermore, a subclass mapping algorithm was performed to visualize the therapeutic responses based on the previously reported 47 melanoma patients with detailed immunotherapy records. The heatmap depicted that patients in the high P-F score group were more responsive to the anti-PD-1 immunotherapy in the TCGA-PAAD cohort (Bonferroni corrected $p = 0.049$) (**Figure 8E**). The consistent phenomenon was also validated in the ICGC-PACA-CA and E-MTAB-6134 cohorts (**Supplementary Figures S9, S10**).

Currently, the systemic chemotherapy regimens including FOLFIRINOX or gemcitabine plus paclitaxel are still the mainstay of therapy for PAAD patients (Mizrahi et al., 2020). Therefore, we subsequently investigated the utility of the P-F score in speculating the response to the commonly used chemotherapeutic agents. As shown in **Figure 8F**, the estimated IC50 levels of paclitaxel and 5-fluorouracil were significantly lower in the low P-F score group than those in the high P-F score group, which indicated that the patients in the low P-F score group might be more sensitive to these two drugs. Besides, significantly decreased estimated IC50 levels of paclitaxel, 5-fluorouracil, and gemcitabine were noticed in the low P-F score group in the ICGC-PACA-CA and E-MTAB-6134 cohorts, respectively (**Supplementary Figure S9C** and **Supplementary Figure S10C**). Given the lack of therapeutic data in the ICGC-PACA-CA, E-MTAB-6134, GSE57495, GSE21501, and GSE85916 datasets, we only stratified the patients from the TCGA-PAAD cohort based on distinct chemotherapeutic regimens to evaluate whether the P-F score determined differently in survival. Subsequently, the patients who have received chemotherapy in the TCGA-PAAD cohort were assigned based on the high and low P-F scores. There was no significant difference observed in survival between the high and low P-F score groups (**Figure 8G**). In the subgroup of patients who had been treated with 5-fluorouracil, cisplatin, or gemcitabine, the Kaplan–Meier curves also showed no statistically significant difference in survival between the high and low P-F score groups (**Figures 8H–J**). When treated with 5-fluorouracil, the patients in the low P-F score group tend to have relatively better survival than those in the high P-F score group,

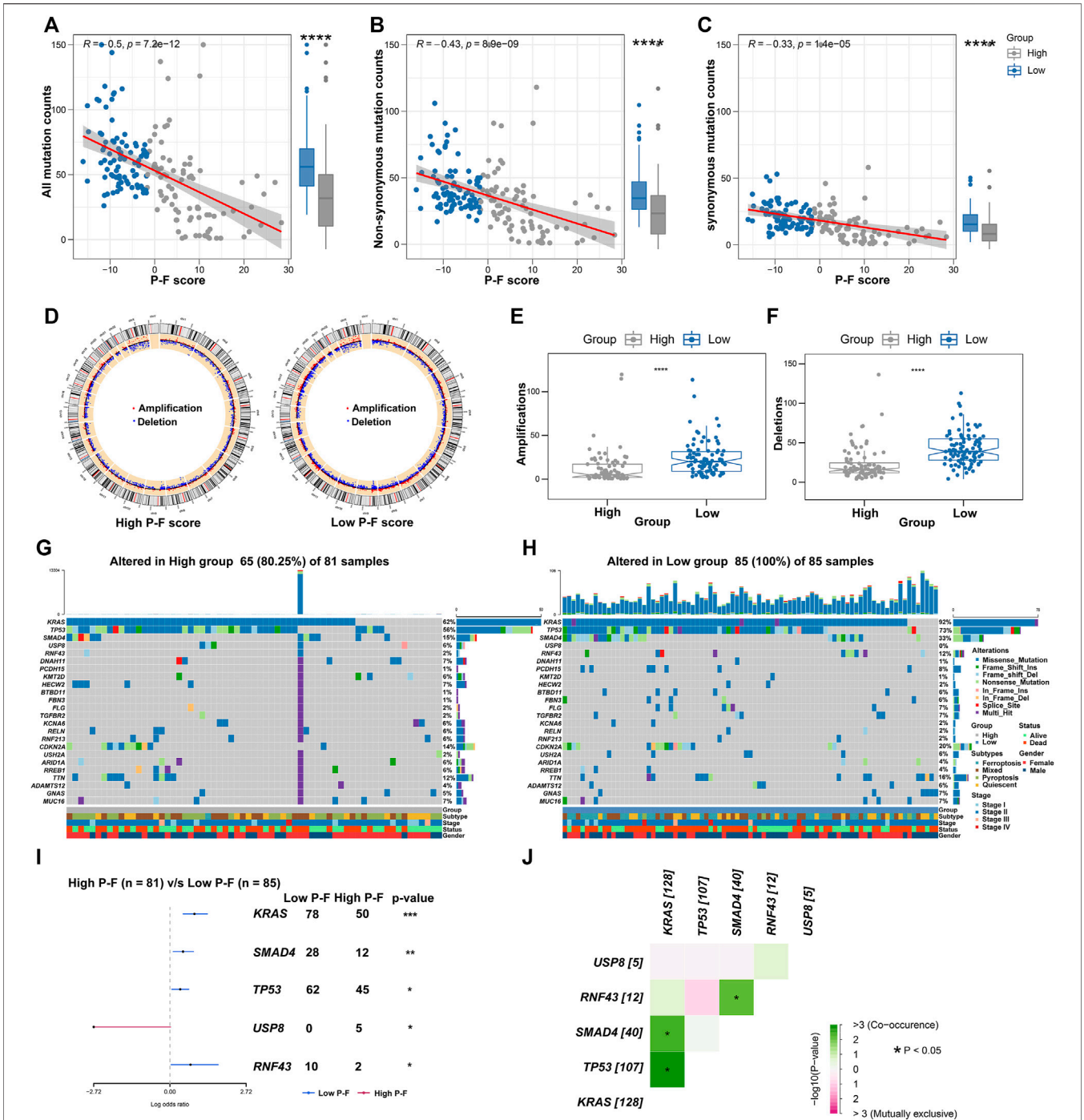

FIGURE 7 | Correlations between the P-F score and tumor mutation status. Correlations between all mutation counts **(A)**, non-synonymous mutation counts **(B)**, synonymous mutation counts **(C)**, and P-F score, and their distributions in the distinct score groups. **(D)** Circos plots depicted the locations of CNV alteration in the high and low P-F score groups. The red dots indicated the amplifications, and the blue dots indicated the deletions. The amplifications **(E)** and deletions **(F)** of chromosome were evaluated in distinct score groups. The oncoplot depicted the landscape of 24 genes with most frequently genomic alteration in the high **(G)** and low **(H)** score groups. **(I)** Forest plot showed the mutated genes that were significantly different between the two groups. **(J)** Interactions among the mutated genes that were significantly different between the high and low P-F score groups (*$p < 0.05$; **$p < 0.01$; ***$p < 0.001$; and ****$p < 0.0001$).

though no statistically significant difference was observed (log-rank $p = 0.076$). These results together suggested that the patients with high P-F scores might be more responsive to immunotherapy, while the patients with low P-F scores might benefit more from chemotherapeutic agents such as paclitaxel or 5-fluorouracil. Because of the limited number of patients who have been

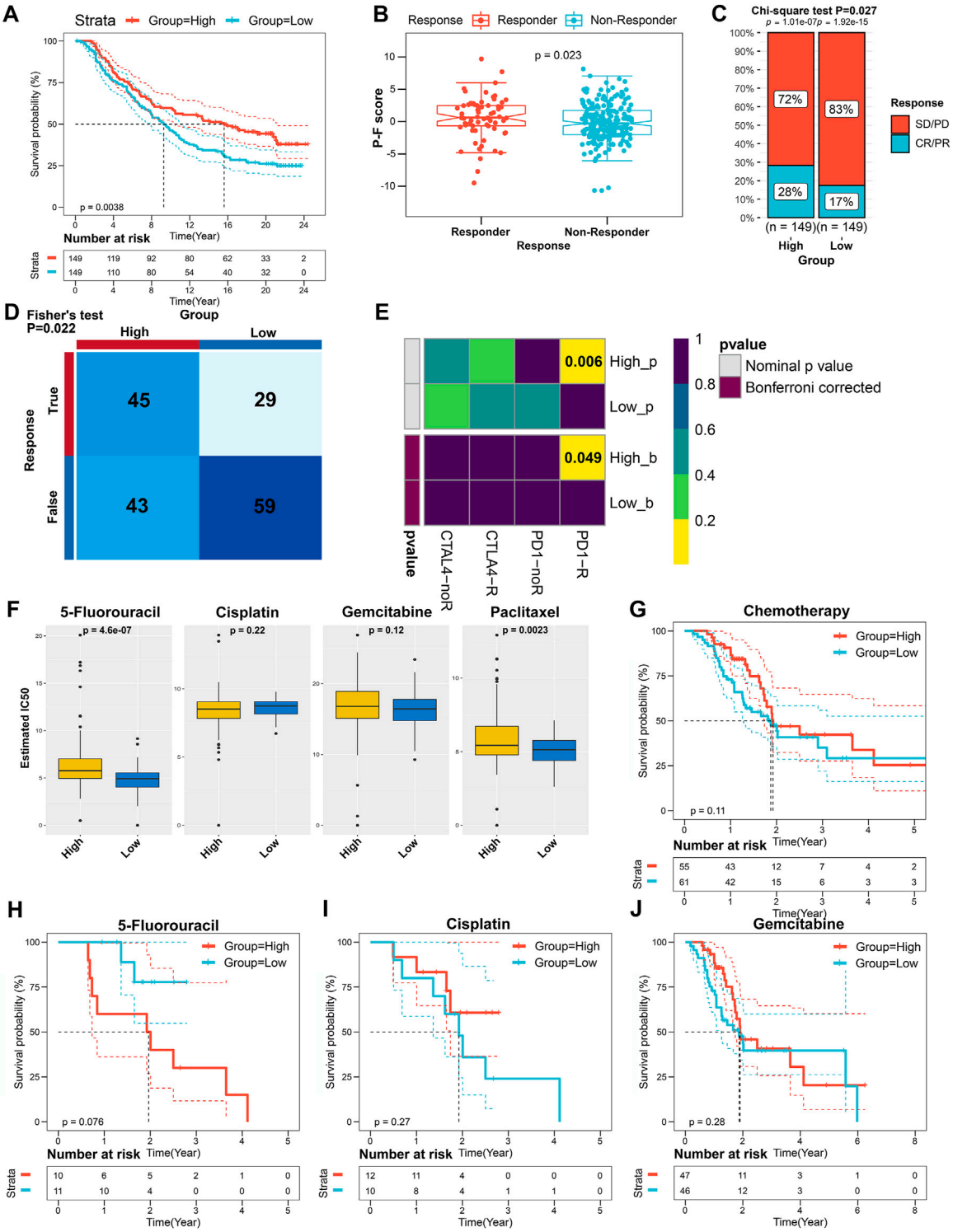

FIGURE 8 | The role of the P-F score in predicting the benefits from immunotherapy and chemotherapy. **(A)** Kaplan–Meier curve for patients with distinct P-F scores from the IMvigor210 cohort (log-rank $p = 0.0038$). **(B)** Evaluation of the P-F scores among patients with distinct anti-PD-L1 treatment responses (Wilcoxon test $p = 0.023$). **(C)** Clinical responses to the anti-PD-L1 immunotherapy of patients in high or low P-F score groups from the IMvigor210 cohort (SD, stable disease; PD, progressive disease; CR, complete response; PR, partial response). **(D)** The responses to anti-PD-1 and anti-CTLA4 immunotherapies of PAAD patients with high or low P-F scores in the TCGA-PAAD cohort were predicted by using the TIDE algorithm (Fisher's test $p = 0.022$). **(E)** Heatmap visualized the responses to anti-PD-1 and anti-CTLA4 immunotherapies between the distinct P-F score groups. **(F)** The estimated IC50 levels of 5-fluorouracil, cisplatin, gemcitabine, and paclitaxel between the two groups. **(G)** Kaplan–Meier curve for patients who have received chemotherapy in the TCGA-PAAD cohort (log-rank $p = 0.11$). Kaplan–Meier curves for patients in the TCGA-PAAD cohort who have been treated with 5-fluorouracil **(H)** (log-rank $p = 0.076$), cisplatin **(I)** (log-rank $p = 0.27$), or gemcitabine **(J)** (log-rank $p = 0.28$).

treated with 5-fluorouracil and paclitaxel in the TCGA-PAAD cohort, further large-scale clinical trials are urgently required to investigate the prognostic value of the P-F score in the chemotherapy for PAAD. Based on the value of $|\log_2 FC|$, the top 150 upregulated DEGs and 150 downregulated DEGs between the high and low P-F score groups were uploaded to the CMap small molecular drug database to search the underlying drugs. As shown in **Supplementary Figure S11**, a total of 55 potential small molecular drugs and 30 drug mechanisms were identified, in which the HDAC inhibitors accounted for the highest proportion among the inhibitors (**Supplementary Table S11**). Taken together, these findings have highlighted the potential value of the P-F score in selecting more suitable therapeutic strategy for PAAD patients.

DISCUSSION

To facilitate the development of individualized therapy for PAAD patients, persistent progress in classifying clinically relevant subtypes of PAAD is urgently needed. In this study, we have established a scoring system (P-F score) based on the consensus clustering of pyroptosis- and ferroptosis-related gene expression profiles in PAAD patients. The results of this study indicated that the P-F score could work as a reliably independent prognostic factor and predictive indicator to estimate the therapeutic responses to immunotherapy and chemotherapy. The PAAD patients with high P-F scores were characterized with escalated immune and stromal score, active immune phenotype, lower tumor purity, and genomic alterations when compared with those in patients with low P-F scores. Furthermore, the patients in the high P-F score group were more responsive to the anti-PD-L1 representative immunotherapy, while the patients in the low P-F score group might be more sensitive to the chemotherapeutic agents like paclitaxel or 5-fluorouracil.

Currently, the exploration of non-apoptotic cell death processes has accelerated the advances in treating malignancies (Chen et al., 2021a). Pyroptosis and ferroptosis have shown complex effects in the biology and therapy of cancer that vary in genetic backgrounds (Friedmann Angeli et al., 2019; Chen et al., 2021b; Wu et al., 2021). Although the roles of pyroptosis and ferroptosis in tumor biology and antitumor immunity have been widely studied, the potential clinical translation is still hampered by the substantial lack in proofs derived from human samples (Tang et al., 2020b). PAAD has occupied over 85% of pancreatic cancer, which represents the malignancy from exocrine pancreas (Ryan et al., 2014). Hence, we mainly focused on developing a scoring system that integrates the pyroptosis and ferroptosis profiles of PAAD to better stratify pancreatic cancer. In this study, the PAAD samples were initially stratified into 4 cell death subtypes based on the median expression levels of coexpressed pyroptosis- and ferroptosis-related genes. The patients in the pyroptosis subtype had relatively best survival, while the relatively worse survival was found in the mixed subtype. The TMB that reflects the mutation accumulation in cancer has shown negative correlation with the OS of patients, even when accounting for distinct cancer types (Pleasance et al., 2020). Across the 4 cell death subtypes, the patients in the ferroptosis and mixed subtypes presented higher TMB than that of patients in other subtypes. These findings together suggested the pyroptosis and ferroptosis might act synergistically to facilitate tumor progression in PAAD, even though patients with independently high expression of pyroptosis-related genes demonstrated the best outcome. Therefore, a comprehensive characterization of the distinct cell death processes would be a better approach to stratify PAAD for further individualized assessment and therapy.

Given the heterogeneity among different patients, it was more practical to quantify the distinct cell death processes in an individual tumor sample. In the present study, the P-F score was established by utilizing the Boruta algorithm. Patients with high P-F scores exhibited a longer survival time, suggesting that the P-F score might work as an indicator of favorable prognosis. The high predictive efficacy of the P-F score in PAAD for 1-, 2-, 3-, 4-, and 5-year survival times was confirmed by the analysis of ROCs. Through the univariate and multivariate Cox regression analyses, the P-F score was identified as an independent protective factor for OS. Meanwhile, good accuracy of the P-F score in predicting OS was further validated in the TCGA-PAAD, ICGC-PACA-CA, and E-MTAB-6134 cohorts *via* time-dependent AUCs. Our data collectively confirmed the well predictive ability of the P-F score, which could have a clinical application in assessing the OS of PAAD patients. As a key driving force for pancreatic tumorigenesis, *KRAS* mutations were found in nearly all PAAD (Waters and Der, 2018). Intriguingly, significantly elevated genomic mutations were noticed in the low P-F score group. For instance, the mutation frequencies of *KRAS* in the low and high P-F score groups were 92 and 62%, respectively. Recently, the activation of ferroptosis by high-iron diets or depletion of Gpx4 has been proven to promote *KRAS*-driven pancreatic tumorigenesis (Dai et al., 2020). Notably, nearly all the patients in the ferroptosis subtype were allocated in the low P-F score group. These findings suggested that *KRAS* mutations might drive the cell death profile toward a pattern of low P-F score in PAAD. Therefore, the P-F scoring system established in this study could effectively stratify PAAD in the fields of prognosis and genomic alterations.

As an emerging novel therapeutic choice, ICBs have displayed promising effects in multiple malignancies. Given the immune-privileged nature of PAAD, the majority of PAAD patients do not respond well to the ICBs. Accordingly, identifying the portion of patients who might benefit from the ICBs is an urgent demand for clinical practice. Through functional enrichment analysis, the genes that were involved in immunostimulating pathways, including T-cell activation and positive regulation of the immune effector process, were enriched in the high P-F score group. Additionally, a more activated immune phenotype with significantly higher intratumoral infiltrations of activated $CD4^+$ memory T cells, $CD8^+$ T cells, and γδ T cells was found in the high P-F score group, while the low P-F score group was associated with significantly higher infiltration of immunosuppressive Tregs. Emerging evidences have indicated that the preexisting anticancer immunity could positively regulate the response to immunotherapy, while the tumor-infiltrating Tregs could not only suppress the native anticancer immune response but also weaken the efficiencies of ICBs (Kim and Chen, 2016; Chen et al., 2019; Gonzalez-Navajas et al., 2021). The patients from the IMvigor210 cohort who received anti-PD-L1 treatment were evaluated. In line with these

findings, a significantly higher response rate to anti-PD-L1 immunotherapy was observed in patients with high P-F scores. The high TMB has been routinely regarded as an indicator in predicting the response to ICB treatment (Cristescu et al., 2018; Chan et al., 2019). However, the high TMB was recently proven to fail in predicting response to treatment with ICBs across all solid cancer types (McGrail et al., 2021). Hence, the P-F score might be used as an alternative biomarker in predicting the response to ICB treatment. Overall, these results suggested that the patients with high P-F score might benefit more from the single agent of ICB treatment. Considering the enriched intratumoral Tregs in the low P-F score group, the depletion or suppression of Tregs might work in synergy with ICB treatment. In this content, there are ongoing clinical trials (ClinicalTrials.gov: NCT03447314, and NCT03739710) to validate the effects of the combination of ICBs and targeting Tregs in advanced solid tumors. These reasonable speculations in this study need future clinical trial-based validation in a large PAAD cohort.

Recently, some studies have explored the pyroptosis- or ferroptosis-related molecular subgrouping in various cancers, including PAAD, lung adenocarcinoma, and hepatocellular carcinoma (Tang et al., 2020a; Fu and Song, 2021; Liu et al., 2021). Some strengths could be noticed in our study. This study is more valuable and convincing when compared with other studies that only focused on pyroptosis- or ferroptosis-related genes (Tang et al., 2020a; Fu and Song, 2021; Liu et al., 2021). Different from one recent study that clustered the hepatocellular carcinoma based on the prognosis-related genes associated with ferroptosis and pyroptosis, this study stratified cell death subtypes based on dual analysis of pyroptosis- and ferroptosis-related genes and further established a scoring system depending on the DEGs among different cell death subtypes (Huo et al., 2021). The P-F scoring system established in our study could provide a better understanding of the crosstalk between the pyroptosis and ferroptosis in PAAD. Although an earlier study that focused more on the association between the immune populations and prognosis has provided an integrated immunophenotypic classification of PAAD, our study further broadened the genetic and immunologic variables to prognostic and therapeutic decision-making values (Wartenberg et al., 2018). Meanwhile, there are some limitations in this study. First, as limited by lacking therapeutic data of a PAAD-related immunotherapy cohort, we validated the availability of the P-F score in predicting the benefits from immunotherapy through utilizing the IMvigor210 cohort, an immunotherapy cohort of urothelial cancer. Besides, therapeutic data in the ICGC-PACA-CA, E-MTAB-6134, GSE57495, GSE21501, and GSE85916 datasets are incomplete. As a result, we just investigated the effect of the P-F score in the patients who have received chemotherapy in the TCGA-PAAD cohort. Notwithstanding its limitations, our study does establish an integrated P-F scoring system in PAAD. Large-scale clinical trials are required to further verify the value of the P-F score in predicting the benefits from immunotherapy and chemotherapy for PAAD.

In conclusion, we comprehensively analyzed the landscape of pyroptosis and ferroptosis in PAAD, establishing an integrated P-F scoring system. Distinct genomic alterations, immune infiltrations, and survival were revealed between the high and low P-F score groups. Functionally, the P-F score has superior capacity in predicting the outcomes and responses to the treatments with chemotherapeutic agents or immunotherapies of PAAD patients. Collectively, the systematic evaluation of the tumor cell death profiles conducted by this study has potential values for prognostic evaluation and therapeutic decision-making for PAAD patients.

DATA AVAILABILITY STATEMENT

Publicly available datasets were analyzed in this study. These data can be found here: The RNA-sequence (RNA-Seq) data with matched clinical information of all available PAAD patients were extracted from The Cancer Genome Atlas (TCGA) (https://www.cancer.gov/tcga) (n = 176) and International Cancer Genome Consortium (ICGC) (https://daco.icgc.org/) (n = 165) databases. Additionally, the E-MTAB-6134 dataset with completely clinical information of 288 PAAD patients and datasets without detailed clinical information including GSE57495, GSE21501, and GSE85916 were all extracted from the Array Express database (https://www.ebi.ac.uk/arrayexpress). The TCGA dataset was utilized as the training cohort, and the other datasets were set as validation cohorts. Based on the Creative Commons 3.0 license downloaded from http://research-pub.gene.com/IMvigor210CoreBiologie, the IMvigor210 dataset was extracted from a freely available data package. The IMvigor210 dataset containing 298 patients of urothelial cancer who had received immunotherapy was performed to validate the prediction value of the P-F score. The corresponding information of somatic mutations in TCGA-PAAD patients was extracted from UCSC Xena (https://xena.ucsc.edu/).

AUTHOR CONTRIBUTIONS

Research design: HT and HS; data collection: TY, HT, and CL; data analysis: HT, WN, and YW; manuscript preparation: TY, HT, CL, and WN; chart preparation: TY, HT, CL, and KZ; revisions: TY, HT, CL, WN, YW, KZ, and HS. All the authors have read and approved the final draft for submission.

FUNDING

This work was financially supported by the National Natural Science Foundation of China (82003195), the China Postdoctoral Science Foundation (2020M680150), and postdoctoral research project, West China Hospital, Sichuan University (2020HXBH002).

SUPPLEMENTARY MATERIAL

The Supplementary Material for this article can be found online at: https://www.frontiersin.org/articles/10.3389/fcell.2022.826879/full#supplementary-material

REFERENCES

Bersuker, K., Hendricks, J. M., Li, Z., Magtanong, L., Ford, B., Tang, P. H., et al. (2019). The CoQ Oxidoreductase FSP1 Acts Parallel to GPX4 to Inhibit Ferroptosis. *Nature* 575 (7784), 688–692. doi:10.1038/s41586-019-1705-2

Brahmer, J. R., Tykodi, S. S., Chow, L. Q. M., Hwu, W.-J., Topalian, S. L., Hwu, P., et al. (2012). Safety and Activity of Anti-PD-L1 Antibody in Patients with Advanced Cancer. *N. Engl. J. Med.* 366 (26), 2455–2465. doi:10.1056/NEJMoa1200694

Chan, T. A., Yarchoan, M., Jaffee, E., Swanton, C., Quezada, S. A., Stenzinger, A., et al. (2019). Development of Tumor Mutation burden as an Immunotherapy Biomarker: Utility for the Oncology Clinic. *Ann. Oncol.* 30 (1), 44–56. doi:10.1093/annonc/mdy495

Chen, X., Kang, R., Kroemer, G., and Tang, D. (2021a). Broadening Horizons: the Role of Ferroptosis in Cancer. *Nat. Rev. Clin. Oncol.* 18 (5), 280–296. doi:10.1038/s41571-020-00462-0

Chen, X., Kang, R., Kroemer, G., and Tang, D. (2021b). Targeting Ferroptosis in Pancreatic Cancer: a Double-Edged Sword. *Trends Cancer* 7 (10), 891–901. doi:10.1016/j.trecan.2021.04.005

Chen, Y.-P., Wang, Y.-Q., Lv, J.-W., Li, Y.-Q., Chua, M. L. K., Le, Q.-T., et al. (2019). Identification and Validation of Novel Microenvironment-Based Immune Molecular Subgroups of Head and Neck Squamous Cell Carcinoma: Implications for Immunotherapy. *Ann. Oncol.* 30 (1), 68–75. doi:10.1093/annonc/mdy470

Cookson, B. T., and Brennan, M. A. (2001). Pro-inflammatory Programmed Cell Death. *Trends Microbiol.* 9 (3), 113–114. doi:10.1016/s0966-842x(00)01936-3

Cristescu, R., Mogg, R., Ayers, M., Albright, A., Murphy, E., Yearley, J., et al. (2018). Pan-tumor Genomic Biomarkers for PD-1 Checkpoint Blockade-Based Immunotherapy. *Science* 362 (6411). doi:10.1126/science.aar3593

Dai, E., Han, L., Liu, J., Xie, Y., Zeh, H. J., Kang, R., et al. (2020). Ferroptotic Damage Promotes Pancreatic Tumorigenesis through a TMEM173/STING-dependent DNA Sensor Pathway. *Nat. Commun.* 11 (1), 6339. doi:10.1038/s41467-020-20154-8

Doll, S., Freitas, F. P., Shah, R., Aldrovandi, M., da Silva, M. C., Ingold, I., et al. (2019). FSP1 Is a Glutathione-independent Ferroptosis Suppressor. *Nature* 575 (7784), 693–698. doi:10.1038/s41586-019-1707-0

Dong, Z., Bian, L., Wang, M., Wang, L., and Wang, Y. (2021). Identification of a Pyroptosis-Related Gene Signature for Prediction of Overall Survival in Lung Adenocarcinoma. *J. Oncol.* 2021, 1–15. doi:10.1155/2021/6365459

Du, J., Wang, T., Li, Y., Zhou, Y., Wang, X., Yu, X., et al. (2019). DHA Inhibits Proliferation and Induces Ferroptosis of Leukemia Cells through Autophagy Dependent Degradation of Ferritin. *Free Radic. Biol. Med.* 131, 356–369. doi:10.1016/j.freeradbiomed.2018.12.011

Escobar-Hoyos, L. F., Penson, A., Kannan, R., Cho, H., Pan, C.-H., Singh, R. K., et al. (2020). Altered RNA Splicing by Mutant P53 Activates Oncogenic RAS Signaling in Pancreatic Cancer. *Cancer Cell* 38 (2), 198–211. doi:10.1016/j.ccell.2020.05.010

Friedmann Angeli, J. P., Krysko, D. V., and Conrad, M. (2019). Ferroptosis at the Crossroads of Cancer-Acquired Drug Resistance and Immune Evasion. *Nat. Rev. Cancer* 19 (7), 405–414. doi:10.1038/s41568-019-0149-1

Fu, X.-W., and Song, C.-Q. (2021). Identification and Validation of Pyroptosis-Related Gene Signature to Predict Prognosis and Reveal Immune Infiltration in Hepatocellular Carcinoma. *Front. Cel Dev. Biol.* 9, 748039. doi:10.3389/fcell.2021.748039

Gao, J., Qiu, X., Xi, G., Liu, H., Zhang, F., Lv, T., et al. (2018). Downregulation of GSDMD Attenuates Tumor Proliferation via the Intrinsic Mitochondrial Apoptotic Pathway and Inhibition of EGFR/Akt Signaling and Predicts a Good Prognosis in Non-small C-ell L-ung C-ancer. *Oncol. Rep.* 40 (4), 1971–1984. doi:10.3892/or.2018.6634

Geeleher, P., Cox, N. J., and Huang, R. (2014). Clinical Drug Response Can Be Predicted Using Baseline Gene Expression Levels and *In Vitro* Drug Sensitivity in Cell Lines. *Genome Biol.* 15 (3), R47. doi:10.1186/gb-2014-15-3-r47

González-Navajas, J. M., Fan, D. D., Yang, S., Yang, F. M., Lozano-Ruiz, B., Shen, L., et al. (2021). The Impact of Tregs on the Anticancer Immunity and the Efficacy of Immune Checkpoint Inhibitor Therapies. *Front. Immunol.* 12, 625783. doi:10.3389/fimmu.2021.625783

Gordon-Dseagu, V. L., Devesa, S. S., Goggins, M., and Stolzenberg-Solomon, R. (2018). Pancreatic Cancer Incidence Trends: Evidence from the Surveillance, Epidemiology and End Results (SEER) Population-Based Data. *Int. J. Epidemiol.* 47 (2), 427–439. doi:10.1093/ije/dyx232

Hassannia, B., Vandenabeele, P., and Vanden Berghe, T. (2019). Targeting Ferroptosis to Iron Out Cancer. *Cancer Cell* 35 (6), 830–849. doi:10.1016/j.ccell.2019.04.002

Huo, J., Cai, J., Guan, G., Liu, H., and Wu, L. (2021). A Ferroptosis and Pyroptosis Molecular Subtype-Related Signature Applicable for Prognosis and Immune Microenvironment Estimation in Hepatocellular Carcinoma. *Front. Cel Dev. Biol.* 9, 761839. doi:10.3389/fcell.2021.761839

Jiang, P., Gu, S., Pan, D., Fu, J., Sahu, A., Hu, X., et al. (2018). Signatures of T Cell Dysfunction and Exclusion Predict Cancer Immunotherapy Response. *Nat. Med.* 24 (10), 1550–1558. doi:10.1038/s41591-018-0136-1

Jin, M.-Z., and Wang, X.-P. (2021). Immunogenic Cell Death-Based Cancer Vaccines. *Front. Immunol.* 12, 697964. doi:10.3389/fimmu.2021.697964

Johnson, A. M., Kleczko, E. K., and Nemenoff, R. A. (2020). Eicosanoids in Cancer: New Roles in Immunoregulation. *Front. Pharmacol.* 11, 595498. doi:10.3389/fphar.2020.595498

Ju, A., Tang, J., Chen, S., Fu, Y., and Luo, Y. (2021). Pyroptosis-Related Gene Signatures Can Robustly Diagnose Skin Cutaneous Melanoma and Predict the Prognosis. *Front. Oncol.* 11, 709077. doi:10.3389/fonc.2021.709077

Kambara, H., Liu, F., Zhang, X., Liu, P., Bajrami, B., Teng, Y., et al. (2018). Gasdermin D Exerts Anti-inflammatory Effects by Promoting Neutrophil Death. *Cel Rep.* 22 (11), 2924–2936. doi:10.1016/j.celrep.2018.02.067

Kang, R., Zeng, L., Zhu, S., Xie, Y., Liu, J., Wen, Q., et al. (2018). Lipid Peroxidation Drives Gasdermin D-Mediated Pyroptosis in Lethal Polymicrobial Sepsis. *Cell Host & Microbe* 24 (1), 97–108. doi:10.1016/j.chom.2018.05.009

Karki, R., and Kanneganti, T.-D. (2019). Diverging Inflammasome Signals in Tumorigenesis and Potential Targeting. *Nat. Rev. Cancer* 19 (4), 197–214. doi:10.1038/s41568-019-0123-y

Kim, J. M., and Chen, D. S. (2016). Immune Escape to PD-L1/pd-1 Blockade: Seven Steps to success (Or Failure). *Ann. Oncol.* 27 (8), 1492–1504. doi:10.1093/annonc/mdw217

Kursa, M. B., and Rudnicki, W. R. (2010). Feature Selection with theBorutaPackage. *J. Stat. Soft.* 36 (11), 1–13. doi:10.18637/jss.v036.i11

Lamb, J., Crawford, E. D., Peck, D., Modell, J. W., Blat, I. C., Wrobel, M. J., et al. (2006). The Connectivity Map: Using Gene-Expression Signatures to Connect Small Molecules, Genes, and Disease. *Science* 313 (5795), 1929–1935. doi:10.1126/science.1132939

Li, X.-Y., Zhang, L.-Y., Li, X.-Y., Yang, X.-T., and Su, L.-X. (2021). A Pyroptosis-Related Gene Signature for Predicting Survival in Glioblastoma. *Front. Oncol.* 11, 697198. doi:10.3389/fonc.2021.697198

Li, Y., Wang, L., Pappan, L., Galliher-Beckley, A., and Shi, J. (2012). IL-1β Promotes Stemness and Invasiveness of colon Cancer Cells through Zeb1 Activation. *Mol. Cancer* 11, 87. doi:10.1186/1476-4598-11-87

Liang, J.-y., Wang, D.-s., Lin, H.-c., Chen, X.-x., Yang, H., Zheng, Y., et al. (2020). A Novel Ferroptosis-Related Gene Signature for Overall Survival Prediction in Patients with Hepatocellular Carcinoma. *Int. J. Biol. Sci.* 16 (13), 2430–2441. doi:10.7150/ijbs.45050

Liu, L.-P., Lu, L., Zhao, Q.-Q., Kou, Q.-J., Jiang, Z.-Z., Gui, R., et al. (2021). Identification and Validation of the Pyroptosis-Related Molecular Subtypes of Lung Adenocarcinoma by Bioinformatics and Machine Learning. *Front. Cel Dev. Biol.* 9, 756340. doi:10.3389/fcell.2021.756340

Liu, Y., Zhang, X., Zhang, J., Tan, J., Li, J., and Song, Z. (2020). Development and Validation of a Combined Ferroptosis and Immune Prognostic Classifier for Hepatocellular Carcinoma. *Front. Cel Dev. Biol.* 8, 596679. doi:10.3389/fcell.2020.596679

Man, S. M., and Kanneganti, T.-D. (2015). Regulation of Inflammasome Activation. *Immunol. Rev.* 265 (1), 6–21. doi:10.1111/imr.12296

Mayakonda, A., Lin, D.-C., Assenov, Y., Plass, C., and Koeffler, H. P. (2018). Maftools: Efficient and Comprehensive Analysis of Somatic Variants in Cancer. *Genome Res.* 28 (11), 1747–1756. doi:10.1101/gr.239244.118

McGrail, D. J., Pilié, P. G., Rashid, N. U., Voorwerk, L., Slagter, M., Kok, M., et al. (2021). High Tumor Mutation burden Fails to Predict Immune Checkpoint Blockade Response across All Cancer Types. *Ann. Oncol.* 32 (5), 661–672. doi:10.1016/j.annonc.2021.02.006

Miguchi, M., Hinoi, T., Shimomura, M., Adachi, T., Saito, Y., Niitsu, H., et al. (2016). Gasdermin C Is Upregulated by Inactivation of Transforming Growth Factor β Receptor Type II in the Presence of Mutated Apc, Promoting Colorectal Cancer Proliferation. *PLoS One* 11 (11), e0166422. doi:10.1371/journal.pone.0166422

Mizrahi, J. D., Surana, R., Valle, J. W., and Shroff, R. T. (2020). Pancreatic Cancer. *The Lancet* 395 (10242), 2008–2020. doi:10.1016/S0140-6736(20)30974-0

Neoptolemos, J. P., Kleeff, J., Michl, P., Costello, E., Greenhalf, W., and Palmer, D. H. (2018). Therapeutic Developments in Pancreatic Cancer: Current and Future Perspectives. *Nat. Rev. Gastroenterol. Hepatol.* 15 (6), 333–348. doi:10.1038/s41575-018-0005-x

Newman, A. M., Liu, C. L., Green, M. R., Gentles, A. J., Feng, W., Xu, Y., et al. (2015). Robust Enumeration of Cell Subsets from Tissue Expression Profiles. *Nat. Methods* 12 (5), 453–457. doi:10.1038/nmeth.3337

Ou, W., Mulik, R. S., Anwar, A., McDonald, J. G., He, X., and Corbin, I. R. (2017). Low-density Lipoprotein Docosahexaenoic Acid Nanoparticles Induce Ferroptotic Cell Death in Hepatocellular Carcinoma. *Free Radic. Biol. Med.* 112, 597–607. doi:10.1016/j.freeradbiomed.2017.09.002

Pizato, N., Luzete, B. C., Kiffer, L. F. M. V., Corrêa, L. H., de Oliveira Santos, I., Assumpção, J. A. F., et al. (2018). Omega-3 Docosahexaenoic Acid Induces Pyroptosis Cell Death in Triple-Negative Breast Cancer Cells. *Sci. Rep.* 8 (1), 1952. doi:10.1038/s41598-018-20422-0

Pleasance, E., Titmuss, E., Williamson, L., Kwan, H., Culibrk, L., Zhao, E. Y., et al. (2020). Pan-cancer Analysis of Advanced Patient Tumors Reveals Interactions between Therapy and Genomic Landscapes. *Nat. Cancer* 1 (4), 452–468. doi:10.1038/s43018-020-0050-6

Powles, T., Eder, J. P., Fine, G. D., Braiteh, F. S., Loriot, Y., Cruz, C., et al. (2014). MPDL3280A (Anti-PD-L1) Treatment Leads to Clinical Activity in Metastatic Bladder Cancer. *Nature* 515 (7528), 558–562. doi:10.1038/nature13904

Roh, W., Chen, P.-L., Reuben, A., Spencer, C. N., Prieto, P. A., Miller, J. P., et al. (2017). Integrated Molecular Analysis of Tumor Biopsies on Sequential CTLA-4 and PD-1 Blockade Reveals Markers of Response and Resistance. *Sci. Transl. Med.* 9 (379). doi:10.1126/scitranslmed.aah3560

Rooney, M. S., Shukla, S. A., Wu, C. J., Getz, G., and Hacohen, N. (2015). Molecular and Genetic Properties of Tumors Associated with Local Immune Cytolytic Activity. *Cell* 160 (1-2), 48–61. doi:10.1016/j.cell.2014.12.033

Ryan, D. P., Hong, T. S., and Bardeesy, N. (2014). Pancreatic Adenocarcinoma. *N. Engl. J. Med.* 371 (11), 1039–1049. doi:10.1056/NEJMra1404198

Sharma, P., and Allison, J. P. (2015). The Future of Immune Checkpoint Therapy. *Science* 348 (6230), 56–61. doi:10.1126/science.aaa8172

Siegel, R. L., Miller, K. D., and Jemal, A. (2020). Cancer Statistics, 2020. *CA A. Cancer J. Clin.* 70 (1), 7–30. doi:10.3322/caac.21590

Stockwell, B. R., Friedmann Angeli, J. P., Bayir, H., Bush, A. I., Conrad, M., Dixon, S. J., et al. (2017). Ferroptosis: A Regulated Cell Death Nexus Linking Metabolism, Redox Biology, and Disease. *Cell* 171 (2), 273–285. doi:10.1016/j.cell.2017.09.021

Subramanian, A., Narayan, R., Corsello, S. M., Peck, D. D., Natoli, T. E., Lu, X., et al. (2017). A Next Generation Connectivity Map: L1000 Platform and the First 1,000,000 Profiles. *Cell* 171 (6), 1437–1452. doi:10.1016/j.cell.2017.10.049

Sultana, A., Smith, C. T., Cunningham, D., Starling, N., Neoptolemos, J. P., and Ghaneh, P. (2007). Meta-analyses of Chemotherapy for Locally Advanced and Metastatic Pancreatic Cancer. *Jco* 25 (18), 2607–2615. doi:10.1200/JCO.2006.09.2551

Tan, Y., Chen, Q., Li, X., Zeng, Z., Xiong, W., Li, G., et al. (2021). Pyroptosis: a New Paradigm of Cell Death for Fighting against Cancer. *J. Exp. Clin. Cancer Res.* 40 (1), 153. doi:10.1186/s13046-021-01959-x

Tang, D., Chen, X., Comish, P. B., and Kang, R. (2021). The Dual Role of Ferroptosis in Pancreatic Cancer: a Narrative Review. *J. Pancreatology* 4 (2). doi:10.1097/jp9.0000000000000067

Tang, R., Hua, J., Xu, J., Liang, C., Meng, Q., Liu, J., et al. (2020a). The Role of Ferroptosis Regulators in the Prognosis, Immune Activity and Gemcitabine Resistance of Pancreatic Cancer. *Ann. Transl Med.* 8 (21), 1347. doi:10.21037/atm-20-2554a

Tang, R., Xu, J., Zhang, B., Liu, J., Liang, C., Hua, J., et al. (2020b). Ferroptosis, Necroptosis, and Pyroptosis in Anticancer Immunity. *J. Hematol. Oncol.* 13 (1), 110. doi:10.1186/s13045-020-00946-7

Vidal-Vanaclocha, F., Fantuzzi, G., Mendoza, L., Fuentes, A. M., Anasagasti, M. J., Martin, J., et al. (2000). IL-18 Regulates IL-1beta -dependent Hepatic Melanoma Metastasis via Vascular Cell Adhesion Molecule-1. *Proc. Natl. Acad. Sci.* 97 (2), 734–739. doi:10.1073/pnas.97.2.734

Wang, B., and Yin, Q. (2017). AIM2 Inflammasome Activation and Regulation: A Structural Perspective. *J. Struct. Biol.* 200 (3), 279–282. doi:10.1016/j.jsb.2017.08.001

Wang, Q., Wang, Y., Ding, J., Wang, C., Zhou, X., Gao, W., et al. (2020). A Bioorthogonal System Reveals Antitumour Immune Function of Pyroptosis. *Nature* 579 (7799), 421–426. doi:10.1038/s41586-020-2079-1

Wang, W., Green, M., Choi, J. E., Gijón, M., Kennedy, P. D., Johnson, J. K., et al. (2019). CD8+ T Cells Regulate Tumour Ferroptosis during Cancer Immunotherapy. *Nature* 569 (7755), 270–274. doi:10.1038/s41586-019-1170-y

Wang, X., Liu, K., Gong, H., Li, D., Chu, W., Zhao, D., et al. (2021). Death by Histone Deacetylase Inhibitor Quisinostat in Tongue Squamous Cell Carcinoma via Apoptosis, Pyroptosis, and Ferroptosis. *Toxicol. Appl. Pharmacol.* 410, 115363. doi:10.1016/j.taap.2020.115363

Wartenberg, M., Cibin, S., Zlobec, I., Vassella, E., Eppenberger-Castori, S., Terracciano, L., et al. (2018). Integrated Genomic and Immunophenotypic Classification of Pancreatic Cancer Reveals Three Distinct Subtypes with Prognostic/Predictive Significance. *Clin. Cancer Res.* 24 (18), 4444–4454. doi:10.1158/1078-0432.CCR-17-3401

Waters, A. M., and Der, C. J. (2018). KRAS: The Critical Driver and Therapeutic Target for Pancreatic Cancer. *Cold Spring Harb Perspect. Med.* 8 (9), a031435. doi:10.1101/cshperspect.a031435

Wu, D., Wei, C., Li, Y., Yang, X., and Zhou, S. (2021). Pyroptosis, a New Breakthrough in Cancer Treatment. *Front. Oncol.* 11, 698811. doi:10.3389/fonc.2021.698811

Xia, X., Wang, X., Cheng, Z., Qin, W., Lei, L., Jiang, J., et al. (2019). The Role of Pyroptosis in Cancer: Pro-cancer or Pro-"host"? *Cell Death Dis* 10 (9), 650. doi:10.1038/s41419-019-1883-8

Xu, H., Ye, D., Ren, M., Zhang, H., and Bi, F. (2021). Ferroptosis in the Tumor Microenvironment: Perspectives for Immunotherapy. *Trends Mol. Med.* 27 (9), 856–867. doi:10.1016/j.molmed.2021.06.014

Yang, W. S., SriRamaratnam, R., Welsch, M. E., Shimada, K., Skouta, R., Viswanathan, V. S., et al. (2014). Regulation of Ferroptotic Cancer Cell Death by GPX4. *Cell* 156 (1-2), 317–331. doi:10.1016/j.cell.2013.12.010

Yoshihara, K., Shahmoradgoli, M., Martínez, E., Vegesna, R., Kim, H., Torres-Garcia, W., et al. (2013). Inferring Tumour Purity and Stromal and Immune Cell Admixture from Expression Data. *Nat. Commun.* 4, 2612. doi:10.1038/ncomms3612

Zhang, Z., Zhang, Y., and Lieberman, J. (2021). Lighting a Fire: Can We Harness Pyroptosis to Ignite Antitumor Immunity? *Cancer Immunol. Res.* 9 (1), 2–7. doi:10.1158/2326-6066.CIR-20-0525

Zhang, Z., Zhang, Y., Xia, S., Kong, Q., Li, S., Liu, X., et al. (2020). Gasdermin E Suppresses Tumour Growth by Activating Anti-tumour Immunity. *Nature* 579 (7799), 415–420. doi:10.1038/s41586-020-2071-9

Zhu, S., Ding, S., Wang, P., Wei, Z., Pan, W., Palm, N. W., et al. (2017). Nlrp9b Inflammasome Restricts Rotavirus Infection in Intestinal Epithelial Cells. *Nature* 546 (7660), 667–670. doi:10.1038/nature22967

Zhuo, S., Chen, Z., Yang, Y., Zhang, J., Tang, J., and Yang, K. (2020). Clinical and Biological Significances of a Ferroptosis-Related Gene Signature in Glioma. *Front. Oncol.* 10, 590861. doi:10.3389/fonc.2020.590861

Conflict of Interest: The authors declare that the research was conducted in the absence of any commercial or financial relationships that could be construed as a potential conflict of interest.

Publisher's Note: All claims expressed in this article are solely those of the authors and do not necessarily represent those of their affiliated organizations, or those of the publisher, the editors, and the reviewers. Any product that may be evaluated in this article, or claim that may be made by its manufacturer, is not guaranteed or endorsed by the publisher.

frontiers in Cell and Developmental Biology

ORIGINAL RESEARCH
published: 22 February 2022
doi: 10.3389/fcell.2022.792676

Construction and Validation of a Ferroptosis-Related lncRNA Signature as a Novel Biomarker for Prognosis, Immunotherapy and Targeted Therapy in Hepatocellular Carcinoma

Ze Zhang[1,2,3,4†], *Wenwen Zhang*[2,3,4†], *Yafei Wang*[1,2,3,4], *Tao Wan*[2,3,4], *Bingyang Hu*[2,3,4], *Chonghui Li*[2,3,4], *Xinlan Ge*[2,3,4] *and Shichun Lu*[2,3,4*]

[1]*Medical School of Chinese People's Liberation Army (PLA), Beijing, China,* [2]*Faculty of Hepato-Pancreato-Biliary Surgery, Chinese PLA General Hospital, Beijing, China,* [3]*Institute of Hepatobiliary Surgery of Chinese PLA, Beijing, China,* [4]*Key Laboratory of Digital Hepatobiliary Surgery, PLA, Beijing, China*

OPEN ACCESS

Edited by:
Lian Xiang Luo,
Guangdong Medical University, China

Reviewed by:
Cecilia Battistelli,
Sapienza University of Rome, Italy
Gang Chen,
First Affiliated Hospital of Wenzhou Medical University, China

***Correspondence:**
Shichun Lu
lsc620213@126.com

[†]*These authors have contributed equally to this work*

Specialty section:
This article was submitted to Cell Death and Survival, a section of the journal Frontiers in Cell and Developmental Biology

Received: *11 October 2021*
Accepted: *26 January 2022*
Published: *22 February 2022*

Citation:
Zhang Z, Zhang W, Wang Y, Wan T, Hu B, Li C, Ge X and Lu S (2022) Construction and Validation of a Ferroptosis-Related lncRNA Signature as a Novel Biomarker for Prognosis, Immunotherapy and Targeted Therapy in Hepatocellular Carcinoma. Front. Cell Dev. Biol. 10:792676. doi: 10.3389/fcell.2022.792676

Recently, immunotherapy combined with targeted therapy has significantly prolonged the survival time and improved the quality of life of patients with hepatocellular carcinoma (HCC). However, HCC treatment remains challenging due to the high heterogeneity of this malignancy. Sorafenib, the first-line drug for the treatment of HCC, can inhibit the progression of HCC by inducing ferroptosis. Ferroptosis is associated with the formation of an immunosuppressive microenvironment in tumours. Moreover, long non-coding RNAs (lncRNAs) are strongly associated with ferroptosis and the progression of HCC. Discovery of ferroptosis-related lncRNAs (FR-lncRNAs) is critical for predicting prognosis and the effectiveness of immunotherapy and targeted therapies to improve the quality and duration of survival of HCC patients. Herein, all cases from The Cancer Genome Atlas (TCGA) database were divided into training and testing groups at a 6:4 ratio to construct and validate the lncRNA signatures. Least Absolute Shrinkage and Selection Operator (LASSO) regression and Cox regression analyses were used to screen the six FR-lncRNAs (including MKLN1-AS, LINC01224, LNCSRLR, LINC01063, PRRT3-AS1, and POLH-AS1). Kaplan–Meier (K–M) and receiver operating characteristic (ROC) curve analyses demonstrated the optimal predictive prognostic ability of the signature. Furthermore, a nomogram indicated favourable discrimination and consistency. For further validation, we used real-time quantitative polymerase chain reaction (qRT-PCR) to analyse the expression of LNCSRLR, LINC01063, PRRT3-AS1, and POLH-AS1 in HCC tissues. Moreover, we determined the ability of the signature to predict the effects of immunotherapy and targeted therapy in patients with HCC. Gene set enrichment analysis (GSEA) and somatic mutation analysis showed that ferroptosis-related pathways, immune-related pathways, and TP53 mutations may be strongly associated with the overall survival (OS) outcomes of HCC patients. Overall, our study suggests that a new risk model of six FR-lncRNAs has a significant prognostic value for HCC and that it could contribute to precise and individualised HCC treatment.

Keywords: hepatocellular carcinoma, ferroptosis, long non-coding RNAs, prognostic, immunotherapy, targeted therapy, TCGA

INTRODUCTION

Liver cancer ranks sixth in the world in terms of incidence and is the fourth most common cause of cancer-related deaths (Villanueva, 2019). HCC is the most common malignancy of the liver, accounting for approximately 90% of liver cancer cases (Llovet et al., 2021). In the early stages of HCC, curative resection, transplantation, and local ablation are the preferred treatment options, but most patients with HCC are diagnosed at an advanced stage and cannot be cured using the above approaches (Llovet et al., 2021). Despite the many advances in the treatment of HCC, such as immunotherapy and targeted therapies, the median survival time for patients with advanced HCC is only 11–13 months (Villanueva, 2019). Given the high mortality rate of HCC, it is imperative to further explore biomarkers that can predict the effectiveness of HCC immunotherapy or targeted therapy, discover new prognosis-related biomarkers, and identify new therapeutic targets to prolong the survival time of patients with HCC.

Ferroptosis is a type of regulated cell death which, unlike apoptosis, pyroptosis, and necroptosis, is caused by the accumulation of lipid peroxide (Stockwell et al., 2017). Recent studies have shown that ferroptosis is associated with the progression and treatment response of various types of tumours (Chen et al., 2021a). For instance, ferroptosis can induce inflammation-related immunosuppression in the tumour immune microenvironment (TIME), thereby promoting tumour progression, whereas mutations in TP53 and RAS genes are closely related to ferroptosis (Chen et al., 2021a). However, the regulatory mechanisms of ferroptosis in HCC remain to be investigated and are far from being applied for the treatment of HCC (Nie et al., 2018; Capelletti et al., 2020). Therefore, identifying the main regulators associated with ferroptosis is a crucial way to broaden the therapeutic approach to HCC.

Long non-coding RNAs (LncRNAs) are most commonly defined as RNAs that are more than 200 nucleotides in length and do not encode proteins (Quinn and Chang, 2016). In HCC, lncRNAs are specifically involved in protein synthesis, degradation, and epigenetic regulation (Mai et al., 2019). HCC-related lncRNAs can regulate the protein modifications of transcription factors and influence protein function by regulating the corresponding cellular signalling pathways (Li et al., 2017; Yan et al., 2017; Zhang et al., 2018). Furthermore, recent studies have demonstrated that GABPB1 and its antisense lncRNA GABPB1-AS1 are closely linked to erastin-induced ferroptosis and that GABPB1 and GABPB1-AS1 can be used as treatment targets for HCC patients (Qi et al., 2019). However, the mechanism underlying the role of FR-lncRNAs in HCC is unclear, and its importance in the therapeutic and prognostic value of HCC needs to be further elucidated.

In this study, we identified and validated a prognostic signature based on ferroptosis-related (FR)-lncRNAs. We also explored the association between the risk model and immune cell infiltration, immune function, sensitivity of immune checkpoint inhibitor (ICI) treatment, and sorafenib treatment. Furthermore, we used gene set enrichment analysis (GSEA) to reveal the pathways enriched in the high- and low-risk groups of the signature. Finally, we validated the significantly differentially expressed lncRNAs in this signature between the tumour and para-tumour tissues *in vitro*. In conclusion, this new prognostic signature is more accurate and convenient than previous signatures in predicting the prognosis and treatment outcomes of HCC patients.

METHODS

Patient Datasets and Processing

Gene expression profiles and clinical data from patients with HCC were downloaded from The Cancer Genome Atlas (TCGA) database. Considering the likelihood of non-cancer deaths, patients with a survival time of ≤30 days and missing expression data were excluded ($n = 35$), leaving 342 HCC patients in the final cohort. The flow chart of the analysis process is presented in **Figure 1**. A total of 342 HCC cases were randomly assigned to the training and testing sets at a ratio of 6:4 for systematic analysis employing the R project "caret" package. Both the training and testing sets needed to comply with the following requirements: 1) cases were randomly classified into training and test groups, and 2) the clinical characteristics of the subjects in both groups were similar. Gene transfer format (GTF) files were downloaded from Ensembl for annotation to distinguish messenger RNAs (mRNAs) from lncRNAs for subsequent analysis. The data of ferroptosis genes (FRGs) were downloaded from FerrDb (Zhou and Bao, 2020) and led to the identification of 259 FRGs. (**Supplementary Table S1**). Correlation analysis was performed between the FRGs and all the lncRNAs. Those with ferroptosis gene correlation coefficients higher than 0.4 and p values lesser than 0.001 were considered FR-lncRNAs. To identify the differentially expressed FR-lncRNAs, we used the R package "limma" for differential expression analysis of FR-lncRNAs. Significantly differentially expressed FR-lncRNAs fulfilled the following criteria: $p < 0.05$ and $|\log2FC| \geq 1$.

Construction of a Prognostic Risk Signature

We screened lncRNAs associated with OS in patients with HCC using univariate Cox regression analysis. $p < 0.05$ was considered statistically significant. For the training group, LASSO regression analysis was performed using the R project "glmnet" package to further select the screened lncRNAs. To prevent over-fitting, 1,000 rounds of cross-validation were used to adjust the parameter selection, and the partial likelihood deviation met the minimum criteria. We then performed a multivariate Cox regression analysis and identified six FR-lncRNAs. Subsequently, we calculated the six FR-lncRNAs corresponding coefficients to construct a prognostic risk score profile for HCC. The formula was established as follow:

$$\begin{aligned}\text{Risk score} = {} & \text{coef lncRNA1} \times \text{lncRNA1 expression} \\ & + \text{coef lncRNA2} \times \text{lncRNA2 expression} + \cdots \\ & + \text{coef lncRNA N} \times \text{lncRNA N expression.}\end{aligned}$$

Confirmation of the lncRNA Signature

Patients were classified into high- or low-risk groups according to the median risk score threshold. The "survival" package in R was used to perform Kaplan–Meier (K–M) survival analysis in both datasets to verify the predictive ability of the signature. Time-

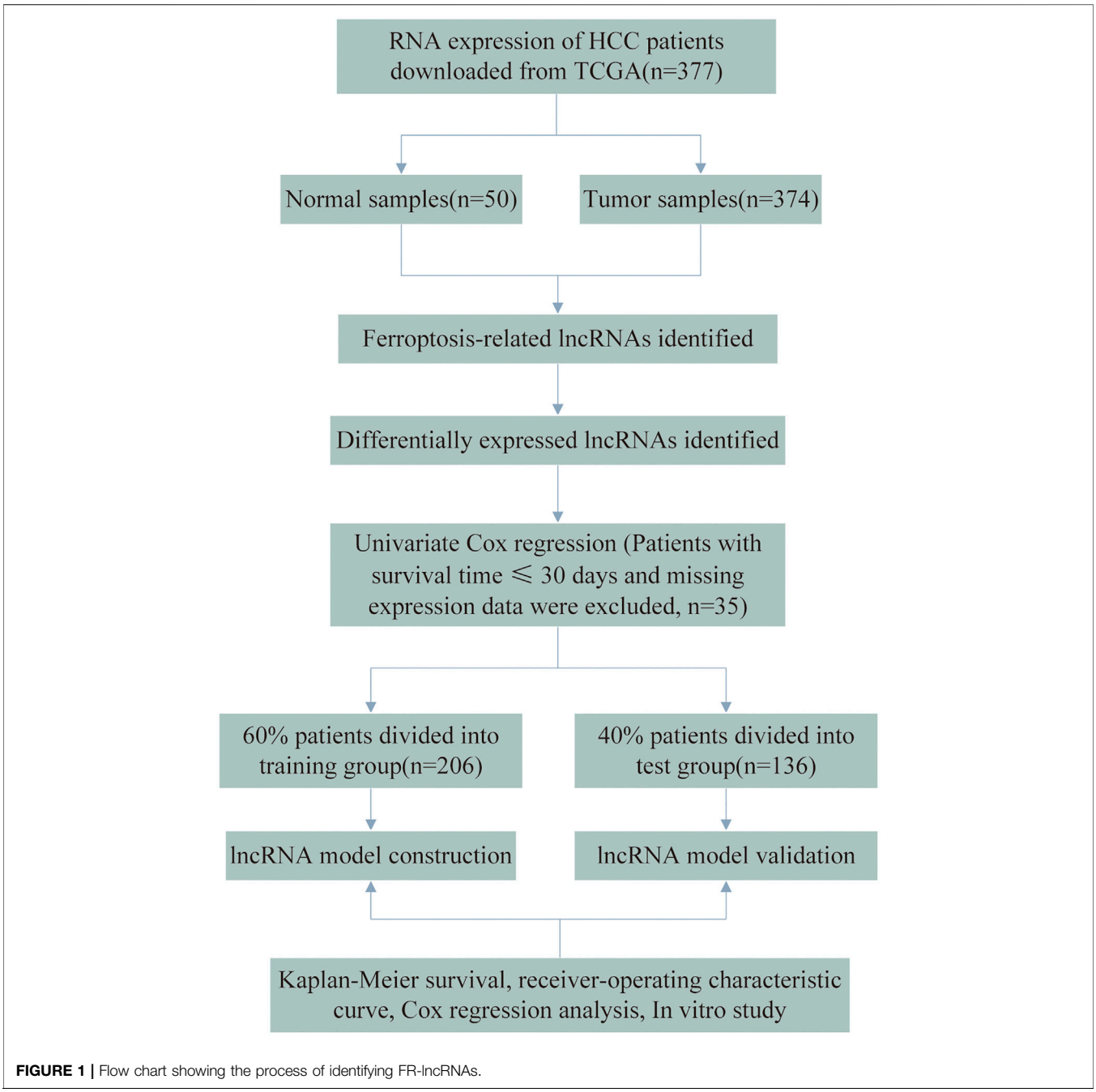

FIGURE 1 | Flow chart showing the process of identifying FR-lncRNAs.

dependent ROC curves were constructed, and the area under the time-dependent ROC curve (AUC) values for 1, 3, and 5 years were calculated. Moreover, multivariate Cox regression analysis was conducted to assess whether the risk score model could be used as an independent predictor of OS in HCC patients. The predictive efficacy of this six-FR-lncRNA signature was further confirmed in the testing and whole cohorts.

Nomogram Construction and Assessment

The R package "rms" and "regplot" were used to construct the nomogram based on the six-FR-lncRNA signature, which integrated the signature, age, and stage. We have estimated the prognosis of HCC patients at 1, 3, and 5 years in the nomogram. Finally, calibration curves were plotted to assess the accuracy and reliability of the nomogram.

RNA Isolation and qRT-PCR Analysis

Eleven fresh pathologically confirmed HCC tumour samples were paired with their para-tumour tissues for RNA extraction and qRT-PCR. None of these patients had been previously diagnosed with any other type of human cancer and had not received anti-cancer treatment. All specimens were rapidly

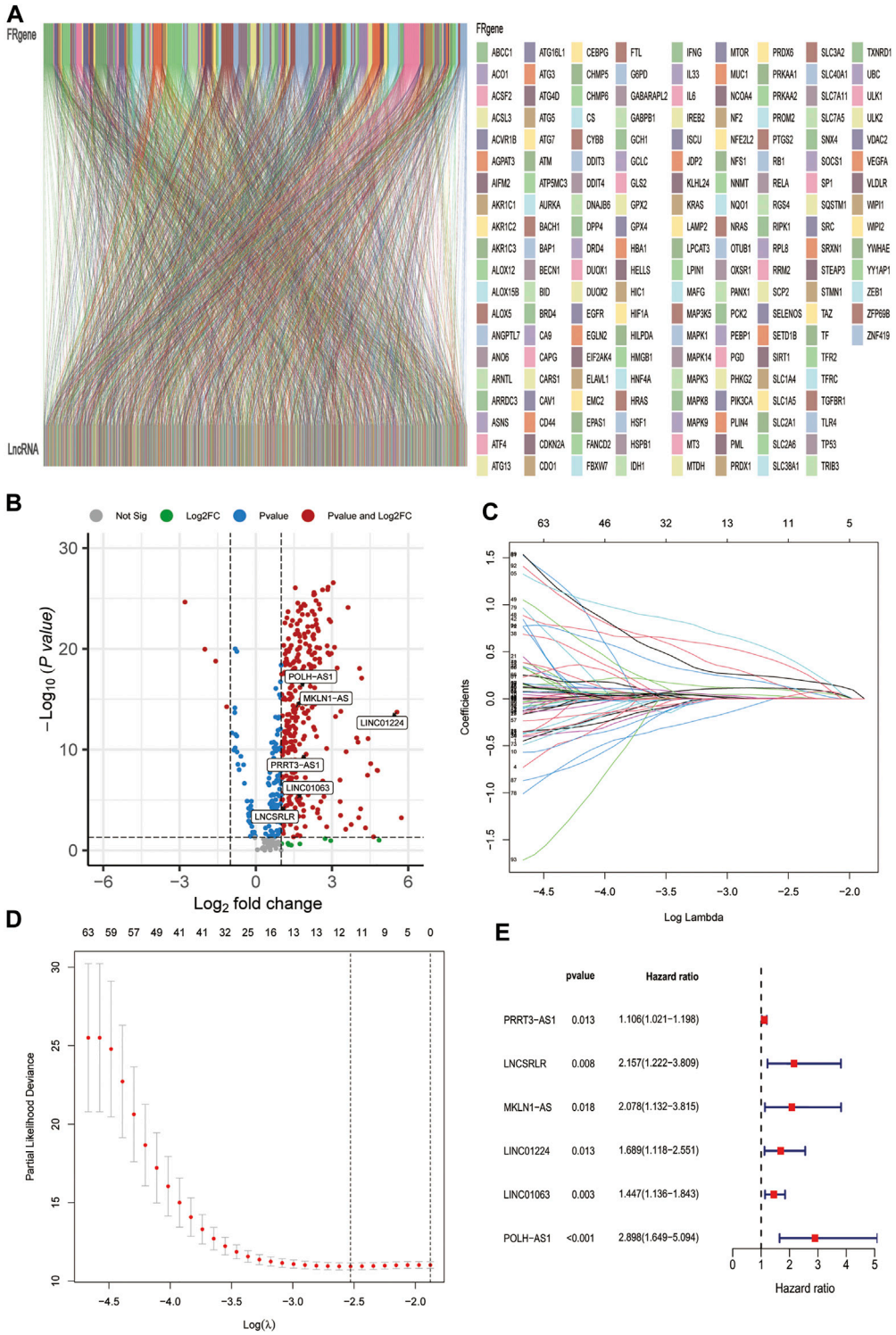

FIGURE 2 | Identification of FR-lncRNAs in HCC patients and construction of the ferroptosis-related lncRNA prognostic signature. **(A)** Sankey relational diagram for FRGs and FR-lncRNAs. **(B)** Volcano plot of the differentially expressed FR-lncRNAs **(C)** LASSO coefficient profiles of 115 FR-lncRNAs. **(D)** To construct a prognostic signature, 11 best candidate FR-lncRNAs were obtained. **(E)** Forest map showed six FR-lncRNAs identified by multivariate Cox regression in the training group.

TABLE 1 | Clinical characteristics of 342 patients with hepatocellular carcinoma.

Character	Training dataset	Test dataset	Entire dataset	*p*-value
	n = 206	*n* = 136	*n* = 342	
Age				0.803
≤65	133	83	216	
>65	73	53	126	
Gender				0.544
Female	61	48	109	
Male	145	88	233	
Grade				0.636
G1-G2	122	92	214	
G3-G4	81	42	123	
Unknow	3	2	5	
TNM stage				0.964
I-II	145	93	238	
III-IV	50	33	83	
Unknow	11	10	21	
Tumor stage				0.996
T1-T2	154	99	252	
T3-T4	51	36	87	
Unknow	2	1	3	

frozen in liquid nitrogen (−196°C) immediately after tissue excision. Total cellular RNA was extracted using the TRIzol reagent (Invitrogen, California, United States). Complementary DNA (cDNA) was synthesised using the PrimeScript Reverse Transcriptase Reagent Kit (Takara Bio, Inc., Japan). Amplification and detection were performed using TB Green® Premix Ex Taq™ II (Takara, Tokyo, Japan) in the ABI Step One Plus Real-Time PCR system (Applied Biosystems). β-Actin was used as an endogenous control. The expression level of PRRT3-AS1, LNCSRLR, LINC01063, and POLH-AS1 was normalised to that of β-actin using the $2^{-\Delta\Delta Ct}$ method. The primer sequences are listed in **Supplementary Table S2**. This study was approved by the ethics committee of the Chinese PLA General Hospital (approval no. S2018-111-01). Written informed consent was obtained from all patients.

Estimation of the Immune Cell Types and Analysis of Tumour Immune Infiltration Cell Types

Quantitative translation of the tumour tissue transcriptome data into the absolute abundance of immune and stromal cells by Cell-type Identification By Estimating Relative Subsets Of RNA Transcripts (CIBERSORT) analysis was conducted to assess the proportion of 22 human immune cell subpopulations (Newman et al., 2015; Becht et al., 2016). Differences in each type of immune cell were compared between the high-risk and low-risk groups to assess differences in the tumour immune microenvironment between the two groups. Then, we implemented a single sample GSEA (ssGSEA) approach using the gene set variation analysis (GSVA) and "GSEABase" packages to analyse the immune functions and inflammatory infiltration profiles (Newman et al., 2019). Immune infiltrating cells and functions were compared between the high- and low-risk groups using the Wilcoxon test.

Analysis of the Expression of Immune Checkpoint Genes and Sensitivity to Clinical Treatment in the High- and Low-Risk Groups

We analysed the expression of 47 immune checkpoint genes between the high- and low-risk groups. Then, we used the tumour immune dysfunction and exclusion (TIDE) algorithm to predict the effectiveness of immunotherapy (Jiang et al., 2018). We also calculated the half-inhibitory concentration (IC50) of sorafenib in the entire dataset. The difference in the IC50 of sorafenib between the two groups was compared using Wilcoxon signed-rank test and the results were obtained by using the R packages "pRRophetic" and "ggplot2."

Somatic Variant Analysis

Gene somatic mutation data based on the whole-exome sequencing platform of TCGA-Liver Hepatocellular Carcinoma (LIHC) datasets were downloaded from the Genomic Data Commons (GDC) database on August 22, 2021. The downloaded Mutation Annotation Format (MAF) files of simple nucleotide variation (workflow type: varScan2 variant aggregation and masking) were analysed using the R package "maftools."

Construction of the lncRNA-FRG Co-Expression Network, Copy Number Variations of FRGs Associated With the Signature, and Functional Analysis

According to the results of the previous co-expression analysis, Cytoscape (version 3.8.2) was used to visualise the co-expression network of prognostic FR-lncRNAs and FRGs. CNV data were obtained through the UCSC Xena program, which is publicly available under specific guidelines. The landscape of genomic CNV in chromosomes was plotted using the "RCircos" R package. GSEA software, version 4.1.0 was used to reveal the signal transduction pathways (Subramanian et al., 2005). The gene sets used in this work were c2.cp.kegg.v7.4.symbols.gmt (Kanehisa et al., 2017) and h.all.v7.4.symbols.gmt (Subramanian et al., 2005). A nominal *p*-value of <0.05 was used as the screening criterion.

Statistical Analysis

We used R version 4.1.0 (Institute for Statistics and Mathematics, Vienna, Austria), GraphPad Prism 8 (GraphPad Software Inc., La Jolla, CA, United States), and SPSS 25.0 (SPSS, IL, United States) to analyse our data. Survival analysis was performed using K–M and log-rank tests. The *t*-test or Mann–Whitney *U* test was used to compare two independent groups. Categorical data were analysed using the χ^2 test. TIDE scores between the high-risk group and low-risk group were compared using the Wilcoxon test. $p < 0.05$ was considered statistically significant ($^*p < 0.05$, $^{**}p < 0.01$, $^{***}p < 0.001$).

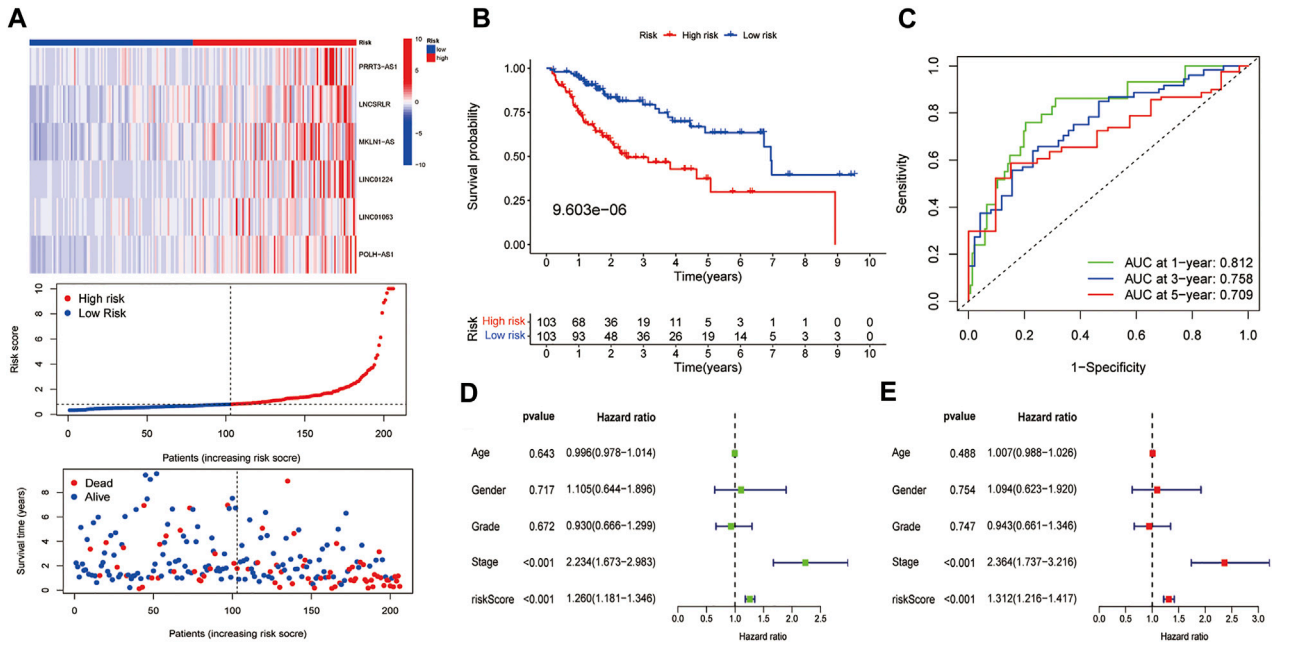

FIGURE 3 | Preliminary examination of the model constructed from the training dataset. **(A)** The heatmap of the expression of six lncRNAs, risk scores, and survival status of each patient. **(B)** K–M survival analysis. **(C)** ROC analysis of the 1, 3, and 5 years OS of HCC patients. The **(D)** univariate and **(E)** multivariate Cox regression results in the training dataset.

RESULTS

Screening of FR-lncRNAs and Differential Expression Analysis

The data of 374 HCC samples and 50 normal samples were downloaded from the LIHC project of TCGA. Then, data annotation was performed according to the GTF file from Ensembl and divided into lncRNA and mRNA data, followed by FRG and lncRNA co-expression analysis and FR-lncRNA co-expression network visualization using the Sankey diagram in **Figure 2A**. Finally, 548 FR-lncRNAs were identified totally ($|r| > 0.4$, $p < 0.001$), of which 336 were identified as differentially expressed FR-lncRNAs according to the standard $p < 0.05$, and $|\log2FC| > 1$ (**Figure 2B**). Among these differentially expressed FR-lncRNAs, 332 were upregulated and four were downregulated.

Construction and Confirmation of the FR-lncRNAs Signature

A total of 342 HCC patients were included according to the inclusion criteria. We performed univariate Cox regression analysis and screened 115 differentially expressed FR-lncRNAs associated with OS ($p < 0.05$) (**Supplementary Table S3**). The 342 HCC patients (entire dataset) were assigned to the training and testing groups at a ratio of 6:4 randomly, and the clinical features were similar between the three groups (**Table 1**). Then, LASSO regression and Cox proportional hazard model analyses were applied to identify the best model in the training dataset (**Figures 2C,D**). Furthermore, multivariate analysis identified six FR-lncRNAs risk scores for HCC (**Supplementary Table S4**), according to the following formula:

$$\begin{aligned} Riskscore = {} & PRRT3-AS1 * 0.101 + LNCSRLR * 0.769 \\ & + MKLN1-AS * 0.732 + LINC01224 * 0.524 \\ & + LINC01063 * 0.370 + POLH-AS1 * 1.06 \end{aligned}$$

Figure 2E shows the relationship between each lncRNA and OS. The expression of six FR-lncRNAs was significantly upregulated in HCC by comparing HCC and normal tissues in the TCGA transcriptome profiles (**Figure 2B**).

We then calculated risk values for each case and categorised all cases as low and high risk based on the median threshold of the training dataset. As shown in the heat map, the expression of the six lncRNAs was higher in the high-risk group of HCC patients than in the low-risk group, gradually increasing patients' mortality as risk score increased (**Figure 3A**). In the training dataset, K–M analysis showed that the survival rate of the low-risk group was significantly higher than that of the high-risk group ($p = 9.603e-06$) (**Figure 3B**). Then, we constructed an ROC curve and the results showed that the AUC values of 1, 3, and 5 years OS were 0.812, 0.758, and 0.709, respectively (**Figure 3C**). Furthermore, univariate and multivariate Cox regression analyses were performed on age, gender, tumour stage, histological grade, and risk score to verify whether the ferroptosis-related risk score could be used independently as an indicator of survival in OS. The results of univariate Cox regression analysis showed that tumour stage ($p < 0.001$) and risk score ($p < 0.001$) were associated with prognosis (**Figure 3D**).

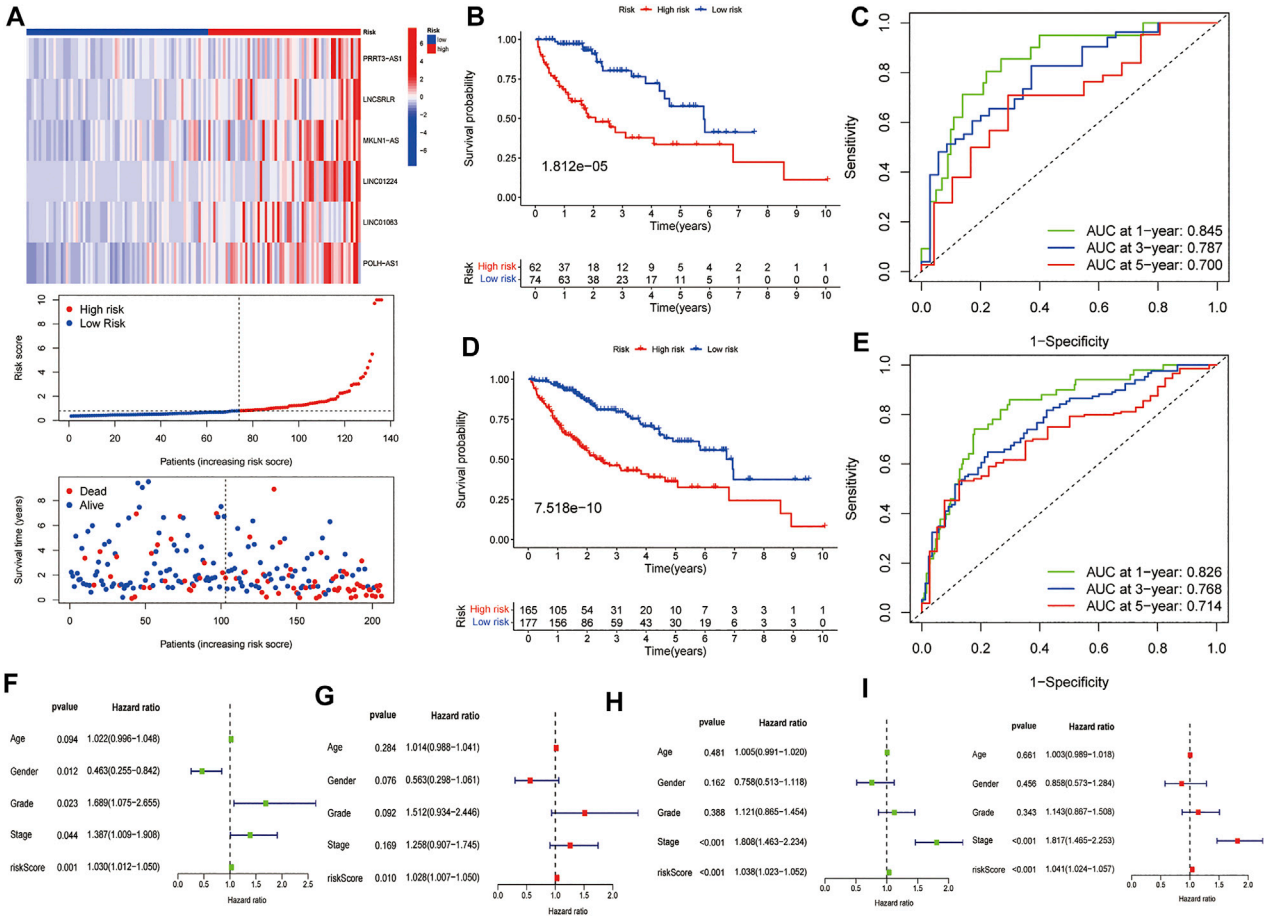

FIGURE 4 | Further validation of the model in the testing group and the entire cohort. **(A)** The heatmap of the expression of six FR-lncRNAs, risk scores, and scattergram of every patient, **(B)** K–M curves for the OS and **(C)** ROC analysis of the 1, 3, and 5 years OS of HCC patients in the testing group. **(D)** K–M curves for the OS and **(E)** ROC curves of the 1, 3, and 5 years OS of HCC patients in the entire group. The **(F)** univariate and **(G)** multivariate Cox regression results in the testing group. The **(H)** univariate and **(I)** multivariate Cox regression results in the entire group.

Multivariate Cox regression analysis illustrated that tumour stage ($p < 0.001$) or risk score ($p < 0.001$) could be used as an independent predictor of prognosis for HCC patients (**Figure 3E**).

Validation of the FR-lncRNA Signature

We used the test dataset and entire dataset to further validate the accuracy and reliability of the prognostic signature. In the test dataset, the distributions of expression profiles of the six-lncRNA, risk score, and OS status were consistent with those of the training dataset (**Figure 4A**). Similarly, K–M analysis of the testing set (**Figure 4B**) and entire data set (**Figure 4D**) showed that patients in the low-risk group had a higher survival rate than those in the high-risk group. The AUC values of the 1, 3, and 5 years OS in the test dataset were 0.845, 0.787, and 0.700, respectively (**Figure 4C**) and the AUC values of the 1, 3, and 5 years OS in the entire dataset were 0.826, 0.768, and 0.714, respectively (**Figure 4E**). Subsequently, we compared the accuracy of our signature with that of published articles according to the values of the AUC and concordance index (C-index) (**Supplementary Figure S1**). The efficacy of our signature is better than that of other studies using an identical protocol. Consistent with the results of the training group, therefore, the FR-lncRNA risk score could be used as an independent predictor of OS based on univariate and multivariate Cox regression analyses of the test dataset and the entire dataset (**Figures 4F–I**). Furthermore, to determine whether the risk score model could be used as the best predictor of survival, we included age, sex, tumour stage, and pathological grade as candidate predictive indicators. We analysed the AUC curves for 1-year prognosis in the three datasets and found that our signature possessed the highest AUC values among these factors (**Figures 5A–C**).

Significantly higher expression of MKLN1-AS and LINC01224 in HCC tissues compared to normal liver tissues has been demonstrated in previous studies (Dan Gong et al., 2020; Gao et al., 2020). We used qRT-PCR to detect the expression of the other four FR-lncRNAs in HCC tissues and adjacent normal tissues. The results showed that the expression levels of LNCSRLR (**Figure 5D**), LINC01063 (**Figure 5E**), PRRT3-AS1 (**Figure 5F**),

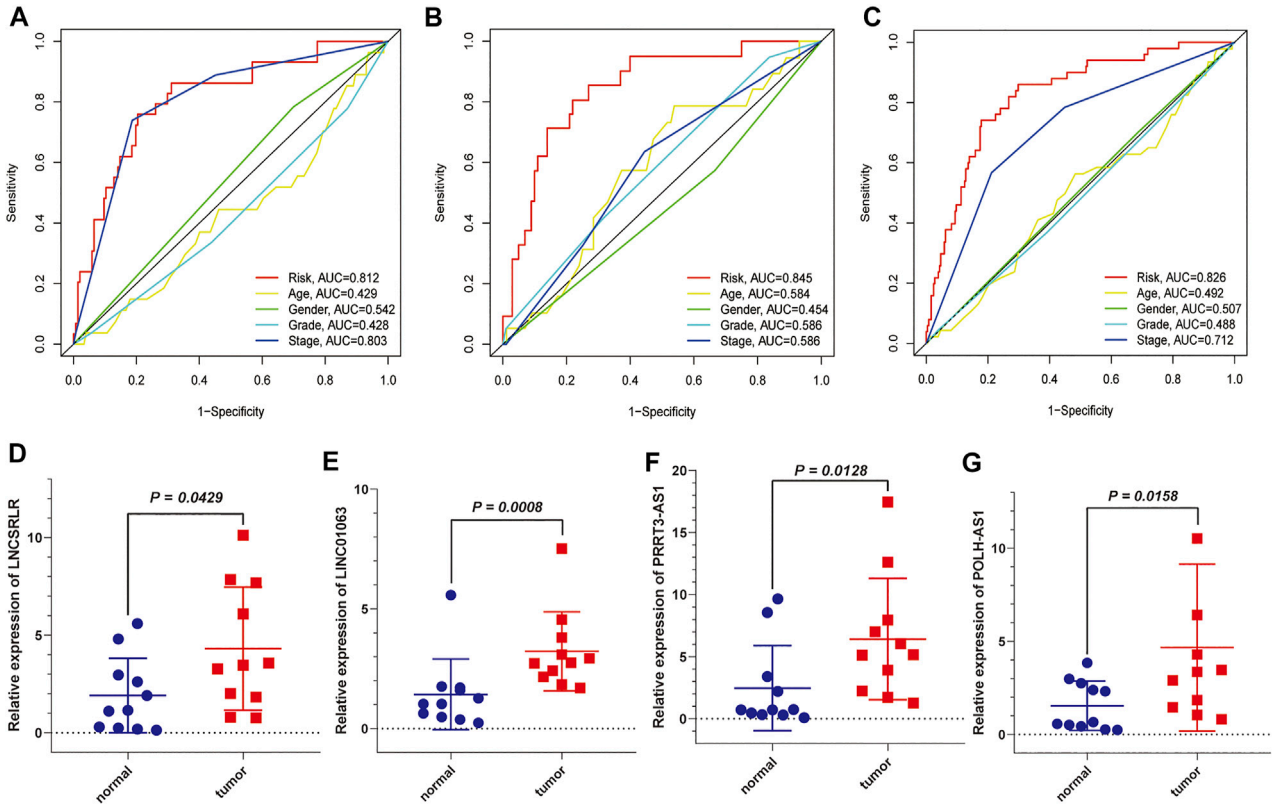

FIGURE 5 | The AUC values of the six FR-lncRNAs model and clinical characteristics predicting 1-year survival and further validation by external experiments. **(A)** Training set. **(B)** Testing set. **(C)** Entire set. **(D)** LNCSRLR, **(E)** LINC01063, **(F)** PRRT3-AS1, and **(G)** POLH-AS1 are highly expressed in HCC tissues compared to normal tissues.

and POLH-AS1 (**Figure 5G**) were higher in HCC tissues than in normal tissues.

A Nomogram Combining the Risk Score, Age, and Tumour Stage to Predict Survival Time in Patients With HCC

Our prognostic nomogram integrated the six-lncRNA signature, age, and tumour stage. Then, we used the prognostic nomogram to predict the prognosis of HCC patients at 1, 3, and 5 years after diagnosis. (**Figure 6A**). Moreover, calibration plots of 1, 3 and 5 years survival probabilities also showed good agreement between nomogram predictions and actual observations (**Figure 6B**). Similar results have been observed for the testing set (**Figure 6C**) and the entire dataset (**Figure 6D**).

Differences in Immune Cell Infiltration, Expression of Immune Checkpoint Genes and Sensitivity to Clinical Treatments Between High- and Low-Risk Groups

The entire dataset was used to explore the relationship between the signature and immune cell infiltration, the expression of immune checkpoint genes, and clinical treatments. The differences in the infiltration of 22 immune cell types in the tumour tissue of all HCC patients are shown in **Figure 7A**. Patients with HCC in the high-risk group had higher ratios of M0 macrophages, follicular helper T cells, memory B cells, memory activated CD4 T cells, and regulatory T cells (Tregs) than those in the low-risk group ($p < 0.05$); meanwhile, patients with HCC in the low-risk group had higher ratios of activated NK cells, M1 macrophages, monocytes, naïve B cells, resting mast cells, and memory resting CD4 T cells than those in the high-risk group ($p < 0.05$) (**Figure 7B**). To explore the relationship between the expression of the six lnc-RNAs and immune infiltration level in HCC, lollipop plots were constructed showing Spearman's correlation coefficient and statistical significance in **Supplementary Figure S2**. Notably, the six lnc-RNAs were positively correlated with the populations of M0 macrophages and Tregs and negatively correlated with the populations of monocytes and M2 macrophages ($p < 0.05$).

We also applied the ssGSEA method to the RNA sequencing data of HCC samples to assess immune cell infiltration and related functions. The populations of immune cells, including activated dendritic cells (aDCs), B cells, immature dendritic cells (iDCs), macrophages, mast cells, neutrophils, Natural Killer (NK) cells, plasmacytoid *dendritic* cells (pDCs), and Tregs, were found

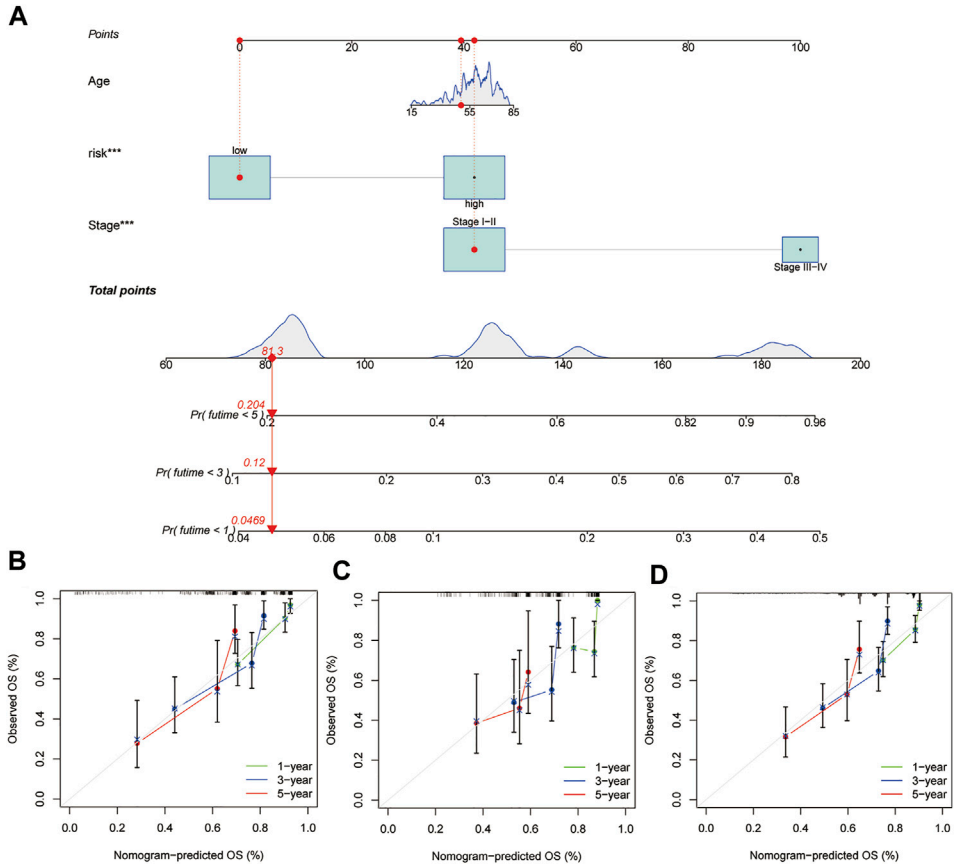

FIGURE 6 | Construction of a nomogram in the training group and calibration maps were used to predict the 1, 3, and 5 years survival. **(A)** Nomogram constructed using the training group dataset. Assessing the accuracy of the nomogram using calibration maps in the **(B)** training group, **(C)** testing group, and **(D)** entire group.

to be markedly different between the two groups (**Figure 7C**). Moreover, immune signature comparisons revealed that low-risk patients had higher cytolytic activity, type-I IFN response, and type-II IFN response than high-risk patients, whereas the opposite was observed for MHC class I (**Figure 7D**).

Given the importance of ICIs in the treatment of HCC, we further analysed the differential expression of immune checkpoint genes between the high- and low-risk groups. We found that patients in the high-risk group had higher expression of immune checkpoint genes, such as PDCD-1 (PD-1), CTLA4, LAG3, HAVCR2 (TIM3), and TIGIT (**Figure 8A**), compared to that in the low-risk group. We then used TIDE to assess the potential clinical efficacy of immunotherapy in the two groups. A higher TIDE prediction score represents a higher potential for immune evasion, suggesting that patients are less likely to benefit from ICI treatment. Our results indicated that the high-risk group had a lower TIDE score than that of the low-risk group, implying that patients in the high-risk group could benefit more from ICI therapy than patients in the low-risk group (**Figure 8B**). In addition to ICI treatment, we attempted to identify the association between the signature and the efficacy of sorafenib for the treatment of HCC. We found that the low-risk group was associated with lower IC50 for sorafenib ($p < 0.01$), which suggested that the signature could be used as a potential predictor of sorafenib treatment sensitivity (**Figure 8C**).

Gene Mutation Analysis

We processed simple nucleotide variation data using the "maftools" package in R. A waterfall plot displayed the top 20 mutated genes in patients with HCC (**Figures 9A,B**). A higher proportion of somatic mutations (TP53) were found in the high-risk group (FDR <0.01, $p < 0.001$) after a Fisher's exact test was used to analyse the mutation differences between two groups. **Figures 9C,D** summarise the mutation information for the high- and low-risk groups, respectively.

Construction of Co-Expression Network, CNV Analysis of FR Genes Associated With the Signature, and GSEA

To explore the interaction between the six FR-lncRNAs and gene expression in HCC, Cytoscape was used to visualise the lncRNA and mRNA co-expression network (**Figure 10A**). The Sankey diagram showed the relationship between FR-lncRNAs, FRGs, and OS in patients with HCC (**Figure 10B**). It was found that the

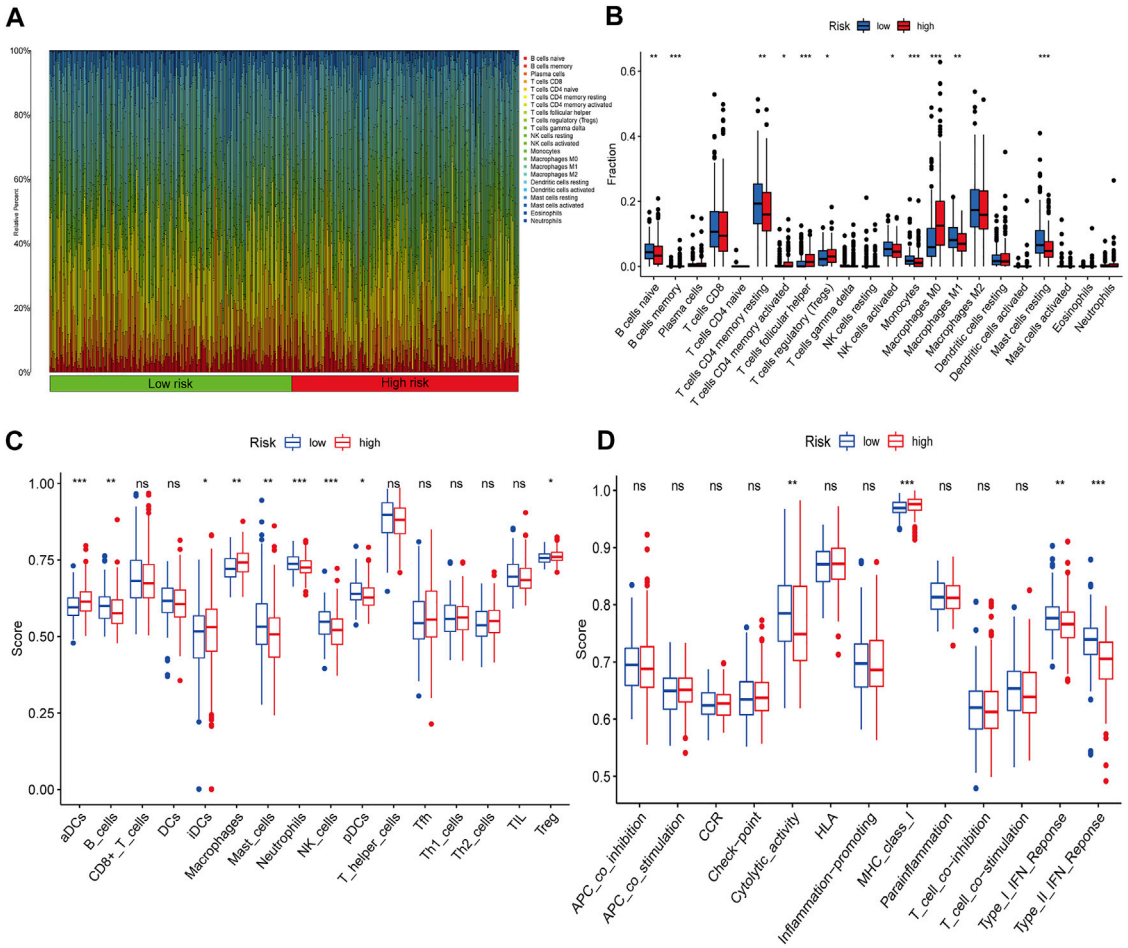

FIGURE 7 | Immune profiles between different risk groups. **(A)** Relative proportions of immune cells in HCC patients. **(B)** Comparison of immune cell subtypes in the high- and low-risk groups. ssGSEA results show the differences in **(C)** immune cell infiltration and **(D)** immune function between the two groups.

FRGs associated with signature had different levels of CNV events. RB1 harboured the most CNV events. Meanwhile, YY1AP1, RPL8, HSF1, MAFG, PGD, and STMN1 also had relatively high CNV events (**Figure 10C**). **Figure 10D** shows the location of CNV events in the FRGs related to the signature on the chromosome. Then, we performed GSEA to explore the biological effects of the six FR-lncRNAs signature, and the entire group dataset was used for GSEA analysis. The results revealed that the high-risk group showed significant enrichment in *Kyoto Encyclopedia of Genes and Genomes* (KEGG) pathways related to cancer processes, such as base excision repair, cell cycle, endocytosis, mismatch repair, nucleotide excision repair, and the WNT signal transduction pathway. Correspondingly, ferroptosis and metabolism-related pathways, such as beta-alanine metabolism, drug metabolism cytochrome P450, fatty acid metabolism, and retinol metabolism were significantly enriched in the low-risk group (**Figure 10E**). Furthermore, GSEA of the hallmark gene sets indicated that PI3K-AKT-MTOR, TGF-β, NOTCH, P53, and WNT-β-Catenin pathways were enriched in the high-risk group significantly, whereas fatty acid metabolism, bile acid metabolism, and xenobiotic metabolism pathways were highly enriched in the low-risk group (**Figure 10F**).

DISCUSSION

The prognosis for patients with HCC is poor, mainly because a large proportion of patients are diagnosed with HCC at an advanced stage (Llovet et al., 2021). Recently, despite the great success achieved using a combination of anti-PD-L1 with anti-VEGF therapies in advanced HCC, there are still a majority of patients who either do not respond to these treatments or do not have a lasting clinical benefit because of high tumour heterogeneity or treatment resistance(Finn et al., 2020; Pinter et al., 2020). Therefore, to maximize the benefits to patients and improve the effectiveness of systematic therapy, it is necessary to explore reliable molecular biomarkers to predict the effectiveness of immunotherapy, targeted therapies, and the prognosis of HCC patients.

LncRNAs play a key role in chromatin structure, cell growth, gene expression, differentiation, and development, and mutations

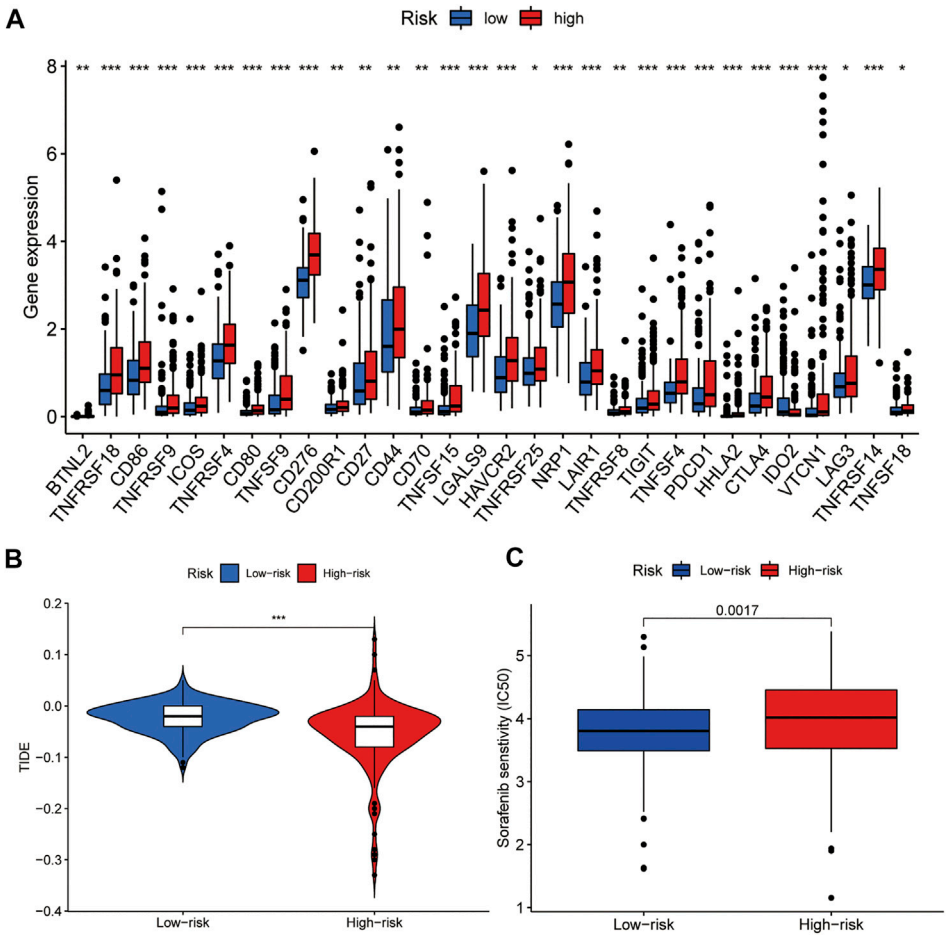

FIGURE 8 | Comparison of the expression of immune checkpoint genes and sensitivity to clinical treatment between high- and low-risk groups. **(A)** Expression of immune checkpoint genes among the two groups. **(B)** TIDE score of the two groups. **(C)** The signature can be used as a potential predictor of sorafenib sensitivity, as low-risk scores are associated with a lower IC50 for sorafenib.

or dysregulation of their expression are associated with a variety of diseases, particularly malignancies (Esteller, 2011; Bhan et al., 2017). Recent studies have revealed that lncRNAs are associated with the following six cancer hallmarks: proliferation, growth suppression, motility, immortality, angiogenesis, and viability (Schmitt and Chang, 2016). For the treatment of HCC, lncRNAs can be used as biomarkers to predict the efficacy of surgery, radiotherapy, chemotherapy, and immunotherapy, and are expected to be a potential tool for individualised HCC diagnosis and treatment (Yuan et al., 2021). Moreover, the TP53 mutation is involved in the expression of specific lncRNAs and gains oncogenic function by creating a complex network of interacting pathways (Di Agostino, 2020). For example, lincRNA-p21 serves as a transcriptional repressor in the p53 pathway and was the first lncRNA identified as being transcriptionally induced by wild-type p53 (Huarte et al., 2010). In 26 resected pancreatic cancer specimens, lncRNA1611 was significantly highly expressed in the cancerous pancreatic tissue of 22 patients compared to normal pancreatic tissue and was positively correlated with TP53 mutation (Wang et al., 2015). However, few studies have documented the relationship between TP53 mutation and lncRNA expression (Lin et al., 2019). Furthermore, several recent studies have found that lncRNAs are strongly associated with ferroptosis in cancer (Xie and Guo, 2021; Yao et al., 2021; Zhang et al., 2021; Zuli Wang et al., 2021). However, to date, the number of FR-associated lncRNAs identified in HCC is scarce, and research on FR-associated lncRNAs in HCC is limited.

RNA-targeted therapies are developing rapidly, such as the expression of HOTAIR-*sbid*, a mutant of lncRNA HOTAIR, which has been shown to reduce cell motility, invasiveness, and response to TGF β-induced epithelial-mesenchymal transition (Wang et al., 2020; Battistelli et al., 2021). In the era of precision medicine, by exploring FR-lncRNAs, we aimed to obtain a risk model that could predict the efficacy of clinical treatments and patient prognosis. We successfully constructed and validated a new biomarker comprising six FR-lncRNAs in patients with HCC based on TCGA dataset. Statistical analysis showed that this risk model has good robustness and predictive power and that it can independently predict OS in patients

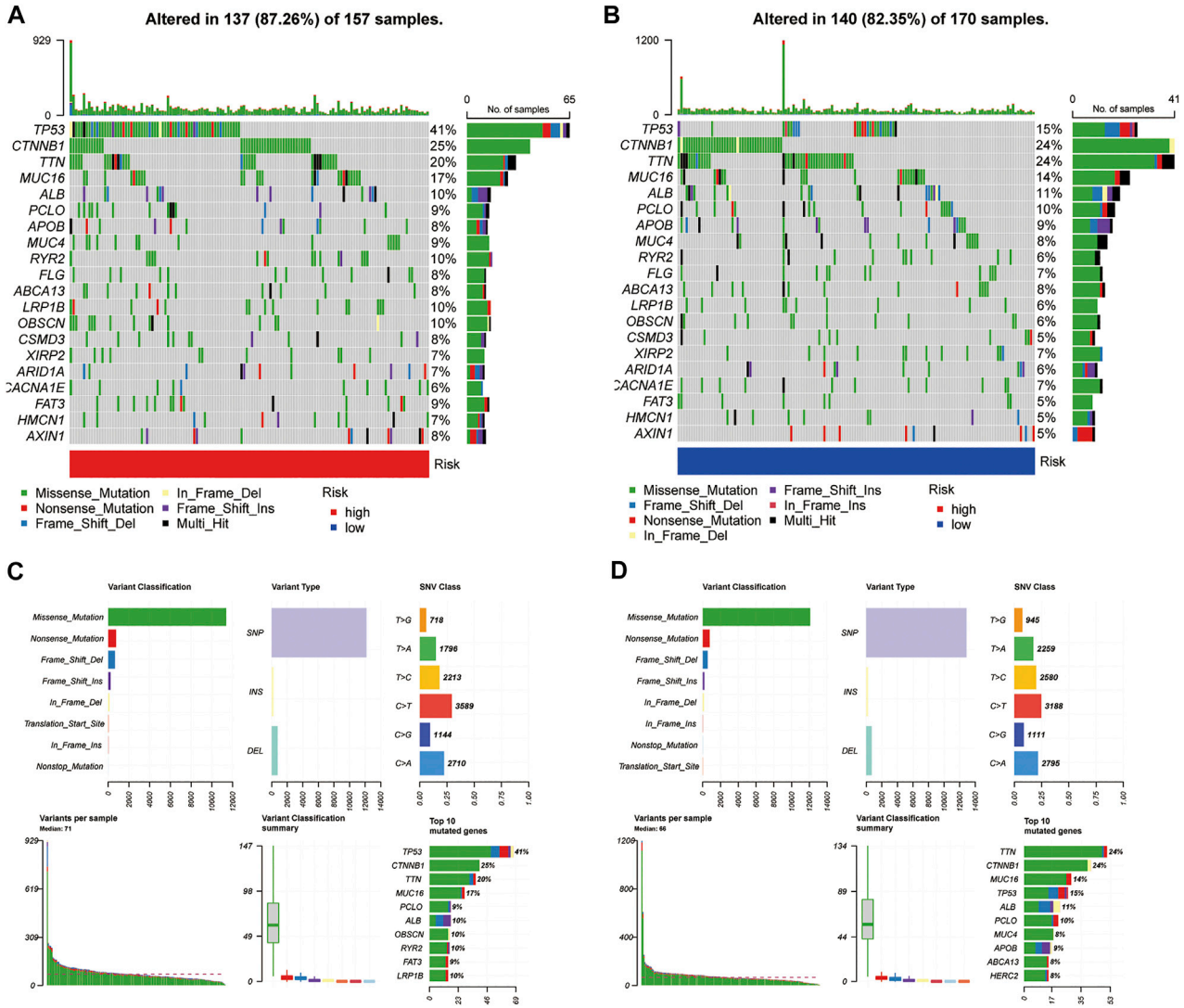

FIGURE 9 | Somatic mutation analysis. **(A,B)** Oncoplots of the mutated genes in the **(A)** high-risk and **(B)** low-risk groups. [**(C,D)**, above] Missense mutations, SNPs, and C > T mutations were the most common mutation types in both groups. [**(C,D)**, below] Variants per sample, variant classification summary, and top ten mutated genes.

with HCC. Furthermore, the predictive accuracy of our signature surpassed that of the previously reported prediction signature of HCC dependent on FR-lncRNAs or FRGs (Liang et al., 2020; Chen et al., 2021; Liang Wang et al., 2021; Liang et al., 2021; Nie et al., 2021; Wan et al., 2021; Xu et al., 2021). The nomogram consisting of age, stage, and six FR-lncRNAs risk scores could be used to visually predict the OS of individual patients with HCC at 1, 3, and 5 years. According to the calibration plots, the nomogram has good prediction accuracy and the predicted results match the actual results well.

Sorafenib and immunotherapy can inhibit the progression of tumours, including HCC, by inducing ferroptosis (Louandre et al., 2013; Nie et al., 2018; Friedmann Angeli et al., 2019; Wang et al., 2019). Ferroptosis can promote exposure to tumour antigens, thereby enhancing the immunogenicity of the TIME and efficacy of immunotherapy (Zhang et al., 2019). Meanwhile, ICIs act primarily through the activation of an anti-tumour immune response driven by cytotoxic T cells, and this anti-tumour effect can induce ferroptosis in cancer cells (Chen et al., 2021a). Moreover, CD36 expressed by $CD8^+$ T cells leads to an accumulation of lipid peroxides in $CD8^+$ T cells through the uptake of fatty acids in the tumour environment, which in turn leads to an elevated iron ion content, increased ferroptosis processes, and reduced secretion of cytotoxic cytokines (Ma et al., 2021). Therefore, HCC patients with different ferroptosis characteristics and immunophenotypes may respond differently to sorafenib or immunotherapy. In our study, the proportion of Tregs, M0 macrophages, follicular helper T cells, and memory B cell subsets in the CIBERSORT analysis showed significant infiltration in the high-risk group. The results of the

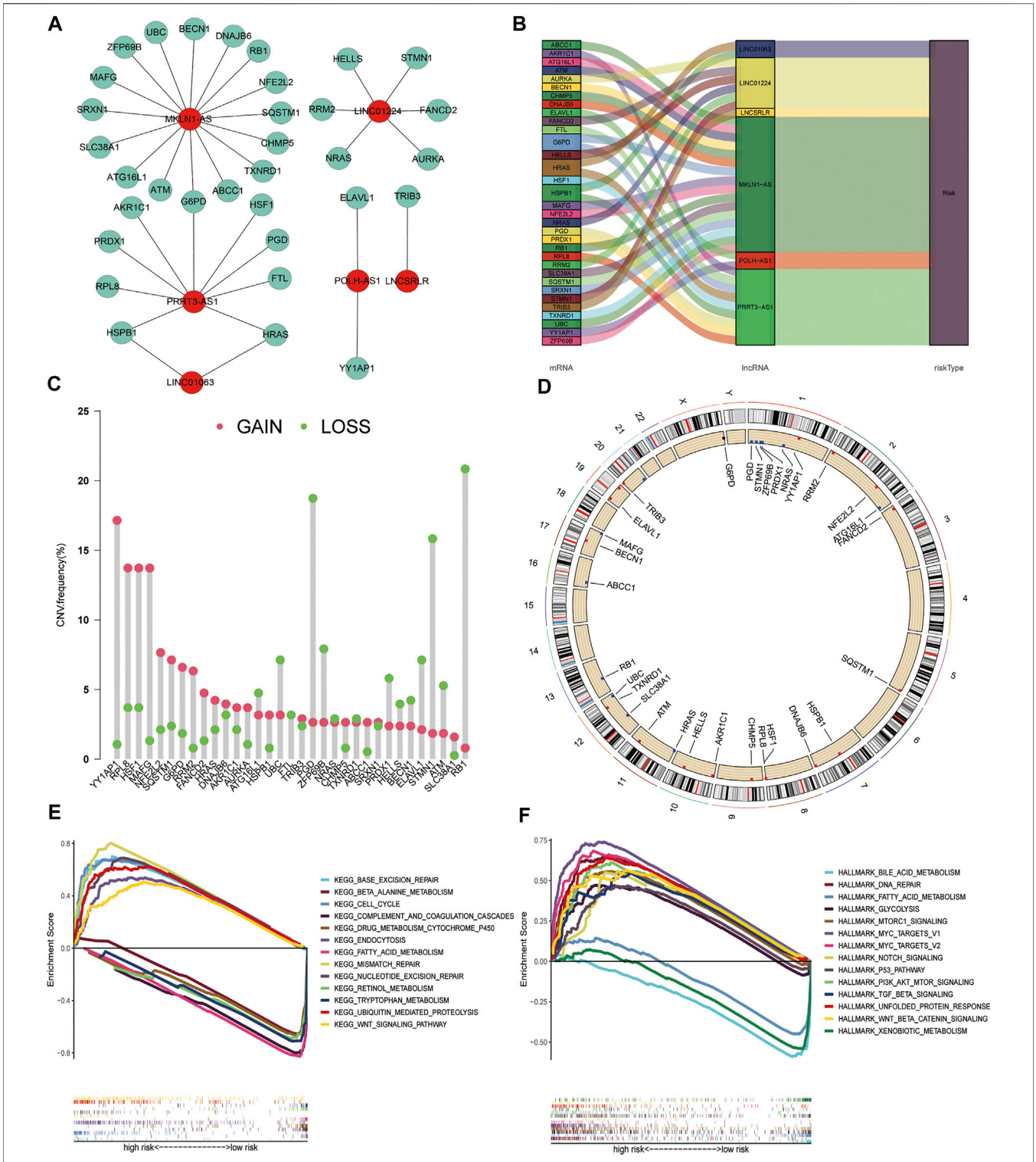

FIGURE 10 | Construction of the co-expression network, copy number variations of ferroptosis genes associated with the signature, and Gene set enrichment analysis. **(A)** Diagram of the co-expression network. **(B)** The Sankey plot shows the degree of association between the FR-lncRNAs and FRGs. **(C)** The CNV frequency of FRGs associated with the signature. **(D)** The location of CNV changes of FRGs on chromosomes. **(E)** KEGG. **(F)** Hallmark gene set. ($p < 0.05$).

ssGSEA analysis showed that the proportion of aDCs, iDCs, macrophages, and Tregs was significantly increased in the TIME of the high-risk group. In addition, immune checkpoint-associated genes were more highly expressed in patients of the high-risk group compared to the low-risk group, which may provide a basis for identifying patients who may respond to ICI therapy. In contrast, the infiltration of activated NK cells and M1 macrophages, which are immune-promoting cell subsets, was significantly increased in the low-risk group in the CIBERSORT analysis. Similarly, the results of the ssGSEA analysis showed that the low-risk group had a significantly higher proportion of B cells, neutrophils, and NK cells in the TIME, and significantly enhanced type-I IFN response, type-II IFN response, and cytolytic activity. Furthermore, the risk model could predict the sensitivity of HCC patients to sorafenib and ICI treatment. The results indicated that patients in the low-risk group were more sensitive to sorafenib than those in the high-risk group. Conversely, the high-risk group was more sensitive to immunotherapy. Importantly, these results may contribute to personalised immunotherapy and targeted therapy for patients with HCC.

Additionally, more patients in the high-risk group had TP53 somatic mutations than in the low-risk group (41% vs. 15%). TP53 mutations affect the cell cycle in approximately 30% of all HCC cases, and patients with this mutation tend to have a poor prognosis (Villanueva, 2019). Interestingly, the effect of TP53 mutations on ferroptosis showed different results depending on the mutation site (Jiang et al., 2015; Jennis et al., 2016). Furthermore, TP53 gene mutations can affect the recruitment and activity of bone marrow cells and T cells, leading to immune evasion and the promotion of cancer progression (Blagih et al., 2020). P53 functions in immune cells, leading to a variety of outcomes that can hinder or support tumour development (Blagih et al., 2020). Thus, a higher frequency of TP53 mutations in the high-risk group of HCC patients may be associated with the status of ferroptosis and an immunosuppressive phenotype. We also found that the FRGs related to our signature were all subject to varying degrees of CNVs, with the highest frequency of loss in the RB1 gene and the highest frequency of gains in YY1AP1. Although "RB1 loss of function" was present in <30% of HCC samples, both genes play an important role in HCC prognosis and treatment.

GSEA analysis results showed that the ferroptosis-related signalling pathways, such as P53 and TGF-β, were enriched in the high-risk group significantly, whereas fatty acid metabolism and drug metabolism cytochrome P450 signalling pathways were enriched in the low-risk group (Chen et al., 2021a; Chen et al., 2021b). Immune-related signalling pathways, such as mismatch repair, the Notch, P53, PI3K-AKT-MTOR, TGF-β, and WNT-β-Catenin pathways were significantly enriched in the high-risk group. These results provide further evidence for differences in ferroptosis and TIME characteristics between the two groups, which may serve as new therapeutic targets.

In the constructed FR-lncRNAs risk model, it was demonstrated that the expression of MKLN1-AS and LINC01224 was significantly upregulated in cell lines and HCC tissues and that the higher expression of MKLN1-AS and LINC01224 was associated with poorer prognosis (Dan Gong et al., 2020; Gao et al., 2020). In addition, MKLN1-AS, LINC01063, and PRRT3-AS1 can act as predictors of prognosis in patients with HCC through autophagy-related or immune-related pathways (Deng et al., 2020; Kong et al., 2020; Yang et al., 2021). However, the roles of MKLN1-AS, LINC01063, PRRT3-AS1, and LINC01224 in the ferroptosis pathway have not yet been reported. LNCSRLR can be used as a biomarker of prognosis in patients with laryngeal squamous cell carcinoma; however, its role in HCC is unknown (Shiqi Gong et al., 2020). The function or pathway of POLH-AS1 has not yet been reported. Furthermore, the expression levels of LNCSRLR, LINC01063, PRRT3-AS1, and POLH-AS1 in HCC tissues have not been determined. We demonstrated that the expression of LNCSRLR, LINC01063, PRRT3-AS1, and POLH-AS1 was higher in HCC tissues than in normal tissues using qPCR.

Our study has certain limitations. First, further basic experiments are needed to validate the relationship between the lncRNAs screened using co-expression analysis and ferroptosis. Our study provides the basis for further in-depth research. Second, we were unable to retrieve a dataset that simultaneously reported six-lncRNA expression levels, clinical characteristics, and survival status of HCC patients. Therefore, we did not perform an external validation of the signature.

In conclusion, we constructed a novel FR-lncRNA signature with favourable specificity and sensitivity for predicting survival time in patients with HCC. A nomogram constructed using age, clinical TNM staging, and risk scores for the six FR-lncRNAs can be a simple tool to predict the survival time of HCC patients. More importantly, our signature can also predict the efficacy of immunotherapy and targeted therapies, which is important for reducing patient suffering, improving the effectiveness of drug treatment, and saving healthcare resources.

DATA AVAILABILITY STATEMENT

The datasets presented in this study can be found in online repositories. The names of the repository/repositories and accession number(s) can be found in the article/ **Supplementary Material**.

ETHICS STATEMENT

The studies involving human participants were reviewed and approved by the ethic committee of the Chinese PLA General Hospital (Approval No. S2018-111-01). The patients/participants provided their written informed consent to participate in this study.

AUTHOR CONTRIBUTIONS

ZZ collected and analysed the data. ZZ and WZ were the major contributors in writing the manuscript. YW and XG provided technical support. WZ and CL provided guidance and advice for this article. SL, who provided the financial and ideas support, and

critically reviewed the manuscript, was our corresponding author. SL, TW, and BH participated in the operation, took care of patients, and communicated with patients. ZZ and WZ were responsible for writing the manuscript. SL was responsible for the analysis of data, data interpretation, and revision. All authors read and approved the final manuscript.

FUNDING

This study was funded by the National Key R&D Program of China (2017YFA0103003 and 2017YFA0103000), and the National Natural Science Foundation of China (81670950).

ACKNOWLEDGMENTS

We appreciate the TCGA and FerrDb database for providing their platforms and contributors for uploading their meaningful datasets. We appreciate the contributions of Dr. Jin Shang to provide technical guidance and assistance.

SUPPLEMENTARY MATERIAL

The Supplementary Material for this article can be found online at: https://www.frontiersin.org/articles/10.3389/fcell.2022.792676/full#supplementary-material

REFERENCES

Battistelli, C., Garbo, S., Riccioni, V., Montaldo, C., Santangelo, L., Vandelli, A., et al. (2021). Design and Functional Validation of a Mutant Variant of the LncRNA HOTAIR to Counteract Snail Function in Epithelial-To-Mesenchymal Transition. *Cancer Res.* 81 (1), 103–113. doi:10.1158/0008-5472.Can-20-1764

Becht, E., Giraldo, N. A., Lacroix, L., Buttard, B., Elarouci, N., Petitprez, F., et al. (2016). Estimating the Population Abundance of Tissue-Infiltrating Immune and Stromal Cell Populations Using Gene Expression. *Genome Biol.* 17 (1), 218. doi:10.1186/s13059-016-1070-5

Bhan, A., Soleimani, M., and Mandal, S. S. (2017). Long Noncoding RNA and Cancer: A New Paradigm. *Cancer Res.* 77 (15), 3965–3981. doi:10.1158/0008-5472.Can-16-2634

Blagih, J., Buck, M. D., and Vousden, K. H. (2020). p53, Cancer and the Immune Response. *J. Cel Sci* 133 (5), jcs237453. doi:10.1242/jcs.237453

Capelletti, M. M., Manceau, H., Puy, H., and Peoc'h, K. (2020). Ferroptosis in Liver Diseases: An Overview. *Int. J. Mol. Sci.* 21 (14), 4908. doi:10.3390/ijms21144908

Chen, X., Kang, R., Kroemer, G., and Tang, D. (2021a). Broadening Horizons: the Role of Ferroptosis in Cancer. *Nat. Rev. Clin. Oncol.* 18 (5), 280–296. doi:10.1038/s41571-020-00462-0

Chen, X., Yu, C., Kang, R., Kroemer, G., and Tang, D. (2021b). Cellular Degradation Systems in Ferroptosis. *Cell Death Differ* 28 (4), 1135–1148. doi:10.1038/s41418-020-00728-1

Chen, Z.-A., Tian, H., Yao, D.-M., Zhang, Y., Feng, Z.-J., and Yang, C.-J. (2021). Identification of a Ferroptosis-Related Signature Model Including mRNAs and lncRNAs for Predicting Prognosis and Immune Activity in Hepatocellular Carcinoma. *Front. Oncol.* 11, 738477. doi:10.3389/fonc.2021.738477

Deng, X., Bi, Q., Chen, S., Chen, X., Li, S., Zhong, Z., et al. (2020). Identification of a Five-Autophagy-Related-lncRNA Signature as a Novel Prognostic Biomarker for Hepatocellular Carcinoma. *Front. Mol. Biosci.* 7, 611626. doi:10.3389/fmolb.2020.611626

Di Agostino, S. (2020). The Impact of Mutant P53 in the Non-coding RNA World. *Biomolecules* 10 (3), 472. doi:10.3390/biom10030472

Esteller, M. (2011). Non-coding RNAs in Human Disease. *Nat. Rev. Genet.* 12 (12), 861–874. doi:10.1038/nrg3074

Finn, R. S., Qin, S., Ikeda, M., Galle, P. R., Ducreux, M., Kim, T.-Y., et al. (2020). Atezolizumab Plus Bevacizumab in Unresectable Hepatocellular Carcinoma. *N. Engl. J. Med.* 382 (20), 1894–1905. doi:10.1056/NEJMoa1915745

Friedmann Angeli, J. P., Krysko, D. V., and Conrad, M. (2019). Ferroptosis at the Crossroads of Cancer-Acquired Drug Resistance and Immune Evasion. *Nat. Rev. Cancer* 19 (7), 405–414. doi:10.1038/s41568-019-0149-1

Gao, W., Chen, X., Chi, W., and Xue, M. (2020). Long Non-coding RNA MKLN1-AS Aggravates Hepatocellular Carcinoma Progression by Functioning as a Molecular Sponge for miR-654-3p, Thereby Promoting Hepatoma-derived Growth Factor Expression. *Int. J. Mol. Med.* 46 (5), 1743–1754. doi:10.3892/ijmm.2020.4722

Gong, D., Feng, P.-C., Ke, X.-F., Kuang, H.-L., Pan, L.-L., Ye, Q., et al. (2020). Silencing Long Non-coding RNA LINC01224 Inhibits Hepatocellular Carcinoma Progression via MicroRNA-330-5p-Induced Inhibition of CHEK1. *Mol. Ther. - Nucleic Acids* 19, 482–497. doi:10.1016/j.omtn.2019.10.007

Gong, S., Xu, M., Zhang, Y., Shan, Y., and Zhang, H. (2020). The Prognostic Signature and Potential Target Genes of Six Long Non-coding RNA in Laryngeal Squamous Cell Carcinoma. *Front. Genet.* 11, 413. doi:10.3389/fgene.2020.00413

Huarte, M., Guttman, M., Feldser, D., Garber, M., Koziol, M. J., Kenzelmann-Broz, D., et al. (2010). A Large Intergenic Noncoding RNA Induced by P53 Mediates Global Gene Repression in the P53 Response. *Cell* 142 (3), 409–419. doi:10.1016/j.cell.2010.06.040

Jennis, M., Kung, C.-P., Basu, S., Budina-Kolomets, A., Leu, J. I.-J., Khaku, S., et al. (2016). An African-specific Polymorphism in the TP53 Gene Impairs P53 Tumor Suppressor Function in a Mouse Model. *Genes Dev.* 30 (8), 918–930. doi:10.1101/gad.275891.115

Jiang, L., Kon, N., Li, T., Wang, S.-J., Su, T., Hibshoosh, H., et al. (2015). Ferroptosis as a P53-Mediated Activity during Tumour Suppression. *Nature* 520 (7545), 57–62. doi:10.1038/nature14344

Jiang, P., Gu, S., Pan, D., Fu, J., Sahu, A., Hu, X., et al. (2018). Signatures of T Cell Dysfunction and Exclusion Predict Cancer Immunotherapy Response. *Nat. Med.* 24 (10), 1550–1558. doi:10.1038/s41591-018-0136-1

Kanehisa, M., Furumichi, M., Tanabe, M., Sato, Y., and Morishima, K. (2017). KEGG: New Perspectives on Genomes, Pathways, Diseases and Drugs. *Nucleic Acids Res.* 45 (D1), D353–d361. doi:10.1093/nar/gkw1092

Kong, W., Wang, X., Zuo, X., Mao, Z., Cheng, Y., and Chen, W. (2020). Development and Validation of an Immune-Related lncRNA Signature for Predicting the Prognosis of Hepatocellular Carcinoma. *Front. Genet.* 11, 1037. doi:10.3389/fgene.2020.01037

Li, D., Liu, X., Zhou, J., Hu, J., Zhang, D., Liu, J., et al. (2017). Long Noncoding RNA HULC Modulates the Phosphorylation of YB-1 through Serving as a Scaffold of Extracellular Signal-Regulated Kinase and YB-1 to Enhance Hepatocarcinogenesis. *Hepatology* 65 (5), 1612–1627. doi:10.1002/hep.29010

Liang, J.-y., Wang, D.-s., Lin, H.-c., Chen, X.-x., Yang, H., Zheng, Y., et al. (2020). A Novel Ferroptosis-Related Gene Signature for Overall Survival Prediction in Patients with Hepatocellular Carcinoma. *Int. J. Biol. Sci.* 16 (13), 2430–2441. doi:10.7150/ijbs.45050

Liang, J., Zhi, Y., Deng, W., Zhou, W., Li, X., Cai, Z., et al. (2021). Development and Validation of Ferroptosis-Related lncRNAs Signature for Hepatocellular Carcinoma. *PeerJ* 9, e11627. doi:10.7717/peerj.11627

Lin, T., Hou, P.-F., Meng, S., Chen, F., Jiang, T., Li, M.-L., et al. (2019). Emerging Roles of P53 Related lncRNAs in Cancer Progression: A Systematic Review. *Int. J. Biol. Sci.* 15 (6), 1287–1298. doi:10.7150/ijbs.33218

Llovet, J. M., Kelley, R. K., Villanueva, A., Singal, A. G., Pikarsky, E., Roayaie, S., et al. (2021). Hepatocellular Carcinoma. *Nat. Rev. Dis. Primers* 7 (1), 6. doi:10.1038/s41572-020-00240-3

Louandre, C., Ezzoukhry, Z., Godin, C., Barbare, J.-C., Mazière, J.-C., Chauffert, B., et al. (2013). Iron-dependent Cell Death of Hepatocellular Carcinoma Cells Exposed to Sorafenib. *Int. J. Cancer* 133 (7), 1732–1742. doi:10.1002/ijc.28159

Ma, X., Xiao, L., Liu, L., Ye, L., Su, P., Bi, E., et al. (2021). CD36-mediated Ferroptosis Dampens Intratumoral CD8+ T Cell Effector Function and Impairs Their Antitumor Ability. *Cel Metab.* 33 (5), 1001–1012.e5. doi:10.1016/j.cmet.2021.02.015

Mai, H., Zhou, B., Liu, L., Yang, F., Conran, C., Ji, Y., et al. (2019). Molecular Pattern of lncRNAs in Hepatocellular Carcinoma. *J. Exp. Clin. Cancer Res.* 38 (1), 198. doi:10.1186/s13046-019-1213-0

Newman, A. M., Liu, C. L., Green, M. R., Gentles, A. J., Feng, W., Xu, Y., et al. (2015). Robust Enumeration of Cell Subsets from Tissue Expression Profiles. *Nat. Methods* 12 (5), 453–457. doi:10.1038/nmeth.3337

Newman, A. M., Steen, C. B., Liu, C. L., Gentles, A. J., Chaudhuri, A. A., Scherer, F., et al. (2019). Determining Cell Type Abundance and Expression from Bulk Tissues with Digital Cytometry. *Nat. Biotechnol.* 37 (7), 773–782. doi:10.1038/s41587-019-0114-2

Nie, J., Lin, B., Zhou, M., Wu, L., and Zheng, T. (2018). Role of Ferroptosis in Hepatocellular Carcinoma. *J. Cancer Res. Clin. Oncol.* 144 (12), 2329–2337. doi:10.1007/s00432-018-2740-3

Nie, Y., Li, J., Wu, W., Guo, D., Lei, X., Zhang, T., et al. (2021). A Novel Nine-lncRNA Risk Signature Correlates with Immunotherapy in Hepatocellular Carcinoma. *Front. Oncol.* 11, 706915. doi:10.3389/fonc.2021.706915

Pinter, M., Jain, R. K., and Duda, D. G. (2021). The Current Landscape of Immune Checkpoint Blockade in Hepatocellular Carcinoma. *JAMA Oncol.* 7, 113. doi:10.1001/jamaoncol.2020.3381

Qi, W., Li, Z., Xia, L., Dai, J., Zhang, Q., Wu, C., et al. (2019). LncRNA GABPB1-AS1 and GABPB1 Regulate Oxidative Stress during Erastin-Induced Ferroptosis in HepG2 Hepatocellular Carcinoma Cells. *Sci. Rep.* 9 (1), 16185. doi:10.1038/s41598-019-52837-8

Quinn, J. J., and Chang, H. Y. (2016). Unique Features of Long Non-coding RNA Biogenesis and Function. *Nat. Rev. Genet.* 17 (1), 47–62. doi:10.1038/nrg.2015.10

Schmitt, A. M., and Chang, H. Y. (2016). Long Noncoding RNAs in Cancer Pathways. *Cancer Cell* 29 (4), 452–463. doi:10.1016/j.ccell.2016.03.010

Stockwell, B. R., Friedmann Angeli, J. P., Bayir, H., Bush, A. I., Conrad, M., Dixon, S. J., et al. (2017). Ferroptosis: A Regulated Cell Death Nexus Linking Metabolism, Redox Biology, and Disease. *Cell* 171 (2), 273–285. doi:10.1016/j.cell.2017.09.021

Subramanian, A., Tamayo, P., Mootha, V. K., Mukherjee, S., Ebert, B. L., Gillette, M. A., et al. (2005). Gene Set Enrichment Analysis: a Knowledge-Based Approach for Interpreting Genome-wide Expression Profiles. *Proc. Natl. Acad. Sci.* 102 (43), 15545–15550. doi:10.1073/pnas.0506580102

Villanueva, A. (2019). Hepatocellular Carcinoma. *N. Engl. J. Med.* 380 (15), 1450–1462. doi:10.1056/NEJMra1713263

Wan, S., Lei, Y., Li, M., and Wu, B. (2021). A Prognostic Model for Hepatocellular Carcinoma Patients Based on Signature Ferroptosis-Related Genes. *Hepatol. Int.* [Epub ahead of print] doi:10.1007/s12072-021-10248-w

Wang, F., Zuroske, T., and Watts, J. K. (2020). RNA Therapeutics on the Rise. *Nat. Rev. Drug Discov.* 19 (7), 441–442. doi:10.1038/d41573-020-00078-0

Wang, L., Ge, X., Zhang, Z., Ye, Y., Zhou, Z., Li, M., et al. (2021). Identification of a Ferroptosis-Related Long Noncoding RNA Prognostic Signature and its Predictive Ability to Immunotherapy in Hepatocellular Carcinoma. *Front. Genet.* 12, 682082. doi:10.3389/fgene.2021.682082

Wang, Q., Jiang, H., Ping, C., Shen, R., Liu, T., Li, J., et al. (2015). Exploring the Wnt Pathway-Associated LncRNAs and Genes Involved in Pancreatic Carcinogenesis Driven by Tp53 Mutation. *Pharm. Res.* 32 (3), 793–805. doi:10.1007/s11095-013-1269-z

Wang, W., Green, M., Choi, J. E., Gijón, M., Kennedy, P. D., Johnson, J. K., et al. (2019). CD8+ T Cells Regulate Tumour Ferroptosis during Cancer Immunotherapy. *Nature* 569 (7755), 270–274. doi:10.1038/s41586-019-1170-y

Wang, Z., Chen, X., Liu, N., Shi, Y., Liu, Y., Ouyang, L., et al. (2021). A Nuclear Long Non-coding RNA LINC00618 Accelerates Ferroptosis in a Manner Dependent upon Apoptosis. *Mol. Ther.* 29 (1), 263–274. doi:10.1016/j.ymthe.2020.09.024

Xie, B., and Guo, Y. (2021). Molecular Mechanism of Cell Ferroptosis and Research Progress in Regulation of Ferroptosis by Noncoding RNAs in Tumor Cells. *Cell Death Discov.* 7 (1), 101. doi:10.1038/s41420-021-00483-3

Xu, Z., Peng, B., Liang, Q., Chen, X., Cai, Y., Zeng, S., et al. (2021). Construction of a Ferroptosis-Related Nine-lncRNA Signature for Predicting Prognosis and Immune Response in Hepatocellular Carcinoma. *Front. Immunol.* 12, 719175. doi:10.3389/fimmu.2021.719175

Yan, X., Zhang, D., Wu, W., Wu, S., Qian, J., Hao, Y., et al. (2017). Mesenchymal Stem Cells Promote Hepatocarcinogenesis via lncRNA-MUF Interaction with ANXA2 and miR-34a. *Cancer Res.* 77 (23), 6704–6716. doi:10.1158/0008-5472.Can-17-1915

Yang, S., Zhou, Y., Zhang, X., Wang, L., Fu, J., Zhao, X., et al. (2021). The Prognostic Value of an Autophagy-Related lncRNA Signature in Hepatocellular Carcinoma. *BMC Bioinformatics* 22 (1), 217. doi:10.1186/s12859-021-04123-6

Yao, J., Chen, X., Liu, X., Li, R., Zhou, X., and Qu, Y. (2021). Characterization of a Ferroptosis and Iron-Metabolism Related lncRNA Signature in Lung Adenocarcinoma. *Cancer Cel Int* 21 (1), 340. doi:10.1186/s12935-021-02027-2

Yuan, D., Chen, Y., Li, X., Li, J., Zhao, Y., Shen, J., et al. (2021). Long Non-coding RNAs: Potential Biomarkers and Targets for Hepatocellular Carcinoma Therapy and Diagnosis. *Int. J. Biol. Sci.* 17 (1), 220–235. doi:10.7150/ijbs.50730

Zhang, F., Li, F., Lu, G.-H., Nie, W., Zhang, L., Lv, Y., et al. (2019). Engineering Magnetosomes for Ferroptosis/Immunomodulation Synergism in Cancer. *ACS Nano* 13 (5), 5662–5673. doi:10.1021/acsnano.9b00892

Zhang, J., Li, Z., Liu, L., Wang, Q., Li, S., Chen, D., et al. (2018). Long Noncoding RNA TSLNC8 Is a Tumor Suppressor that Inactivates the interleukin-6/STAT3 Signaling Pathway. *Hepatology* 67 (1), 171–187. doi:10.1002/hep.29405

Zhang, Y., Guo, S., Wang, S., Li, X., Hou, D., Li, H., et al. (2021). LncRNA OIP5-AS1 Inhibits Ferroptosis in Prostate Cancer with Long-Term Cadmium Exposure through miR-128-3p/SLC7A11 Signaling. *Ecotoxicology Environ. Saf.* 220, 112376. doi:10.1016/j.ecoenv.2021.112376

Zhou, N., and Bao, J. (2020). FerrDb: a Manually Curated Resource for Regulators and Markers of Ferroptosis and Ferroptosis-Disease Associations. *Database (Oxford)* 2020, baaa021. doi:10.1093/database/baaa021

Conflict of Interest: The authors declare that the research was conducted in the absence of any commercial or financial relationships that could be construed as a potential conflict of interest.

Publisher's Note: All claims expressed in this article are solely those of the authors and do not necessarily represent those of their affiliated organizations, or those of the publisher, the editors and the reviewers. Any product that may be evaluated in this article, or claim that may be made by its manufacturer, is not guaranteed or endorsed by the publisher.

frontiers in Genetics

ORIGINAL RESEARCH
published: 01 March 2022
doi: 10.3389/fgene.2022.847940

Development and Validation of a Ferroptosis-Related lncRNAs Prognosis Model in Oral Squamous Cell Carcinoma

Tao Li[1,2], *Yi Wang*[1], *Xianwang Xiang*[1] *and Chuanjun Chen*[1]*

[1]Department of Oral and Maxillofacial Surgery, The First Affiliated Hospital of USTC, Division of Life Sciences and Medicine, University of Science and Technology of China, Hefei, China, [2]WanNan Medical College, Wuhu, China

Objectives: Ferroptosis is an iron-dependent form of programmed cell death, which affects the prognosis of many cancers. Some long non-coding RNA (lncRNA) can affect the prognosis of cancer by regulating the process of ferroptosis. However, the role of ferroptosis-related lncRNA (frlncRNA) in oral squamous cell carcinoma (OSCC) is not yet clear.

Materials and Methods: The data of OSCC patients were downed from The Cancer Genome Atlas (TCGA). After univariate and multivariate Cox regression analysis, the prognosis-related ferroptosis-related lncRNAs were obtained to construct a prognostic model. Calculated the risk score to divide patients into high and low risk groups, and evaluated the predictive ability of the model and the differential expression of immunity in the high and low risk groups.

Results: The prognostic model for OSCC was constructed based on 8 prognostic-related frlncRNAs which co-expressed with 25 mRNAs. Kaplan-Meier analyses displayed that the risk score is inversely proportional to patient survival. Receiver operating characteristic (ROC) and decision curve analysis (DCA) indicated that the risk score is superior to other clinical characteristics, and independent prognostic analysis demonstated that risk score is independent factor for the overall survival (OS) rate. The results of immunological analysis showed differences in immune cells, functions, immune checkpoints, and m6A expression between high and low risk groups.

Conclusion: We constructed an OSCC patients prognosis model based on 8 frlncRNAs, which can provide prognostic evaluation and immune analysis for OSCC patients, and provided new direction for OSCC targeted therapy.

Keywords: ferroptosis, lncRNA, OSCC, immunity, prognosis model

OPEN ACCESS

Edited by:
Lian Xiang Luo,
Guangdong Medical University, China

Reviewed by:
Xing Liang,
Stanford University, United States
Yanqing Liu,
Columbia University, United States
Ling Li,
University of North Dakota, United States

***Correspondence:**
Chuanjun Chen
ccj6318@sina.com.cn

Specialty section:
This article was submitted to Human and Medical Genomics, a section of the journal Frontiers in Genetics

Received: *03 January 2022*
Accepted: *07 February 2022*
Published: *01 March 2022*

Citation:
Li T, Wang Y, Xiang X and Chen C (2022) Development and Validation of a Ferroptosis-Related lncRNAs Prognosis Model in Oral Squamous Cell Carcinoma. Front. Genet. 13:847940. doi: 10.3389/fgene.2022.847940

INTRODUCTION

Oral cancer is one of the common malignant tumors. Recent global estimates show that there will be 377,713 new cases and 177,757 deaths from oral cancer in 2020 (Sung et al., 2021). OSCC is the most common, accounting for more than 90% of all oral cancers (Chi et al., 2015). Although treatment methods are constantly improving, the prognosis of OSCC is still poor, only about 50% in 5 years

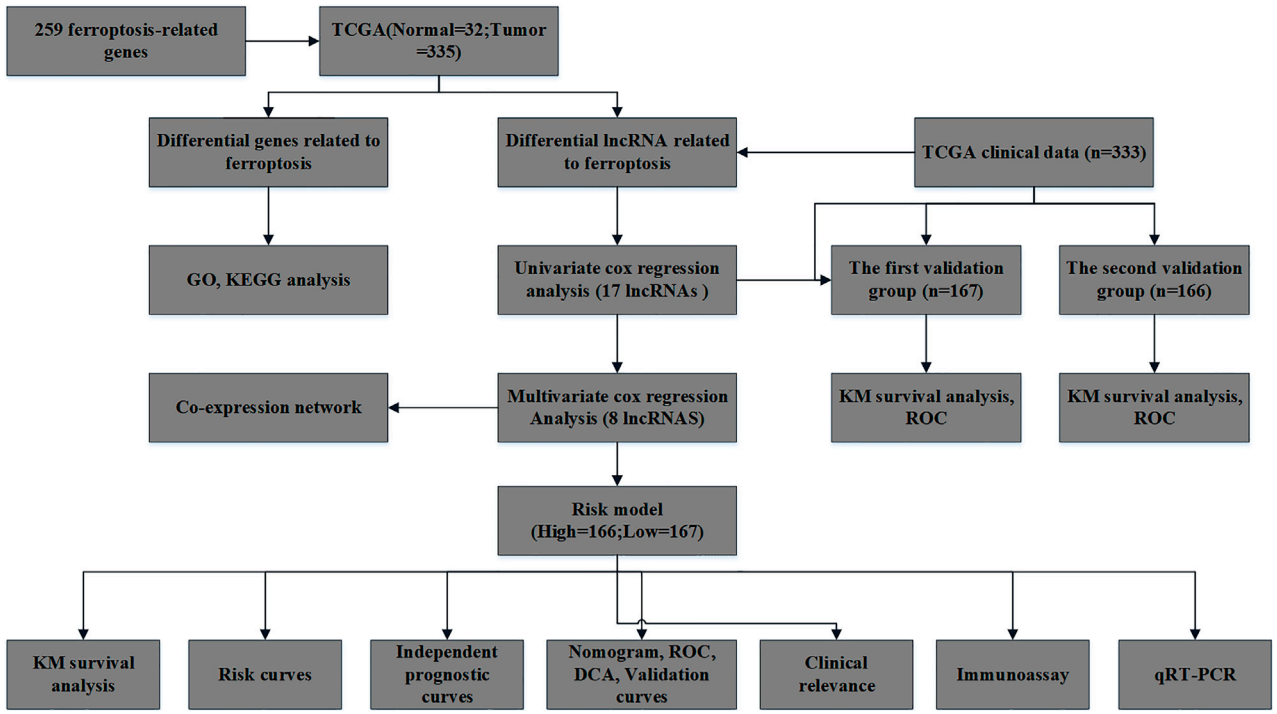

FIGURE 1 | The flowchart of this study.

(Kurihara-Shimomura et al., 2020). At present, the evaluation of prognosis and survival in OSCC is still based on the traditional TNM staging standard. However, due to the differences in the genetic signs of patients with the same TNM staging status, their response to treatment and individual differences may affect the prognosis assessment of patients with OSCC. Therefore, studying the biological, genetic and epigenetic changes of OSCC, especially the underlying mechanism of aggressive phenotype, is essential to improve the prognosis of OSCC patients. Studies have found that programmed cell death (PCD) is related to the occurrence, progression and metastasis of tumors (Lee et al., 2018). Ferroptosis is a new type of PCD, which is different from previous apoptosis and autophagy in its unique mechanism, that is, iron-dependent reactive oxygen species (ROS) accumulation and irresistible lipid metabolism. Oxidation leads to cell death (Dixon et al., 2012). It is well known that inducing cell death is a feasible cancer treatment. Ferroptosis has also been identified as a potential prevention or treatment strategy that triggers cancer cell death, especially for malignant tumors that are resistant to traditional therapies (Roh et al., 2016). Fukuda M et al. reported that ferroptosis plays an important role in oral cancer. Some genes that promote the proliferation of OSCC cells, such as GPX4 and SREBP, seem to protect cells from ferroptosis (Fukuda et al., 2021).

LncRNAs are non-protein coding genes larger than 200 nucleotides to distinguish them from small non-coding RNAs (Kopp and Mendell, 2018). In recent years, with the development of high-throughput sequencing technology, it has been discovered that a large number of non-coding genes play an important role in the occurrence and development of tumors (Gao et al., 2020). Studies have shown that lncRNAs are involved in cell growth, invasion and metastasis. It also plays an important role in OSCC, such as: lncRNACASC9 promotes autophagy apoptosis of OSCC cells by inhibiting the AKT/mTOR signaling pathway to increase autophagy (Yang et al., 2019); lncRNAUCA1 exerts its oncogene effect in OSCC cells through the UCA1/miR-184/SF1 axis (Fang et al., 2017).

The role and prognostic value of frlncRNAs in OSCC are currently unclear. Here, we screened frlncRNAs related to the prognosis of OSCC to construct a prognostic model and study its possible mechanism. Meanwhile, we also analyzed the functional enrichment analysis of differential genes, the differences in the expression of immune cell infiltration, immune checkpoint and m6A between high and low risk groups. It is hoped that new biomarkers can be provided for the targeted therapy of OSCC. The flow chart of this study is shown in **Figure 1**.

MATERIALS AND METHODS

Data acquisition

The RNA sequencing (RNA-seq) data of OSCC patients were downed from TCGA database on 2021.09.29, including 32 samples with normal RNA sequences, 335 samples with OSCC, In addition, we collected 333 cases corresponding clinical datas of tumor samples from TCGA. The clinical data included survival status, survival time, gender, age, tumor stage, pathological grade, T stage, N stage and M stage.

Identification of frlncRNAs

The human GTF interpretation file were downloaded from Ensembl (http://asia.ensembl.org). 19,573 mRNAs and 14,056 lncRNAs were differentiated and extracted by operating the Strawberry Perl software. A total of 259 ferroptosis-related genes (**Supplementary Table S1**) included driver genes, suppressor genes and marker genes were extracted from the FerrDb database (http://www.zhounan.org/ferrdb). The correlation between ferroptosis-related genes and all lncRNAs was analyzed through the R limma package to obtain frlncRNAs and ferroptosis-related mRNAs(frmRNAs). The filter standard was set that correlation coefficient >0.4 and p-value < 0.001, respectively.

Screening Differentially Expressed Genes and Enrichment Analysis

The "limma" package of R software was used to screen of differentially expressed genes (DEG) related to ferroptosis between the normal group and the tumor group. The standard is the false discovery rate (FDR) < 0.05 and |logFC| >1. The packages of "colorspace," "stringi" and "colorspace" were to perform Gene Ontology (GO) analysis and Kyoto Encyclopedia of Genes and Genomes (KEGG) pathway analysis on differentially expressed genes, with p-value < 0.05 and Q-value < 0.05 as the screening conditions.

Construction and Evaluation of the Prognostic Model of frlncRNAs

The most prognostic frlncRNAs were screened by univariate and multivariate COX regression analysis. Over and above that, patients were classified into low-risk (< median) or high-risk (> median) groups according to the median of risk score. The risk scores of OSCC parents were calculated on the basis of the following formula. N represents the finally optioned lncRNA.

$$\text{Risk score} = \text{Exp}_{\text{lncRNA1}} \times \beta_{\text{lncRNA1}} + \text{Exp}_{\text{lncRNA2}} \times \beta_{\text{lncRNA2}} + \cdots + \text{Exp}_{\text{lncRNAn}} \times \beta_{\text{lncRNAn}} \quad (1)$$

The Kaplan–Meier (K-M) survival curves was used to compare the overall survival (OS) between high-risk and low-risk group, receiver operating characteristic (ROC) curves and decision curve analysis (DCA) were used to evaluate whether the predictive power of risk score was better than that of other clinical characteristics. Univariate and multivariate COX regression analyses were used to determine whether risk scores was independent of other clinical characteristics as a prognostic factor in patients with OSCC. Finally, all independent prognostic parameters were incorporated into the construction of the nomogram to predict the 1, 2, and 3 years overall survival of patients. The accuracy of the nomogram's predictions was assessed by the calibration curve.

Internal Validation and Clinical Relevance Analysis

The 333 cliniacal data were randomly divided into two groups to validate the predictive ability of the model according to the ratio of 1:1 through the package "caret" of R (**Table 1**). In order to compare differences in clinical characteristics between high and low risk groups, the clinical data were divided into several subgroups. Moreover, we also compared the differences in the expression of frlncRNAs in various clinical features.

Establishment of a Co-expression Network of lncRNA-mRNA Related to Ferroptosis

Investigated the relationship between frlncRNAs and frmRNAs, and constructed an lncRNA-mRNA co-expression network through Cytoscape.

Immunoassay

Immune cell infiltration files were downloaded from (http://timer.cistrome.org).The difference between immune cells in the high and low risk groups were evaluated by the *TIMER, CIBERSORT, CIBERSORT-ABS, QUANTISEQ, MCPCOUNTER, XCELL* and *EPIC*. In addition, we also compared the differences in immune function, immune checkpoint and m6A between high and low risk groups.

RNA Extraction and Quantitative PCR

There were four pairs of OSCC and adjacent samples collected from the First Affiliated Hospital of University of Science and Technology of China, and stored in liquid nitrogen at -196°C. According to the manufacturer's instructions, total RNA was extracted by Trizol reagent (Yisheng Biotechnology, China), cDNA was synthesized by HiScript II 1st Strand cDNA Synthesis Kit (+gDNA wiper) (Vazyme, China), Hieff® qPCR SYBR Green Master Mix (Low Rox) (Yisheng Biotechnology, China) was used for amplification, GAPDH was set as an endogenous control. we selected 4 lncRNAs (STARD4-AS1, MIAT, AC099850.3, AL512274.1) of the model for qPCR. The relative quantification method of $2^{-\Delta\Delta CT}$ was used to normalize the expression of lncRNA. Each group was repeated three times and the mean value was used for analysis. All patients gave informed consent and signed an informed consent form. The primer sequences of these four lncRNAs are provided in **Supplementary Table S2**.

Statistical Analysis

All data were analyzed using Rstudio or SPSS 20.0. Paired samples were used by independent t-test or one-way analysis of variance. Kaplan-Meier survival analysis was used to assess the difference in survival between the high and low risk groups of OSCC patient prognosis model based on frlncRNAs. ROC and DCA curves were used to evaluate the predictive performance of OSCC prognostic model. The statistical significance was set at $p < 0.05$.

RESULTS

Enrichment Analysis of Differential mRNAs Related to Ferroptosis

We found 62 differential mRNAs related to ferroptosis (17 down-regulated and 45 up-regulated) (**Supplementary Table S3**); BP participated in response to oxidative stress and cellular response to

TABLE 1 | The clinical datas in different groups.

Variables	TCGA(Total)	Validation	
	(*n* = 333)	The first validation group (*n* = 167)	The second validation group (*n* = 166)
Age (%)			
<=65	210 (63.06)	108 (64.67)	102 (61.45)
>65	123 (36.94)	59 (35.33)	64 (38.55)
Gender (%)			
FEMALE	100 (30.03)	55 (32.93)	45 (27.11)
MALE	233 (69.07)	112 (67.07)	121 (72.89)
Grade (%)			
G1-2	257 (77.18)	127 (76.05)	130 (78.31)
G3-4	67 (20.12)	36 (21.55)	31 (18.67)
GX + unknow	9 (2.70)	4 (2.40)	5 (3.01)
Stage(%)			
StageI-II	75 (22.52)	40 (23.95)	35 (21.08)
StageIII-IV	223 (66.97)	108 (64.67)	115 (69.28)
unknow	35 (10.51)	19 (11.38)	16 (9.64)
T (%)			
T1-T2	134 (40.24)	66 (39.52)	68 (40.96)
T3-T4	172 (51.65)	86 (51.50)	86 (51.81)
TX + unknow	27 (8.11)	15 (8.98)	12 (7.23)
M (%)			
M0	121 (36.34)	65 (38.92)	56 (33.73)
MX + unknow	212 (63.66)	102 (61.08)	110 (66.27)
N (%)			
N0	120 (36.04)	63 (37.72)	57 (34.34)
N1-3	158 (47.45)	73 (43.71)	85 (51.20)
NX + unknow	55 (16.51)	31 (18.56)	24 (14.46)

chemical stress; MF regulated organic anion transmembrane transporter activity; CC participated in basal plasma membrane,basal part of cell and apical part of cell (**Figure 2A**). KEGG analysis results demonstated that overexpressed genes were mainly involved in MicroRNAs in cancer, HIF-1 signaling pathway, Ferroptosis, Fluid shear stress and atherosclerosis, Kaposi sarcoma–associated herpesvirus infection, mTOR signaling pathway, Cysteine and methionine metabolism, Central carbon metabolism in cancer, Biosynthesis of amino acids and Pancreatic cancer (**Figure 2B**).

Prognostic-Related frlncRNAs Risk Model and Co-expression Network

A total of 377 differential frlncRNAs were identified, which of 17 were associated with prognosis after univariate analysis ($p < 0.05$) (**Supplementary Table S4**; **Figure 2C**). Multivariate COX regression analysis was performed to select the optimal prognostic frlncRNAs, according to Akaike Information Criterion (AIC), finally 8 frlncRNAs were used to construct the OSCC prognostic model (**Table 2**), and patients were divided into high-risk groups ($n = 166$) and low-risk groups ($n = 167$) based on the median risk score. A total of 25 frmRNAs were co-expressed with these 8 frlncRNAs, of which 6 were co-expressed with AC099850.3 (**Supplementary Table S5**; **Figure 2D**).

The evaluation of Prognosis Model

In independent prognostic analysis, the univariate and multivariate COX analysis showed the risk score of frlncRNAs (HR: 1.721, 95CI 1.438–2.059), age (HR: 1.037 95CI: 1.020–1.055) and tumor stage (HR: 1.595, 95CI: 1.279–1.988) were independent prognostic factors of OS in patients with OSCC ($p < 0.05$, **Figures 3A,B**). There were more deaths can be observed in the high-risk group from **Figures 3C,D**. We as well observed that STARD4-AS1, MIAT and AL512274.1 were more expressed in the low-risk group; on the contrary, AC099850.3, AC090246.1, ALMS1-IT1, AC021087.4, and HOTARM1 were more expressed in the high-risk group (**Figure 3E**). In addition, as shown in **Figure 4A**, Kaplan-Meier analysis illustrated that the expression of high-risk lncRNAs characteristics was significantly different from the low-risk group in OS ($p < 0.001$), and the patients' risk score was inversely proportional to the survival rate of OSCC patients. It can be seen that there are some numbers under the **Figure 4A**. For e.g., when the time node is 1, the number corresponding to red is 110, which represents the number of people who survived in the high-risk group when the follow-up time is 1 year. We assessed the sensitivity and specificity of the risk model through AUC (the area under the ROC curve), the AUC of the model to predict 1, 2, and 3 years OS was 0.690, 0.672, and 0.677, respectively (**Figure 4B**). And the ROC (**Figure 4C**) and DCA (**Figure 4D**) curves of the risk score of frlncRNAs indicated that risk score was better than traditional clinical pathology features in predicting the prognosis of OSCC. We included the independent factors of age, tumor stage, and risk score in the multivariate independent prognostic analysis into the nomogram (**Figure 4E**) to predict 1, 2, and 3 years survival, and used the calibration curve to verify. The results (**Figures 4F–H**) displayed that the calibration curves were close to the ideal slope, which meaned that age, tumor, and risk scores together can accurately predict 1-, 3-, and 5 years OS of patients.

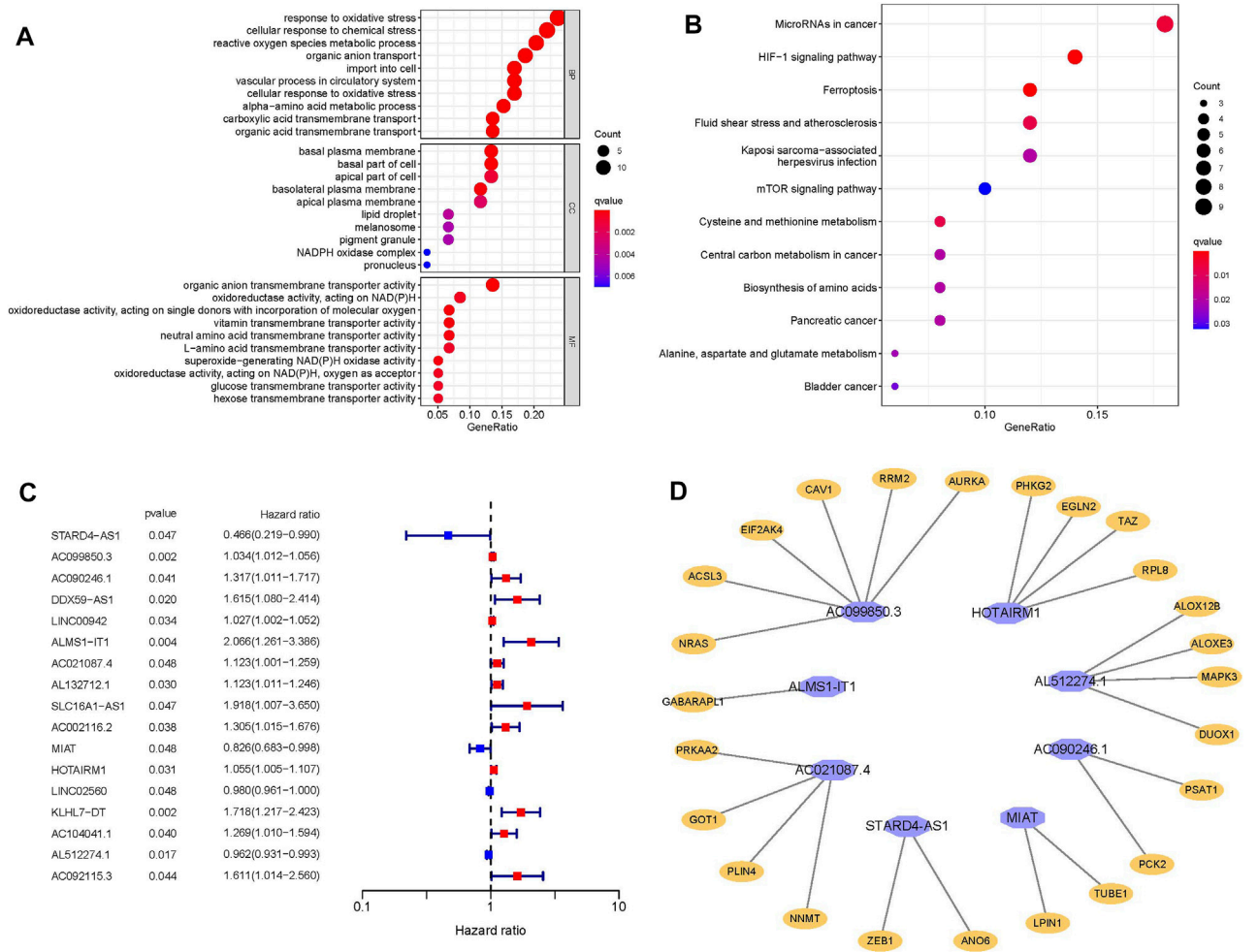

FIGURE 2 | (A) Go enrichment analysis. **(B)** KEGG enrichment analysis. **(C)** Forest plot represents 17 lncRNAs related to OSSC prognosis obtained by univariate analysis. **(D)** The prognostic-related lncRNAs and their co-expressed mRNA obtained from multivariate COX regression analysis, purple represents lncRNA, orange represents mRNA.

TABLE 2 | 8 frlncRNAs by multivariate Cox regression analysis.

LncRNA	Coef	HR	HR.95L	HR.95H	*p-value*
STARD4-AS1	−0.559	0.572	0.270	1.212	0.145
AC099850.3	0.028	1.029	1.007	1.052	0.011
AC090246.1	0.362	1.436	1.051	1.962	0.023
ALMS1-IT1	0.557	1.746	1.034	2.947	0.037
AC021087.4	0.140	1.151	1.027	1.288	0.016
MIAT	−0.238	0.788	0.640	0.970	0.024
HOTAIRM1	0.047	1.050	0.995	1.106	0.079
AL512274.1	−0.038	0.962	0.931	0.996	0.030

The clinical Relevance Analysis and Internal Validation

The clinical variables were divided into several subgroups. We compared the differences in the OS of patients in the high and low risk groups in various clinical variables through Kaplan-Meier analysis. It can be seen that the OS of patients in the high risk group is lower in all subgroups including (age, gender, grade, stage, Tstage, N stage, M stage; $p < 0.5$, **Figures 5A–M**). Furthermore, The results of the Kaplan-Meier analysis of the first validation group and the second validation group illustrated that the OS of the high-risk group was lower ($p < 0.5$, **Figures 5N,P**), and the AUC of the risk score in both groups was greater than that of other clinical characteristics, which indicated that the predictive performance of the risk model was good (**Figures 5O,Q**). We also analyzed the differences in the expression of frlncRNAs among different clinical features(**Figures 6A–F**). It can be observed that ALMS1-IT1 was differentially expressed in males and females (**Figure 6B**). In addition, its expression is differential in N stage (**Figure 6D**); AL512274.1 had differences in the expression of grade, stage, and N stage (**Figures 6C,D,F**); AC099850.3 was differentially expressed on different grades (**Figure 6C**).

Immunity and Gene Expression and qPCR

The immune response heatmap based on *TIMER, CIBERSORT, CIBERSORT-ABS, QUANTISEQ, MCPCOUNTER, XCELL*, and

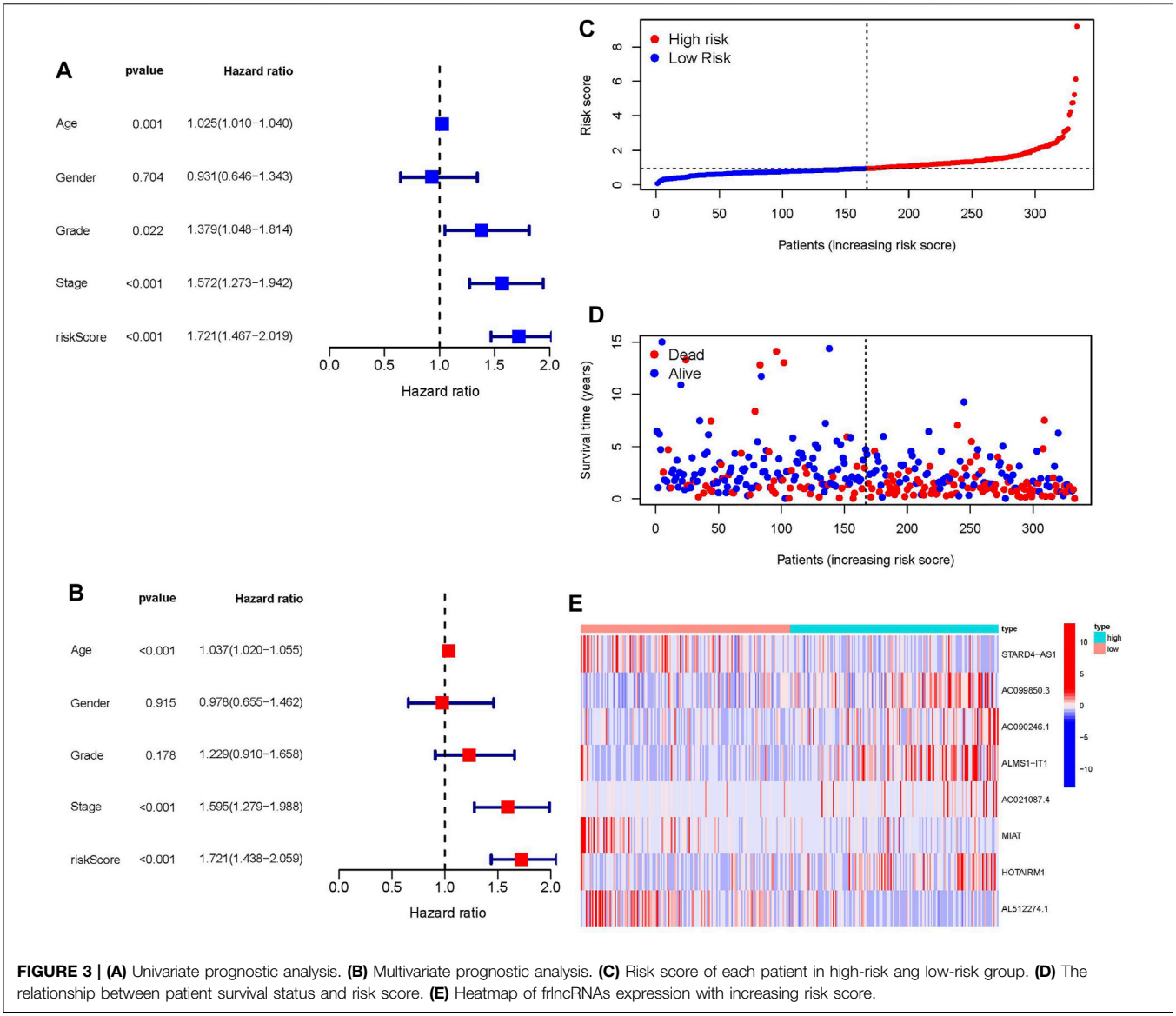

FIGURE 3 | (A) Univariate prognostic analysis. **(B)** Multivariate prognostic analysis. **(C)** Risk score of each patient in high-risk ang low-risk group. **(D)** The relationship between patient survival status and risk score. **(E)** Heatmap of frlncRNAs expression with increasing risk score.

EPIC algorithms is shown in the **Figure 6G**. Analysis of differences in immune function based on TCGA-OSCC data showed that APC_co_inhibition, CCR, Check-point, Cytolytic_activity, HLA, Inflammation-promoting, Parainflammation, T_cell_co-inhibition, T_cell_co-stimulation and Type_II_IFN_Reponse were all highly expressed in the low-risk group (**Figure 7A**). At the same time, the comparison of m6A-related gene expression in high and low groups suggested that the expressions of WTAP, METTL14, YTHDF1, HNRNPC, YTHDC2, RBM15 and ALKBH5 were different ($p < 0.05$, **Figure 7B**). In view of the importance of checkpoint inhibitor-based immunotherapy, we further explored the differences in immune checkpoint expression between the two groups. The results demonstrated that between the two groups *CD48*, *TNFRSF9*, *CD40LG*, *CD160*, *CTLA4*, *KIR3DL1, CD200R1*, *CD28, PDCD1*, *ADORA2A*, *CD27*, *TIGIT*, *TNFRSF4*, *BTLA*, *ICOS*, *CD244*, and *IDO2* were expressed higher in the low-risk group;*CD70, CD276, TNFSF9* were the opposite ($p < 0.05$, **Figure 7C**). As shown in **Figures 7D–G**, MIAT, AL512274.1 and STARD4-AS1 were more highly expressed in adjacent tissues than tumor, and AC099850.3 was highly expressed in tumor tissues, which is consistent with our model.

DISCUSSION

Ferroptosis is an iron-dependent cell death program, which has been shown to be related to tumor development and response to anti-tumor therapy (Chen et al., 2021a). LncRNA is an active participant in the immune regulation of 33 cancer types (Li et al., 2020a). Morever, many lncRNAs are involved in the progression of malignant tumors and tumor resistance, and have become new biomarkers and therapeutic targets in cancer diagnosis and treatment (Wang et al., 2019a). The excellent predictive ability

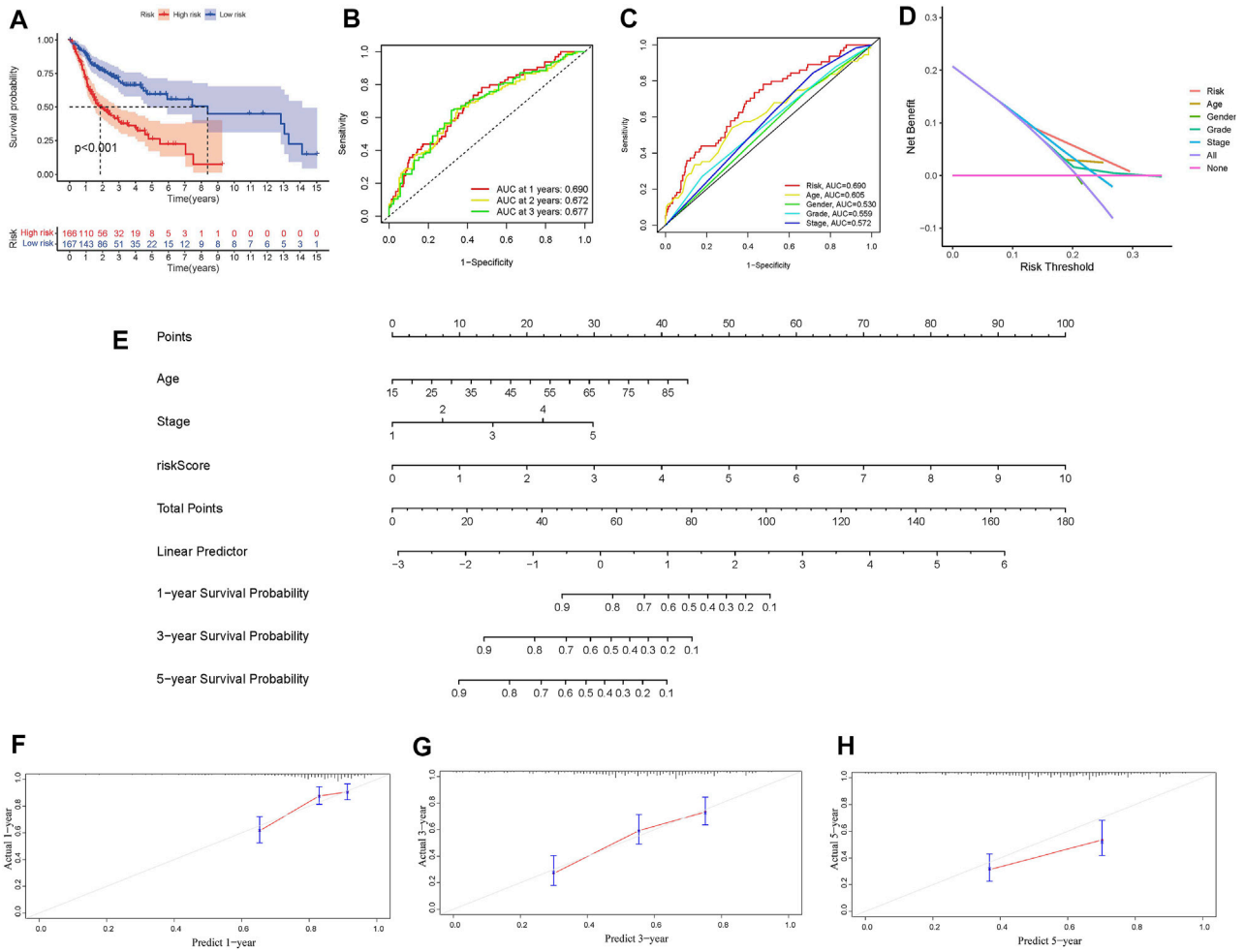

FIGURE 4 | (A) Survival analysis of overall survival rate of high and low risk groups. **(B)** Prognosis model 1, 2 and 3 years ROC curve and AUC. **(C)** Comparison of frlncRNAs risk score and other clinicopathological characteristics of AUC. **(D)** DCA curve. **(E)** Nomogram. **(F–G)** Calibration curves for 1year, 3years, and 5 years forecasts of nomogram.

of frlncRNAs in cancer has been confirmed in a variety of cancers (Chen et al., 2021b; Lu et al., 2021; Jin et al., 2021; Li et al., 2021). However, the mechanism of frlncRNAs in OSCC is still unclear. Therefore, we conducted research on the correlation between frlncRNAs and the prognosis of OSSC. Based on 8 frlncRNAs, we constructed an OSSC risk prognosis model and divided patients into high and low risk groups according to risk scores. ROC, DCA, independent prognostic analysis to verify its predictive ability, the results showed that its predictive ability is better than other clinical features. These 8 frlncRNAs contained 5 risk factors: AC099850.3, AC090246.1, ALMS1-IT1, AC021087.4, and HOTARM1; three protection factors: STARD4-AS1, MIAT and AL512274.1. Among them, AC099850.3 is the most co-expressed lncRNA, which is related to six differently expressed mRNAs, namely (CAV1, NRAS, ACSL3, AURKA, EIF2AK4 and RRM2), and its high expression level is closely related to the reduction in the survival rate of patients with tongue cancer (Zhou et al., 2019). The high expression of ALMS1-IT1 can lead to poor prognosis of many cancers, such as head and neck squamous cell carcinoma (Xing et al., 2019), small cell lung cancer (Luan et al., 2021). The mechanism of its regulation is not yet fully understood. There are studies have shown that in small cell lung cancer, ALMS1-IT1 regulates AVL9 by adsorbing miRNAs, and participates in the regulation of cell cycle-related CDK pathways, thereby affecting tumor progression (Luan et al., 2021). HOTAIRM1 plays different roles in different diseases. It promotes autophagy and proliferation of acute myeloid leukemia cells with mutant nucleophosphoprotein by regulating the expression of EGR1 and ULK3 (Jing et al., 2021). HOTAIRM1 is down-regulated in liver cancer. The specific mechanism may be related to inhibiting the Wnt pathway to inhibit the proliferation of hepatocellular carcinoma cells and promote their apoptosis, thereby inhibiting the progression of liver cancer (Zhang et al., 2018). It is worth noting that as an oncogene, MIAT can proliferate and migrate in various cancer cells such as hepatocellular carcinoma (Huang et al., 2018), osteosarcoma (Zhang et al., 2019), and papillary thyroid carcinoma (Wang et al., 2019b). However, in our study, single-factor and multi-

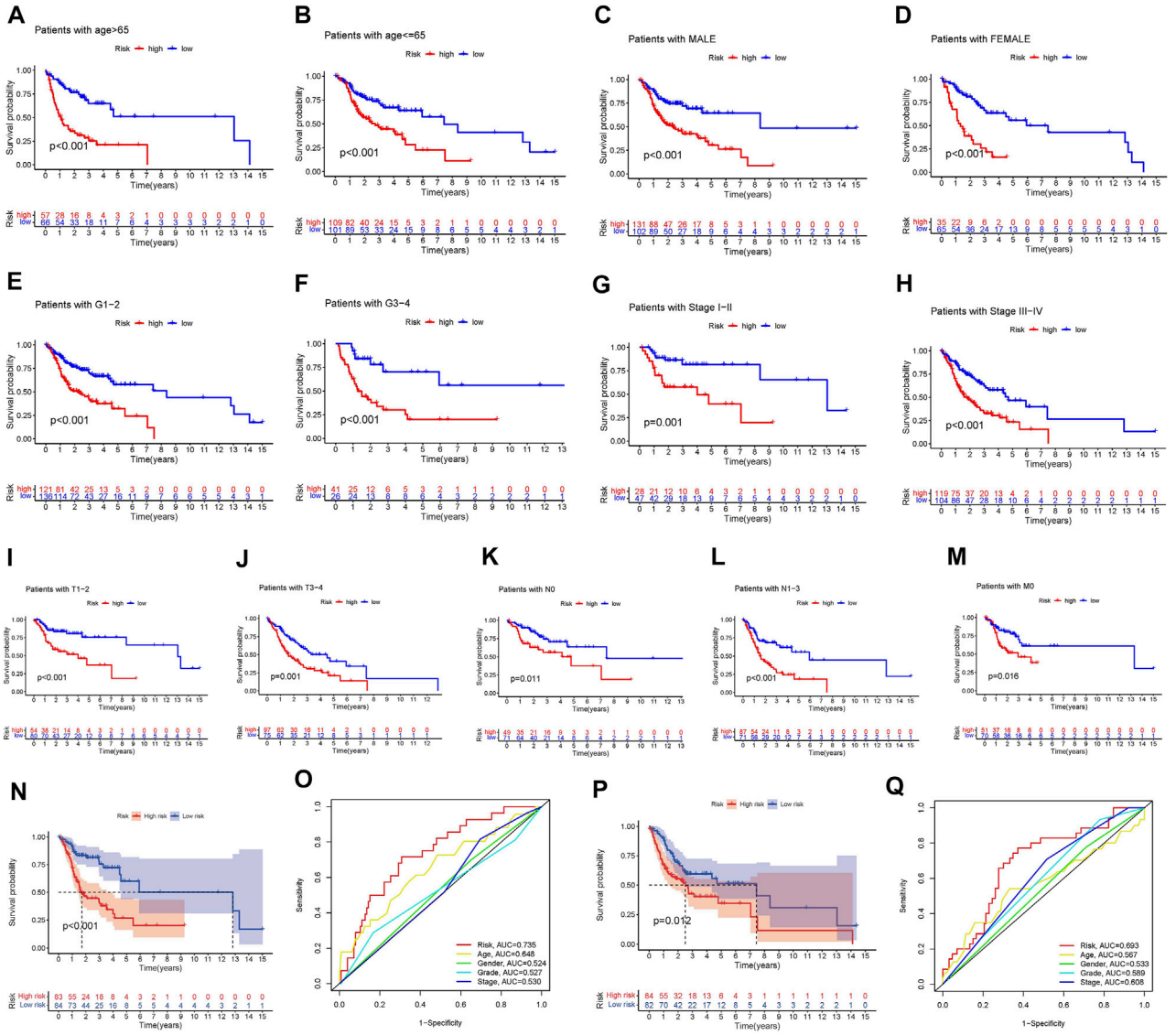

FIGURE 5 | (A–M) Kaplan-Meier analysis Survival analysis of high and low groups among various subclinical characteristics. (**A**: age > 65; **B**: age <= 65; **C**: MALE; **D:** FEMALE; **E**: G1-2; **F**: G3-4; **G**: Stage I-II; **H**: Stage III-IV; **I**: T1-2; **J**: T3-4; **K:** N0; **L**: N1-3; **M**: M0) **(N)** Kaplan-Meier analysis of the first validation group. **(O)** Comparison of the predictive ability of the risk score with other clinical characteristics in the first validation group. **(P)** Kaplan-Meier analysis of the second validation group. **(Q)** Comparison of the predictive ability of the risk score with other clinical characteristics in the first validation group.

factor COX regression analysis showed that MIAT is a protective factor for the prognosis of OSCC. Furthermore, as shown in **Figure 7E**, MIAT expressed higher in adjacent tissues, which is consistent with our model. The role of AL512274.1 in cancer is still unclear, but studies have found that its co-expressed mRNA (MAPK3) is involved in the control of cell proliferation, differentiation and autophagy (Cagnol and Chambard, 2010; Jiang et al., 2021). STARD4-AS1, AC090246.1, AC021087.4 have not seen relevant studies in oral cancer and other tumors, and the specific mechanism is worthy of further investigation.

Considering that immunotherapy is playing an increasingly important role in cancer treatment. We compared the differences in immunity between high and low risk groups. As the **Figure 7C** displays that, except for CD70, CD276 and TNFSF9, almost all other differential genes in the immune checkpoint were expressed in the low-risk group, while m6A except YTHDC2 were mainly expressed in the high-risk group. Studies have reported that CD70 is highly expressed in oral cancer, and its specific CAR-T cells can specifically recognize and effectively eliminate CD70-positive HNSCC cells (Park et al., 2018). In addition, CD276 is highly expressed in head and neck squamous cell carcinoma and the blockade of CD276 significantly inhibited the lymph node metastasis of head and neck squamous cell carcinoma, which is one of the most challenging problems in the treatment of head and neck squamous cell carcinoma, indicating that targeting

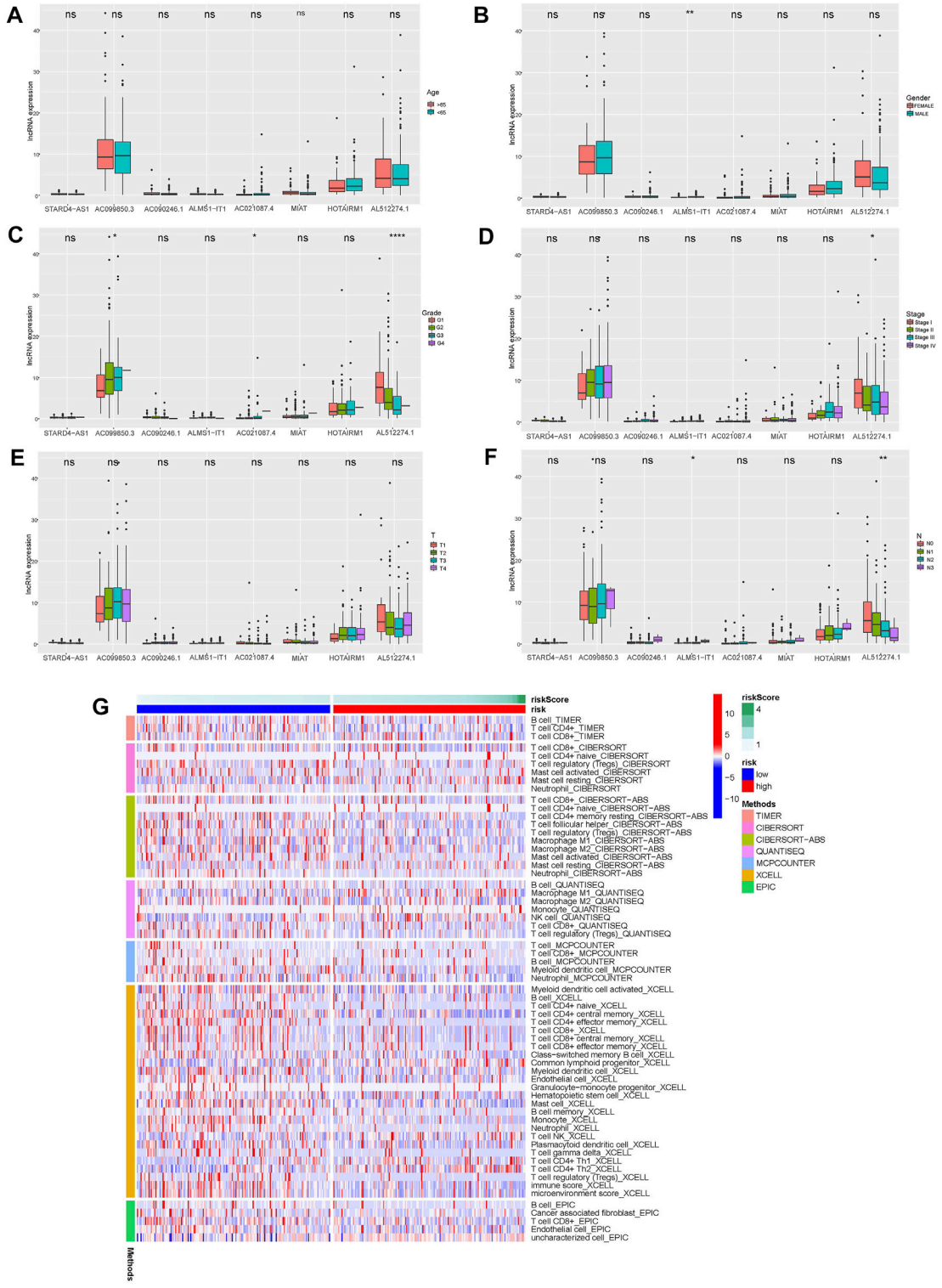

FIGURE 6 | (A–F) Differences in the expression of 8 frlncRNAs among clinical variables (**A**: age; **B**: Gender; **C**: Grade; **D**: Stage; **E**: T stage; **F**: N stage; $*p < 0.05$; $**p < 0.01$; $***p < 0.001$; $****p < 0.001$). **G**: Heat map of immune cell expression in high and low risk groups.

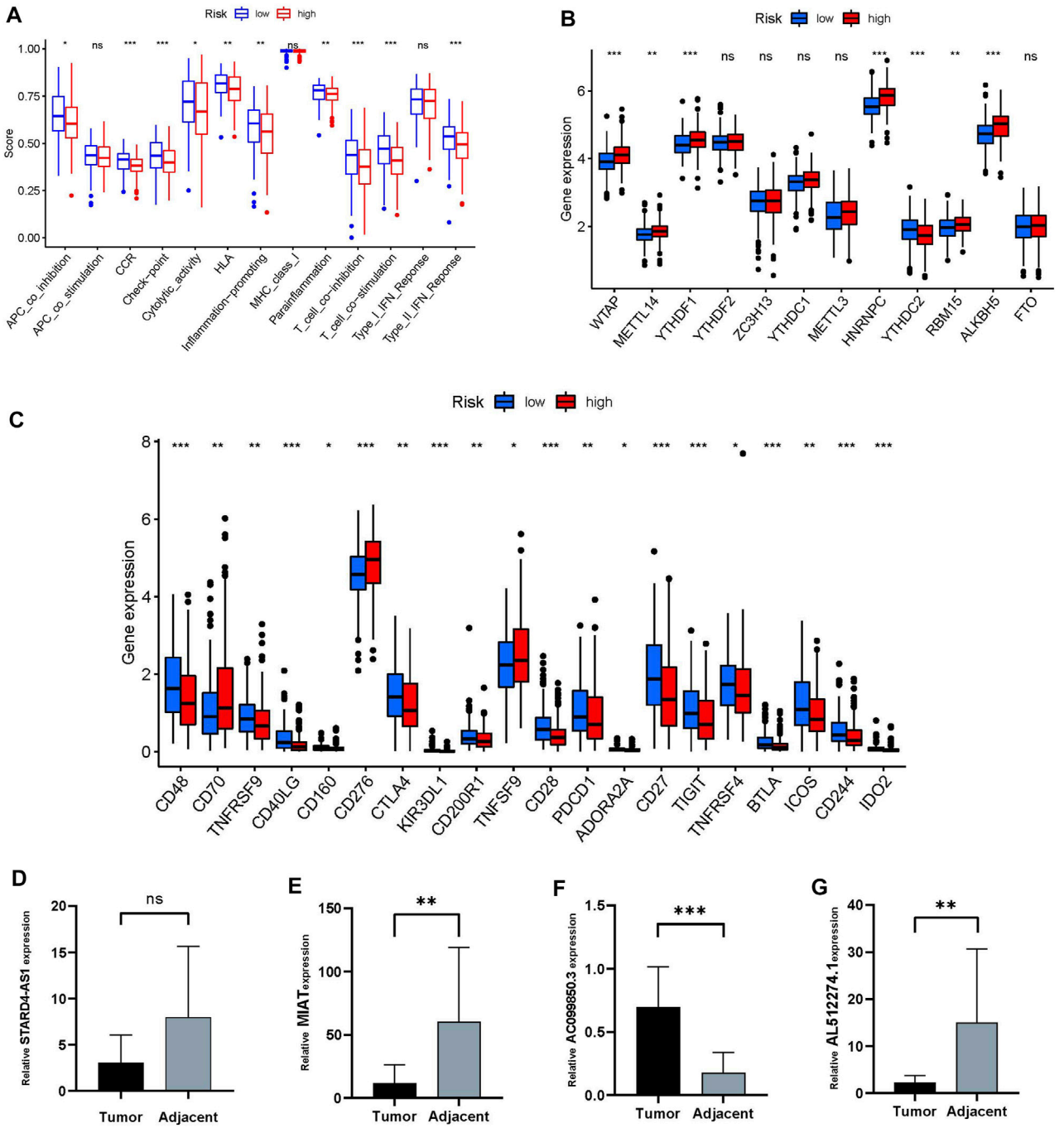

FIGURE 7 | Differences in immune status between high and low risk groups. **(A)** immune function. **(B)** Differences in m6A expression between high and low risk groups. **(C)** Differences in immune checkpoints between the two groups. **(D–G)** The relative expression of four frlncRNAs (STARD4-AS1, MIAT, AC099850.3, AL512274.1) between tumor and adjacent tissue (*$p < 0.05$;**$p < 0.01$; ***$p < 0.001$)

CD276 can enhance anti-tumor immunity (Wang et al., 2021). There are no studies on TNFSF9 and YTHDC2 in oral cancer. Yang Li reported that YTHDC2 is a tumor suppressor gene in the head and neck, which is highly expressed in normal tissues but low in tumors (Li et al., 2020b). In general, frlncRNAs have shown excellent performance in our research and are expected to become new biomarkers for the treatment of OSCC. However, there are some deficiencies in this study. First, the establishment and validation of the risk model is based on the TCGA database and its grouping, and there is a lack of external validation to provide more evidence for evaluating its clinical utility. Second, the number of experimental validations is limited, and the role

and mechanism of most frlncRNAs in the progression of OSCC in this study are not clear, and further investigation is needed.

CONCLUSION

We constructed an OSCC patients prognosis model based on 8 frlncRNAs, which can provide prognostic evaluation and immune analysis for OSCC patients, and provided new direction for OSCC targeted therapy.

DATA AVAILABILITY STATEMENT

The original contributions presented in the study are included in the article/**Supplementary Material**, further inquiries can be directed to the corresponding author.

ETHICS STATEMENT

The studies involving human participants were reviewed and approved by the Ethics Committee in Medical Research of the First Affiliated Hospital of University of Science and Technology of China First Affiliated Hospital of University of Science and Technology of China. The patients/participants provided their written informed consent to participate in this study.

AUTHOR CONTRIBUTIONS

TL conceived the project, designed the research and drafted the manuscript. CC directed this research. TL and XX collected public data and specimens, analyzed, and tested. CC and YW revised the manuscript. All authors reviewed the manuscript.

FUNDING

This work was supported by the Fundamental Research Funds for the Central Universities (No. WK9110000146).

SUPPLEMENTARY MATERIAL

The Supplementary Material for this article can be found online at: https://www.frontiersin.org/articles/10.3389/fgene.2022.847940/full#supplementary-material

REFERENCES

Cagnol, S., and Chambard, J.-C. (2010). ERK and Cell Death: Mechanisms of ERK-Induced Cell Death - Apoptosis, Autophagy and Senescence. *FEBS J.* 277 (1), 2–21. doi:10.1111/j.1742-4658.2009.07366.x

Chen, X., Kang, R., Kroemer, G., and Tang, D. (2021). Broadening Horizons: the Role of Ferroptosis in Cancer. Nature Reviews. *Nat. Rev. Clin. Oncol.* 18 (5), 280–296. doi:10.1038/s41571-020-00462-0

Chen, Z.-A., Tian, H., Yao, D.-M., Zhang, Y., Feng, Z.-J., and Yang, C.-J. (2021). Identification of a Ferroptosis-Related Signature Model Including mRNAs and lncRNAs for Predicting Prognosis and Immune Activity in Hepatocellular Carcinoma. *Front. Oncol.* 11, 738477. doi:10.3389/fonc.2021.738477

Chi, A. C., Day, T. A., and Neville, B. W. (2015). Oral Cavity and Oropharyngeal Squamous Cell Carcinoma-An Update. *CA: a Cancer J. clinicians* 65 (5), 401–421. doi:10.3322/caac.21293

Dixon, S. J., Lemberg, K. M., Lamprecht, M. R., Skouta, R., Zaitsev, E. M., Gleason, C. E., et al. (2012). Ferroptosis: an Iron-dependent Form of Nonapoptotic Cell Death. *Cell* 149 (5), 1060–1072. doi:10.1016/j.cell.2012.03.042

Fang, Z., Zhao, J., Xie, W., Sun, Q., Wang, H., and Qiao, B. (2017). LncRNA UCA1 Promotes Proliferation and Cisplatin Resistance of Oral Squamous Cell Carcinoma by Sunppressing miR-184 Expression. *Cancer Med.* 6 (12), 2897–2908. doi:10.1002/cam4.1253

Fukuda, M., Ogasawara, Y., Hayashi, H., Okuyama, A., Shiono, J., Inoue, K., et al. (2021). Down-regulation of Glutathione Peroxidase 4 in Oral Cancer Inhibits Tumor Growth through SREBP1 Signaling. *Anticancer Res.* 41 (4), 1785–1792. doi:10.21873/anticanres.14944

Gao, N., Li, Y., Li, J., Gao, Z., Yang, Z., Li, Y., et al. (2020). Long Non-coding RNAs: The Regulatory Mechanisms, Research Strategies, and Future Directions in Cancers. *Front. Oncol.* 10, 598817. doi:10.3389/fonc.2020.598817

Huang, X., Gao, Y., Qin, J., and Lu, S. (2018). lncRNA MIAT Promotes Proliferation and Invasion of HCC Cells via Sponging miR-214. *Am. J. Physiology-Gastrointestinal Liver Physiol.* 314 (5), G559–G565. doi:10.1152/ajpgi.00242.2017

Jiang, Q., Xue, D., Shi, F., and Qiu, J. (2021). Prognostic Significance of an Autophagy-Related Long Non-coding RNA Signature in Patients with Oral and Oropharyngeal Squamous Cell Carcinoma. *Oncol. Lett.* 21 (1), 29. doi:10.3892/ol.2020.12290

Jin, Y., Wang, Z., He, D., Zhu, Y., Gong, L., Xiao, M., et al. (2021). Analysis of Ferroptosis-Mediated Modification Patterns and Tumor Immune Microenvironment Characterization in Uveal Melanoma. *Front. Cell Dev. Biol.* 9, 685120. doi:10.3389/fcell.2021.685120

Jing, Y., Jiang, X., Lei, L., Peng, M., Ren, J., Xiao, Q., et al. (2021). Mutant NPM1-Regulated lncRNA HOTAIRM1 Promotes Leukemia Cell Autophagy and Proliferation by Targeting EGR1 and ULK3. *J. Exp. Clin. Cancer Res.* 40 (1), 312. doi:10.1186/s13046-021-02122-2

Kopp, F., and Mendell, J. T. (2018). Functional Classification and Experimental Dissection of Long Noncoding RNAs. *Cell* 172 (3), 393–407. doi:10.1016/j.cell.2018.01.011

Kurihara-Shimomura, M., Sasahira, T., Shimomura, H., and Kirita, T. (2020). Peroxidan Plays a Tumor-Promoting Role in Oral Squamous Cell Carcinoma. *Ijms* 21 (15), 5416. doi:10.3390/ijms21155416

Lee, S. Y., Ju, M. K., Jeon, H. M., Jeong, E. K., Lee, Y. J., Kim, C. H., et al. (2018). Regulation of Tumor Progression by Programmed Necrosis. *Oxid Med. Cell Longev* 2018, 3537471. doi:10.1155/2018/3537471

Li, H., Liu, L., Huang, T., Jin, M., Zheng, Z., Zhang, H., et al. (2021). Establishment of a Novel Ferroptosis-Related lncRNA Pair Prognostic Model in colon Adenocarcinoma. *Aging* 13 (19), 23072–23095. doi:10.18632/aging.203599

Li, Y., Jiang, T., Zhou, W., Li, J., Li, X., Wang, Q., et al. (2020). Pan-cancer Characterization of Immune-Related lncRNAs Identifies Potential Oncogenic Biomarkers. *Nat. Commun.* 11 (1), 1000. doi:10.1038/s41467-020-14802-2

Li, Y., Zheng, J.-N., Wang, E.-H., Gong, C.-J., Lan, K.-F., and Ding, X. (2020). The m6A Reader Protein YTHDC2 Is a Potential Biomarker and Associated with Immune Infiltration in Head and Neck Squamous Cell Carcinoma. *PeerJ* 8, e10385. doi:10.7717/peerj.10385

Lu, L., Liu, L.-P., Zhao, Q.-Q., Gui, R., and Zhao, Q.-Y. (2021). Identification of a Ferroptosis-Related LncRNA Signature as a Novel Prognosis Model for Lung Adenocarcinoma. *Front. Oncol.* 11, 675545. doi:10.3389/fonc.2021.675545

Luan, T., Zhang, T. Y., Lv, Z. H., Guan, B. X., Xu, J. Y., Li, J., et al. (2021). The lncRNA ALMS1-IT1 May Promote Malignant Progression of Lung Adenocarcinoma via AVL9-mediated Activation of the Cyclin-dependent Kinase Pathway. *FEBS open bio* 11 (5), 1504–1515. doi:10.1002/2211-5463.13140

Park, Y. P., Jin, L., Bennett, K. B., Wang, D., Fredenburg, K. M., Tseng, J. E., et al. (2018). CD70 as a Target for Chimeric Antigen Receptor T Cells in Head and Neck Squamous Cell Carcinoma. *Oral Oncol.* 78, 145–150. doi:10.1016/j.oraloncology.2018.01.024

Roh, J.-L., Kim, E. H., Jang, H. J., Park, J. Y., and Shin, D. (2016). Induction of Ferroptotic Cell Death for Overcoming Cisplatin Resistance of Head and Neck Cancer. *Cancer Lett.* 381 (1), 96–103. doi:10.1016/j.canlet.2016.07.035

Sung, H., Ferlay, J., Siegel, R. L., Laversanne, M., Soerjomataram, I., Jemal, A., et al. (2021). Global Cancer Statistics 2020: GLOBOCAN Estimates of Incidence and Mortality Worldwide for 36 Cancers in 185 Countries. *CA A. Cancer J. Clin.* 71 (3), 209–249. doi:10.3322/caac.21660

Wang, C., Li, Y., Jia, L., Kim, J. K., Li, J., Deng, P., et al. (2021). CD276 Expression Enables Squamous Cell Carcinoma Stem Cells to Evade Immune Surveillance. *Cell stem cell* 28 (9), 1597–1613. doi:10.1016/j.stem.2021.04.011

Wang, R., Zhao, L., Ji, L., Bai, L., and Wen, Q. (2019). Myocardial Infarction Associated Transcript (MIAT) Promotes Papillary Thyroid Cancer Progression via Sponging miR-212. *Biomed. Pharmacother.* 118, 109298. doi:10.1016/j.biopha.2019.109298

Wang, X., Li, H., and Shi, J. (2019). LncRNA HOXA11-AS Promotes Proliferation and Cisplatin Resistance of Oral Squamous Cell Carcinoma by Suppression of miR-214-3p Expression. *Biomed. Res. Int.* 2019, 8645153. doi:10.1155/2019/8645153

Xing, L., Zhang, X., and Chen, A. (2019). Prognostic 4-lncRNA-Based Risk Model Predicts Survival Time of Patients with Head and Neck Squamous Cell Carcinoma. *Oncol. Lett.* 18 (3), 3304–3316. doi:10.3892/ol.2019.10670

Yang, Y., Chen, D., Liu, H., and Yang, K. (2019). Increased Expression of lncRNA CASC9 Promotes Tumor Progression by Suppressing Autophagy-Mediated Cell Apoptosis via the AKT/mTOR Pathway in Oral Squamous Cell Carcinoma. *Cell Death Dis* 10 (2), 41. doi:10.1038/s41419-018-1280-8

Zhang, C., Xie, L., Liang, H., and Cui, Y. (2019). LncRNA MIAT Facilitates Osteosarcoma Progression by Regulating Mir-128-3p/VEGFC axis. *IUBMB life* 71 (7), 845–853. doi:10.1002/iub.2001

Zhang, Y., Mi, L., Xuan, Y., Gao, C., Wang, Y. H., Ming, H. X., et al. (2018). LncRNA HOTAIRM1 Inhibits the Progression of Hepatocellular Carcinoma by Inhibiting the Wnt Signaling Pathway. *Eur. Rev. Med. Pharmacol. Sci.* 22 (15), 4861–4868. doi:10.26355/eurrev_201808_15622

Zhou, R.-S., Zhang, E.-X., Sun, Q.-F., Ye, Z.-J., Liu, J.-W., Zhou, D.-H., et al. (2019). Integrated Analysis of lncRNA-miRNA-mRNA ceRNA Network in Squamous Cell Carcinoma of Tongue. *BMC cancer* 19 (1), 779. doi:10.1186/s12885-019-5983-8

Conflict of Interest: The authors declare that the research was conducted in the absence of any commercial or financial relationships that could be construed as a potential conflict of interest.

Publisher's Note: All claims expressed in this article are solely those of the authors and do not necessarily represent those of their affiliated organizations, or those of the publisher, the editors, and the reviewers. Any product that may be evaluated in this article, or claim that may be made by its manufacturer, is not guaranteed or endorsed by the publisher.

frontiers in Cell and Developmental Biology

REVIEW
published: 03 March 2022
doi: 10.3389/fcell.2022.845232

The Role of Ferroptosis in the Treatment and Drug Resistance of Hepatocellular Carcinoma

Siqi Zhao†, Wubin Zheng†, Chao Yu†, Gaoxin Xu, Xinyi Zhang, Chao Pan, Yongheng Feng, Kunxing Yang, Jin Zhou* and Yong Ma**

Department of General Surgery, Nanjing First Hospital, Nanjing Medical University, Nanjing, China

OPEN ACCESS

Edited by:
Lian Xiang Luo, Guangdong Medical University, China

Reviewed by:
Liang He, University of California, San Francisco, United States
Xiang Wang, National Institute of Arthritis and Musculoskeletal and Skin Diseases (NIH), United States
Yixuan Guo, The University of Utah, United States

***Correspondence:**
Kunxing Yang
2472701653@qq.com
Jin Zhou
georgenjmu@163.com
Yong Ma
yma0917@163.com

†These authors have contributed equally to this work and share first authorship

Specialty section:
This article was submitted to Cell Death and Survival, a section of the journal Frontiers in Cell and Developmental Biology

Received: *05 January 2022*
Accepted: *04 February 2022*
Published: *03 March 2022*

Citation:
Zhao S, Zheng W, Yu C, Xu G, Zhang X, Pan C, Feng Y, Yang K, Zhou J and Ma Y (2022) The Role of Ferroptosis in the Treatment and Drug Resistance of Hepatocellular Carcinoma. Front. Cell Dev. Biol. 10:845232. doi: 10.3389/fcell.2022.845232

Cell death is a fundamental feature of multicellular organisms' development and a key driver of degenerative diseases. Ferroptosis is a new regulatory cell death mediated by iron-dependent lipid peroxidation, which is different from apoptosis and necrosis in morphology, pathophysiology and mechanism. Recent studies have found that ferroptosis is involved in the development of many diseases including hepatocellular carcinoma (HCC). As further research progresses, specific mechanisms of ferroptosis in HCC are being revealed. In this review, we summarize these recent advances about the treatment of drug-resistance in HCC and the latest ferroptosis-related treatment for HCC.

Keywords: ferroptosis, drug resistance, treatment, hepatocellular carcinoma, regulatory cell death

INTRODUCTION

HCC is an invasive cancer prevalent worldwide, with a mortality rate ranked second among all the cancers, which was just behind lung cancer and colon cancer (Bray et al., 2018). The 5-years survival rate of HCC patients is less than 10%, and the average life expectancy is only 6 months for those patients who were not eligible for surgery. And the existing treatments, including radiofrequency therapy, radiotherapy therapy, and chemotherapy, do not significantly improve the prognosis of HCC patients. Currently, in terms of HCC chemotherapy, the US Food and Drug Administration (FDA) has approved a variety of small molecule multi-kinase inhibitors, such as sorafenib, for the treatment of advanced HCC (Boland and WU, 2018). However, the therapeutic effect of most patients is still limited due to the frequent drug resistance of those inhibitors. Therefore, different modulation strategies and administration routes have been proposed to enhance the antitumor activity of these agents.

Dixon identified an iron-dependent form of cell death in 2012 and defined this modality as ferroptosis. It is now considered that ferroptosis is triggered by both exogenous and endogenous pathways, either by inhibition of cell membrane transporters (cystine/glutamate transporter system) or by activation of iron transporters, serum transferrin, and lactoferrin. Endogenous pathways are activated by blocking intracellular antioxidant enzymes such as glutathione peroxidase 4 (GPX4) (Tang and KROEMER, 2020). Unlike other known modes of cell death, such as apoptosis, necrosis, and autophagy, ferroptosis has unique morphological, biochemical, and genetic characteristics, such as mitochondrial atrophy, increased membrane density, iron, and ROS accumulation.

Recent studies have found that ferroptosis is involved in the proliferation, invasion, and migration of HCC cells, and is also closely related to drug-resistance in HCC, of which the specific mechanism is being gradually revealed.

TABLE 1 | The regulators of ferroptosis in HCC.

Gene/Axis/Compound/Drug	Mechanism	Target	Influence to ferroptosis	References
Ubiquitin-like Modifier Enzyme 1 (UBA1)	Inhibit NRF2 expression by inhibiting of UBA1	NRF2	-	Shan et al. (2020)
Disulfiram (DSF)	DSF inhibits the signaling pathways of NRF2 and MAPK kinase	NRF2	+	Ren et al. (20211021)
p62	p62 can down-regulate Keap1 expression and reduce NRF2 degradation	Keap1	-	Sun et al. (2016a)
Xanthine Oxidoreductase (XOR)	XOR can down-regulate NRF2 expression	Keap1	+	Sun et al. (2020)
Tripartite motif-containing 25 (TRIM25)	TRIM25 can activate NRF2	Keap1	-	Liu et al. (2020)
Malic enzymes (ME)	Transcriptionally activating ME1 by NRF2 when cells encounter further episodes of ROS insult	induced by NRF2		Lee et al. (2021)
Sigma-1 receptor (S1R)	S1R can regulate NRF2 thus inhibiting ROS accumulation	NRF2	-	Bai et al. (2019)
Catenin beta-1 (CTNNB1)	CTNNB1 may have synergistic effect with NRF2 mutation	NRF2	Unknown	Zavattari et al. (2015); Tao et al. (2021)
miR-101 (miRNA)	Target the 3′-UTR of NRF2 and negatively regulate NRF2	NRF2	+	Gao et al. (2017); Raghunath et al. (2018)
miR-144 (miRNA)	Activation of Nrf2	NRF2	-	Raghunath et al. (2018)
miR-340 (miRNA)	Target at the 3′-UTR of NRF2 and negatively regulate NRF2	NRF2	+	Shi et al. (2014); Raghunath et al., 2018)
miR-122 (miRNA)	Inhibited by NRF2	Inhibited by NRF2	Unknown	Aydin et al. (2019)
miR-129-3p (miRNA)	Induced by NRF2	Induced by NRF2	Unknown	Sun et al. (2019)
miR-141 (miRNA)	Upregulate NRF2	Keap1	-	Raghunath et al. (2018)
miR-200a (miRNA)	Increase NRF2 and inhibit TFR1 expression	Keap1	-	Greene et al. (2013); Raghunath et al. (2018)
Kral (lncRNA)	Induce Keap1 to regulate NRF2	Keap1	+	Wu et al. (2018)
Glutathione S-transferase zeta 1 (GSTZ1)	Inhibit NRF2/GPX4 axis	NRF2	+	Wang et al. (2021a)
Quiescin sulfhydryl oxidase 1 (QSOX1)	Inhibit NRF2	NRF2	+	Sun et al. (2021)
miR-200b (miRNA)	Adjust ferritin heavy chain 1(FtH1) and ferritin light chain (FtL)	Ferritin	Unknown	Greene et al. (2013)
miR-122 (miRNA)	Reduce iron by adjusting Nocturnin	Nocturnin	Unknown	Zhang et al. (2020)
PVT1 (lncRNA)	Increase lipid peroxidation and iron deposition *in vivo* and *in vitro*	TFR1	+	Lu et al. (2020)
miR-152 (miRNA)	Inhibit TFR1 expression	TFR1	-	Kindrat et al. (2016)
miR-22 (miRNA)	Inhibit TFR1 expression	TFR1	-	Greene et al. (2013)
miR-320 (miRNA)	Inhibit TFR1 expression	TFR1	-	Greene et al. (2013)
miR-107 (miRNA)		Inhibited by iron		Zou et al. (2016)
miR-30d (miRNA)		Inhibited by iron		Zou et al. (2016)
Formosaanin C	Inducing ferritinophagy and lipid ROS formation	/	+	Lin et al. (2020)
CDGSH iron sulfur domain2 (CISD2)	Excessive iron ion accumulation	Fe	-	Li et al. (2021b)
O-GlcNAcylation	Increase the iron concentration through transcriptional elevation of TFRC	TRFC	+	Zhu et al. (2021)
Solasonine	Increase lipid ROS levels by suppression of GPX4 and GSS	GPX4	+	Jin et al. (2020)

(Continued on following page)

TABLE 1 | (*Continued*) The regulators of ferroptosis in HCC.

Gene/Axis/Compound/Drug	Mechanism	Target	Influence to ferroptosis	References
Heteronemin	Decrease GPX4 expression and induced the formation of ROS	GPX4	+	Chang et al. (2021)
Selenoproteins	Constitute GPX4	GPX4	-	Ingold et al. (2018)
Sigma-1 receptor (S1R)	Inhibit the expression of GPX4	GPX4	-	Bai et al. (2019)
Circ-interleukin-4 receptor (CircIL4R)	As a miR-541-3p sponge to regulate its target GPX4	GPX4	-	Xu et al. (2020)
Ketamine	Decrease expression of lncPVT1 (directly interacted with miR-214-3p to impede its role as a sponge of GPX4) and GPX4	GPX4	+	He et al. (2021)
Legumain	Promote chaperone-mediated autophagy of GPX4	GPX4	+	Chen et al. (2021)
vitamin D receptor (VDR)	Transregulation of GPX4	GPX4	-	Hu et al. (2020)
Ceruloplasmin (CP)	Accumulation of intracellular ferrous iron (Fe^{2+}) and lipid ROS	Fe	-	Shang et al. (2020)
miR-22 (miRNA)	Increase ROS	SIRT-1	+	Pant et al. (2017)
miR-92 (miRNA)	Increase ROS	unknown	+	Cardin et al. (2012)
miR-145 (miRNA)	Elimination of insulin-induced PKM2 and ROS elevation	PKM2	-	Li et al. (2014)
miR-222 (miRNA)	Unknown	ER (endoplasmic reticulum)	-	Dai et al. (2010)
Let-7 (miRNA)	Directly acts on the 3′-UTR of Bach1 and negatively regulates expression of this protein, and thereby up-regulates modulation of heme oxygenase 1 (HMOX1) gene expression	Heme oxygenase-1	-	Hou et al. (2012)
miR-221 (miRNA)	Unknown	ER	-	Dai et al. (2010)
miR-21 (miRNA)	Increase ROS	unknown	+	Shu et al. (2016)
miR-181 (miRNA)	Increase ROS	Unknown	+	Zhang et al. (2020)
miR-200a-3p (miRNA)	Inhibite p38/p53/miR-200 feedback loop and increased ROS	p53	+	Xiao et al. (2015)
miR-125b (miRNA)	Increase ROS	HK2	+	Li et al. (2017)
miR-26a (miRNA)	Regulate fatty acid and cholesterol homeostasis and decreasing ROS	Triglyceride, totalcholesterol, malondialdehyde	-	Ali et al. (2018)
miR-885-5p (miRNA)	Induce TIGAR (TP53-induced glycolysis and apoptosis regulator)expression through a p53-independent pathway and decreasing ROS	TIGAR	-	Zou et al. (2019)
miR-150-3p (miRNA)	Induced by ROS	/	/	Wan et al. (2017)
miR-1915-3p (miRNA)	Induced by ROS	/	/	Wan et al. (2017)
miR-34a-3p (miRNA)	Induced by ROS	/	/	Beccafico et al. (2015)
miR-34a-5p (miRNA)	Induced by ROS	/	/	Wan et al. (2017)
miR-638 (miRNA)	Induced by ROS	/	/	Wan et al. (2017)
H19 (ncRNA)	Decrease ROS	MAPK/ERK signaling pathway	-	Ding et al. (2018)
GABPB1-AS1 (lncRNA)	Downregulate the gene encoding Peroxiredoxin-5 (PRDX5) peroxidase and the eventual suppression of the cellular antioxidant capacity	/	+	Qi et al. (2019)
miR-18a (miRNA)	Downregulate the expression of Glutamate-Cysteine Ligase Subunit Catalytic (GCLC), the rate-limiting enzyme of GSH synthesis	GSH	+	Anderton et al. (2017)

(Continued on following page)

TABLE 1 | (*Continued*) The regulators of ferroptosis in HCC.

Gene/Axis/Compound/Drug	Mechanism	Target	Influence to ferroptosis	References
miR-152 (miRNA)	Reduce GSH levels by targeting Glutathione S-transferase	GSH	+	Huang et al. (2010)
miR-503 (miRNA)	Unknown	GSH	+	Wang et al. (2014)
Neat1 (lncRNA)	Increase GST to increase GSH consumption	GST	+	Wang et al. (2018)
Metallothionein-1G (MT-1G)	Induce depletion of GSH	GSH	-	Sun et al. (2016b)
Deleted in azoospermia-associated protein 1 (DAZAP1)	Interact with the 3′UTR (untranslated region) of SLC7A11 mRNA and positively regulate its stability	SLC7A11	-	Wang et al. (2021b)
Transforming growth factor β1 (TGF-β1)	Upregulate of Smad3 inhibits SLC7A11 expression	SLC7A11	+	Kim et al. (2020)
sulfasalazine	Inhibit SLC7A11	SLC7A11	+	Song et al. (2017)
Actinomycin D	Inhibit of SLC7A11 expression by inhibition of CD133 synthesis	SLC7A11	+	Song et al. (2017)
Circ0097009 (circRNA)	Regulate of SLC7A11 expression by expression of miR-1261	SLC7A11	-	Lyu et al. (2021)
METTL14	SLC7A11 mRNA was modified at 5′UTR and degraded	SLC7A11	+	Fan et al. (2021)
transcription factors YAP/TAZ	Induce the expression of SLC7A11	SLC7A11	-	Gao et al. (2021)
IFN-γ	Down-regulate the mRNA and protein levels of SLC3A2 and SLC7A11	SLC7A11	+	Kong et al. (2021)
activating transcription factor 3 (ATF3)	Bind to the SLC7A11 promoter and repressing SLC7A11 expression in a p53-independent manner	SLC7A11	+	Wang et al. (2020)
miR-182-5p and miR-378a-3p (miRNA)	Directly bind to the 3′UTR of GPX4 and SLC7A11 mRNA, downregulation of GPX4 and SLC7A11	GPX4, SLC7A11	+	Ding et al. (2020)
LINC00618 (lncRNA)	Increase the levels of lipid ROS and iron, decreasing the expression of SLC7A11	ROS,SLC7A11	+	Wang et al. (2021c)
microRNA-17-5p (miRNA)	Activate the p38 MAPK pathway, which in turn facilitates the phosphorylation of HSPB1	HSPB1	unknown	Yang et al. (2010)
heat shock protein beta-1 (HSPB1)	Reduce iron-mediated production of lipid ROS	ROS	-	Sun et al. (2015)
protein kinase p38α (Mapk14)	Decrease the expression of HSPB1 to reduce the accumulation of intracellular ROS	HSPB1	+	Sakurai et al. (2013)
dual specificity phosphatase 1 (DUSP1)	Inhibit the phosphorylation of P38 MAPK and HSPB1	HSPB1	+	Hao et al. (2015)
Astragalus	Directly down-regulate MT1G	MT1G	+	Liu et al. (2021b)
microRNA-205 and microRNA-211-5p (miRNA)	Target the 3′UTR of ACSL4 inhibits ACSL4 expression at mRNA and protein levels	ACSL4	-	Cui et al. (2014); Qin et al. (2020)
Lactic acid	Produce sterol regulatory element binding protein 1 (SREBP1) and downstream stearoyl-coA desaturase-1 (SCD1) to enhance the production of iron-resistant monounsaturated fatty acids (PUFA). SCD1 acts synergistically with acyl-CoA synthase 4 (ACSL4)	ACSL4,PUFA	-	Zhao et al. (2020)
NADPH-cytochrome P450 reductase (POR) and NADH-cytochrome b5 reductase (CYB5R1)	React with iron to generate reactive hydroxyl radicals for the peroxidation of the polyunsaturated fatty acid (PUFA) chains of membrane phospholipids, thereby disrupting membrane integrity	PUFA	+	Yan et al. (2021)
DJ-1/PARK7 (cancer-associated protein)	DJ-1 depletion inhibits the transsulfuration pathway by disrupting the formation of the S-adenosyl homocysteine hydrolase tetramer and impairing its activity	homocysteine	-	Cao et al. (2020)
hydroxycarboxylic acid receptor 1 (HCAR1)/monocarboxylate transporter 1 (MCT1)	Enhance the production of anti-ferroptosis monounsaturated fatty acids	MUFA	-	Zhao et al. (2020)

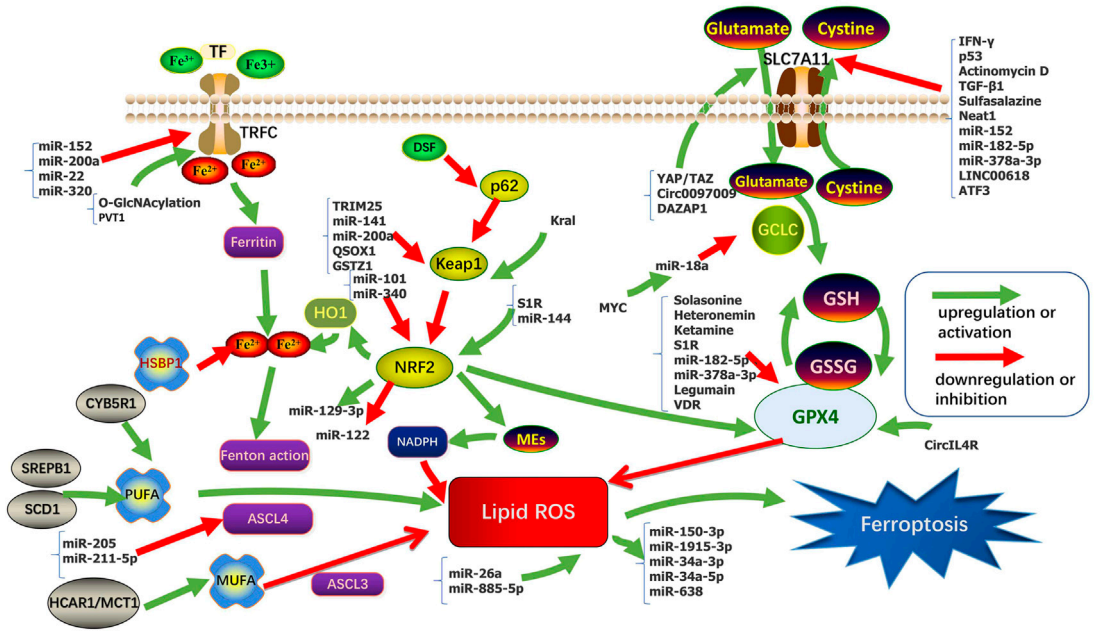

FIGURE 1 | Regulation pathways and key molecular mechanisms of ferroptosis in HCC.

REGULATION OF FERROPTOSIS IN HCC

Sensitivity to ferroptosis is closely related to many biological processes, such as (anti-)oxidant metabolism, iron metabolism, lipid metabolism, energy metabolism, and regulation of non-coding RNAs (ncRNAs). NcRNAs participate in the regulation of tumorigenesis *via* various biological processes such as chromatin modification, alternative splicing, competition with endogenous RNAs, and interaction with proteins. Intervention in these key links may regulate the sensitivity of HCC cells to ferroptosis. The regulation of ferroptosis found in HCC in recent years was sorted out in **Table 1** and **Figure 1**.

(Anti-)Oxidant Metabolism

(Anti-)oxidant Metabolism plays an important role in ferroptosis. Glutathione (GSH) metabolism and anti-oxidant capacity regulate sensitivity to ferroptosis. GSH is a tripeptide antioxidant that acts as a cofactor of Se-dependent GPX4 to reduce lipid hydroperoxides (Yant et al., 2003; Lu, 2009). Inhibition of cystine required for GSH synthesis eventually leads to depletion of intracellular GSH levels (Dixon et al., 2012; Dixon and STOCKWELL, 2014). GPX4 converts GSH between the reduced and oxidized states and converts lipid hydroperoxides to lipid alcohols. This process prevents the formation of Fe^{2+} dependent toxic lipid ROS (Labunskyy et al., 2014; Forcina and DIXON, 2019). GPX4 is the only reported enzyme that can directly reduce complex phospholipid peroxides and is the downstream target gene of NRF2 (Nuclear factor E2-related factor 2) (Forcina and DIXON, 2019; Friedmann Angeli et al., 2019). Erastin, a classical ferroptosis-inducing drug, depletes GSH and indirectly inactivates GPX4, leading to accumulation of toxic lipid ROS and subsequent lipid peroxidation (Dixon et al., 2012; Dixon and STOCKWELL, 2014), ultimately leading to ferroptosis.

At present, most studies on NRF2 in HCC involve the p62-Keap1 (Kelch-like ECH-associated protein 1)-NRF2 axis. The p62-Keap1-NRF2 signaling pathway is involved in the process of cell avoiding ferroptosis. NRF2 is a key regulator of the antioxidant response, including the expression of the Cystine/glutamate exchange system (system X^{C-}) (Hassannia et al., 2019). Inhibition or knockdown of NRF2 enhances erastin- or sorafenib-induced ferroptosis in HCC *in vitro* and *in vivo* (Hassannia et al., 2019). The System X^{C-} consists of solute carrier family 7 member 11 (SLC7A11, xCT) and solute carrier family 3 member 2 (SLC3A2, 4F2hc) by disulfide bonded, which import the extracellular oxidized form of cysteine and cystine, in exchange for intracellular glutamate. SLC7A11 indirectly inactivates GPX4 by reducing cysteine uptake, thereby limiting GSH synthesis, increasing lipid ROS, and ultimately leading to ferroptosis (Sato et al., 1999; Cao and DIXON, 2016). NRF2 has antioxidant elements and is regulated by Keap1. Its gene transcription is partially under the control of ROS. Sun et al. (2016a) found p62 expression prevents NRF2 degradation by Keap1 inactivation and enhances the subsequent nuclear accumulation of NRF2. They also demonstrate that NRF2-mediated anti-ferroptosis activity depends on the induction of NADPH (Reduced Nicotinamide Adenine Dinucleotide Phosphate) quinone oxidoreductase 1 (NQO1), heme oxygenase-1(HO-1), and ferritin heavy chain-1 (FTH1).

In morphology, ferroptosis mainly occurred in cells with reduced mitochondrial size, increased bilayer membrane density, and decreased or disappeared mitochondrial crest (Dixon et al., 2012; Yang and STOCKWELL, 2008; Yagoda et al., 2007). Mitochondria are the main source of ROS.

Excessive ROS can cause significant oxidative stress and lead to cell and tissue damage (Czaja et al., 2013). Gao et al. (2019) showed that ROS derived from mitochondria are involved in cysteine deprivation induced ferroptosis. Li et al. (2021) found depletes cysteine can enhance sorafenib-induced ferroptosis and lipid ROS production, and increase oxidative stress and mitochondrial ROS accumulation. And they point out that sorafenib exerts its anti-HCC function partly by targeting the mitochondrial function. Huang et al. (2021a) found the use of ZZW-115 (Nuclear protein 1 inhibitor) induced ferroptosis and subsequent mitochondrial morphological changes, including the disintegration of mitochondrial network and severe mitochondrial metabolic disorders, which were compatible with the process of ferroptosis, and this process can be complementary to TFAM (a core mitochondrial transcription factor) (Zhao, 2019).

Iron Metabolism

Iron is a redox-active metal that can participate in the formation of free radicals and the propagation of lipid peroxidation. Elevated iron levels increase susceptibility to ferroptosis. Iron overload or excessive activity of heme oxygenase 1 (HMOX1) increases the labile iron pool (LIP) that cause ferroptosis. Excessive iron increases ROS through Fenton reaction (through reaction with hydrogen peroxide (H_2O_2), ferrous iron (Fe^{2+}) is oxidized into trivalent iron (Fe^{3+}), forming highly active hydroxyl radical) (Hassannia et al., 2019), ROS is reversely neutralized by iron (Arefieva et al., 2021). Iron metabolism mainly involves the interaction between transferrin (TF) and its receptor (TFR), the input of iron through divalent metal transporter 1 (DMT1), the storage of iron as ferritin and iron-sulfur clusters (ISC), and the output of iron through iron transporter (FPN) (Abeyawardhane and LUCAS, 2019; Wang et al., 2019a).

The protection of the p62-Keap1-NRF2 signaling pathway on ferroptosis in HCC cells also involves the regulation of Fe homeostasis. An early study showed an increase in TFR1 and a decrease in ferritin (FTL and FTH1) expression in ferroptosis sensitive cells compared with iron-resistant cells (Yang and STOCKWELL, 2008). Sun et al. (2016a) showed that it was FTH1, not FTL or TFR1, that was regulated by NRF2 in ferroptosis. FTH1 inhibited ferroptosis by storing and transporting Fe^{2+} in HCC cells. In addition, excess iron in the liver may play a role in carcinogenesis by promoting tumor growth and altering the immune system (Kowdley, 2004). It is important to note that induction of ferroptosis in the liver may have different roles in tumorigenesis and cancer therapy.

Lipid Metabolism

Ferroptosis is iron-dependent regulatory necrosis induced by lipid peroxidation that occurs in cell membranes, a peroxidation reaction by polyunsaturated fatty acids catalyzed by the synthesis of acyl-CoA synthetase long-chain family member 4 (ACSL4) (Doll et al., 2017; Conrad and PRATT, 2019). Some polyunsaturated fatty acids (PUFAs) such as phosphatidylethanolamine (PE) and phosphatidylcholine (PC) are responsible for inducing ferroptosis by lipid peroxidation. Since *de novo* synthesis of PUFAs is strictly limited in mammals, various PUFAs are produced by the PUFAs biosynthesis pathway through the uptake of essential fatty acids from the blood and lymphatic fluid by cells. Free polyunsaturated fatty acids can be incorporated into cell membranes by various enzymes, such as ACLS4 and LPCAT3 (lysophosphatidylcholine acyltransferase 3), and lipid peroxidation can be induced by enzyme-induced and non-enzyme-induced mechanisms, resulting in ferroptosis (Lin et al., 2021). In this regard, knockdown of ACLS4, which preferably converts arachidonoyl (AA) to acylated AA, or loss of LPCAT3, which catalyzes the insertion of acylated AA into PLs (phospholipids), and make cells resistant to ferroptosis (Dixon et al., 2015; Yuan et al., 2016; Doll et al., 2017; Kagan et al., 2017). Magtanong et al. (2019) found that acyl-CoA synthetase long-chain family member 3 (ACSL3) converts monounsaturated fatty acids (MUFAs) into its acyl-CoA ester for incorporation into membrane phospholipids, thereby protecting cancer cells from ferroptosis. However, the levels of fatty acids (include MUFAs and PUFAs) in human serum are much higher than those in classical media containing fetal bovine serum (FBS), so how cells maintain the level of free fatty acid pools in cells is important to determine whether cells experience ferroptosis (Kamphorst et al., 2013; Magtanong et al., 2019).

Energy Metabolism

Cellular energy metabolism is directly related to ferroptosis because it regulates antioxidant defense by mediating the synthesis of biological macromolecules and biological reductants such as NADPH (Zheng and CONRAD, 2020). Tumor cells typically exhibit upregulated glycolysis and PPP (pentose phosphate pathway) activity, which not only reduces ROS production by inhibiting mitochondrial respiration but also replenishes NADPH supply, thereby helps maintaining redox homeostasis to ensure cell survival. In energy metabolism, previous studies have reported that Cytochrome P450 oxidoreductase (POR) is a key mediator of ferroptosis, which promotes ferroptosis through the peroxidation of saturated phospholipids in cell membranes (Zou et al., 2020). Glucose 6-phosphate dehydrogenase (G6PD) is a key enzyme in PPP and plays a key role in NADPH production (Yang et al., 2019). G6PD may negatively regulate ferroptosis in HCC by regulating POR (Cao et al., 2021). Lu et al. (2018) pointed out that G6PD induces epithelial-mesenchymal transition (EMT) by activating the Signal Transducers and Activators of Transcription 3(STAT3) pathway, thereby promoting migration and invasion of HCC. Therefore, it can be concluded that disruption of tumor energy metabolism pathway not only changes the sensitivity of mutant tumor cells to ferroptosis, but also reduces their antioxidant defense ability to promote ferroptosis, and even affects tumor migration and invasion.

Regulation of Ferroptosis by Non-Coding RNAs

According to length and shapes, ncRNAs are divided into various types including microRNAs (miRNAs), PIWI-interacting RNAs (piRNAs), small nuclear RNAs (snRNAs), small nucleolar RNAs

TABLE 2 | Common chemotherapeutic agents in HCC.

Chemotherapeutic agent	Mode of action	References
Sorafenib	Tyrosine-kinase inhibitor	Shaaban et al. (2014)
5-Flurouracil	Inhibition of thymidylate synthase	Longley et al. (2003)
Cisplatin	DNA damage	Shaaban et al. (2014)
Gemcitabine	Nucleotide analogue mis-incorporated into DNA	Heinemann et al. (1988); Mini et al. (2006)
Capecitabine	Inhibition of DNA synthesis	Walko and LINDLEY (2005)
Doxorubicin	Generation of free radicals and the intercalation into DNA	Gewirtz, (1999)
Epirubicin	Inhibitor of DNA topoisomerase II	Shaaban et al. (2014)
Lenvatinib	An inhibitor of VEGF receptors 1–3, FGF receptors 1–4, PDGF receptor α, RET, and KIT	Kudo et al. (2018)

TABLE 3 | The adjustment of hepatocellular cancer-related chemotherapy resistance.

Gene/Axis/Compound/Drug	Mechanism	Target	Influence to drug resistance	References
Aspirin	Silences of ACSL4 and induction of GADD45B expression	ACSL4	synergized with sorafenib	Xia et al. (2017)
GSTZ1	Inhibit NRF2/GPX4 axis	GPX4	synergized with sorafenib	Wang et al. (2021a)
QSOX1	Inhibit NRF2	NRF2	synergized with sorafenib	Wang et al. (2021a)
MT-1G	Knockout of MT-1G increases glutathione consumption and lipid peroxidation	MT-1G	synergized with sorafenib	Sun et al. (2016b)
Malic enzymes (MEs)	Produce NADPH and neutralizes ROS	NRF2	synergized with sorafenib	Lee et al. (2021)
Astragalus	Directly down-regulate MT-1G	MT-1G	synergized with sorafenib	Liu et al. (2021b)
Secreted protein acidic and rich in cysteine (SPARC)	LDH release and ROS accumulation	ROS	synergized with sorafenib	Hua et al. (2021)
Artesunate	Degradation of ferritin, lipid peroxidation	lysosomal	synergized with sorafenib	Li et al. (2021c)
disulfiram/copper	Inhibit NRF2 and MAPK kinase signaling pathways	NRF2	synergized with sorafenib	Ren et al. (20211021)
Haloperidol	Antagonize sigma receptor 1	S1R	synergized with sorafenib	Bai et al. (2017)
CISD2	Excessive iron ion accumulation	FE	synergized with sorafenib	Li et al. (2021b)
Transcription factors YAP/TAZ	Induce SLC7A11 expression	SLC7A11	Antagonism with sorafenib	Gao et al. (2021)
Apoptosis-inducing factor mitochondria-associated 2 (AIFM2)	Activation of membrane repair mechanisms that regulate membrane germination and fission	unknown	Antagonism with sorafenib	Dai et al. (2020)
Sigma-1 receptor (S1R)	Inhibit the accumulation of ROS	NRF2	Antagonism with sorafenib	Bai et al. (2019)
DAZAP1	Interact with the 3′UTR (untranslated region) of SLC7A11 mRNA and positively regulated its stability	SLC7A11	Antagonism with sorafenib	Wang et al. (2021b)
Sulfasalazine	Inhibit SLC7A11	SLC7A11	associated with drug resistance of cisplatin, doxorubicin and sorafenib	Song et al. (2017)
miR-340 (miRNA)	Targetes NRF2	NRF2	synergized with cisplatin	Shi et al. (2014)
Apigenin	Inhibit Mir-101/Nrf2 pathway	NRF2	synergized with doxorubicin	Gao et al. (2017)
KRAL (lncRNA)	Induce Keap1 to regulation NRF2	NRF2	synergized with 5-Fluorouracil (5-FU)	Wu et al. (2018)
miR-144 (miRNA)	Targete NRF2	NRF2	synergized with 5-Fluorouracil (5-FU)	Zhou et al. (2016)
ATP-binding cassette C5 (ABCC5)	Stabilize SLC7A11 protein to increase intracellular GSH and attenuate lipid peroxidation accumulation	SLC7A11	Antagonism with sorafenib	Huang et al. (2021b)
Ungeremine	Increase ROS production	ROS	related	Mbaveng et al. (2019)
XCanthine oxidoreductase (XOR)	NRF2 degradation	NRF2	related	Sun et al. (2020)

(snoRNAs), long ncRNAs (lncRNAs), circular RNAs (circRNAs), transfer RNAs (tRNAs), and ribosomal RNAs (rRNAs) (Wang et al., 2019b; Alzhrani et al., 2020). MiRNAs exhibit functions by binding to the 3′-untranslated regions of target mRNAs and suppressing their expression (Majidinia et al., 2020). MiRNA can regulate ferroptosis and control cancer progression by regulating GSH, iron levels, NRF2, and ROS. LncRNAs mainly act as the regulatory factors of transcription factors in the nucleus or as miRNAs of sponges in the cytoplasm to regulate ferroptosis (Wu et al., 2020). However, there were few studies on the relationship between ferroptosis and circRNA, tRNA, rRNA, piRNA, snRNA, and snoRNA. Studies have reported that the tRNA mutations in HCC leads to decreased expression of selenoproteins, except for GPX4 and GPX1 (glutathione peroxidase 1), and introduces some weak changes in ferroptosis (Kipp et al., 2013; Becker et al., 2014; De Spirt et al., 2016). The regulation of ferroptosis found in HCC about ncRNAs in recent years was sorted out in **Table 1** and **Figure 1**. Wider and deeper studies are needed to explore the function of ncRNAs in ferroptosis.

TREATMENT OF FERROPTOSIS IN HCC

Ferroptosis Associated With Chemotherapy Resistance in HCC

Although the treatments have become more diversified in recent years, the average life expectancy of HCC was lagged far behind those of other cancers. The result of systemic chemotherapy has been particularly disappointing, not only because of the chemotherapeutic resistance of HCC, but also the severe results of major side effects, making the treatment of advanced HCC depends on the degree of underlying liver dysfunction, the burden of malignancy, and the patient's general profile or expectations. Treatment options for advanced HCC are limited comparing to early HCC. In this context, several therapeutic agents have been developed over the past 50 years to provide better responses and improve the average life expectancy in patients with HCC. Some common chemotherapeutic agents in HCC are summarized in **Table 2**. However, In two randomized clinical trials of advanced HCC patients in stage III, Sorafenib, which is a commonly used chemotherapy drug, only increased overall survival by 2.8 and 2.3 months compared to the placebo, suggested limited effect to drug-resistant HCC in advanced HCC (Llovet et al., 2008; Cheng et al., 2009). Therefore, overcome the resistance of sorafenib and find more effective new drugs has become an urgency for advanced HCC patients and postoperative adjuvant chemotherapy patients. Different regulatory strategies and delivery routes have been proposed to enhance the antitumor activity of these drugs (Kodama et al., 2008; Hung et al., 2012; Li et al., 2013; Song et al., 2013). Although some ferroptosis inducers, for example, Erastin, are very effective in killing cancer cells *in vitro*, their pharmacokinetic properties, such as solubility and metabolic stability, are not suitable for the usage *in vivo* (Yang et al., 2014). It is now believed that sorafenib can induce a new type of regulated cell death-ferroptosis (Louandre et al., 2013), distinct from apoptosis, necrosis, and autophagy (Dixon et al., 2012), not only sorafenib, Guo et al. (2018) killed a variety of tumor cells with cisplatin, which can simultaneously cause apoptosis and ferroptosis. Wu et al. (2018) found that some ncRNAs affect the sensitivity of 5-Fu-resistant cells by regulating some key steps of ferroptosis.

In recent years, the adjustment of HCC-related chemotherapy resistance is shown in **Table 3**.

Ferroptosis Associated With Radiotherapy Tolerance in HCC

Radiation therapy is an important non-surgical treatment for cancer, but the clinical problems such as low efficacy and severe side effects remained unsolved. Gene therapy can synergistically increase the effect of radiation therapy through its antitumor mechanisms, which may reduce the dose. Radiotherapy induces ferroptosis by down-regulation of SLC7A11 and up-regulation of ACSL4, resulting in GSH production, increasing lipid synthesis, and subsequent oxidative damage (Lang et al., 2019; Lei et al., 2020). Studies have found that collectrin (CLTRN), as a target of radiation, is regulated by NRF1 (nuclear respiratory factor 1)/RAN (RAS oncogene family)/DLD (dihydrolipoamide dehydrogenase) protein complex and enhances the radiosensitivity of HCC cells through ferroptosis (Yuan et al., 2021). A combination of gene therapy and radiation therapy is one way forward, allowing the radiation doses to be reduced and the side effects to be reduced. It is worth considering whether the application of iron death inhibitors to non-tumor cells can increase their radiation tolerance to reduce the adverse effects of radiotherapy.

Ferroptosis Associated With Emerging Therapies in HCC

The use of nano drugs to induce ferroptosis will become a new anticancer strategy (Shen et al., 2018). More and more anticancer nano drugs have been approved by FDA, and the development of drugs with higher efficacy and safety will become an emerging road for future cancer treatment (Bobo et al., 2016). Tang et al. (2019) synthesized manganese-doped mesoporous silica nanoparticles (MMSNs) from manganese and silica. This reaction resulted in the inactivation of GPX4 and the increase of intracellular lipid peroxides through the consumption of intracellular GSH induced by the degradation of MMSNs. Ou et al. (2017) used natural omega-3 fatty acid docosahexaenoic acid (LDL-DHA) reconstructed into Low-density lipoprotein nanoparticles to selectively kill HCC cells. LDL-DHA induces ferroptosis by increasing tissue lipid hydroperoxide levels and inhibition of GPX4 expression. Tian et al. (2022) reported a novel cascade copper-based metal-organic framework (MOF) therapeutic nanocatalyst using HKUST-1 (a kind of metal organic framework) combining meloxicam (Mel), a cyclooxygenase-2 (COX-2) inhibitor, and sorafenib (Sol). Down-regulation of COX-2 induces PINK1/Parkin-mediated mitochondrial autophagy, chemodynamic Therapy (CDT) -mediated cytotoxic ROS, accumulated lipid peroxides (LPO) and Sol through inhibition system X^{C-}, the three interacted to

activate ferroptosis and increase the sensitivity of HCC cells to chemotherapy. Liu et al. (2021a) constructed mil-101 (Fe) nanoparticles (NPs) loaded with sorafenib and iRGD (iRGD peptide (amino acid sequence: CRGDK/RGPD/EC) [MIL-101 (Fe) @ SOR], which co-administration significantly promoted the development of ferroptosis. Ma et al. (2017) enhanced the sensitivity of cancer cells to cisplatin by loading cisplatin prodrug onto iron oxide nanoparticles to increase ROS production. Du et al. (2021) designed an exosome with three parts, including surface functionalization of CD47, membrane loading of ferroptosis inducer Er (Erastin), and core of photosensitizer RB (Rose Bengal), and demonstrated potent antitumor therapeutic effects with surprisingly low toxicity.

DISCUSSION

In this review, we summarize recent advances in potential regulators of ferroptosis in HCC and look into the ways ferroptosis can be used to create new therapies in the future. We demonstrate multiple advances in the drug resistance assessments in HCC treatment, the use of multiple genes or compounds to sensitize sorafenib, and the treatment of ferroptosis in HCC in some emerging areas, Nanoparticles such as MMSNs and LDL-DHA prepared in the tumor microenvironment and engineered exosomes with ferroptosis inducers are utilized to induce ferroptosis to bring better prognosis for patients.

The combination of ferroptosis with other therapies, such as immunotherapies, is also promising. Recently, it has been reported that anti-PD-L1 (programmed cell death-Ligand 1) immune checkpoint blockade can induce cancer cell ferroptosis responses by down-regulating SLC7A11 expression in cancer cells as a result of IFN-γ (Interferon γ) secreted by $CD8^+$ T cells (Wang et al., 2019c). Therefore, we believe that therapeutic expansion in ferroptosis may realize effective treatment for patients with advanced HCC.

There are still some issues to be resolved: Although lipid peroxidation is an important factor affecting ferroptosis, what is the actual mechanism of ferroptosis downstream of phospholipid peroxidation? There are many mechanisms of ferroptosis, and many metabolic factors affect the death of tumor cells, the formation of drug resistance, and the avoidance of immune-induced metastasis. It is still unknown that which metabolic factor plays a more important decisive role. *In vivo* pharmacokinetics of some ferroptosis inducers are still not suitable for *in vivo* usage, especially how ferroptosis drugs work in liver-specific biotransformation in the treatment of HCC. The fatty acid pool of cells affects the progress of ferroptosis in cells, how to use the change of fatty acid in the blood to determine the progress of ferroptosis in cells? and how to create a fatty acid microenvironment that is conducive to killing tumor cells in the liver?

AUTHOR CONTRIBUTIONS

SZ reviewed articles, collected data, and wrote the main manuscript text. WZ conceived and designed this study. CY and GX made the chart and figure. XZ, YF, and CP critically analyzed the data and gave valuable advice. KY, JZ, and YM critically revised it for important intellectual content. All authors contributed to the article and approved the submitted version.

FUNDING

This research was supported by Jiangsu Natural Science Foundation (SBK2019021253).

REFERENCES

Abeyawardhane, D. L., and Lucas, H. R. (2019). Iron Redox Chemistry and Implications in the Parkinson's Disease Brain [J]. *Oxid Med. Cel Longev* 2019, 4609702. doi:10.1155/2019/4609702

Ali, O., Darwish, H. A., Eldeib, K. M., and Abdel Azim, S. A. (2018). miR-26a Potentially Contributes to the Regulation of Fatty Acid and Sterol Metabolism *In Vitro* Human HepG2 Cell Model of Nonalcoholic Fatty Liver Disease. *Oxid Med. Cel Longev* 2018, 8515343. doi:10.1155/2018/8515343

Alzhrani, R., Alsaab, H. O., Petrovici, A., Bhise, K., Vanamala, K., Sau, S., et al. (2020). Improving the Therapeutic Efficiency of Noncoding RNAs in Cancers Using Targeted Drug Delivery Systems. *Drug Discov. Today* 25 (4), 718–730. doi:10.1016/j.drudis.2019.11.006

Anderton, B., Camarda, R., Balakrishnan, S., Balakrishnan, A., Kohnz, R. A., Lim, L., et al. (2017). MYC -driven Inhibition of the Glutamate-cysteine Ligase Promotes Glutathione Depletion in Liver Cancer. *EMBO Rep.* 18 (4), 569–585. doi:10.15252/embr.201643068

Arefieva, O. D., Vasilyeva, M. S., Zemnukhova, L. A., and Timochkina, A. S. (2021). Heterogeneous Photo-Fenton Oxidation of Lignin of rice Husk Alkaline Hydrolysates Using Fe-Impregnated Silica Catalysts. *Environ. Tech.* 42 (14), 2220–2228. doi:10.1080/09593330.2019.1697376

Aydin, Y., Kurt, R., Song, K., Lin, D., Osman, H., Youngquist, B., et al. (2019). Hepatic Stress Response in HCV Infection Promotes STAT3-Mediated Inhibition of HNF4A-miR-122 Feedback Loop in Liver Fibrosis and Cancer Progression. *Cancers (Basel)* 11 (10). doi:10.3390/cancers11101407

Bai, T., Lei, P., Zhou, H., Liang, R., Zhu, R., Wang, W., et al. (2019). Sigma-1 Receptor Protects against Ferroptosis in Hepatocellular Carcinoma Cells. *J. Cel Mol Med* 23 (11), 7349–7359. doi:10.1111/jcmm.14594

Bai, T., Wang, S., Zhao, Y., Zhu, R., Wang, W., and Sun, Y. (2017). Haloperidol, a Sigma Receptor 1 Antagonist, Promotes Ferroptosis in Hepatocellular Carcinoma Cells. *Biochem. Biophysical Res. Commun.* 491 (4), 919–925. doi:10.1016/j.bbrc.2017.07.136

Beccafico, S., Morozzi, G., Marchetti, M. C., Riccardi, C., Sidoni, A., Donato, R., et al. (2015). Artesunate Induces ROS- and P38 MAPK-Mediated Apoptosis and Counteracts Tumor Growthin Vivoin Embryonal Rhabdomyosarcoma Cells. *Carcin* 36 (9), 1071–1083. doi:10.1093/carcin/bgv098

Becker, N.-P., Martitz, J., Renko, K., Stoedter, M., Hybsier, S., Cramer, T., et al. (2014). Hypoxia Reduces and Redirects Selenoprotein Biosynthesis. *Metallomics* 6 (5), 1079–1086. doi:10.1039/c4mt00004h

Bobo, D., Robinson, K. J., Islam, J., Thurecht, K. J., and Corrie, S. R. (2016). Nanoparticle-Based Medicines: A Review of FDA-Approved Materials and Clinical Trials to Date. *Pharm. Res.* 33 (10), 2373–2387. doi:10.1007/s11095-016-1958-5

Boland, P., and Wu, J. (2018). Systemic Therapy for Hepatocellular Carcinoma: beyond Sorafenib. *Chin. Clin. Oncol.* 7 (5), 50. doi:10.21037/cco.2018.10.10

Bray, F., Ferlay, J., Soerjomataram, I., Siegel, R. L., Torre, L. A., and Jemal, A. (2018). Global Cancer Statistics 2018: GLOBOCAN Estimates of Incidence and

Mortality Worldwide for 36 Cancers in 185 Countries. *CA: A Cancer J. Clinicians* 68 (6), 394–424. doi:10.3322/caac.21492

Cao, F., Luo, A., and Yang, C. (2021). G6PD Inhibits Ferroptosis in Hepatocellular Carcinoma by Targeting Cytochrome P450 Oxidoreductase. *Cell Signal.* 87, 110098. doi:10.1016/j.cellsig.2021.110098

Cao, J., Chen, X., Jiang, L., Lu, B., Yuan, M., Zhu, D., et al. (2020). DJ-1 Suppresses Ferroptosis through Preserving the Activity of S-Adenosyl Homocysteine Hydrolase. *Nat. Commun.* 11 (1), 1251. doi:10.1038/s41467-020-15109-y

Cao, J. Y., and Dixon, S. J. (2016). Mechanisms of Ferroptosis. *Cell Mol Life Sci* 73 (11-12), 2195–2209. doi:10.1007/s00018-016-2194-1

Cardin, R., Romilda, C., Piciocchi, M., Marika, P., Sinigaglia, A., Alessandro, S., et al. (2012). Oxidative DNA Damage Correlates with Cell Immortalization and Mir-92 Expression in Hepatocellular Carcinoma. *BMC Cancer* 12, 177. doi:10.1186/1471-2407-12-177

Chang, W. T., Bow, Y. D., Fu, P. J., Li, C. Y., Wu, C. Y., Chang, Y. H., et al. (2021). A Marine Terpenoid, Heteronemin, Induces Both the Apoptosis and Ferroptosis of Hepatocellular Carcinoma Cells and Involves the ROS and MAPK Pathways. *Oxid Med. Cel Longev* 2021, 7689045. doi:10.1155/2021/7689045

Chen, C. a., Wang, D., Yu, Y., Zhao, T., Min, N., Wu, Y., et al. (2021). Legumain Promotes Tubular Ferroptosis by Facilitating Chaperone-Mediated Autophagy of GPX4 in AKI. *Cell Death Dis* 12 (1), 65. doi:10.1038/s41419-020-03362-4

Cheng, A.-L., Kang, Y.-K., Chen, Z., Tsao, C.-J., Qin, S., Kim, J. S., et al. (2009). Efficacy and Safety of Sorafenib in Patients in the Asia-Pacific Region with Advanced Hepatocellular Carcinoma: a Phase III Randomised, Double-Blind, Placebo-Controlled Trial. *Lancet Oncol.* 10 (1), 25–34. doi:10.1016/s1470-2045(08)70285-7

Conrad, M., and Pratt, D. A. (2019). The Chemical Basis of Ferroptosis. *Nat. Chem. Biol.* 15 (12), 1137–1147. doi:10.1038/s41589-019-0408-1

Cui, M., Xiao, Z., Sun, B., Wang, Y., Zheng, M., Ye, L., et al. (2014). Involvement of Cholesterol in Hepatitis B Virus X Protein-Induced Abnormal Lipid Metabolism of Hepatoma Cells via Up-Regulating miR-205-Targeted ACSL4. *Biochem. Biophysical Res. Commun.* 445 (3), 651–655. doi:10.1016/j.bbrc.2014.02.068

Czaja, M. J., Ding, W.-X., Donohue, T. M., Friedman, S. L., Kim, J.-S., Komatsu, M., et al. (2013). Functions of Autophagy in normal and Diseased Liver. *Autophagy* 9 (8), 1131–1158. doi:10.4161/auto.25063

Dai, E., Zhang, W., Cong, D., Kang, R., Wang, J., and Tang, D. (2020). AIFM2 Blocks Ferroptosis Independent of Ubiquinol Metabolism. *Biochem. Biophysical Res. Commun.* 523 (4), 966–971. doi:10.1016/j.bbrc.2020.01.066

Dai, R., Li, J., Liu, Y., Yan, D., Chen, S., Duan, C., et al. (2010). miR-221/222 Suppression Protects against Endoplasmic Reticulum Stress-Induced Apoptosis via p27(Kip1)- and MEK/ERK-mediated Cell Cycle Regulation. *Biol. Chem.* 391 (7), 791–801. doi:10.1515/BC.2010.072

De Spirt, S., Eckers, A., Wehrend, C., Micoogullari, M., Sies, H., Stahl, W., et al. (2016). Interplay between the Chalcone Cardamonin and Selenium in the Biosynthesis of Nrf2-Regulated Antioxidant Enzymes in Intestinal Caco-2 Cells. *Free Radic. Biol. Med.* 91, 164–171. doi:10.1016/j.freeradbiomed.2015.12.011

Ding, C., Ding, X., Zheng, J., Wang, B., Li, Y., Xiang, H., et al. (2020). miR-182-5p and miR-378a-3p Regulate Ferroptosis in I/R-induced Renal Injury. *Cel Death Dis* 11 (10), 929. doi:10.1038/s41419-020-03135-z

Ding, K., Liao, Y., Gong, D., Zhao, X., and Ji, W. (2018). Effect of Long Non-coding RNA H19 on Oxidative Stress and Chemotherapy Resistance of CD133+ Cancer Stem Cells via the MAPK/ERK Signaling Pathway in Hepatocellular Carcinoma. *Biochem. Biophysical Res. Commun.* 502 (2), 194–201. doi:10.1016/j.bbrc.2018.05.143

Dixon, S. J., Lemberg, K. M., Lamprecht, M. R., Skouta, R., Zaitsev, E. M., Gleason, C. E., et al. (2012). Ferroptosis: An Iron-dependent Form of Nonapoptotic Cell Death. *Cell* 149 (5), 1060–1072. doi:10.1016/j.cell.2012.03.042

Dixon, S. J., and Stockwell, B. R. (2014). The Role of Iron and Reactive Oxygen Species in Cell Death. *Nat. Chem. Biol.* 10 (1), 9–17. doi:10.1038/nchembio.1416

Dixon, S. J., Winter, G. E., Musavi, L. S., Lee, E. D., Snijder, B., Rebsamen, M., et al. (2015). Human Haploid Cell Genetics Reveals Roles for Lipid Metabolism Genes in Nonapoptotic Cell Death. *ACS Chem. Biol.* 10 (7), 1604–1609. doi:10.1021/acschembio.5b00245

Doll, S., Proneth, B., Tyurina, Y. Y., Panzilius, E., Kobayashi, S., Ingold, I., et al. (2017). ACSL4 Dictates Ferroptosis Sensitivity by Shaping Cellular Lipid Composition. *Nat. Chem. Biol.* 13 (1), 91–98. doi:10.1038/nchembio.2239

Du, J., Wan, Z., Wang, C., Lu, F., Wei, M., Wang, D., et al. (2021). Designer Exosomes for Targeted and Efficient Ferroptosis Induction in Cancer via Chemo-Photodynamic Therapy. *Theranostics* 11 (17), 8185–8196. doi:10.7150/thno.59121

Fan, Z., Yang, G., Zhang, W., Liu, Q., Liu, G., Liu, P., et al. (2021). Hypoxia Blocks Ferroptosis of Hepatocellular Carcinoma via Suppression of METTL14 Triggered YTHDF2-dependent Silencing of SLC7A11. *J. Cell. Mol. Medi* 25 (21), 10197–10212. doi:10.1111/jcmm.16957

Forcina, G. C., and Dixon, S. J. (2019). GPX4 at the Crossroads of Lipid Homeostasis and Ferroptosis. *Proteomics* 19 (18), e1800311. doi:10.1002/pmic.201800311

Friedmann Angeli, J. P., Krysko, D. V., and Conrad, M. (2019). Ferroptosis at the Crossroads of Cancer-Acquired Drug Resistance and Immune Evasion. *Nat. Rev. Cancer* 19 (7), 405–414. doi:10.1038/s41568-019-0149-1

Gao, A.-M., Zhang, X.-Y., and Ke, Z.-P. (2017). Apigenin Sensitizes BEL-7402/ADM Cells to Doxorubicin through Inhibiting miR-101/Nrf2 Pathway. *Oncotarget* 8 (47), 82085–82091. doi:10.18632/oncotarget.18294

Gao, M., Yi, J., Zhu, J., Minikes, A. M., Monian, P., Thompson, C. B., et al. (2019). Role of Mitochondria in Ferroptosis. *Mol. Cel* 73 (2), 354–363. doi:10.1016/j.molcel.2018.10.042

Gao, R., Kalathur, R. K. R., Coto-Llerena, M., Ercan, C., Buechel, D., Shuang, S., et al. (2021). YAP/TAZ and ATF4 Drive Resistance to Sorafenib in Hepatocellular Carcinoma by Preventing Ferroptosis. *EMBO Mol. Med.* 13 (12), e14351. doi:10.15252/emmm.202114351

Gewirtz, D. (1999). A Critical Evaluation of the Mechanisms of Action Proposed for the Antitumor Effects of the Anthracycline Antibiotics Adriamycin and Daunorubicin. *Biochem. Pharmacol.* 57 (7), 727–741. doi:10.1016/s0006-2952(98)00307-4

Greene, C. M., Varley, R. B., and Lawless, M. W. (2013). MicroRNAs and Liver Cancer Associated with Iron Overload: Therapeutic Targets Unravelled. *Wjg* 19 (32), 5212–5226. doi:10.3748/wjg.v19.i32.5212

Guo, J., Xu, B., Han, Q., Zhou, H., Xia, Y., Gong, C., et al. (2018). Ferroptosis: A Novel Anti-tumor Action for Cisplatin. *Cancer Res. Treat.* 50 (2), 445–460. doi:10.4143/crt.2016.572

Hao, P.-P., Li, H., Lee, M.-J., Wang, Y.-P., Kim, J.-H., Yu, G.-R., et al. (2015). Disruption of a Regulatory Loop between DUSP1 and P53 Contributes to Hepatocellular Carcinoma Development and Progression. *J. Hepatol.* 62 (6), 1278–1286. doi:10.1016/j.jhep.2014.12.033

Hassannia, B., Vandenabeele, P., and Vanden Berghe, T. (2019). Targeting Ferroptosis to Iron Out Cancer. *Cancer Cell* 35 (6), 830–849. doi:10.1016/j.ccell.2019.04.002

He, G.-N., Bao, N.-R., Wang, S., XI, M., Zhang, T.-H., and Chen, F.-S. (2021). Ketamine Induces Ferroptosis of Liver Cancer Cells by Targeting lncRNA PVT1/miR-214-3p/GPX4. *Dddt* 15, 3965–3978. doi:10.2147/dddt.s332847

Heinemann, V., Hertel, L. W., Grindey, G. B., and Plunkett, W. (1988). Comparison of the Cellular Pharmacokinetics and Toxicity of 2',2'-difluorodeoxycytidine and 1-Beta-D-Arabinofuranosylcytosine. *Cancer Res.* 48 (14), 4024–4031.

Hou, W., Tian, Q., Steuerwald, N. M., Schrum, L. W., and Bonkovsky, H. L. (2012). The Let-7 microRNA Enhances Heme Oxygenase-1 by Suppressing Bach1 and Attenuates Oxidant Injury in Human Hepatocytes. *Biochim. Biophys. Acta* 1819 (11-12), 1113–1122. doi:10.1016/j.bbagrm.2012.06.001

Hu, Z., Zhang, H., Yi, B., Yang, S., Liu, J., Hu, J., et al. (2020). VDR Activation Attenuate Cisplatin Induced AKI by Inhibiting Ferroptosis. *Cel Death Dis* 11 (1), 73. doi:10.1038/s41419-020-2256-z

Hua, H. W., Jiang, H. S., Jia, L., Jia, Y. P., Yao, Y. L., Chen, Y. W., et al. (2021). SPARC Regulates Ferroptosis Induced by Sorafenib in Human Hepatocellular Carcinoma [J]. *Cancer Biomark* 32 (4), 425–433. doi:10.3233/CBM-200101

Huang, C., Santofimia-Castaño, P., Liu, X., Xia, Y., Peng, L., Gotorbe, C., et al. (2021). NUPR1 Inhibitor ZZW-115 Induces Ferroptosis in a Mitochondria-dependent Manner. *Cell Death Discov.* 7 (1), 269. doi:10.1038/s41420-021-00662-2

Huang, J., Wang, Y., Guo, Y., and Sun, S. (2010). Down-regulated microRNA-152 Induces Aberrant DNA Methylation in Hepatitis B Virus-Related

Hepatocellular Carcinoma by Targeting DNA Methyltransferase 1. *Hepatology* 52 (1), 60–70. doi:10.1002/hep.23660

Huang, W., Chen, K., Lu, Y., Zhang, D., Cheng, Y., Li, L., et al. (2021). ABCC5 Facilitates the Acquired Resistance of Sorafenib through the Inhibition of SLC7A11-Induced Ferroptosis in Hepatocellular Carcinoma. *Neoplasia* 23 (12), 1227–1239. doi:10.1016/j.neo.2021.11.002

Hung, C.-S., Lin, S.-F., Liu, H.-H., Kuo, L.-J., Li, L.-T., Su, H.-Y., et al. (2012). Survivin-mediated Therapeutic Efficacy of Gemcitabine through Glucose-Regulated Protein 78 in Hepatocellular Carcinoma. *Ann. Surg. Oncol.* 19 (8), 2744–2752. doi:10.1245/s10434-011-2188-z

Ingold, I., Berndt, C., Schmitt, S., Doll, S., Poschmann, G., Buday, K., et al. (2018). Selenium Utilization by GPX4 Is Required to Prevent Hydroperoxide-Induced Ferroptosis. *Cell* 172 (3), 409–422. doi:10.1016/j.cell.2017.11.048

Jin, M., Shi, C., Li, T., Wu, Y., Hu, C., and Huang, G. (2020). Solasonine Promotes Ferroptosis of Hepatoma Carcinoma Cells via Glutathione Peroxidase 4-induced Destruction of the Glutathione Redox System. *Biomed. Pharmacother.* 129, 110282. doi:10.1016/j.biopha.2020.110282

Kagan, V. E., Mao, G., Qu, F., Angeli, J. P. F., Doll, S., Croix, C. S., et al. (2017). Oxidized Arachidonic and Adrenic PEs Navigate Cells to Ferroptosis. *Nat. Chem. Biol.* 13 (1), 81–90. doi:10.1038/nchembio.2238

Kamphorst, J. J., Cross, J. R., Fan, J., De Stanchina, E., Mathew, R., White, E. P., et al. (2013). Hypoxic and Ras-Transformed Cells Support Growth by Scavenging Unsaturated Fatty Acids from Lysophospholipids. *Proc. Natl. Acad. Sci.* 110 (22), 8882–8887. doi:10.1073/pnas.1307237110

Kim, D. H., Kim, W. D., Kim, S. K., Moon, D. H., and Lee, S. J. (2020). TGF-β1-mediated Repression of SLC7A11 Drives Vulnerability to GPX4 Inhibition in Hepatocellular Carcinoma Cells. *Cel Death Dis* 11 (5), 406. doi:10.1038/s41419-020-2618-6

Kindrat, I., Tryndyak, V., De Conti, A., Shpyleva, S., Mudalige, T. K., Kobets, T., et al. (2016). MicroRNA-152-mediated Dysregulation of Hepatic Transferrin Receptor 1 in Liver Carcinogenesis. *Oncotarget* 7 (2), 1276–1287. doi:10.18632/oncotarget.6004

Kipp, A. P., Frombach, J., Deubel, S., and Brigelius-Flohé, R. (2013). Selenoprotein W as Biomarker for the Efficacy of Selenium Compounds to Act as Source for Selenoprotein Biosynthesis. *Methods Enzymol.* 527, 87–112. doi:10.1016/b978-0-12-405882-8.00005-2

Kodama, Y., Fumoto, S., Nishi, J., Nakashima, M., Sasaki, H., Nakamura, J., et al. (2008). Absorption and Distribution Characteristics of 5-Fluorouracil (5-FU) after an Application to the Liver Surface in Rats in Order to Reduce Systemic Side Effects. *Biol. Pharm. Bull.* 31 (5), 1049–1052. doi:10.1248/bpb.31.1049

Kong, R., Wang, N., Han, W., Bao, W., and Lu, J. (2021). Ifnγ-mediated Repression of System Xc − Drives Vulnerability to Induced Ferroptosis in Hepatocellular Carcinoma Cells. *J. Leukoc. Biol.* 110 (2), 301–314. doi:10.1002/jlb.3ma1220-815rrr

Kowdley, K. V. (2004). Iron, Hemochromatosis, and Hepatocellular Carcinoma. *Gastroenterology* 127 (5 Suppl. 1), S79–S86. doi:10.1016/j.gastro.2004.09.019

Kudo, M., Finn, R. S., Qin, S., Han, K.-H., Ikeda, K., Piscaglia, F., et al. (2018). Lenvatinib versus Sorafenib in First-Line Treatment of Patients with Unresectable Hepatocellular Carcinoma: a Randomised Phase 3 Non-inferiority Trial. *The Lancet* 391 (10126), 1163–1173. doi:10.1016/s0140-6736(18)30207-1

Labunskyy, V. M., Hatfield, D. L., and Gladyshev, V. N. (2014). Selenoproteins: Molecular Pathways and Physiological Roles. *Physiol. Rev.* 94 (3), 739–777. doi:10.1152/physrev.00039.2013

Lang, X., Green, M. D., Wang, W., Yu, J., Choi, J. E., Jiang, L., et al. (2019). Radiotherapy and Immunotherapy Promote Tumoral Lipid Oxidation and Ferroptosis via Synergistic Repression of SLC7A11. *Cancer Discov.* 9 (12), 1673–1685. doi:10.1158/2159-8290.cd-19-0338

Lee, D., Zhang, M. S., Tsang, F. H. C., Bao, M. H. R., Xu, I. M. J., Lai, R. K. H., et al. (2021). Adaptive and Constitutive Activations of Malic Enzymes Confer Liver Cancer Multilayered Protection against Reactive Oxygen Species. *Hepatology* 74 (2), 776–796. doi:10.1002/hep.31761

Lei, G., Zhang, Y., Koppula, P., Liu, X., Zhang, J., Lin, S. H., et al. (2020). The Role of Ferroptosis in Ionizing Radiation-Induced Cell Death and Tumor Suppression. *Cell Res* 30 (2), 146–162. doi:10.1038/s41422-019-0263-3

Li, B., Wei, S., Yang, L., Peng, X., Ma, Y., Wu, B., et al. (2021). CISD2 Promotes Resistance to Sorafenib-Induced Ferroptosis by Regulating Autophagy in Hepatocellular Carcinoma. *Front. Oncol.* 11, 657723. doi:10.3389/fonc.2021.657723

Li, Q., Liu, X., Yin, Y., Zheng, J. T., Jiang, C. F., Wang, J., et al. (2014). Insulin Regulates Glucose Consumption and Lactate Production through Reactive Oxygen Species and Pyruvate Kinase M2. *Oxid Med. Cel Longev* 2014, 504953. doi:10.1155/2014/504953

Li, T., Dong, Z.-R., Guo, Z.-Y., Wang, C.-H., Tang, Z.-Y., Qu, S.-F., et al. (2013). Aspirin Enhances IFN-α-Induced Growth Inhibition and Apoptosis of Hepatocellular Carcinoma via JAK1/STAT1 Pathway. *Cancer Gene Ther.* 20 (6), 366–374. doi:10.1038/cgt.2013.29

Li, W., Hao, J., Zhang, L., Cheng, Z., Deng, X., and Shu, G. (2017). Astragalin Reduces Hexokinase 2 through Increasing miR-125b to Inhibit the Proliferation of Hepatocellular Carcinoma Cells *In Vitro* and *In Vivo*. *J. Agric. Food Chem.* 65 (29), 5961–5972. doi:10.1021/acs.jafc.7b02120

Li, Y., Xia, J., Shao, F., Zhou, Y., Yu, J., Wu, H., et al. (2021). Sorafenib Induces Mitochondrial Dysfunction and Exhibits Synergistic Effect with Cysteine Depletion by Promoting HCC Cells Ferroptosis. *Biochem. Biophysical Res. Commun.* 534, 877–884. doi:10.1016/j.bbrc.2020.10.083

Li, Z.-j., Dai, H.-q., Huang, X.-w., Feng, J., Deng, J.-h., Wang, Z.-x., et al. (2021). Artesunate Synergizes with Sorafenib to Induce Ferroptosis in Hepatocellular Carcinoma. *Acta Pharmacol. Sin* 42 (2), 301–310. doi:10.1038/s41401-020-0478-3

Lin, P. L., Tang, H. H., Wu, S. Y., Shaw, N. S., and Su, C. L. (2020). Saponin Formosanin C-Induced Ferritinophagy and Ferroptosis in Human Hepatocellular Carcinoma Cells. *Antioxidants (Basel)* 9 (8). doi:10.3390/antiox9080682

Lin, Z., Liu, J., Kang, R., Yang, M., and Tang, D. (2021). Lipid Metabolism in Ferroptosis [J]. *Adv. Biol.* 5 (8), e2100396. doi:10.1002/adbi.202100396

Liu, X., Zhu, X., Qi, X., Meng, X., and Xu, K. (2021). Co-Administration of iRGD with Sorafenib-Loaded Iron-Based Metal-Organic Framework as a Targeted Ferroptosis Agent for Liver Cancer Therapy. *Ijn* 16, 1037–1050. doi:10.2147/ijn.s292528

Liu, Y., Tao, S., Liao, L., Li, Y., Li, H., Li, Z., et al. (2020). TRIM25 Promotes the Cell Survival and Growth of Hepatocellular Carcinoma through Targeting Keap1-Nrf2 Pathway. *Nat. Commun.* 11 (1), 348. doi:10.1038/s41467-019-14190-2

Liu, Z., Ma, H., and Lai, Z. (2021). Revealing the Potential Mechanism of Astragalus Membranaceus Improving Prognosis of Hepatocellular Carcinoma by Combining Transcriptomics and Network Pharmacology. *BMC Complement. Med. Ther.* 21 (1), 263. doi:10.1186/s12906-021-03425-9

Llovet, J. M., Ricci, S., Mazzaferro, V., Hilgard, P., Gane, E., Blanc, J.-F., et al. (2008). Sorafenib in Advanced Hepatocellular Carcinoma. *N. Engl. J. Med.* 359 (4), 378–390. doi:10.1056/nejmoa0708857

Longley, D. B., Latif, T., Boyer, J., Allen, W. L., Maxwell, P. J., and Johnston, P. G. (2003). The Interaction of Thymidylate Synthase Expression with P53-Regulated Signaling Pathways in Tumor Cells. *Semin. Oncol.* 30 (3 Suppl. 6), 3–9. doi:10.1016/s0093-7754(03)00119-2

Louandre, C., Ezzoukhry, Z., Godin, C., Barbare, J.-C., Mazière, J.-C., Chauffert, B., et al. (2013). Iron-dependent Cell Death of Hepatocellular Carcinoma Cells Exposed to Sorafenib. *Int. J. Cancer* 133 (7), 1732–1742. doi:10.1002/ijc.28159

Lu, J., Xu, F., and Lu, H. (2020). LncRNA PVT1 Regulates Ferroptosis through miR-214-Mediated TFR1 and P53. *Life Sci.* 260, 118305. doi:10.1016/j.lfs.2020.118305

Lu, M., Lu, L., Dong, Q., Yu, G., Chen, J., Qin, L., et al. (2018). Elevated G6PD Expression Contributes to Migration and Invasion of Hepatocellular Carcinoma Cells by Inducing Epithelial-Mesenchymal Transition. *Acta Biochim. Biophys. Sin (Shanghai)* 50 (4), 370–380. doi:10.1093/abbs/gmy009

Lu, S. C. (2009). Regulation of Glutathione Synthesis. *Mol. Aspects Med.* 30 (1-2), 42–59. doi:10.1016/j.mam.2008.05.005

Lyu, N., Zeng, Y., Kong, Y., Chen, Q., Deng, H., Ou, S., et al. (2021). Ferroptosis Is Involved in the Progression of Hepatocellular Carcinoma through the circ0097009/miR-1261/SLC7A11 axis. *Ann. Transl Med.* 9 (8), 675. doi:10.21037/atm-21-997

Ma, P. a., Xiao, H., Yu, C., Liu, J., Cheng, Z., Song, H., et al. (2017). Enhanced Cisplatin Chemotherapy by Iron Oxide Nanocarrier-Mediated Generation of Highly Toxic Reactive Oxygen Species. *Nano Lett.* 17 (2), 928–937. doi:10.1021/acs.nanolett.6b04269

Magtanong, L., Ko, P.-J., To, M., Cao, J. Y., Forcina, G. C., Tarangelo, A., et al. (2019). Exogenous Monounsaturated Fatty Acids Promote a Ferroptosis-

Resistant Cell State. *Cel Chem. Biol.* 26 (3), 420–432. doi:10.1016/j.chembiol.2018.11.016

Majidinia, M., Karimian, A., Alemi, F., Yousefi, B., and Safa, A. (2020). Targeting miRNAs by Polyphenols: Novel Therapeutic Strategy for Aging. *Biochem. Pharmacol.* 173, 113688. doi:10.1016/j.bcp.2019.113688

Mbaveng, A. T., Bitchagno, G. T. M., Kuete, V., Tane, P., and Efferth, T. (2019). Cytotoxicity of Ungeremine towards Multi-Factorial Drug Resistant Cancer Cells and Induction of Apoptosis, Ferroptosis, Necroptosis and Autophagy. *Phytomedicine* 60, 152832. doi:10.1016/j.phymed.2019.152832

Mini, E., Nobili, S., Caciagli, B., Landini, I., and Mazzei, T. (2006). Cellular Pharmacology of Gemcitabine. *Ann. Oncol.* 17 (Suppl. 5), v7–v12. doi:10.1093/annonc/mdj941

Ou, W., Mulik, R. S., Anwar, A., Mcdonald, J. G., He, X., and Corbin, I. R. (2017). Low-density Lipoprotein Docosahexaenoic Acid Nanoparticles Induce Ferroptotic Cell Death in Hepatocellular Carcinoma. *Free Radic. Biol. Med.* 112, 597–607. doi:10.1016/j.freeradbiomed.2017.09.002

Pant, K., Yadav, A. K., Gupta, P., Islam, R., Saraya, A., and Venugopal, S. K. (2017). Butyrate Induces ROS-Mediated Apoptosis by Modulating miR-22/SIRT-1 Pathway in Hepatic Cancer Cells. *Redox Biol.* 12, 340–349. doi:10.1016/j.redox.2017.03.006

Qi, W., Li, Z., Xia, L., Dai, J., Zhang, Q., Wu, C., et al. (2019). LncRNA GABPB1-AS1 and GABPB1 Regulate Oxidative Stress during Erastin-Induced Ferroptosis in HepG2 Hepatocellular Carcinoma Cells. *Sci. Rep.* 9 (1), 16185. doi:10.1038/s41598-019-52837-8

Qin, X., Zhang, J., Lin, Y., Sun, X.-m., Zhang, J.-n., and Cheng, Z.-q. (2020). Identification of MiR-211-5p as a Tumor Suppressor by Targeting ACSL4 in Hepatocellular Carcinoma. *J. Transl Med.* 18 (1), 326. doi:10.1186/s12967-020-02494-7

Raghunath, A., Sundarraj, K., Arfuso, F., Sethi, G., and Perumal, E. (2018). Dysregulation of Nrf2 in Hepatocellular Carcinoma: Role in Cancer Progression and Chemoresistance. *Cancers (Basel)* 10 (12). doi:10.3390/cancers10120481

Ren, X., Li, Y., Zhou, Y., Hu, W., Yang, C., Jing, Q., et al. (202110212). Overcoming the Compensatory Elevation of NRF2 Renders Hepatocellular Carcinoma Cells More Vulnerable to Disulfiram/copper-Induced Ferroptosis. *Redox Biol.* 46, 102122. doi:10.1016/j.redox.2021.102122

Sakurai, T., Kudo, M., Umemura, A., He, G., Elsharkawy, A. M., Seki, E., et al. (2013). p38α Inhibits Liver Fibrogenesis and Consequent Hepatocarcinogenesis by Curtailing Accumulation of Reactive Oxygen Species. *Cancer Res.* 73 (1), 215–224. doi:10.1158/0008-5472.can-12-1602

Sato, H., Tamba, M., Ishii, T., and Bannai, S. (1999). Cloning and Expression of a Plasma Membrane Cystine/Glutamate Exchange Transporter Composed of Two Distinct Proteins. *J. Biol. Chem.* 274 (17), 11455–11458. doi:10.1074/jbc.274.17.11455

Shaaban, S., Negm, A., Ibrahim, E. E., and Elrazak, A. A. (2014). Chemotherapeutic Agents for the Treatment of Hepatocellular Carcinoma: Efficacy and Mode of Action. *Oncol. Rev.* 8 (1), 246. doi:10.4081/oncol.2014.246

Shan, Y., Yang, G., Huang, H., Zhou, Y., Hu, X., Lu, Q., et al. (2020). Ubiquitin-Like Modifier Activating Enzyme 1 as a Novel Diagnostic and Prognostic Indicator that Correlates with Ferroptosis and the Malignant Phenotypes of Liver Cancer Cells. *Front. Oncol.* 10, 592413. doi:10.3389/fonc.2020.592413

Shang, Y., Luo, M., Yao, F., Wang, S., Yuan, Z., and Yang, Y. (2020). Ceruloplasmin Suppresses Ferroptosis by Regulating Iron Homeostasis in Hepatocellular Carcinoma Cells. *Cell Signal* 72, 109633. doi:10.1016/j.cellsig.2020.109633

Shen, Z., Song, J., Yung, B. C., Zhou, Z., Wu, A., and Chen, X. (2018). Emerging Strategies of Cancer Therapy Based on Ferroptosis. *Adv. Mater.* 30 (12), e1704007. doi:10.1002/adma.201704007

Shi, L., Chen, Z. G., Wu, L. L., Zheng, J. J., Yang, J. R., Chen, X. F., et al. (2014). miR-340 Reverses Cisplatin Resistance of Hepatocellular Carcinoma Cell Lines by Targeting Nrf2-dependent Antioxidant Pathway. *Asian Pac. J. Cancer Prev.* 15 (23), 10439–10444. doi:10.7314/apjcp.2014.15.23.10439

Shu, X. L., Fan, C. B., Long, B., Zhou, X., and Wang, Y. (2016). The Anti-cancer Effects of Cisplatin on Hepatic Cancer Are Associated with Modulation of miRNA-21 and miRNA-122 Expression. *Eur. Rev. Med. Pharmacol. Sci.* 20 (21), 4459–4465.

Song, D. S., Bae, S. H., Song, M. J., Lee, S. W., Kim, H. Y., Lee, Y. J., et al. (2013). Hepatic Arterial Infusion Chemotherapy in Hepatocellular Carcinoma with portal Vein Tumor Thrombosis. *Wjg* 19 (29), 4679–4688. doi:10.3748/wjg.v19.i29.4679

Song, Y., Jang, J., Shin, T.-H., Bae, S. M., Kim, J.-s., Kim, K. M., et al. (2017). Sulfasalazine Attenuates Evading Anticancer Response of CD133-Positive Hepatocellular Carcinoma Cells. *J. Exp. Clin. Cancer Res.* 36 (1), 38. doi:10.1186/s13046-017-0511-7

Sun, J., Zhou, C., Zhao, Y., Zhang, X., Chen, W., Zhou, Q., et al. (2021). Quiescin Sulfhydryl Oxidase 1 Promotes Sorafenib-Induced Ferroptosis in Hepatocellular Carcinoma by D Riving EGFR Endosomal Trafficking and Inhibiting NRF2 Activation [J]. *Redox Biol.* 41, 101942. doi:10.1016/j.redox.2021.101942

Sun, Q., Zhang, Z., Lu, Y., Liu, Q., Xu, X., Xu, J., et al. (2020). Loss of Xanthine Oxidoreductase Potentiates Propagation of Hepatocellular Carcinoma Stem Cells. *Hepatology* 71 (6), 2033–2049. doi:10.1002/hep.30978

Sun, W., Yi, Y., Xia, G., Zhao, Y., Yu, Y., Li, L., et al. (2019). Nrf2-miR-129-3p-mTOR Axis Controls an miRNA Regulatory Network Involved in HDACi-Induced Autophagy. *Mol. Ther.* 27 (5), 1039–1050. doi:10.1016/j.ymthe.2019.02.010

Sun, X., Niu, X., Chen, R., He, W., Chen, D., Kang, R., et al. (2016). Metallothionein-1G Facilitates Sorafenib Resistance through Inhibition of Ferroptosis. *Hepatology* 64 (2), 488–500. doi:10.1002/hep.28574

Sun, X., Ou, Z., Chen, R., Niu, X., Chen, D., Kang, R., et al. (2016). Activation of the P62-Keap1-NRF2 Pathway Protects against Ferroptosis in Hepatocellular Carcinoma Cells. *Hepatology* 63 (1), 173–184. doi:10.1002/hep.28251

Sun, X., Ou, Z., Xie, M., Kang, R., Fan, Y., Niu, X., et al. (2015). HSPB1 as a Novel Regulator of Ferroptotic Cancer Cell Death. *Oncogene* 34 (45), 5617–5625. doi:10.1038/onc.2015.32

Tang, D., and Kroemer, G. (2020). Ferroptosis. *Curr. Biol.* 30 (21), R1292–R1297. doi:10.1016/j.cub.2020.09.068

Tang, H., Chen, D., Li, C., Zheng, C., Wu, X., Zhang, Y., et al. (2019). Dual GSH-Exhausting Sorafenib Loaded Manganese-Silica Nanodrugs for Inducing the Ferroptosis of Hepatocellular Carcinoma Cells. *Int. J. Pharm.* 572, 118782. doi:10.1016/j.ijpharm.2019.118782

Tao, J., Krutsenko, Y., Moghe, A., Singh, S., Poddar, M., Bell, A., et al. (2021). Nuclear Factor Erythroid 2-related Factor 2 and β-Catenin Coactivation in Hepatocellular Cancer: Biological and Therapeutic Implications. *Hepatology* 74 (2), 741–759. doi:10.1002/hep.31730

Tian, H., Zhao, S., Nice, E. C., Huang, C., He, W., Zou, B., et al. (2022). A Cascaded Copper-Based Nanocatalyst by Modulating Glutathione and Cyclooxygenase-2 for Hepatocellular Carcinoma Therapy. *J. Colloid Interf. Sci.* 607 (Pt 2), 1516–1526. doi:10.1016/j.jcis.2021.09.049

Walko, C. M., and Lindley, C. (2005). Capecitabine: A Review. *Clin. Ther.* 27 (1), 23–44. doi:10.1016/j.clinthera.2005.01.005

Wan, Y., Cui, R., Gu, J., Zhang, X., Xiang, X., Liu, C., et al. (2017). Dentification of Four Oxidative Stress-Responsive MicroRNAs, miR-34a-5p, miR-1915-3p, miR-638, and M iR-150-3p, in Hepatocellular Carcinoma. *Oxid Med. Cel Longev*, 2017, 5189138. doi:10.1155/2017/5189138

Wang, D., Zhang, N., Ye, Y., Qian, J., Zhu, Y., and Wang, C. (2014). Role and Mechanisms of microRNA-503 in Drug Resistance Reversal in HepG2/ADM Human Hepatocellular Carcinoma Cells. *Mol. Med. Rep.* 10 (6), 3268–3274. doi:10.3892/mmr.2014.2591

Wang, F., Lv, H., Zhao, B., Zhou, L., Wang, S., Luo, J., et al. (2019). Iron and Leukemia: New Insights for Future Treatments. *J. Exp. Clin. Cancer Res.* 38 (1), 406. doi:10.1186/s13046-019-1397-3

Wang, J., Zhu, S., Meng, N., He, Y., Lu, R., and Yan, G.-R. (2019). ncRNA-Encoded Peptides or Proteins and Cancer. *Mol. Ther.* 27 (10), 1718–1725. doi:10.1016/j.ymthe.2019.09.001

Wang, L., Liu, Y., Du, T., Yang, H., Lei, L., Guo, M., et al. (2020). ATF3 Promotes Erastin-Induced Ferroptosis by Suppressing System Xc-. *Cell Death Differ* 27 (2), 662–675. doi:10.1038/s41418-019-0380-z

Wang, Q., Bin, C., Xue, Q., Gao, Q., Huang, A., Wang, K., et al. (2021). GSTZ1 Sensitizes Hepatocellular Carcinoma Cells to Sorafenib-Induced Ferroptosis via Inhibition of NRF2/GPX4 axis. *Cel Death Dis* 12 (5), 426. doi:10.1038/s41419-021-03718-4

Wang, Q., Guo, Y., Wang, W., Liu, B., Yang, G., Xu, Z., et al. (2021). RNA Binding Protein DAZAP1 Promotes HCC Progression and Regulates Ferroptosis by Interacting with SLC7A11 mRNA. *Exp. Cel Res.* 399 (1), 112453. doi:10.1016/j.yexcr.2020.112453

Wang, S., Zhang, Q., Wang, Q., Shen, Q., Chen, X., Li, Z., et al. (2018). NEAT1 Paraspeckle Promotes Human Hepatocellular Carcinoma Progression by Strengthening IL-6/STAT3 Signaling. *Oncoimmunology* 7 (11), e1503913. doi:10.1080/2162402x.2018.1503913

Wang, W., Green, M., Choi, J. E., Gijón, M., Kennedy, P. D., Johnson, J. K., et al. (2019). CD8+ T Cells Regulate Tumour Ferroptosis during Cancer Immunotherapy. *Nature* 569 (7755), 270–274. doi:10.1038/s41586-019-1170-y

Wang, Z., Chen, X., Liu, N., Shi, Y., Liu, Y., Ouyang, L., et al. (2021). A Nuclear Long Non-coding RNA LINC00618 Accelerates Ferroptosis in a Manner Dependent upon Apoptosis. *Mol. Ther.* 29 (1), 263–274. doi:10.1016/j.ymthe.2020.09.024

Wu, L., Pan, C., Wei, X., Shi, Y., Zheng, J., Lin, X., et al. (2018). lncRNA KRAL Reverses 5-fluorouracil Resistance in Hepatocellular Carcinoma Cells by Acting as a ceRNA against miR-141. *Cell Commun Signal* 16 (1), 47. doi:10.1186/s12964-018-0260-z

Wu, Z.-y., Trenner, M., Boon, R. A., Spin, J. M., and Maegdefessel, L. (2020). Long Noncoding RNAs in Key Cellular Processes Involved in Aortic Aneurysms. *Atherosclerosis* 292, 112–118. doi:10.1016/j.atherosclerosis.2019.11.013

Xia, H., Lee, K. W., Chen, J., Kong, S. N., Sekar, K., Deivasigamani, A., et al. (2017). Simultaneous Silencing of ACSL4 and Induction of GADD45B in Hepatocellular Carcinoma Cells Amplifies the Synergistic Therapeutic Effect of Aspirin and Sorafenib. *Cel Death Discov.* 3, 17058. doi:10.1038/cddiscovery.2017.58

Xiao, Y., Yan, W., Lu, L., Wang, Y., Lu, W., Cao, Y., et al. (2015). p38/p53/miR-200a-3p Feedback Loop Promotes Oxidative Stress-Mediated Liver Cell Death. *Cell Cycle* 14 (10), 1548–1558. doi:10.1080/15384101.2015.1026491

Xu, Q., Zhou, L., Yang, G., Meng, F., Wan, Y., Wang, L., et al. (2020). CircIL4R Facilitates the Tumorigenesis and Inhibits Ferroptosis in Hepatocellular Carcinoma by Regulating the miR-541-3p/GPX4 axis. *Cell Biol Int* 44 (11), 2344–2356. doi:10.1002/cbin.11444

Yagoda, N., Von Rechenberg, M., Zaganjor, E., Bauer, A. J., Yang, W. S., Fridman, D. J., et al. (2007). RAS-RAF-MEK-dependent Oxidative Cell Death Involving Voltage-dependent Anion Channels. *Nature* 447 (7146), 864–868. doi:10.1038/nature05859

Yan, B., Ai, Y., Sun, Q., Ma, Y., Cao, Y., Wang, J., et al. (2021). Membrane Damage during Ferroptosis Is Caused by Oxidation of Phospholipids Catalyzed by the Oxidoreductases POR and CYB5R1. *Mol. Cel* 81 (2), 355–369. doi:10.1016/j.molcel.2020.11.024

Yang, F., Yin, Y., Wang, F., Wang, Y., Zhang, L., Tang, Y., et al. (2010). miR-17-5p Promotes Migration of Human Hepatocellular Carcinoma Cells through the P38 Mitogen-Activated Protein Kinase-Heat Shock Protein 27 Pathway. *Hepatology* 51 (5), 1614–1623. doi:10.1002/hep.23566

Yang, H. C., Wu, Y. H., Yen, W. C., Liu, H. Y., Hwang, T. L., Stern, A., et al. (2019). The Redox Role of G6PD in Cell Growth, Cell Death, and Cancer. *Cells* 8 (9). doi:10.3390/cells8091055

Yang, W. S., Sriramaratnam, R., Welsch, M. E., Shimada, K., Skouta, R., Viswanathan, V. S., et al. (2014). Regulation of Ferroptotic Cancer Cell Death by GPX4. *Cell* 156 (1-2), 317–331. doi:10.1016/j.cell.2013.12.010

Yang, W. S., and Stockwell, B. R. (2008). Synthetic Lethal Screening Identifies Compounds Activating Iron-dependent, Nonapoptotic Cell Death in Oncogenic-RAS-Harboring Cancer Cells. *Chem. Biol.* 15 (3), 234–245. doi:10.1016/j.chembiol.2008.02.010

Yant, L. J., Ran, Q., Rao, L., Van Remmen, H., Shibatani, T., Belter, J. G., et al. (2003). The Selenoprotein GPX4 Is Essential for Mouse Development and Protects from Radiation and Oxidative Damage Insults. *Free Radic. Biol. Med.* 34 (4), 496–502. doi:10.1016/s0891-5849(02)01360-6

Yuan, H., Li, X., Zhang, X., Kang, R., and Tang, D. (2016). Identification of ACSL4 as a Biomarker and Contributor of Ferroptosis. *Biochem. Biophysical Res. Commun.* 478 (3), 1338–1343. doi:10.1016/j.bbrc.2016.08.124

Yuan, Y., Cao, W., Zhou, H., Qian, H., and Wang, H. (2021). CLTRN, Regulated by NRF1/RAN/DLD Protein Complex, Enhances Radiation Sensitivity of Hepatocellular Carcinoma Cells through Ferroptosis Pathway. *Int. J. Radiat. Oncology*Biology*Physics* 110 (3), 859–871. doi:10.1016/j.ijrobp.2020.12.062

Zavattari, P., Perra, A., Menegon, S., Kowalik, M. A., Petrelli, A., Angioni, M. M., et al. (2015). Nrf2, but Not β-catenin, Mutation Represents an Early Event in Rat Hepatocarcinogenesis. *Hepatology* 62 (3), 851–862. doi:10.1002/hep.27790

Zhang, X., Wang, L., Li, H., Zhang, L., Zheng, X., and Cheng, W. (2020). Crosstalk between Noncoding RNAs and Ferroptosis: New Dawn for Overcoming Cancer Progression. *Cel Death Dis* 11 (7), 580. doi:10.1038/s41419-020-02772-8

Zhao, L. (2019). Mitochondrial DNA Degradation: A Quality Control Measure for Mitochondrial Genome Maintenance and Stress Response. *Enzymes* 45, 311–341. doi:10.1016/bs.enz.2019.08.004

Zhao, Y., Li, M., Yao, X., Fei, Y., Lin, Z., Li, Z., et al. (2020). HCAR1/MCT1 Regulates Tumor Ferroptosis through the Lactate-Mediated AMPK-SCD1 Activity and its Therapeutic Implications. *Cel Rep.* 33 (10), 108487. doi:10.1016/j.celrep.2020.108487

Zheng, J., and Conrad, M. (2020). The Metabolic Underpinnings of Ferroptosis. *Cel Metab.* 32 (6), 920–937. doi:10.1016/j.cmet.2020.10.011

Zhou, S., Ye, W., Zhang, Y., Yu, D., Shao, Q., Liang, J., et al. (2016). miR-144 Reverses Chemoresistance of Hepatocellular Carcinoma Cell Lines by Targeting Nrf2-dependent Antioxidant Pathway. *Am. J. Transl Res.* 8 (7), 2992–3002.

Zhu, G., Murshed, A., Li, H., Ma, J., Zhen, N., Ding, M., et al. (2021). O-GlcNAcylation Enhances Sensitivity to RSL3-Induced Ferroptosis via the YAP/TFRC Pathway in Liver Cancer. *Cel Death Discov.* 7 (1), 83. doi:10.1038/s41420-021-00468-2

Zou, C., Zou, C., Cheng, W., Li, Q., Han, Z., Wang, X., et al. (2016). Heme Oxygenase-1 Retards Hepatocellular Carcinoma Progression through the microRNA Pathway. *Oncol. Rep.* 36 (5), 2715–2722. doi:10.3892/or.2016.5056

Zou, S., Rao, Y., and Chen, W. (2019). miR-885-5p Plays an Accomplice Role in Liver Cancer by Instigating TIGAR Expression via Targeting its Promoter. *Biotechnol. Appl. Biochem.* 66 (5), 763–771. doi:10.1002/bab.1767

Zou, Y., Li, H., Graham, E. T., Deik, A. A., Eaton, J. K., Wang, W., et al. (2020). Cytochrome P450 Oxidoreductase Contributes to Phospholipid Peroxidation in Ferroptosis. *Nat. Chem. Biol.* 16 (3), 302–309. doi:10.1038/s41589-020-0472-6

Conflict of Interest: The authors declare that the research was conducted in the absence of any commercial or financial relationships that could be construed as a potential conflict of interest.

Publisher's Note: All claims expressed in this article are solely those of the authors and do not necessarily represent those of their affiliated organizations, or those of the publisher, the editors and the reviewers. Any product that may be evaluated in this article, or claim that may be made by its manufacturer, is not guaranteed or endorsed by the publisher.

frontiers in Cell and Developmental Biology

ORIGINAL RESEARCH
published: 01 March 2022
doi: 10.3389/fcell.2022.847513

Identification of Ferroptosis-Related Genes as Biomarkers for Sarcoma

Zhiyuan Guan[1†], Shengfu Liu[2†], Liying Luo[3†], Zhong Wu[1], Shan Lu[3]*, Zhiqiang Guan[4]* and Kun Tao[2]**

[1]Department of Orthopedics, The Shanghai tenth People's Hospital of Tongji University, Shanghai, China, [2]Nanjing Medical University, Nanjing, China, [3]Department of Nursing, Xuzhou Municipal Hospital Affiliated with Xuzhou Medical University, Jiangsu, China, [4]Department of Dermatology, Xuzhou Municipal Hospital Affiliated with Xuzhou Medical University, Xuzhou, China

Sarcomas are seen as mixed-up nature with genetic and transcriptional heterogeneity and poor prognosis. Although the genes involved in ferroptosis are still unclear, iron loss is considered to be the core of glioblastoma, tumor progression, and tumor microenvironment. Here, we developed and tested the prognosis of SARC, which is a genetic marker associated with iron residues. The ferroptosis-related gene expression, one-way Cox analysis, and least-selection absolute regression algorithm (LASSO) are used to track prognostic-related genes and create risk assessment models. Finally, immune system infiltration and immune control point analysis are used to study the characteristics of the tumor microenvironment related to risk assessment. Moreover, LncRNA–miRNA–mRNA network was contributed in our studies. We determined the biomarker characteristics associated with iron degradation in gene 32 and developed a risk assessment model. ROC analysis showed that its model was accurately predicted, with 1, 2, 3, 4, and 5 years of overall survival in TCGA cohort of SARC patients. A comparative analysis of settings found that overall survival (OS) was lower in the high-risk than that in the low-risk group. The nomogram survival prediction model also helped to predict the OS of SARC patients. The nomogram survival prediction model has strong predictive power for the overall survival of SARC patients in TCGA dataset. GSEA analysis shows that high-risk groups are rich in inflammation, cancer-related symptoms, and pathological processes. High risk is related to immune cell infiltration and immune checkpoint. Our prediction model is based on SARC ferritin-related genes, which may support SARC prediction and provide potential attack points.

Keywords: ferroptosis, sarcoma, prognosis, tumor microenvironment, bioinformatics

OPEN ACCESS

Edited by:
Lian Xiang Luo, Guangdong Medical University, China

Reviewed by:
Huichao Deng, Howard Hughes Medical Institute (HHMI), United States
Ling Li, University of North Dakota, United States
Guoshuai Feng, Washington University in St. Louis, United States

****Correspondence:***
Shan Lu
lushan@163.com
Zhiqiang Guan
Gzq199207@163.com
Kun Tao
doctk@163.com
Zhiyuan Guan
gzy_2008@bjmu.edu.cn

†These authors have contributed equally to this work

Specialty section:
This article was submitted to Cell Death and Survival, a section of the journal Frontiers in Cell and Developmental Biology

Received: *02 January 2022*
Accepted: *31 January 2022*
Published: *01 March 2022*

Citation:
Guan Z, Liu S, Luo L, Wu Z, Lu S, Guan Z and Tao K (2022) Identification of Ferroptosis-Related Genes as Biomarkers for Sarcoma. Front. Cell Dev. Biol. 10:847513. doi: 10.3389/fcell.2022.847513

INTRODUCTION

SARC (sarcoma) is a type of stromal cancer with more than 100 subtypes. Sarcomas occur in all age groups and are more general in teens and young adults than in the elderly (Reed et al., 2019). SARC also includes many malignant tumors with different symptoms, behaviors, and results. For example, chemotherapy has only a known effect on a few sarcomas. Although confirmed sarcoma can be removed by surgery or radiotherapy, the incidence of metastatic sarcoma within 5 years is still as high as 50% (Brennan et al., 2014). Only 5% of metastatic patients have a 5-year survival period (Zhu et al., 2020).

Although some of the diagnostic markers of SARC can effectively predict the progress of SARC, they are still at the molecular stage and not yet used in clinical practice. Therefore, diagnostic markers related to undiscovered genes are of great significance for the diagnosis and prediction-related analysis of SARC.

Ferroptosis, an iron-dependent form of programmed cell death, which is linked to pathophysiological conditions. Sensitivity to lipid peroxidation is attributed to many metabolic pathways, such as fatty acid metabolism, iron processing, methionine metabolism, and mitochondrial respiration (Zheng and Conrad, 2020; Jiang et al., 2021). Notably, ferroptosis is related to stroke, ischemic heart disease, liver and kidney damage (Benjamin et al., 2017). In particular, there is strong evidence that high levels of ferroptosis play an important role in the suppression of tumor growth, and the activation of iron levels will enhance the therapeutic effect of anticancer drugs (Li and Li, 2020). Cancer cells store large amounts of iron and active oxygen to stimulate metabolism and growth(Battaglia et al., 2020). Gene dysregulation involved in iron nucleocytosis may promote cancer cell proliferation, invasion, and metastasis (Jung et al., 2019). In addition, CD8 + T cells cause iron loss by controlling the link between cancer cell death mechanism and immune system activation, thereby inhibiting tumor growth (Tang et al., 2020).

In the past, there was an association between many subtypes of sarcoma and apoptosis-related genes such as GPX4, which induces iron loss by increasing MDA, ROS, and intracellular iron levels in osteosarcoma cells (Lin H et al., 2021). LOX promotes tumor deposition and catalyzes the production of lipid hydrogen peroxide in the plasma membrane. In the process of ptosis, ALOX15 protein is always present in the cell membrane (Shintoku et al., 2017). Pharmacological lipid peroxidation inhibitors (such as ferrostatin-1 and lipid peroxidin-1), reactive oxygen species scavengers (such as alpha-tocopherol and glutathione), and iron chelator deferoxamine can inhibit the accumulation of reactive oxygen species; lipid peroxidation oxidizes and heals swamps (Dächert et al., 2020). However, the side effects of ferroptosis limit their applications in treating sarcomas (Blatt, 1994). Therefore, sarcoma iron gout needs more understanding.

These studies focused on genes related to iron-related diseases. We perform extensive bioinformatics analyses based on The Cancer Genome Atlas (TCGA) clinical data to analyze the gene expression levels, DNA methylation, and copy number transfer models. The SARC risk assessment system in TCGA dataset was developed and validated by detecting regulated iron-related genes. In addition, the function and gene clusters were performed to identify possible pathways and mechanisms of ferroptosis metabolism. Our results indicate that four genetic markers can be used as independent predictors of OS in sarcoma patients.

MATERIALS AND METHODS

Analysis of the Ferroptosis-Related Genes in SARC

Ferroptosis-related genes are obtained from the genset (the Molecular Feature Database (MSigDB) version 7.1) (Subramanian et al., 2005; Liberzon et al., 2015), including the 15 gene sets (Mou et al., 2020; Zhang S et al., 2020). After removing overlapping genes, we got a set of genes related to ferroptosis-related gene (FRG), including 32 genes.

Datasets and Data Processing

As of 30 November 2021, we have obtained data on RNA sequences and summary of 260 SARC patients' clinical characteristics from TCGA database. The RNA sequence data of 88 normal human ovarian samples were downloaded from the GTEx database. The RNA-seq data and clinical information from the external validation cohort were extracted from the GEO database (GSE21050).

A total of 32 FRGs were obtained from previous studies (Lin W et al., 2021; Ye et al., 2021). The "limma" packages demonstrate the difference between FRG expression in SARC and normal tissues. Then, we contribute 32 protein–protein interaction networks (PPI) to search for interaction finder (STRING).

Gene Mutation, Methylation, and Copy Number Variation

The "maftool" package is used to create single-nucleotide variation, copy number variation, and 32 FRG cascade plots for SARC patients. GSCA Lite is used to keep methylation alive and analyze the changes in copy number.

Gene Functional Enrichment Analysis

Genetic ontology (GO), which includes biological process (BP), cell composition (CC), and molecular function classification (MF), uses the "ggplot2" software package in R. In the same way, Kyoto Encyclopedia and Genome uses this software package to analyze (KEGG) genes. A hypergeometric distribution test was applied to detect enrichment terms, and p values were adjusted by the false discovery rate (FDR) method with a cutoff FDR <0.05.

Development of Ferroptosis-Related Prognostic (FRG) Model

Cox regression analysis (COX analysis) is used to investigate the effects of FRGs on prognosis of SARC. The Kaplan–Mayer curve uses the logarithmic test and one-way regression of Cox proportional hazards to generate p (HR) values with 95% confidence intervals (CIs). PRGs with important prognostic value were selected in further analysis. Based on these prognostic-related PRGs, LASSO–Cox regression analysis was used to contribute a prognostic model. According to the average risk score, TCGA–SARC patients were divided into low-risk and high-risk subgroups, and Kaplan–Meier analysis was used to compare the overall survival rates of the two subgroups. Time receiver performance (ROC) analysis is used to evaluate the prediction accuracy and risk assessment of each gene. Taking into account the clinical characteristics, we developed a nomosis prediction schedule to predict the overall survival rate at 1, 3, and 5 years. A forest was used to show the p-value, HR, and 95% CI of each variable through the "forest plot" R package.

To evaluate whether the risk score system can serve as an independent predictive index, univariate and multivariate Cox regression analyses were performed with clinicopathologic parameters. All independent prognostic parameters were used to construct a nomogram to predict the 1-, 3- and 5-year OS probabilities by the "rms" package. The concordance index

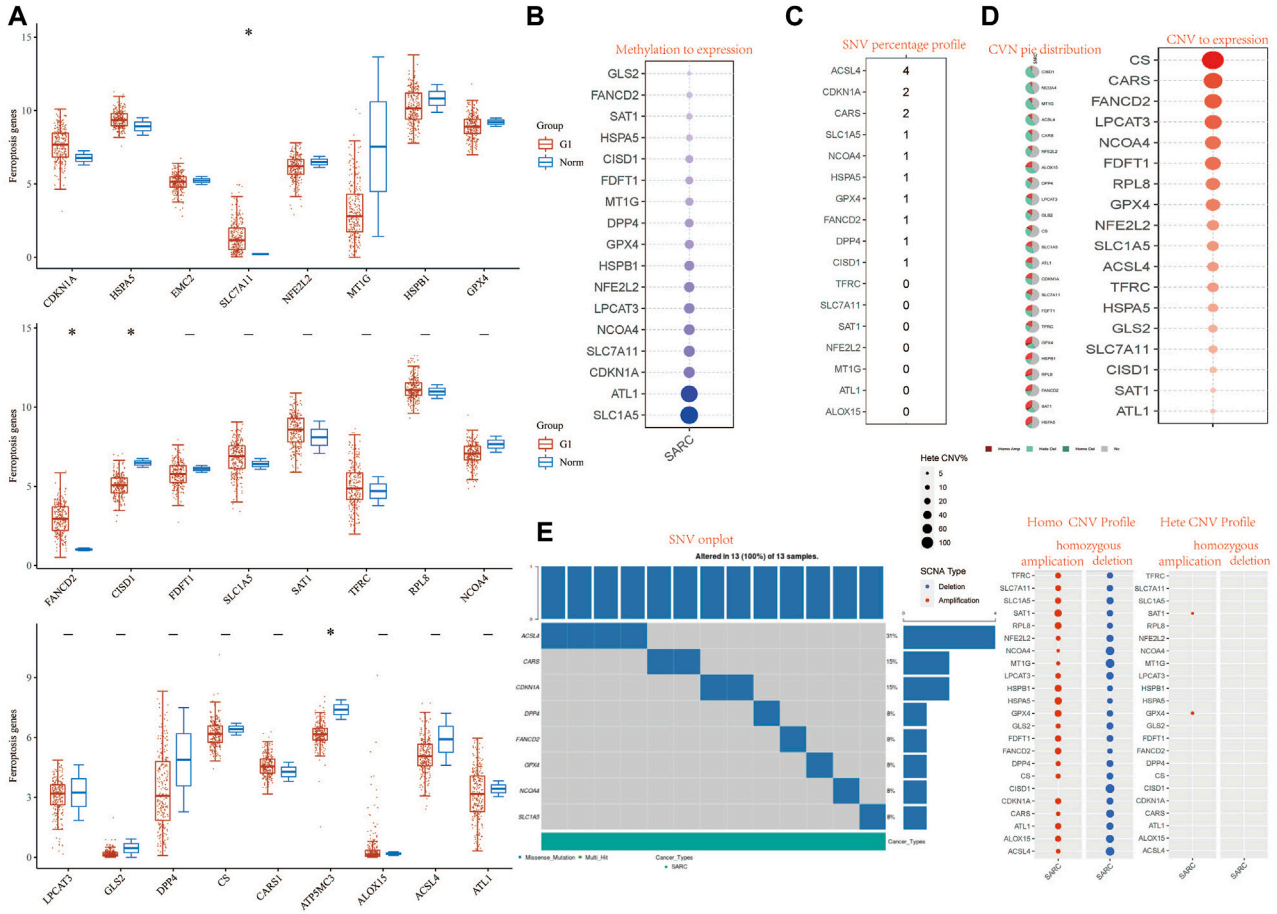

FIGURE 1 | Landscape of genetic and expression variation of FRG in SARC. **(A)** The expression of 32 FRG in SARC, Tumor, blue; normal, red. The upper and lower ends of the boxes represent the interquartile range of values. The lines in the boxes represent median value. **(B)** Methylation to expression. **(C)** SNV percentage profile. **(D)** CNV pie distribution and CNV to expression of 32 FRG in the SARC cohort. **(E)** SNV onplot, homo CNV profile, and hete CNV profile of 32 FRG in the SARC cohort. ***p< 0.001. FRG, ferroptosis-related gene; SARC, sarcoma; SNP, single nucleotide polymorphism; INS, insertion; DEL, deletion; SNV, single-nucleotide variation; CNV, copy number variation.

(C-index), calibration, and ROC analyses were used to evaluate the discriminative ability of the nomogram (Alba et al., 2017).

Immune Related Analysis in Ferroptosis-Related Prognostic (FRG) Model

We used the tumor immune assessment function to analyze the relationship between prognostic FRGs and immune system infiltration, and comprehensively analyze the immune cells infiltrating the portal. The TIM gene module can monitor the relation between the expression of SARC gene and the degree of immune infiltration. Spearman correlation analysis was used to calculate the correlation between gene expression, and the results of tumor mutation burden (TMB) and microsatellite instability (MSI). p values less than 0.05 are considered statistically significant.

Endogenous RNA Network Analysis

To elucidate the possible role of FRGs in SARC, a competitive endogenous RNA (ceRNA) network.miRTarBase (http://mirtarbase.cuhk.edu.cn/) and TarBase V.8 (https://carolina.imis.athenainnovation.gr/diana_tools/web/index.php?r=tarbasev8%2Findex) were contributed and utilized to predict the possible miRNA targets. According to the identified miRNA, it is assumed that StarBase (http://starbase.sysu.edu.cn/) is LncBase v.2 (https://carolina.imis.athena-innovation.gr/diana_tools/web/index.php?r = lncbasev2/index-predicted) is used to predict the interaction between lncRNA and miRNA. In all analyses, p< 0.05 was considered to be statistically significant.

GSEA

The aforementioned software package R was used to calculate the DEG training package. Then GSEA (http://software.broadinstitute.org/gsea/index.jsp) was used to identify the characteristics of high- and low-risk groups.

TIMER Database Analysis

The result of the infiltration estimation generated by the TIMER algorithm consists of 6 specific subgroups of immune cells, including B cells, CD4 + T cells, CD8 + T cells, macrophages,

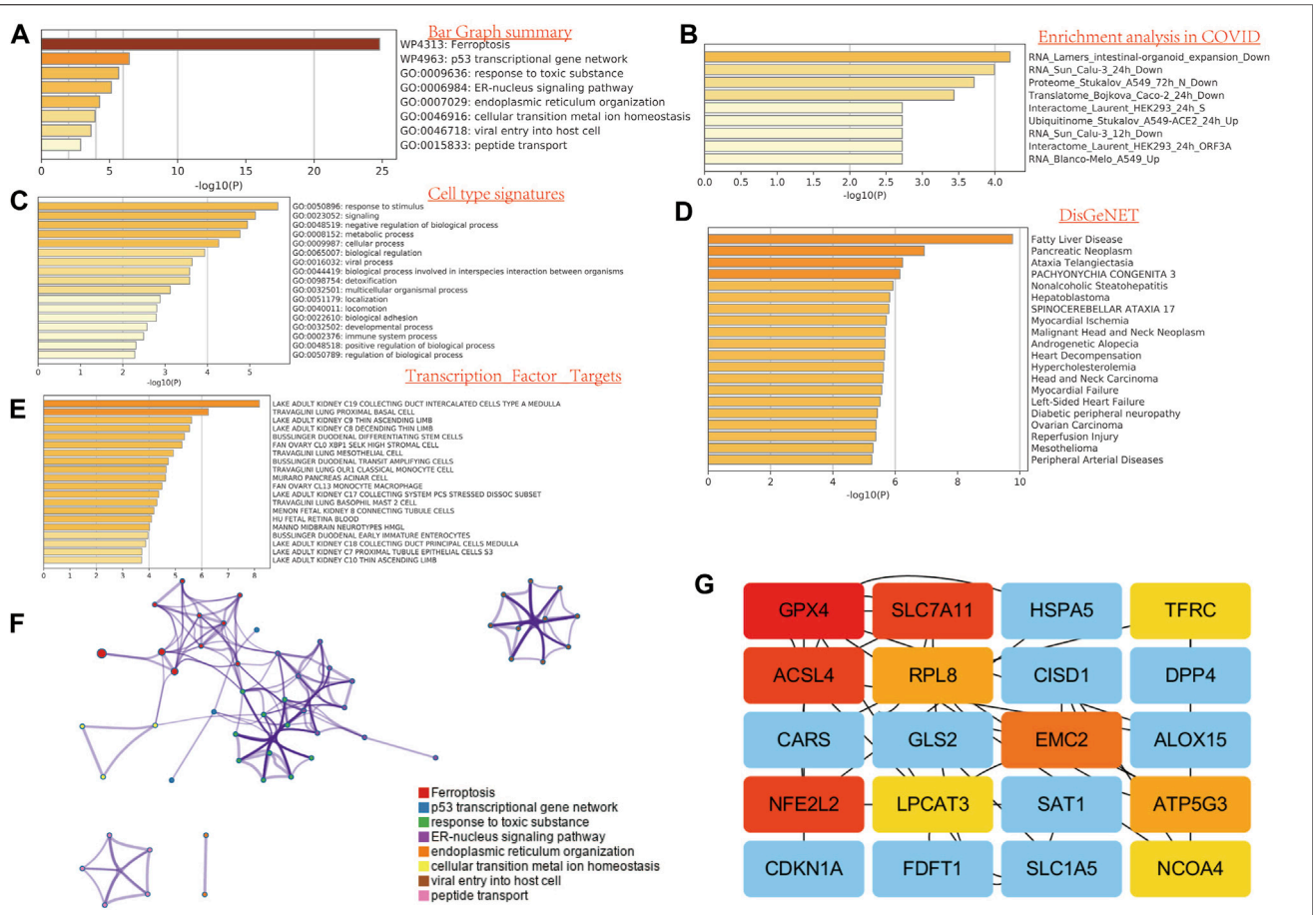

FIGURE 2 | Functional enrichment analysis of FRG in SARC. **(A)** Bar graph summary. **(B)** Enrichment analysis in COVID. **(C)** Cell type signature. **(D)** DisGeNET. E, transcription factor targets. **(E)** GO enrichment analysis. **(F)** Network analysis. **(G)** Network analysis between top 20 genes.

neutrophils, and dendritic cells (Sturm et al., 2019; Li et al., 2020). We extracted the results of the penetration assessment and evaluated the different results of the penetration assessment of immune cell subsets between high-risk and low-risk populations (Newman et al., 2015).

Statistical Analysis

All statistical analyses in this study were performed using software R (version 3.6.3) and GraphPad Prism (version 8.0.2). Kaplan–Mayer survival analysis uses the logarithmic series test. Risk factors (HR) and 95% confidence intervals (CI) should be provided when relevant. Both groups were compared with Student's t-test and the Kruskal–Wallis test. A two-tailed p value less than 0.05 was considered statistically significant without specific annotation.

RESULTS

Expression of FRGs in SARC

First, we use TCGA data to study the expression of 32 FRGs in SARC and normal tissues. The total amount of SARC is 4 FRGs. For example, the expression of SLC7A11, FANCD2, and CISD1 was higher in tumor tissues than that in normal tissues, but ATP5MC3 was lower. A GeneMANIA network showed that FANCD2, SLC7A11, CISD1, and ATP5MC3 were performed to detect these FRG interactions. The minimum required interaction score is 0.9. The heat map of results showed that FANCD2, SLC7A11, CISD1, and ATP5MC3 are key genes (**Figure 1**, **SupplementaryFigure S1**, **Supplementary Table S1**).

Landscape of Genetic Variation, Methylation, and Copy Number Variation

We first analyzed the relationship between FRG and methylation. In all FRGs, we found that the methylation rate of SLC1A5 and ATL1 is associated with a methylation level (**Figure 1B**). Then we analyzed the percentage plot of individual nucleotide variation on the chart. The ACSL4 mutation frequency is high (**Figure 1C**). We summarized the copy number and frequency of 32 FRG somatic mutations in SARC. As shown in **Figures 1D,E**, we found that CISD1 and NCOA4 have a higher level of CNV pie distribution, and CS, CARS, FANCD2,

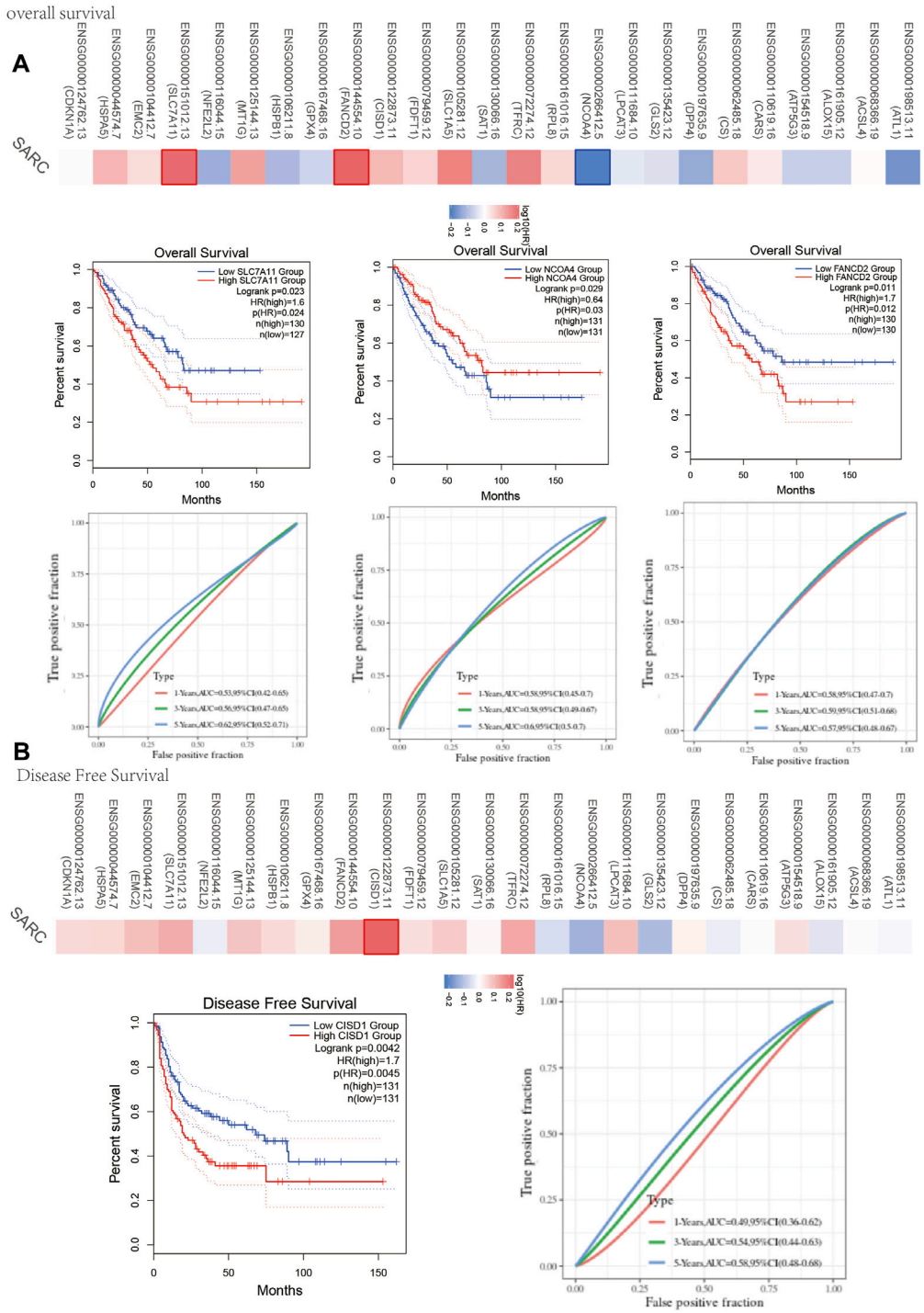

FIGURE 3 | Prognosis value of FRG in SARC. **(A)** The overall survival curve of SLC7A11, NCOA4, and FANCD2 in SARC patients in the high-/low-expression group. **(B)** Disease free survival curve of CISD1 in SARC patients in the high-/low-expression group. FRG, ferroptosis-related gene; SARC, sarcoma.

and LPCAT3 have a higher CNV expression level. ALOX15 has a high circulating distribution of CVN (copy number change), while CISD1, ACSL4, and ALOX15 show high levels of homozygous SARC deletion. **Supplementary Figure S5C** shows that TP53 and RB1 have higher levels of genomic alteration. The mutation count, TMB, fraction genome altered, aneuploidy score, MSIsensor score, radiation therapy, and Onc Tree code, and cancer type details also show significant

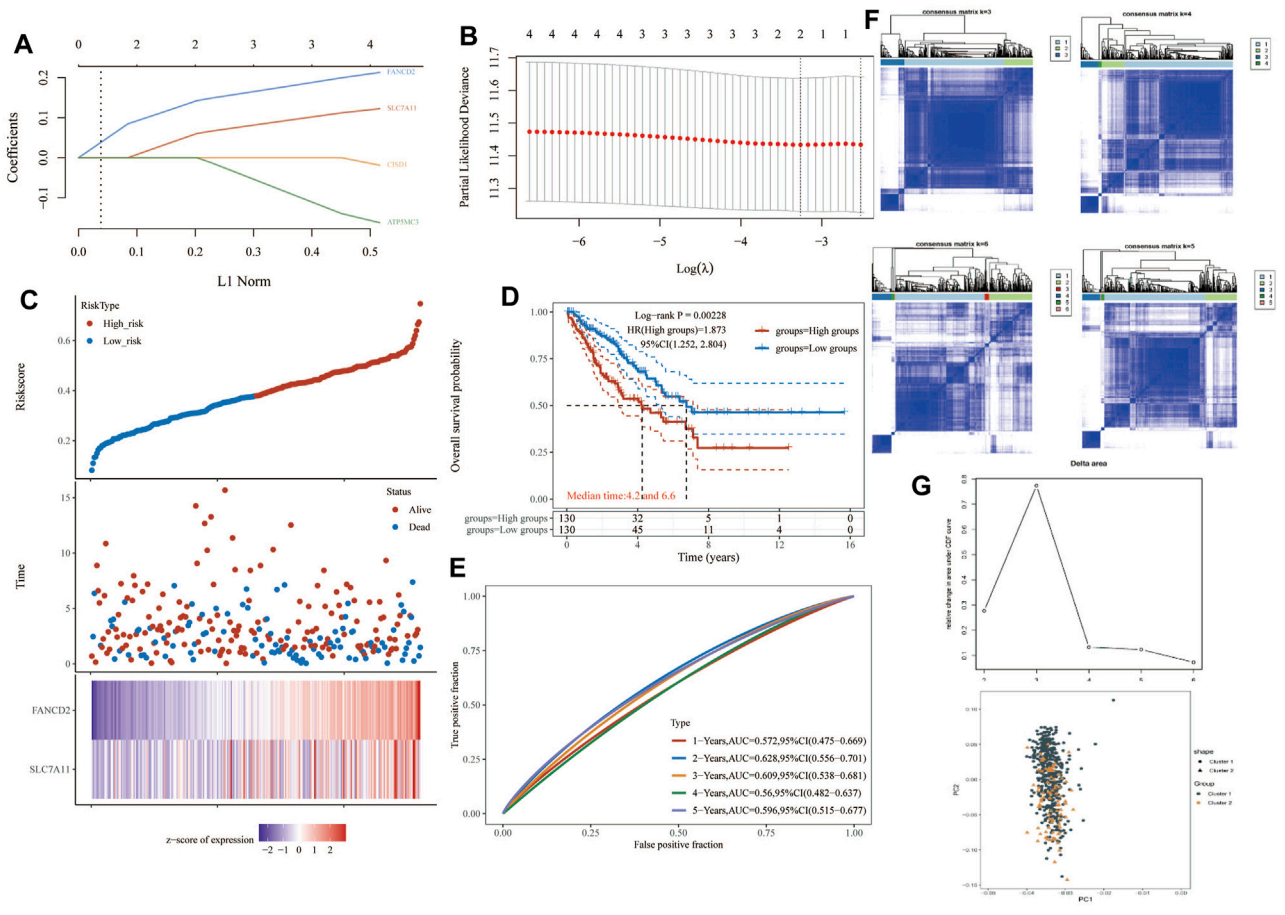

FIGURE 4 | Construction of a prognostic FRG model. **(A)** LASSO coefficient profiles of the four PRGs. **(B)** Plots of the ten-fold cross-validation error rates. **(C)** Distribution of risk score, survival status, and the expression of four prognostic PRGs in SARC. **(D,E)** Overall survival curves for SARC patients in the high-/low-risk group and the ROC curve of measuring the predictive value. **(F,G)** Prognostic FRG model. FRG, ferroptosis-related gene; SARC, sarcoma.

difference in genome changes of FRGs (**Supplementary Table S3**).

Functional Enrichment Analysis

To illustrate the role of FRGs, we uses GO and KEGG databases to analyze the FRGs pathway. We found that these 32 FRGs are mainly involved in the p53 transcriptional gene network, response to toxic substance, ER–nucleus signaling pathway, endoplasmic reticulum organization, cellular transition metal ion homeostasis, and peptide transport are involved in the process of ferroptosis in GO assay (**Figure 2A**). For COVID related GO enrichment analysis, RNA lamers intestinal organoid expansion, RNA Sun calu-3 24 h, proteome stukalov, translatome luarant also play an important role in the ferroptosis related pathway. The cell type signature for example response to stimulus, signaling and negative regulation of biological process and transcription factor target such as lake adult kidney c19 collecting duct intercalated cells types a medulla also play potential role in ferroptisis related pathway. In addition, the analysis of the KEGG pathway showed that the 32 FRGs are mainly involved in the TOR, RTX and EMT (**Figure 2A**). We also compiled the percentage of the global channel, the percentage of the heat map, and the connection network in **Supplementary Figure S4** (**Supplementary Tables S3–4**).

Ferroptosis-Related Prognostic Gene Model

One-way Cox regression analysis was used to select the prognostic FRGs for the genetic prognostic model. As a result, a total of 4 genes with prognostic values were identified. Kaplan–Mayer survival curves are shown in **Figures 3A,B**. For overall survival, we found that the high expression of SLC7A11(p = 0.023) and FANCD2 (p = 0.011) was correlated with good prognosis, but that of NCOA4 was linked with poor prognosis. For disease-free survival, we found that high expression of CISD1 (p = 0.0042) links with better prognosis (**Figure 2C**). Based on these 4 prognostic FRGs, LASSO–Cox regression analysis was performed to construct a prognostic gene model (**Figure 4**). According to risk assessment, SARC patients are divided into two groups. The risk results, survival status, and expression distribution of these genes are shown in **Figure 4**. The higher the risk score, the higher the risk of

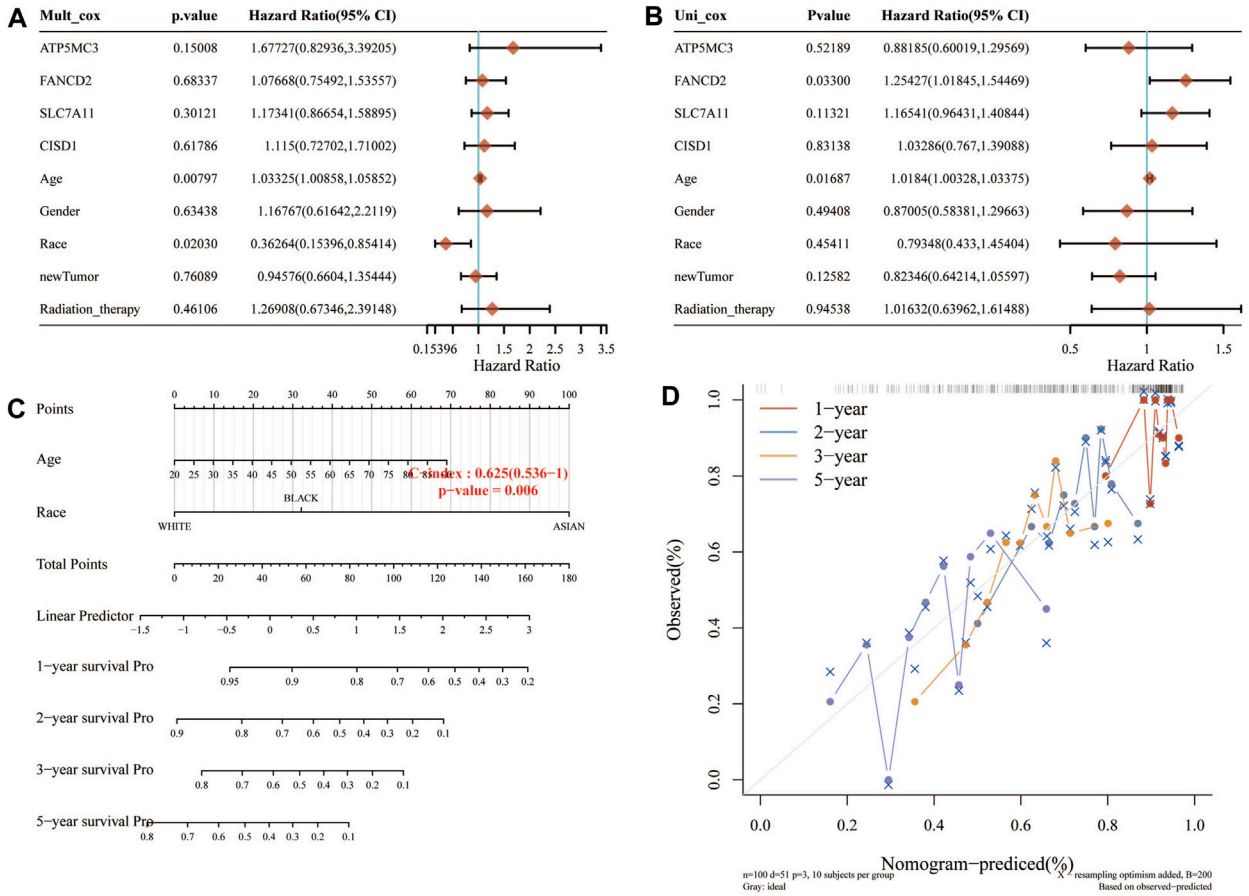

FIGURE 5 | Construction of a predictive nomogram. **(A,B)** Hazard ratio and *p*-value of the constituents involved in univariate and multivariate Cox regression analyses considering clinical the parameters and four prognostic FRG in SARC. **(C,D)** Nomogram to predict the 1-, 2-, 3-, and 5-year overall survival rate of SARC patients. Calibration curve for the overall survival nomogram model in the discovery group. A dashed diagonal line represents the ideal nomogram. FRG, ferroptosis-related gene; SARC, sarcoma.

death and the shorter the survival time (**Figure 4C**). The Kaplan–Meier curve shows that the overall survival rate of high-risk patients is not only higher than that of low-risk patients (average time = 4.2 and 6.6 years, $p = 0.000228$, **Figure 4D**) but also 1 year, 2, 3, 4 year annual, and 5-year ROC curves are 0.572, 0.628, 0.609, 0.56, and 0.596, respectively.

Building a Predictive Nomogram

Considering the clinicopathologic and prognostic characteristics of FRGs, we also compiled the prognostic nomogram of the survival prediction table. One-dimensional and multi-dimensional analyses showed that NOD1 and pT staging, pN staging, and pM staging are independent factors affecting the prognosis of SARC patients (**Figure 5**). The chart with predictable names shows that the 1, 2, 3, and 5-year overall survival of the entire cohort can be better predicted than the ideal model (index C: 0.625 (0.536–1), $p< 0.01$).

Immune Infiltration and Immune Survival in SARC

Immunohistochemical results suggested SLC7A11 and FANCD2 staining in melanoma (**Figure 6A**). Ferroptosis plays an important role in the creation of tumor immune microenvironment. In our study, we also used the TIMER database to clarify the relationship between the expression of prognostic FRG (FANCD2, SLC7A11, CISD1, and ATP5MC3) and SARC immune filtration and somatic copy number variation. For example, B cells in FANCD2 are significantly expanded, lacking $CD4^+$ T cells and macrophage branching. However, FANCD2 have no significant difference in SLC7A11, CISD1, and ATP5MC3 (**Figure 6**). SLC7A11 was negatively correlated with CD4+ T cells, and FAND2 was negatively correlated with CD4+ T cells and macrophages. The data show that FANCD2 and CISD1 are positively correlated with B cells. CISD1 was also positively correlated with CD8+ T cells but negatively correlated with CD4+ T cells. ATP5G3 was negatively correlated with macrophages (**Figure 7A**). Immune survival

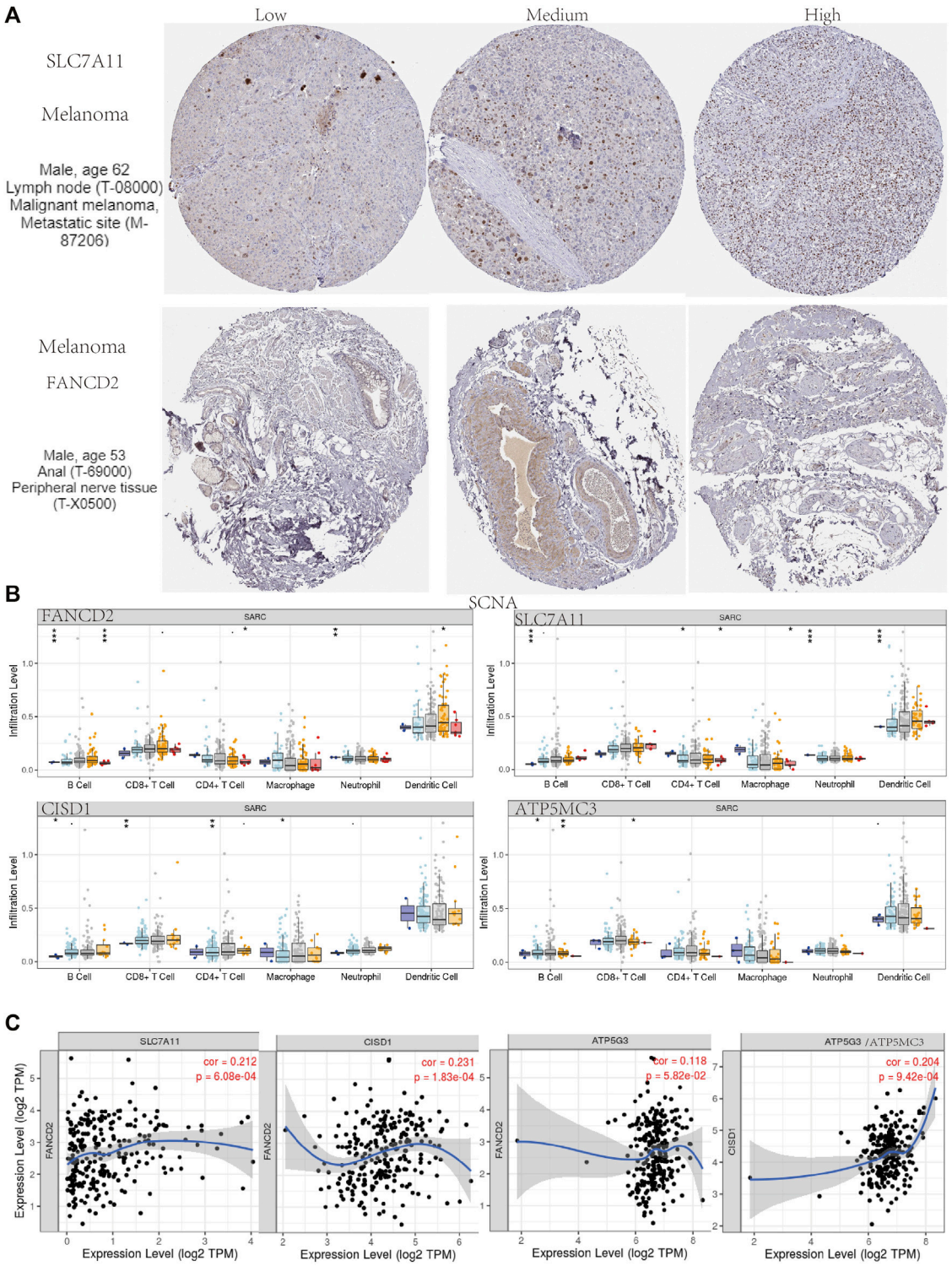

FIGURE 6 | Human Protein Atlas immunohistochemical analysis of SARC. **(A)** SCNA of SARC in FANCD2, SLC7A11, CISD1, and ATP5MC3. **(B)** Correlation analysis among FANCD2, SLC7A11, CISD1, and ATP5MC3 **(C)**.

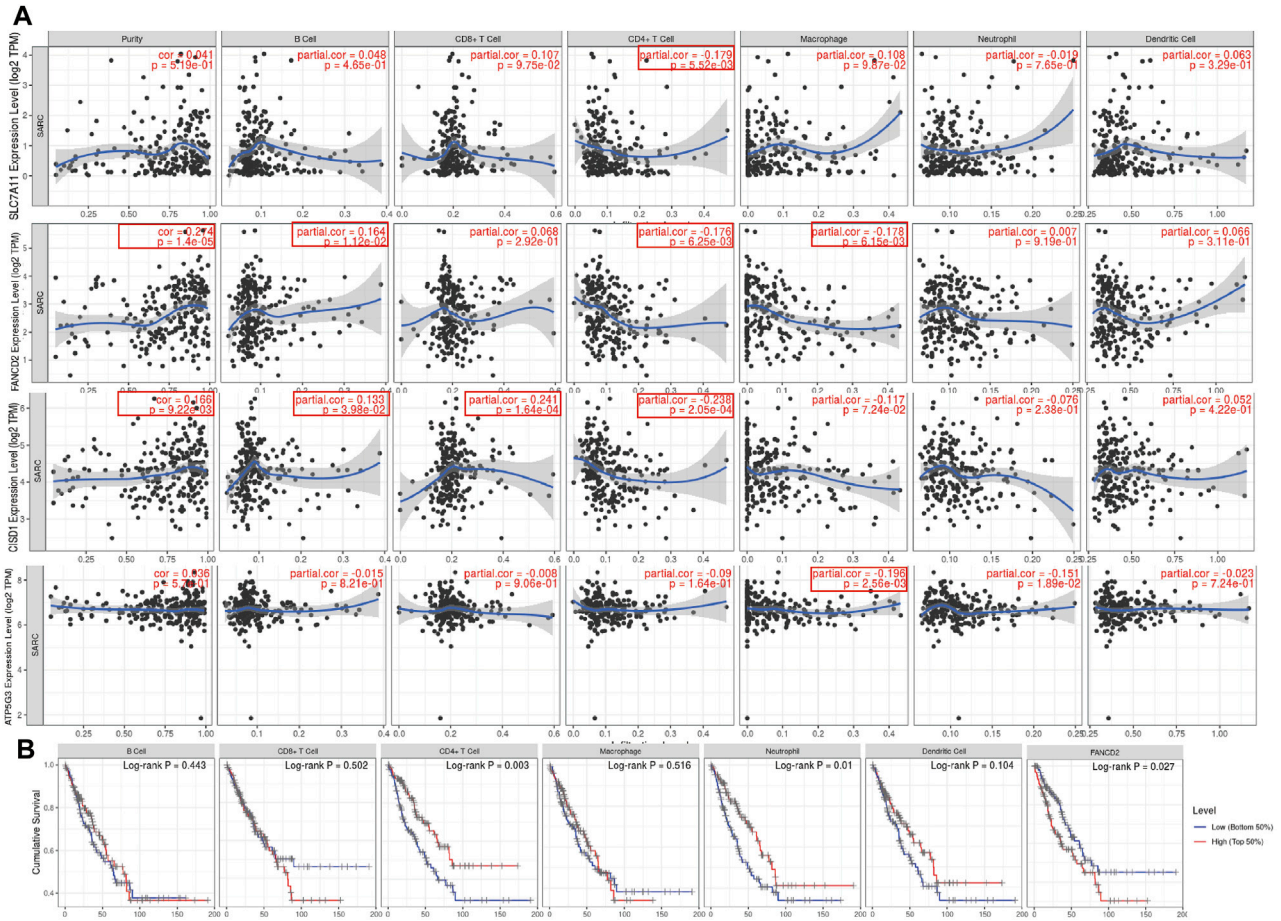

FIGURE 7 | Association between seven prognostic PRG and immune infiltration (TIMER). **(A)** The association between the abundance of immune cells and the expression of FANCD2, SLC7A11, CISD1, and ATP5MC3 in SARC. FRG, ferroptosis-related gene; SARC, sarcoma. **(B)** Cumulative survival of B cell, CD8+ T cell, CD4+ T cell, marcrophage, neutrophil, and dendritic cell of FRGs in SARC.

(**Figure 7B**) shows that lower CD4 + T cells and neutrophils level also have better prognosis. Moreover, a lower FANCD2 level also predicted poor prognosis .

Drug Sensitivity, TMB, and MSI in SARC

The instability of TMB and microsatellites can be used as biomarkers to predict the effect of tumor immunotherapy (Campbell et al., 2017; Latham et al., 2019; Samstein et al., 2019; Chan et al., 2020). The aforementioned analysis shows that FRGs are negatively correlated with tumor immune system infiltration. To determine whether this FRG can also be used as a biomarker for drug screening, we analyzed the correlation between FRG and TMB and MSI in SARC. The results show that MSI is positively correlated with SLC7A11 (p = 0.010) and FANCD2 (p = 7.06E-5). In addition, the TMB also negatively correlated with FANCD1, SLC7A11, CISD1, and ATP5MC3. SLC7A11 has negatively correlated with ESTIMATE score (p = 7.45E-7), immune score (p = 3.7E-5), and Stromal Score (p = 5.16E-8). FANCD2 was negatively correlated with Stromal Score (p = 0.018). CISD1 negatively correlated with ESTIMATE score (p = 0.044) and Stromal Score (p = 4.81E-4). Immune score shows that FANCD2 was correlated with neutrophils, macrophages, and CD4+ T cells. CISD1 were correlated with neutrophils and $CD4^+$ T cells. ATP5MC3 correlated with neutrophils and macrophages (**Figure 8**). The immune checkpoint and immune pathway are shown in **Supplementary Figure S2**. Analyzing the correlation between gene expression and available drugs is key to setting treatment goals. In our study, we analyzed 14 genes that are significantly related to some or most anticancer drugs, such as FANCD2, HSPA5, NFE2L2, ACSL4, and DPP4 in the Cancer Therapeutic Response Portal Database (**Supplementary Figure S2**).

Contribute an miRNA–LncRNA–mRNA Network

To elucidate the molecular mechanism of FRGs in SARC, we constructed an mRNA–miRNA–lncRNA interaction network. We first investigate the correlation hub gene, and Ven plot found that 101 hub genes have been analyzed, as shown in **Supplementary Figure S3A** and **Table 1**. The ferroptosis-related gene pathway analysis found the energy produced by the oxidation of organic compounds and cellular respiration in the BP pathway and mitochondrial inner membrane,

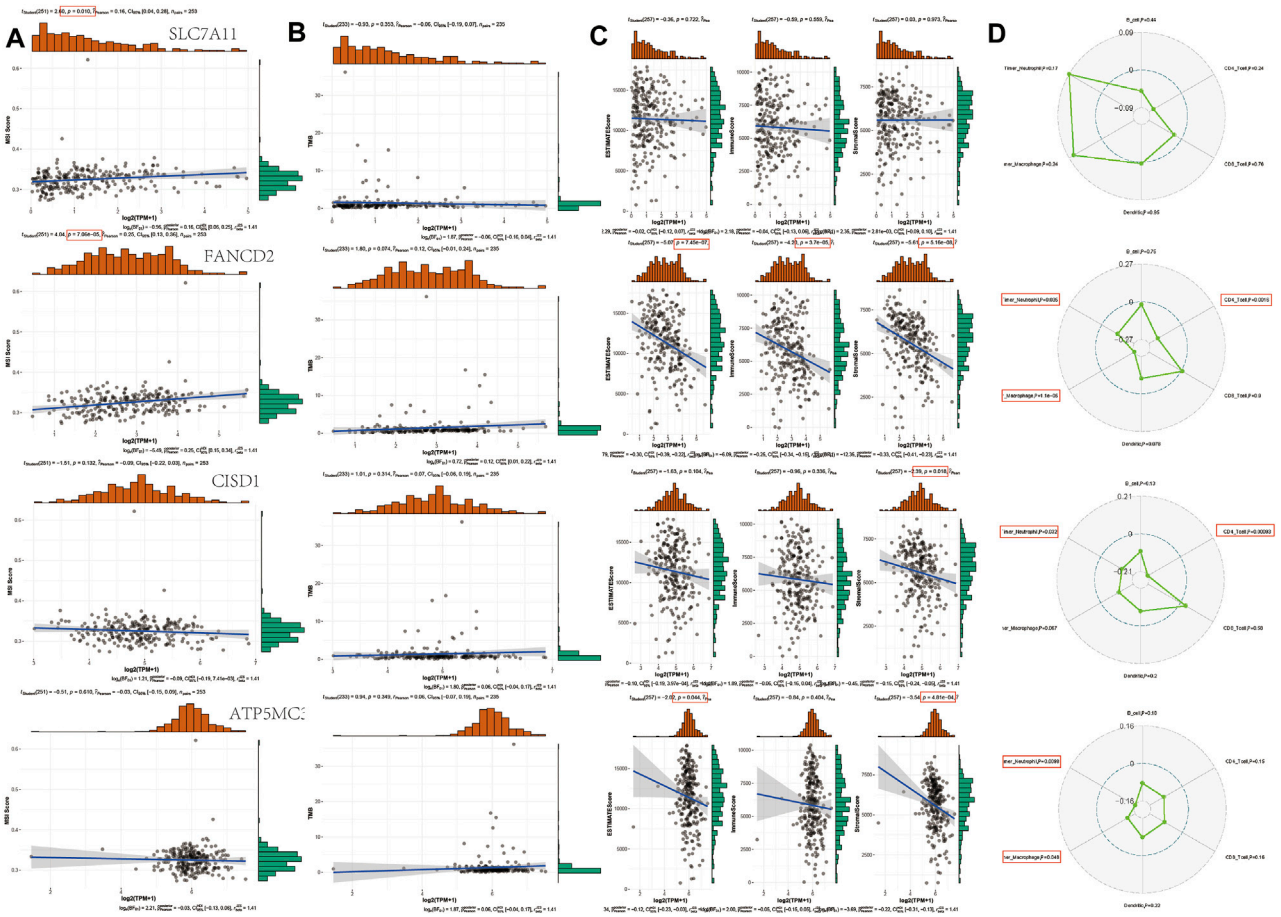

FIGURE 8 | TMB, MSI, and ESTIMATE Score analysis of FRG in SARC. **(A)** Correlation between 4 prognostic FRGs and MSI in SARC. **(B)** Correlation between 4 prognostic FRGs and TMB in SARC. **(C)** Correlation between 4 prognostic FRGs and ESTIMATE Score in SARC. **(D)** Correlation between 4 prognostic FRGs and immune score in SARC. TMB, tumor mutation burden; MSI, microsatellite instability; LUAD, lung adenocarcinoma; FRG, ferroptosis-related gene; CTRP, Cancer Therapeutics Response Portal; GDSC, Genomics of Drug Sensitivity in Cancer.

mitochondrial protein complex in CC pathway, electron transfer activity, NADH dehydrogenase activity in MF and Parkinson disease, oxidative phosphorylation, and non-alcoholic fatty liver disease in KEGG (**Supplementary Figure S3A,B**).

The data identified 5 miRNAs such as hsa-mir-140-3p, hsa-mir-221-3p, hsa-mir-222-3p, and has-miR-16-5p as the targeting mRNA binding to CISD1, ATP5MC3, SLC7A11, and FANCD2 in ENCORI dataset. The high levels of hsa-mir-29c-3p, hsa-mir-15b-5p, hsa-mir-425-5p, and hsa-mir-424-5p were correlated with poor prognosis in SARC (**Supplementary Figure S6** and **Table 2** and **3**). Based on this result, we also checked its upstream lncRNA target to construct an miRNA–lncRNA axis. As shown in **Supplementary Figure S4**, we found the miRNA–LncRNA network in has-mir-29c-3p with 11 lncRNA in **Supplementary Figure S4A**. We also analyzed the expression level of SARC in **Supplementary Figure S4B**. The higher level of 3 lncRNA such as TPL1P1 (p = 0.0017), HSP90AB3P (p = 0.00044), and GAPDHP (p = 0.0068) were correlated with poor prognosis (**Supplementary Figure S4**). According to mirTarBase and TarBase V.8, Has-mir-29c-3p has been identified as the target of the ceRNA network (**Supplementary Figure S6**). We found that 52 common lncRNAs have been found in mirTarBase and TarBase V.8., and the LncRNA–miRNA–mRNA network has also been contributed in SARC (**Supplementary Figure S6**).

DISCUSSION

Ferroptosis is a recently found form of cell-regulated death related to the metabolism pathway in human health (Liang et al., 2019). Accumulation of iron (II) and lipid peroxidation play important roles in causing ferroptosis. Iron chelators and lipophilic antioxidants can inhibit ferroptosis (Su et al., 2020). However, there is increasing evidence that iron poisoning plays an important role in neuro-diseases, including neurodegenerative diseases and cardiovascular diseases (Zhou et al., 2020). In addition, a thorough FRG landscape analysis of soft tissue sarcoma revealed a new type of FRG related to cancer and

TABLE 1 | Hub gene analysis by GO analysis.

node_name	MCC	DMNC	MNC	Degree	EPC	Bottleneck	Eccentricity	Closeness	Radiality	Betweenness	Stress	Clustering coefficient
SAT1	2	0	1	4	13.791	1	0.16667	8.05	5	2	24	0
HSPA5	3	0.61557	2	6	14.376	3	0.2	9.73333	5.66667	76	2,544	0.13333
SLC1A5	2	0.61557	2	4	12.805	1	0.16667	7.58333	4.80952	0	0	0.33333
GLS2	2	0.61557	2	4	13.12	1	0.16667	7.58333	4.80952	0	0	0.33333
FDFT1	1	0	1	2	9.216	1	0.14286	6.17619	4.04762	0	0	0
TFRC	3	0	1	6	12.628	4	0.2	9.28333	5.57143	96	3,016	0
DPP4	1	0	1	2	9.464	1	0.16667	6.58333	4.61905	0	0	0
HSPB1	2	0	1	4	11.097	2	0.16667	7.46667	4.80952	40	1704	0
CS	1	0	1	2	8.169	1	0.14286	5.66905	3.85714	0	0	0
NCOA4	3	0	1	6	13.921	22	0.25	10.58333	6.09524	212	6,504	0
NFE2L2	6	0.61795	3	10	15.15	3	0.2	10.9	5.80952	71.66667	1776	0.08889
CDKN1A	1	0	1	2	11.024	1	0.16667	7.21667	4.85714	0	0	0
CARS	1	0	1	2	9.431	1	0.14286	6.25952	4.09524	0	0	0
CISD1	3	0.61557	2	6	13	4	0.2	9.11667	5.52381	84	2,912	0.13333
RPL8	4	0.61557	2	8	12.874	2	0.16667	9	5.04762	52	1,640	0.07143
EMC2	5	0.61795	3	8	12.739	2	0.16667	8.83333	5	42	1,568	0.14286
ATP5G3	4	0.61795	3	6	12.671	1	0.16667	8.33333	4.95238	2	24	0.26667
GPX4	11	0.47549	6	14	15.35	22	0.25	12.66667	6.28571	259.3333	7,152	0.10989
ALOX15	2	0.61557	2	4	14.017	1	0.2	8.48333	5.38095	0	0	0.33333
SLC7A11	6	0.61795	3	10	15.039	3	0.2	10.65	5.71429	78	1896	0.13333
LPCAT3	3	0.61557	2	6	14.695	1	0.2	9.15	5.47619	13.33333	640	0.13333
ACSL4	6	0.56839	4	8	15.093	1	0.2	9.98333	5.61905	7.66667	104	0.21429

TABLE 2 | Prediction of miRNA binding to ATP5MC3.

Gene name	miRNA name	PITA	RNA22	miRmap	microT	miRanda	PicTar	TargetScan	Number
ATP5MC3	hsa-miR-425-5p	1	0	1	1	1	1	1	6
ATP5MC3	hsa-miR-15a-5p	1	0	1	1	1	0	0	4
ATP5MC3	hsa-miR-16-5p	1	0	1	1	1	0	0	4
ATP5MC3	hsa-miR-27a-3p	1	0	1	0	1	0	1	4
ATP5MC3	hsa-miR-29a-3p	1	0	1	0	1	0	1	4
ATP5MC3	hsa-miR-29b-3p	1	0	1	0	1	0	1	4
ATP5MC3	hsa-miR-139-5p	1	0	1	0	1	0	1	4
ATP5MC3	hsa-miR-15b-5p	1	0	1	1	1	0	0	4
ATP5MC3	hsa-miR-27b-3p	1	0	1	0	1	0	1	4
ATP5MC3	hsa-miR-195-5p	1	0	1	1	1	0	0	4
ATP5MC3	hsa-miR-29c-3p	1	0	1	0	1	0	1	4
ATP5MC3	hsa-miR-424-5p	1	0	1	1	1	0	0	4
ATP5MC3	hsa-miR-425-5p	1	0	1	1	1	0	0	4
CISD1	hsa-miR-140-3p	1	1	0	1	0	0	1	4
FANCD2	hsa-miR-221-3p	1	0	1	0	1	1	0	4
FANCD2	hsa-miR-222-3p	1	0	1	0	1	1	0	4
SLC7A11	hsa-miR-26a-5p	1	0	1	1	1	1	1	6
SLC7A11	hsa-miR-26b-5p	1	0	1	1	1	1	1	6
SLC7A11	hsa-miR-27a-3p	1	0	1	1	1	1	1	6
SLC7A11	hsa-miR-27b-3p	1	0	1	1	1	1	1	6
SLC7A11	hsa-miR-329-3p	2	0	2	2	0	0	0	6
SLC7A11	hsa-miR-362-3p	2	0	2	2	0	0	0	6
SLC7A11	hsa-miR-1297	1	0	1	1	1	1	1	6

prognosis (Huang et al., 2021). Ferroptosis has recently become a treatment target and potential biomarkers for sarcoma (Chen et al., 2021).

We performed this study for the first time using gene information of SARC from open databases. First, we chose 32 genes, which are related to ferroptosis. Among them, four ferroptosis genes were analyzed using Cox and LASSO regression to select potential prognostic markers of one variant and then to construct a prognostic model. Among them, the expression level of two genes (SLC7A11 and FANCD2) was negatively correlated with OS, and the expression level of one gene (NCOA4) was positively correlated with OS. These data are consistent with previous results. Sun et al. found that the inhibition of GSH and SLC7A11 is the main cause of EMT and iron

TABLE 3 | Prognostic values of potential upstream miRNAs of in TCGA sarcoma cancer cohort.

miRNA	Cancer	Cox coefficient	*p*-value	FDR Corrected	Rank	Median Expression	Mean Expression
hsa-miR-29c-3p	ATP5MC3	–0.356	0.0011	0.0125	40	273.42	444.98
hsa-miR-15b-5p	ATP5MC3	0.262	0.014	0.0625	97	196.27	270.8
hsa-miR-425-5p	ATP5MC3	0.233	3.30E-02	9.88E-02	152	83.61	111.13
hsa-miR-424-5p	ATP5MC3	0.191	0.046	0.12	174	145.56	238.01
hsa-miR-362-3p	SLC7A11	0.19	0.062	0.144	196	2.62	4.12
hsa-miR-26a-5p	SLC7A11	0.171	0.11	0.212	234	1,544.81	4,683.31
hsa-miR-16-5p	ATP5MC3	0.149	1.20E-01	2.21E-01	238	395.86	429.71
hsa-miR-29a-3p	ATP5MC3	–0.127	0.23	0.355	295	2,448.34	3,355.48
hsa-miR-195-5p	ATP5MC3	–0.115	0.24	0.365	299	31.24	42.44
hsa-miR-222-3p	FANCD2	0.112	2.90E-01	4.16E-01	316	72.38	117.04
hsa-miR-26b-5p	SLC7A11	0.1	0.33	0.461	324	334.61	427.63
hsa-miR-221-3p	FANCD2	0.095	3.70E-01	5.00E-01	335	280.69	469.1
hsa-miR-140-3p	CISD1	0.071	0.46	0.586	354	1,235.76	1,534.06
hsa-miR-27b-3p	ATP5MC3	–0.063	0.56	0.669	381	895.4	1,123.92
hsa-miR-27b-3p	SLC7A11	–0.063	0.56	0.669	381	895.4	1,123.92
hsa-miR-27a-3p	ATP5MC3	0.059	0.58	0.685	383	836.55	992.59
hsa-miR-27a-3p	SLC7A11	0.059	0.58	0.685	383	836.55	992.59
hsa-miR-29b-3p	ATP5MC3	–0.024	0.82	0.872	427	223.34	393.42
hsa-miR-139-5p	ATP5MC3	0.003	0.98	0.984	449	41.27	61.09
hsa-miR-15a-5p	ATP5MC3	–0.001	9.90E-01	9.92E-01	454	201.56	223.4

deficiency in A549 cells (Sun et al., 2021). SLC7A11 is becoming a potential new cancer treatment target. This article briefly introduces the structure and function of SLC7A11 (Lin et al., 2020). FANCD2 has played a new role in reducing ferroptosis. FANCD2 can be used as a target for the development of new cancer therapies aimed at reducing the side effects of ferroptosis (Song et al., 2016). ATP5MC3 is better predictor in a risk prognosis model and also be defined as potential drug for treatment of prostate cancer.

We also analyzed the functional enrichment of these FRGs and found that these 32 FRGs are mainly involved in the regulation of the p53 gene transcription network, response to toxic substance, ER–nucleus signaling pathway, endoplasmic reticulum organization, cellular transition metal ion homeostasis, and peptide transport (Kang et al., 2019). It has been confirmed that the level of glutathione in intestinal tissue is the most influential metabolic pathway related to glutathione/GPx 4 after exposure to microcystin (Zhang et al., 2021). Colitis mice is evidently induced by ferroptosis, which is mediated by stress signals from the endoplasmic reticulum (Xu et al., 2020). The enigmatic lipid peroxidation product is believed to be the direct agent of ferritin metabolism, a special death program caused by glutathione peroxidase 4 (GPX4) insufficiency (Kagan et al., 2017).

In recent years, it has fundamentally changed the way cancer is treated (Dupont et al., 2021), which pointed out that by integrating multi-dimensional biological data and clinical characteristics, highly heterogeneous tumors can be classified into more specific subtypes for personalized treatment (Zhang H et al., 2020). In fact, the accumulation of evidence based on molecular profiling has established itself in the subgroup of cancer patients representing different phenotypes, prognosis, and treatment response (Tan et al., 2019). According to the characteristics of immunogen expression, patients with sarcoma can be divided into two subtypes: prognosis and clinical importance. Patients with high-risk immune subtypes are more sensitive to immune checkpoint blockers (Francescutti and Skitzki, 2012; Tsukahara et al., 2016).

In addition, we developed a ferritin-related gene-based nomogram prediction model for predicting OS in SARC patients. The calibration table and ROC analysis show that the nomogram has a reliable predictive ability for the queue TCGA operating system. The Nomap model can be used to determine the patient's prognosis and make follow-up plans.

GSEA showed that the drug is more sensitive to immune response and tumor progression in the high-risk group. In Kaposi's sarcoma, chemotherapy with vincristine, bleomycin, and etoposide appears to improve overall survival, survival, and quality of life (Macken et al., 2018). Methotrexate also plays an important role high-grade osteosarcoma in children and young adults (van Dalen et al., 2011; Abe et al., 2021). The overall biological response in Ewing's sarcoma exposure shows differences in response (Aryee et al., 2013).

miRNA and lncRNA play a role in a variety of biological and pathological processes, such as apoptosis, cell cycle, migration, invasion, regulating proliferation, metastasis, EMT, and resistance to drugs. It plays an important role and has been extensively studied. mRNAs are target through transcription or post-transcription (Wang et al., 2020). Therefore, the LncRNA–miRNA–mRNA network was contributed in our studies. Perilous studies found that LncRNA TTN-AS1 regulates apoptosis and drug resistance in osteosarcoma cells through the miR-134-5p/MBTD1 axis (Fu et al., 2019). Zhang et al. also investigated that LncRNA axis SNHG3/miRNA-151a-3p/RAB22A regulates osteosarcoma invasion and migration (Zheng et al., 2019).

Advances in cancer treatment are increasingly recognizing a more promising approach to ferroptosis in the development of effective combination therapies (Friedmann Angeli et al., 2019). As first-line treatment options for patients with SARC are developed, the biology of the tumor and the tumor microenvironment should be considered in order to obtain optimal benefit from treatment strategies. The

expression of NCOA4 may be a potential new factor that promotes the stratification of SARC and/or immunotherapy in patients with iron hook, which may be an important factor in predicting the recurrence of SARC patients. In addition, the modulation of SLC7A11 overexpressed in many types of cancers and is associated with patients' poor prognosis (Lin et al., 2020). In addition, FANCD2 genes were correlated with the diagnostic and prognostic factors of low-grade glioma and breast cancer (Fagerholm et al., 2013; Liu et al., 2020). CISD1 was also regarded as a potentially effective tool for prognostic of pancreatic cancer (Yang et al., 2022). It means that ferroptosis-related genes show great potential during many cancer therapies (Xu et al., 2019).

The major limitation in this study is the lack of available analysis of data heterogeneity and platform differences based on a large number of normal and tumor samples. Our study shows that the disease-related level and extreme harshness of TNM staging are not independent prediction-related factors for OS in SARC patients. This difference may be due to heterogeneity of the data or different classification and classification models (Warren and Harrison, 2018). In addition, the group cancer type information in TCGA database is mainly limited to sarcoma groups, so it is difficult to extrapolate these results to different types and locations of sarcomas. The development of this field also requires further efforts to verify the results of bioinformatics predictions, including the detection of Western blotting proteins or immunohistochemical staining, to promote the analysis of iron dependence *in vivo* and *in vitro* and immunotherapy functions.

CONCLUSION

In general, ferroptosis induction and immunotherapy are now the main advances in the treatment of SARC. With a deeper understanding of bleomycin therapy biology and resistance mechanisms, ferroptosis-based combination therapy has received more and more attention. We first found that the high expression of SLC7A11, FANCD2, CISD1, and ATP3MC3 genes related to ferroptosis, which is related to the signal transduction of the infiltrating immune cell receptor in SARC. Therefore, it is expected that SLC7A11, FANCD2, CISD1, and ATP3MC3 will be used as new markers to identify patients who may undergo adequate ferroptosis induction therapy or combined immunotherapy.

DATA AVAILABILITY STATEMENT

The original contributions presented in the study are included in the article/**Supplementary Material**; further inquiries can be directed to the corresponding authors.

AUTHOR CONTRIBUTIONS

Conception and design: ZG and SL. Acquisition, analysis, and interpretation of the data: ZG, SL, ZW, SFL, and ZG. Drafting and writing: ZG. Final approval of the article: ZG, SL, ZW, SFL, ZG, and KT.

ACKNOWLEDGMENTS

We would like to thank all participants and our hospital.

SUPPLEMENTARY MATERIAL

The Supplementary Material for this article can be found online at: https://www.frontiersin.org/articles/10.3389/fcell.2022.847513/full#supplementary-material

REFERENCES

Abe, K., Higurashi, T., Takahashi, M., Maeda-Minami, A., Kawano, Y., Miyazaki, S., et al. (2021).Concomitant Use of High-Dose Methotrexate and Glycyrrhizin Affects Pharmacokinetics of Methotrexate, Resulting in Hepatic Toxicity. In Vivo.35 (4), 2163–2169. doi:10.21873/invivo.12487

Alba, A. C., Agoritsas, T., Walsh, M., Hanna, S., Iorio, A., Devereaux, P. J., et al. (2017). Discrimination and Calibration of Clinical Prediction Models.*Jama.*318 (14), 1377–1384. doi:10.1001/jama.2017.12126

Aryee, D. N. T., Niedan, S., Ban, J., Schwentner, R., Muehlbacher, K., Kauer, M., et al. (2013).Variability in Functional P53 Reactivation by PRIMA-1Met/APR-246 in Ewing Sarcoma.*Br. J. Cancer.*109 (10), 2696–2704. doi:10.1038/bjc.2013.635

Battaglia, A. M., Chirillo, R., Aversa, I., Sacco, A., Costanzo, F., and Biamonte, F. (2020).Ferroptosis and Cancer: Mitochondria Meet the "Iron Maiden" Cell Death. *Cells.*9 (6), 1505.doi:10.3390/cells9061505

Benjamin, E. J., Blaha, M. J., Chiuve, S. E., Cushman, M., Das, S. R., Deo, R., et al. (2017).Heart Disease and Stroke Statistics-2017 Update: A Report from the American Heart Association. *Circulation.*135 (10), e146–e603.doi:10.1161/CIR.0000000000000485

Blatt, J. (1994). Deferoxamine in Children with Recurrent Neuroblastoma.*Anticancer Res.*14 (5b), 2109–2112.

Brennan, M. F., Antonescu, C. R., Moraco, N., and Singer, S. (2014). Lessons Learned from the Study of 10,000 Patients with Soft Tissue Sarcoma. *Ann. Surg.*260 (3), 416–421. doi:10.1097/SLA.0000000000000869

Campbell, B. B., Light, N., Fabrizio, D., Zatzman, M., Fuligni, F., de Borja, R., et al. (2017).Comprehensive Analysis of Hypermutation in Human Cancer.*Cell.*171 (5), 1042–1056. doi:10.1016/j.cell.2017.09.048

Chan, J. Y., Lim, J. Q., Yeong, J., Ravi, V., Guan, P., Boot, A., et al. (2020). Multiomic Analysis and Immunoprofiling Reveal Distinct Subtypes of Human Angiosarcoma. *J. Clin. Invest.*130 (11), 5833–5846. doi:10.1172/jci139080

Chen, M., Jiang, Y., and Sun, Y. (2021).KDM4A-mediated Histone Demethylation of SLC7A11 Inhibits Cell Ferroptosis in Osteosarcoma. *Biochem.biophysical Res. Commun.*550, 77–83. doi:10.1016/j.bbrc.2021.02.137

Dächert, J., Ehrenfeld, V., Habermann, K., Dolgikh, N., and Fulda, S. (2020). Targeting Ferroptosis in Rhabdomyosarcoma Cells.*Int. J. Cancer.*146 (2), 510–520. doi:10.1002/ijc.32496

Dupont, C. A., Riegel, K., Pompaiah, M., Juhl, H., and Rajalingam, K. (2021).Druggable Genome and Precision Medicine in Cancer: Current Challenges. *Febs J.*288 (21), 6142–6158. doi:10.1111/febs.15788

Fagerholm, R., Sprott, K., Heikkinen, T., Bartkova, J., Heikkilä, P., Aittomäki, K., et al. (2013).Overabundant FANCD2, Alone and Combined with NQO1, Is a Sensitive Marker of Adverse Prognosis in Breast Cancer. *Ann. Oncol.*24 (11), 2780–2785. doi:10.1093/annonc/mdt290

Francescutti, V., and Skitzki, J. J. (2012).Sarcomas and the Immune System: Implications for Therapeutic Strategies. *Surg. Oncol. Clin. North America.*21 (2), 341–355. doi:10.1016/j.soc.2011.11.002

Friedmann Angeli, J. P., Krysko, D. V., and Conrad, M. (2019).Ferroptosis at the Crossroads of Cancer-Acquired Drug Resistance and Immune Evasion.*Nat. Rev. Cancer.*19 (7), 405–414. doi:10.1038/s41568-019-0149-1

Fu, D., Lu, C., Qu, X., Li, P., Chen, K., Shan, L., et al. (2019).LncRNA TTN-AS1 Regulates Osteosarcoma Cell Apoptosis and Drug Resistance via the miR-134-5p/MBTD1 axis.*Aging.*11 (19), 8374–8385. doi:10.18632/aging.102325

Huang, W., Duan, Y., Yang, X., Shang, C., Chen, X., Zhang, H., et al. (2021).Identification of Novel Prognostic Risk Signatures of Soft Tissue Sarcoma Based on Ferroptosis-Related Genes.*Front. Oncol.*11, 629868.doi:10.3389/fonc.2021.629868

Jiang, X., Stockwell, B. R., and Conrad, M. (2021).Ferroptosis: Mechanisms, Biology and Role in Disease. *Nat. Rev. Mol. Cel Biol.*22 (4), 266–282. doi:10.1038/s41580-020-00324-8

Jung, M., Mertens, C., Tomat, E., and Brüne, B. (2019).Iron as a Central Player and Promising Target in Cancer Progression. *Int. J. Mol. Sci.*20 (2), 273.doi:10.3390/ijms20020273

Kagan, V. E., Mao, G., Qu, F., Angeli, J. P. F., Doll, S., Croix, C. S., et al. (2017).Oxidized Arachidonic and Adrenic PEs Navigate Cells to Ferroptosis. *Nat. Chem. Biol.*13 (1), 81–90. doi:10.1038/nchembio.2238

Kang, R., Kroemer, G., and Tang, D. (2019).The Tumor Suppressor Protein P53 and the Ferroptosis Network.*Free Radic. Biol. Med.*133, 162–168. doi:10.1016/j.freeradbiomed.2018.05.074

Latham, A., Srinivasan, P., Kemel, Y., Shia, J., Bandlamudi, C., Mandelker, D., et al. (2019).Microsatellite Instability Is Associated with the Presence of Lynch Syndrome Pan-Cancer. *J. Clin. Oncol.*37 (4), 286–295. doi:10.1200/jco.18.00283

Li, D., and Li, Y. (2020).The Interaction between Ferroptosis and Lipid Metabolism in Cancer.*Sig Transduct Target.Ther.*5 (1), 108.doi:10.1038/s41392-020-00216-5

Li, T., Fu, J., Zeng, Z., Cohen, D., Li, J., Chen, Q., et al. (2020).TIMER2.0 for Analysis of Tumor-Infiltrating Immune Cells.*Nucleic Acids Res.*48 (W1), W509–W514.doi:10.1093/nar/gkaa407

Liang, C., Zhang, X., Yang, M., and Dong, X. (2019).Recent Progress in Ferroptosis Inducers for Cancer Therapy.*Adv. Mater.*31 (51), e1904197.doi:10.1002/adma.201904197

Liberzon, A., Birger, C., Thorvaldsdóttir, H., Ghandi, M., Mesirov, J. P., and Tamayo, P. (2015).The Molecular Signatures Database Hallmark Gene Set Collection.*Cel Syst.*1 (6), 417–425. doi:10.1016/j.cels.2015.12.004

Lin, H., Chen, X., Zhang, C., Yang, T., Deng, Z., Song, Y., et al. (2021).EF24 Induces Ferroptosis in Osteosarcoma Cells through HMOX1. *Biomed.Pharmacother.*136, 111202.doi:10.1016/j.biopha.2020.111202

Lin, W., Chen, Y., Wu, B., Chen, Y., and Li, Z. (2021). Identification of the Pyroptosis-related Prognostic Gene Signature and the Associated Regulation axis in Lung Adenocarcinoma.*Cell Death Discov.*7 (1), 161.doi:10.1038/s41420-021-00557-2

Lin, W., Wang, C., Liu, G., Bi, C., Wang, X., Zhou, Q., et al. (2020). SLC7A11/xCT in Cancer: Biological Functions and Therapeutic Implications. *Am. J. Cancer Res.*10 (10), 3106–3126.

Liu, H., Gao, L., Xie, T., Li, J., Zhai, T.-s., and Xu, Y. (2021). Identification and Validation of a Prognostic Signature for Prostate Cancer Based on Ferroptosis-Related Genes.*Front. Oncol.*11, 623313.doi:10.3389/fonc.2021.623313

Liu, Y., Xu, Z., Jin, T., Xu, K., Liu, M., and Xu, H. (2020).Ferroptosis in Low-Grade Glioma: A New Marker for Diagnosis and Prognosis. *Med. Sci. Monit.*26, e921947.doi:10.12659/MSM.921947

Macken, M., Dale, H., Moyo, D., Chakmata, E., Depani, S., Israels, T., et al. (2018).Triple Therapy of Vincristine, Bleomycin and Etoposide for Children with Kaposi Sarcoma: Results of a Study in Malawian Children. *Pediatr.Blood Cancer.*65 (2), e26841.doi:10.1002/pbc.26841

Mou, Y., Zhang, Y., Wu, J., Hu, B., Zhang, C., Duan, C., et al. (2020). The Landscape of Iron Metabolism-Related and Methylated Genes in the Prognosis Prediction of Clear Cell Renal Cell Carcinoma.*Front. Oncol.*10, 788.doi:10.3389/fonc.2020.00788

Newman, A. M., Liu, C. L., Green, M. R., Gentles, A. J., Feng, W., Xu, Y., et al. (2015). Robust Enumeration of Cell Subsets from Tissue Expression Profiles.*Nat. Methods.*12 (5), 453–457. doi:10.1038/nmeth.3337

Reed, D. R., Naghavi, A., and Binitie, O. (2019).Sarcoma as a Model for Adolescent and Young Adult Care.*J. Oncol. Pract.*15 (5), 239–247. doi:10.1200/jop.18.00684

Samstein, R. M., Lee, C.-H., Shoushtari, A. N., Hellmann, M. D., Shen, R., Janjigian, Y. Y., et al. (2019). Tumor Mutational Load Predicts Survival after Immunotherapy across Multiple Cancer Types. *Nat. Genet.*51 (2), 202–206. doi:10.1038/s41588-018-0312-8

Shintoku, R., Takigawa, Y., Yamada, K., Kubota, C., Yoshimoto, Y., Takeuchi, T., et al. (2017).Lipoxygenase-mediated Generation of Lipid Peroxides Enhances Ferroptosis Induced by Erastin and RSL3. *Cancer Sci.*108 (11), 2187–2194. doi:10.1111/cas.13380

Song, X., Xie, Y., Kang, R., Hou, W., Sun, X., Epperly, M. W., et al. (2016).FANCD2 Protects against Bone Marrow Injury from Ferroptosis. *Biochem.biophysical Res. Commun.*480 (3), 443–449. doi:10.1016/j.bbrc.2016.10.068

Sturm, G., Finotello, F., Petitprez, F., Zhang, J. D., Baumbach, J., Fridman, W. H., et al. (2019).Comprehensive Evaluation of Transcriptome-Based Cell-type Quantification Methods for Immuno-Oncology. *Bioinformatics (Oxford, England).*35 (14), i436–i445.doi:10.1093/bioinformatics/btz363

Su, Y., Zhao, B., Zhou, L., Zhang, Z., Shen, Y., Lv, H., et al. (2020).Ferroptosis, a Novel Pharmacological Mechanism of Anti-cancer Drugs.*Cancer Lett.*483, 127–136. doi:10.1016/j.canlet.2020.02.015

Subramanian, A., Tamayo, P., Mootha, V. K., Mukherjee, S., Ebert, B. L., Gillette, M. A., et al. (2005).Gene Set Enrichment Analysis: a Knowledge-Based Approach for Interpreting Genome-wide Expression Profiles. *Proc. Natl. Acad. Sci.*102 (43), 15545–15550. doi:10.1073/pnas.0506580102

Sun, L., Dong, H., Zhang, W., Wang, N., Ni, N., Bai, X., et al. (2021).Lipid Peroxidation, GSH Depletion, and SLC7A11 Inhibition Are Common Causes of EMT and Ferroptosis in A549 Cells, but Different in Specific Mechanisms. *DNA Cel. Biol.*40 (2), 172–183. doi:10.1089/dna.2020.5730

Tan, T. Z., Rouanne, M., Tan, K. T., Huang, R. Y.-J., and Thiery, J.-P. (2019). Molecular Subtypes of Urothelial Bladder Cancer: Results from a Meta-Cohort Analysis of 2411 Tumors. *Eur. Urol.*75 (3), 423–432. doi:10.1016/j.eururo.2018.08.027

Tang, R., Xu, J., Zhang, B., Liu, J., Liang, C., Hua, J., et al. (2020).Ferroptosis, Necroptosis, and Pyroptosis in Anticancer Immunity.*J. Hematol. Oncol.*13 (1), 110.doi:10.1186/s13045-020-00946-7

Tsukahara, T., Emori, M., Murata, K., Mizushima, E., Shibayama, Y., Kubo, T., et al. (2016).The Future of Immunotherapy for Sarcoma.*Expert Opin. Biol. Ther.*16 (8), 1049–1057. doi:10.1080/14712598.2016.1188075

van Dalen, E. C., van As, J. W., and de Camargo, B. (2011). Methotrexate for High-Grade Osteosarcoma in Children and Young Adults.*Cochrane Database Syst. Rev.*2011 (5), Cd006325. doi:10.1002/14651858.CD006325.pub3

Wang, J.-y., Yang, Y., Ma, Y., Wang, F., Xue, A., Zhu, J., et al. (2020).Potential Regulatory Role of lncRNA-miRNA-mRNA axis in Osteosarcoma. *Biomed.Pharmacother.*121, 109627.doi:10.1016/j.biopha.2019.109627

Warren, A. Y., and Harrison, D. (2018).WHO/ISUP Classification, Grading and Pathological Staging of Renal Cell Carcinoma: Standards and Controversies. *World J. Urol.*36 (12), 1913–1926. doi:10.1007/s00345-018-2447-8

Xu, M., Tao, J., Yang, Y., Tan, S., Liu, H., Jiang, J., et al. (2020).Ferroptosis Involves in Intestinal Epithelial Cell Death in Ulcerative Colitis. *Cell Death Dis.*11 (2), 86. doi:10.1038/s41419-020-2299-1

Xu, T., Ding, W., Ji, X., Ao, X., Liu, Y., Yu, W., et al. (2019). Molecular Mechanisms of Ferroptosis and its Role in Cancer Therapy.*J. Cel Mol Med.*23 (8), 4900–4912. doi:10.1111/jcmm.14511

Yang, J., Wei, X., Hu, F., Dong, W., and Sun, L. (2022).Development and Validation of a Novel 3-gene Prognostic Model for Pancreatic Adenocarcinoma Based on Ferroptosis-Related Genes.*Cancer Cel Int.*22 (1), 21.doi:10.1186/s12935-021-02431-8

Ye, Y., Dai, Q., and Qi, H. (2021).A Novel Defined Pyroptosis-Related Gene Signature for Predicting the Prognosis of Ovarian Cancer. *Cel Death Discov.*7 (1), 71.doi:10.1038/s41420-021-00451-x

Zhang, H., Ahearn, T. U., Lecarpentier, J., Barnes, D., Beesley, J., Qi, G., et al. (2020). Genome-wide Association Study Identifies 32 Novel Breast Cancer Susceptibility Loci from Overall and Subtype-specific Analyses.*Nat. Genet.*52 (6), 572–581. doi:10.1038/s41588-020-0609-2

Zhang, S., Chang, W., Wu, H., Wang, Y. H., Gong, Y. W., Zhao, Y. L., et al. (2020). Pan-cancer Analysis of Iron Metabolic Landscape across the Cancer Genome Atlas.*J.Cel Physiol*235 (2), 1013–1024. doi:10.1002/jcp.29017

Zhang, Y., Wu, D., Fan, Z., Li, J., Gao, L., Wang, Y. e., et al. (2021). Microcystin-LR Induces Ferroptosis in Intestine of Common Carp (Cyprinus carpio). *Ecotoxicology Environ. Saf.*223, 112610.doi:10.1016/j.ecoenv.2021.112610

Zheng, J., and Conrad, M. (2020).The Metabolic Underpinnings of Ferroptosis.*Cel Metab.*32 (6), 920–937. doi:10.1016/j.cmet.2020.10.011

Zheng, S., Jiang, F., Ge, D., Tang, J., Chen, H., Yang, J., et al. (2019).LncRNA SNHG3/miRNA-151a-3p/RAB22A axis Regulates Invasion and Migration of Osteosarcoma.*Biomed.Pharmacother.*112, 108695.doi:10.1016/j.biopha.2019.108695

Zhou, R.-P., Chen, Y., Wei, X., Yu, B., Xiong, Z.-G., Lu, C., et al. (2020).Novel Insights into Ferroptosis: Implications for Age-Related Diseases. *Theranostics.*10 (26), 11976–11997. doi:10.7150/thno.50663

Zhu, M. M. T., Shenasa, E., and Nielsen, T. O. (2020).Sarcomas: Immune Biomarker Expression and Checkpoint Inhibitor Trials. *Cancer Treat.Rev.*91, 102115.doi:10.1016/j.ctrv.2020.102115

Conflict of Interest: The authors declare that the research was conducted in the absence of any commercial or financial relationships that could be construed as a potential conflict of interest.

Publisher's Note: All claims expressed in this article are solely those of the authors and do not necessarily represent those of their affiliated organizations, or those of the publisher, the editors, and the reviewers. Any product that may be evaluated in this article, or claim that may be made by its manufacturer, is not guaranteed or endorsed by the publisher.

frontiers in Genetics

ORIGINAL RESEARCH
published: 08 March 2022
doi: 10.3389/fgene.2022.865073

Nobiletin Induces Ferroptosis in Human Skin Melanoma Cells Through the GSK3β-Mediated Keap1/Nrf2/HO-1 Signalling Pathway

Senling Feng[1†], Yongheng Zhou[2†], Hongliang Huang[1†], Ying Lin[3], Yifeng Zeng[2], Shanshan Han[3], Kaikai Huang[3], Quanzhi Liu[3], Wenting Zhu[1], Zhongwen Yuan[1] and Baoying Liang[3]**

[1]Key Laboratory for Major Obstetric Diseases of Guangdong Province, Department of Pharmacy, The Third Affiliated Hospital of Guangzhou Medical University, Guangzhou, China, [2]Department of Pharmacy, The Fourth Affiliated Hospital of Guangzhou Medical University, Guangzhou, China, [3]Guangdong Provincial Clinical Research Center for Chinese Medicine Dermatology, Department of Dermatology, Guangdong Provincial Hospital of Traditional Chinese Medicine, The Second Affiliated Hospital of Guangzhou University of Traditional Chinese Medicine, Guangzhou, China

OPEN ACCESS

Edited by:
Lian Xiang Luo,
Guangdong Medical University, China

Reviewed by:
Zheng Xiang,
Liaoning University, China
Qiaosi Tang,
Calico Life Sciences LLC,
United States
Yi-You Huang,
Hainan University, China

***Correspondence:**
Zhongwen Yuan
2018681079@gzhmu.edu.cn
Baoying Liang
byliangmust@163.com

†These authors have contributed equally to this work

Specialty section:
This article was submitted to Human and Medical Genomics, a section of the journal Frontiers in Genetics

Received: 29 January 2022
Accepted: 21 February 2022
Published: 08 March 2022

Citation:
Feng S, Zhou Y, Huang H, Lin Y, Zeng Y, Han S, Huang K, Liu Q, Zhu W, Yuan Z and Liang B (2022) Nobiletin Induces Ferroptosis in Human Skin Melanoma Cells Through the GSK3β-Mediated Keap1/Nrf2/HO-1 Signalling Pathway. Front. Genet. 13:865073. doi: 10.3389/fgene.2022.865073

Melanoma is an aggressive malignant skin tumour with an increasing global incidence. However, current treatments have limitations owing to the acquired tumour drug resistance. Ferroptosis is a recently discovered form of programmed cell death characterised by iron accumulation and lipid peroxidation and plays a critical role in tumour growth inhibition. Recently, ferroptosis inducers have been regarded as a promising therapeutic strategy to overcome apoptosis resistance in tumour cells. In this study, we reported that nobiletin, a natural product isolated from citrus peel, and exhibited antitumour activity by inducing ferroptosis in melanoma cells. Subsequently, we further explored the potential mechanism of nobiletin-induced ferroptosis, and found that the expression level of glycogen synthase kinase 3β (GSK3β) in the skin tissue of patients with melanoma was significantly reduced compared to that in the skin of normal tissue. Additionally, nobiletin increased GSK3β expression in melanoma cells. Moreover, the level of Kelch-like Ech-associated protein-1 (Keap1) was increased, while the level of nuclear factor erythroid 2-related factor 2 (Nrf2), and haem oxygenase-1 (HO-1) was decreased in nobiletin-treated melanoma cells, suggesting that the antioxidant defence system was downregulated. Furthermore, knockdown of GSK3β significantly reduced nobiletin-induced ferroptosis and upregulated the Keap1/Nrf2/HO-1 signalling pathway, while the opposite was observed in cells overexpressing GSK3β. In addition, molecular docking assay results indicated that nobiletin showed strong binding affinities for GSK3β, Keap1, Nrf2, and HO-1. Taken together, our results demonstrated that nobiletin could induce ferroptosis by regulating the GSK3β-mediated Keap1/Nrf2/HO-1 signalling pathway in human melanoma cells. Hence, nobiletin stands as a promising drug candidate for melanoma treatment with development prospects.

Keywords: nobiletin, ferroptosis, melanoma, GSK3β, Keap1/Nrf2/HO-1

INTRODUCTION

Melanoma is a highly aggressive skin malignancy that arises from the malignant proliferation of melanocytes (Eddy and Chen, 2020). The global incidence of melanoma continues to increase at an annual rate of approximately 3–7%, standing as an important public health problem (Leiter et al., 2020). Melanoma is often successfully treated with surgery when it is detected at an early stage (Scala et al., 2019). However, no effective treatments are available for advanced or metastatic melanoma. In recent years, although targeted therapy and immunotherapy have been used for the treatment of melanoma and have led to improved clinical outcomes, their high cost and the development of tumour resistance to these treatments limit their clinical application (Falcone et al., 2020; Swayden et al., 2020; Matias et al., 2021). Therefore, the identification and development of novel, effective, and accessible therapeutic approaches for melanoma that overcome the limitations of current treatments is urgently needed.

Ferroptosis is an iron-dependent form of regulated cell death characterised by the accumulation of lipid peroxides. This type of cell death is distinct from typical cell death processes, such as necrosis, autophagy, and apoptosis (Hirschhorn and Stockwell, 2019). Iron is an important microelement in the human body and plays a crucial role in metabolism. Through the Fenton reaction, excessive iron can produce reactive oxygen species (ROS) and activate lipoxygenase to promote lipid peroxidation, which leads to ferroptosis. The cyst(e)/glutathione (GSH)/glutathione peroxidase 4 (GPX4) axis has been recognised as an important pathway for regulating ferroptosis (Zheng and Conrad, 2020). While GSH is an important antioxidant and a free radical scavenger (Kennedy et al., 2020), GPX4 can specifically catalyse the conversion of lipid peroxides into lipid alcohols through the oxidation of GSH. GSH depletion leads to the inactivation of GPX4, promoting the accumulation of lipid peroxides to trigger ferroptosis (Ursini and Maiorino, 2020). Emerging evidence supports the critical role of ferroptosis in tumour suppression and suggests that ferroptosis may be a potential therapeutic target for refractory cancer for overcoming the apoptosis resistance of tumour cells (Lin et al., 2020; Chen et al., 2021).

Cancer cells can activate antioxidant systems to resist ferroptosis. Nuclear factor erythroid 2-related factor 2 (Nrf2) is an important transcription factor involved in the response against endogenous antioxidant stress and is regulated by Kelch-like Ech-associated protein-1 (Keap1). Nrf2 can inhibit lipid peroxidation by upregulating multiple antioxidant enzymes such as haem oxygenase-1 (HO-1) (Loboda et al., 2016). Consequently, inhibiting the Keap1/Nrf2/HO-1 antioxidant pathway may be a suitable strategy to promote ferroptosis in cancer cells.

Glycogen synthase kinase 3β (GSK3β) is a ubiquitously expressed serine/threonine protein kinase involved in the regulation of various cellular biological processes, including glycogen metabolism, signal transduction, cell cycle regulation, and cell proliferation (Theeuwes et al., 2017). Accumulating evidence suggests that GSK3β is a crucial regulator of the oxidative stress response associated with the occurrence and development of cancer (Domoto et al., 2020; He et al., 2020). Recent studies have shown that overexpression of GSK3β promotes erastin-induced ferroptosis and increases the sensitivity of breast cancer cells to chemotherapeutic agents (Wu et al., 2020). However, the role of GSK3β in ferroptosis remains unclear and requires further elucidation.

In recent years, several studies have suggested that some natural products, such as artemisinin (Chen G. Q. et al., 2020), quercetin (Wang et al., 2021), gallic acid (Khorsandi et al., 2020), and erianin (Chen P. et al., 2020), can sensitise cells to ferroptosis and show significant antitumour effects. Nobiletin, a polymethoxyflavone extracted from citrus peel, exhibits a variety of biological activities, including anti-inflammatory, antioxidant, anti-diabetic, and neuroprotective effects (Nguyen-Ngo et al., 2020). Previous studies have reported that nobiletin has strong antitumour effects on several types of cancers, such as breast, ovarian, gastric, colorectal, and lung cancers (Goh et al., 2019). The main mechanisms involve inhibiting cell proliferation, arresting the cell cycle, inducing apoptosis, limiting angiogenesis, and reducing inflammatory effects (Ashrafizadeh et al., 2020). Nevertheless, the effect of nobiletin on ferroptosis is still unclear and requires further investigation.

In this study, we aimed to elucidate the role of nobiletin in ferroptosis, and investigate the underlying mechanisms and pathways involved. The findings of this study could help in identifying targets for the treatment of melanoma.

MATERIALS AND METHODS

Cell Culture

The human melanoma cell line SK-MEL-28 was obtained from Guangzhou Cellcook Biotechnology Co., Ltd (Guangzhou, China). SK-MEL-28 cells were cultured in high-glucose Dulbecco's modified Eagle's medium supplemented with 10% foetal bovine serum and 1% antibiotic solution (penicillin/streptomycin) at 37°C in a humidified atmosphere of 5% CO_2. The cell culture medium was replaced every 1–2 days. The cells were passaged using trypsin containing ethylenediaminetetraacetic acid and then used for the assays.

Cell Viability Assay

The cytotoxicity of nobiletin towards SK-MEL-28 cells was measured using the Cell Counting Kit-8 (CCK-8) assay. After trypsinisation and resuspension, approximately 5,000 cells per well were seeded in 96-well plates and treated with dimethyl sulfoxide or different concentrations of nobiletin dissolved in dimethyl sulfoxide. To assess the cytotoxicity caused by nobiletin, we treated SK-MEL-28 cells with different concentrations of nobiletin (2, 4, 8, 10, 20, 50, 100, and 200 μM). SK-MEL-28 cells were treated with 5, 15, and 45 μM nobiletin for 48 h, and with 15 μM nobiletin for 24, 48, and 72 h. Subsequently, 10 μl of CCK-8 solution and 90 μl of medium containing 10% foetal bovine serum were added to each well and incubated at 37°C

with 5% CO_2 for 2 h. The absorbance at 450 nm was measured using a plate reader.

Colony Formation Assay

The nobiletin-treated cells were seeded into 6-well plates at a density of approximately 1×10^3 cells/well. A clonogenic assay was used to study the effect of nobiletin on colony formation in SK-MEL-28 cells. After 10 days of treatment (5, 15, and 45 μM nobiletin). Washing with ice-cold phosphate-buffered saline (PBS), the clones were fixed with 4% paraformaldehyde for 20–30 min and then stained with 0.1% crystal violet for 15 min. Subsequently, the excess crystal violet solution was removed by slowly washing the cells with tap water. Colonies were photographed and quantified under a microscope and the colony numbers were counted using the software of Quantity one-Colony counting (BIO-RAD, California, United States).

RNA Isolation and Reverse Transcription Quantitative Polymerase Chain Reaction

Trizol reagent was used to extract total RNA, which was reverse-transcribed into cDNA using PrimeScript™RT reagent Kit with gDNA Eraser (TaKaRa, Beijing, China) according to the manufacturer's instruction. In brief, the collected cells were lysed with RNAzol RT reagent. RNA was separated by adding RNase-free ddH2O to the lysate. After centrifuging, the aqueous layer was collected. The RNA was precipitated and washed by ethanol. After removing ethanol, the RNA was dried and re-suspended in RNase-free ddH2O. The concentration of RNA was quantified by NanoDrop 2000/2000C spectrophotometer (Thermo scientific, Thermo Fisher Technology (China) Co., LTD). Next, 1 μg RNA was diluted to 12 μl by RNase-free ddH2O, and reverse transcription was conducted using TB Green™ Premix Ex Taq™ II kit (Takara, Beijing, China). RT-qPCR was performed to evaluate the mRNA expression level of the transcripts encoding *GSK3β, Keap1, Nrf2,* and *HO-1*. The primers were purchased from BGI-Shenzhen. Sequences were 5′-GTAACTTGCCCTCACCCTCC-3′ and 5′-GCAGGCAGGACAACTCTCTT-3′ for *GSK3β* (NM_002093.4); 5′-GTCCCCTACAGCCAAGGTCC-3′ and 5′-CCCTCAATGGACACCACCTC-3′ for *Keap1* (NM_203500.2); 5′-CCAAGACCTCCTTGAGTGCG-3′ and 5′-ATCAAATCC ATGTCCTGTCCCT-3′ for *Nrf2* (NM_001313900.1); 5′-CTC CTCTCGAGCGTCCTCAG-3′ and 5′-AAATCCTGGGGCATG CTGTC-3′ for *HO-1* (NM_002133.3); and 5′-ATTCCTATGTGG GCGACGAG-3′ and 5′-AGGACTCCATGCCCAGGAA-3′ for β-actin (NM_001101.5). Next, the $2^{-\Delta\Delta Ct}$ method was employed to access the relative mRNA expression.

Western Blotting

Antibodies were purchased from Cell Signaling Technology, Inc (Danvers, MA, United States), including caspase-3 (#9662), LC3B (D11,XP® Rabbit mAb #3868), GSK-3β (D5C5Z,XP® Rabbit mAb 12456) and phospho-GSK-3β (Ser9,D85E12,XP® Rabbit mAb 5558). The dilution ratio of primary antibody was 1:1,000. The dilution ratio of the second antibody was 1:10,000. Protein concentrations were determined using a bicinchoninic acid Protein Assay Kit (Shanghai Biyuntian Biotechnology Co., LTD), according to the manufacturer's instructions. Briefly, protein samples were separated using sodium dodecyl sulphate–polyacrylamide gel electrophoresis and transferred to polyvinylidene difluoride membranes. The membranes were blocked in 5% skimmed milk at 25°C for 1 h and incubated with primary antibodies at 4°C overnight. Then, the membranes were washed and incubated with horseradish peroxidase-conjugated secondary antibody for 1 h. Next, the membranes were washed three times with tris-buffered saline with Tween-20 solution. Protein bands were detected using an enhanced chemiluminescence detection system (Bio-rad GelDoc XR System gel imaging System). β-actin and lamin B were used as the control for experimental data analysis.

Malondialdehyde Assay

Cellular MDA content was detected using an MDA activity assay kit (Shanghai Biyuntian Biotechnology Co., LTD), according to the manufacturer's instructions. Briefly, MDA detection reagents were added to the standard substance (control group), anhydrous ethanol (blank group), and test samples (experimental group). All the samples were incubated at 95°C for 40 min. The cooled mixtures were then centrifuged at 1,000 g for 10 min. The absorbance of the supernatant was measured at 532 nm using a spectrophotometer (Spectramax® paradigm®Multi-mode Detection platform, Molecular Devices, California, United States). The relative concentration of MDA in the cells was expressed as a percentage of that in the control group after blank correction.

ROS Measurement

ROS levels were measured using the peroxide-sensitive fluorescent probe 2′-7′ dichlorofluorescin diacetate (DCFH-DA) (Invitrogen, Carlsbad, CA, United States), in accordance with the manufacturer's protocol. Briefly, cells were seeded into 6-well plates and treated with nobiletin. After treatment, the cells were washed twice with PBS and labelled with DCFH-DA at 37°C for 30 min. The cells were then collected, and the fluorescence intensity was detected using a flow cytometer (BD FACS Aria, BD Biosciences, San Jose, CA) with excitation and emission settings of 488 and 525 nm, respectively.

GSH Assay

GSH levels were measured using a GSH assay kit (Shanghai Westang BIO-TECH CO., LTD) according to the manufacturer's instructions. The cells were seeded in 96-well plates and treated with nobiletin. The cells were then incubated at 37°C for 30 min with monochlorobimane (32 μM) in PBS. The absorbance was measured using the microplate reader (Thermo Scientific, Thermo Fisher Technology (China) Co., LTD) at 450 nm immediately.

Iron Assay

Iron levels were measured using the iron Assay Kit (Colorimetric, ab83366). Cells were seeded in 6-well plates and treated with nobiletin for 24 h. For total iron (Fe2+ and Fe3+) iron reducer was added, and after adding serum-free medium containing iron

probe, the cells were incubated at 37°C for 60 min. The absorbance was measured using the microplate reader at 593 nm.

Immunohistochemistry

Skin tissue samples were obtained from The Fourth Affiliated Hospital of Guangzhou Medical University (Guangzhou, China). All samples were collected with the informed consent of the patients. The experiments were approved by ethics committee of The Fourth Affiliated Hospital of Guangzhou Medical University (ethics number: 2022-H-001). Skin tissues were fixed, dehydrated, embedded in paraffin, and sectioned into 4 μm-thick slices. After deparaffination and rehydration, the slices were subjected to antigen retrieval using sodium citrate buffer. Then, the slices were blocked in normal goat serum at 37°C for 30 min and incubated with primary antibodies (GSK3β) at 4°C overnight. Next, the slices were washed three times with PBS and incubated with secondary antibodies at 37°C for 30 min. Subsequently, a chromogenic agent was added to the slices, which were redyed, dehydrated, and sealed. The slides of skin tissues were viewed under the inverted fluorescence microscope (Nikon ECLIPSE Ti2).

Small Interfering RNA (siRNA) Transfection

GSK3β siRNA (Cell Signalling Technology, Inc.) was used to knock down the expression of GSK3β. Briefly, cells were seeded in 6-well plates and cultured for 24 h. Transfection was performed when the cell confluency reached 70–80%. Solution A was prepared by adding 5 μl of 20 mM siRNA into 200 μl serum-free opti-Minimum Essential Medium, while for solution B, 5 μl of Lipofectamine 2000 was added to 200 μl serum-free opti-Minimum Essential Medium. Solutions A and B were then mixed and incubated at 25°C for 20 min. After discarding the medium and washing the cells twice with PBS, 600 μl of serum-free medium and the mixture of solution A and B were added to the wells and incubated at 37°C with 5% CO_2 for 4–6 h. Subsequently, the medium was discarded, and 3 ml of medium containing 10% foetal bovine serum was added to the wells. Then, the cells were cultured for 24 h. Finally, dimethyl sulfoxide and 15 μM nobiletin solution were added into different wells as control group and experimental group, respectively, followed by incubation for 24 h. The cultured cells were collected and used in the experiments.

Transfection of an Expression Vector Encoding GSK3β

Cells were seeded into 6-well plates. Twenty-4 hours later, the cells were transfected with the expression plasmid for GSK3β (pCDH-CMV-GSK3β-EF1-copGFP-T2A-Puro-COA,
Guangzhou IGEbio Co. LTD; abbreviated in the manuscript as pCMV-GSK3β), using either Lipofectamine™ 2000 (Invitrogen) following the manufacturer's specifications. The overexpression of GSK3β was monitored by determining its mRNA levels and protein levels after 48 h upon transfection. When assaying the cell viability caused by overexpression of GSK3β, nobiletin was added 48 h after transfection and cell viability determined using the CCK-8 assay. An empty vector was transfected in parallel with Pcmv-GSK3β and was used as negative control.

Molecular Docking Analysis

We got the 3D structure PDB files of GSK3β (PDB ID: 5k5n) from the RSCB PDB database (TTPSww.Rcsb.org/), and used PyMOL software to remove ligands or solvent molecules in target proteins; Using AutoDock Tools 1.5. Hydrogenation, charge calculation and other operations for protein molecules and small molecule compounds, small molecule compounds are flexible keys can be rotated by default and saved as PBDQT file. The ligand was set as flexible and the receptor was set as rigid to conduct semi-flexible docking. Genetic Algorithm Parameters algorithm was selected to run molecular docking. All the residues in proteins were protonated at pH 7.0. Partial charges of the atoms were assigned by the Sybyl force field. A scoring function was used to evaluate docking affinity.

Statistical Analysis

GraphPad Prism 8 software was used for data processing and analysis. All experiments were repeated three times and all data are presented as mean ± standard deviation (SD). The data were statistically analysed using the independent-samples t-test, one-way analysis of variance, and Dunnett-t test with the level of statistical significance set at $^{*}p < 0.05$, $^{**}p < 0.01$, and $^{***}p < 0.001$ compared to corresponding control.

RESULTS

Nobiletin Inhibits Cell Growth and Colony Formation in SK-MEL-28 Cells

The CCK-8 assay results revealed that nobiletin has moderate inhibitory activity against SK-MEL-28 cells with an IC_{50} value of 53.63 μM (**Figure 1A**). Subsequently, The results indicated that nobiletin significantly reduced the viability of SK-MEL-28 cells compared to that of dimethyl sulfoxide-treated cells in a concentration- and time-dependent manner (**Figures 1B,C**). And nobiletin significantly decreased the number of colonies in a concentration-dependent manner (**Figures 1D,E**).

Nobiletin Induces Ferroptosis in SK-MEL-28 Cells

Expression of caspase 3, LC3B, and GPX4 are indicators of apoptosis, autophagy, and ferroptosis, respectively. To investigate which form of cell death nobiletin induced, we measured the protein levels of caspase-3, LC3B, and GPX4 in SK-MEL-28 cells after drug treatment. As shown in **Figures 2A,B**, there were no significant differences in caspase 3 and LC3B protein levels between nobiletin-treated and untreated SK-MEL-28 cells. In contrast, GPX4 protein levels were reduced in nobiletin-treated cells compared to untreated cells. This effect could be reversed by the addition of the ferroptosis inhibitor Lip-1. Altogether, these results suggest that nobiletin induces ferroptosis rather than apoptosis or autophagy.

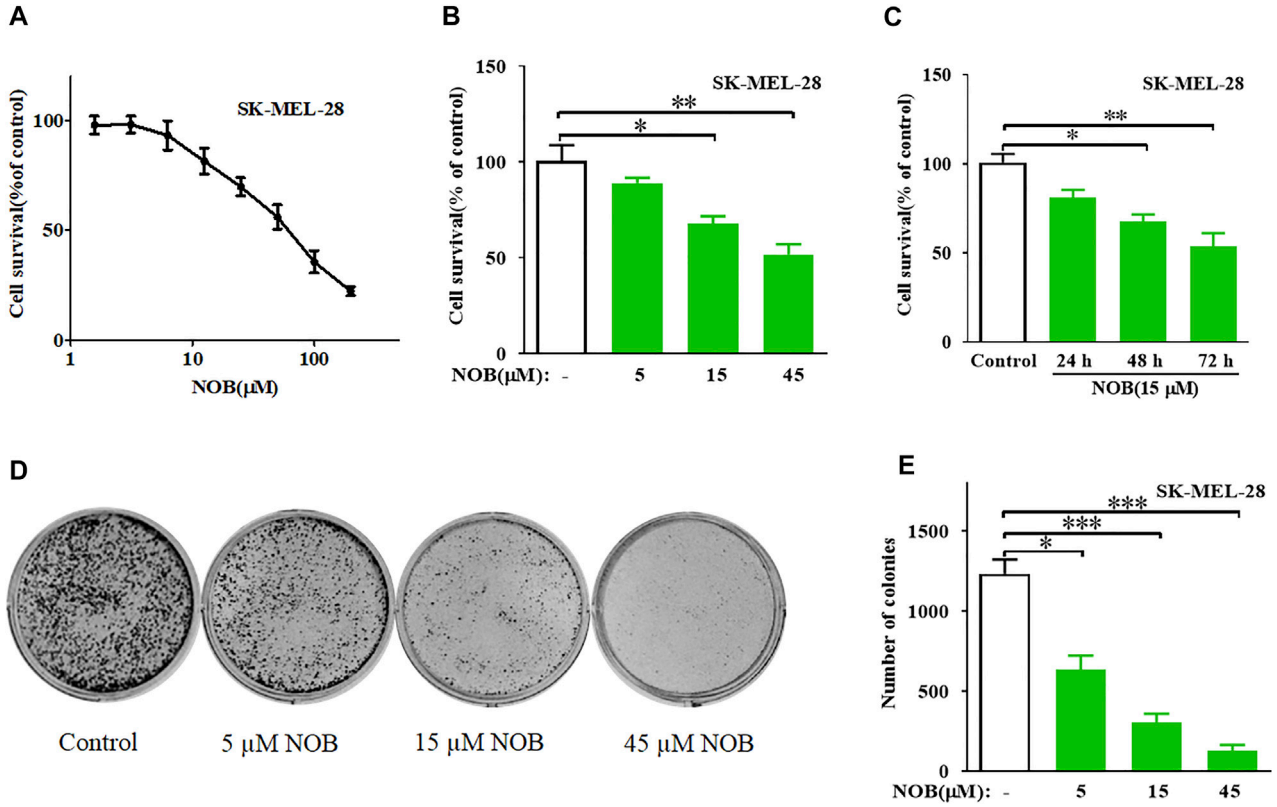

FIGURE 1 | Nobiletin inhibits cell growth and colony formation in melanoma cells. **(A)** Cytotoxicity of nobiletin in SK-MEL-28 cells. **(B,C)** Nobiletin inhibited cell growth of SK-MEL-28 cells in a concentration-dependent and time-dependent manner. **(B)** Cell viability of SK-MEL-28 cells treated with indicate concentration of nobiletin (5, 15, and 45 μM) for 48 h. **(C)** Cell viability of SK-MEL-28 cells treated with nobiletin (15 μM) for 24, 48, and 72 h **(D,E)** Nobiletin inhibited the colony formation ability of SK-MEL-28 cells in a concentration-dependent manner. **(D)** Representative images of cell colonies after treatment with nobiletin (5, 15, and 45 μM) for 10 days. **(E)** Quantitative analyses of colonies numbers. $n = 3$, $^{*}p < 0.05$, $^{**}p < 0.01$, and $^{***}p < 0.001$.

To further confirm whether nobiletin induced ferroptosis in SK-MEL-28 cells, we assessed cell viability and the levels of MDA, ROS, GSH, and iron after nobiletin treatment. As shown in **Figure 2C**, the viability of SK-MEL-28 cells was significantly reduced by nobiletin, whereas pre-treatment with the ferroptosis inhibitors Fer-1 or Lip-1 prevented this effect. Hence, inhibition of ferroptosis could reduce the cytotoxicity of nobiletin-induced SK-MEL-28 cells. Moreover, nobiletin significantly increased the levels of MDA, ROS, and iron, as well as decreased the levels of GSH in a concentration-dependent manner (**Figures 2D–H**). Taken together, these findings strongly suggest that nobiletin induces ferroptosis in SK-MEL-28 cells.

GSK3β Is Low Expressed in Cutaneous Melanoma Tissues and Nobiletin Enhances GSK3β Expression Level in SK-MEL-28 Cells

The results of immunohistochemistry showed that GSK3β expression in the skin tissue of patients with melanoma was significantly reduced compared to that of normal skin tissue (**Figure 3A**). Therefore, we hypothesized that GSK3β may be involved in the mechanism of nobiletin-induced ferroptosis in melanoma cells. RT-qPCR analysis results revealed that nobiletin significantly increased the mRNA levels of *GSK3β* in SK-MEL-28 cells with increasing concentration and time (**Figures 3B,C**). Western blotting results confirmed that a similar tendency was observed for GSK3β protein levels (**Figures 3D–G**). Therefore, the results revealed that nobiletin enhanced the expression of GSK3β at the mRNA and protein level in a concentration- and time-dependent manner.

Nobiletin Inhibits the Keap1/Nrf2/HO-1 Axis in SK-MEL-28 Cells

To explore the role of the antioxidant defence system in nobiletin-induced ferroptosis, we investigated the activation level of the Keap1/Nrf2/HO-1 signalling pathway. Nobiletin increased the mRNA levels of *Keap1* and decreased the mRNA levels of *Nrf2* and *HO-1* in a concentration-dependent manner (**Figures 4A–C**). The protein levels of Keap1, total Nrf2, nuclear Nrf2, and HO-1 in SK-MEL-28 cells followed the same tendencies as their corresponding transcripts (**Figures 4D–H**). These results indicated that nobiletin enhanced Keap1 expression and inhibited the Nrf2/HO-1 signalling pathway, thereby downregulating the antioxidant defence system in SK-MEL-28 cells.

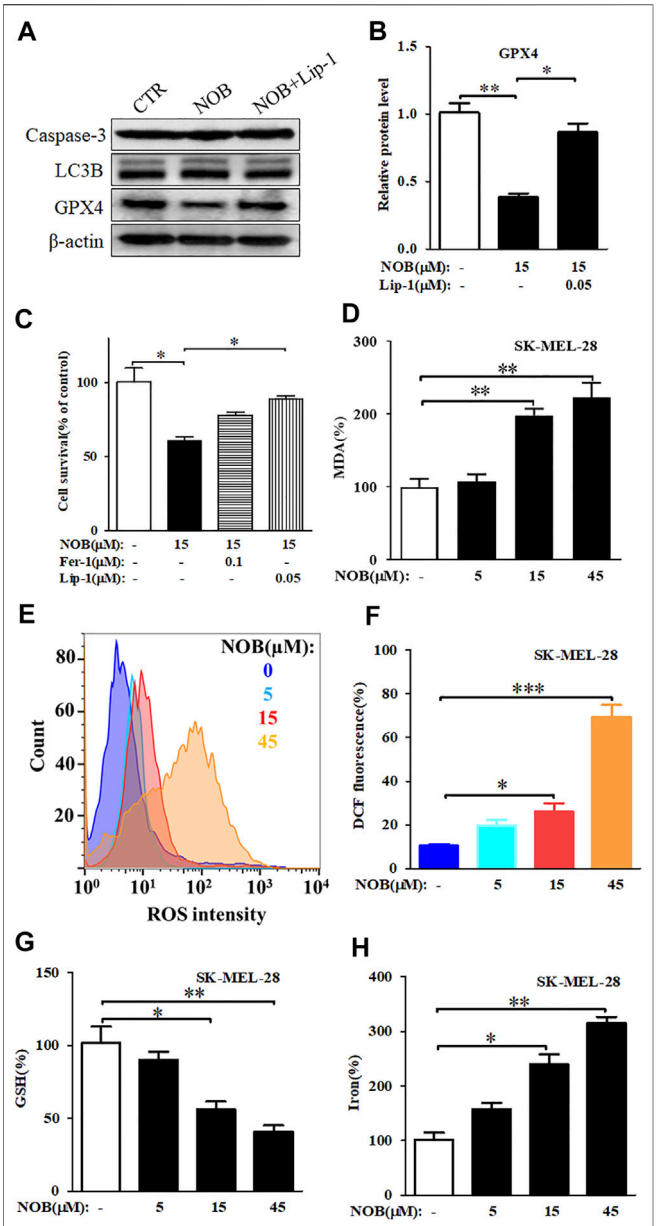

FIGURE 2 | Nobiletin induces ferroptosis in melanoma cells. **(A)** Western blot analysis of Caspase 3, LC3B, and GPX4 expression levels in SK-MEL-28 cells cultured with nobiletin (15 μM) or nobiletin in combination with Lip-1. **(B)** The protein levels of GPX4 in SK-MEL-28 cells treated with nobiletin (15 μM) or nobiletin in combination with Lip-1. **(C)** Cell viability of SK-MEL-28 cells treated with nobiletin (15 μM), nobiletin in combination with Fer-1 or Lip-1. **(D–H)** The levels of MDA, ROS, GSH, and iron in SK-MEL-28 cells treated with indicate concentration of nobiletin (5, 15, 45 μM). $n = 3$, $^{*}p < 0.05$, $^{**}p < 0.01$, and $^{***}p < 0.001$.

Nobiletin Induces Ferroptosis by Regulating the GSK3β-Mediated Keap1/Nrf2/HO-1 Signalling Pathway in SK-MEL-28 Cells

To investigate the relationship between GSK3β and the Keap1/Nrf2/HO-1 signalling pathway, we knocked down the expression of GSK3β in SK-MEL-28 cells and detected the protein and mRNA levels of Keap1, Nrf2, and HO-1. As shown in **Figures 5A–C**, the mRNA and protein levels of Keap1 were decreased, while the levels of Nrf2 and HO-1 were increased in nobiletin-treated SK-MEL-28 cells in which GSK3β was silenced compared to those in GSK3β-expressing nobiletin-treated SK-MEL-28 cells. These results suggest that GSK3β mediates the regulation of the Keap1/Nrf2/HO-1 signalling pathway in nobiletin-treated melanoma cells.

To further elucidate the role of GSK3β in nobiletin-induced ferroptosis, we assessed the viability of SK-MEL-28 cells with low GSK3β expression after nobiletin treatment. Knockdown of GSK3β significantly reduced nobiletin-induced cell death in SK-MEL-28 cells (**Figure 5D**). Subsequently, the levels of MDA, ROS, GSH, and iron were detected in SK-MEL-28 cells with reduced expression of GSK3β. As shown in **Figures 5E–I**, GSK3β knockdown decreased MDA, ROS, and iron levels, whereas it increased GSH levels in nobiletin-treated cells. The results showed that GSK3β knockdown significantly reduced nobiletin-induced ferroptosis in SK-MEL-28 cells.

Furthermore, we over-expressed GSK3β in SK-MEL-28 cells using pCMV-GSK3β. High expression of GSK3β could downregulate the Keap1/Nrf2/HO-1 signalling pathway (**Figures 6A–C**) and promote nobiletin-induced ferroptosis (**Figures 6D–I**). Taken together, these results indicate that nobiletin triggers ferroptosis by regulating the GSK3β-mediated Keap1/Nrf2/HO-1 signalling pathway in SK-MEL-28 cells.

Nobiletin Presents Strong Binding Affinities With GSK3β

To further explore the binding mechanism between nobiletin and GSK3β, molecular docking analysis was performed. As shown in **Figure 7**, the conformations of 6QH(Ligand) fitted well with the binding site pocket of GSK3β, the docking scores (kJ/mol) was −7.57, 6QH(Ligand) formed hydrogen bonds with VAL-135 and TYR-134 in GSK3β.The conformation of LY294002 and Perifosine forms hydrogen bonds with Val135 and ASP-200 in GSK3β, and the binding site scores (kJ/mol) of LY294002 and Perifosine are −5.49 and 6.02, respectively. Nobiletin formed hydrogen bonds with Val135 in GSK3β, Compared with LY294002, the docking score (kJ/mol) of nobiletin and GSK3β was -5.61, indicating that the binding site of nobiletin and GSK3β fitted well with the binding site pocket of GSK3β. These results revealed that nobiletin showed strong binding affinities with GSK3β.

DISCUSSION

Melanoma is regarded as the most dangerous skin malignancy and has an increasing incidence worldwide (Carr et al., 2020). Advanced melanomas, most of which metastasise, are characterised by high aggressiveness, low survival rates, and high drug resistance, and in most cases remain incurable (Damsky et al., 2010). Hence, it is urgent to identify new and effective therapeutic agents for melanoma. Here, we report that

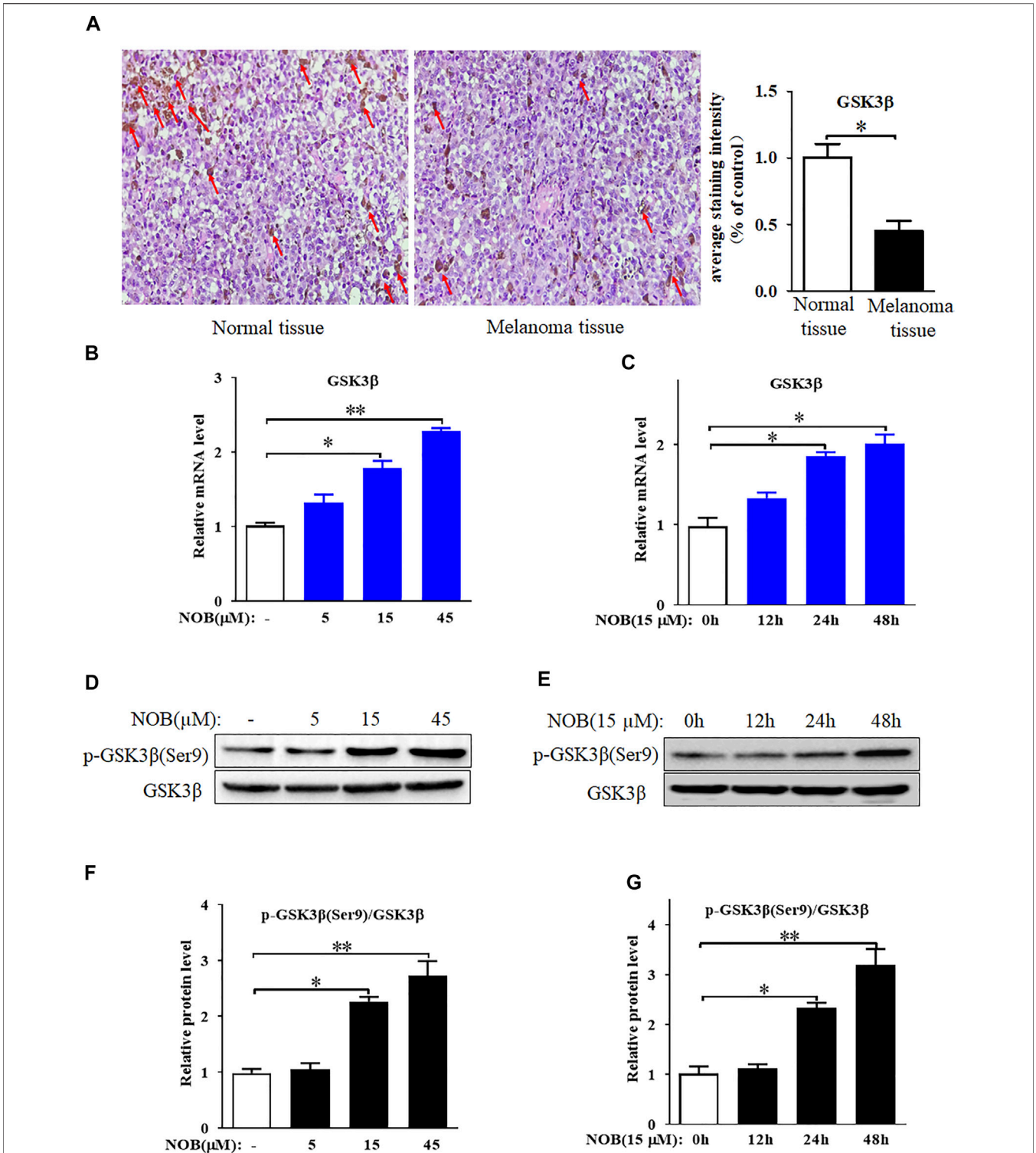

FIGURE 3 | GSK3β is low expressed in cutaneous melanoma tissues and nobiletin enhances GSK3β expression level in SK-MEL-28 cells. **(A)** GSK3β expression in skin tissue of normal person or melanoma patient was detected by immunohistochemical staining. **(B–G)** Nobiletin significantly increased the mRNA and protein levels of GSK3β in SK-MEL-28 cells in a concentration-dependent and time-dependent manner. $n = 3$, $^{*}p < 0.05$, $^{**}p < 0.01$.

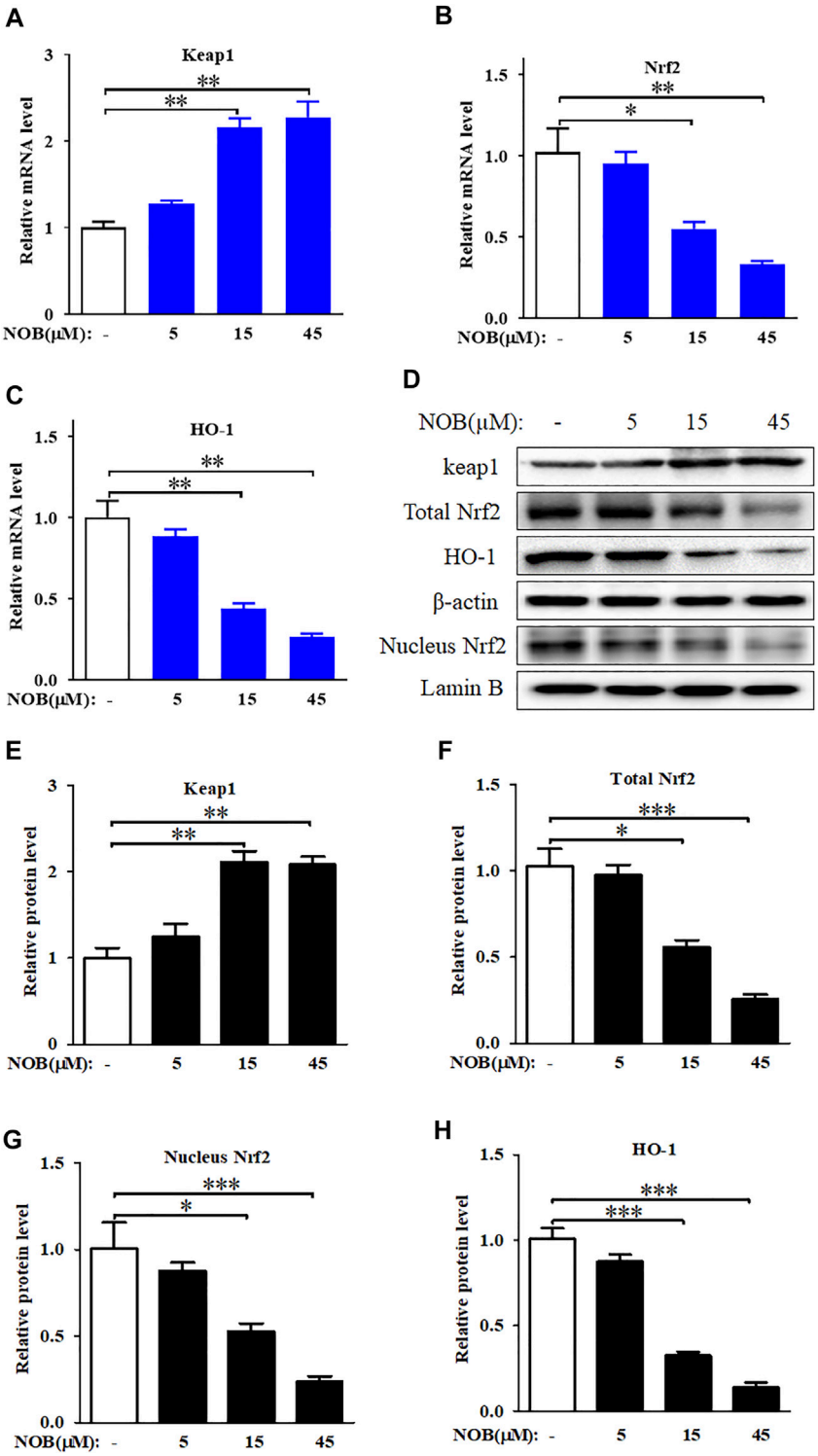

FIGURE 4 | Nobiletin inhibits Keap1/Nrf2/HO-1 axis in melanoma cells. **(A–C)** The mRNA levels of Keap1, Nrf2, and HO-1 in SK-MEL-28 cells treated with indicate concentration of nobiletin (5, 15, and 45 μM). **(D,H)** The protein levels of Keap1, total Nrf2, nucleus Nrf2, and HO-1 in SK-MEL-28 cells treated with nobiletin (5, 15, and 45 μM). $n = 3$, $^{*}p < 0.05$, $^{**}p < 0.01$, and $^{***}p < 0.001$.

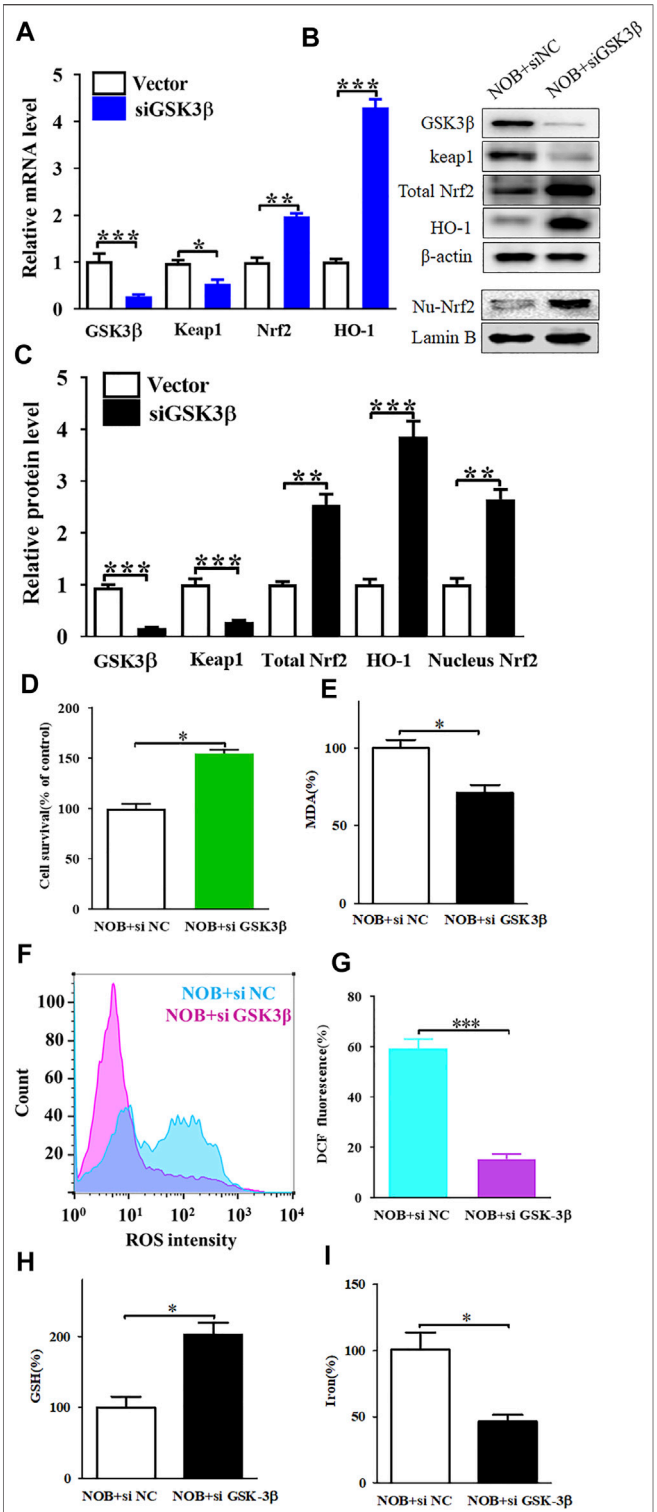

FIGURE 5 | Gene knockdown of GSK3β upregulates of Keap1/Nrf2/HO-1 signaling pathway and significantly reduces nobiletin-induced ferroptosis. **(A)** The mRNA levels of Keap1, Nrf2, and HO-1 in SK-MEL-28 cells with reduced expression of GSK3β. **(B,C)** The protein levels of Keap1, total Nrf2, nucleus Nrf2, and HO-1 in SK-MEL-28 cells with reduced expression of GSK3β. **(D)** Cell viability of SK-MEL-28 cells with reduced expression of GSK3β after nobiletin-treatment. **(E–I)** The levels of MDA, ROS, GSH, and iron in SK-MEL-28 cells with reduced expression of GSK3β after nobiletin-treatment. $n = 3$, $^{*}p < 0.05$, $^{**}p < 0.01$, and $^{***}p < 0.001$.

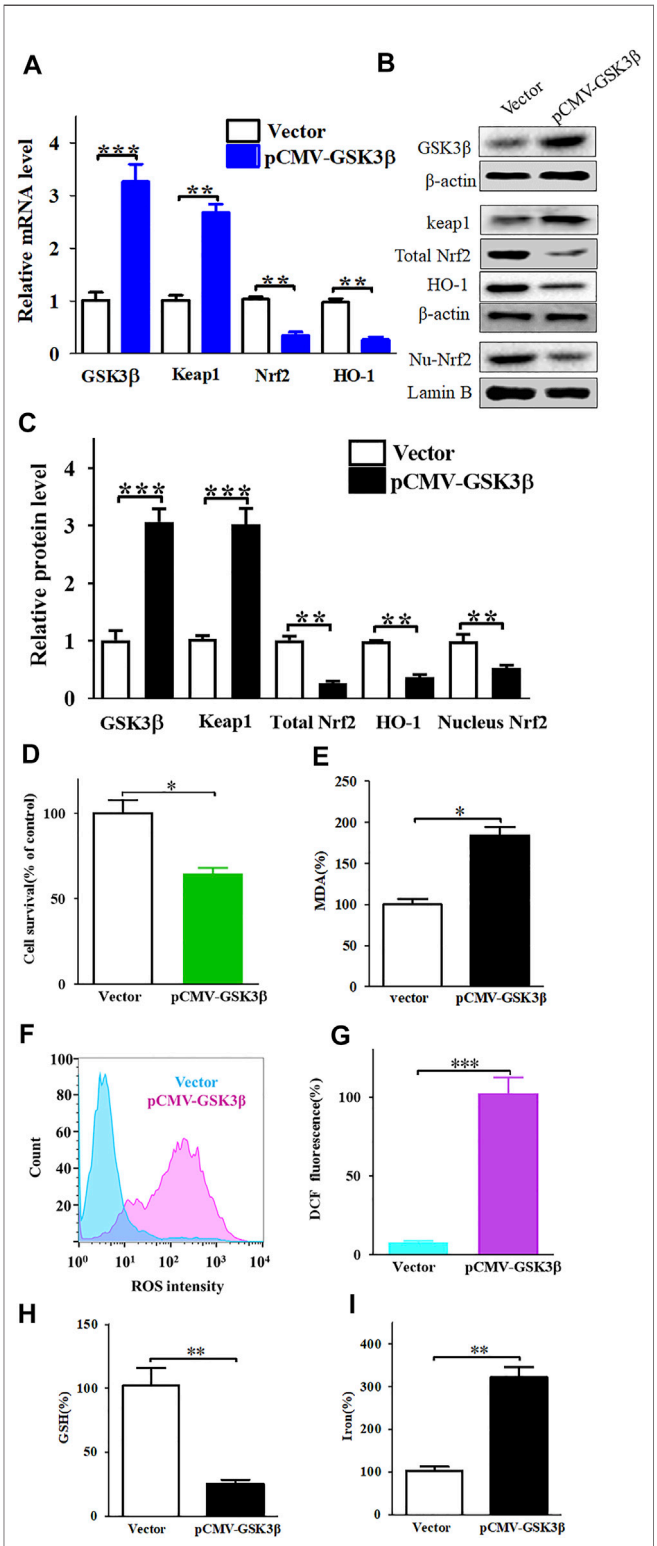

FIGURE 6 | Enhanced expression of GSK3β downregulates of Keap1/Nrf2/HO-1 signaling pathway and significantly increases nobiletin-induced ferroptosis. **(A)** The mRNA levels of Keap1, Nrf2, and HO-1 in SK-MEL-28 cells with enhanced expression of GSK3β. **(B,C)** The protein levels of Keap1, total Nrf2, nucleus Nrf2 and HO-1 in SK-MEL-28 cells with enhanced expression of GSK3β. **(D)** Cell viability of SK-MEL-28 cells with enhanced expression of GSK3β after nobiletin-treatment. **(E–I)** The levels of MDA, ROS, GSH, and iron in SK-MEL-28 cells with enhanced expression of GSK3β after nobiletin-treatment. $n = 3$, $^{*}p < 0.05$, $^{**}p < 0.01$, and $^{***}p < 0.001$.

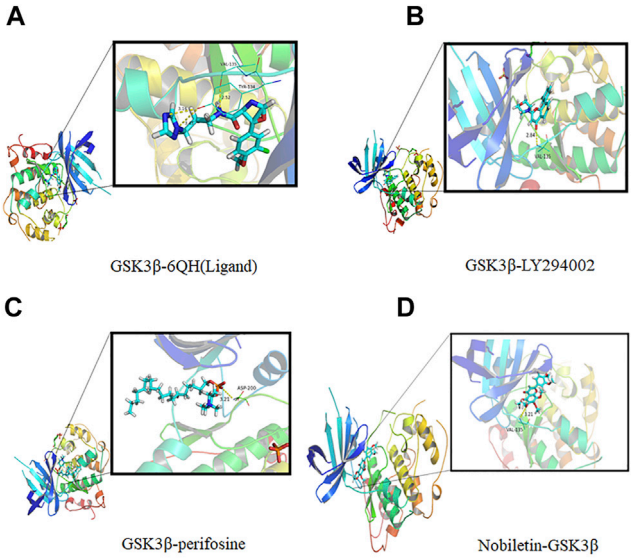

E

Protein	Ligand	Compound	Affinity (kJ/mol)	H-bond position
GSK3β (PDB ID:5k5n)	6QH	6QH(Ligand)	-7.57	VAL-135、TYR-134
		LY294002	-5.49	VAL-135
		Perifosine	-6.02	ASP-200
		Nobiletin	-5.61	VAL-135

FIGURE 7 | Molecular docking analysis of nobiletin with GSK3β. **(A–D)** The complex structure of GSK3β with 6QH(Ligand), LY294002, Perifosine, and nobiletin. **(E)** Docking scores of the complexes.

the natural product nobiletin exhibits antitumour activity by triggering ferroptosis in human skin melanoma cells. The main mechanism involved the inhibition of the Keap1/Nrf2/HO-1 signalling pathway by increasing the expression level of GSK3β.

Nobiletin is a polymethoxyflavone extracted from the peel of citrus fruits that has been reported to show strong antitumour activity in different types of cancers (Uesato et al., 2014; Jiang et al., 2018; Goh et al., 2019). Previous studies have reported that nobiletin can inhibit the growth of tumour cells by inducing cell cycle arrest and apoptosis (Ashrafizadeh et al., 2020). Wei *et al.* demonstrated that nobiletin could induce cell cycle arrest in the G0/G1 phase and promote apoptosis via the SRC/AKT/STAT3/YY1AP1 pathway in human renal carcinoma cells (Wei et al., 2019). Additionally, Ma *et al.* reported that nobiletin could stimulate G2 cell cycle arrest, trigger apoptosis, and regulate the expression of proteins such as Bcl-2, Bax, caspase-3, and COX-2 in hepatic cancer cells. Finally, Moon and Cho found that nobiletin induced apoptosis through a protective autophagy pathway mediated by intracellular endoplasmic reticulum stress in the human gastric cancer cell line SNU-16 (Moon and Cho, 2016). Nevertheless, most of the previous studies have focused on apoptosis or cell cycle arrest rather than ferroptosis induced by nobiletin.

In contrast to the existing studies, we focused on the effects of nobiletin on ferroptosis in melanoma cells. Ferroptosis is a recently identified form of programmed cell death that is mainly caused by the accumulation of iron and lipid peroxides

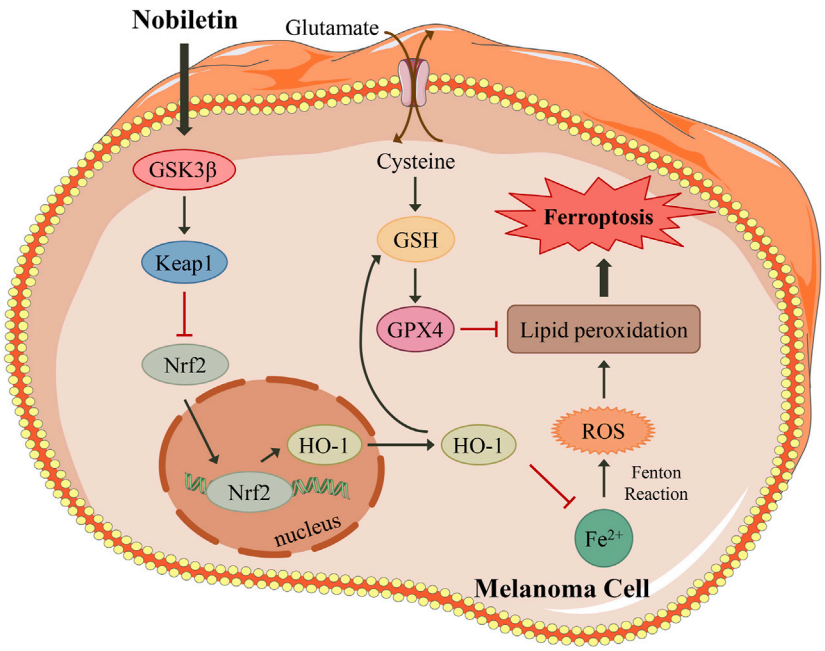

FIGURE 8 | A proposed model illustrating that nobiletin induces ferroptosis in melanoma cells. Nobiletin increases the expression of GSK3β, which activates Keap1 and inhibits the Nrf2/HO-1 axis. Nobiletin leads to the accumulation of iron and ROS. In another side, inhibiton of Keap1/Nrf2/HO-1 axis suppresses GSH, and then inactivates GPX4. Both ROS accumulation and GPX4 inactivation give rise to lipid peroxidation, thereby inducing ferroptosis. In summary, nobiletin induces ferroptosis by regulation of the GSK3β-mediated Keap1/Nrf2/HO-1 signaling pathway in human melanoma cells.

within the cells (Dixon et al., 2012). GSH depletion and lipid ROS formation also play crucial roles in the induction of ferroptosis (Tang D. et al., 2021). GPX4 is an indispensable regulator of intracellular lipid homeostasis, and its inactivation can result in ROS accumulation and lipid peroxidation, which induce ferroptosis (Forcina and Dixon, 2019). It has been reported that ferroptosis is closely associated with tumour therapy outcomes (Lin et al., 2020; Chen et al., 2021). In recent years, ferroptosis has attracted increasing attention, as drugs triggering ferroptosis would permit to overcome the acquired apoptosis-resistance of cancer cells (Tang Z. et al., 2021; Su et al., 2020). In the present study, we found that nobiletin inactivated GPX4 but had no effect on caspase 3 and LC3B levels in SK-MEL-28 cells, indicating that nobiletin may induce cell death through ferroptosis rather than through apoptosis or autophagy. Next, we investigated whether nobiletin treatment induced ferroptosis in human melanoma cells. As expected, nobiletin-induced cell death could be reduced by pre-treatment with the ferroptosis inhibitors Fer-1 or Lip-1. In addition, nobiletin could trigger events characteristic of ferroptosis, including lipid peroxidation, ROS accumulation, GSH depletion, and excess iron accumulation in SK-MEL-28 cells. In conclusion, these results indicate that ferroptosis contributes to the inhibition of the growth of nobiletin-treated melanoma cells. The underlying mechanism still needs to be fully elucidated.

GSK3β, a serine/threonine protein kinase, is a key enzyme involved in various diseases, including cancer (Domoto et al., 2020; He et al., 2020). Although the role of GSK3β in cancer has been extensively studied, it still remains controversial. Although some studies have reported that inhibiting the activity of GSK3β can suppress the growth of various types of cancers such as brain cancer (Furuta et al., 2017), breast cancer (Ugolkov et al., 2016), colorectal cancer (Salim et al., 2013), ovarian cancer (Cao et al., 2006), and leukaemia (Wang et al., 2008), indicating that GSK3β exerts a tumour promoter role, GSK3β has been regarded as a tumour suppressor factor in other studies. For example, high GSK3β levels are associated with better prognosis in gastric cancer. In breast cancer, overexpression of GSK-3β enhances erastin-induced ferroptosis (Wu et al., 2020). Moreover, inhibition of GSK3β, which increased β-catenin and SNAIL activity, contributed to the invasion of NAV2-associated cutaneous melanoma cells (Hu et al., 2019). In our study, GSK3β expression level in the skin tissue of patients with melanoma was significantly decreased compared with that of normal skin. Furthermore, enhanced expression of GSK3β was observed in SK-MEL-28 cells treated with nobiletin, indicating that GSK3β might be a key regulator of nobiletin-induced ferroptosis.

Nrf2 plays a critical role in maintaining the intracellular redox balance. Keap1 is an endogenous inhibitor of Nrf2, which can bind to Nrf2 in the cytoplasm and promote its ubiquitination and subsequent degradation. Increased oxidative stress induces the modification of Keap1, which causes its dissociation from Nrf2. Nrf2 then translocates into the nucleus and binds to the antioxidant response elements, thereby increasing the expression level of antioxidant enzymes such as HO-1. The Keap1/Nrf2/HO-1 signalling pathway is recognised as an important antioxidant system that protects cancer cells from ferroptosis (Lippmann et al., 2020). In *KRAS*-mutant colorectal cancer cells, inhibition of the Nrf2/HO-1 axis contributed to the promotion of ferroptosis induced by RSL3, a GPX4 inhibitor (Yang et al., 2021). Here, we revealed that nobiletin could inhibit the Keap1/Nrf2/HO-1 axis in SK-MEL-28 cells, which might be the potential mechanism of nobiletin-induced ferroptosis.

GSK3β is also regarded as a regulator of Nrf2, as inactivation of GSK3β increases the nuclear accumulation of Nrf2, thereby upregulating the antioxidant defence system (Salazar et al., 2006). However, the interaction between GSK3β and the Keap1/Nrf2/HO-1 axis in ferroptosis remains unclear. Our research revealed that GSK3β could mediate the regulation of the Keap1/Nrf2/HO-1 signalling pathway in nobiletin-treated melanoma cells. Moreover, knockdown of GSK3β significantly reduced nobiletin-induced ferroptosis, accompanied by upregulation of the Keap1/Nrf2/HO-1 signalling pathway, while the opposite was observed in cells with enhanced expression of GSK3β. Furthermore, the results of molecular docking analysis indicated that nobiletin had strong binding affinities for GSK3β, Keap1, Nrf2, and HO-1. Collectively, our results demonstrated that the mechanism of nobiletin-induced ferroptosis involved regulation of the GSK3β-mediated Keap1/Nrf2/HO-1 signalling pathway in human melanoma cells.

In summary, our research demonstrated that nobiletin triggered ferroptosis in human melanoma cells, as well as increased lipid peroxidation, ROS accumulation, GSH depletion, GPX4 inactivation, and iron accumulation. The mechanism involved the inhibition of the Keap1/Nrf2/HO-1 signalling pathway by increasing the expression level of GSK3β (**Figure 8**). Our results identify nobiletin as a novel ferroptosis inducer and suggest that it may be a promising drug candidate for the treatment of melanoma. To promote the clinical application of nobiletin, *in vivo* experiments and clinical trials are urgently needed in the future.

DATA AVAILABILITY STATEMENT

The datasets presented in this study can be found in online repositories. The names of the repository/repositories and accession number(s) can be found in the article/Supplementary Material.

ETHICS STATEMENT

The studies involving human participants were reviewed and approved by the Medical Ethics Committee of the Fourth Affiliated Hospital of Guangzhou Medical University (2022-H-001). The patients/participants provided their written informed consent to participate in this study. Written informed consent was obtained from the individual(s) for the publication of any potentially identifiable images or data included in this article.

AUTHOR CONTRIBUTIONS

SF, ZY, and BL designed the research. HH and BL carried out the experiments and performed data analysis. YZ, YL, SH, KH, QL, and WZ participated part of the experiments. YZ, SF, and BL wrote the manuscript. ZY and YZ revised the manuscript. All of the authors have read and approved the final manuscript.

FUNDING

This work was supported by National Natural Science Foundation of China (No. 82104446); Basic and Applied Basic Research Foundation of Guangdong Province (No. 2019A1515111109); Yiwen Talent Project; Academician He Lin New Medical Research Foundation (No. 2021HLKY02); Guangdong Provincial Clinical Research Center for Chinese Medicine Dermatology (PFK 2021-03); Scientific Research Project, Traditional Chinese Medicine Bureau of Guangdong Provincial (No. 20221162).

ACKNOWLEDGMENTS

We would like to thank Editage (www.editage.cn) for English language editing.

REFERENCES

Ashrafizadeh, M., Zarrabi, A., Saberifar, S., Hashemi, F., Hushmandi, K., Hashemi, F., et al. (2020). Nobiletin in Cancer Therapy: How This Plant Derived-Natural Compound Targets Various Oncogene and Onco-Suppressor Pathways. *Biomedicines* 8, 110. doi:10.3390/biomedicines8050110

Cao, Q., Lu, X., and Feng, Y.-J. (2006). Glycogen Synthase Kinase-3β Positively Regulates the Proliferation of Human Ovarian Cancer Cells. *Cell Res* 16, 671–677. doi:10.1038/sj.cr.7310078

Carr, S., Smith, C., and Wernberg, J. (2020). Epidemiology and Risk Factors of Melanoma. *Surg. Clin. North America* 100, 1–12. doi:10.1016/j.suc.2019.09.005

Chen, G.-Q., Benthani, F. A., Wu, J., Liang, D., Bian, Z.-X., and Jiang, X. (2020). Artemisinin Compounds Sensitize Cancer Cells to Ferroptosis by Regulating Iron Homeostasis. *Cell Death Differ* 27, 242–254. doi:10.1038/s41418-019-0352-3

Chen, P., Wu, Q., Feng, J., Yan, L., Sun, Y., Liu, S., et al. (2020). Erianin, a Novel Dibenzyl Compound in Dendrobium Extract, Inhibits Lung Cancer Cell Growth and Migration via Calcium/calmodulin-dependent Ferroptosis. *Sig Transduct Target. Ther.* 5, 51. doi:10.1038/s41392-020-0149-3

Chen, X., Kang, R., Kroemer, G., and Tang, D. (2021). Broadening Horizons: the Role of Ferroptosis in Cancer. *Nat. Rev. Clin. Oncol.* 18, 280–296. doi:10.1038/s41571-020-00462-0

Damsky, W. E., Rosenbaum, L. E., and Bosenberg, M. (2010). Decoding Melanoma Metastasis. *Cancers* 3, 126–163. doi:10.3390/cancers3010126

Dixon, S. J., Lemberg, K. M., Lamprecht, M. R., Skouta, R., Zaitsev, E. M., Gleason, C. E., et al. (2012). Ferroptosis: an Iron-dependent Form of Nonapoptotic Cell Death. *Cell* 149, 1060–1072. doi:10.1016/j.cell.2012.03.042

Domoto, T., Uehara, M., Bolidong, D., and Minamoto, T. (2020). Glycogen Synthase Kinase 3β in Cancer Biology and Treatment. *Cells* 9, 1388. doi:10.3390/cells9061388

Eddy, K., and Chen, S. (2020). Overcoming Immune Evasion in Melanoma. *Ijms* 21, 8984. doi:10.3390/ijms21238984

Falcone, I., Conciatori, F., Bazzichetto, C., Ferretti, G., Cognetti, F., Ciuffreda, L., et al. (2020). Tumor Microenvironment: Implications in Melanoma Resistance to Targeted Therapy and Immunotherapy. *Cancers* 12, 2870. doi:10.3390/cancers12102870

Forcina, G. C., and Dixon, S. J. (2019). GPX4 at the Crossroads of Lipid Homeostasis and Ferroptosis. *Proteomics* 19, 1800311. doi:10.1002/pmic.201800311

Furuta, T., Sabit, H., Dong, Y., Miyashita, K., Kinoshita, M., Uchiyama, N., et al. (2017). Biological Basis and Clinical Study of Glycogen Synthase Kinase- 3β-Targeted Therapy by Drug Repositioning for Glioblastoma. *Oncotarget* 8, 22811–22824. doi:10.18632/oncotarget.15206

Goh, J. X. H., Tan, L. T., Goh, J. K., Chan, K. G., Pusparajah, P., Lee, L. H., et al. (2019). Nobiletin and Derivatives: Functional Compounds from Citrus Fruit Peel for colon Cancer Chemoprevention. *Cancers* 11, 867. doi:10.3390/cancers11060867

He, R., Du, S., Lei, T., Xie, X., and Wang, Y. (2020). Glycogen Synthase Kinase 3β in Tumorigenesis and Oncotherapy (Review). *Oncol. Rep.* 44, 2373–2385. doi:10.3892/or.2020.7817

Hirschhorn, T., and Stockwell, B. R. (2019). The Development of the Concept of Ferroptosis. *Free Radic. Biol. Med.* 133, 130–143. doi:10.1016/j.freeradbiomed.2018.09.043

Hu, W., Li, X., Cheng, R., Ke, J., Liu, Y., Ma, M., et al. (2019). NAV2 Facilitates Invasion of Cutaneous Melanoma Cells by Targeting SNAI2 through the GSK-3β/β-Catenin Pathway. *Arch. Dermatol. Res.* 311 (5), 399–410. doi:10.1007/s00403-019-01909-w

Jiang, Y.-P., Guo, H., and Wang, X.-B. (2018). Nobiletin (NOB) Suppresses Autophagic Degradation via Over-expressing AKT Pathway and Enhances Apoptosis in Multidrug-Resistant SKOV3/TAX Ovarian Cancer Cells. *Biomed. Pharmacother.* 103, 29–37. doi:10.1016/j.biopha.2018.03.126

Kennedy, L., Sandhu, J. K., Harper, M.-E., and Cuperlovic-Culf, M. (2020). Role of Glutathione in Cancer: from Mechanisms to Therapies. *Biomolecules* 10, 1429. doi:10.3390/biom10101429

Khorsandi, K., Kianmehr, Z., Hosseinmardi, Z., and Hosseinzadeh, R. (2020). Anti-cancer Effect of Gallic Acid in Presence of Low Level Laser Irradiation: ROS Production and Induction of Apoptosis and Ferroptosis. *Cancer Cel Int* 20, 18. doi:10.1186/s12935-020-1100-y

Leiter, U., Keim, U., and Garbe, C. (2020). Epidemiology of Skin Cancer: Update 2019. *Adv. Exp. Med. Biol.* 1268, 123–139. doi:10.1007/978-3-030-46227-7_6

Lin, X., Ping, J., Wen, Y., and Wu, Y. (2020). The Mechanism of Ferroptosis and Applications in Tumor Treatment. *Front. Pharmacol.* 11, 1061. doi:10.3389/fphar.2020.01061

Lippmann, J., Petri, K., Fulda, S., and Liese, J. (2020). Redox Modulation and Induction of Ferroptosis as a New Therapeutic Strategy in Hepatocellular Carcinoma. *Translational Oncol.* 13, 100785. doi:10.1016/j.tranon.2020.100785

Loboda, A., Damulewicz, M., Pyza, E., Jozkowicz, A., and Dulak, J. (2016). Role of Nrf2/HO-1 System in Development, Oxidative Stress Response and Diseases: an Evolutionarily Conserved Mechanism. *Cell. Mol. Life Sci.* 73, 3221–3247. doi:10.1007/s00018-016-2223-0

Matias, M., Pinho, J. O., Penetra, M. J., Campos, G., Reis, C. P., and Gaspar, M. M. (2021). The Challenging Melanoma Landscape: from Early Drug Discovery to Clinical Approval. *Cells* 10, 3088. doi:10.3390/cells10113088

Moon, J., and Cho, S. (2016). Nobiletin Induces Protective Autophagy Accompanied by ER-Stress Mediated Apoptosis in Human Gastric Cancer SNU-16 Cells. *Molecules* 21, 914. doi:10.3390/molecules21070914

Nguyen-Ngo, C., Salomon, C., Quak, S., Lai, A., Willcox, J. C., and Lappas, M. (2020). Nobiletin Exerts Anti-diabetic and Anti-inflammatory Effects in an *In Vitro* Human Model and *In Vivo* Murine Model of Gestational Diabetes. *Clin. Sci.* 134, 571–592. doi:10.1042/CS20191099

Salazar, M., Rojo, A. I., Velasco, D., de Sagarra, R. M., and Cuadrado, A. (2006). Glycogen Synthase Kinase-3β Inhibits the Xenobiotic and Antioxidant Cell Response by Direct Phosphorylation and Nuclear Exclusion of the Transcription Factor Nrf2. *J. Biol. Chem.* 281, 14841–14851. doi:10.1074/jbc.M513737200

Salim, T., Sjölander, A., and Sand-Dejmek, J. (2013). Nuclear Expression of Glycogen Synthase Kinase-3β and Lack of Membranous β-catenin Is

Correlated with Poor Survival in colon Cancer. *Int. J. Cancer* 133, 807–815. doi:10.1002/ijc.28074

Scala, J., Vojvodic, A., Vojvodic, P., Vlaskovic-Jovicevic, T., Peric-Hajzler, Z., Matovic, D., et al. (2019). New Trends in Cutaneous Melanoma Surgery. *Open Access Maced. J. Med. Sci.* 7, 3090–3092. doi:10.3889/oamjms.2019.828

Su, Y., Zhao, B., Zhou, L., Zhang, Z., Shen, Y., Lv, H., et al. (2020). Ferroptosis, a Novel Pharmacological Mechanism of Anti-cancer Drugs. *Cancer Lett.* 483, 127–136. doi:10.1016/j.canlet.2020.02.015

Swayden, M., Chhouri, H., Anouar, Y., and Grumolato, L. (2020). Tolerant/persister Cancer Cells and the Path to Resistance to Targeted Therapy. *Cells* 9, 2601. doi:10.3390/cells9122601

Tang, D., Chen, X., Kang, R., and Kroemer, G. (2021). Ferroptosis: Molecular Mechanisms and Health Implications. *Cel Res* 31, 107–125. doi:10.1038/s41422-020-00441-1

Tang, Z., Huang, Z., Huang, Y., Chen, Y., Huang, M., Liu, H., et al. (2021). Ferroptosis: the Silver Lining of Cancer Therapy. *Front. Cel Dev. Biol.* 9, 765859. doi:10.3389/fcell.2021.765859

Theeuwes, W. F., Gosker, H. R., Langen, R. C. J., Verhees, K. J. P., Pansters, N. A. M., Schols, A. M. W. J., et al. (2017). Inactivation of Glycogen Synthase Kinase-3β (GSK-3β) Enhances Skeletal Muscle Oxidative Metabolism. *Biochim. Biophys. Acta (Bba) - Mol. Basis Dis.* 1863, 3075–3086. doi:10.1016/j.bbadis.2017.09.018

Uesato, S., Yamashita, H., Maeda, R., Hirata, Y., Yamamoto, M., Matsue, S., et al. (2014). Synergistic Antitumor Effect of a Combination of Paclitaxel and Carboplatin with Nobiletin from Citrus Depressa on Non-small-cell Lung Cancer Cell Lines. *Planta. Med.* 80, 452–457. doi:10.1055/s-0034-1368321

Ugolkov, A., Gaisina, I., Zhang, J.-S., Billadeau, D. D., White, K., Kozikowski, A., et al. (2016). GSK-3 Inhibition Overcomes Chemoresistance in Human Breast Cancer. *Cancer Lett.* 380, 384–392. doi:10.1016/j.canlet.2016.07.006

Ursini, F., and Maiorino, M. (2020). Lipid Peroxidation and Ferroptosis: the Role of GSH and GPx4. *Free Radic. Biol. Med.* 152, 175–185. doi:10.1016/j.freeradbiomed.2020.02.027

Wang, Z., Smith, K. S., Murphy, M., Piloto, O., Somervaille, T. C. P., and Cleary, M. L. (2008). Glycogen Synthase Kinase 3 in MLL Leukaemia Maintenance and Targeted Therapy. *Nature* 455, 1205–1209. doi:10.1038/nature07284

Wang, Z. X., Ma, J., Li, X. Y., Wu, Y., Shi, H., Chen, Y., et al. (2021). Quercetin Induces P53-independent Cancer Cell Death through Lysosome Activation by the Transcription Factor EB and Reactive Oxygen Species-dependent Ferroptosis. *Br. J. Pharmacol.* 178, 1133–1148. doi:10.1111/bph.15350

Wei, D., Zhang, G., Zhu, Z., Zheng, Y., Yan, F., Pan, C., et al. (2019). Nobiletin Inhibits Cell Viability via the SRC/AKT/STAT3/YY1AP1 Pathway in Human Renal Carcinoma Cells. *Front. Pharmacol.* 10, 690. doi:10.3389/fphar.2019.00690

Wu, X., Liu, C., Li, Z., Gai, C., Ding, D., Chen, W., et al. (2020). Regulation of GSK3β/Nrf2 Signaling Pathway Modulated Erastin-Induced Ferroptosis in Breast Cancer. *Mol. Cel Biochem.* 473, 217–228. doi:10.1007/s11010-020-03821-8

Yang, J., Mo, J., Dai, J., Ye, C., Cen, W., Zheng, X., et al. (2021). Cetuximab Promotes RSL3-Induced Ferroptosis by Suppressing the Nrf2/HO-1 Signalling Pathway in KRAS Mutant Colorectal Cancer. *Cell Death Dis* 12, 1079. doi:10.1038/s41419-021-04367-3

Zheng, J., and Conrad, M. (2020). The Metabolic Underpinnings of Ferroptosis. *Cel Metab.* 32, 920–937. doi:10.1016/j.cmet.2020.10.011

Conflict of Interest: The authors declare that the research was conducted in the absence of any commercial or financial relationships that could be construed as a potential conflict of interest.

Publisher's Note: All claims expressed in this article are solely those of the authors and do not necessarily represent those of their affiliated organizations, or those of the publisher, the editors and the reviewers. Any product that may be evaluated in this article, or claim that may be made by its manufacturer, is not guaranteed or endorsed by the publisher.

frontiers in Genetics

ORIGINAL RESEARCH
published: 08 March 2022
doi: 10.3389/fgene.2022.787884

Identification and Validation of a Ferroptosis-Related Long Non-Coding RNA (FRlncRNA) Signature to Predict Survival Outcomes and the Immune Microenvironment in Patients With Clear Cell Renal Cell Carcinoma

Zhongbao Zhou[1†], Zhenpeng Yang[2†], Yuanshan Cui[3], Shuai Lu[2], Yongjin Huang[1], Xuanyan Che[1], Liqing Yang[4] and Yong Zhang[1]**

[1]Department of Urology, Beijing TianTan Hospital, Capital Medical University, Beijing, China, [2]Department of General Surgery, Beijing Shijitan Hospital, Capital Medical University, Beijing, China, [3]Department of Urology, The Affiliated Yantai Yuhuangding Hospital of Qingdao University, Yantai, China, [4]Department of Neurology, The Affiliated Yantai Yuhuangding Hospital of Qingdao University, Yantai, China

OPEN ACCESS

Edited by:
Lei Huang,
University of Massachusetts Medical School, United States

Reviewed by:
Xiaming Liu,
Huazhong University of Science and Technology, China
Jinyi Tong,
Nanjing Medical University, China
Zhuoyuan Xin,
Jilin University, China
Jie Pan,
Stanford University, United States

***Correspondence:**
Yong Zhang
doctorzzb@163.com
Liqing Yang
lyl-happy-2007@163.com

†These authors share first authorship

Specialty section:
This article was submitted to Cancer Genetics and Oncogenomics, a section of the journal Frontiers in Genetics

Received: 01 October 2021
Accepted: 05 January 2022
Published: 08 March 2022

Citation:
Zhou Z, Yang Z, Cui Y, Lu S, Huang Y, Che X, Yang L and Zhang Y (2022) Identification and Validation of a Ferroptosis-Related Long Non-Coding RNA (FRlncRNA) Signature to Predict Survival Outcomes and the Immune Microenvironment in Patients With Clear Cell Renal Cell Carcinoma. Front. Genet. 13:787884. doi: 10.3389/fgene.2022.787884

Background: The incidence of clear cell renal cell carcinoma (ccRCC) is increasing worldwide, contributing to 70–85% of kidney cancer cases. Ferroptosis is a novel type of programmed cell death and could predict prognoses in cancers. Here, we developed a ferroptosis-related long non-coding RNA (FRlncRNA) signature to improve the prognostic prediction of ccRCC.

Methods: The transcriptome profiles of FRlncRNAs and clinical data of ccRCC were obtained from The Cancer Genome Atlas and ICGC databases. Patients were randomly assigned to training cohorts, testing cohorts, and overall cohorts. The FRlncRNA signature was constructed by Lasso regression and Cox regression analysis, and Kaplan–Meier (K-M) analysis was used to access the prognosis of each group. The accuracy of this signature was evaluated by the receiver operating characteristic (ROC) curve. The visualization of functional enrichment was carried out by the gene set enrichment analysis (GSEA). Internal and external datasets were performed to verify the FRlncRNA signature.

Results: A FRlncRNA signature comprising eight lncRNAs (AL590094.1, LINC00460, LINC00944, AC024060.1, HOXB-AS4, LINC01615, EPB41L4A-DT, and LINC01550) was identified. Patients were divided into low- and high-risk groups according to the median risk score, in which the high-risk group owned a dramatical shorter survival time than that of the low-risk group. Through ROC analysis, it was found that this signature had a greater predictive capability than traditional evaluation methods. The risk score was an independent risk factor for overall survival suggested by multivariate Cox analysis (HR = 1.065, 95%CI = 1.036–1.095, and $p < 0.001$). We constructed a clinically predictive nomogram based on this signature and its clinical features, which is of accurate prediction about the survival rate of patients. The GSEA showed that primary pathways were the P53

signaling pathway and tumor necrosis factor–mediated signaling pathway. The major FRlncRNAs (LINC00460, LINC00944, LINC01550, and EPB41L4A-DT) were verified with the prognosis of ccRCC in the GEPIA and K-M Plotter databases. Their major target genes (BNIP3, RRM2, and GOT1) were closely related to the stage, grade, and survival outcomes of ccRCC by the validation of multiple databases. Additionally, we found two groups had a significant distinct pattern of immune function, immune checkpoint, and immune infiltration, which may lead to different survival benefits.

Conclusions: The FRlncRNA signature was accurate and act as reliable tools for predicting clinical outcomes and the immune microenvironment of patients with ccRCC, which may be molecular biomarkers and therapeutic targets.

Keywords: ferroptosis, clear cell renal cell carcinoma, long non-coding RNAs, prognostic signature, overall survival, immune microenvironment

INTRODUCTION

Renal cell carcinoma (RCC) is a common solid tumor in kidney cancer, accounting for about 90% of renal malignancies (Ferlay et al., 2018; Compérat et al., 2019). The European Association of Urology (EAU) guidelines reported that the incidence of RCC has increased by approximately 2% per year in the past 2 decades (Bex et al., 2018). One of the most common pathological types in RCC is clear cell renal cell carcinoma (ccRCC), which accounts for about 75% of RCC (Ferlay et al., 2018). So it is very meaningful to identify molecular biomarkers to monitor the progression and early metastasis of ccRCC.

Ferroptosis is a novel type of programmed cell death, which is mainly characterized by lipid peroxidation (Chen et al., 2020). Ferroptosis is involved in the synthesis and metabolism of many molecules, including amino acids, polyunsaturated fatty acids, glutathione, phospholipids, and others (Stockwell et al., 2017; Xie and Guo, 2021). Additionally, ferroptosis can be inhibited by iron chelators, lipid peroxidation inhibitors, and reduction in intracellular polyunsaturated fatty acids (Dixon et al., 2015). Valashedi et al. reported that ferroptosis can inhibit tumor formation and progression, which may be beneficial in the treatment of cancer (Valashedi et al., 2021). The correlation between the expression of ferroptosis-related genes (FRGs) and tumorigenesis has not been deeply investigated.

Long noncoding RNAs (lncRNAs) have been shown to participate in various considerable biological processes, such as cell proliferation and differentiation, gene regulation and translation, RNA splicing, regulation of microRNAs, and protein folding (Panni et al., 2020). The mechanism of ferroptosis during cancer development was rarely reported. Ferroptosis regulated by lncRNAs was known to participate in the various progression stages of ccRCC, such as invasion, metastasis, prognosis, and chemoresistance. The limitation of multiple studies is that they only target the single or a few lncRNAs investigated for ccRCC (Ju et al., 2020; Zhu et al., 2020; Yang et al., 2021). To date, novel biomarkers have not been reported to be explored *via* the lncRNAs' expression profiles of The Cancer Genome Atlas (TCGA) database to predict the prognosis of ccRCC. Therefore, we developed a ferroptosis-related long non-coding RNA (FRlncRNA) signature using TCGA database to find new biomarkers to predict prognosis of ccRCC.

MATERIALS AND METHODS

Datasets and Sample Extraction

The FPKM-RNA sequence and clinical information of ccRCC were downloaded from the TCGA-KIRC data portal (https://portal.gdc.cancer.gov/), where it contained a total of 537 ccRCC tissues and 72 adjacent tissues. The clinical information mainly included age, gender, clinical stage, T stage, N stage, M stage, survival status, survival time, and survival prognosis. The exclusion criteria were as follows: 1) The pathological diagnosis did not meet ccRCC; 2) The RNA sequence and clinical data were incomplete; and 3) The follow-up time did not exceed 30 days. Subsequently, the expression data of these RNAs were sorted, annotated, and then assigned to protein-coding genes and lncRNAs using the Ensembl human genome browser (http://asia.ensembl.org/info/data/index.html) and Perl program. The extracted data were normalized and processed by log2 transformation. The expression data of 89 ccRCC patients from the ICGC database (https://dcc.icgc.org/analysis) were obtained for the external validation of the FRlncRNA signature. The "limma" package in R software was utilized to correct the transcriptome data we have downloaded.

Screening of FRlncRNAs and Differentially Expressed Genes

The FerrDb database (http://www.zhounan.org/ferrdb/legacy/index.html) was used to obtain the FRG dataset, containing a total of 214 FRGs (Supplementary data) where 203 FRGs were found in the TCGA dataset. Among them, 62 FRGs were differentially expressed in ccRCC. The relation between FRGs and lncRNAs was analyzed by the Pearson correlation analysis. LncRNAs would be included in this study when the square of the correlation coefficient (R^2) was greater than 0.3, and concomitantly, the p-value was lower than 0.001. Finally, the

TABLE 1 | The characteristics of ccRCC patients included in this study.

Variable		Overall cohorts (n = 507)	Training cohorts (n = 243)	Testing cohorts (n = 264)	ICGC cohorts (n = 89)
Age (year, Mean ± SD)		60.26 ± 12.08	60.21 ± 12.46	60.31 ± 11.72	60.48 ± 10.06
Gender (n, %)	Male	333 (65.7)	163 (67.1)	170 (64.4)	50 (56.2)
	Female	174 (34.3)	80 (32.9)	94 (35.6)	39 (43.8)
Stage (n, %)	Stage I	253 (49.9)	116 (47.7)	137 (51.9)	0 (0.0)
	Stage II	53 (10.5)	28 (11.5)	25 (9.5)	0 (0.0)
	Stage III	116 (22.9)	59 (24.3)	57 (21.6)	0 (0.0)
	Stage IV	82 (16.2)	39 (16.0)	43 (16.3)	0 (0.0)
	Unknown	3 (0.5)	1 (0.5)	2 (0.7)	89 (100.0)
T stage (n, %)	T1	259 (51.1)	119 (49.0)	140 (53.0)	51 (57.3)
	T2	65 (12.8)	34 (14.0)	31 (11.7)	9 (10.2)
	T3	172 (33.9)	84 (34.6)	88 (33.3)	27 (30.3)
	T4	11 (2.2)	6 (2.4)	5 (2.0)	2 (2.2)
N stage (n, %)	N0	225 (44.4)	90 (37.0)	135 (51.1)	40 (44.9)
	N1	16 (3.2)	10 (4.1)	6 (2.3)	0
	NX	266 (52.4)	143 (58.9)	123 (46.6)	49 (55.1)
M stage (n, %)	M0	401 (79.1)	198 (81.5)	203 (76.9)	35 (39.3)
	M1	78 (15.4)	38 (15.6)	40 (15.2)	4 (4.5)
	MX	26 (5.1)	7 (2.9)	19 (7.2)	50 (56.2)
	Unknown	2 (0.4)	0 (0.0)	2 (0.7)	0 (0.0)
Survival status (n, %)	Alive	162 (34.0)	77 (31.7)	85 (32.2)	60 (67.4)
	Dead	345 (66.0)	166 (68.3)	179 (67.8)	29 (32.6)
Survival years (Mean ± SD)		3.25 ± 2.18	3.00 ± 2.03	3.48 ± 2.29	4.17 ± 1.69

SD, standard deviation.

"limma" package in R software was applied to extract a total of 1,669 FRlncRNAs (Supplementary data).

Identification of the Prognostic FRlncRNA Signature

To establish an effective prognostic prediction model, we randomly divided 537 ccRCC patients into training cohorts and testing cohorts in a 1:1 ratio. Finally, 243 people were included in the training cohorts, and 264 people were included in the testing cohorts, according to the exclusion criteria. The detailed patient grouping process is shown in **Supplementary Figure S1**. The basic characteristics of each group are showed in **Table 1** (Details in Supplementary data). The FRlncRNA signature was built according to the training cohorts, and the capability of predicting prognosis was evaluated *via* the testing cohorts, overall cohorts, and ICGC cohorts. The prognostic capability of FRlncRNAs in the training cohorts was assessed by the univariate Cox regression analysis. If $p < 0.05$, it would be included in the least absolute shrinkage and selection operator (Lasso) regression using the "glmnet" package in R software to avoid overfitting. The risk score of each patient, established by incorporating the Lasso regression into the multivariate Cox regression analysis, was calculated according to the function, $\sum^{n}{}_{i=1}\beta_i *$ (expression of $lncRNA_i$), where β represented the regression coefficient. Patients were classed into high- and low-risk groups based on the median risk score, and the survival rate between two groups was compared using the log-rank test.

The risk score of each patient in the test cohorts, overall cohorts, and ICGC cohorts was calculated using the same way to confirm the stability of the established model. The survival outcomes of each cohort were analyzed by the Kaplan–Meier (K-M) survival curve. The "ROC package" in R software was employed to analyze the specificity and sensitivity of the established model based on the ROC curve and its area under the curve (AUC) value.

Construction and Evaluation of the Prognostic Nomogram

A prognostic nomogram according to the aforementioned risk score and traditional prognosis-related clinical variables (age, grade, and stage) was established to statistically predict the prognosis of ccRCC patients. Subsequently, the reliability and accuracy of the nomogram were evaluated *via* the concordance index (C-index), calibration curve, and ROC curve. The basic characteristics of patients were included into the multivariate Cox regression analysis to determine whether the risk score was an independent predictor of prognosis.

Functional Enrichment Analysis

The gene set enrichment analysis (GSEA) software was employed to perform the explanation of the functional enrichment of these FRlncRNAs. The pathway components of the high-risk group and the differences of the pathway activity and expression patterns, which were downloaded from MSigDB and GSEA 4.1.0, were analyzed in the pathway analysis dataset including c2. cp.kegg. v7.4. symbols and c5. go.bp. v7.4. symbols. A two-tailed *p*-value less than 0.05 was considered to be significant. To clarify how target genes of these FRlncRNAs participated in the development of ccRCC, we performed a functional analysis of related FRGs. The "clusterProfiler" package (Yu et al., 2012) and "org.Hs.eg.db" package in R software were used for functional

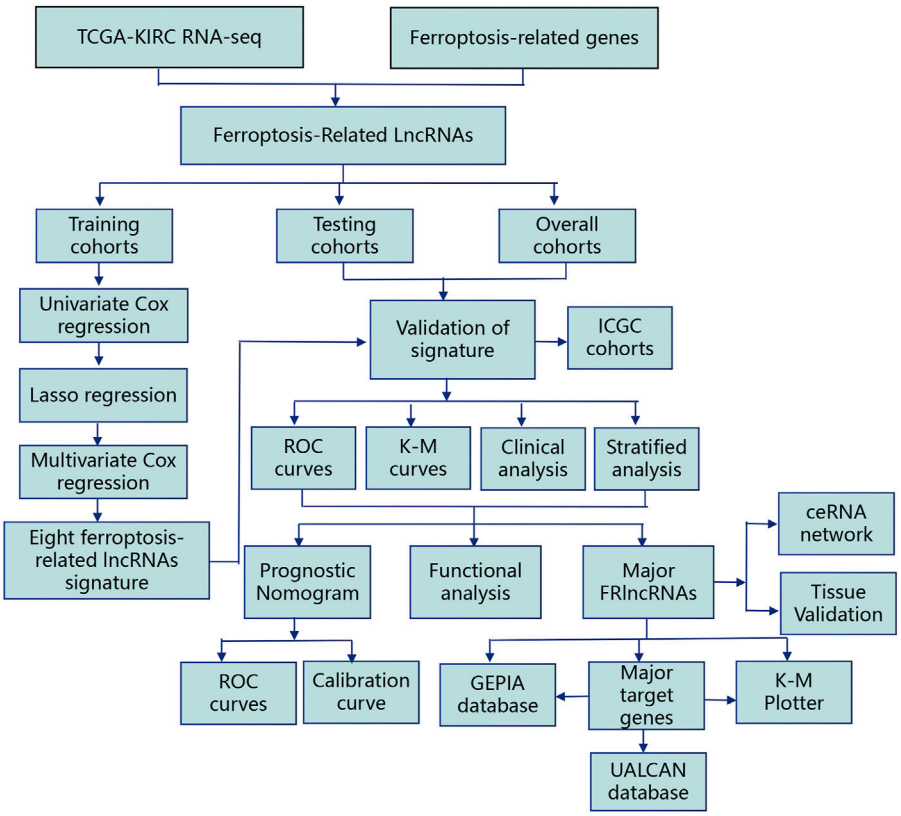

FIGURE 1 | Analysis flow chart of this research.

enrichment of target genes based on the Kyoto Encyclopedia of Genes and Genomes (KEGG) signaling pathway and gene ontology (GO) enrichment analysis. The cut-off criterion was set as p less than 0.05 and a q value more than 0.05.

Interaction Network Construction and Verification

When the co-expression coefficient was greater than 0.3 and the p-value was less than 0.001 using the "limma" package, we believed that there was a good correlation between FRlncRNAs and FRGs. Cytoscape 3.6.0 software was used to visualize the network between eight FRlncRNAs and related FRGs. After that, we further identified the major FRlncRNAs and related FRGs by searching the relevant literature and multiple databases. We also explored the ceRNA network of major FRlncRNAs. The gene expression profiling interactive analysis (GEPIA, http://gepia.cancer-pku.cn/) contained RNA-seq and clinical data compiled by TCGA and GTEx after standardized analysis. The UALCAN online database (http://ualcan.path.uab.edu/index.html) reported the differences of the target gene expression between normal tissues and ccRCC-graded tissues. The K-M Plotter database (http://kmplot.com/analysis/) included data on the correlation between the gene expression and prognostic data of 530 patients with ccRCC. The expression levels of the major FRlncRNAs-FRGs and the prognostic correlation were verified in the above three databases.

RNA Extraction, Reverse Transcription, and Quantitative Real-time PCR (qRT-PCR)

A total RNA extraction micro kit (RNT411-03, Mabio, Guangdong, China; http://www.mabiotech.cn/en/list-643-1.html) was used to extract the total RNA from tumor tissues and normal tissues based on the operation instructions, and then, a spectrophotometer was employed to detect the concentration and check the quality of total RNA. Then, a cDNA synthesis kit with random primers (AG11711, AG, Changsha, China; https://agbio.com.cn/product/evo-m-mlv-rt-kit-with-gdna-clean-for-qpcr-ii/?v=b838b393d55f) was used in a 20 μ1 reaction volume with 1 μg total RNA for cDNA synthesis. The mRNA expression was detected by the Script SYBR Green PCR kit (AG11702, AG, Changsha, China; https://agbio.com.cn/product/sybr-green-premix-pro-taq-hs-qpcr-kit-ii/?v=b838b393d55f) *via* an ABI7900HT Fast Real-time PCR machine, with the following conditions: pre-denaturation at 95°C for 30 s, followed by 40 cycles of denaturation at 95°C for 5 s, and annealing and extension at 60°C for 30 s. GAPDH was the internal control for mRNA, and the 2-ΔΔCt function was used to calculate the gene expression level (DiMagno, 2007). QRT-PCR primer sequences used in our experiments are listed as follows:

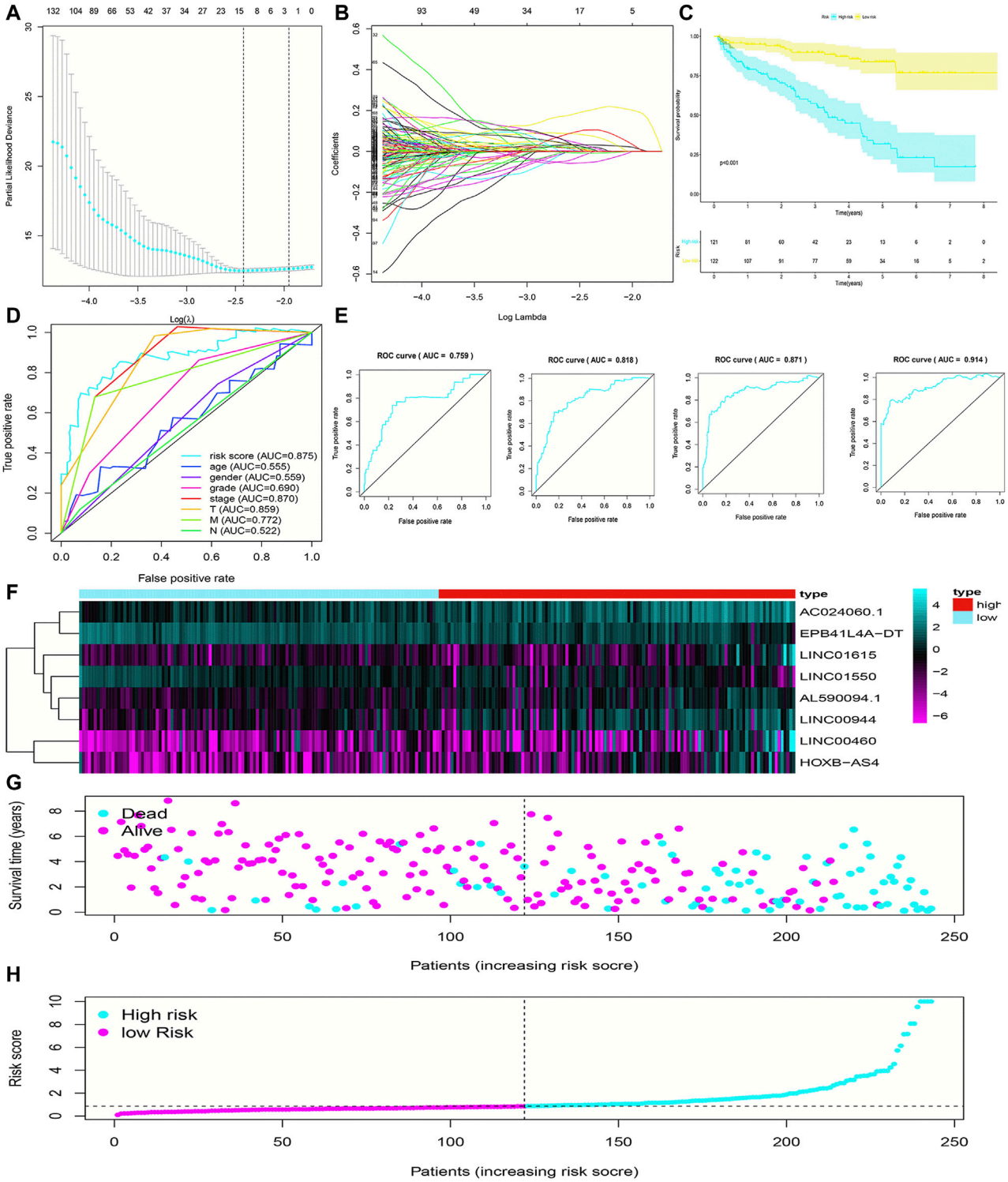

FIGURE 2 | Construction and evaluation of the FRlncRNA signature in training cohorts. The LASSO regression analysis was performed to avoid overfitting in training cohorts after univariate Cox regression analysis. LASSO coefficient values and vertical dashed lines were calculated at the best log(lambda) value **(A)** and LASSO coefficient profiles **(B)** of the prognostic-related lncRNAs were displayed. **(C)** K-M curves showed that the high-risk group had worse survival probability than the low-risk group in the training cohorts. **(D)** ROC curves for this signature and their AUC values in training cohorts. **(E)** ROC curves and their AUC values represented 1-, 3-, 5-, and 10-year predictions in training cohorts. **(F)** Heatmap of the eight FRlncRNA expression profiles showed the expression of FRlncRNAs in the high-risk and low-risk groups in training cohorts. **(G)** Scatter plot showed the correlation between the survival status and risk score of ccRCC patients. **(H)** Risk score distribution plot showed the distribution of high-risk and low-risk ccRCC patients.

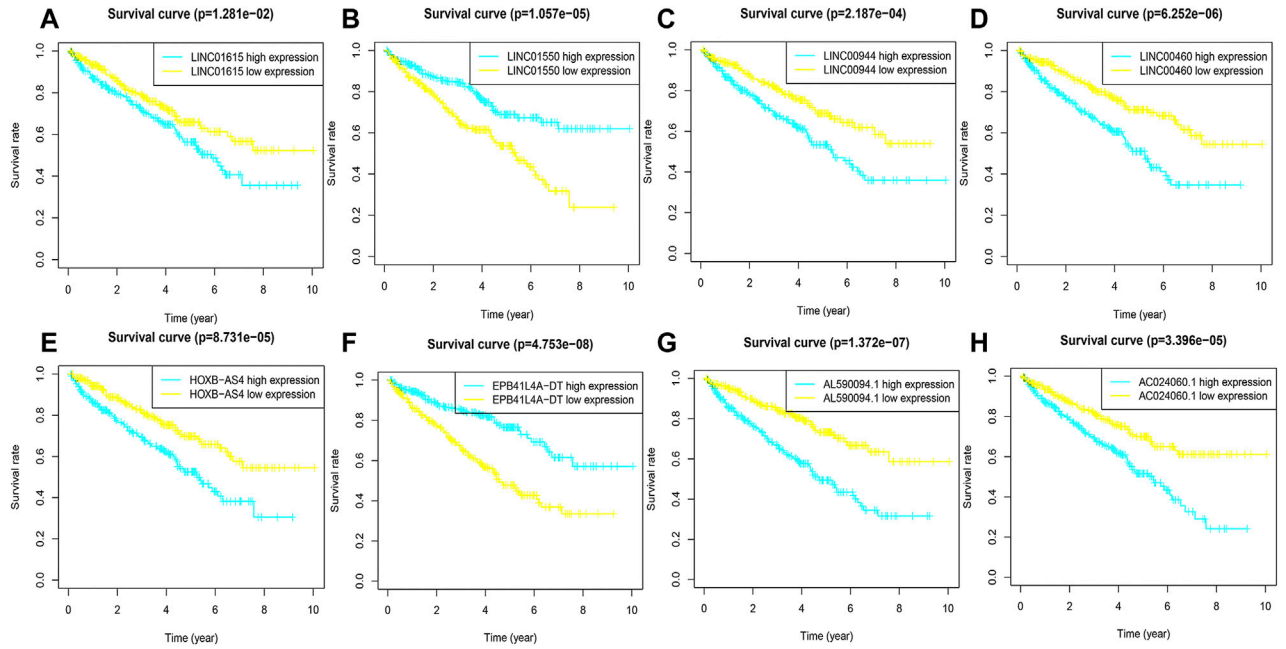

FIGURE 3 | K-M curves of eight FRlncRNAs in the prognostic signature. **(A-H)** The K-M survival curves of AC024060.1, AL590094.1, HOXB-AS4, LINC00460, LINC00944, and LINC01615 showed the high expression group had worse OS than the low expression group in the training cohorts ($p < 0.05$) and the K-M curves of EPB41L4A-DT and LINC01550 showed the high expression group had better OS than the low expression group in the training cohorts ($p < 0.05$).

GAPDH forward primer (F): 5′-TGACTTCAACAGCGACAC CCA-3'; GAPDH reverse primer (R): 5′-CACCCTGTTGCTGTA GCCAAA-3'; LINC00460 F: 5′-TAAACCTAGGGGCCGGTCG-3'; LINC00460 R: 5′-AACGGTCCAGAGCAGACAAAA-3'; LINC00944 F: 5′-AGACGCACATCAGGAAGACAG-3'; LINC00944 R: 5′-TGAGTTACAGGGACCGAAGC-3'; LINC01550 F: 5′-GGTGCAGTCTCCTCAGAACTAC-3'; LINC01550 R: 5′-GGGAGAGGGAGAACGACTGT-3'; EPB41L4A-DT F: 5′-CGGAGCAGGTGCAATCTGT-3'; and EPB41L4A-DT R: 5′-TCAAAACTACGTCTGATGCCAAA-3'.

Statistical Analysis

The two-tailed Student's t-test was calculated for the difference within groups or among groups. Categorical variables were presented as proportions, and the chi-square test was used for the comparisons between groups. Multivariate or univariate Cox proportional hazard regression analysis was calculated for evaluating the prognostic significance. The log-rank test and K-M curve assessed the prognostic results. R software (version 3.6.0) was used to draw the heatmap, GSEA, survivorship curve, ROC curve, nomogram, and calibration plot. A two-tailed *p*-value less than or equal to 0.05 was considered as the statistical significance.

RESULTS

Construction and Verification of the FRlncRNA Signature

The flowchart of this work is showed in **Figure 1**. The univariate Cox regression analysis was used to analyze the expression of FRlncRNAs in the training cohorts. A total of 678 lncRNAs were found to be closely related with the prognosis of ccRCC. High overfitting of these prognostic-related lncRNAs were eliminated by Lasso Cox analysis, and 15 FRlncRNAs were identified (**Figure 2A**; Supplementary data). Then, multivariate Cox regression analysis extracted a prognostic signature containing eight FRlncRNAs and their coefficients (**Supplementary Table S1**; **Figure 2B**), calculated with the following formula: Risk score = (0.190*AL590094.1) + (0.047*LINC00460) + (0.204* LINC00944) + (0.168*AC024060.1) + (0.116*HOXB-AS4) + (0.048* LINC01615)—(0.134* EPB41L4A-DT)—(0.345* LINC01550). Based on the hazard ratio (HR) score gained by the multivariate Cox regression analysis, AC024060.1, AL590094.1, HOXB-AS4, LINC00460, LINC00944, and LINC01615, whose HRs were greater than 1, were risk factors, but EPB41L4A-DT and LINC01550, whose HRs were less than 1, were protective factors (**Supplementary Table S1**).

To evaluate the sensitivity and stability of the prognostic risk score, the training cohorts were divided into the low-risk group (122 cases) and the high-risk group (121 cases) based on the median of risk scores (0.86). The results of the K-M curve showed that the survival ability of patients in the high-risk group was significantly lower than that in the low-risk group ($p < 0.001$) (**Figure 2C**). The accuracy of the prognostic signature was evaluated by the ROC curve, and the AUC value was 0.875 (**Figure 2D**). The AUC values of 1, 3, 5, and 10 years of overall survival (OS) were 0.759, 0.818, 0.871, and 0.914, respectively (**Figure 2E**). The heatmap showed remarkable differences in the expression of eight FRlncRNAs between the high-risk group and the low-risk group (**Figure 2F**). The

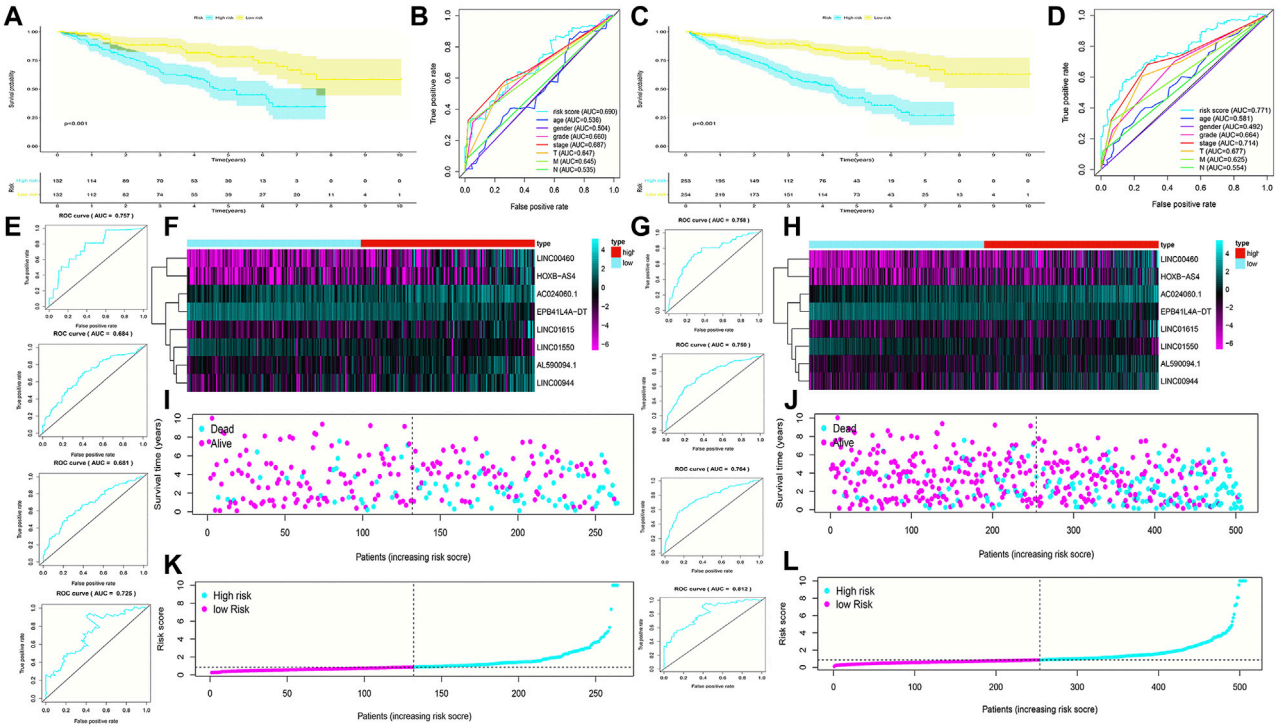

FIGURE 4 | Validation of the prognostic signature for ccRCC patients in testing cohorts and overall cohorts. K-M curves showed that the high-risk group had worse OS than the low-risk group in the testing cohorts **(A)** and overall cohorts **(C)**. ROC curves for the prognostic signature and their AUC values in the testing cohorts **(B)** and overall cohorts **(D)**. ROC curves and their AUC values represented 1-, 3-, 5-, and 10-year predictions in the testing cohorts **(E)** and overall cohorts **(G)**. Heatmap of eight FRlncRNA expression profiles showed the expression of FRlncRNAs in high-risk and low-risk groups in the testing cohorts **(F)** and overall cohorts **(H)**. Scatter plot showed the outcomes between the survival status and risk score of ccRCC patients in high- and low-risk groups in the testing cohorts **(I)** and overall cohorts **(J)**. Risk score distribution plot showed the distribution of high- and low-risk ccRCC patients in the testing cohorts **(K)** and overall cohorts **(L)**.

scatter plot indicated that ccRCC patients with a high risk score had a lower survival rate than those with a low-risk score (**Figure 2G**). Moreover, the distribution map of the risk score was consistent with the categorization of patient groups (**Figure 2H**). The prognostic effect of eight FRlncRNAs evaluated by K-M curves displayed that higher expressions of AC024060.1, AL590094.1, HOXB-AS4, LINC00460, LINC00944, and LINC01615 and lower expressions of EPB41L4A-DT and LINC01550 were linked to inferior OS ($p < 0.01$) (**Figures 3A–H**). The prognostic risk-related model we constructed exhibited a good stability and sensitivity in predicting the OS of ccRCC patients.

Validation of the FRlncRNA Signature

To validate the predictive capacity of the FRlncRNA signature, risk scores of patients were calculated in the testing cohorts and overall cohorts, and patients were classified into the low-risk group and the high-risk group based on the median of risk scores (0.85 and 0.86, respectively). The OS in the testing cohorts ($p < 0.001$) (**Figure 4A**) and overall cohorts ($p < 0.001$) (**Figure 4C**) were analyzed by K-M curves, demonstrating that these results were in line with the training cohorts. The ROC curves of testing cohorts (AUC = 0.690) (**Figure 4B**) and overall cohorts (AUC = 0.771) (**Figure 4D**) illustrated that the FRlncRNA signature has an accurate predictive capability about the OS of ccRCC patients, which was further validated by ROC time curves and their AUC values, such as the AUC value in testing cohorts, 1-year AUC = 0.757, 3-year AUC = 0.684, 5-year AUC = 0.681, and 10-year AUC = 0.725 (**Figure 4E**) and the AUC value in overall cohorts (1-year AUC = 0.758, 3-year AUC = 0.750, 5-year AUC = 0.764, and 10-year AUC = 0.812) (**Figure 4G**). The consistent expression profiles of eight FRlncRNAs in the training cohorts are shown in the heatmap (**Figures 4F,H**). A lower survival rate was observed in the high-risk group than the low-risk group, and distribution maps of the risk score validated a higher risk score in the high-risk group (**Figures 4I–L**). In addition, ICGC cohorts were used to evaluate the constructed model, which showed a good ability to predict the survival rate of patients with ccRCC (**Supplementary Figure 2A–E**). These results showed that the FRlncRNA signature can be a good indicator in predicting the prognosis of patients compared with other existing signatures reported in recent studies (**Supplementary Table S2**) (Canxuan and Dan, 2021; Hong et al., 2021; Ma et al., 2021; Xing et al., 2021; Yu et al., 2021; Zheng et al., 2021). Taken together, our data implied that the FRlncRNA signature showed a stable prognostic-predictive ability.

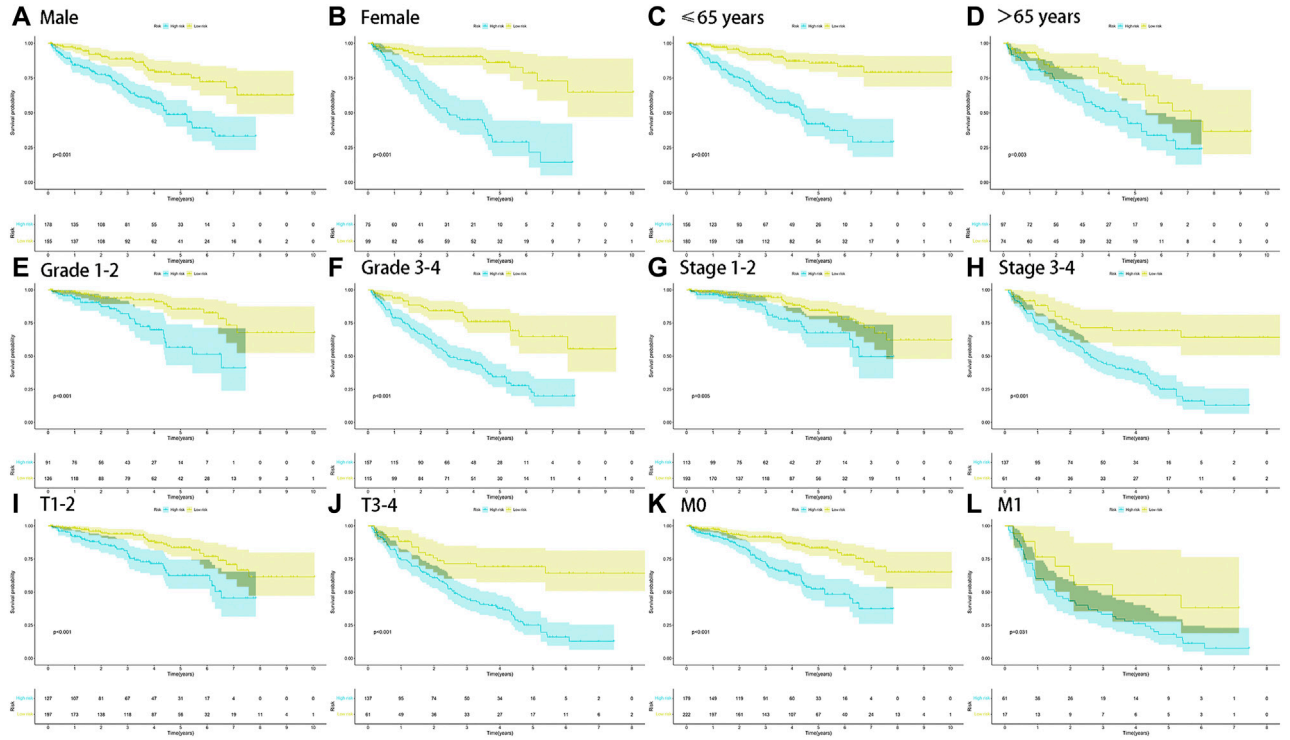

FIGURE 5 | Survival outcomes of ccRCC patients stratified by various clinicopathological features. K-M curves showed the survival outcomes of high- and low-risk ccRCC patients stratified according to the gender (MALE vs. FEMALE) **(A,B)**, age (≤65 years vs. >65 years) **(C,D)**, grade (grade I-II vs. grade III-IV) **(E,F)**, stage (stage I-II vs. stage III-IV) **(G,H)**, T stage (T1-2 vs. T3-4) **(I,J)**, and M stage (M0 vs. M1) **(K,L)**, respectively (all $p < 0.05$).

Stratified Analysis of Prognosis-Related Clinicopathological Characteristics

The stratified analysis of clinicopathological characteristics was performed to assess the predictive ability of the FRlncRNA signature and the stability of its OS prediction in the high-risk and low-risk groups including gender (female and male), age (≤65 years old and >65 years old), grade (I-II and III-IV), stage (I-II and III-IV stage), T stage (T1-2 stage and T3-4 stage), and M stage (M0 stage and M1 stage). The results of the K–M curve in different clinical characteristics suggested that the OS of the high-risk group was worse than that of the low-risk group ($p < 0.01$) (**Figures 5A–L**).

Construction and Evaluation of the Prognostic Nomogram

The risk score was demonstrated by the univariate and multivariate Cox regression analyses to be an independent prognostic factor ($p < 0.05$) (**Supplementary Table S3**, **Figures 6A,B**). Subsequently, clinicopathological characteristics including the age, grade and stage, and risk score were applied to construct the nomogram using the "rms" package in R software to predict the 1-, 3-, and 5-year OS of ccRCC patients (**Figure 6C**). The increasing risk score deteriorated the prognosis of ccRCC. The results of the multivariate ROC curve suggested that the AUC value was 0.771, which was higher than that of the grade (0.664) and stage (0.714), implying that the nomogram had the ability of accurate prediction for survival outcomes of ccRCC (**Figure 6D**). We used the calibration curve to observe whether the actual prognostic value was consistent with the predicted value of the nomogram and found that the calibration curves of 1-, 3-, and 5-year survival rates were consistent with the nomogram (**Figure 6E**). The clinical influences of the risk score for ccRCC patients in the training, testing, and overall cohorts are showed in **Supplementary Table S4**.

Functional Analysis of the FRlncRNA Signature and FRlncRNA-Related FRGs

The underlying molecular mechanisms of the FRlncRNA signature involved in the high-risk group were further verified by GSEA . Signaling pathways including the P53 signaling pathway [enrichment score (ES) 0.49; normalized enrichment score (NES) 1.76; nominal (NOM) p-value 0.03], the cytokine–cytokine receptor interaction signaling pathway (ES 0.39; NES 1.71; NOM p-value 0.03), the tumor necrosis factor–mediated signaling pathway (ES 0.50; NES 1.87; NOM p-value 0.005), and regulation of the T helper 1 type immune response signaling pathway (ES 0.64; NES 1.98; NOM p-value 0.007) were markedly enriched in the high-risk group (**Figure 7**).

The top 30 terms from the GO analysis of FRlncRNA-related FRGs are demonstrated in the dot plot (**Figures 8A–C**). GO analysis

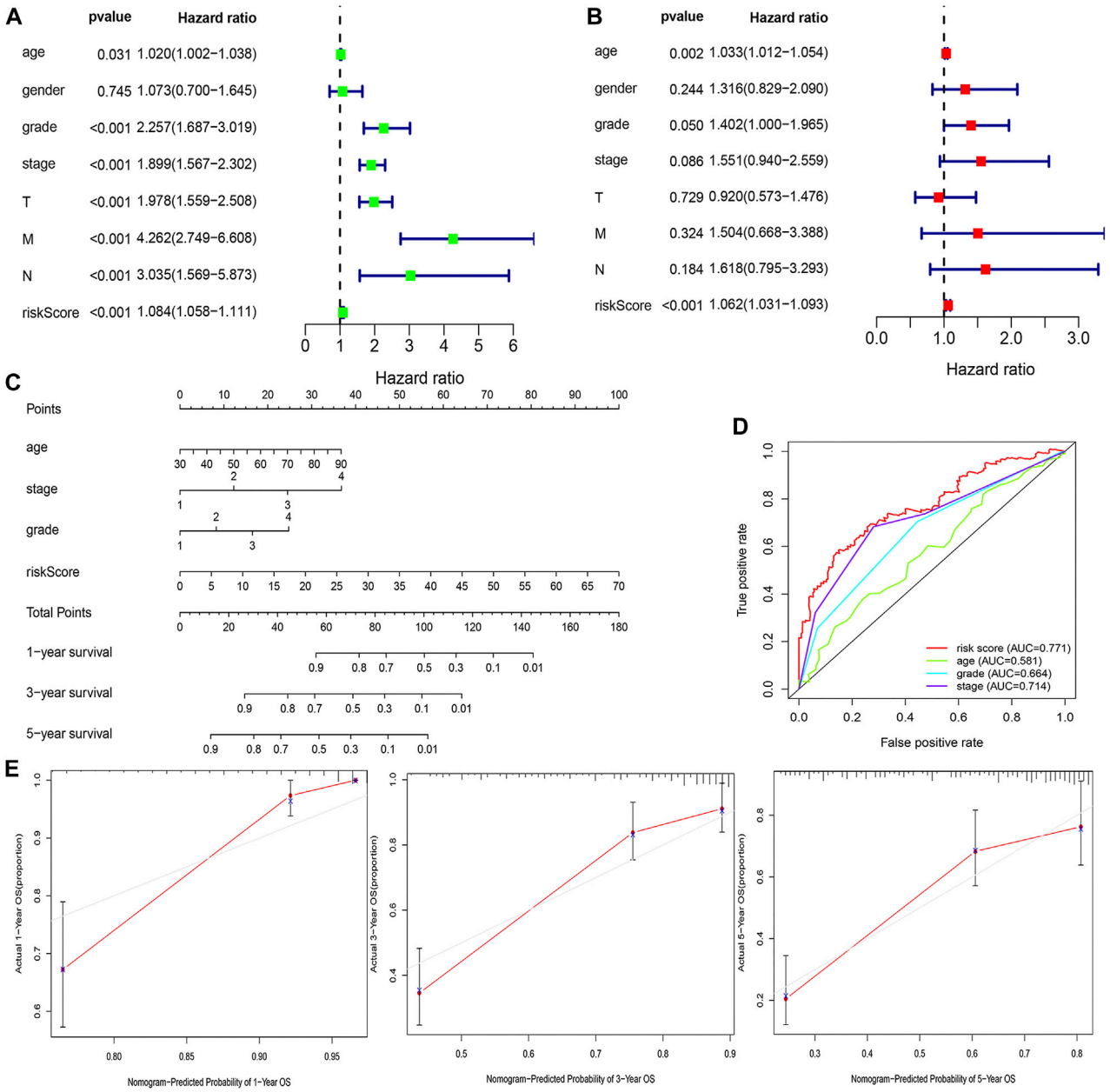

FIGURE 6 | Estimation of the clinical value of the FRlncRNA signature in ccRCC patients. The univariate Cox regression analysis showed that risk score and clinicopathological features including gender, age, grade, stage, T stage, N stage, and M stage were prognostic-related variables **(A)**. The multivariate Cox regression analysis showed the risk score was an independent prognostic factor **(B)**. Construction of a prognostic nomogram based on the risk score and clinicopathological parameters to predict 1-, 3-, 5-year OS of ccRCC patients **(C)**. The multivariate ROC curve showed predictive accuracy of the risk score was similar to other clinicopathological features **(D)**. The calibration curves of the nomogram displayed the concordance between predicted and observed 1-, 3-, and 5-year OS **(E)**.

consisted of biological process (BP) analysis mainly including positive regulation of the catabolic process and intrinsic apoptotic signaling pathway; cellular component (CC) analysis mainly containing focal adhesion, cell-substrate adherens junction, and cell-substrate junction; and molecular function (MF) analysis mostly composing of protein serine/threonine kinase activity, ubiquitin protein ligase binding, and iron ion binding. The "pathway-gene network" and "pathway-gene clustering," as shown in **Figures 8D–F**, were plotted to represent the complex relationship between FRlncRNA-related FRGs and KEGG pathways.

Construction of the Co-Expression Network and Verification of Major Genes

The co-expression network between eight FRlncRNAs and 49 FRGs (R^2 > 0.3 and p < 0.001) is shown in **Figure 9A**. The

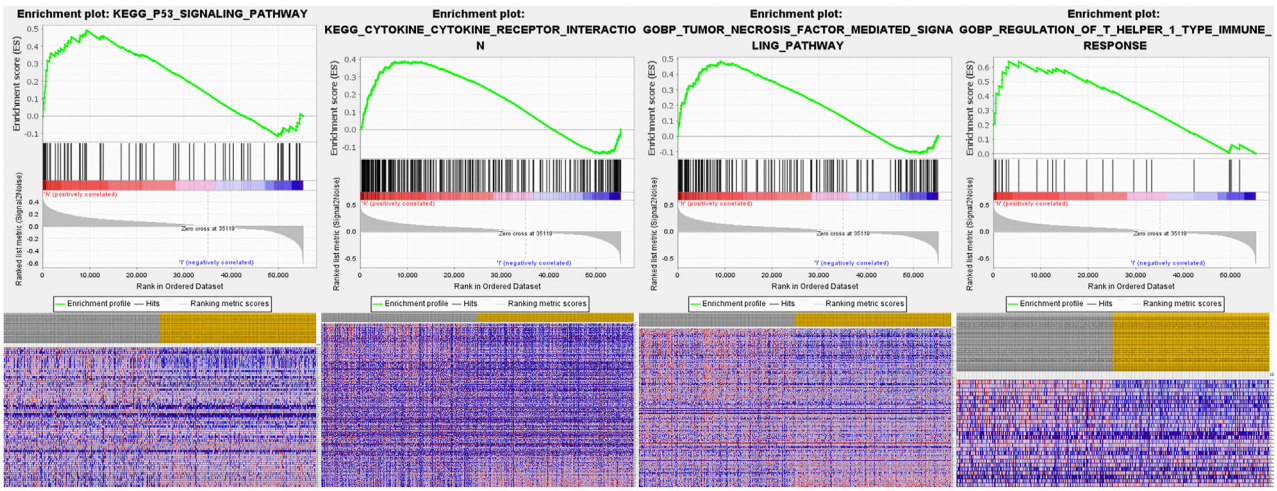

FIGURE 7 | GSEA analysis of the high-risk group in ccRCC patients based on the prognostic signature.

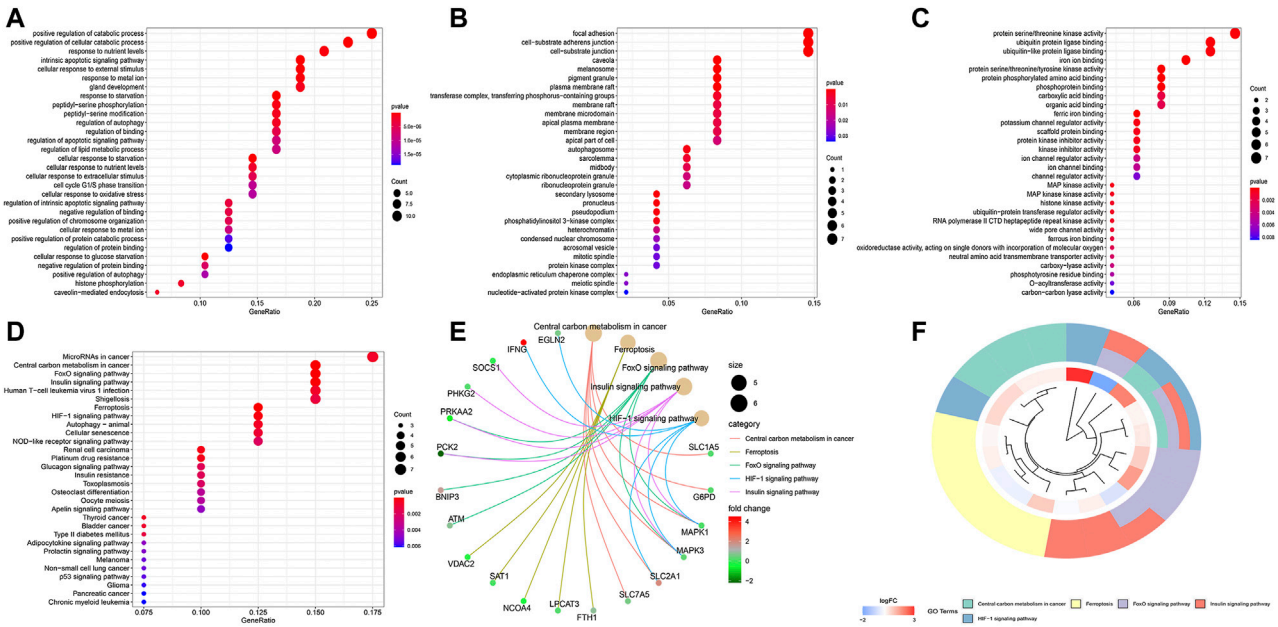

FIGURE 8 | Functional enrichment analysis of FRG-associated eight FRlncRNAs. **(A)** biological process, **(B)** cellular component, **(C)** molecular function, **(D)** dotplot of the KEGG signal pathway showing the counts of genes, **(E)** Cnetplot of the KEGG signal pathway showing the "pathway-gene" network, and **(F)** Circos plot of the KEGG pathway enrichment results.

Sankey diagram showed the interrelation between eight FRlncRNAs, 49 FRGs, and the risk type (**Figure 9B**). By analyzing the results of differential expression analysis ($p < 0.01$) and searching relevant literatures (Shijie Zhang et al., 2021; Chen and Zheng, 2021; Xuan et al., 2021) and databases, we selected four FRlncRNAs (LINC00460, LINC00944, LINC01550, and EPB41L4A-DT) for further study. Compared with normal tissues, LINC00460 (logFC = 5.039, p = 1.74E-19) and LINC00944 (logFC = 3.906, p = 2.46E-32) were significantly upregulated in ccRCC tissues, and LINC01550 (logFC = 0.359, p = 0.005) and EPB41L4A-DT (logFC = 0.2400, p = 0.003) were significantly downregulated in ccRCC tissues. To more accurately predict their action pathways, the ceRNA network (lncRNA–miRNA–mRNA) of four FRlncRNAs was explored (**Supplementary Figure S3**).

Two databases (GEPIA and K-M Plotter) were employed to investigate four FRlncRNAs including expression levels and survival outcomes. The expression levels of LINC00460

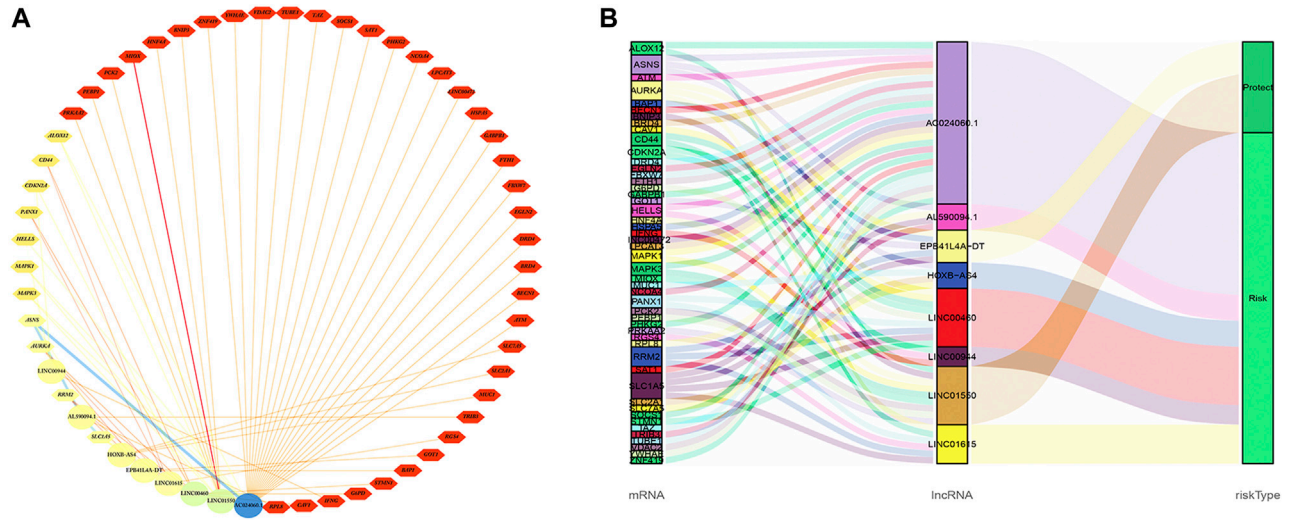

FIGURE 9 | Co-expression network of eight FRlncRNAs and 49 FRGs **(A)**. The Sankey diagram showed the connective degree between 49 FRGs and eight FRlncRNAs (risk/protective) **(B)**.

(Pr = 7.18E-09) and LINC00944 (Pr = 2.54E-11) increased gradually with the increase of stages but those of LINC01550 (Pr = 0.000122) and EPB41L4A-DT (Pr = 1.06E-10) decreased gradually with the increase in stages, suggesting that four FRlncRNAs were strongly correlated with tumor progression (**Figures 10A–H**). High expression levels of LINC00460 and LINC00944 and low expression levels of LINC01550 and EPB41L4A-DT were related to the poor prognosis ($p < 0.05$) (**Figures 10I–P**). Similarly, lower 5-year OS ($p < 0.05$) was noted in 530 ccRCC patients from the K-M Plotter database with an increasing expression of LINC00460 or decreasing expressions of LINC01550 and EPB41L4A-DT (**Figures 10Q–S**).

Through linear correlation analysis (R > 0.3 and $p < 0.001$) and literature retrieval (Shao et al., 2019; Xiong et al., 2021a; Hong et al., 2021), we selected three target genes (BNIP3, RRM2, and GOT1) for further verification. BNIP3 ($p < 0.05$) and RRM2 ($p < 0.05$) were significantly upregulated in ccRCC tissues, but GOT1 ($p < 0.05$) was significantly downregulated in ccRCC tissues (**Figures 11A–C**). The expression levels of BNIP3 and GOT1 decreased gradually with the increase in grades, but RRM2 increased gradually with the increase in clinical grades and stages, which revealed that three target genes were closely related to tumor progression (**Figures 11D–I**). High expression levels of RRM2 and low expression levels of BNIP3 and GOT1 were related to poor prognosis after the analysis of GEPIA and K-M Plotter databases ($p < 0.05$) (**Figures 11J–O**). The linear correlation analysis found that RRM2, BNIP3, and GOT1 may be potential targets of LINC00460 (R = 0.35; $p < 2.2E-16$), LINC01550 (R = 0.57; $p < 2.2E-16$), and EPB41L4A-DT (R = 0.33; $p < 3.8E-15$), respectively, which also needed further experimental verification (**Figures 11P–R**).

Tumor Tissue Validation

The expression levels of four FRlncRNAs were verified by qRT-PCR in the tumor and adjacent normal tissues collected from twenty ccRCC patients (**Supplementary Table S5**). LINC01550 and EPB41L4A-DT in tumor tissues were downregulated, while LINC00460 and LINC00944 were upregulated, showing the statistical significance (**Figures 12A–D**, t-test, $p < 0.05$; **Figures 12E–H**, paired t-test, $p < 0.05$). These results were consistent with our previous verification results, but more samples were still needed for verification.

Immune Analysis

We summarized the result of 507 ccRCC patients calculated by various algorithms and compared all the immune cell subtypes in two groups. Infiltration proportion of partial cell subtypes had an obvious difference between two groups, among which mainly T cell NK, B cell, T cell follicular helper, and T cell regulatory (Tregs) had a higher infiltration proportion in the high-risk group, while T cell $CD4^+$, neutrophils and endothelial cells had a lower proportion (**Figure 13A**). The immune functions of the high-risk group and low-risk group were analyzed, respectively, using "GSVA" and "GSEABase" packages in R software and found that almost all items (APC co-stimulation, CCR, check-point, cytolytic activity, inflammation promoting, para inflammation, T-cell co-inhibition, T-cell co-stimulation, Type I IFN response) in the high-risk group were upregulated ($p < 0.05$, **Figure 13B**), indicating a significant change in the immunophenotype in the high-risk group. We further explored the expression of immune checkpoint-related markers in two groups and found some markers (CTLA4, CD40LG, LAG3, CD44, CD27, CD160, TNFRSF18, CD40, TNFSF4, CD244, TMIGD2, LAIR1, TIGIT, TNFRSF9, PDCD1, CD86, IDO2, CD200R1, BTLA4, TNFSF9, LGALS9, CD70, CD48, CD80, TNFRSF25, ICOS, TNFSF14, CD28, and TNFRSF8) in the high-risk group were upregulated, and some markers (NRP1, KIR3DL1, HHLA2, TNFSF18, HAVCR2, and TNFSF15) were downregulated, indicating an immunosuppressive and exhausted phenotype in the high-risk group (**Figure 13C**). Based on the above analyses, we found two groups had a significant distinct pattern of immune infiltration, which may lead to different survival benefits.

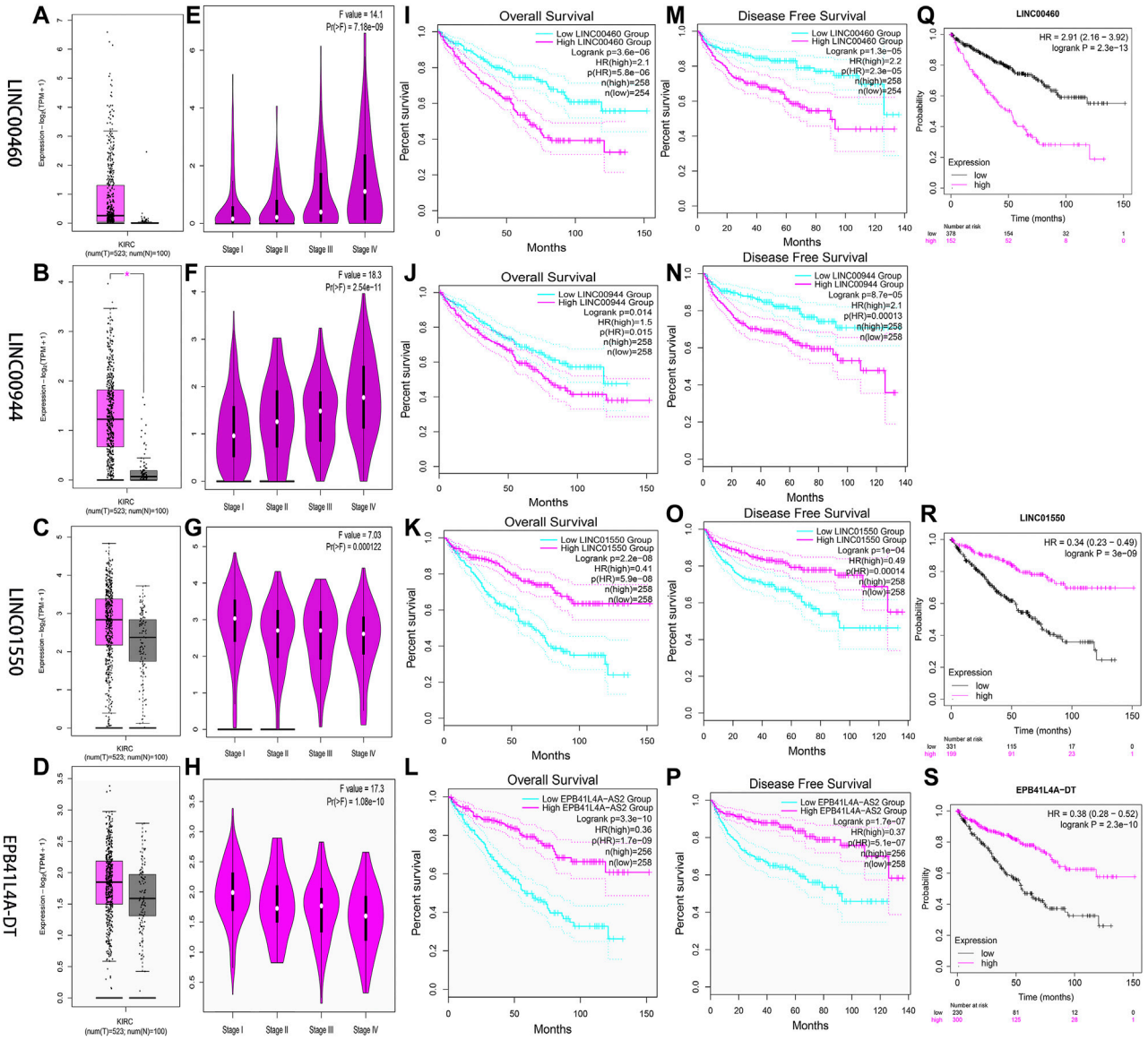

FIGURE 10 | Verification of expression and prognosis of four FRlncRNAs (LINC00460, LINC00944, LINC01550, and EPB41L4A-DT) from the GEPIA **(A-P)** and K-M Plotter databases **(Q-S)**. The expression levels of LINC00460 and LINC00944 increased gradually with the increase of stages, but LINC01550 and EPB41L4A-DT decreased gradually with the increase of stages. The high expression levels of LINC00460 and LINC00944 and low expression levels of LINC01550 and EPB41L4A-DT were associated with poor prognosis ($p < 0.05$).

DISCUSSION

Although breakthroughs have been made in surgical methods and postoperative auxiliary regimens for ccRCC in recent years, the prognosis of patients with advanced ccRCC and metastatic ccRCC was still of concern (Atkins and Tannir, 2018; Toth and Cho, 2020). Furthermore, some ccRCC patients with the same TNM stage or similar risk factors may represent different clinical outcomes due to complicated pathogenic molecules. It was necessary to discover molecular biomarkers that can predict the prognosis of the tumor (Attalla et al., 2020). Ferroptosis was reported to be closely associated with the biological process of ccRCC, for example proliferation, invasion, and metastasis (Miess et al., 2018; Markowitsch et al., 2020; Tang and Xiao, 2020), in which crucial regulatory roles of lncRNAs were identified in the ferroptosis-related biological process of malignant tumor cells (Mao et al., 2018; Wang et al., 2019; Wu and Liu, 2021). So an FRlncRNA signature was established and evaluated in predicting clinical outcomes.

Fifteen FRlncRNAs related with prognosis of ccRCC were initially identified in the training group, and a prognostic signature was constructed containing eight FRlncRNAs using multivariate Cox regression along with the Lasso regression. The OS of patients with high-risk scores was shorter than that of

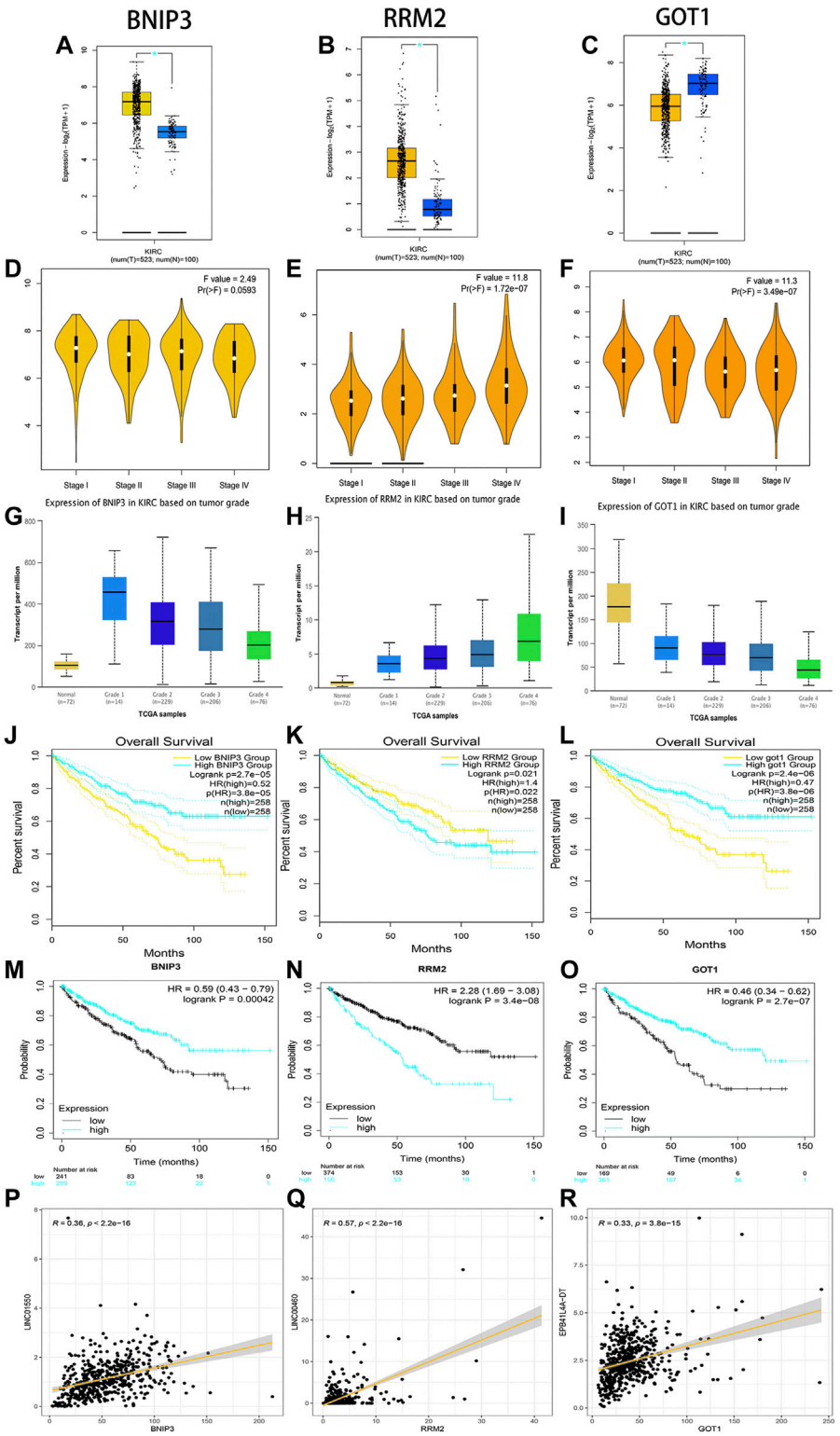

FIGURE 11 | Verification of expression and prognosis of three target genes (BNIP3, RRM2, and GOT1) from the GEPIA, UALCAN, and K-M Plotter databases. BNIP3 and RRM2 were significantly upregulated in ccRCC tissues, but GOT1 was significantly downregulated in ccRCC tissues **(A-C)**. The expression levels of BNIP3 and GOT1 decreased gradually with the increase of grades, but RRM2 increased gradually with the increase of grades and stages **(D-I)**. The high expression levels of RRM2 and low expression levels of BNIP3 and GOT1 were associated with poor prognosis **(J-O)**. Linear correlation analysis found that RRM2, BNIP3, and GOT1 may be potential target genes of LINC00460, LINC01550, and EPB41L4A-DT, respectively **(P-R)**.

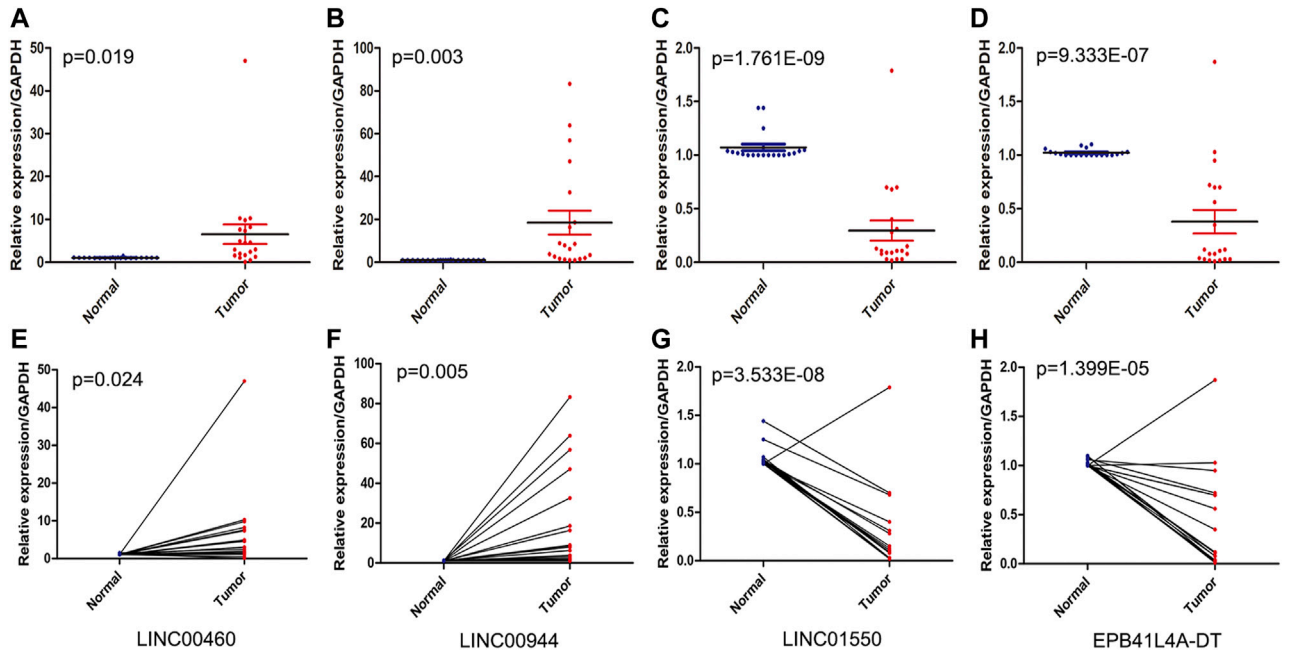

FIGURE 12 | QRT-PCR analysis of the expression of four FRlncRNAs (LINC00460 **(A, E)**, LINC00944 **(B, F)**, LINC01550 **(C, G)**, and EPB41L4A-DT **(D,H)**) from twenty patients with ccRCC.

patients with low-risk scores. The FRlncRNA signature validated by the ROC curve was greatly sensitive and act as specific prognosis markers for ccRCC, which further verifications were performed in the testing cohorts, overall cohorts, and ICGC cohorts. The FRlncRNA signature was also related to different OS in various subgroups of ccRCC, for instance age, gender, grade, stage, T stage, and M stage. Importantly, this signature was proved to be an independent risk factor in predicting survival outcomes. Next, we set up a nomogram including the risk score to calculate 1-, 3-, and 5-year survival rates of ccRCC patients, which had a higher sensitivity compared with the conventional grade and stage standard. After co-expression network construction and differential expression analysis, we selected four FRlncRNAs (LINC00460, LINC00944, LINC01550, and EPB41L4A-DT) which were closely related with FRGs for further study. The expression levels of four FRlncRNAs were verified by qRT-PCR from twenty ccRCC patients, which found that LINC01550 and EPB41L4A-DT in tumor tissues were downregulated, while LINC00460 and LINC00944 were upregulated. The expression levels of LINC00460, LINC00944, LINC01550, and EPB41L4A-DT differed across the four stages, suggesting that four FRlncRNAs were closely related to the tumor stage. Two external databases confirmed that four FRlncRNAs were significantly correlated with the prognosis of ccRCC. The correlation analysis identified that RRM2, BNIP3, and GOT1 may be potential targets of LINC00460, LINC01550, and EPB41L4A-DT, respectively. BNIP3 and RRM2 strikingly increased in ccRCC tissues, while GOT1 significantly reduced. BNIP3 and GOT1 were downregulated gradually with the increase in the grade, but RRM2 increased gradually with the increase in the grade and stage, which revealed that three target genes were closely related with tumor progression. The high expression level of RRM2 and low expression levels of BNIP3/GOT1 were related to poor prognosis, which was consistent with the prognosis of three FRlncRNAs after the analysis of GEPIA and K-M Plotter databases.

Based on the functional annotation and pathway enrichment analysis of the FRlncRNA signature, the mechanism of FRlncRNAs regulating ccRCC development was intuitively outlined. The results suggest that FRlncRNAs can positively regulate the P53 signaling pathway, tumor necrosis factor (TNF)-mediated signaling pathway, cytokine–cytokine receptor interaction, and T helper 1 type immune response signaling pathway. In addition, the GSEA found FRlncRNA-related FRGs were significantly enriched on the microRNA in cancer, iron ion binding, ferroptosis, focal adhesion, positive regulation of the catabolic process, and hypoxia-inducible transcription factor 1 (HIF-1) signaling pathway. We further constructed the ceRNA network to reveal the potential pathway of four major FRlncRNAs through acting on microRNA. P53, as an important regulatory factor in the development of cancer, often played a role as a target protein in ccRCC (Huang et al., 2020; Patergnani et al., 2020; Chen et al., 2021a; Sekino et al., 2021a). P53 knockout decreased sensitivity to sunitinib, and p53-positive cases tended to be associated with poor progression-free survival after first-line sunitinib treatment (Sekino et al., 2021b). The TNF-family-related signature of ccRCC also was proved to be closely related to the prognostic value, immune infiltration, and tumor mutation burden (Wenhao Zhang et al., 2021).

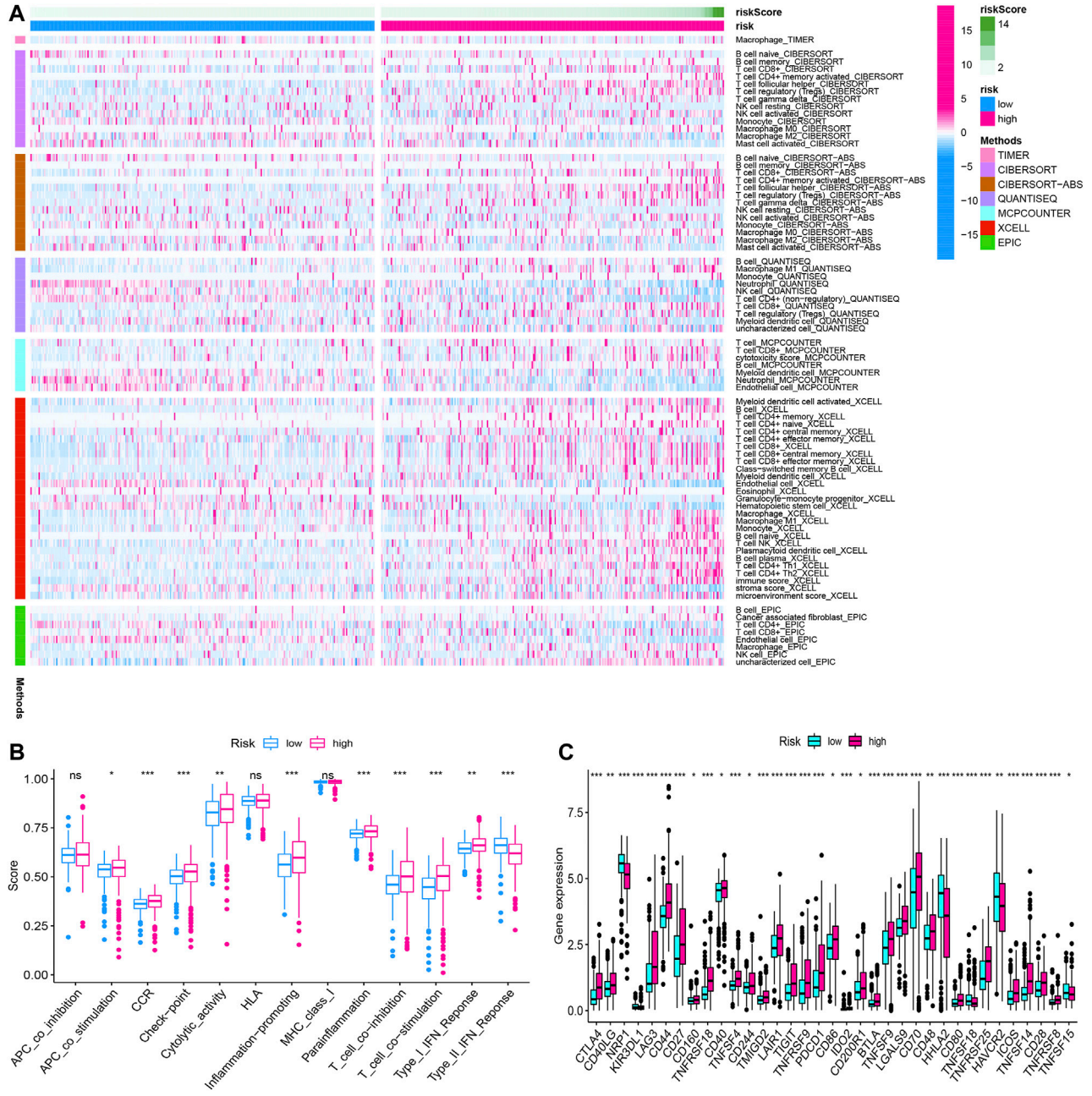

FIGURE 13 | The immune infiltration, **(A)** immune function, **(B)** immune checkpoint, and **(C)** of the high- and low-risk groups for BLCA patients in the overall cohorts. *$p < 0.05$; **$p < 0.01$; ***$p < 0.001$.

Ferroptosis was first reported in non–small cell lung cancer cells (Dixon et al., 2012). Subsequently, researchers examined the sensitivity of 117 cancer cells to erastin-induced ferroptosis cell death and found that RCC was particularly sensitive to GPX4-regulated ferroptosis (Yang et al., 2014). Miess et al. reported that the induction of silencing of glutathione peroxidase, GPx3, and GPx4 genes by siRNA was lethal to renal cancer cells (Miess et al., 2018). The impaired fatty acid degradation might drive ccRCC cells to become extremely dependent on GSH synthesis to prevent the accumulation of lipid peroxides and maintain cell viability owing to HIF-induced lipid uptake. These findings suggested that ccRCC cells were sensitive to ferroptosis-mediated cell death by inhibiting or even blocking GSH synthesis of tumor cells (Tang and Xiao, 2020). Notably, RCC cells re-expressing Von Hippel-Lindau developed resistance to ferroptosis. Yang et al. reported that TAZ, an effector of the Hippo pathway, regulated the sensitivity of RCC cells to ferroptosis (Yang et al., 2019). Therefore, modulating ferroptosis may have therapeutic potentials.

Currently, four FRlncRNAs (LINC01615, LINC01550, EPB41L4A-DT, and LINC00944) have been reported to be related to cancer development. Among them, LINC01615 was not only an optimal diagnostic lncRNA biomarker for head and neck squamous cell carcinoma but also closely related to survival time (Hu et al., 2020). LINC01615 has also been identified to be associated with the extracellular matrix and had further impacts on the metastasis of hepatocellular carcinoma (Ji et al., 2019). In addition, Chen et al. identified that the increased expression of LINC01550 seriously impeded cell proliferation and invasion abilities and caused cell apoptosis and G1 and S-phase arrest of the melanoma cells, which indicated that LINC01550 may act as a potential therapeutic target for melanoma (Chen et al., 2021b). Importantly, the overexpressed lncRNA EPB41L4A-DT in the renal cancer cell line 786-O, cell proliferation assays, flow cytometry, and clonogenic assay showed that upregulating EPB41L4A-DT may inhibit the proliferation of renal cancer cells (Xu et al., 2016). The knockdown of LINC00944 in 786-O and 769-P RCC cells could significantly decrease proliferation and migration and also promoted phosphorylation of Akt (Chen and Zheng, 2021). The above results further confirmed the accuracy of our model, but the potential mechanism of LINC01615 and LINC01550 in the occurrence and development of RCC needed to be further studied.

Besides, two FRlncRNAs (AC024060.1 and LINC00460) have been included in related clinical prediction models and demonstrated a good predictive power for the prognosis of cancer patients. Among them, AC024060.1 may predict the prognosis and progression of patients with bladder cancer as an immune-related lncRNA (Wang et al., 2021). Also, AC024060.1 as an autophagy-related lncRNA may be involved in the diagnosis and prognosis of bladder cancer (Wan et al., 2021). Moreover, Zhang et al. constructed a prognostic model based on ceRNA-related lncRNA and found that LINC00460 may provide insight into the prognostic biomarkers and therapeutic targets of ccRCC (Zhang et al., 2020). Little is known about prognostic effects of AL590094.1 and HOXB-AS4 on the prognosis of cancer. Therefore, more research is needed to explore the influence of FRlncRNAs on the prognosis of ccRCC mediated by ferroptosis.

There are some basic experimental studies on the biological function of two target genes (RRM2 and BNIP3) regulated by FRlncRNAs for renal cancer. Xiong et al. reported that RRM2 could regulate the sensitivity of renal cancer to sunitinib and PD-1 blockade *via* the stabilization of ANXA1 and the activation of the AKT pathway, and the effectiveness of the PD-1 blockade was improved by the deletion of RRM2 (Xiong et al., 2021b). Shao et al. identified that BNIP3 inactivation in renal cancer was probably caused by histone deacetylation, rather than methylation, and the histone deacetylation inhibitor can restore the expression of BNIP3 in renal cancer, subsequently resulting in growth inhibition and apoptotic promotion (Shao et al., 2019). These findings were consistent with our results, which may also need further experimental verification. As FRGs, GOT1 has only been proved to be a biomarker of ccRCC patients in clinical prediction models, which also needs further basic experiments to explore (Chang et al., 2021; Hong et al., 2021).

Ferroptosis is a type of cell death providing novel insights into tumor therapy. However, there are still many crucial questions less well studied, such as the interaction between ferroptosis and other cell deaths and the host immunogenicity. Thus, this study examined ferroptosis biomarkers can serve as a predictive factor to ccRCC prognosis, which may offer consultations for therapeutic modalities. Nevertheless, the current study still has some shortcomings. First, due to the shortage of the single and small amount data source, a certain deviation may occur in this study. Second, to illustrate the prognostic function of ferroptosis-related signals, more prospectives are required to cooperate with our retrospective study. Third, with the in-depth study of FRGs, the study needs to be updated regularly. Fourth, relevant functional assays should be conducted to examine the ways that FRlncRNAs influence the development and progression of ccRCC and explore underlying molecular mechanisms. Fifth, this model divided patients into the high-risk group and low-risk group according to the median risk score, although better sensitivity and specificity were obtained; the accuracy was worse than the optimal cutoff value.

CONCLUSION

The FRlncRNA signature was accurate and act as reliable tools for predicting clinical outcomes and the immune microenvironment of patients with ccRCC, which may be molecular biomarkers and therapeutic targets.

DATA AVAILABILITY STATEMENT

The original contributions presented in the study are included in the article/**Supplementary Material**, further inquiries can be directed to the corresponding author.

ETHICS STATEMENT

The studies involving human participants were reviewed and approved by the ethics committee of Yantai Yuhuangding Hospital (KY-E-2021–06-07). The patients/participants provided their written informed consent to participate in this study.

AUTHOR CONTRIBUTIONS

Conception and design of the research: All authors; Acquisition of data:ZZ, YZ, CY, LS, HY, CX; Analysis and interpretation of data: ZZ, YZ, CY, LS; Statistical analysis: ZZ, YZ, CX, YL. LS; Drafting manuscript: ZZ, YZ, CY; Obtaining funding: ZY, YL. All authors read and approved the final manuscript.

FUNDING

This work was supported by Beijing Municipal Administration of Hospitals' Ascent Plan, Code: DFL20190502; Beijing Municipal Administration of Hospitals Clinical Medicine Development of Special Funding Support, Code: ZYLX201820; Shandong Provincial Natural Science Foundation, Code: ZR2021MH186; Yantai science and technology project, Code: 2019YD025.

ACKNOWLEDGMENTS

The authors thank the National Cancer Institute for providing the TCGA-KIRC dataset. The authors also thank the ICGC database and GSEA database.

SUPPLEMENTARY MATERIAL

The Supplementary Material for this article can be found online at: https://www.frontiersin.org/articles/10.3389/fgene.2022.787884/full#supplementary-material

REFERENCES

Atkins, M. B., and Tannir, N. M. (2018). Current and Emerging Therapies for First-Line Treatment of Metastatic Clear Cell Renal Cell Carcinoma. *Cancer Treat. Rev.* 70, 127–137. doi:10.1016/j.ctrv.2018.07.009

Attalla, K., Weng, S., Voss, M. H., and Hakimi, A. A. (2020). Epidemiology, Risk Assessment, and Biomarkers for Patients With Advanced Renal Cell Carcinoma. *Urol. Clin. North America* 47, 293–303. doi:10.1016/j.ucl.2020.04.002

Bex, A., Albiges, L., Ljungberg, B., Bensalah, K., Dabestani, S., Giles, R. H., et al. (2018). Updated European Association of Urology Guidelines for Cytoreductive Nephrectomy in Patients With Synchronous Metastatic Clear-Cell Renal Cell Carcinoma. *Eur. Urol.* 74, 805–809. doi:10.1016/j.eururo.2018.08.008

Canxuan, L., and Dan, L. (2021). A Robust Ferroptosis-Related Gene Signature Predicts Overall Survival in Clear Cell Renal Cell Carcinoma. *Future Oncol.* 17, 4321–4341. doi:10.2217/fon-2021-0275

Chang, K., Yuan, C., and Liu, X. (2021). Ferroptosis-Related Gene Signature Accurately Predicts Survival Outcomes in Patients With Clear-Cell Renal Cell Carcinoma. *Front. Oncol.* 11, 649347. doi:10.3389/fonc.2021.649347

Chen, C., and Zheng, H. (2021). LncRNA LINC00944 Promotes Tumorigenesis but Suppresses Akt Phosphorylation in Renal Cell Carcinoma. *Front. Mol. Biosci.* 8, 697962. doi:10.3389/fmolb.2021.697962

Chen, J., Xu, D., Cao, J.-w., Zuo, L., Han, Z.-t., Tian, Y.-j., et al. (2021a). TRIM47 Promotes Malignant Progression of Renal Cell Carcinoma by Degrading P53 through Ubiquitination. *Cancer Cell Int.* 21, 129. doi:10.1186/s12935-021-01831-0

Chen, J., Li, P., Chen, Z., Wang, S., Tang, S., Chen, X., et al. (2021b). Elevated LINC01550 Induces the Apoptosis and Cell Cycle Arrest of Melanoma. *Med. Oncol.* 38, 32. doi:10.1007/s12032-021-01478-x

Chen, X., Li, J., Kang, R., Klionsky, D. J., and Tang, D. (2020). Ferroptosis: Machinery and Regulation. *Autophagy* 2021 Sep; 17 (9), 2054–2081. doi:10.1080/15548627.2020.1810918

Compérat, E. M., Burger, M., Gontero, P., Mostafid, A. H., Palou, J., Rouprêt, M., et al. (2019). Grading of Urothelial Carcinoma and the New "World Health Organisation Classification of Tumours of the Urinary System and Male Genital Organs 2016". *Eur. Urol. Focus.* 5, 457–466. doi:10.1016/j.euf.2018.01.003

DiMagno, M. J. (2007). Nitric Oxide Pathways and Evidence-Based Perturbations in Acute Pancreatitis. *Pancreatology* 7, 403–408. doi:10.1159/000108956

Dixon, S. J., Lemberg, K. M., Lamprecht, M. R., Skouta, R., Zaitsev, E. M., Gleason, C. E., et al. (2012). Ferroptosis: an Iron-Dependent Form of Nonapoptotic Cell Death. *Cell.* 149, 1060–1072. doi:10.1016/j.cell.2012.03.042

Dixon, S. J., Winter, G. E., Musavi, L. S., Lee, E. D., Snijder, B., Rebsamen, M., et al. (2015). Human Haploid Cell Genetics Reveals Roles for Lipid Metabolism Genes in Nonapoptotic Cell Death. *ACS Chem. Biol.* 10, 1604–1609. doi:10.1021/acschembio.5b00245

Ferlay, J., Colombet, M., Soerjomataram, I., Dyba, T., Randi, G., Bettio, M., et al. (2018). Cancer Incidence and Mortality Patterns in Europe: Estimates for 40 Countries and 25 Major Cancers in 2018. *Eur. J. Cancer* 103, 356–387. doi:10.1016/j.ejca.2018.07.005

Hong, Y., Lin, M., Ou, D., Huang, Z., and Shen, P. (2021). A Novel Ferroptosis-Related 12-gene Signature Predicts Clinical Prognosis and Reveals Immune Relevancy in clear Cell Renal Cell Carcinoma. *BMC Cancer* 21, 831. doi:10.1186/s12885-021-08559-0

Hu, Y., Guo, G., Li, J., Chen, J., and Tan, P. (2020). Screening Key lncRNAs with Diagnostic and Prognostic Value for Head and Neck Squamous Cell Carcinoma Based on Machine Learning and mRNA-lncRNA Co-expression Network Analysis. *Cancer Biomark.* 27, 195–206. doi:10.3233/cbm-190694

Huang, S., Yan, Q., Xiong, S., Peng, Y., Zhao, R., and Liu, C. (2020). Chromodomain Helicase DNA-Binding Protein 5 Inhibits Renal Cell Carcinoma Tumorigenesis by Activation of the P53 and RB Pathways. *Biomed. Res. Int.* 2020, 5425612. doi:10.1155/2020/5425612

Ji, D., Chen, G. F., Liu, X., Zhu, J., Sun, J. Y., Zhang, X. Y., et al. (2019). Identification of LINC01615 as Potential Metastasis-Related Long Noncoding RNA in Hepatocellular Carcinoma. *J. Cell Physiol.* 234, 12964–12970. doi:10.1002/jcp.27963

Ju, X., Sun, Y., Zhang, F., Wei, X., Wang, Z., and He, X. (2020). Long Non-Coding RNA LINC02747 Promotes the Proliferation of Clear Cell Renal Cell Carcinoma by Inhibiting miR-608 and Activating TFE3. *Front. Oncol.* 10, 573789. doi:10.3389/fonc.2020.573789

Ma, S., Zhao, M., Fan, J., Chang, M., Pan, Z., Zhang, Z., et al. (2021). Analysis of Ferroptosis-Related Gene Expression and Prognostic Factors of Renal Clear Cell Carcinoma Based on TCGA Database. *Int. J. Gen. Med.* 14, 5969–5980. doi:10.2147/ijgm.s323511

Mao, C., Wang, X., Liu, Y., Wang, M., Yan, B., Jiang, Y., et al. (2018). A G3BP1-Interacting lncRNA Promotes Ferroptosis and Apoptosis in Cancer via Nuclear Sequestration of P53. *Cancer Res.* 78, 3484–3496. doi:10.1158/0008-5472.CAN-17-3454

Markowitsch, S. D., Schupp, P., and Lauckner, J. (2020). Artesunate Inhibits Growth of Sunitinib-Resistant Renal Cell Carcinoma Cells Through Cell Cycle Arrest and Induction of Ferroptosis. *Cancers (Basel).* 12, 3150. doi:10.3390/cancers12113150

Miess, H., Dankworth, B., Gouw, A. M., Rosenfeldt, M., Schmitz, W., Jiang, M., et al. (2018). The Glutathione Redox System Is Essential to Prevent Ferroptosis Caused by Impaired Lipid Metabolism in clear Cell Renal Cell Carcinoma. *Oncogene* 37, 5435–5450. doi:10.1038/s41388-018-0315-z

Panni, S., Lovering, R. C., Porras, P., and Orchard, S. (2020). Non-Coding RNA Regulatory Networks. *Biochim. Biophys. Acta (Bba) - Gene Regul. Mech.* 1863, 194417. doi:10.1016/j.bbagrm.2019.194417

Patergnani, S., Guzzo, S., Mangolini, A., dell'Atti, L., Pinton, P., and Aguiari, G. (2020). The Induction of AMPK-Dependent Autophagy Leads to P53 Degradation and Affects Cell Growth and Migration in Kidney Cancer Cells. *Exp. Cell Res.* 395, 112190. doi:10.1016/j.yexcr.2020.112190

Sekino, Y., Han, X., Kobayashi, G., Babasaki, T., Miyamoto, S., Kobatake, K., et al. (2021a). BUB1B Overexpression Is an Independent Prognostic Marker and Associated with CD44, P53, and PD-L1 in Renal Cell Carcinoma. *Oncology* 99, 240–250. doi:10.1159/000512446

Sekino, Y., Takemoto, K., Murata, D., Babasaki, T., Kobatake, K., Kitano, H., et al. (2021b). P53 Is Involved in Sunitinib Resistance and Poor Progression-Free Survival After Sunitinib Treatment of Renal Cell Carcinoma. *Anticancer Res.* 41, 4287–4294. doi:10.21873/anticanres.15233

Shao, Y., Liu, Z., Liu, J., Wang, H., Huang, L., Lin, T., et al. (2019). Expression and Epigenetic Regulatory Mechanism of BNIP3 in Clear Cell Renal Cell Carcinoma. *Int. J. Oncol.* 54, 348–360. doi:10.3892/ijo.2018.4603

Stockwell, B. R., Friedmann Angeli, J. P., Bayir, H., Bush, A. I., Conrad, M., Dixon, S. J., et al. (2017). Ferroptosis: A Regulated Cell Death Nexus Linking Metabolism, Redox Biology, and Disease. *Cell.* 171, 273–285. doi:10.1016/j.cell.2017.09.021

Tang, S., and Xiao, X. (2020). Ferroptosis and Kidney Diseases. *Int. Urol. Nephrol.* 52, 497–503. doi:10.1007/s11255-019-02335-7

Toth, A. T., and Cho, D. (2020). Emerging Therapies for Advanced Clear Cell Renal Cell Carcinoma. *J. Kidneycancer VHL.* 7, 17–26. doi:10.15586/jkcvhl.v7i4.156

Valashedi, M. R., Nikoo, A., and Najafi-Ghalehlou, N. (2021). Pharmacological Targeting of Ferroptosis in Cancer Treatment. *Curr. Cancer Drug Targets* 21. doi:10.2174/1568009621666211202091523

Wan, J., Guo, C., Fang, H., Xu, Z., Hu, Y., and Luo, Y. (2021). Autophagy-Related Long Non-Coding RNA Is a Prognostic Indicator for Bladder Cancer. *Front. Oncol.* 11, 647236. doi:10.3389/fonc.2021.647236

Wang, J., Shen, C., Dong, D., Zhong, X., Wang, Y., and Yang, X. (2021). Identification and Verification of an Immune-Related lncRNA Signature for Predicting the Prognosis of Patients with Bladder Cancer. *Int. Immunopharmacology* 90, 107146. doi:10.1016/j.intimp.2020.107146

Wang, M., Mao, C., Ouyang, L., Liu, Y., Lai, W., Liu, N., et al. (2019). Long Noncoding RNA LINC00336 Inhibits Ferroptosis in Lung Cancer by Functioning as a Competing Endogenous RNA. *Cell Death Differ.* 26, 2329–2343. doi:10.1038/s41418-019-0304-y

Wu, H., and Liu, A. (2021). Long Non-Coding RNA NEAT1 Regulates Ferroptosis Sensitivity in Non-Small-Cell Lung Cancer. *J. Int. Med. Res.* 49, 300060521996183. doi:10.1177/0300060521996183

Xie, B., and Guo, Y. (2021). Molecular Mechanism of Cell Ferroptosis and Research Progress in Regulation of Ferroptosis by Noncoding RNAs in Tumor Cells. *Cell Death Discov.* 7, 101. doi:10.1038/s41420-021-00483-3

Xing, X.-L., Yao, Z.-Y., Ou, J., Xing, C., and Li, F. (2021). Development and Validation of Ferroptosis-Related lncRNAs Prognosis Signatures in Kidney Renal Clear Cell Carcinoma. *Cancer Cell Int.* 21, 591. doi:10.1186/s12935-021-02284-1

Xiong, W., Zhang, B., and Yu, H. (2021a). RRM2 Regulates Sensitivity to Sunitinib and PD-1 Blockade in Renal Cancer by Stabilizing ANXA1 and Activating the AKT Pathway. *Adv. Sci. (Weinh).* 2021 Sep; 8 (18), e2100881. doi:10.1002/advs.202100881

Xiong, W., Zhang, B., Yu, H., Zhu, L., Yi, L., and Jin, X. (2021b). RRM2 Regulates Sensitivity to Sunitinib and PD-1 Blockade in Renal Cancer by Stabilizing ANXA1 and Activating the AKT Pathway. *Adv. Sci. (Weinh).* 8, e2100881. doi:10.1002/advs.202100881

Xu, S., Wang, P., You, Z., Meng, H., Mu, G., Bai, X., et al. (2016). The Long Non-coding RNA EPB41L4A-AS2 Inhibits Tumor Proliferation and Is Associated With Favorable Prognoses in Breast Cancer and Other Solid Tumors. *Oncotarget* 7, 20704–20717. doi:10.18632/oncotarget.8007

Xuan, Y., Chen, W., Liu, K., Gao, Y., Zuo, S., Wang, B., et al. (2021). A Risk Signature with Autophagy-Related Long Noncoding RNAs for Predicting the Prognosis of Clear Cell Renal Cell Carcinoma: Based on the TCGA Database and Bioinformatics. *Dis. Markers.* 2021, 8849977. doi:10.1155/2021/8849977

Yang, W.-H., Ding, C.-K. C., Sun, T., Rupprecht, G., Lin, C.-C., Hsu, D., et al. (2019). The Hippo Pathway Effector TAZ Regulates Ferroptosis in Renal Cell Carcinoma. *Cell Rep.* 28, 2501–2508. doi:10.1016/j.celrep.2019.07.107

Yang, W. S., SriRamaratnam, R., Welsch, M. E., Shimada, K., Skouta, R., Viswanathan, V. S., et al. (2014). Regulation of Ferroptotic Cancer Cell Death by GPX4. *Cell.* 156, 317–331. doi:10.1016/j.cell.2013.12.010

Yang, Y., Gong, P., Yao, D., Xue, D., and He, X. (2021). LncRNA HCG18 Promotes Clear Cell Renal Cell Carcinoma Progression by Targeting miR-152-3p to Upregulate RAB14. *Cmar.* 13, 2287–2294. doi:10.2147/cmar.s298649

Yu, G., Wang, L.-G., Han, Y., and He, Q.-Y. (2012). clusterProfiler: an R Package for Comparing Biological Themes Among Gene Clusters. *OMICS: A J. Integr. Biol.* 16, 284–287. doi:10.1089/omi.2011.0118

Yu, X., Wu, H., and Wang, H. (2021). *Identification of 8 Feature Genes Related to Clear Cell Renal Cell Carcinoma Progression Based on Co-Expression Analysis. Kidney Blood Press Res.* 2021 Sep; 47(2), 113–124. doi:10.1159/000520832

Zhang, D., Zeng, S., and Hu, X. (2020). Identification of a Three-Long Noncoding RNA Prognostic Model Involved Competitive Endogenous RNA in Kidney Renal clear Cell Carcinoma. *Cancer Cell Int.* 20, 319. doi:10.1186/s12935-020-01423-4

Shijie Zhang, S., Zhang, F., Niu, Y., and Yu, S. (2021). Aberration of lncRNA LINC00460 Is a Promising Prognosis Factor and Associated with Progression of Clear Cell Renal Cell Carcinoma. *Cmar.* 13, 6489–6497. doi:10.2147/cmar.s322747

Wenhao Zhang, W., Li, C., Wu, F., Li, N., Wang, Y., Hu, Y., et al. (2021). Analyzing and Validating the Prognostic Value of a TNF-Related Signature in Kidney Renal Clear Cell Carcinoma. *Front. Mol. Biosci.* 8, 689037. doi:10.3389/fmolb.2021.689037

Zheng, B., Niu, Z., Si, S., Zhao, G., Wang, J., Yao, Z., et al. (2021). Comprehensive Analysis of New Prognostic Signature Based on Ferroptosis-Related Genes in clear Cell Renal Cell Carcinoma. *Aging* 13, 19789–19804. doi:10.18632/aging.203390

Zhu, K., Miao, C., Tian, Y., Qin, Z., Xue, J., Xia, J., et al. (2020). lncRNA MIR4435-2HG Promoted clear Cell Renal Cell Carcinoma Malignant Progression via miR-513a-5p/KLF6 axis. *J. Cell Mol. Med.* 24, 10013–10026. doi:10.1111/jcmm.15609

Conflict of Interest: The authors declare that the research was conducted in the absence of any commercial or financial relationships that could be construed as a potential conflict of interest.

Publisher's Note: All claims expressed in this article are solely those of the authors and do not necessarily represent those of their affiliated organizations, or those of the publisher, the editors, and the reviewers. Any product that may be evaluated in this article, or claim that may be made by its manufacturer, is not guaranteed or endorsed by the publisher.

frontiers | Frontiers in Genetics

ORIGINAL RESEARCH
published: 26 April 2022
doi: 10.3389/fgene.2022.849437

Novel Prognostic Signature for Acute Myeloid Leukemia: Bioinformatics Analysis of Combined CNV-Driven and Ferroptosis-Related Genes

Chunjiao Han[1†], Jiafeng Zheng[2†], Fangfang Li[3†], Wei Guo[1,2] and Chunquan Cai[4*]*

[1]Clinical School of Paediatrics, Tianjin Medical University, Tianjin, China, [2]Department of Pulmonology, Tianjin Children's Hospital/Tianjin University Children's Hospital, Tianjin, China, [3]Department of Rheumatology and Immunology, Tianjin Children's Hospital/Tianjin University Children's Hospital, Tianjin, China, [4]Department of Institute of Pediatrics, Tianjin Children's Hospital/Tianjin University Children's Hospital, Tianjin, China

OPEN ACCESS

Edited by:
Ying Li,
The University of Texas Health Science Center at San Antonio, United States

Reviewed by:
Xianzhe Li,
The Sixth Affiliated Hospital of Sun Yat-sen University, China
Zi-Jun Xu,
Jiangsu University Affiliated People's Hospital, China

***Correspondence:**
Wei Guo
guowei79656@126.com
Chunquan Cai
15122656313@126.com

[†]These authors have contributed equally to this work and share first authorship

Specialty section:
This article was submitted to Human and Medical Genomics, a section of the journal Frontiers in Genetics

Received: 06 January 2022
Accepted: 22 March 2022
Published: 26 April 2022

Citation:
Han C, Zheng J, Li F, Guo W and Cai C (2022) Novel Prognostic Signature for Acute Myeloid Leukemia: Bioinformatics Analysis of Combined CNV-Driven and Ferroptosis-Related Genes. Front. Genet. 13:849437. doi: 10.3389/fgene.2022.849437

Background: Acute myeloid leukemia (AML), which has a difficult prognosis, is the most common hematologic malignancy. The role of copy number variations (CNVs) and ferroptosis in the tumor process is becoming increasingly prominent. We aimed to identify specific CNV-driven ferroptosis-related genes (FRGs) and establish a prognostic model for AML.

Methods: The combined analysis of CNV differential data and differentially expressed genes (DEGs) data from The Cancer Genome Atlas (TCGA) database was performed to identify key CNV-driven FRGs for AML. A risk model was constructed based on univariate and multivariate Cox regression analysis. The Gene Expression Omnibus (GEO) dataset was used to validate the model. Gene Ontology (GO) and Kyoto Encyclopedia of Genes and Genomes (KEGG) enrichment analyses were conducted to clarify the functional roles of DEGs and CNV-driven FRGs.

Results: We identified a total of 6828 AML-related DEGs, which were shown to be significantly associated with cell cycle and immune response processes. After a comprehensive analysis of CNVs and corresponding DEGs and FRGs, six CNV-driven FRGs were identified, and functional enrichment analysis indicated that they were involved in oxidative stress, cell death, and inflammatory response processes. Finally, we screened 2 CNV-driven FRGs (DNAJB6 and HSPB1) to develop a prognostic risk model. The overall survival (OS) of patients in the high-risk group was significantly shorter in both the TCGA and GEO (all $p < 0.05$) datasets compared to the low-risk group.

Conclusion: A novel signature based on CNV-driven FRGs was established to predict the survival of AML patients and displayed good performance. Our results may provide potential targets and new research ideas for the treatment and early detection of AML.

Keywords: acute myeloid leukemia, copy number variations, ferroptosis, prognosis, gene signature

INTRODUCTION

AML is a heterogeneous malignancy that is characterized by imbalanced hematopoietic stem cells and uncontrolled differentiation. It accounts for 15–20% of leukemia in children and has a higher incidence during adolescence (Arber et al., 2016). Despite intensive treatment, the long-term survival rate of children with AML is still only 45–55% (Carver et al., 2003). Cytogenetic outcomes and molecular is considered the most important prognostic factors at present (Döhner et al., 2017), however, the current genetic methods still can't achieve accurate prognosis prediction. Our study is aimed to construct a novel prognostic model as well as an improvement of risk-adapted therapy for patients.

Ferroptosis is a newly discovered iron-dependent programmed cell death, which is unlike apoptosis, autophagy, necrosis, pyroptosis, and other cell death forms (Grimwade et al., 2016). It results in cell death by inducing excessive membrane lipid peroxidation (Herold et al., 2018). It is reported that ferroptosis induction can inhibit the growth of tumor cells especially with resistance to traditional therapies (Herold et al., 2014; Döhner et al., 2017). For refractory and relapsed AML, resistance to apoptosis is an important therapeutic measure (Hong et al., 2021; Huang et al., 2021). Currently, as a potential therapeutic target for cancer treatment, ferroptosis has attracted worldwide attention. Some studies have suggested that some ferroptosis-related genes can be prognosis biomarkers (Huot et al., 1996; Herold et al., 2014; Döhner et al., 2017). The upregulation of phospholipid hydroperoxidase GPx4 is associated with poor prognosis of AML (Jakob et al., 1993). In addition, a study found that low AKR1C2 and SOCS1 expression was highly correlated with more favorable overall survival and disease-free survival in AML patients (Jiang et al., 2020).

CNV refers to the duplication, inversion, or deletion of a DNA sequence of more than one kilobase (Jiang et al., 2020). Recently, CNV has been recognized as an important source of genetic variation which was found to play an important role in many cancers. The previous study suggested that the presence of CNV affects not only protein expression but also long non-coding RNAs and miRNAs (Kerr et al., 1994). Cytogenetic CNV abnormalities have been included in WHO classification (2016) (Kim et al., 2012) and other risk stratification strategies (Liang et al., 2009; Li et al., 2013; Kuett et al., 2015), and constitute the single strongest prognostic factor for complete remission (CR) and overall survival (OS) of AML. A study has found CNVs in 23 patients (76.7%) with NK-AML in Korea (Jiang et al., 2020). It showed that CNV increase is an independent predictive factor for shorter event-free survival and may affect the success of Ara-C and anthracycline-based chemotherapy. However, most previous studies focused on CNV or transcriptome changes, there is still a lack of comprehensive research on how CNV drives AML.

Although FRGs and CNV can be used as prognostic markers of AML respectively, the relationship between FRGs and CNV has not been reported at present, which aroused our interest. In the present study, we used transcriptomics and CNVs profiles to identify CNV driven FRGs and aimed to construct a prognostic model of AML. Our study may contribute to a better understanding of the underlying mechanisms and provide a new therapeutic target for the treatment of AML.

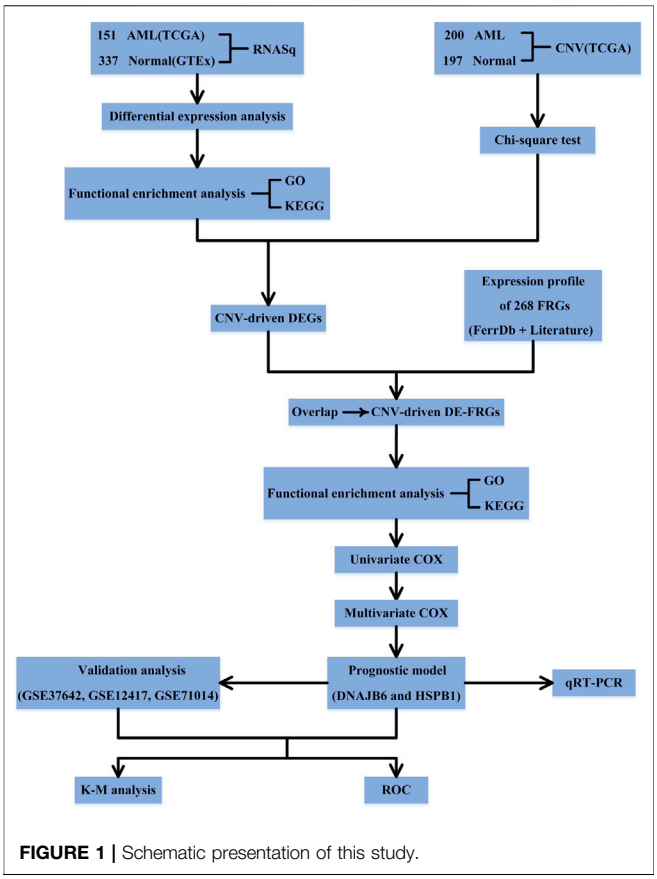

FIGURE 1 | Schematic presentation of this study.

MATERIALS AND METHODS

Data Source

Gene expression profiles of 151 bone marrow samples from AML patients were downloaded from the TCGA database. Since sequencing data of control samples were not available from the TCGA database, we obtained RNA sequencing data of 337 normal peripheral blood samples from the GTEx database. The GSE37642 (Mitra et al., 2008; Liang et al., 2016; Meng et al., 2016; Nibourel et al., 2017) was obtained from the GEO database. The GSE37642 dataset (platform: GPL570; https://www.ncbi.nlm.nih.gov/geo/query/acc.cgi?acc=GSE37642) contains transcriptional data from 136 AML patients with complete survival information, which was used for external validation analysis of the prognostic signature. Furthermore, the GSE12417 (platform: GPL570; n = 73; https://www.ncbi.nlm.nih.gov/geo/query/acc.cgi?acc=GSE12417) and GSE71014 (platform: GPL10558; n = 104; https://www.ncbi.nlm.nih.gov/geo/query/acc.cgi?acc=GSE71014) datasets were downloaded as complementary

external validation sets to perform validation analyses on a larger sample base.

Figure 1 shows the schematic presentation of this study.

Collection of FRGs

We downloaded 259 FRGs from the FerrDb online database (http://www.zhounan.org/ferrdb/). Meanwhile, a total of 60 FRGs were also obtained from the report of Yingkai Hong et al. (Herold et al., 2014). After de-duplication (retention of unique values), a total of 268 FRGs were obtained for our study (**Supplementary Table S1**).

Differential Expression Analysis

Gene expression profiles of AML (n = 151) and normal (n = 337) samples from TCGA and GTEx were subjected to normalize Between Arrays function for normalization, and subsequently, differential expression analysis (AML vs. normal) was performed using the R package limma. The significance threshold was set to $|\log_2 \text{fold change (FC)}| \geq 1$ and $p < 0.05$. A volcano map showing the distribution of the identified DEGs was plotted based on the R package ggplot2. In addition, we also verified that the identified DEGs were able to distinguish between normal and AML samples by Principal Component Analysis (PCA) to imply the applicability of the samples.

Functional Enrichment Analysis

To reveal the functions of target genes, R package clusterProfiler (Papaemmanuil et al., 2016) was used to conduct Gene Ontology (GO) annotation and Kyoto Encyclopedia of Genes and Genomes (KEGG) pathway enrichment analyses. The GO terms were comprised of the following three divisions: biological process (BP), cellular component (CC), and molecular function (MF). $p < 0.05$ was regarded as statistically significant.

Integrative Analysis of Gene Expression and CNVs

The CNV data of AML patients (n = 200) and normal subjects (n = 197) were downloaded from the TCGA database (sequencing platform Affymetrix SNP 6.0). Genes in CNV regions were annotated using Genome Research Consortium Human build 38 (GRCh38) as the reference genome. CNVs alteration rates between normal and tumor samples were then compared using the Chi-square test, and CNVs data with $p < 0.05$ were chosen for the next analysis. Then the CNVs data and DEGs data of the same sample were merged to construct a matrix. By using the Kolmogorov-Smirnov test, those genes showing the same tendency both in CNVs and differential gene expression (CNV increase-upregulated; CNV decrease-downregulated) were selected as CNV-driven DEGs. Moreover, CNV-driven DEGs and identified FRGs were analyzed for overlap, and the common genes in both gene lists were defined as CNV-driven DE-FRGs.

Construction, Evaluation, and Validation of the Prognostic Model

The TCGA-AML dataset containing 132 AML samples with complete survival information was used for prognostic gene screening and prognostic model construction and evaluation. The GSE37642 (n = 136), GSE12417 (n = 73), and GSE71014 (n = 104) datasets were used as an independent external validation set for prognostic model validation analysis. Prognostic genes were screened by Cox regression analysis. Briefly, target genes were included in univariate Cox regression analysis, and variables satisfying $p < 0.1$ were included in stepwise regression multivariate Cox analysis. The variables obtained from multivariate Cox regression analysis were identified as the optimal variables for the construction of the prognostic model. The risk score for each AML patient was calculated using the regression coefficient (coef) calculated from the multivariate Cox analysis and the expression of prognostic genes. The formula for calculating the risk score as shown below:

$$\begin{aligned} risk\ score = {} & coef_{gene_1} \times expression_{gene_1} \\ & + coef_{gene_2} \times expression_{gene_2} + \cdots \\ & + coef_{gene_n} \times expression_{gene_n} \end{aligned}$$

The samples were classified into high- and low-risk groups based on the median value of the risk score in each dataset (TCGA dataset and independent external validation set). The difference in OS between the two risk subgroups was assessed based on the R package survival using Kaplan-Meier (K-M) analysis. Receiver operating characteristic (ROC) curves were plotted by survROC package to assess the accuracy of the risk score for prognostic prediction in patients with TCGA-AML and GSE37642/GSE12417/GSE71014 datasets-AML.

Independent Prognostic Analysis of the Risk Score

Clinical characteristics of AML (age and sex) available in the TCGA database were included in the Cox regression analysis along with the risk score. Univariate Cox regression analyses with $p < 0.05$ output would be performed further in multivariate Cox analyses. Ultimately, variables with $p < 0.05$ generated by multivariate Cox regression analysis were considered as independent prognostic factors for AML.

Patient and Tissue Preparation

We selected the blood of 10 AML patients and 10 healthy people to carry on the quantitative PCR test to the genes screened in this study. The experimental verification data are obtained from the sample database of the Institute of Pediatrics of Tianjin Children's Hospital, and no samples are obtained directly from the children's body, so they do not need to be approved by the institutional ethics committee. All experimental operations are carried out in accordance with the relevant guidelines and regulations, and have been repeatedly verified by professional laboratory researchers.

RNA Isolation and Quantitative Real-Time Polymerase Chain Reaction

Whole-cell RNA was extracted via the RNAiso Plus (TaKaRa, Japan). Quantitative real-time polymerase chain reaction (qRT-

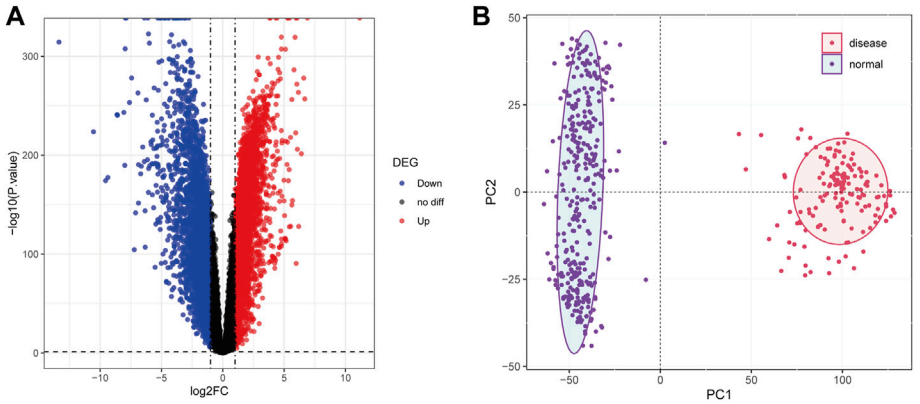

FIGURE 2 | Differential expression analysis. **(A)**: The volcanic map was used to show the differential genes between the samples of AML patients and normal people. Abscissa denotes log2FC, ordinate denotes-log10 (*p* value). Each dot in the picture represents a gene, and the red and blue dots represent significant differential expression, and the red dots indicate upregulated expression in the disease samples, blue dots indicate downregulation, and black dots indicate no significant difference. The horizontal guide represents-log10 (*p*-value) = 0.05. The vertical guide represents log2FC = ±1. **(B)**: Principal component analysis diagram. The dots in the picture represent the sample, the red represents the AML patient, and the purple represents the normal person sample. PC1 and PC2 represent the first and second principal components respectively.

PCR) was performed to detect DNAJB6 and HSPB1 expression using American Bio rad Bole T100 gradient PCR instrument. The following primers were used for qRT-PCR: DNAJB6 primers: upstream primer F: 5′-TATGAAGTGCTGTCGGATGCTAAG A-3'; downstream primer R: 5′-GAAGACATCATCTGGGTT ACGGA-3'. The conditions for PCR to DNAJB6 were: the size of the amplified product was 144bp, annealing temperature was 55–60°C. The sequences of HSPB1 primers used were: upstream primer F: 5′-GCAGTCCAACGAGATCACCA-3′ and downstream primer R: 5′-TTACTTGGCGGCAGTCTCATC-3′. The conditions for PCR to HSPB1 were: the size of the amplified product was 97bp, annealing temperature was 55–60°C. qRT-PCR was conducted in triplicate for each sample. All gene expression levels were normalized to that of GAPDH using the $2^{-\Delta\Delta Ct}$ method. Uupaired *t*-test (two-tailed) was used for the comparison analyses.

Statistical Analysis

All analyses in this study were performed in R software. A log-rank test was used to check the significant difference in OS between groups. An area under the ROC curve (AUC) served as an indicator of prognostic accuracy. Unless otherwise specified, a *p*-value less than 0.05 was considered statistically significant.

RESULTS

Exploration of AML-Related DEGs

The normalized expression profiles of TCGA-AML (n = 151) and GTEx-normal (n = 337) were selected as the basis for differential expression analysis. By R package limma, we identified 6,828 DEGs between AML and normal samples. Among them, a total of 3,330 met $\log_2$ FC ≥ 1 and $p < 0.05$ and 3,498 matched $\log_2$ FC ≤ -1 and $p < 0.05$ (**Figure 2A**; **Supplementary Table S2**). Furthermore, PCA performed based on the obtained DEGs demonstrated that samples from different groups were clustered in the same category (**Figure 2B**).

To explore the potential mechanisms of the above AML-related DEGs, we performed GO and KEGG function enrichment analysis for upregulated DEGs and downregulated DEGs, respectively, using the clusterProfiler package. **Figures 3A–C** illustrated the top5 terms that were significantly enriched in the three categories of GO, BP, CC, and MF, based on upregulated and downregulated DEGs. In the BP category, specifically, upregulated DEGs were significantly associated with "ribonucleoprotein complex biogenesis", "RNA splicing", "RNA splicing, via transesterification reactions" (**Figure 3A**); besides, these genes were found to be closely correlated with the cell cycle ("DNA replication", "chromosome segregation", "mitotic nuclear division", etc.). Moreover, upregulated DEGs might be played mainly in CCs such as "chromosomal region", "spindle", "chromosome, centromeric region" (**Figure 3B**) for MFs such as "histone binding", "DNA-dependent ATPase activity", "helicase activity" (**Figure 3C**). The results of the detailed GO analysis for the upregulated DEGs could be reviewed in **Supplementary Table S3**. For the down-regulated DEGs, they were significantly correlated with immune responses ("regulation of immune effector process", "negative regulation of immune system process", "immune response-activating signal transduction", etc.) and biological processes of immune cells ("neutrophil degranulation", "T cell activation", "T-cell differentiation", "lymphocyte proliferation", etc.) (**Figure 3A**). Also, these genes were able to perform the molecular functions of "carbohydrate binding", "organic acid binding", and "MHC protein binding" (**Figure 3C**) in "specific granule", "secretory granule lumen", and "cytoplasmic vesicle lumen" (**Figure 3B**). Detailed GO analysis results for downregulated DEGs were displayed in **Supplementary Table S4**. The top5 pathways

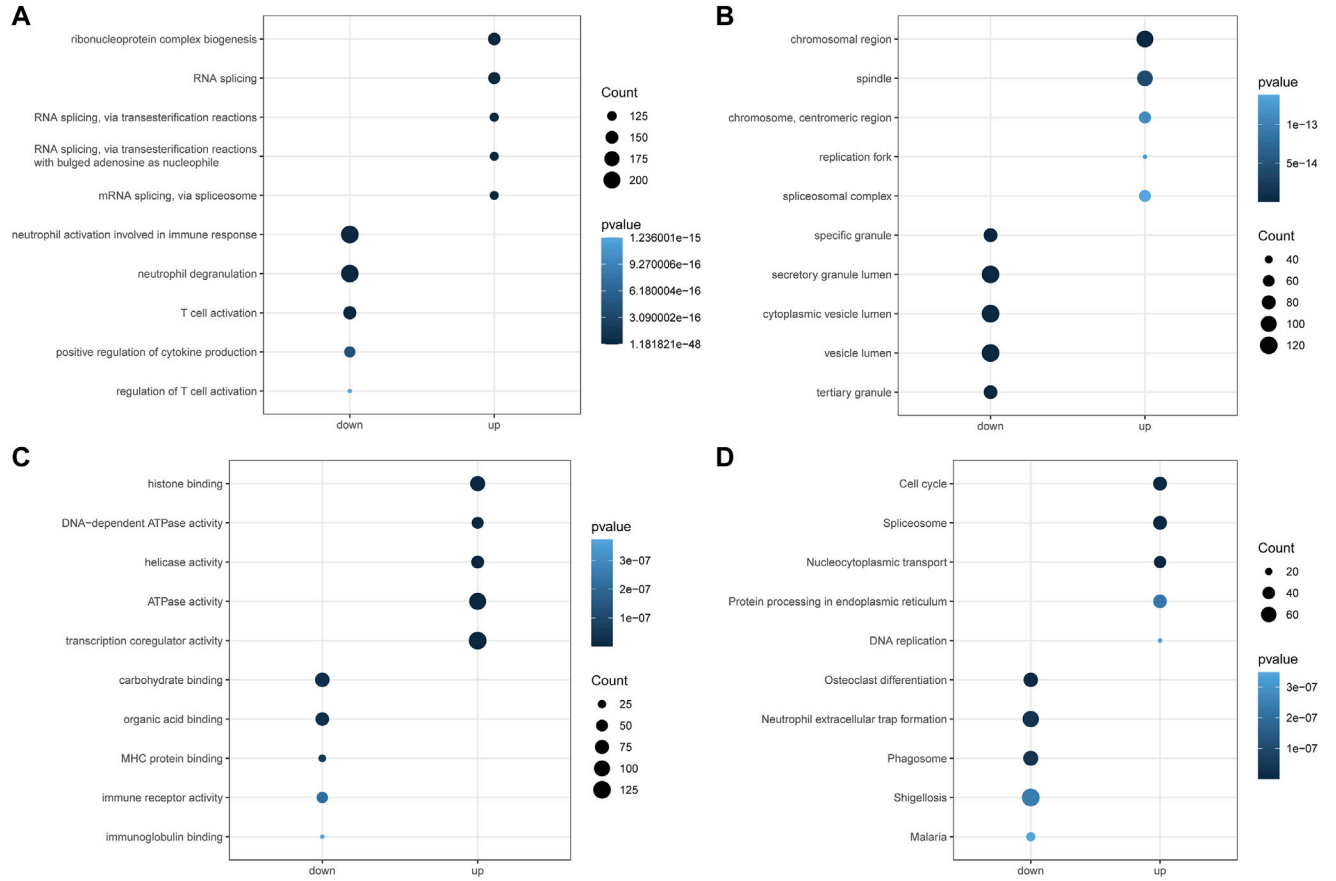

FIGURE 3 | Functional enrichment analysis of differential genes by GO and KEGG. **(A)**: Gene ontology analysis for the biological process (BP) of the AML-related DEGs. **(B)**: Gene ontology analysis for the cellular component (CC) of the AML-related DEGs. **(C)**: Gene ontology analysis for the molecular function (MF) of the AML-related DEGs. **(D)**: Kyoto Encyclopedia of Genome and Genome (KEGG) enrichment analysis of the 6828 AML-related DEGs. Down represents the functional enrichment of downregulated genes, while up represents the enrichment analysis of up-regulated genes. The vertical axis represents the functional item, the size of the dot represents the number of enriched genes, and the color represents the *p*-value.

significantly enriched in KEGG analysis were shown in **Figure 3D**, with upregulated DEGs involved in "Cell cycle", "Spliceosome", "Nucleocytoplasmic transport", "Protein processing in endoplasmic reticulum", and "DNA replication" (**Supplementary Table S5**); downregulated DEGs were closely associated with "Osteoclast differentiation", "Neutrophil extracellular trap formation", "Phagosome", "Shigellosis", and "Malaria" (**Supplementary Table S6**).

Identification of CNV-Driven DE-FRGs in AML Patients

By applying the Chi-square test, 4637 CNV genes associated with AML were identified ($p < 0.05$; **Supplementary Table S7**). The distribution of AML-related CNVs in chromosomes was presented in **Figure 4A**. Then CNV-driven DEGs were screened using the Kolmogorov-Smirnov test. We selected 337 CNV-driven DEGs, of which 127 were upregulated in AML with increased CNV (**Supplementary Table S8**) and the remaining 210 were downregulated with decreased CNV (**Supplementary Table S9**). Subsequently, by overlap analysis (**Figure 4B**), a total of 6 CNV-driven DE-FRGs, namely ALOX15B, MTDH, DNAJB6, HSPB1, ATF4, and PLIN2, were identified in the above list of CNV-driven DEGs and the list of 268 FRGs (**Supplementary Table S1**).

To illustrate the potential functional and biological effects of these CNV-driven DE-FRGs, GO (**Supplementary Table S10**) and KEGG (**Supplementary Table S11**) analyses were performed (**Figure 4C**). Results showed that CNV-driven DE-FRGs were significantly enriched in the BP category in terms related to oxidative stress response and its mediated cell death, such as "negative regulation of cellular response to oxidative stress", "negative regulation of oxidative stress-induced cell death", "negative regulation of response to oxidative stress", and "regulation of oxidative stress-induced cell death". KEGG analysis showed that these genes were involved in "MAPK signaling pathway", "Cocaine addiction", "VEGF signaling pathway", "Arachidonic acid metabolism", and "Cortisol synthesis and secretion". These results suggested that CNV-driven DE-FRGs were probably implicated in the cell cycle

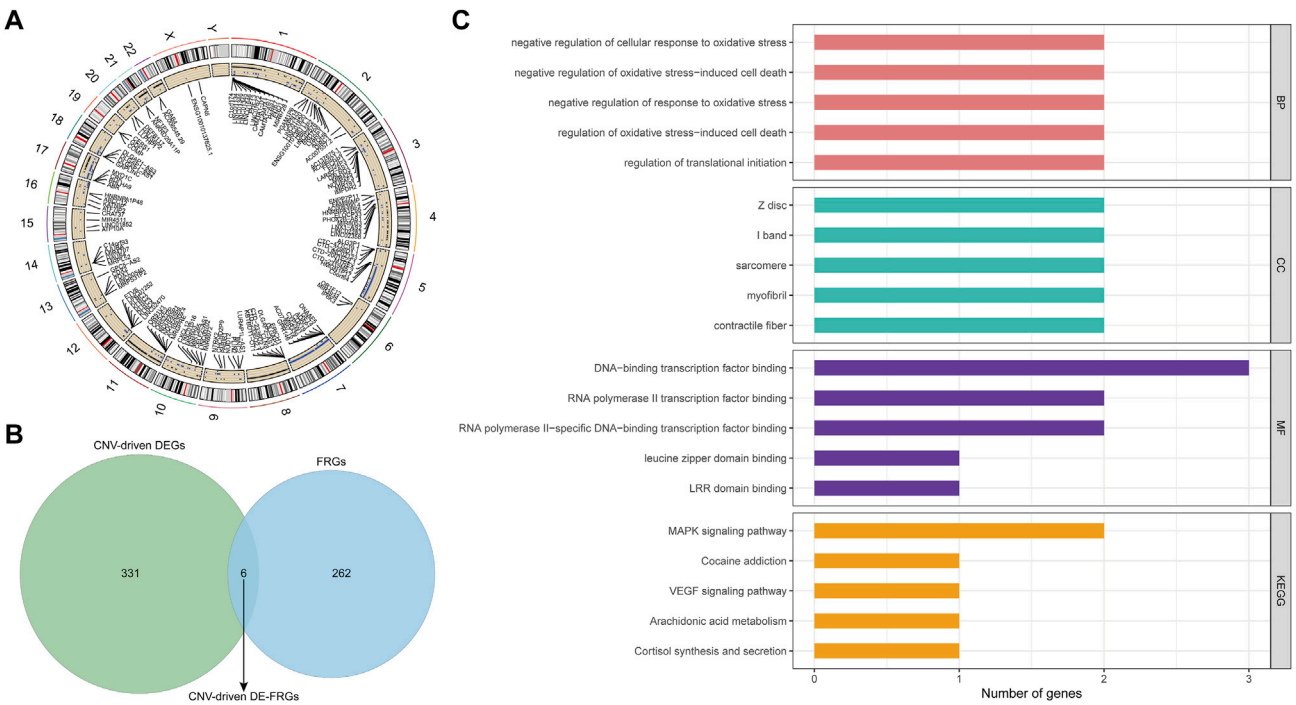

FIGURE 4 | Identification and function analysis of the CNV-driven differential ferroptosis-related genes in AML. **(A)**: Distribution of AML-related CNVs visualized by circus plot. The outside circle represents 24 chromosomes including sex chromosomes; the inside circle represents the distribution of CNVs (the blue dots represent CNV deletions). **(B)**: ferroptosis-related genes and CNV driving genes were intersected and Venn diagram was drawn. Finally, six differential ferroptosis-related genes driven by CNV were obtained: ALOX15B, MTDH, DNAJB6, HSPB1, ATF4, and PLIN2. **(C)**: The functions of 6 CNV-driven differential ferroptosis-related genes were analyzed by GO and KEGG functional enrichment analysis. The first five functional items were sorted according to the count value, the horizontal axis represented the number of enriched genes, and the vertical axis represented the functional items.

dysregulation and the inflammatory immune response during the disease process.

Construction of a Prognostic Signature Based on CNV-Driven DE-FRGs

We matched the expression profiles of the identified CNV-driven DE-FRGs in 132 TCGA-AML samples containing complete survival data. Univariate Cox regression analysis was applied to identify the CNV-driven DE-FRGs associated with survival time in AML patients. $p < 0.1$ was set as the cut-off value, and a total of 2 variables associated with survival in TCGA-AML patients were screened, namely DNAJB6 and HSPB1 (**Figure 5A**). HR > 1 for HSPB1 (HR = 1.2222, 95% CI. 0.992–1.506, $p = 0.059$) may be an oncogenic gene in AML, whereas DNAJB6 (HR = 0.514, 95% CI: 0.345–0.767, $p = 0.001$) with HR < 1 was expected to be a protective factor for AML. Further, the Cox model consisting of DNAJB6 and HSPB1 (**Figure 5B**) was identified as the optimal prognostic signature for AML by sophisticated calculations of multivariate Cox analysis with stepwise regression.

Evaluation of a Two-Gene Prognostic Signature-based Risk System

We assessed the efficacy of prognostic signature consisting of DNAJB6 and HSPB1 for predicting AML prognosis by risk scoring system. The risk score for each TCGA-AML patient was calculated according to the following formula: risk score = (−0.65 * expression of DNAJB6) + (0.19 * expression of HSPB1). All TCGA-AML samples were divided into high- (n = 66) and low- (n = 66) risk groups according to the median risk score (median = 1.029) (**Supplementary Table S12**). **Figure 5C** demonstrated the risk profile and AML survival distribution in the TCGA database, suggesting that low-risk AML patients had relatively longer OS than high-risk patients. Moreover, the heatmap showed that DNAJB6 was relatively less expressed in the high-risk group compared to the low-risk group, while HSPB1 tended to be more highly expressed in the high-risk group (**Figure 5C**). K-M survival analysis confirmed that the low-risk group had better OS and the high-risk score was linked to poor outcomes (**Figure 5D**). The ROC curve assessed the accuracy of the risk score to predict OS in TCGA-AML patients at 1, 3, and 5 years 1 year OS had an AUC of 0.726, 3 years of 0.634, and 5 years of 0.741 (**Figure 5E**). These results indicated that our risk score had a more reliable performance in predicting the prognosis of AML patients.

Validation of the Two-Gene Prognostic Signature in the GEO Database

The risk scores for AML patients in the GSE37642 (n = 136), GSE12417 (n = 73), and GSE71014 (n = 104) datasets were

calculated using the above equations, and the samples were divided into high-risk and low-risk groups based on the optimal threshold for risk scores (**Figures 6A–C**). The predictive validity of the risk scores in the independent external validation set was consistent with that in TCGA database. Patients in the low-risk group had significantly longer survival times compared with the high-risk group (**Figures 6D–F**). Meanwhile, ROC curve analysis showed that the AUC of risk score in predicting patients" OS at 1, 3, and 5 years was 0.631, 0.682, and 0.675 in the GSE37642 dataset (**Figure 6G**). 0.640, 0.621, and 0.589, respectively, in the GSE12417 dataset (**Figure 6H**). 0.652, 0.782, and 0.766,

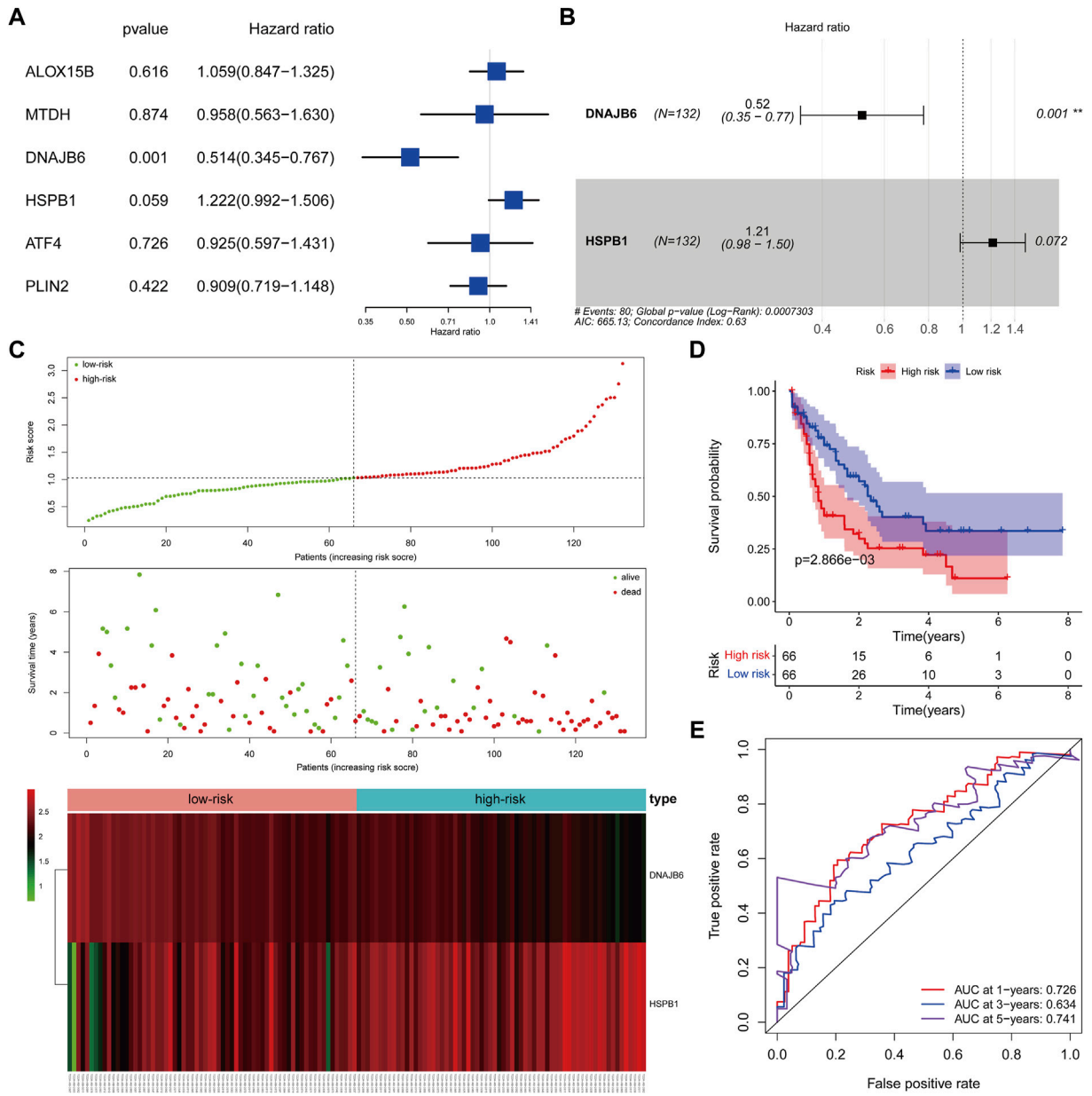

FIGURE 5 | Clinical prognostic biomarker analysis. **(A)**: Forest map shows univariate Cox analysis. **(B)**: forest map shows multivariate Cox analysis, Hazard ratio >1, high-risk gene, that is, the higher the gene expression, the higher the patient risk; conversely, Hazard ratio <1, low-risk gene, that is, the lower the gene expression, the higher the patient risk. **(C)**: The risk model draws a risk curve, with red dots representing high-risk patients and green dots representing low-risk patients. The ordinate is the risk score and the survival time respectively, and the dotted line is the median risk score and the corresponding number of diseases. Gene expression heatmap of high-risk and low-risk groups. **(D)**: According to the K-M survival curve drawn by the risk score, the Abscissa represents the survival time, the ordinate indicates the survival rate, the red curve represents the high-risk group, and the blue curve represents the low-risk group. **(E)**: ROC curve (1, 3, 5 years), the AUC area of the model was calculated to evaluate the effectiveness of the model.

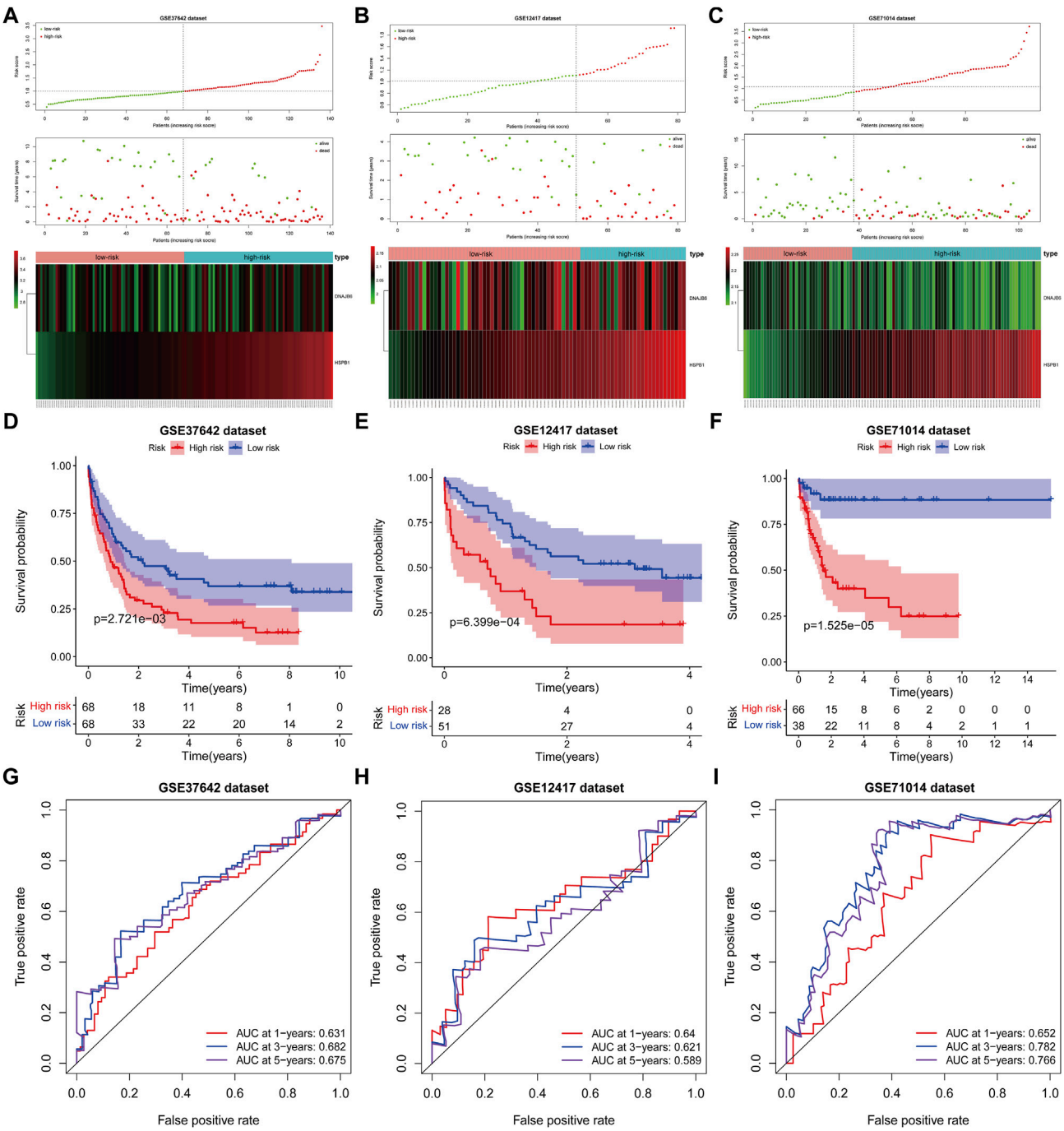

FIGURE 6 | The prognostic risk model was validated in the GEO database. **(A–C)**: The distribution of risk score, survival time, life status, and the prognostic 2-CNV-driven DE-FRGs expression patterns in the GSE37642 dataset, GSE12417 dataset and GSE71014 dataset. The risk scores are arranged in ascending order from left to right and each dot indicates an AML individual. The black dotted line is the optimum cutoff dividing patients into low and high-risk groups. The colors from green to red in the heatmap indicate the expression level from low to high. **(D–F)**: Kaplan-Meier plots compare overall survival between patients in low- and high-risk groups in the GSE37642 dataset, GSE12417 dataset and GSE71014 dataset. *p*-values were calculated by log-rank test. **(G–I)**: The receiver operating characteristic (ROC) curves of the prognostic signature for 1-, 3-, and 5-years survival in the GSE37642 dataset, GSE12417 dataset and GSE71014 dataset.

TABLE 1 | Univariate Cox analysis.

	HR	HR.95L	HR.95H	*p*-value
Age	1.03482198014829	1.01882519224958	1.05106993696686	1.66E-05
Gender	0.962366615022004	0.619557528552139	1.49485634348315	0.864443099593092
Risk score	2.55281810175952	1.70387284566633	3.82474565355407	5.54E-06

TABLE 2 | Multivariate Cox analysis.

	HR	HR.95L	HR.95H	*p*-value
Age	1.03132276756969	1.01480193820568	1.04811255365579	0.000181619864716146
Risk score	2.26714423194939	1.47977186168049	3.47346986489139	0.000169704374503001

respectively, in the GSE71014 dataset (**Figure 6I**). This evidence suggested that our risk score had more satisfactory predictive validity and some general applicability.

Risk Score was an Independent Prognostic Factor for AML

We explored the relationship between risk score and clinical characteristics (age and gender) in the TCGA-AML dataset by the Wilcoxon test. The results revealed that the risk score was significantly different between age subgroups (p = 0.02), and the risk score was positively correlated with age, with higher risk levels at older ages (**Supplementary Figure 1A**). Besides, the risk scores were higher in the male subgroup than in the female group, but which was not statistically significant (p = 0.084; **Supplementary Figure 1B**).

Further, Cox regression analysis was utilized to evaluate whether the risk score could predict the outcome of AML patients independently of clinical characteristics (age and gender). Univariate Cox analysis noted that age and risk score were significantly associated with prognosis in AML patients (p < 0.05; **Table 1**). Ultimately, multivariate Cox analysis indicated that age and risk score were the independent factors of AML prognosis (**Table 2**).

Validation of Prognostic Gene Expression in PCR Expression Test

We collected the blood of 10 AML patients and 10 healthy individuals and analyzed the mRNA expression levels of two prognostic genes by PCR. The results showed that the expression of the DNAJB6 gene and the HSPB1 gene in AML patients were both lower than that in healthy people (p < 0.0001; **Figures 7A,P** < 0.0001; **Figure 7B**). There was a significant statistical difference in the expression level after statistical analysis.

DISCUSSION

With the progress of AML treatment such as the combination of chemotherapy and stem cell transplantation, the outcomes of AML patients have great improvement. However, the prognosis of AML patients still cannot be accurately judged. The defect of apoptosis is a common cause of chemoresistance (Poeta et al., 2008). Ferroptosis is different from apoptosis which can provide us with new ideas for inducing cancer cell death (Radtke et al., 2009). Some reports have determined that leukemia cells are more sensitive to the ferroptosis inducer erastin than other cancer cell types (Seth and Singh, 2015; Reyna et al., 2017). In addition, CNV has been reported to be associated with chemotherapy response

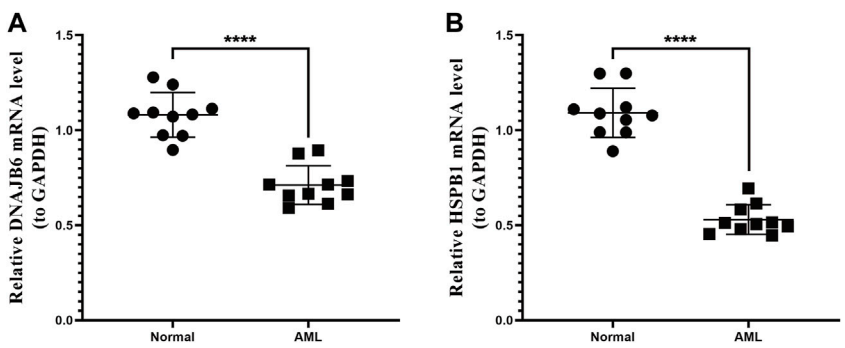

FIGURE 7 | qRT-PCR expression test. The two genes selected in the model were verified by qRT-PCR expression test. **(A)**: Expression of DNAJB6 gene in normal human and AML patients. **(B)**: Expression of HSPB1 gene in normal human and AML patients. *p*-values were calculated by the independent sample *t*-test.

and many studies on CNV in AML have been carried out (Song et al., 2016; Shen et al., 2018; Jiang et al., 2020; Shao et al., 2021). However, none of them has comprehensively evaluated the role of gene expression derived from CNV. Both ferroptosis and CNV can be used as prognostic markers, but the relationship between them in AML has not been reported. Therefore, we combined ferroptosis and CNV aiming to improve the prognostic prediction and management efficiency in AML patients.

We combined analysis of CNV differential data and differentially expressed genes (DEGs) data to identify key CNV-driven FRGs for AML by using publicly available AML datasets. A total of 6 CNV-driven DE-FRGs (ALOX15B, MTDH, DNAJB6, HSPB1, ATF4, and PLIN2) were identified by overlap analysis, and functional enrichment analysis indicated that they were involved in oxidative stress, cell death, and inflammatory response processes. Finally, 2 CNV-driven FRGs (DNAJB6 and HSPB1) were identified by Univariate analysis and COX model. The OS of patients in the high-risk group was significantly shorter in the datasets compared to the low-risk group.

DNAJB6 encodes a highly conserved DNAJ/Hsp40 family chaperone protein and interacts with Hsp70 chaperone protein (Stevens et al., 2019). Glutathione peroxidase 4 (GPX4, an antioxidant enzyme) is a defensive protein which is a kind of the GSH peroxidase (Sun et al., 2015). GPx4 inhibits lipid reactive oxygen species (ROS) production by decreasing phospholipid hydroperoxide and plays an important role in inhibiting iron cell apoptosis (Reyna et al., 2017). Overexpressing DNAJB6a can has the ability to downregulate GPX4 and promote ferroptosis (Tang et al., 2011). It is reported that DNAJB6 expression was downregulated in ESCC tissues and it acts as an anti-oncogene in ESCC (Tang et al., 2011). In addition, Mitra A et al. also reported that DNAJB6a can weaken malignant activity of breast carcinoma (Vosberg et al., 2016). However, Zhang et al. found that DNAJB6 is an oncogene that can aggravate the invasion of colorectal cancer (Wei et al., 2020). In our study, we found the expression of DNAJB6 oncogene was lower in the low-risk group compared with the high-risk group associated with poor prognosis. At the same time, according to the hazard ratio (HR) of univariate analysis, the HR of DNAJB6 is 0.514, indicating that DNAJB6 is a protective factor in AML. Our result is consistent with previous study about ESCC and breast cancer.

HSPB1 (also named Hsp27), a member of the small heat shock protein family, is involved in regulating cytoskeletal tissue or stabilizing abnormally folded proteins to prevent aggregation (Yang et al., 2013; Yan et al., 2021). Its abnormal expression in cancer is associated with aggressive tumor behavior, increased chemoresistance, and poor prognosis (Carver et al., 2003). It is overexpressed in many cancers such as prostate, breast, gastric, ovarian, bladder and pancreas (Carver et al., 2003). However, our study showed that HSPB1 is downregulated in AML. In addition, the HR of univariate analysis indicated that HSPB1 is a negative factor in AML. The result revealed that the higher the gene expression, the higher the risk of patients. A study demonstrated that HSPB1 is a negative regulator of ferroptotic cancer cell death (Yang et al., 2014). Phosphorylated HSPB1 can not only inhibit apoptosis and induce autophagy (Yu et al., 2012; Yang and Stockwell, 2016), but also reduce cellular iron uptake and lipid ROS production (Yang et al., 2014). It is of great significance for us to study its treatment for ferroptosis-mediated cancer.

Currently, some studies have found ferroptosis-related gene signatures which can predict prognosis genes that can predict AML (Yu et al., 2015). Huang et al. (Yu et al., 2015) developed a 12 FRG-based prognostic risk model comprised of 10 risk-related genes (GPX4, CD44, FH, CISD1, SESN2, LPCAT3, AIFM2, ACSL5, HSPB1, and SOCS1) and 2 protective genes (ACSL6 and G3BP1) to predict clinical outcomes. The 12 FRGs are divided into 4 categories according to their functions: lipid metabolism (GPX4, LPCAT3, ACSL5, ACSL6), antioxidant (CD44, SESN2, AIFM2), iron metabolism (CISD1, HSPB1), and cancer metabolism (SOCS1, FH, G3BP1). Although their prediction value is better than our result by comparing ROC, it is easy to exclude some prognostic genes of AML by using a single marker to construct a prognostic model. In our study, two genes are CNV-driven ferroptosis-related genes which were obtained by CNV and ferroptosis binding analysis. The prognostic model composed of these two genes is more conducive to clinical analysis and judgement.

Recently, some scholars have studied AML and found that atorvastatin has activity on AML by up regulating comprehensive stress pathway and inhibiting oxidative phosphorylation (Yusuf et al., 2020). This study showed that atorvastatin inhibited the oxygen consumption rate of AML cells, which has specific significance for chemotherapy-resistant AML primordial cells dependent on oxidative phosphorylation. This study found that HSPB1 gene is enriched in the pathway of oxidative stress. The expression of HSPB1 gene can be considered to have an impact on the progression of AML. It can be speculated that there may be a compensation mechanism between oxidative phosphorylation of HSPB1 and atorvastatin quinone. In addition, studies have shown that leukemia cells rely on aldhyde dehydrogenase 3a2 (aldh3a2) enzyme to oxidize long-chain fatty aldehydes to prevent cell oxidative damage (Zhang et al., 2015), but do not rely on normal myeloid cell counterparts. At the same time, aldehyde is a by-product of oxidative phosphorylation and increased nucleotide synthesis in cancer. It is produced by lipid peroxide and is the basis of non-caspase dependent cell death and iron death. At present, the dependence of leukemia cells on aldh3a2 has been observed in a variety of mouse and human myeloid leukemia. In addition, the inhibition of aldh3a2 and GPx4 has comprehensive lethality. GPx4 inhibits lipid ROS and then block the ferroptosis process. GPx4 inhibition is a known trigger of iron death, but GPx4 inhibition itself has little effect on AML cells. Inhibition of aldh3a2 provides a therapeutic opportunity for the unique metabolic state of AML cells, and may become a new idea for the treatment of AML in the future.

HSPB1 gene is enriched in multiple oxidative stress pathways, and it is an iron death driving gene. It can be speculated that GPx4 inhibition and HSPB1 gene expression are related to the development of AML. Studies have shown that DNAJB6 can promote the iron death process of ESCC (Tang et al., 2011). In ESCC, the overexpression of DNAJB6 is accompanied by a significant decrease in GPx4 protein level. The study also shows that DNAJB6 plays an anticancer role in the process of ESCC through iron death mechanism. This

study also shows that DNAJB6 is a protective factor of AML. In addition, a study on bone marrow damage (Zhou and Chen, 2021)showed that Fanconi anemia complement group D2 (FANCD2), a nuclear protein involved in DNA damage repair, can prevent iron apoptosis mediated damage in bone marrow stromal cells (BMSC). Knockout of FANCD2 increases biochemical events related to iron death (e.g., ferrous accumulation, glutathione consumption and malondialdehyde production). Mechanistically, FANCD2 is involved in regulating the expression of genes and/or proteins of iron metabolism (such as fth1, TF, TFRC, HAMP, HSPB1, slc40a1 and steam3) and lipid peroxidation (such as GPx4). However, progressive BMF in FA patients is closely related to AML. Therefore, the mechanism of the linkage of HSPB1, GPx4 and FANCD2 in AML related diseases needs to be further explored.

This study also has some limitations. Our prognostic model was constructed by existing public datasets, although it is validated by PCR expression test, more prospective investigations are needed to validate its predictive power. In the future, we should continue to pay attention to the role of these two genes in AML pathology by experimental and clinical studies. We believe that our prognostic model based on CNV-driven FRGs is of great significance in predicting the survival of AML patients and will offer novel insight for AML research.

DATA AVAILABILITY STATEMENT

The original contributions presented in the study are included in the article/**Supplementary Material**, further inquiries can be directed to the corresponding authors.

AUTHOR CONTRIBUTIONS

CH and JZ contributed to the conception of the study. JZ and FL contributed significantly to analysis and manuscript preparation. CH performed the data analyses and wrote the manuscript. WG and CC helped perform the analysis with constructive discussions. All authors contributed to the article and approved the final manuscript.

FUNDING

This work was supported by National Natural Science Foundation of China [Grant number 81771589], the Program of Tianjin Science and Technology Plan [Grant number 18ZXDBSY00170; 20JCZXJC00170], Tianjin Natural Science Foundation [Grant number 21JCYBJC00460], the Public Health and Technology Project of Tianjin [grant number TJWJ2021ZD007] and General project of Tianjin Children's Hospital [grant number Y2020013]. We are grateful for the financial support from the "Tianjin Medical Key Discipline (Specialist) Construction Project".

SUPPLEMENTARY MATERIAL

The Supplementary Material for this article can be found online at: https://www.frontiersin.org/articles/10.3389/fgene.2022.849437/full#supplementary-material

Supplementary Figure S1 | Clinical significance of the prognostic signature in TCGA set. Risk score in the different ages **(A)** and gender **(B)** *P*-values were calculated by the Wilcoxon test.

REFERENCES

Arber, D. A., Orazi, A., Hasserjian, R., Thiele, J., Borowitz, M. J., Le Beau, M. M., et al. (2016). The 2016 Revision to the World Health Organization Classification of Myeloid Neoplasms and Acute Leukemia. *Blood* 127 (20), 2391–2405. doi:10.1182/blood-2016-03-643544

Carver, J., Rekas, A., Thorn, D., and Wilson, M. (2003). Small Heat-Shock Proteins and Clusterin: Intra- and Extracellular Molecular Chaperones with a Common Mechanism of Action and Function? *IUBMB Life (International Union Biochem. Mol. Biol. Life)* 55 (12), 661–668. doi:10.1080/15216540310001640498

Döhner, H., Estey, E., Grimwade, D., Amadori, S., Appelbaum, F. R., Büchner, T., et al. (2017). Diagnosis and Management of AML in Adults: 2017 ELN Recommendations from an International Expert Panel. *Blood* 129 (4), 424–447. doi:10.1182/blood-2016-08-733196

Grimwade, D., Ivey, A., and Huntly, B. J. P. (2016). Molecular Landscape of Acute Myeloid Leukemia in Younger Adults and its Clinical Relevance. *Blood* 127 (1), 29–41. doi:10.1182/blood-2015-07-604496

Herold, T., Jurinovic, V., Batcha, A. M. N., Bamopoulos, S. A., Rothenberg-Thurley, M., Ksienzyk, B., et al. (2018). A 29-gene and Cytogenetic Score for the Prediction of Resistance to Induction Treatment in Acute Myeloid Leukemia. *Haematologica* 103 (3), 456–465. doi:10.3324/haematol.2017.178442

Herold, T., Metzeler, K. H., Vosberg, S., Hartmann, L., Röllig, C., Stölzel, F., et al. (2014). Isolated Trisomy 13 Defines a Homogeneous AML Subgroup with High Frequency of Mutations in Spliceosome Genes and Poor Prognosis. *Blood* 124 (8), 1304–1311. doi:10.1182/blood-2013-12-540716

Hong, Y., Lin, M., Ou, D., Huang, Z., and Shen, P. (2021). A Novel Ferroptosis-Related 12-gene Signature Predicts Clinical Prognosis and Reveals Immune Relevancy in clear Cell Renal Cell Carcinoma. *BMC Cancer* 21 (1), 831. doi:10.1186/s12885-021-08559-0

Huang, X., Zhou, D., Ye, X., and Jin, J. (2021). Construction of a Novel Ferroptosis-Related Gene Signature for Predicting Prognosis and Immune Microenvironment in Acute Myeloid Leukemia. *Bosn J. Basic Med. Sci.* doi:10.17305/bjbms.2021.6274

Huot, J., Houle, F., Spitz, D. R., and Landry, J. (1996). HSP27 Phosphorylation-Mediated Resistance against Actin Fragmentation and Cell Death Induced by Oxidative Stress. *Cancer Res.* 56 (2), 273–279.

Jakob, U., Gaestel, M., Engel, K., and Buchner, J. (1993). Small Heat Shock Proteins Are Molecular Chaperones. *J. Biol. Chem.* 268 (3), 1517–1520. doi:10.1016/s0021-9258(18)53882-5

Jiang, B., Zhao, Y., Shi, M., Song, L., Wang, Q., Qin, Q., et al. (2020). DNAJB6 Promotes Ferroptosis in Esophageal Squamous Cell Carcinoma. *Dig. Dis. Sci.* 65 (7), 1999–2008. doi:10.1007/s10620-019-05929-4

Kerr, J. F. R., Winterford, C. M., and Harmon, B. V. (1994). Apoptosis. Its Significance in Cancer and Cancer Therapy. *Cancer* 73 (8), 2013–2026. doi:10.1002/1097-0142(19940415)73:8<2013::aid-cncr2820730802>3.0.co;2-j

Kim, K. I., Kim, T.-k., Kim, I.-W., Ahn, K.-S., Yoon, S.-S., Shin, W. G., et al. (2012). Copy Number Variations in normal Karyotype Acute Myeloid Leukaemia and Their Association with Treatment Response. *Basic Clin. Pharmacol. Toxicol.* 111 (5), 317–324. doi:10.1111/j.1742-7843.2012.00904.x

Kuett, A., Rieger, C., Perathoner, D., Herold, T., Wagner, M., Sironi, S., et al. (2015). IL-8 as Mediator in the Microenvironment-Leukaemia Network in Acute Myeloid Leukaemia. *Sci. Rep.* 5, 18411. doi:10.1038/srep18411

Li, Z., Herold, T., He, C., Valk, P. J. M., Chen, P., Jurinovic, V., et al. (2013). Identification of a 24-gene Prognostic Signature that Improves the European LeukemiaNet Risk Classification of Acute Myeloid Leukemia: an International Collaborative Study. *Jco* 31 (9), 1172–1181. doi:10.1200/jco.2012.44.3184

Liang, H., Yoo, S.-E., Na, R., Walter, C. A., Richardson, A., and Ran, Q. (2009). Short Form Glutathione Peroxidase 4 Is the Essential Isoform Required for Survival and Somatic Mitochondrial Functions. *J. Biol. Chem.* 284 (45), 30836–30844. doi:10.1074/jbc.M109.032839

Liang, L., Fang, J.-Y., and Xu, J. (2016). Gastric Cancer and Gene Copy Number Variation: Emerging Cancer Drivers for Targeted Therapy. *Oncogene* 35 (12), 1475–1482. doi:10.1038/onc.2015.209

Meng, E., Shevde, L. A., and Samant, R. S. (2016). Emerging Roles and Underlying Molecular Mechanisms of DNAJB6 in Cancer. *Oncotarget* 7 (33), 53984–53996. doi:10.18632/oncotarget.9803

Mitra, A., Fillmore, R. A., Metge, B. J., Rajesh, M., Xi, Y., King, J., et al. (2008). Large Isoform of MRJ (DNAJB6) Reduces Malignant Activity of Breast Cancer. *Breast Cancer Res.* 10 (2), R22. doi:10.1186/bcr1874

Nibourel, O., Guihard, S., Roumier, C., Pottier, N., Terre, C., Paquet, A., et al. (2017). Copy-number Analysis Identified New Prognostic Marker in Acute Myeloid Leukemia. *Leukemia* 31 (3), 555–564. doi:10.1038/leu.2016.265

Papaemmanuil, E., Gerstung, M., Bullinger, L., Gaidzik, V. I., Paschka, P., Roberts, N. D., et al. (2016). Genomic Classification and Prognosis in Acute Myeloid Leukemia. *N. Engl. J. Med.* 374 (23), 2209–2221. doi:10.1056/NEJMoa1516192

Poeta, G., Bruno, A., Del Principe, M., Venditti, A., Maurillo, L., Buccisano, F., et al. (2008). Deregulation of the Mitochondrial Apoptotic Machinery and Development of Molecular Targeted Drugs in Acute Myeloid Leukemia. *Ccdt* 8 (3), 207–222. doi:10.2174/156800908784293640

Radtke, I., Mullighan, C. G., Ishii, M., Su, X., Cheng, J., Ma, J., et al. (2009). Genomic Analysis Reveals Few Genetic Alterations in Pediatric Acute Myeloid Leukemia. *Proc. Natl. Acad. Sci. U.S.A.* 106 (31), 12944–12949. doi:10.1073/pnas.0903142106

Reyna, D. E., Garner, T. P., Lopez, A., Kopp, F., Choudhary, G. S., Sridharan, A., et al. (2017). Direct Activation of BAX by BTSA1 Overcomes Apoptosis Resistance in Acute Myeloid Leukemia. *Cancer Cell* 32 (4), 490–505. e410. doi:10.1016/j.ccell.2017.09.001

Seth, R., and Singh, A. (2015). Leukemias in Children. *Indian J. Pediatr.* 82 (9), 817–824. doi:10.1007/s12098-015-1695-5

Shao, R., Wang, H., Liu, W., Wang, J., Lu, S., Tang, H., et al. (2021). Establishment of a Prognostic Ferroptosis-related Gene Profile in Acute Myeloid Leukaemia. *J. Cel Mol Med* 25 (23), 10950–10960. doi:10.1111/jcmm.17013

Shen, Z., Song, J., Yung, B. C., Zhou, Z., Wu, A., and Chen, X. (2018). Emerging Strategies of Cancer Therapy Based on Ferroptosis. *Adv. Mater.* 30 (12), 1704007. doi:10.1002/adma.201704007

Song, X., Xie, Y., Kang, R., Hou, W., Sun, X., Epperly, M. W., et al. (2016). FANCD2 Protects against Bone Marrow Injury from Ferroptosis. *Biochem. Biophysical Res. Commun.* 480 (3), 443–449. doi:10.1016/j.bbrc.2016.10.068

Stevens, A. M., Xiang, M., Heppler, L. N., Tošić, I., Jiang, K., Munoz, J. O., et al. (2019). Atovaquone Is Active against AML by Upregulating the Integrated Stress Pathway and Suppressing Oxidative Phosphorylation. *Blood Adv.* 3 (24), 4215–4227. doi:10.1182/bloodadvances.2019000499

Sun, X., Ou, Z., Xie, M., Kang, R., Fan, Y., Niu, X., et al. (2015). HSPB1 as a Novel Regulator of Ferroptotic Cancer Cell Death. *Oncogene* 34 (45), 5617–5625. doi:10.1038/onc.2015.32

Tang, D., Kang, R., Livesey, K. M., Kroemer, G., Billiar, T. R., Van Houten, B., et al. (2011). High-mobility Group Box 1 Is Essential for Mitochondrial Quality Control. *Cel Metab.* 13 (6), 701–711. doi:10.1016/j.cmet.2011.04.008

Vosberg, S., Herold, T., Hartmann, L., Neumann, M., Opatz, S., Metzeler, K. H., et al. (2016). Close Correlation of Copy Number Aberrations Detected by Next-Generation Sequencing with Results from Routine Cytogenetics in Acute Myeloid Leukemia. *Genes Chromosomes Cancer* 55 (7), 553–567. doi:10.1002/gcc.22359

Wei, J., Xie, Q., Liu, X., Wan, C., Wu, W., Fang, K., et al. (2020). Identification the Prognostic Value of Glutathione Peroxidases Expression Levels in Acute Myeloid Leukemia. *Ann. Transl Med.* 8 (11), 678. doi:10.21037/atm-20-3296

Yan, H.-f., Zou, T., Tuo, Q.-z., Xu, S., Li, H., Belaidi, A. A., et al. (2021). Ferroptosis: Mechanisms and Links with Diseases. *Sig Transduct Target. Ther.* 6 (1), 49. doi:10.1038/s41392-020-00428-9

Yang, L., Cao, L., Yang, M., Tang, D., Kang, R., Min, X., et al. (2013). Hsp27: a Novel Therapeutic Target for Pediatric M4/M5 Acute Myeloid Leukemia. *Oncol. Rep.* 29 (4), 1459–1466. doi:10.3892/or.2013.2274

Yang, W. S., SriRamaratnam, R., Welsch, M. E., Shimada, K., Skouta, R., Viswanathan, V. S., et al. (2014). Regulation of Ferroptotic Cancer Cell Death by GPX4. *Cell* 156 (1-2), 317–331. doi:10.1016/j.cell.2013.12.010

Yang, W. S., and Stockwell, B. R. (2016). Ferroptosis: Death by Lipid Peroxidation. *Trends Cel Biol.* 26 (3), 165–176. doi:10.1016/j.tcb.2015.10.014

Yu, G., Wang, L.-G., Han, Y., and He, Q.-Y. (2012). clusterProfiler: an R Package for Comparing Biological Themes Among Gene Clusters. *OMICS: A J. Integr. Biol.* 16 (5), 284–287. doi:10.1089/omi.2011.0118

Yu, Y., Xie, Y., Cao, L., Yang, L., Yang, M., Lotze, M. T., et al. (2015). The Ferroptosis Inducer Erastin Enhances Sensitivity of Acute Myeloid Leukemia Cells to Chemotherapeutic Agents. *Mol. Cell Oncol.* 2 (4), e1054549. doi:10.1080/23723556.2015.1054549

Yusuf, R. Z., Saez, B., Sharda, A., van Gastel, N., Yu, V. W. C., Baryawno, N., et al. (2020). Aldehyde Dehydrogenase 3a2 Protects AML Cells from Oxidative Death and the Synthetic Lethality of Ferroptosis Inducers. *Blood* 136 (11), 1303–1316. doi:10.1182/blood.2019001808

Zhang, T.-T., Jiang, Y.-Y., Shang, L., Shi, Z.-Z., Liang, J.-W., Wang, Z., et al. (2015). Overexpression of DNAJB6 Promotes Colorectal Cancer Cell Invasion through an IQGAP1/ERK-dependent Signaling Pathway. *Mol. Carcinog.* 54 (10), 1205–1213. doi:10.1002/mc.22194

Zhou, F., and Chen, B. (2021). Prognostic Significance of Ferroptosis-Related Genes and Their Methylation in AML. *Hematology* 26 (1), 919–930. doi:10.1080/16078454.2021.1996055

Conflict of Interest: The authors declare that the research was conducted in the absence of any commercial or financial relationships that could be construed as a potential conflict of interest.

Publisher's Note: All claims expressed in this article are solely those of the authors and do not necessarily represent those of their affiliated organizations, or those of the publisher, the editors and the reviewers. Any product that may be evaluated in this article, or claim that may be made by its manufacturer, is not guaranteed or endorsed by the publisher.

frontiers | Frontiers in Genetics

ORIGINAL RESEARCH
published: 26 April 2022
doi: 10.3389/fgene.2022.880864

Characterization of the Ferroptosis-Related Genes for Prognosis and Immune Infiltration in Low-Grade Glioma

Xiuwei Yan[1,2], Hang Ji[1,2], Zhihui Liu[1,2], Shuai Ma[1,2], Jiawei Dong[1,2], Xiaoyan Jiang[1], Xueyan Hu[2], Fang Wang[1,2], Hongtao Zhao[1,2], Jiaqi Jin[1,2], Jiheng Zhang[1,2], Nan Wang[1,2], Jianyang Du[3] and Shaoshan Hu[1,2]**

[1]Department of Neurosurgery, The Second Affiliated Hospital of Harbin Medical University, Harbin, China, [2]Cancer Center, Department of Neurosurgery, Zhejiang Provincial People's Hospital, Affiliated People's Hospital, Hangzhou Medical College, Hangzhou, China, [3]Department of Neurosurgery, Shandong Provincial Hospital Affiliated to Shandong First Medical University, Jinan, China

OPEN ACCESS

Edited by:
Lei Huang,
University of Massachusetts Medical School, United States

Reviewed by:
Chongming Jiang,
Baylor College of Medicine, United States
Minjie Hu,
Carnegie Institution for Science, United States
Pengpeng Liu,
University of Massachusetts Medical School, United States

***Correspondence:**
Jianyang Du
jianyangdu@126.com
Shaoshan Hu
shaoshanhu421@163.com

Specialty section:
This article was submitted to Human and Medical Genomics, a section of the journal Frontiers in Genetics

Received: 22 February 2022
Accepted: 21 March 2022
Published: 26 April 2022

Citation:
Yan X, Ji H, Liu Z, Ma S, Dong J, Jiang X, Hu X, Wang F, Zhao H, Jin J, Zhang J, Wang N, Du J and Hu S (2022) Characterization of the Ferroptosis-Related Genes for Prognosis and Immune Infiltration in Low-Grade Glioma. Front. Genet. 13:880864. doi: 10.3389/fgene.2022.880864

Background: Although ferroptosis has been validated to play a crucial role in some types of tumors, the influence of ferroptosis-related genes (FRGs) on the immune microenvironment in low-grade glioma (LGG) remains unclear. In this research, we screen the FRGs to assess the prognosis value and immune microenvironment in LGG, to provide reliable diagnosis and treatment evidence for the clinic.

Methods: A total of 1,239 patients of LGG samples were selected for subsequent analyses from The Cancer Genome Atlas, Chinese Glioma Genome Atlas, and the Repository of Molecular Brain Neoplasia Data datasets. Univariate Cox regression analysis was used to screen for prognostic FRGs. Consensus clustering was utilized to determine ferroptosis subtypes of LGG patients. Next, the prognostic model was constructed based on differentially expressed FRGs and validation in the validating datasets. The immune microenvironment, biological pathway, and hypoxia score were explored by single-sample gene set enrichment analysis. The potential response of chemotherapy and immune checkpoint blockade therapy was also estimated. In addition, the correlation between the risk score and autophagy-related genes was examined by the Pearson correlation coefficient.

Results: A total of three ferroptosis subtypes were identified by consensus clustering for prognostic FRGs which exhibited different outcomes, clinicopathological characteristics, and immune microenvironment. Afterward, a prognostic model that performed great predictive ability based on nine prognostic FRGs has been constructed and validated. Moreover, the prognostic model had the potential to screen the sensitivity to chemotherapy and immunotherapy in LGG patients. Finally, we also found that the prognostic model has a great connection to autophagy and hypoxia.

Conclusion: We developed a ferroptosis-related prognostic model which strongly linked to diagnosis, treatment, prognosis, and recurrence of LGG. This study also reveals the connection between ferroptosis and tumor immune microenvironment.

Keywords: ferroptosis, low-grade glioma, ferroptosis-related prognostic model, prognostic prediction, immune microenvironment, autophagy, hypoxia

INTRODUCTION

Low-grade glioma (LGG) belongs to WHO grade II and III gliomas (Louis et al., 2016). It approximately accounts for 15% of the primary intracranial malignant tumors (Sanai et al., 2011). LGG is most commonly seen in young adults aged 35–44 years (Ostrom et al., 2016). At present, the standard therapeutic schedules including surgical resection, adjuvant radiotherapy, and chemotherapy are mainly adopted, but the outcomes are always unfavorable (Semmel et al., 2018). Cancers with same origins, pathologic stages, and clinical stages may have different molecular characterizations (Friedman et al., 2015). Recent studies have identified that molecular pathogenesis is closely related to LGG progression, suggesting the promising prospect of targeted therapy (Bready and Placantonakis, 2019). Consequently, exploring the potential molecular mechanisms will benefit the outcomes of patients with LGG.

Ferroptosis was initially described as a regulated cell death unlike other forms of cell death, in 2012 (Dixon et al., 2012). It is characterized by dysbalance in the regulation of intracellular iron metabolism and membrane lipid peroxidation (Ursini and Maiorino, 2020). The function of ferroptosis in several types of cancer has been reported previously, including breast cancer (Li H. et al., 2022), hepatocellular carcinoma (Chen et al., 2022), gastric cancer (Zhang et al., 2021), head neck squamous cell carcinoma (Lu et al., 2021), lung cancer (Li and Liu, 2022), renal cell carcinoma (Du et al., 2021), ovarian cancer (Li H.-W. et al., 2022), and pancreatic cancer (Liu et al., 2021). Mou et al. (2022) has found that for LGG the SAT1 activation is closely related to ferroptosis upon ROS induction. Based on the sequencing technology, many ferroptosis-related gene (FRG) risk signatures have been developed in LGG to predict prognosis and treatment efficacy (Xu et al., 2021; Zhao et al., 2021; Zheng et al., 2021). However, the influence of FRGs on the tumor microenvironment (TME) in LGG has not been elucidated yet.

In this study, through the screened FRGs from The Cancer Genome Atlas (TCGA), Chinese Glioma Genome Atlas (CGGA), and Repository of Molecular Brain Neoplasia Data (Rembrandt) datasets, a total of 1,239 patients of LGG samples were selected for subsequent analyses. Ferroptosis subtypes with distinct prognosis, immune microenvironment, and clinicopathological and biological processes were identified by consensus clustering. Subsequently, we built the ferroptosis-related prognostic model to quantify the differences between individuals. Beyond that, we also explored the connection between ferroptosis and hypoxia as well as autophagy. Overall, our findings may contribute to the clinical therapeutic strategies for LGG patients.

METHODS

Dataset Acquisition

The flow chart of this study is shown in **Supplementary Figure S1**. The mRNA expression profiles with corresponding clinical data of LGG samples were downloaded from TCGA (https://portal.gdc.cancer.gov/repository), CGGA (http://www.cgga.org.cn), and Rembrandt (http://gliovis.bioinfo.cnio.es) datasets. Then, patients with incomplete survival data and histopathological diagnosis were excluded. Ultimately, a total of 1,239 patients of LGG samples were selected for the subsequent analysis. TCGA dataset (n = 508) served as the training set. The CGGA (n = 592) and the Rembrandt datasets (n = 139) were chosen as the validation sets. The available clinical information about the patients is summarized in **Supplementary Table S2**.

Identification of Prognostic FRGs and Functional Analysis

The FRGs were obtained from the FerrDb online database (http://www.zhounan.org/ferrdb) (Zhou and Bao, 2020). After merging with LGG transcripts of three cohorts, the univariate Cox regression analysis was used to screen for prognostic FRGs from TCGA, CGGA, and Rembrandt datasets (**Supplementary Tables S3–S5**). Gene Ontology (GO) and Kyoto Encyclopedia of Genes and Genomes (KEGG) analyses of the intersecting prognostic FRGs were performed using Metascape (https://metascape.org/gp/index.html#/main/step1) (Zhou et al., 2019).

Classification of Molecular Subtypes by Consistent Clustering

Based on the intersecting prognostic FRGs, the 'ConsensusClusterPlus' package in R was utilized for the consistent clustering to determine ferroptosis subtypes of LGG patients from TCGA, CGGA, and Rembrandt datasets. The k-value (ranging from 2– 9) was used for determining the best cluster number. The overall survival (OS) analysis among different clusters was calculated using the Kaplan–Meier method.

Evaluation of Immune Infiltration in the TME

The immune-stromal component of the TME for each sample was calculated with the ESTIMATE algorithm (Yoshihara et al., 2013), which is commonly represented as three kinds of scores named ImmuneScore, StromalScore, and ESTIMATEScore. Using the single-sample gene set enrichment analysis (ssGSEA), the relative infiltration of 28 immune cells in TME and the activity levels of typical biological pathways in individual samples were calculated.

The anti-tumor immune response can be described as a sequence of gradual procedures, including the release of cancer cell antigens (Step 1), cancer antigen presentation (Step 2), priming and activation (Step 3), trafficking of immune cells to tumors (Step 4), infiltration of immune cells into tumors (Step 5), recognition of cancer cells by T cells (Step 6), and killing of cancer cells (Step 7). In this research, we explored the connection between ferroptosis subtypes and anti-tumor immune response. The anti-tumor activity score of each sample in TCGA was obtained from Tumor Immunophenotype Profiling (TIP, http://biocc.hrbmu.edu.cn/TIP/index.jsp) (Xu et al., 2018).

Mutational Signature Analyses

The tumor mutation burden (TMB) was defined as the total number of somatic mutations per megabase in tumor tissue. Much like the immunosuppressive microenvironment, TMB is also critical in anti-tumor immunotherapy. Therefore, we calculated the TMB of each sample in LGG based on TCGA mutation data. The R package 'maftools' was used to process and present the mutation data (Mayakonda et al., 2018).

Identification and Validation of the Prognostic Model

According to the intersecting prognostic FRGs, we identified the differentially expressed FRGs (DE-FRGs) with adjusted p-value < 0.05 between cluster-1 and cluster-3 using the 'limma' package in R. We further applied the 'glmnet' package in R to perform the least absolute shrinkage and selection operator (LASSO) regression analysis for narrowing the range of genes those were upregulated in DE-FRGs. Then, the risk score for each sample can be calculated using the following formula.

$$riskScore = \sum_{i=1}^{n} Coef(X_i) * Exp(X_i).$$

In the formula, $Coef\ (X_i)$ represents the coefficient of each FRG, and $Exp\ (X_i)$ stands for the gene expression levels of those FRGs. The patients were divided into low- and high-risk groups according to the median risk score. The risk score of patients from CGGA and Rembrandt datasets can also be calculated to validate the efficacy of the prognostic model.

The Kaplan–Meier method was used to draw survival curves. Meanwhile, the area under the curves (AUCs) of receiver operating characteristic (ROC) curves was calculated to evaluate the predictive ability of 1, 3, and 5 years of survival. To explore whether the prognostic model could be used as an independent factor of OS in LGG, univariate and multivariate Cox regression analyses were performed. Next, combining all independent prognostic factors from the previous step, the nomogram was built using the R package 'rms'. The calibration curve was used to evaluate the accuracy of the nomogram.

Prediction of Chemotherapeutic and Immune Checkpoint Blockade Therapy Response

Temozolomide is the most commonly used chemotherapeutic in LGG therapy. Therefore, the chemotherapeutic response of temozolomide for each patient was predicted by the Genomics of Drug Sensitivity in Cancer (https://www.cancerrxgene.org/). The prediction of half-maximal inhibitory concentration (IC_{50}) values was conducted using the R package 'pRRophetic' (Geeleher et al., 2014).

Tumor immune dysfunction and exclusion (TIDE, http://tide.dfci.harvard.edu/) is a calculation method based on the induction of T-cell dysfunction in tumors with high infiltration of cytotoxic T lymphocytes (CTLs) and the prevention of T-cell infiltration in tumors with low CTL levels (Jiang et al., 2018). The subclass mapping method (SubMap, https://www.genepattern.org/) is an unsupervised algorithm that reveals common subtypes between independent datasets (Hoshida et al., 2007). In this study, the TIDE and SubMap algorithms were used to estimate the immune checkpoint blockade (ICB) therapy response of LGG patients.

Gene Set Enrichment Analysis

Gene set enrichment analysis (GSEA) was performed using GSEA software (v4.0.0) to identify signaling pathways regulated by the prognostic model. The hallmark gene set collection is provided by the Molecular Signatures Database (MSigDB) (http://www.broad.mit.edu/gsea, v7.4). Gene sets with | NES | > 1 and nominal p-value < 0.05 were considered significant.

Correlations of the Prognostic Model With the Autophagy and Hypoxia Score

We retrieved the autophagy-related genes (ARGs) from the Human Autophagy Database (http://www.autophagy.lu/autophagy.html). The relationship between ARGs and the risk score was estimated by the Pearson correlation coefficient.

The hypoxia-related gene set was retrieved from the MSigDB. To obtain hypoxia scores, the enrichment fraction of the hypoxia pathway in each sample was quantified by the ssGSEA algorithm.

Statistical Analysis

R software (v3.6.0) and GraphPad Prism (v9.3.1) were used for statistical analyses and visualization. The survival differences of Kaplan–Meier analysis were assessed with the log-rank test through the 'survminer' package in R. Differences among the inter-group were compared using the Wilcox test. The value of $p < 0.05$ was considered statistically significant.

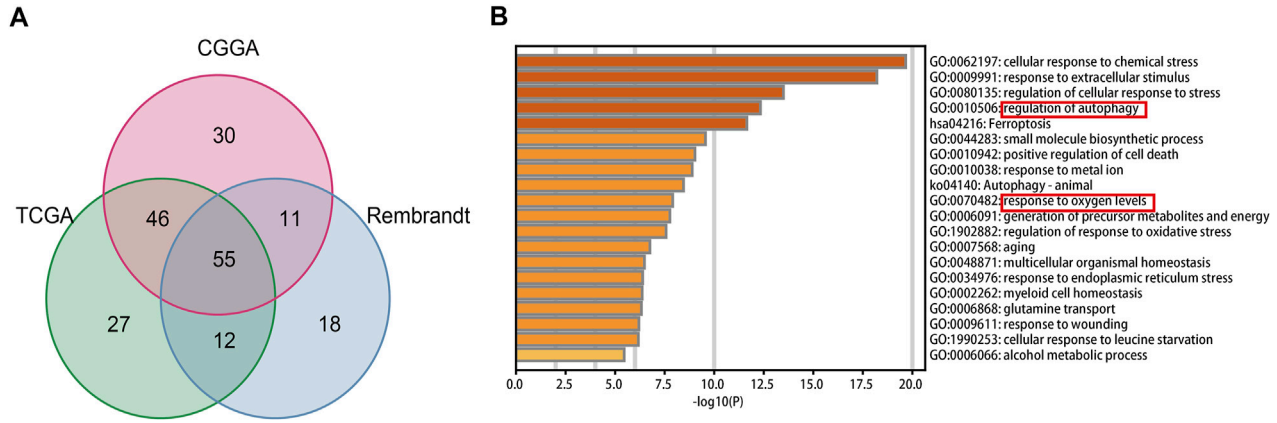

FIGURE 1 | Identification and functional enrichment analyses of the intersecting FRGs in TCGA, CGGA, and Rembrandt datasets. **(A)** Venn diagram to identify the intersecting FRGs from TCGA, CGGA, and Rembrandt datasets. **(B)** GO and KEGG analyses of the intersecting FRGs.

RESULTS

Identification of the Prognosis-Related FRGs in LGG

In total, fifty-five intersecting prognostic FRGs were identified by univariate Cox regression analysis in TCGA, CGGA, and Rembrandt databases (**Figure 1A**, **Supplementary Table S6**). After that, we performed a functional analysis using Metascape Online. As shown in **Figure 1B**, the GO analysis results suggest that the intersecting prognostic FRGs are enriched in response to the regulation of autophagy, metal ion, and oxygen levels. The KEGG pathway analysis revealed that the intersecting prognostic FRGs were enriched in ferroptosis and autophagy signaling pathways.

Consensus Clustering Determined Ferroptosis-Related Clusters of LGG

In this study, we explored the expression levels of fifty-five intersecting prognostic FRGs to construct consensus clusters. The 'ConsensusClusterPlus' package of R was exploited to confirm the ideal cluster numbers by calculating the average cluster consistency and intercluster coefficient variation of each class number. Ultimately, the consensus matrixes (**Figure 2A**) and cumulative distribution function (CDF) curves (**Figure 2B**) showed that $k = 3$ was the stable clustering number of FRGs. The LGG patients in TCGA dataset were divided into three groups named cluster-1 ($n = 99$), cluster-2 ($n = 221$), and cluster-3 ($n = 188$). Compared with cluster-2 and cluster-3, the Kaplan–Meier survival plot showed that patients in cluster-1 had the worst prognosis (**Figure 2C**). In addition, we also got three ferroptosis subtypes in CGGA and Rembrandt databases (**Supplementary Figures S2A,B, S3A,B**). Similar to TCGA dataset, the survival analysis also showed significant differences among different subtypes in the validating datasets (**Supplementary Figures S2C, S3C**). Meanwhile, the heatmap showed clinical and molecular features and different expression levels of fifty-five intersecting prognosis FRGs among different clusters in three datasets (**Supplementary Figures 2D, S2D, S3D**). Next, we further analyzed the distribution of various clinical features in different subgroups of three datasets (**Figure 2E**). In TCGA dataset, patients in cluster-1 have a higher proportion of age >40, WHO III, isocitrate dehydrogenase (IDH) wild type, O6-methylguanine-DNA methyltransferase promoter (MGMTp) unmethylated, and 1p19q non-codeletion which corresponds to the poor prognosis, whereas the cluster-3 patients are lower in these aforementioned features. Similar to TCGA dataset, the clinical traits also present marked differences among different clusters in the CGGA and Rembrandt datasets (**Supplementary Figures S2E, S3E**).

The Immune Microenvironment and Mutational Status in the Subtypes of Ferroptosis

First, we analyzed the immune scores of the three ferroptosis subtypes and found that the ImmuneScore, StromalScore, and ESTIMATEScore were higher in cluster-1 than those of the other two subtypes (**Figure 2F**). Subsequently, a correlation between the immune cell composition and ferroptosis subtypes was explored. As shown in **Figure 2G**, cluster-1 has a higher score of immune cells, followed by cluster-2 and cluster-3. We further analyzed the enrichment of typical biological processes in different clusters. The result revealed that cluster-1 was remarkably enriched in most oncogenic pathways (**Figure 2H**). The aforementioned results were also validated in two validation datasets (**Supplementary Figures S2F–H, S3F–H**).

T cell plays a vital role in anti-tumor immunotherapy. We analyzed the correlations between the ferroptosis subtypes and the activities of the anti-tumor immune response (**Figure 2I**). The anti-tumor activity score of the release of cancer cell antigens (Step 1) and a large proportion of immune cell recruiting (Step 4) were significantly higher in cluster-1. The steps of priming and activation (Step 3), recognition of cancer cells by T cells (Step 6), and killing of cancer cells (Step 7) were higher in cluster-3.

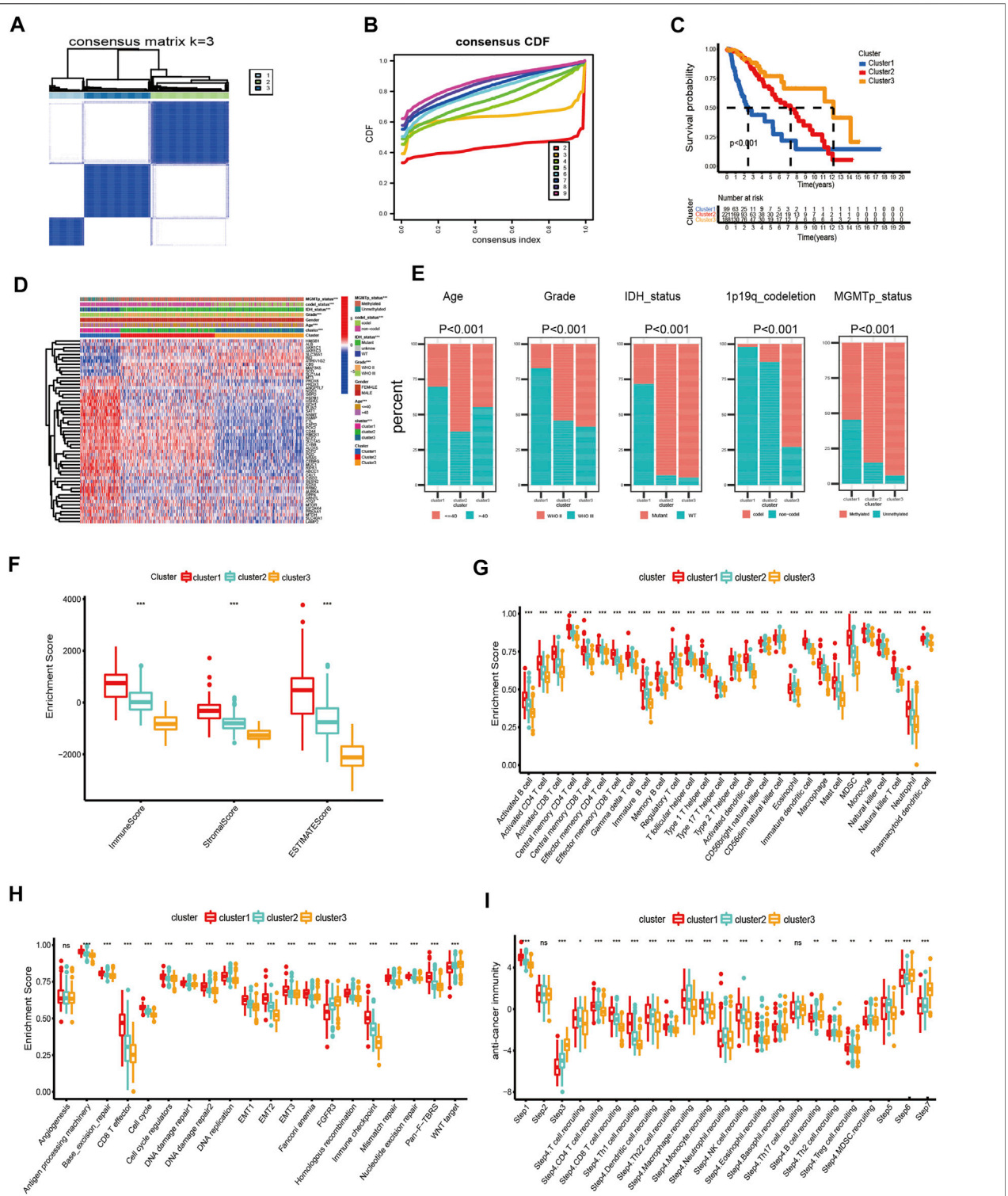

FIGURE 2 | Differential clinicopathological features and immune landscape of LGG among different clusters in TCGA dataset. **(A)** Consensus clustering matrix for $k = 3$. **(B)** Cumulative distribution function curves for $k = 2$–9. **(C)** Kaplan–Meier curve of overall survival among three clusters. **(D)** Heatmap and clinicopathological features of the three clusters. **(E)** Proportion of clinical characteristics in three clusters. **(F–I)** Distribution of ImmuneScore **(F)**, 28 immune cells **(G)**, typical biological pathways **(H)**, and activity score of the anti-tumor immune response **(I)** across the three ferroptosis subtypes. The horizontal line of the box plot represents the median values (*$p < 0.05$, **$p < 0.01$, ***$p < 0.001$; ns, non-significant).

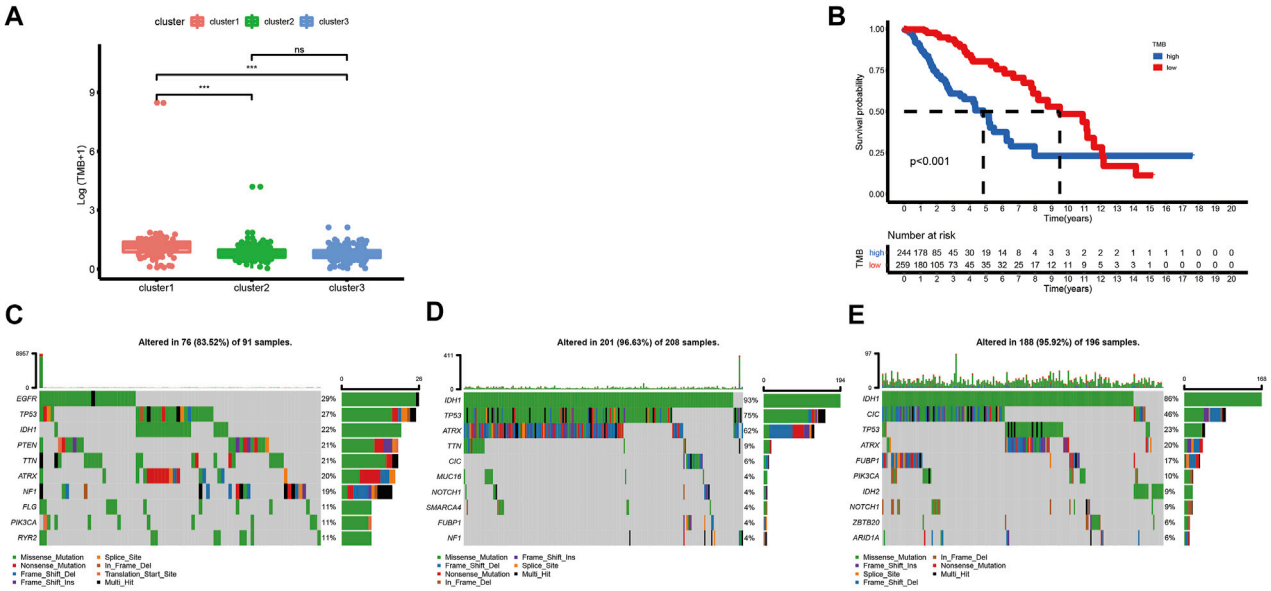

FIGURE 3 | Correlations between the ferroptosis subtypes and somatic variants in TCGA dataset. **(A)** Differences in TMB levels among different ferroptosis subtypes. **(B)** Correlation between TMB and prognosis in LGG patients. **(C-E)** Distribution of the top ten variants of mutated genes among different ferroptosis subtypes. The horizontal line of the box plot represented the median values (*p < 0.05, **p < 0.01, ***p < 0.001; ns, non-significant).

However, cluster-2 has a higher score in the fraction of immune cell recruiting (Step 4) and infiltration of immune cells into tumors (Step 5). In addition, there is no significant difference in cancer antigen presentation (Step 2) among the three subgroups.

Although high TMB is closely associated with a poor prognosis of glioma, it is also associated with better responses to immunotherapy (Bouffet et al., 2016; Touat et al., 2020; Yin et al., 2020). In this research, we calculated TMB scores for each sample with mutations in TCGA database to compare the differences between various clusters. The TMB level of cluster-1 is higher than that of others. However, there is no significant difference between cluster-2 and cluster-3 (**Figure 3A**). Meanwhile, we found that there is a significant correlation between TMB and prognosis in LGG patients (**Figure 3B**). Furthermore, among these three ferroptosis subtypes, cluster-2 had the highest mutation rate (96.63%), followed by cluster-3 (95.92%) and cluster-1 (83.52%). Previous studies have reported that IDH1 and IDH2 mutations were closely related to the prognosis of glioma patients (Yan et al., 2009). In this study, we noticed that the IDH mutation in cluster-3 (86% IDH1 and 9% IDH2) is higher than that in cluster-1 (22% IDH1) and cluster-2 (93% IDH1), indicating the vital role of IDH mutation in LGG patients (**Figures 3C–E**).

Construction and Validation of the Prognostic Model Based on FRGs

There were 49 DE-FRGs obtained from cluster-1 and cluster-3, including 41 upregulated, and 8 downregulated (**Figure 4A**). Taking advantage of the upregulated DE-FRGs, we constructed a new ferroptosis-related prognostic model according to the LASSO regression with the optimal lambda value (**Figures 4B,C**). The calculated coefficient of the nine FRGs is shown in **Supplementary Table S7**. According to the median cut-off value, the model categorized the patients into low- and high-risk groups. The Kaplan–Meier survival curve in TCGA databases indicated that patients in the high-risk group were associated with worse outcomes (**Figure 4D**). The distribution plot of the risk score and survival status showed that the risk score was strongly positively correlated with the death of LGG patients (**Figure 4G**). The AUC values of the prognostic model for FRGs were 0.907 (1-year), 0.902 (2-year), and 0.835 (5-year), which exhibited a remarkable predictive performance (**Figure 5J**).

We validated the applicability of the prognostic model in the CGGA and Rembrandt datasets. Similarly, patients in the low-risk group had better prognosis (**Figures 4E,F,H,I**). The AUC values for 1-year, 2-year, and 5-year survival in the CGGA dataset were 0.688, 0.731, and 0.726, respectively (**Figure 4K**). The AUC values in the Rembrandt dataset were 0.706, 0.793, and 0.762, respectively (**Figure 4L**). All the results prove that our prognostic model reveals favorable specificity and sensitivity.

In addition, we performed subgroup analyses according to age, gender, grade, IDH_status, 1p19q_status, and MGMTp_status in CGGA and TCGA datasets. Patients in the high-risk group were predicted with a worse prognosis in all subgroups (**Figures 5A–L**, and **Supplementary Figures S4A–L**). It is prompted that the prognostics model is better clinically applicable.

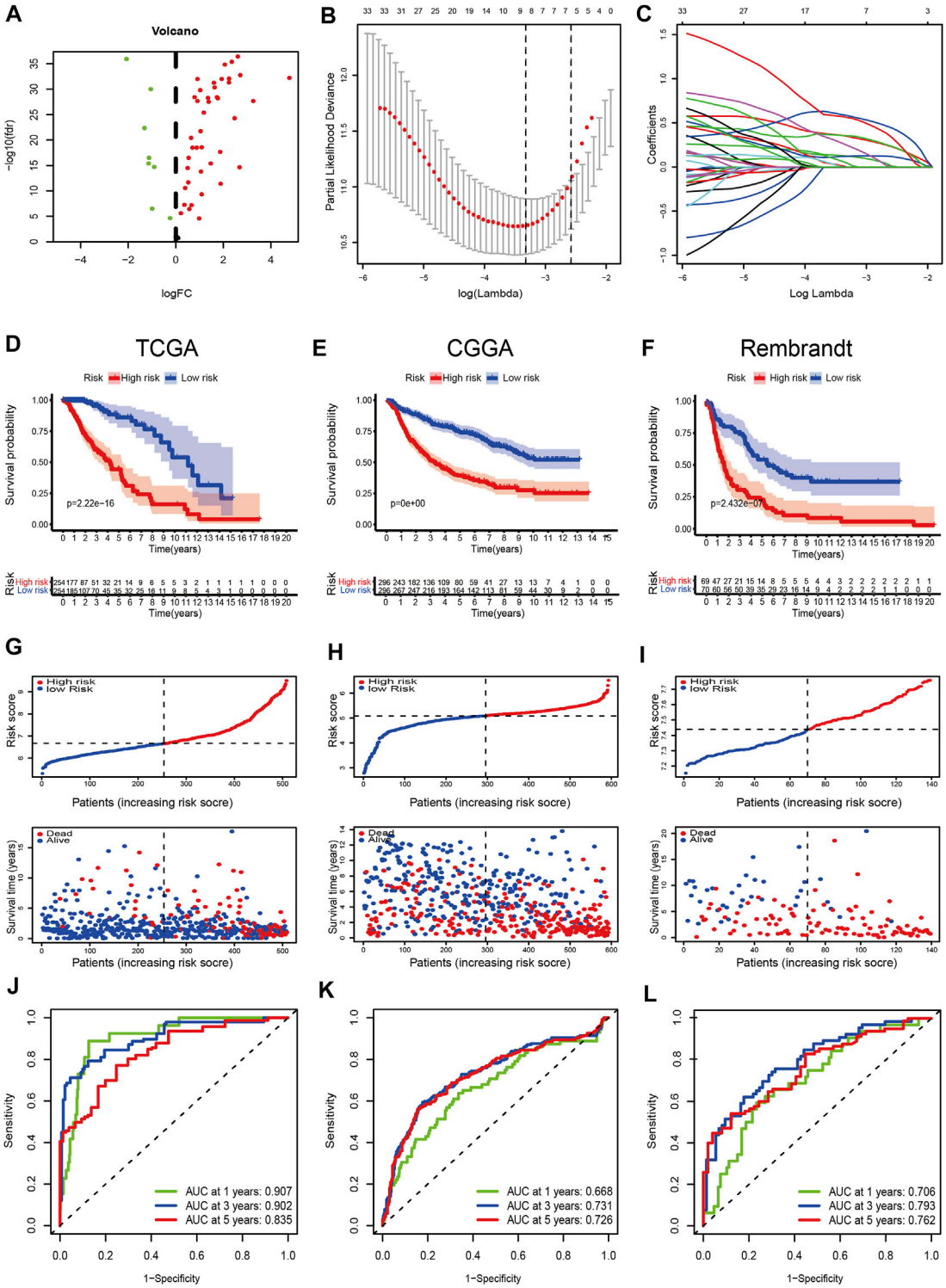

FIGURE 4 | Construction and validation of the prognostic model. **(A)** Volcano plot of DEGs between cluster-1 and cluster-3; red indicates downregulated genes, and green indicates upregulated genes. **(B)** LASSO coefficient profiles of the 41 upregulated DE-FRGs in TCGA dataset. **(C)** Cross-validation for tuning the parameter selection in the LASSO analysis. **(D–F)** Kaplan–Meier curves for survival in the TCGA, CGGA, and Rembrandt datasets. **(G–I)** Distribution plots of the risk score and survival status in the TCGA, CGGA, and Rembrandt datasets. **(J–L)** ROC curve analyses for predicting 1-, 3-, and 5-year OS in the TCGA, CGGA, and Rembrandt datasets.

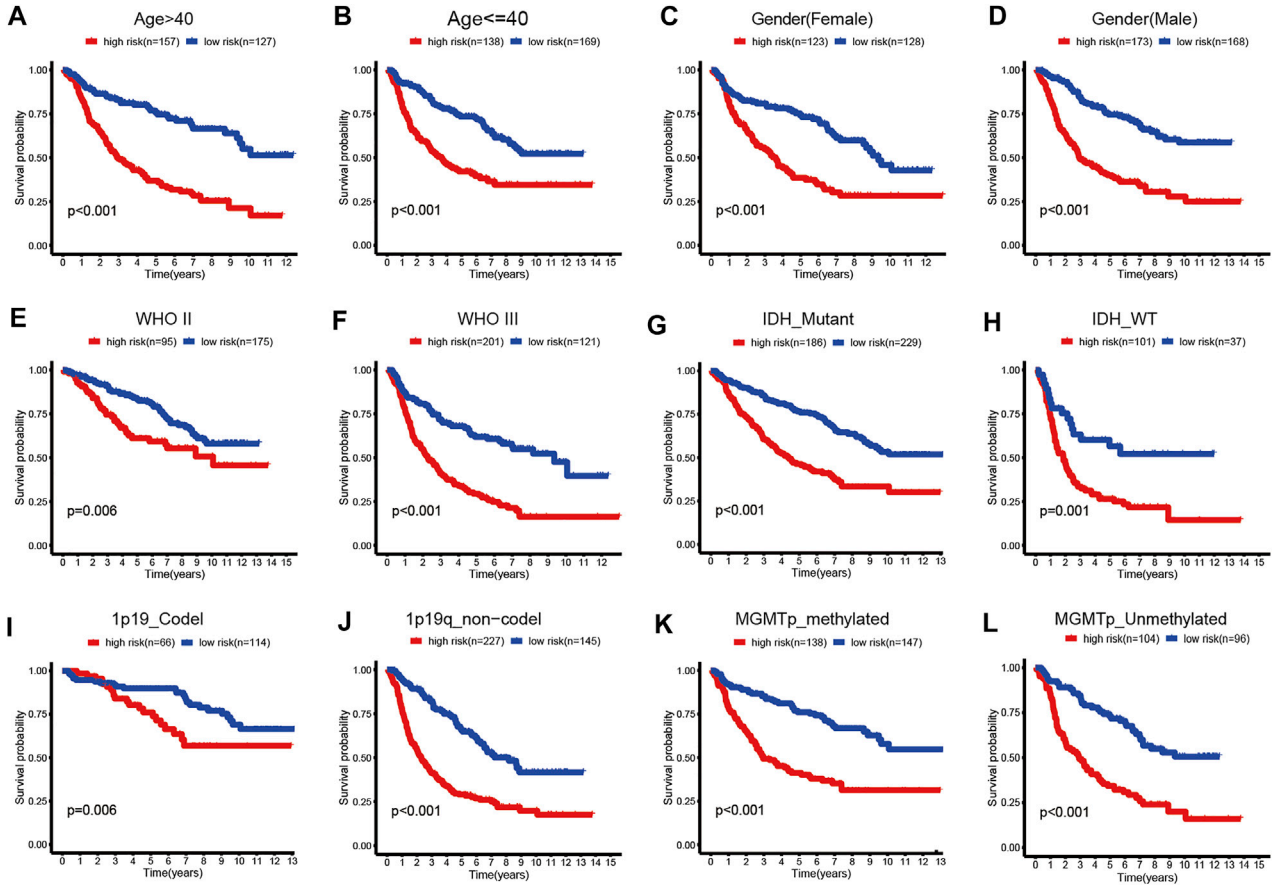

FIGURE 5 | Kaplan–Meier survival curves for the low- and high-risk groups stratified by clinicopathological variables in TCGA dataset. **(A,B)** Age. **(C,D)** Gender. **(E,F)** WHO grade. **(G,H)** IDH_status. **(I,J)** 1p19q_status. **(K,L)** MGMTp_status.

Construction and Validation of a Prognostic Nomogram

To evaluate whether the risk scores can be applied as an independent prognostic biomarker, univariate and multivariate Cox regression analyses were performed in TCGA, CGGA, and Rembrandt datasets (**Figures 6A–C**). The results suggest that the risk score was always an independent prognostic factor in both univariate and multivariate Cox regression analyses. Meanwhile, we constructed a nomogram with the independent prognostic parameters for the OS in TCGA and CGGA datasets (**Figures 6D**, **Supplementary Figure S5A**). Meanwhile, the calibration plot showed that the predicted power was similar to the actual observations (**Figures 6E**, **Supplementary Figure S5B**).

The Immune Microenvironment and Mutational Status in Distinct Risk Groups

We further evaluated the difference in immune scores, immune cell composition, and typical biological processes between the two risk groups in TCGA dataset. As the results reflected, the immune scores and the majority of the immune cell composition were higher in the high-risk group (**Figures 7A,B**). Meanwhile, it is not surprising that most oncogenic pathways were enriched in the high-risk group compared with the low-risk group (**Figure 7C**). The same results were confirmed in the CGGA and the Rembrandt datasets (Supplementary Figures S6A–F).

We next analyzed the differences in somatic mutation among the two risk groups in TCGA dataset. As shown in **Figure 7D**, there was a significant difference in TMB levels between the high- and low-risk groups. The risk score was positively correlated to the level of the TMB (**Figure 7E**). Moreover, patients in the high-risk group have a higher mutation rate than those in the low-risk group (**Figures 7F,G**).

Sensitivity to Chemotherapies and ICB Therapy in Distinct Risk Groups

To further study and characterize drug responses of temozolomide in LGG patients, we assessed differences in drug sensitivity between the high- and low-risk groups by analyzing the IC_{50} of temozolomide. We found that in TCGA, CGGA, and Rembrandt datasets, patients in the high-risk group were more sensitive to temozolomide (**Figures 8A–C**).

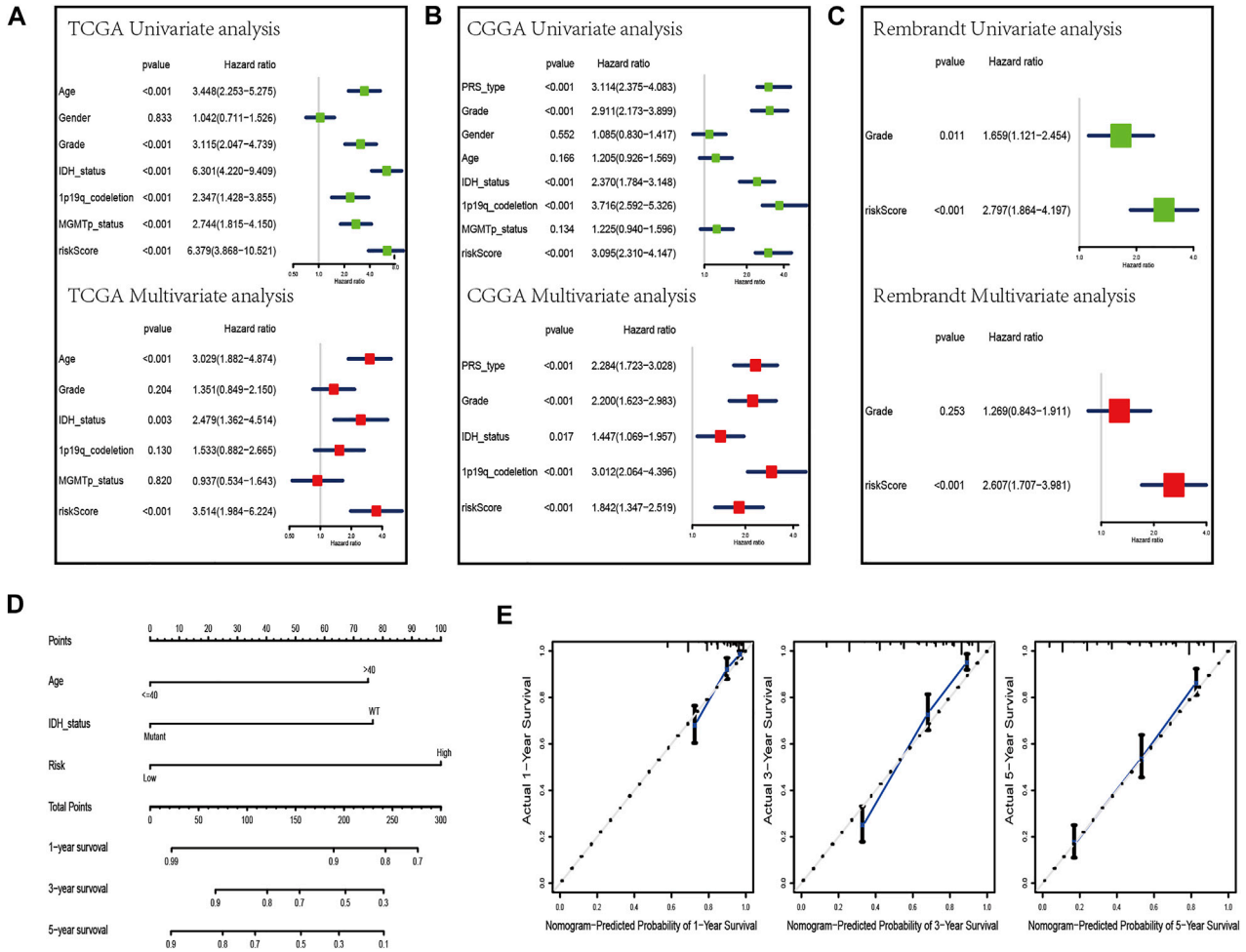

FIGURE 6 | Development of a nomogram by integrating the risk score and clinicopathological characters in the TCGA cohort. **(A–C)** Univariate analysis and multivariate analysis containing risk score and clinical factors in TCGA **(A)**, CGGA **(B)**, and Rembrandt **(C)** datasets. **(D)** Nomogram constructed to predict OS rates at 1, 3, and 5 years. **(E)** Calibration curves predicted 1-, 3-, and 5-year survival.

Immune checkpoint blockades that target CTLA-4 and PD-1/PD-L1 have shown some promise against glioma (Saha et al., 2017; Zhao et al., 2019), but only a fraction of patients respond to treatment. According to the TIDE and SubMap algorithms, the expression profiles of TCGA, CGGA, and Rembrandt datasets were compared with a published dataset containing 47 melanoma patients who responded to immunotherapy. We found that treatment with PD-1 showed better results in the high-risk group (Bonferroni correction $p < 0.05$) (**Figures 8D–F**).

Functional Analysis of the Prognostic Model

We further verified the different functional phenotypes involved in the high- and low-risk groups *via* GSEA. The finding disclosed that several pathways, such as angiogenesis, epithelial–mesenchymal transition, hypoxia, and glycolysis, were significantly activated in the high-risk group (**Figure 9A**). These findings were further validated in the CGGA and Rembrandt datasets (**Figures 9B,C**).

Identification of the Hypoxia Correlation With the Ferroptosis-Related Prognostic Model

Our previous study found that the intersecting FRGs were correlated to biological processes of oxygen metabolism through GO and KEGG analyses. First, the Pearson correlation coefficient was taken advantage of evaluating the connection between ARGs and the risk score of the prognostic model. Among the 210 ARGs, a total of 175 (83.3%) ARGs were significantly correlated with risk scores, of which 126 were positively correlated, and 49 were negatively correlated (**Supplementary Table S8**). The top 10 ARGs positively correlated (*CASP8, CASP4, WIPI1, CASP3, CFLAR, DIRAS3, P4HB, SH3GLB1, CASP1, and HSPA5*) with the risk score and the top 10 negative relationships (*BID, GRID1, MAPK8, PEA15, SAR1A, EEF2, ST13, SIRT1, TSC1, and BAG1*) with the risk score are shown in **Figures 10A, B**.

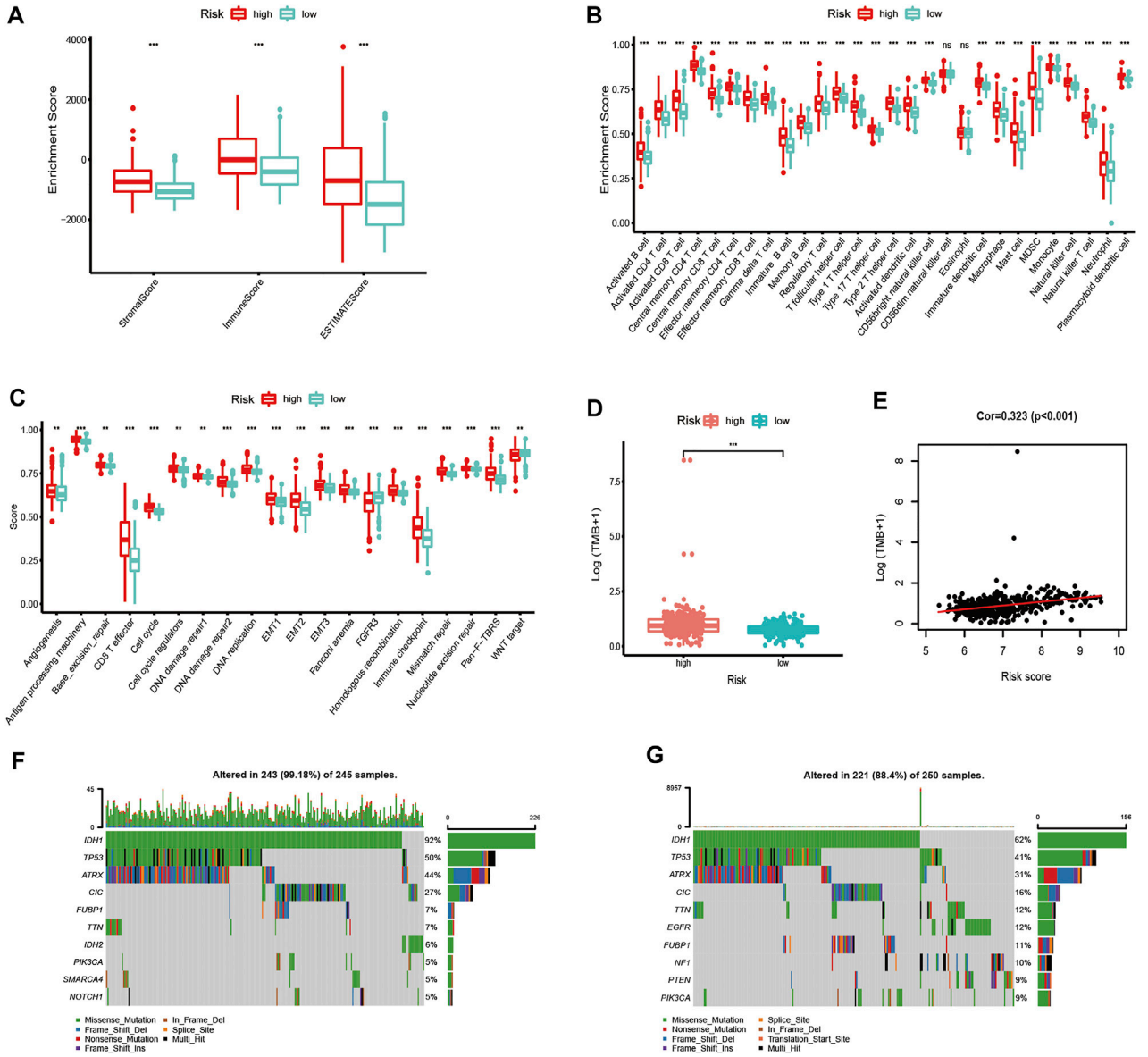

FIGURE 7 | Immune microenvironment, biological process characteristics, and prediction of chemotherapeutic response among distinct risk groups. **(A–D)** Distribution of ImmuneScore **(A)**, 28 immune cells **(B)**, typical biological pathways **(C)**, and TMB levels **(D)** between the high- and low-risk groups in TCGA dataset. **(E)** Correlation between TMB and risk score in LGG patients. **(F,G)** Mutation rates of top 10 mutated genes in low- and high-risk groups. The horizontal line of the box plot represents the median values (*$p < 0.05$, **$p < 0.01$, ***$p < 0.001$; ns, non-significant).

Afterward, the hypoxia enrichment score of each patient was calculated. As shown in **Figure 11A**, patients in the high-risk group had a higher hypoxia score. The risk score was positively correlated to the hypoxia score (**Figure 11B**). Afterward, the patients were divided into two groups by the median of hypoxia scores. The Kaplan-Meier survival curves performed an unfavorable prognosis of the high hypoxia score patients (**Figure 11C**). **Figure 11D** shows that a low-risk score combined with a low hypoxia score group performed better outcomes compared with the other groups.

DISCUSSION

LGGs are a fatal, invading, and heterogeneous group of tumors and usually results in progressive neurological disability and adverse clinical outcomes (Hayhurst, 2017). Different from necrosis, apoptosis, autophagy, and pyroptosis, ferroptosis is a new type of regulated cell death (Dixon et al., 2015), which is closely related to glioma tumorigenesis, progression, and tumor microenvironment (Xu et al., 2021). Therefore, the effective prognostic biomarkers relying on the FRGs will benefit the clinical treatment of patients with LGG.

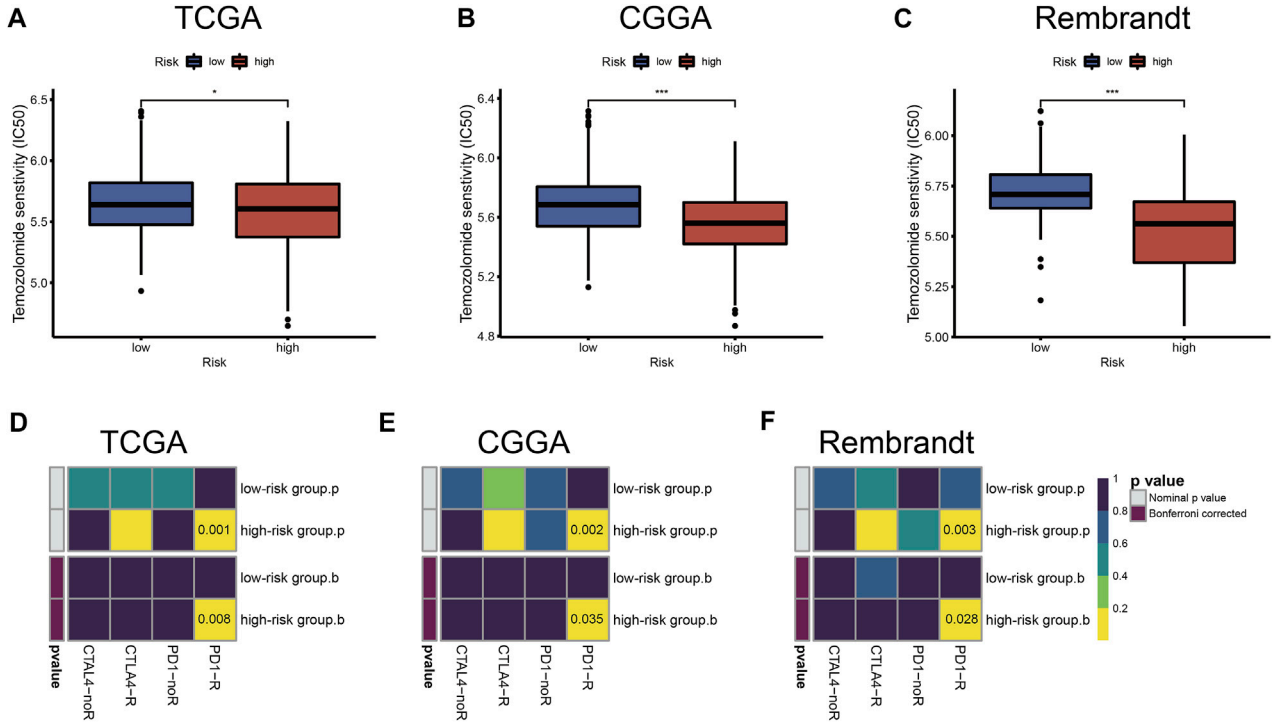

FIGURE 8 | Chemotherapeutics and ICB therapy responses in high- and low-risk groups with LGG. Drug sensitivity of temozolomide in TCGA **(A)**, CGGA **(B)**, and Rembrandt **(C)** datasets. ICB therapy responses to anti-PD1 and anti-CTLA4 treatments of LGG in TCGA **(D)**, CGGA **(E)**, and Rembrandt **(F)** datasets. The horizontal line of the box plot represents the median values (*$p < 0.05$, **$p < 0.01$, ***$p < 0.001$; ns, non-significant).

The present study commits to detecting the correlation between the ferroptosis subtypes and the ferroptosis-related prognostic model and the immune microenvironment. Ulteriorly, we identified potential biomarkers for prognosis prediction and target therapy. According to the prognostic FRGs, the LGG patients were initially sorted into three ferroptosis states, which exhibited different outcomes, clinicopathological features, immune landscape, and biological processes. Later on, we constructed an FRG-based prognostic model associated with LGG patients. Our results revealed that the prognostic model performed a predictive performance with satisfactory sensitivity and specificity. Meanwhile, the prognosis of LGG was affected by the model which was an independent factor. We also studied the immune microenvironment, chemotherapies, and ICB therapy between different risk groups. All the aforementioned results in the validating datasets were verified. Furthermore, the relationship between the prognostic model and autophagy as well as hypoxia was explored.

The immune microenvironment has a great effect on tumor proliferation and molecular heterogeneity (Barthel et al., 2021). In this study, the immune microenvironment of each cluster in TCGA dataset was first evaluated. We found that the immune score and immune cell infiltration in cluster-1 were higher than those in the others. However, the result of cancer immunity cycles showed that the anti-tumor activities of priming and activation (Step 3), recognition of cancer cells by T cells (Step 6), and killing of cancer cells (Step 7) in cluster-1 are lower. Meanwhile, the biological processes including stromal activation (EMT, Pan–F–TBRS) and immune activation (CD8 T effector, antigen processing machinery, and immune checkpoint) pathways in cluster-1 were higher than those in the other two clusters. Considering that glioma is characterized by a 'cold' tumor (Jackson et al., 2019), we deduce that the reason for the patients' poor outcomes in cluster-1 probably derived from the deficiency of 'effective T cells' which affect the immunosuppression microenvironment. We also discovered that cluster-1 with a higher TMB level suggested that patients may gain a positive efficacy from immunotherapy. Although patients in cluster-1 have the highest TMB level, the mutation rate is lower than that in other clusters. Research findings show that IDH mutation has a significant correlation to the prognosis of glioma (Hartmann et al., 2010; Turkalp et al., 2014; Eckel-Passow et al., 2015). In this study, patients in cluster-3 have the highest IDH mutation rate among the three clusters, corresponding to better outcomes. Interestingly, as a potent tumor suppressor, CIC mutation merely occurred in the top 10 mutated genes of cluster-2 (6%) and cluster-3 (46%) (Wong and Yip, 2020). Similarly, PTEN mutation, which results in the loss of tumor-suppressive function in LGG (Endersby and Baker, 2008), exclusively appeared in the top 10 mutated genes of cluster-1.

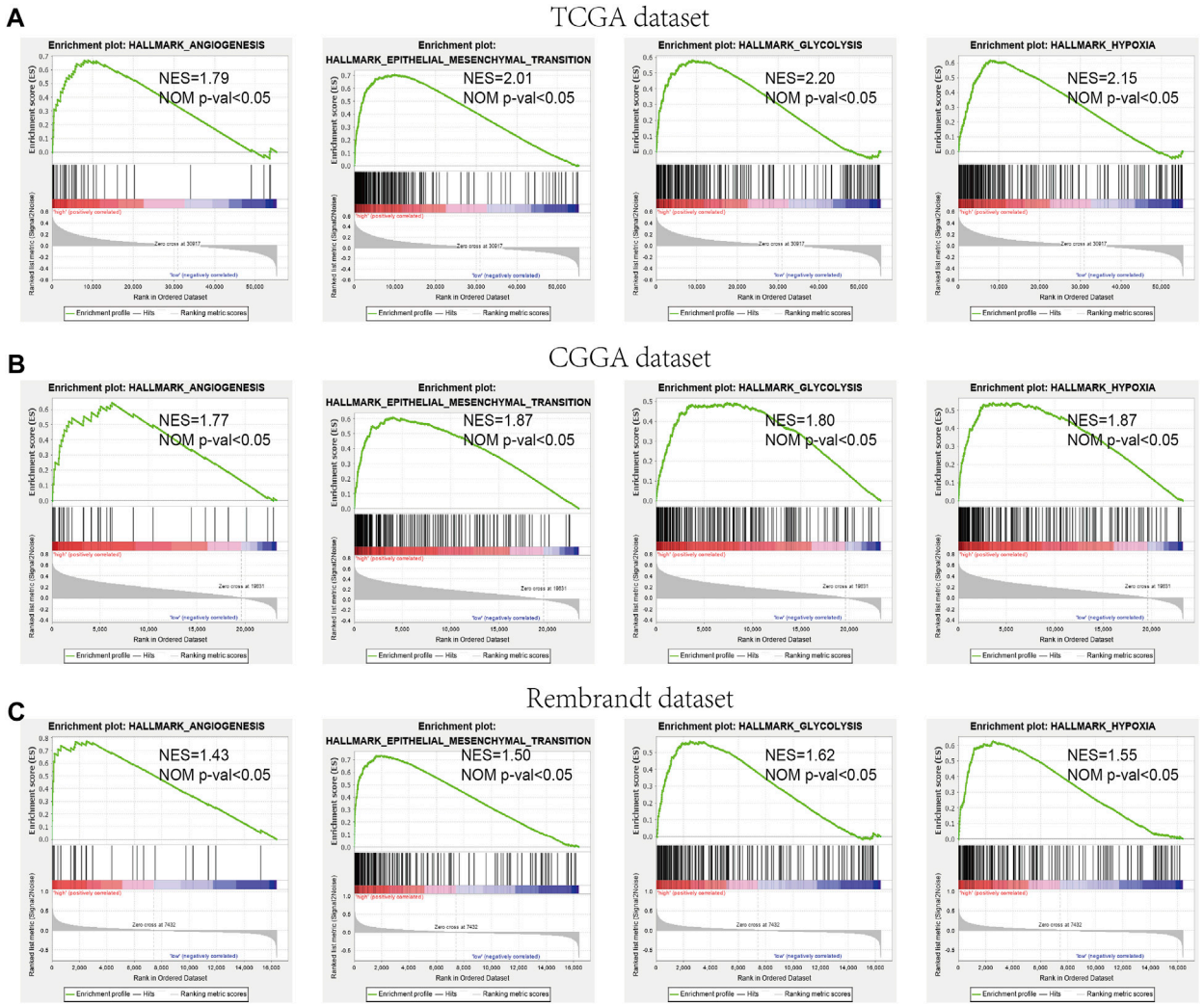

FIGURE 9 | GSEA comparisons of the low- and high-risk groups. **(A–C)** Common functional gene sets enriched in the high-risk group compared to the low-risk group in TCGA **(A)**, CGGA **(B)**, and Rembrandt **(C)** datasets.

For the convenience of the calculation of the TME landscapes in individuals, we evaluated the immune microenvironment among the different risk groups. Similar to the aforementioned results, anti-tumor immune responses are both activated and suppressed in the high-risk group. GSEA revealed that the regulation of "angiogenesis," "epithelial–mesenchymal transition," "hypoxia," and "glycolysis" was enriched in the high-risk group. It indicates that the high-risk group was bound up with the process of tumor proliferation.

Chemotherapy and ICB therapy are crucial adjunctive therapies for glioma. Temozolomide is the first-line drug for glioma treatment. As expected, the patients in the high-risk group are more sensitive to temozolomide therapy than those in the low-risk group. In addition, patients in the high-risk group have a better response to anti-PD-1 therapy. The result is consistent with our findings.

Autophagy is a conserved, self-degradation pathway that is critical for survival, differentiation, development, and homeostasis (Levine and Kroemer, 2008; Onorati et al., 2018). Although ferroptosis is distinct from other types of regulated cell death, activation of autophagy is necessary for the induction of ferroptosis under given conditions (Kang and Tang, 2017; Liu et al., 2020). In this study, according to GO and KEGG analyses, we first verified that the prognostic model has a significant correlation with most ARGs. Studies have proved that hypoxia can promote cell proliferation in tumors and the progression of tumor conversion to the malignant phenotype (Sun et al., 2021). Meanwhile, hypoxia can also protect macrophages from ferroptosis (Fuhrmann et al., 2020). We subsequently explored the relationship between the prognostic model and the hypoxia score. The results revealed that the prediction ability significantly improved with a combination of the risk score and hypoxia score. The aforementioned results contribute a new insight into the multitargeted therapy in LGG.

However, some limitations in this study should be considered. First, as a validating dataset, it had a lack of

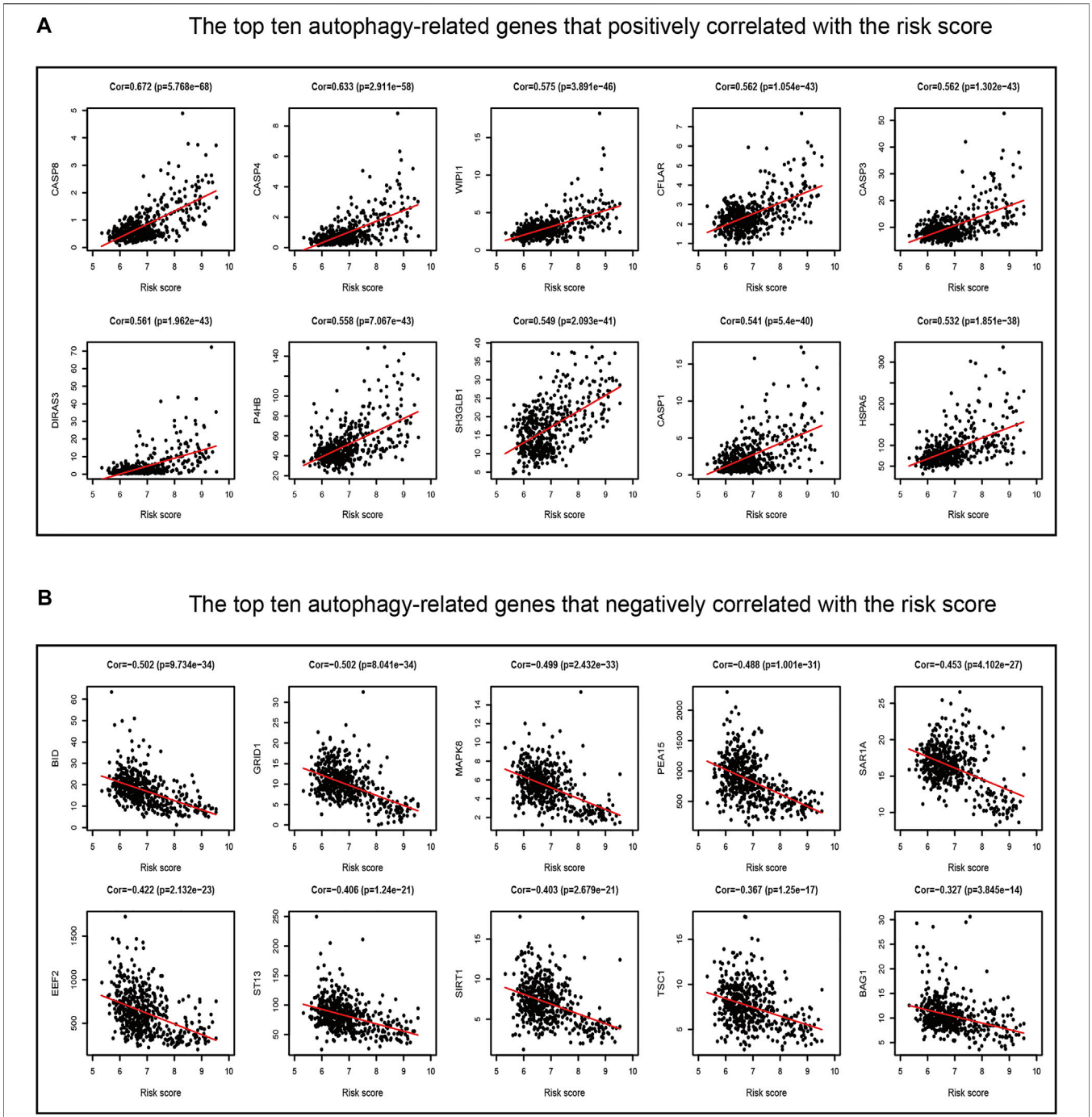

FIGURE 10 | Correlations between the ferroptosis-related prognostic model and ARGs in TCGA dataset. **(A)** Top ten ARGs positively correlated with the risk score. **(B)** Top ten ARGs negatively correlated with the risk score.

corresponding clinicopathological data in the Rembrandt database. Second, this study is based on bioinformatics analysis, and the experimental verification is needed in the future. Last, the transformation of the basic scientific advances into efficient therapeutics should be explored, which will be a formidable challenge.

CONCLUSION

According to the prognostic FRGs from the three datasets, we clustered LGG patients into three subgroups which exhibited different outcomes, clinicopathological features, immune landscape, and biological processes. Subsequently, a novel

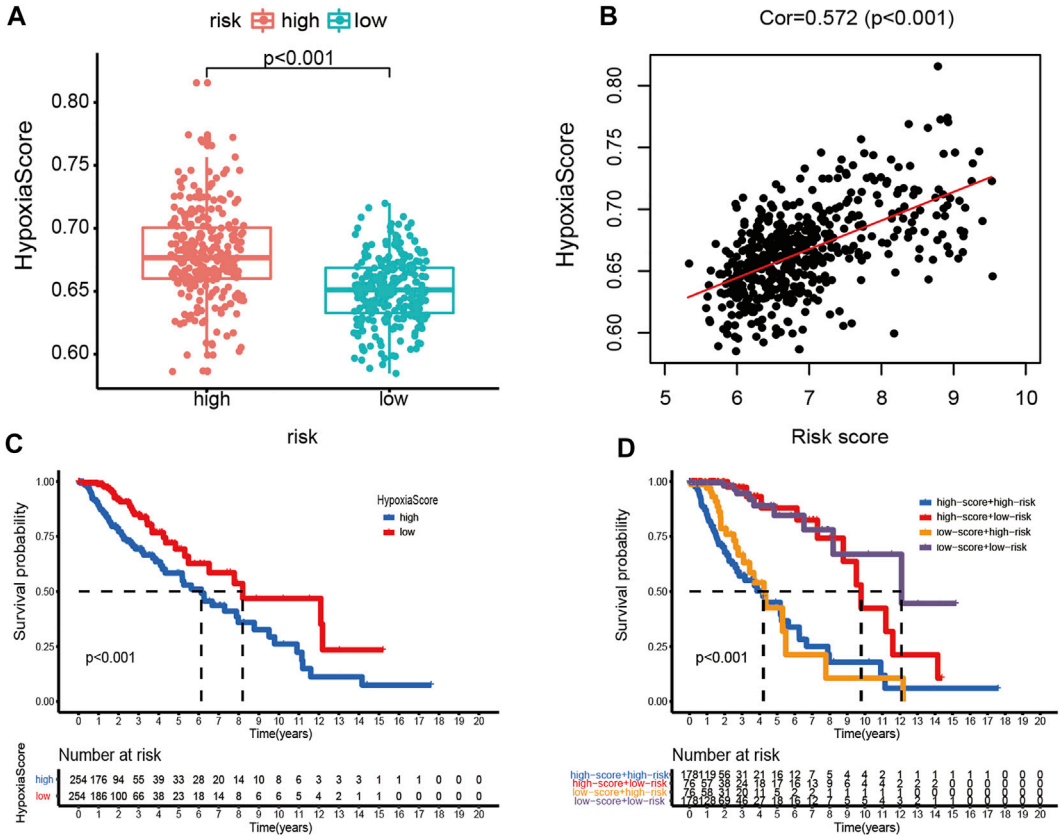

FIGURE 11 | Hypoxia score analysis. **(A)** Hypoxia scores between high- and low-risk groups. **(B)** Correlation between the hypoxia score and risk score in LGG patients. **(C)** Kaplan-Meier survival curves of OC patients with high or low hypoxia score. **(D)** Kaplan-Meier survival curves of four subgroups based on the risk score and hypoxia score.

clinically applicable ferroptosis-related prognostic model was constructed to benefit individualized prediction of diagnosis, treatment, prognosis, and recurrence. Moreover, our study has provided several novel insights into the connection between ferroptosis and the immunosuppressive microenvironment in LGG, which may be beneficial in individualized treatment strategies.

DATA AVAILABILITY STATEMENT

The original contributions presented in the study are included in the article/**Supplementary Material**, further inquiries can be directed to the corresponding authors.

AUTHOR CONTRIBUTIONS

XY, JYD, and SH conceived and designed the study and drafted the manuscript. HJ, JWD, and JZ provided analytical technical support. XY, ZL, and HZ participated in the production of charts and pictures. All authors have read and approved the final manuscript. All authors contributed to the article and approved the submitted version.

FUNDING

This work was funded by the National Natural Science Foundation of China (No. 61575058).

ACKNOWLEDGMENTS

We all authors sincerely acknowledge the contributions from TCGA, CGGA, and Rembrandt databases for offering convenient access to datasets. In addition, we thank Dr. Siwen Wang for the help in statistics and encouragement.

SUPPLEMENTARY MATERIAL

The Supplementary Material for this article can be found online at: https://www.frontiersin.org/articles/10.3389/fgene.2022.880864/full#supplementary-material

REFERENCES

Barthel, L., Hadamitzky, M., Dammann, P., Schedlowski, M., Sure, U., Thakur, B. K., et al. (2021). Glioma: Molecular Signature and Crossroads with Tumor Microenvironment. *Cancer Metastasis Rev.* 41, 53–75. doi:10.1007/s10555-021-09997-9

Bouffet, E., Larouche, V., Campbell, B. B., Merico, D., de Borja, R., Aronson, M., et al. (2016). Immune Checkpoint Inhibition for Hypermutant Glioblastoma Multiforme Resulting from Germline Biallelic Mismatch Repair Deficiency. *J. Clin. Oncol.* 34, 2206–2211. doi:10.1200/jco.2016.66.6552

Bready, D., and Placantonakis, D. G. (2019). Molecular Pathogenesis of Low-Grade Glioma. *Neurosurg. Clin. North America* 30, 17–25. doi:10.1016/j.nec.2018.08.011

Chen, Y., Li, L., Lan, J., Cui, Y., Rao, X., Zhao, J., et al. (2022). CRISPR Screens Uncover Protective Effect of PSTK as a Regulator of Chemotherapy-Induced Ferroptosis in Hepatocellular Carcinoma. *Mol. Cancer* 21, 11. doi:10.1186/s12943-021-01466-9

Dixon, S. J., Lemberg, K. M., Lamprecht, M. R., Skouta, R., Zaitsev, E. M., Gleason, C. E., et al. (2012). Ferroptosis: An Iron-Dependent Form of Nonapoptotic Cell Death. *Cell* 149, 1060–1072. doi:10.1016/j.cell.2012.03.042

Dixon, S. J., Winter, G. E., Musavi, L. S., Lee, E. D., Snijder, B., Rebsamen, M., et al. (2015). Human Haploid Cell Genetics Reveals Roles for Lipid Metabolism Genes in Nonapoptotic Cell Death. *ACS Chem. Biol.* 10, 1604–1609. doi:10.1021/acschembio.5b00245

Du, Y., Zhao, H.-C., Zhu, H.-C., Jin, Y., and Wang, L. (2021). Ferroptosis Is Involved in the Anti-Tumor Effect of Lycorine in Renal Cell Carcinoma Cells. *Oncol. Lett.* 22, 781. doi:10.3892/ol.2021.13042

Eckel-Passow, J. E., Lachance, D. H., Molinaro, A. M., Walsh, K. M., Decker, P. A., Sicotte, H., et al. (2015). Glioma Groups Based on 1p/19q, IDH, and TERT Promoter Mutations in Tumors. *N. Engl. J. Med.* 372, 2499–2508. doi:10.1056/NEJMoa1407279

Endersby, R., and Baker, S. J. (2008). PTEN Signaling in Brain: Neuropathology and Tumorigenesis. *Oncogene* 27, 5416–5430. doi:10.1038/onc.2008.239

Friedman, A. A., Letai, A., Fisher, D. E., and Flaherty, K. T. (2015). Precision Medicine for Cancer with Next-Generation Functional Diagnostics. *Nat. Rev. Cancer* 15, 747–756. doi:10.1038/nrc4015

Fuhrmann, D. C., Mondorf, A., Beifuß, J., Jung, M., and Brüne, B. (2020). Hypoxia Inhibits Ferritinophagy, Increases Mitochondrial Ferritin, and Protects from Ferroptosis. *Redox Biol.* 36, 101670. doi:10.1016/j.redox.2020.101670

Geeleher, P., Cox, N., and Huang, R. S. (2014). pRRophetic: An R Package for Prediction of Clinical Chemotherapeutic Response from Tumor Gene Expression Levels. *PloS one* 9, e107468. doi:10.1371/journal.pone.0107468

Hartmann, C., Hentschel, B., Wick, W., Capper, D., Felsberg, J., Simon, M., et al. (2010). Patients with IDH1 Wild Type Anaplastic Astrocytomas Exhibit Worse Prognosis Than IDH1-Mutated Glioblastomas, and IDH1 Mutation Status Accounts for the Unfavorable Prognostic Effect of Higher Age: Implications for Classification of Gliomas. *Acta Neuropathol.* 120, 707–718. doi:10.1007/s00401-010-0781-z

Hayhurst, C. (2017). Contemporary Management of Low-Ggrade Glioma: A Paradigm Shift in Neuro-Oncology. *Pract. Neurol.* 17, 183–190. doi:10.1136/practneurol-2017-001604

Hoshida, Y., Brunet, J.-P., Tamayo, P., Golub, T. R., and Mesirov, J. P. (2007). Subclass Mapping: Identifying Common Subtypes in Independent Disease Data Sets. *PloS one* 2, e1195. doi:10.1371/journal.pone.0001195

Jackson, C. M., Choi, J., and Lim, M. (2019). Mechanisms of Immunotherapy Resistance: Lessons from Glioblastoma. *Nat. Immunol.* 20, 1100–1109. doi:10.1038/s41590-019-0433-y

Jiang, P., Gu, S., Pan, D., Fu, J., Sahu, A., Hu, X., et al. (2018). Signatures of T Cell Dysfunction and Exclusion Predict Cancer Immunotherapy Response. *Nat. Med.* 24, 1550–1558. doi:10.1038/s41591-018-0136-1

Kang, R., and Tang, D. (2017). Autophagy and Ferroptosis-What Is the Connection? *Curr. Pathobiol Rep.* 5, 153–159. doi:10.1007/s40139-017-0139-5

Levine, B., and Kroemer, G. (2008). Autophagy in the Pathogenesis of Disease. *Cell* 132, 27–42. doi:10.1016/j.cell.2007.12.018

Li, H.-W., Liu, M.-B., Jiang, X., Song, T., Feng, S.-X., Wu, J.-Y., et al. (2022). GALNT14 Regulates Ferroptosis and Apoptosis of Ovarian Cancer through the EGFR/mTOR Pathway. *Future Oncol.* 18, 149–161. doi:10.2217/fon-2021-0883

Li, H., and Liu, L. (2022). Zinc Moderates Circular RNA CircFOXP1 Expression in Order to Regulate Ferroptosis during Lung Adenocarcinoma. *Chemico-Biological Interactions* 352, 109760. doi:10.1016/j.cbi.2021.109760

Li, H., Yang, P., Wang, J., Zhang, J., Ma, Q., Jiang, Y., et al. (2022). HLF Regulates Ferroptosis, Development and Chemoresistance of Triple-Negative Breast Cancer by Activating Tumor Cell-Macrophage Crosstalk. *J. Hematol. Oncol.* 15, 2. doi:10.1186/s13045-021-01223-x

Liu, J., Kuang, F., Kroemer, G., Klionsky, D. J., Kang, R., and Tang, D. (2020). Autophagy-Dependent Ferroptosis: Machinery and Regulation. *Cel Chem. Biol.* 27, 420–435. doi:10.1016/j.chembiol.2020.02.005

Liu, S., Wu, W., Chen, Q., Zheng, Z., Jiang, X., Xue, Y., et al. (2021). TXNRD1: A Key Regulator Involved in the Ferroptosis of CML Cells Induced by Cysteine Depletion *In Vitro*. *Oxidative Med. Cell. longevity* 2021, 7674565. doi:10.1155/2021/7674565

Louis, D. N., Perry, A., Reifenberger, G., von Deimling, A., Figarella-Branger, D., Cavenee, W. K., et al. (2016). The 2016 World Health Organization Classification of Tumors of the Central Nervous System: A Summary. *Acta Neuropathol.* 131, 803–820. doi:10.1007/s00401-016-1545-1

Lu, T., Zhang, Z., Pan, X., Zhang, J., Wang, X., Wang, M., et al. (2021). Caveolin-1 Promotes Cancer Progression via Inhibiting Ferroptosis in Head and Neck Squamous Cell Carcinoma. *J. Oral Pathol. Med.* 51, 52–62. doi:10.1111/jop.13267

Mayakonda, A., Lin, D.-C., Assenov, Y., Plass, C., and Koeffler, H. P. (2018). Maftools: Efficient and Comprehensive Analysis of Somatic Variants in Cancer. *Genome Res.* 28, 1747–1756. doi:10.1101/gr.239244.118

Mou, Y., Zhang, L., Liu, Z., and Song, X. (2022). Abundant Expression of Ferroptosis-Related SAT1 Is Related to Unfavorable Outcome and Immune Cell Infiltration in Low-Grade Glioma. *BMC cancer* 22, 215. doi:10.1186/s12885-022-09313-w

Onorati, A. V., Dyczynski, M., Ojha, R., and Amaravadi, R. K. (2018). Targeting Autophagy in Cancer. *Cancer* 124, 3307–3318. doi:10.1002/cncr.31335

Ostrom, Q. T., Gittleman, H., Xu, J., Kromer, C., Wolinsky, Y., Kruchko, C., et al. (2016). CBTRUS Statistical Report: Primary Brain and Other Central Nervous System Tumors Diagnosed in the United States in 2009-2013. *Neuro-oncology* 18, v1–v75. doi:10.1093/neuonc/now207

Saha, D., Martuza, R. L., and Rabkin, S. D. (2017). Macrophage Polarization Contributes to Glioblastoma Eradication by Combination Immunovirotherapy and Immune Checkpoint Blockade. *Cancer cell* 32, 253–267. doi:10.1016/j.ccell.2017.07.006

Sanai, N., Chang, S., and Berger, M. S. (2011). Low-Grade Gliomas in Adults. *J Neurosurg.* 115, 948–965. doi:10.3171/2011.7.Jns101238

Semmel, D., Ware, C., Kim, J. Y., and Peters, K. B. (2018). Evidence-Based Treatment for Low-Grade Glioma. *Semin. Oncol. Nurs.* 34, 465–471. doi:10.1016/j.soncn.2018.10.008

Sun, X., Zhou, Z., Zhang, Y., Wang, J., Zhao, X., Jin, L., et al. (2021). Identification and Validation of a Hypoxia-Related Prognostic and Immune Microenvironment Signature in Bladder Cancer. *Cancer Cel Int* 21, 251. doi:10.1186/s12935-021-01954-4

Touat, M., Li, Y. Y., Boynton, A. N., Spurr, L. F., Iorgulescu, J. B., Bohrson, C. L., et al. (2020). Mechanisms and Therapeutic Implications of Hypermutation in Gliomas. *Nature* 580, 517–523. doi:10.1038/s41586-020-2209-9

Turkalp, Z., Karamchandani, J., and Das, S. (2014). IDH Mutation in Glioma: New Insights and Promises for the Future. *JAMA Neurol.* 71, 1319–1325. doi:10.1001/jamaneurol.2014.1205

Ursini, F., and Maiorino, M. (2020). Lipid Peroxidation and Ferroptosis: The Role of GSH and GPx4. *Free Radic. Biol. Med.* 152, 175–185. doi:10.1016/j.freeradbiomed.2020.02.027

Wong, D., and Yip, S. (2020). Making Heads or Tails - The Emergence of Capicua (CIC) as an Important Multifunctional Tumour Suppressor. *J. Pathol.* 250, 532–540. doi:10.1002/path.5400

Xu, L., Deng, C., Pang, B., Zhang, X., Liu, W., Liao, G., et al. (2018). TIP: A Web Server for Resolving Tumor Immunophenotype Profiling. *Cancer Res.* 78, 6575–6580. doi:10.1158/0008-5472.Can-18-0689

Xu, S., Wang, Z., Ye, J., Mei, S., and Zhang, J. (2021). Identification of Iron Metabolism-Related Genes as Prognostic Indicators for Lower-Grade Glioma. *Front. Oncol.* 11, 729103. doi:10.3389/fonc.2021.729103

Yan, H., Parsons, D. W., Jin, G., McLendon, R., Rasheed, B. A., Yuan, W., et al. (2009). IDH1 and IDH2 Mutations in Gliomas. *N. Engl. J. Med.* 360, 765–773. doi:10.1056/NEJMoa0808710

Yin, W., Jiang, X., Tan, J., Xin, Z., Zhou, Q., Zhan, C., et al. (2020). Development and Validation of a Tumor Mutation Burden-Related Immune Prognostic Model for Lower-Grade Glioma. *Front. Oncol.* 10, 1409. doi:10.3389/fonc.2020.01409

Yoshihara, K., Shahmoradgoli, M., Martínez, E., Vegesna, R., Kim, H., Torres-Garcia, W., et al. (2013). Inferring Tumour Purity and Stromal and Immune Cell Admixture from Expression Data. *Nat. Commun.* 4, 2612. doi:10.1038/ncomms3612

Zhang, H., Wang, M., He, Y., Deng, T., Liu, R., Wang, W., et al. (2021). Chemotoxicity-Induced Exosomal lncFERO Regulates Ferroptosis and Stemness in Gastric Cancer Stem Cells. *Cell Death Dis* 12, 1116. doi:10.1038/s41419-021-04406-z

Zhao, J., Chen, A. X., Gartrell, R. D., Silverman, A. M., Aparicio, L., Chu, T., et al. (2019). Immune and Genomic Correlates of Response to Anti-PD-1 Immunotherapy in Glioblastoma. *Nat. Med.* 25, 462–469. doi:10.1038/s41591-019-0349-y

Zhao, J., Liu, Z., Zheng, X., Gao, H., and Li, L. (2021). Prognostic Model and Nomogram Construction Based on a Novel Ferroptosis-Related Gene Signature in Lower-Grade Glioma. *Front. Genet.* 12, 753680. doi:10.3389/fgene.2021.753680

Zheng, Y., Ji, Q., Xie, L., Wang, C., Yu, C. N., Wang, Y. L., et al. (2021). Ferroptosis-Related Gene Signature as a Prognostic Marker for Lower-grade Gliomas. *J. Cel Mol Med* 25, 3080–3090. doi:10.1111/jcmm.16368

Zhou, N., and Bao, J. (2020). FerrDb: A Manually Curated Resource for Regulators and Markers of Ferroptosis and Ferroptosis-Disease Associations. *Database : J. Biol. Databases Curation* 2020, baaa021. doi:10.1093/database/baaa021

Zhou, Y., Zhou, B., Pache, L., Chang, M., Khodabakhshi, A. H., Tanaseichuk, O., et al. (2019). Metascape Provides a Biologist-Oriented Resource for the Analysis of Systems-Level Datasets. *Nat. Commun.* 10, 1523. doi:10.1038/s41467-019-09234-6

Conflict of Interest: The authors declare that the research was conducted in the absence of any commercial or financial relationships that could be construed as a potential conflict of interest.

Publisher's Note: All claims expressed in this article are solely those of the authors and do not necessarily represent those of their affiliated organizations, or those of the publisher, the editors, and the reviewers. Any product that may be evaluated in this article, or claim that may be made by its manufacturer, is not guaranteed or endorsed by the publisher.

frontiers | Frontiers in Genetics

ORIGINAL RESEARCH
published: 16 May 2022
doi: 10.3389/fgene.2022.897683

Integrated Analysis Reveals Critical Ferroptosis Regulators and FTL Contribute to Cancer Progression in Hepatocellular Carcinoma

Shaoying Ke, Congren Wang, Zijian Su, Shaoze Lin and Gongle Wu*

Hepatological Surgery Department, First Hospital of Quanzhou Affiliated to Fujian Medical University, Quanzhou, China

Background: The carcinogenesis and prognosis of hepatocellular carcinoma (HCC) involve complex molecular mechanisms, and ferroptosis is related to the development and therapeutic efficacy of HCC, but the specific mechanism and prognostic role of ferroptosis-related genes in HCC have not been elucidated.

Methods: Differentially expressed gene analysis, Cox regression, and unsupervised consensus clustering were applied to identify crucial ferroptosis regulators and establish ferroptosis-related subtypes in HCC. Random forest analysis and survival analysis were adopted to confirm FTL as the hub prognostic and diagnostic ferroptosis regulator in HCC.

Results: The ferroptosis-related subtypes based on the crucial prognostic ferroptosis regulators showed that patients in fescluster A had a higher survival probability ($p < 0.001$) and better clinical characteristics than patients in fescluster B in the TCGA-LIHC cohort. Patients with a high tumor mutation burden (TMB) in fescluster B presented a significantly poorer prognosis. FTL was the core ferroptosis regulator, and its low expression revealed a significant survival advantage compared with its high expression ($p = 0.03$). The expression and predictive value of FTL were both closely related to the clinical features ($p < 0.05$). Expression of FTL accurately distinguished HCC from normal tissues in the TCGA-LIHC cohort, ICGC cohort, and GSE14520 dataset. In addition, higher infiltrating fractions of immune cells, such as activated $CD8^+$ T cells and Gamma delta T cells, mainly enriched immune-related signaling pathways, including the IL2-STAT3 signaling pathway and interferon-gamma response signaling pathway, and higher expression of immune checkpoints, including PDCD1, CTLA4, TIGIT, and CD83, were presented in patients with high FTL expression ($p < 0.05$). Patients with high FTL were more sensitive to some targeted drugs, such as cisplatin, dasatinib, and sorafenib, than those with low FTL ($p < 0.05$). A nomogram based on FTL accurately predicted the prognosis of HCC. Further knockdown of FTL was determined to significantly inhibit cell proliferation and migration in HCC.

Conclusion: Our study validated ferroptosis-related subtypes and FTL with effective prognostic value in HCC and was beneficial for identifying candidates suitable for targeted

OPEN ACCESS

Edited by:
Lian Xiang Luo,
Guangdong Medical University, China

Reviewed by:
Lei Lei Liang,
Shanghai Jiao Tong University, China
Xing Liang,
Stanford University, United States
Mingyue Li,
Wistar Institute, United States

****Correspondence:***
Shaoying Ke
keshaoying9163@sina.com

Specialty section:
This article was submitted to Human and Medical Genomics, a section of the journal Frontiers in Genetics

Received: *16 March 2022*
Accepted: *13 April 2022*
Published: *16 May 2022*

Citation:
Ke S, Wang C, Su Z, Lin S and Wu G (2022) Integrated Analysis Reveals Critical Ferroptosis Regulators and FTL Contribute to Cancer Progression in Hepatocellular Carcinoma. Front. Genet. 13:897683. doi: 10.3389/fgene.2022.897683

drug therapy and immunotherapy, thereby offering further insight into individual treatment strategies to improve disease outcomes in HCC patients.

Keywords: ferroptosis, ferritin light chain, hepatocellular carcinoma, progression, prognosis

INTRODUCTION

Hepatocellular carcinoma (HCC) is the most common type of primary liver cancer, which is the fifth most prevalent malignancy and the second leading cause of cancer-related death globally (Ferlay et al., 2015; Torre et al., 2015). HCC patients reveal various clinical symptoms, including weight loss, hepatalgia, diarrhea, obstructive jaundice, and ascites (Sun and Sarna, 2008; Chen et al., 2014). However, early HCC lacks classic clinical features, and once the signs and symptoms of liver cancer start to appear, most HCC cases are locally advanced and/or distant metastatic, which results in difficult therapy and poor prognosis (Gong and Qin, 2016; Ayuso et al., 2018).

Surgery, including liver transplantation (LT) and liver resection (LR), serves as an effective treatment for HCC. However, LT has strict selection criteria for patients, usually using the Milan standard (solitary tumor ≤5 cm and up to three nodules ≤3 cm) (Zarrinpar and Busuttil, 2013; Jadlowiec and Taner, 2016). LT is the most efficient therapeutic method, but the donor shortage greatly limits its applicability (Forner et al., 2018). Surgical resection is the most common therapy for HCC, but approximately 70% of cases experience a relapse within 5 years after surgical treatment (Hany et al., 2018). Chemotherapy is one of the most important treatment modalities for advanced HCC (Ikeda et al., 2018); however, unsolved issues remain, including drug resistance and metastasis to other organs. Therefore, it is crucial to identify molecular biomarkers that can be used for early diagnosis and prognosis prediction.

Ferroptosis is an iron-dependent form of nonapoptotic programmed cell death driven by disruption of the intracellular balance of glutathione peroxidase 4 (GPX4) degradation of lipid peroxides. In recent years, triggering ferroptosis in cancer has been found to be beneficial to cancer treatment, especially the effectiveness of drug-resistant cancer (Hassannia et al., 2019; Tang et al., 2022). Due to the high metabolic signature of cancer cells, they often show an increased requirement for iron, and their characteristic of "iron addiction" increases the likelihood that they trigger ferroptosis. There is limited effective drug therapy for HCC. Sorafenib is the only drug used for advanced HCC, but it is often unable to be further treated due to drug resistance. Current studies suggest that the negative regulator of ferroptosis, metallothionein-1g (MT-1G) (Sun et al., 2016a), the activation of nuclear factor erythroid 2-related factor 2 (NRF2) (Sun et al., 2016b), and the transcription factor yes-associated protein/transcriptional coactivator with PDZ-binding motif (YAP/TAZ) all inhibit ferroptosis (Gao et al., 2021), which may be the main mechanism of drug resistance in the treatment of HCC by sorafenib (Nie et al., 2018). The NRF2 inhibitor (alkaloid trigonelline) and the negative status of retinoblastoma (Rb) protein both enhance the sensitivity of ferroptosis, which might assist the effectiveness of sorafenib for HCC treatment (Arlt et al., 2013; Louandre et al., 2015). In addition, ferroptosis has a strong relationship with metabolism. Low-density lipoprotein-docosahexaenoic acid (LDL-DHA) induces ferroptosis in HCC by regulating lipid metabolism, and regulation of lactic acid mediated by hydroxycarboxylic acid receptor 1/monocarboxylate transporter 1 (HCAR1/MCT1) also affects ferroptosis (Ou et al., 2017; Zhao et al., 2020). The rapid development of biological information technology has helped us use computers to efficiently assist in the diagnosis and treatment of diseases. Most of the ferroptosis-related genes have been found to be closely related to the differentially expressed genes in HCC, and the ferroptosis and iron metabolism characteristic models are conducive to the diagnosis and prognosis prediction of HCC, as well as guiding the immunity or targeted therapy of HCC patients (Liu et al., 2020a; Liang et al., 2020; Tang et al., 2020). These studies are beneficial to the treatment of advanced HCC by ferroptosis of HCC. However, the mechanism of ferroptosis in HCC remains unclear.

Ferritin is an iron storage protein that participates in iron metabolism. There are two subunits of ferritin heavy chain (FTH) and ferritin light chain (FTL) in mammals, as well as the mitochondrial subunit form (FtMt), which exists only in mitochondria. FTL is composed of 174 amino acids with a molecular weight of 19 kDa, and its structure is more stable than that of FTH. Different FTH/FTL ratios have different functions. Iron storage organs such as the liver or spleen mainly contain FTL, while FTH is mainly related to antioxidant activity. As the main subunit of ferritin, FTL directly affects iron homeostasis (Arber et al., 2016). Current studies have found that FTL may be regulated by the DNA damage response of serine/threonine kinase ATM, hypoxia, atractylodin, and other factors, resulting in ferroptosis (Liu et al., 2020b; Chen et al., 2020; He et al., 2021). FTL may also be involved in the development of tumors, such as the proliferation rate of HeLa cells and glioblastoma multiforme (GBM) cells (Wu et al., 2016) and the drug resistance process of breast cancer (Cozzi et al., 2004). Circulating transcription of FTL is significantly upregulated in samples from HCC patients and maybe a new target for the diagnosis and treatment of HCC (Wang et al., 2009; Sayeed et al., 2020). The decrease in FTL protein is associated with ferroptosis in HCC cells (He et al., 2021), but its role and mechanism remain unknown.

In this study, we performed an integrative analysis of the molecular mechanism and prognostic role of 239 ferroptosis-related genes in HCC. Based on the prognostic ferroptosis regulators, consistent ferroptosis-related clusters were constructed. FTL served as a critical ferroptosis regulator by random forest analysis. Then, we explored the independent prognostic and diagnostic role of FTL and assessed the association of FTL with immune infiltration and immune checkpoints in HCC patients. In addition, we knocked down FTL in HCC cells to measure the oncogenic effect of FTL in HCC. These findings may help to explore the predictive role of FTL in the prognosis, diagnosis, therapeutic treatment, and oncogenesis of HCC patients.

MATERIALS AND METHODS

Acquisition of Ferroptosis-Related Genes

The genes related to ferroptosis were downloaded from a previously published public data center (www.zhounan.org/ferrdb), and noncoding genes were removed from the dataset. The website also divided ferroptosis-related genes into three groups as follows: suppressors, drivers, and markers. We further analyzed the genes closely related to this research.

Identification of Differentially Expressed Genes

We obtained the mRNA-sequencing data and clinical information of HCC patients from the liver hepatocellular carcinoma (LIHC) cohort in The Cancer Genome Atlas (TCGA) database (https://www.cancer.gov/), which included 19,676 annotated mRNA sequences and other clinical data from 370 tumor tissue samples and 50 normal tissue samples. After matching mRNA sequences with ferroptosis-related genes, the differentially expressed genes (DEGs) were selected by limma, an R package, with numerical conditions log2-fold change (FC) > 1 and an adjusted p-value < 0.05.

Identification of Molecular Subgroups by Consistent Clustering

We used the ConsensusClusterPlus package in R software for consistent clustering. The Euclidean squared distance metric and the K-means clustering algorithm were used to classify the TCGA-LIHC cohort into k clusters, with k = 2 to k = 9. The optimal number of clusters was determined by the consistent cumulative distribution function (CDF) graph and the delta region graph (Wilkerson and Hayes, 2010).

Construction and Validation of a Predictive Nomogram

To predict the 1-, 3-, and 5-year survival probability of HCC patients, we combined all independent prognostic factors to construct a nomogram. Calibration curves were generated to assess the consistency between predicted survival rates and actual survival rates.

Survival Analysis

The Kaplan-Meier (K-M) curve was a visualized tool for comparing the overall survival (OS) and progression-free survival (PFS) in different ferroptosis molecular subgroups, with log-rank tests to compare the curves. The receiver operating characteristic (ROC) curve, which was built by the R package "survivalROC," was used to evaluate model prognostic performance by calculating the area under the ROC curve (AUC).

Cell Culture

Human hepatocellular carcinoma cell lines, including SK-HEP1 and HCC-LM3, were obtained from the American Type Culture Collection (ATCC) (Manassas, VA, United States). The cells were cultured in DMEM (containing 10% fetal bovine serum and 100 U/ml penicillin–streptomycin) and placed in a 37°C, 5% CO_2 incubator.

Cell Transfection

We transfected FTL shRNAs into SK-HEP1 and HCC-LM3 cells through Lipofectamine 2000 (Invitrogen, CA, United States), which was synthesized by GeneChem (Shanghai, China). After cultivation in basic DMEM, the cells were cultured in DMEM supplemented with FBS and penicillin–streptomycin.

Western Blotting

The total protein of the two liver cancer cell lines after FTL shRNA transfection was extracted using RIPA lysis buffer (Invitrogen) containing PMSF (Bio–Rad, Shanghai, China), and the protein concentration was determined and quantified. The total protein was treated with 10% sodium dodecyl sulfate–polyacrylamide gel electrophoresis (SDS–PAGE) and transferred to a polyvinylidene fluoride membrane (PVDF) (Invitrogen, Carlsbad, United States). After transfer, the membranes were blocked at room temperature for 2 h, then the primary antibody was added and incubated at 4°C overnight, and the secondary antibody was added and incubated at room temperature for 2 h. Finally, the iBright FL1500 intelligent imaging system (Invitrogen, Carlsbad, United States) was used to analyze the absorbance of the protein bands and calculate the relative protein expression level. The antibodies used in the study are listed in the **Supplementary Material**.

Cell Proliferation Assay

SK-HEP1 and HCC-LM3 cells were digested and counted, seeded in 96-well plates (3,000 cells/plate in 200 μl DMEM), and cultured in a 37°C, 5% CO_2 incubator. After 0, 24, 48, and 72 h, we washed the culture medium off the cells to be tested, added CCK8 solution according to the instructions, and continued to culture the cells for 2 h. The absorbance value (OD) of each group was measured at 450 nm on a microplate reader and recorded for statistical analysis. We also used the 5-ethynyl-2′-deoxyuridine (EdU) reagent (Ruibo, Guangzhou, China) and a viability/cytotoxicity kit (Invitrogen, Carlsbad, United States) according to the manufacturer's protocol.

Immunofluorescence

SK-HEP1 and HCC-LM3 cells were trypsinized for 24 h, rinsed with PBS three times (3 min/time), fixed with 4% paraformaldehyde for 15 min at room temperature, and then stabilized in 0.2% Triton for 10 min to rupture the cell membrane. Nonspecific antigen-binding sites were blocked with 2% BSA for 30 min, and then the cells were incubated with anti-PCNA overnight at 4°C. After washing, the cells were incubated with the anti-rabbit antibody for 60 min, and the nuclei were stained with DAPI for 2 min and then washed with PBS. Finally, a fluorescence microscope was used to observe and photograph the cells, and the expression levels of PCNA were detected.

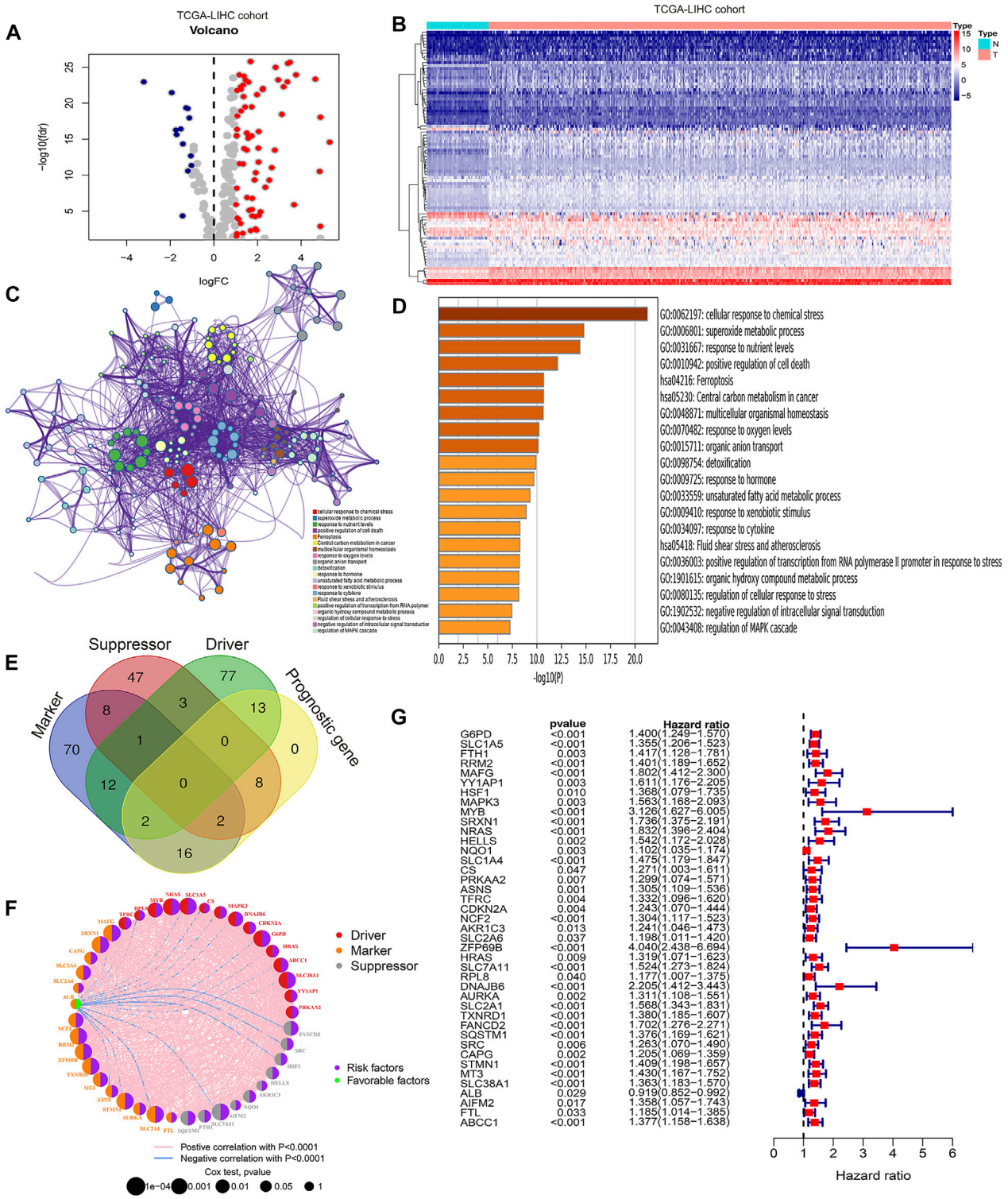

FIGURE 1 | Identification of prognostic related ferroptosis regulators in HCC. **(A)** Volcano plot showing the expression characteristics of differentially expressed genes (DEGs) between tumor tissues and normal tissues in the TCGA-LIHC cohort. **(B)** Heatmap showing DEGs associated with ferroptosis in the TCGA-LIHC cohort. **(C)** Protein–protein network indicating the top 20 regulatory signaling pathways of DEGs via KEGG and GO functional analyses. **(D)** Bar plots showing the top 20 regulatory signaling pathways of DEGs via KEGG and GO functional analyses. **(E)** Venn diagram showing the function of ferroptosis-related genes. **(F)** Protein–protein network indicating the gene function, interaction, and prognostic role of DEGs. **(G)** Forest plot showing the prognostic value of DEGs using univariate Cox analysis.

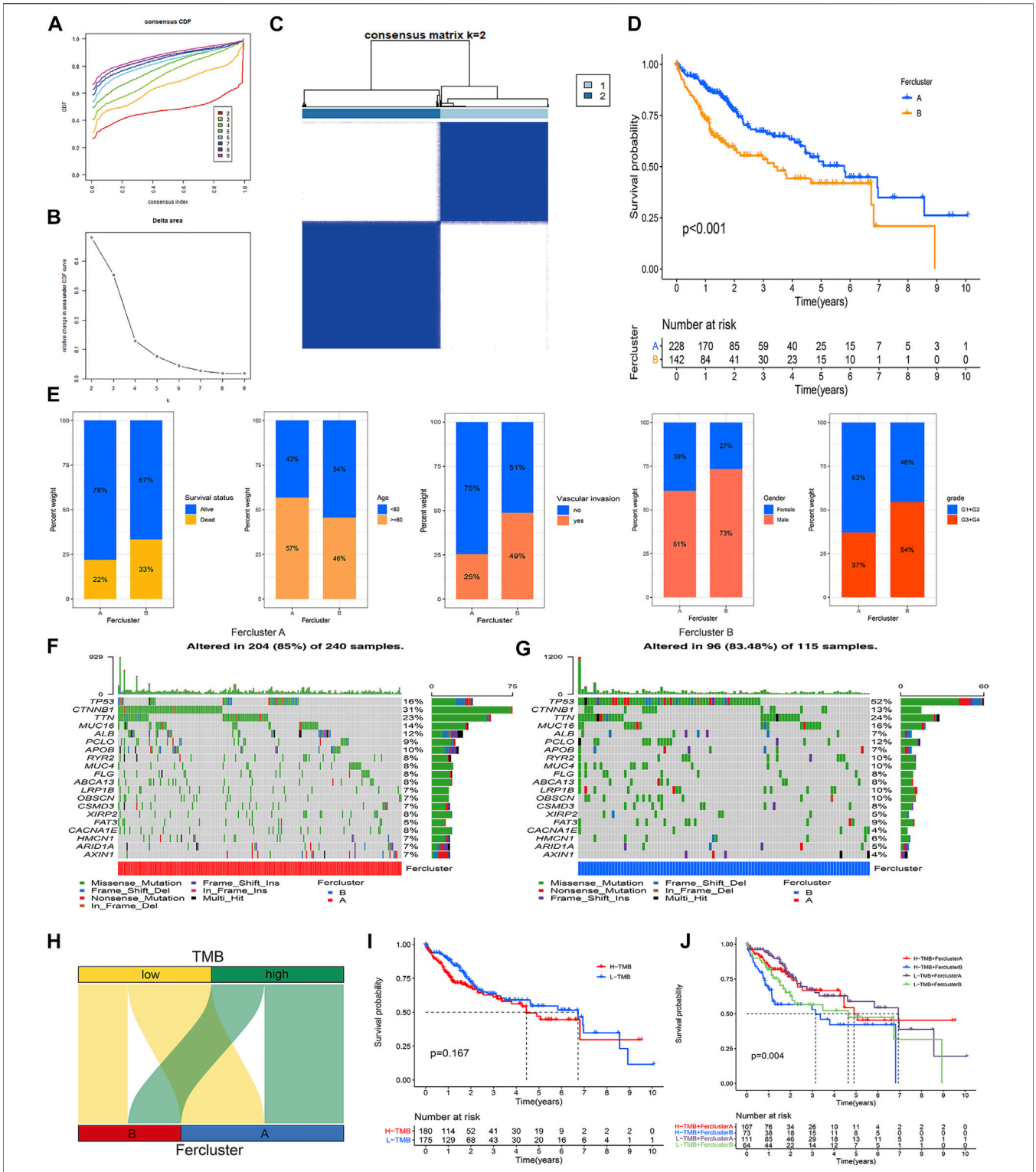

FIGURE 2 | Establishment and clinical assessment of ferroptosis-related subtypes in HCC. **(A)** Consensus cumulative distribution function (CDF) curves with k from 2 to 9. **(B)** Delta area plot showing the relative change in area under the CDF curves between k and k-1 (k = 2–9). **(C)** The result of consensus clustering (k value = 2). **(D)** K-M curve showing the difference in survival probability between fescluster A and fescluster B. **(E)** Characteristics of clinical features in fescluster A and fescluster B. **(F–G)** Characteristics of TMB in fescluster A and fescluster B. **(H)** Venn diagram showing the correlation between TMB and fesclusters. **(I)** K-M curve showing the difference in survival probability between low and high TMB. **(J)** K-M curve showing the difference in survival probability among fescluster A with low TMB, fescluster A with high TMB, fescluster B with low TMB, and fescluster B with high TMB.

Statistical Analysis

The *t*-test was used for the measurement data, the χ^2 test was used for the enumeration data, and the Kaplan-Meier method and log-rank test were used for the survival analysis. For all statistical calculations, the final results were determined to be statistically significant at $p < 0.05$.

RESULTS

Identification of Prognostic Ferroptosis Regulators in HCC

To identify prognostic ferroptosis regulators in HCC, we first conducted differential gene expression analysis between tumor tissues and normal tissues in the TCGA-LIHC cohort, and the expression characteristics of the DEGs are shown in **Figures 1A,B** and **Supplementary Table S1**. Then, we performed Kyoto Encyclopedia of Genes and Genomes (KEGG) analysis and Gene Ontology (GO) analysis to explore the signaling pathways, biological processes, cellular components, and molecular functions of the DEGs. We confirmed "ferroptosis" as a mainly enriched signaling pathway (**Figures 1C,D**) and obtained a total of 239 ferroptosis-related DEGs that were enriched in the ferroptosis pathway. Subsequently, we drew a Venn diagram to identify the role of ferroptosis-related DEGs as markers, suppressors, and drivers in ferroptosis (**Figure 1E**). The gene function, interaction, and prognostic role among the ferroptosis-related DEGs are shown in **Figure 1F**. Using univariate Cox regression, we finally identified 41 prognostic ferroptosis regulators from markers, suppressors, and drivers of ferroptosis (**Figure 1G**).

Establishment of Ferroptosis-Related Subtypes in HCC and Clinical Validation

Unsupervised consensus clustering based on the expression characteristics of the 41 prognostic ferroptosis regulators was performed to establish ferroptosis-related subtypes in HCC. The results revealed that the optimal number of clusters was two (k value = 2) (**Figures 2A–C**). Hence, the patients in the TCGA-LIHC cohort were divided into two clusters, namely, fescluster A and fescluster B. The survival analysis indicated that compared with patients in fescluster B, patients in fescluster A showed a significant survival advantage ($p < 0.001$) (**Figure 2D**). We further explored the differences in clinical features between the two clusters, and the results revealed that patients in fescluster B had a higher proportion of death, age <60 years old, vascular invasion occurrence, and pathological grades G3/G4 than patients in fescluster A, and the patients in both fescluster A and fescluster B were predominantly male (**Figure 2E**). The results indicated that the clinical features of patients in fescluster B were worse than those in fescluster A. In recent years, tumor mutation burden (TMB), which represents the characteristics of the total number of somatic coding mutations in tumors, has been increasingly shown to have predictive value in tumor prognosis as a potential biomarker for non-small-cell lung cancer, liver cancer, and other cancer types (Rizvi et al., 2015; Tang et al., 2021). Based on this, we then confirmed the characteristics of TMB in fescluster A and fescluster B (**Figures 2F,G**) and explored the correlation between TMB and fesclusters (**Figure 2H**). The survival analysis shows that there was no statistically significant difference in survival probability between the high TMB group and the low TMB group ($p > 0.05$) (**Figure 2I**). We further divided the patients into fescluster A with low TMB, fescluster A with high TMB, fescluster B with low TMB, and fescluster B with high TMB, and survival analysis indicated that patients in fescluster A with low TMB showed a significant survival advantage compared with the other groups, while patients in fescluster B with high TMB had the worst prognosis (**Figure 2J**). These results revealed that the established ferroptosis-related subtypes in HCC showed effective prognostic predictive performance in HCC and were closely associated with the clinical characteristics of patients.

FTL Is a Critical Ferroptosis Regulator Associated With Prognosis and Clinical Features in HCC

Next, random forest analysis was used to analyze critical ferroptosis-related genes in HCC, and the results indicated that MT3, NRAS, STMN1, FTL, and SLC1A5 were the five most important ferroptosis regulators in HCC associated with prognosis (**Figure 3A**). According to previous publications, there have been a lot of research on the function of three genes NRAS (Dietrich et al., 2019; Ding et al., 2020), STMN1 (Zhang et al., 2020), and SLC1A5 (Zhao et al., 2021) in HCC, and in this study, our pre-experiment indicated the expression of MT3 didn't affect the proliferation of HCC, so we focused on the role of FTL in HCC. With the FTL expression level at 75% by quartile as the criterion, we divided the high FTL group and the low FTL group in the TCGA-LIHC cohort. The K-M survival curve and ROC curve showed that higher FTL expression predicted poor survival with superior reliability in HCC patients (**Figures 3B,C**). **Figures 3D–H** indicates that the expression level of FTL is closely associated with clinical features ($p < 0.05$), including sex, history grade, and TNM stage, but not age, in HCC. Interestingly, the predictive value of FTL was also closely related to clinical features, including sex, history grade, and TNM stage ($p < 0.05$), but not age in HCC. High expression levels of FTL showed poor survival time in the HCC patients with male sex, TNM stage I-II, and G3-G4 grade ($p < 0.05$), however, in HCC patients with female sex, TNM stage III-IV, and G1-G2 history grade, there was no sign of FTL expression in the prognosis of HCC (**Figure 3I**-L).

Measuring FTL Expression and Validating the Diagnostic Ability of FTL in HCC Patients

To verify the expression level of FTL in normal tissue and tumor tissue in HCC patients, we obtained three different HCC cohorts, including the TCGA-LIHC cohort, ICGC HCC cohort, and GSE14520 cohort. The results indicated that FTL was obviously higher in HCC tissue than in normal tissue (**Figures 4A,E,I**). Then, calibration curves, ROC curves, and decision curve analysis (DCA) were used to validate the diagnostic ability of FTL in HCC patients. The AUC values of the calibration curve and ROC curve were 0.716, 0.769, and 0.694, respectively, in these three cohorts (**Figures 4B,C, F–G, J–K**), indicating good predictive performance of this diagnostic model. The DCA curve of our diagnostic model showed some net benefit

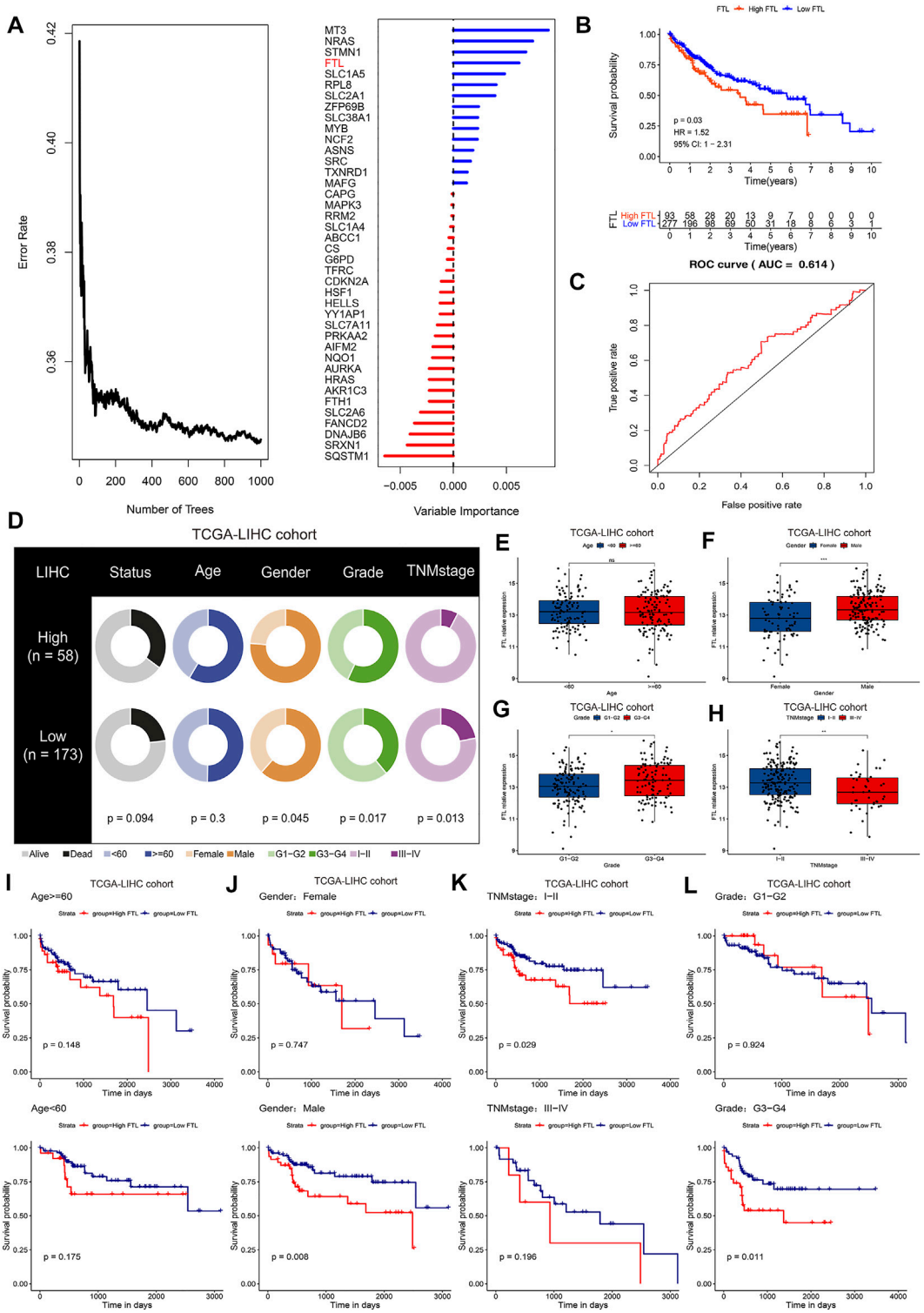

FIGURE 3 | FTL is a critical ferroptosis regulator associated with prognosis and clinical features in HCC. **(A)** Random forest analysis indicating the importance of ferroptosis regulators in predicting overall survival in HCC. **(B)** K-M survival curve showing the different overall survival rates in the high FTL and low FTL groups in the TCGA-LIHC cohort. **(C)** ROC curves evaluating the specificity and sensitivity of FTL in predicting overall survival in HCC. **(D)** Differences in clinical features, including survival status, age, sex, grade, and TNM stage, between the high FTL and low FTL groups in the TCGA-LIHC cohort. **(E–H)** Correlation of FTL expression and clinical features including age, sex, grade, and TNM stage in the TCGA-LIHC cohort. **(I-L)** K-M survival curve showing the different overall survival rates of patients in the high FTL and low FTL groups in different clinical subgroups of the TCGA-LIHC cohort. ns, no significance. *$p < 0.05$, **$p < 0.01$, and ***$p < 0.001$.

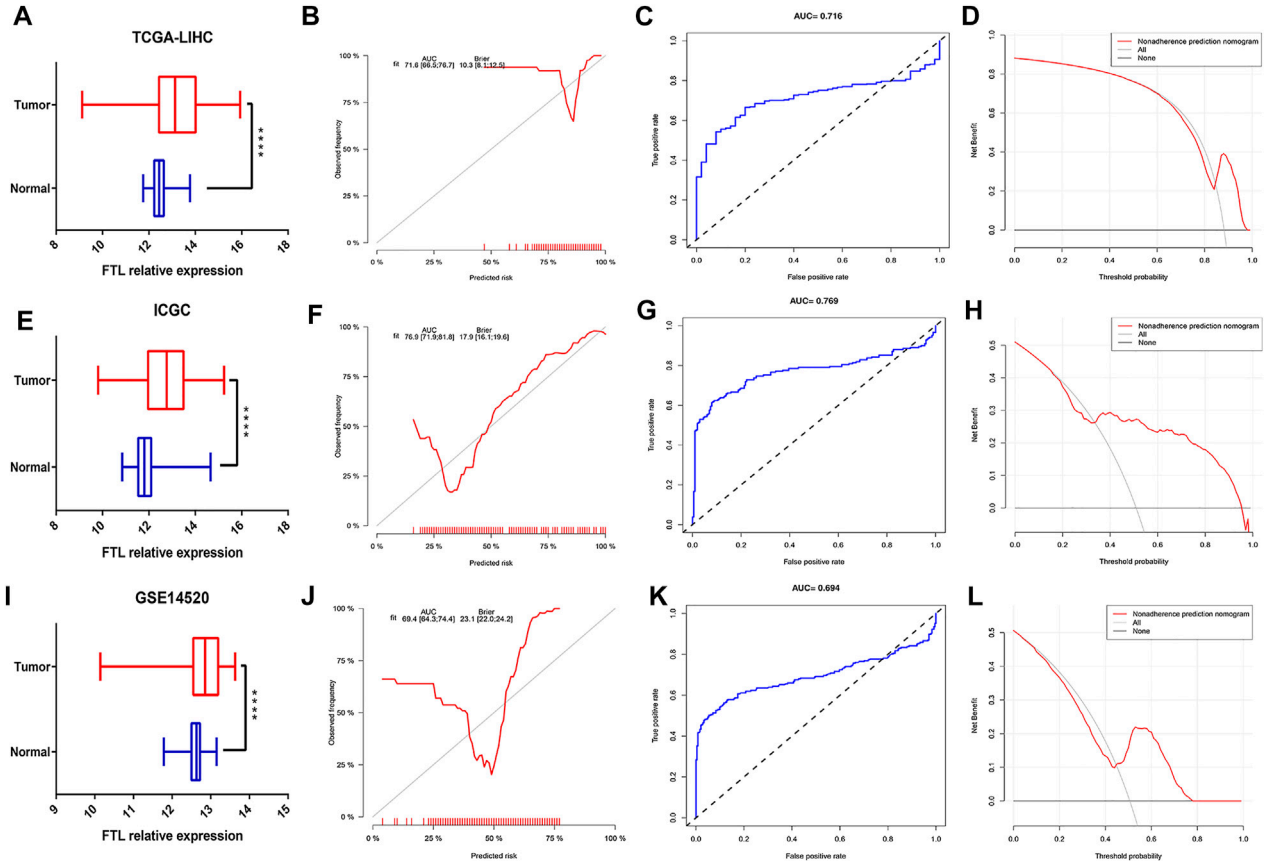

FIGURE 4 | Measurement of FTL expression in tumor samples compared with normal samples and evaluation of the diagnostic ability of FTL in HCC. **(A,E,I)** Box plot showing the FTL mRNA expression level in normal and tumor tissues in HCC from the TCGA-LIHC cohort, ICGC-HCC cohort, and GSE14520 cohort. **(B,F,J)** Calibration curves indicating the diagnostic ability of FTL in HCC patients from the TCGA-LIHC cohort, ICGC-HCC cohort, and GSE14520 cohort. **(C,G,K)** ROC curves assessing the predictive performance of the diagnostic model in the TCGA-LIHC cohort, ICGC-HCC cohort, and GSE14520 cohort. **(D,H,L)** DCA curves validating the predictive potency of the diagnostic model in the TCGA-LIHC cohort, ICGC-HCC cohort, and GSE14520 cohort. ****$p < 0.0001$.

for prediction (**Figures 4D,H,L**). Overall, these results indicated that FTL was more highly expressed in HCC tissue and that the diagnostic model showed good predictive performance for distinguishing between HCC samples and normal samples.

Identification of the Different Immune Microenvironment Between High FTL and Low FTL HCC Patients

To further clarify the immune microenvironment associated with the FTL expression level in HCC, a single sample gene set enrichment analysis (ssGSEA) was used to identify immune cell infiltration and immune activity. The results showed that higher expression indicated more immune cell infiltration, including activated $CD8^+$ T cells and Gamma delta T cells (**Figure 5A**). In addition, the enrichment scores of cytolytic activity, CCR, HLA, and immune checkpoint were significantly increased in high FTL HCC patients (**Figure 5B**). **Figure 5C** shows the relationship between FTL expression and immune checkpoints, including PDCD1, CTLA4, TIGIT, and CD83; these checkpoints were expressed at higher levels in the high FTL group than in the low FTL group (**Figures 5D–G**). GSEA indicated that high FTL expression was also positively associated with immune activation-related signaling pathways, including the IL2-STAT5 signaling pathway, IL6-JAK-STAT3 signaling pathway, and interferon-gamma response signaling pathway (**Figures 5H–J**). This evidence suggests that FTL expression is positively associated with the immune-activation microenvironment in HCC.

Prediction of Chemotherapeutic and Targeted Therapeutic Responses Between High FTL and Low FTL HCC Patients

To predict the chemotherapeutic and targeted therapeutic responses, half the maximum inhibitory concentration (IC50) of 266 anticancer drugs was obtained from the Genomics of Drug Sensitivity in Cancer (GDSC) website. The results showed that traditional chemotherapeutic drugs, including cisplatin, paclitaxel, and vinorelbine, had lower IC50 values in the high FTL group than in the low FTL group in HCC ($p < 0.05$) (**Figures 6A–C**). In addition, HCC patients with higher FTL expression showed lower IC50 values of targeted drugs such as sorafenib, dasatinib, imatinib,

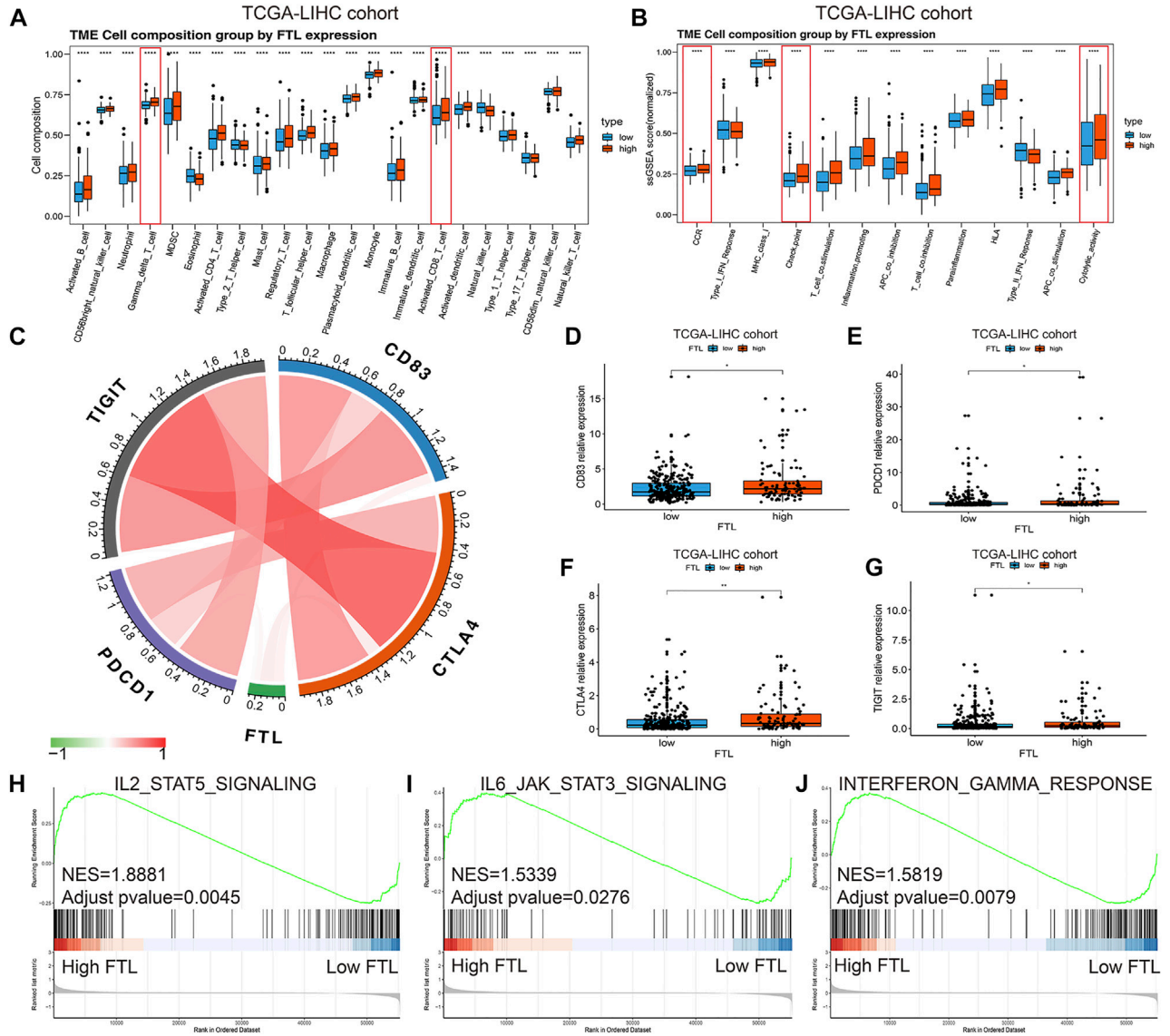

FIGURE 5 | Identification of immune cell infiltration and immune activity between high FTL and low FTL HCC patients. **(A)** Box plot showing immune cell infiltration in HCC patients in the high FTL group compared with the low FTL group. **(B)** Box plot showing the different immune activities between high FTL and low FTL HCC patients. **(C)** Relationship of FTL expression and immune checkpoints, including PDCD1, CTLA4, TIGIT, and CD83, in HCC. **(D–G)** Expression level of checkpoint genes, including PDCD1, CTLA4, TIGIT, and CD83, between high FTL and low FTL HCC patients. **(H–J)** GSEA shows the correlation between FTL expression and immune activation-related signaling pathways, such as the IL2-STAT5 signaling pathway, IL6-JAK-STAT3 signaling pathway, and interferon-gamma response signaling pathway. *$p < 0.05$, **$p < 0.01$, and ****$p < 0.0001$.

roscovitine, sunitinib, thapsigargin, tipifarnib, temsirolimus, and rapamycin ($p < 0.05$) (**Figure 6D–L**). These results indicate that the expression level of FTL is related to the sensitivity of some chemotherapeutic drugs and targeted drug treatments.

Construction and Validation of a Nomogram Integrating Independent Predictive Factors

To evaluate the independent performance of the FTL level in predicting prognosis compared with other clinical features, including age, AFP, weight, vascular invasion, sex, history grade, and TNM stage, univariate and multivariate Cox regression were used. The results showed that age, TNM stage, and FTL level were independent predictive factors in HCC patients (**Figure 7A**). Then, a nomogram predictive model was constructed based on these three independent predictive factors to quantify the survival probability of HCC patients at 1, 3, and 5 years (**Figure 7B**). The calibration curve of the nomogram for predicting the overall survival probability of HCC patients at 1, 3, and 5 years was close to the 45° line (**Figures 7C–E**). DCA was used to evaluate the guiding significance of these independent predictive factors for predicting overall survival time at

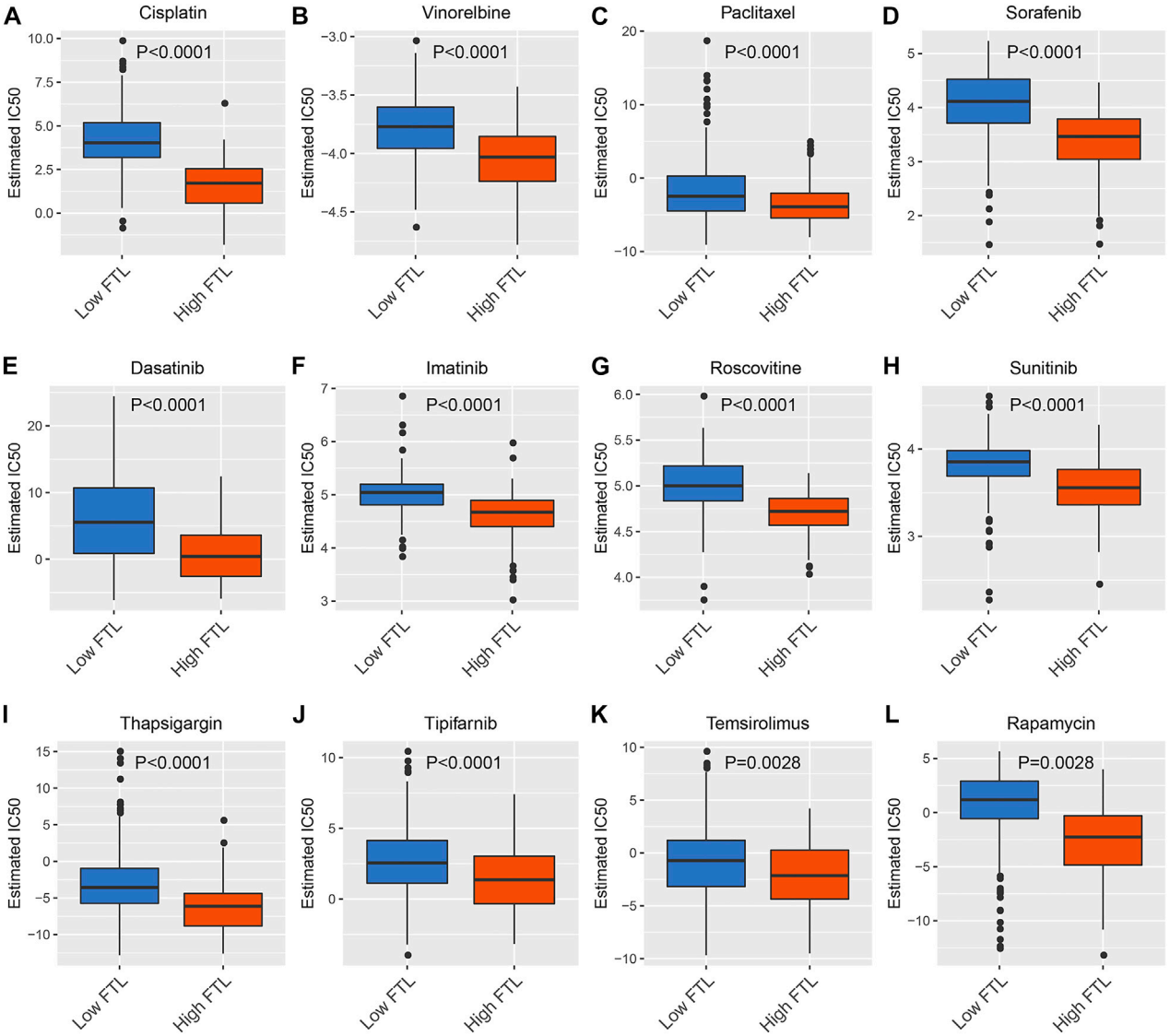

FIGURE 6 | Prediction of chemotherapeutic and targeted therapeutic responses in HCC patients with high FTL and low FTL. **(A–C)** Box plot showing the prediction of the IC50 value of traditional chemotherapeutic drugs, including cisplatin, paclitaxel, and vinorelbine, between the high FTL and low FTL groups of HCC patients. **(D-L)** Box plot showing the prediction of the IC50 value of targeted drugs, including sorafenib, dasatinib, imatinib, roscovitine, sunitinib, thapsigargin, tipifarnib, temsirolimus, and rapamycin, in HCC patients with high FTL compared with the low FTL group.

1, 3, and 5 years, and the results show that the nomogram has superior predictive value in clinical practice (**Figures 7F–H**). These results showed that FTL is an independent prognostic factor and that our nomogram has valuable predictive performance.

Silencing FTL Expression Inhibited HCC Cell Proliferation and Triggered Ferroptosis

To confirm the role of FTL in the tumor progression of HCC, HCC cells including SK-HEP1 and HCC-LM3 were transfected with two different FTL shRNA and scramble shRNA. Western blot indicated the FTL shRNA effectively inhibited FTL expression in SK-HEP1 and HCC-LM3 cells (**Figures 8A,B**). Then CCK8 kit and Edu assay were used to assess the role of FTL on HCC-cell proliferation. The result showed FTL inhibition obviously suppressed the proliferation of SK-HEP1 and HCC-LM3 cells (**Figures 8C–F**). To further explore the role of FTL in HCC-cell proliferation, immunofluorescence was used to measure the expression of PCNA in SK-HEP1 and HCC-LM3 cells. The result indicated FTL inhibition effectively decreased PCNA expression levels in HCC cells (**Figures 8G,H**). Moreover, silencing FTL expression induced lipid peroxidation levels of SK-HEP1 and HCC-LM3 cells (**Figure 8I-L**) and the concentration of iron inSK-HEP1 and HCC-LM3 cells was significantly increased with FTL inhibition (**Figure 8M–N**). These results indicated FTL

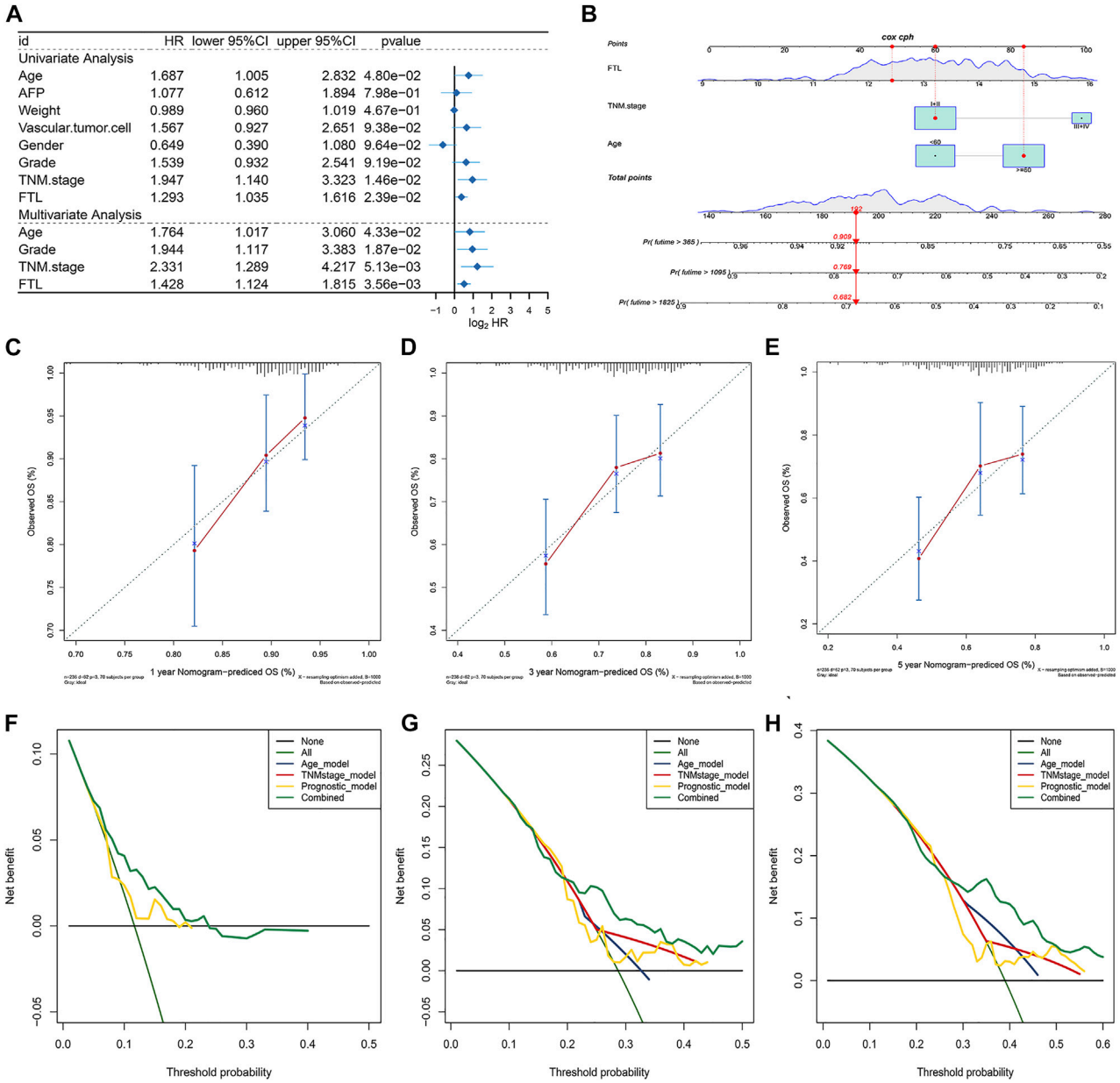

FIGURE 7 | Construction and validation of a nomogram integrating independent predictive factors. **(A)** Univariate and multivariate Cox regression for evaluating the independent prognostic factor from FTL and other clinical features, such as age, AFP, weight, vascular invasion, sex, history grade, and TNM stage. **(B)** Nomogram constructed for predicting the survival probability of patients with HCC at 1, 3, and 5 years. **(C–E)** Calibration curve of the nomogram for the overall survival probability of HCC patients at 1, 3, and 5 years. **(F–H)** DCA curve was used to evaluate the predictive ability of single independent predictive factors compared with the nomogram in HCC patients at 1, 3, and 5 years.

inhibition effectively suppressed HCC-cell proliferation and triggered ferroptosis in HCC cells.

DISCUSSION

Hepatocellular carcinoma is the most common type of liver cancer and the second leading cause of cancer-related death (Ferlay et al., 2015). Early HCC usually has no obvious clinical manifestations, and most of the symptoms are already advanced with a poor prognosis. Current treatment options include surgical resection, liver transplantation, chemotherapy, and targeted drug therapy for advanced HCC. However, surgical treatment is only applicable to patients with early HCC with very strict indications, and HCC patients are often diagnosed as advanced and have drug resistance to chemotherapy and targeted drugs (Llovet et al., 2021). Therefore, it is very important to find targets related to the diagnosis and prognosis of HCC.

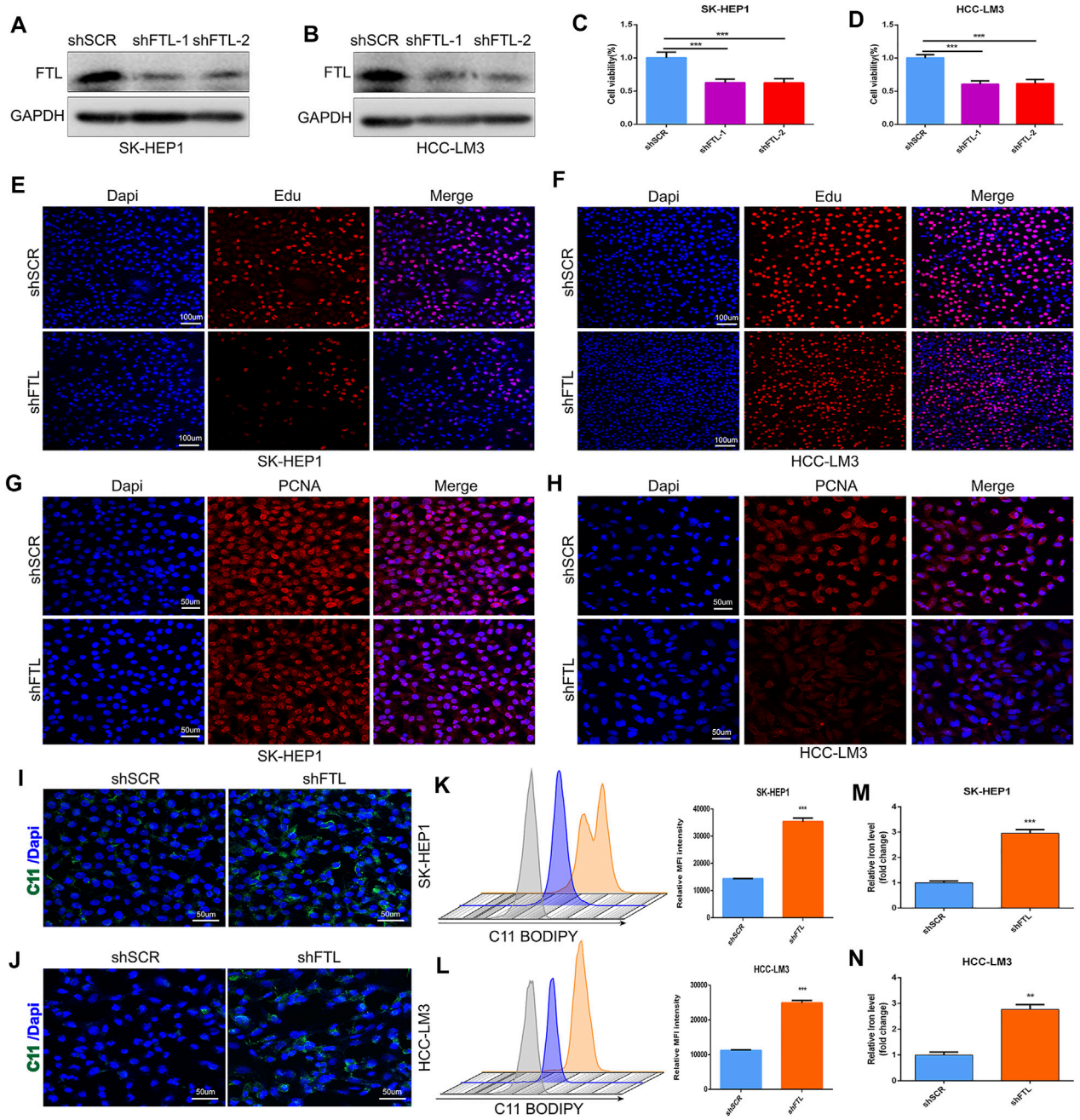

FIGURE 8 | FTL knockdown inhibited HCC-cell proliferation and induced ferroptosis in HCC cells. **(A, B)** Western blot indicated the FTL inhibition efficiency of FTL shRNA administration in SK-HEP1 and HCC-LM3 cells. **(C–F)** The proliferation of SK-HEP1 and HCC-LM3 cells was measured by using CCK8 kit, Edu assay. **(G–H)** The protein level of PCNA was measured by immunofluorescence assay. **(I–L)** The lipid peroxidation level of SK-HEP1 and HCC-LM3 cells was detected by using C11 BODIPY probe. **(M–N)** The concentration of iron level in SK-HEP1 and HCC-LM3 cells with or without shRNA administration. Data are shown as the mean ± SD of at least three independent experiments. $^{**}p < 0.01$ and $^{***}p < 0.001$.

Ferroptosis, first named in 2012 (Hirschhorn and Stockwell, 2019), is a nonapoptotic form of programmed cell death driven by iron-dependent phospholipid peroxidation (Jiang et al., 2021). Iron enrichment in the microenvironment of malignant tumors further promotes the malignancy of tumors, and the liver is an organ prone to oxidative damage (Toyokuni, 2009). Therefore, the study of ferroptosis in HCC is conducive to finding new therapeutic targets for HCC. Sorafenib is the main targeted drug for the treatment of advanced HCC, but its resistance limits its efficacy. At present, it is considered that enhancing the ferroptosis sensitivity of HCC is an effective way to solve sorafenib resistance, such as upregulation of MT-1G or antagonism of NRF2 (Sun et al., 2016a; Sun et al., 2016b).

A series of prognostic models based on the relationship between ferroptosis and HCC is helpful to accurately grasp the condition of HCC. For example, the iron death-related gene model can predict the survival rate of HCC patients, the prognostic model of HCC ferroptosis-related regulators can predict the prognosis of HCC patients and the choice of treatment methods more accurately, and the iron death-related prognostic model constructed by combining the methylation characteristics of some HCC can predict the risk more accurately (Du and Zhang, 2020; Liang et al., 2020; Deng et al., 2021; Xu et al., 2021). In this study, we comprehensively analyzed the potential mechanism and prognostic role of 239 ferroptosis-related genes in HCC. Then, these prognostic ferroptosis regulators were divided into markers, suppressors, and drivers of ferroptosis. Interestingly, based on these prognostic ferroptosis-related genes, HCC was separated into two different subtypes, fesclusters A and B. The overall survival of fescluster B was obviously poor than that of fescluster A. In addition, the fescluster was closely related to sex, age, vascular invasion, histological grade, and survival status in HCC. More importantly, we found that FTL was a critical ferroptosis regulator in HCC. A high expression level of FTL predicted a worse survival rate, and FTL functioned as an independent prognostic and diagnostic factor in HCC.

The tumor microenvironment (TME) is the cellular environment influencing the process of tumors and is composed of immune cells (both innate and acquired immune cells), nonimmune stromal cells (such as fibroblasts, endothelial cells, and various tissue-associated cells), and extracellular matrix proteins (Monteran and Erez, 2019; Wculek et al., 2020; Pansy et al., 2021). Among them, all kinds of cells interact with each other and cancer cells through the secretion of various cytokines, chemokines, and other signals, so they play a key role in the regulation of the tumor immune response. The TME plays an important role in the regulation of HCC (Leonardi et al., 2012; Wu et al., 2019). For example, hepatic stellate cells (HSCs) promote tumorigenicity by eliminating HCC necrosis, and some secreted cytokines and chemokines are essential for the stem-like characteristics of HCC cells (Amann et al., 2009; Xiong et al., 2018). While immune cells can inhibit the development of HCC, immune cell defects lead to immunosuppression of HCC (Piñeiro Fernández et al., 2019; Chen et al., 2021). In this study, we found that a high FTL expression level indicated increased infiltration of immune cells, such as activated $CD8^+$ T cells and Gamma delta T cell. High FTL expression was also associated with immune-related signaling pathways, including the IL2-STAT5 signaling pathway and the interferon-gamma response signaling pathway. In addition, the enrichment scores of cytolytic activity, CCR HLA, and immune checkpoint were significantly increased in high FTL HCC patients. Moreover, immune checkpoints, including PDCD1, CTLA4, TIGIT, and CD83, were positively associated with FTL expression levels in HCC. This evidence suggests that FTL may function as a predictor of the immune response and that patients with high FTL levels may obtain more clinical benefits from immunotherapy in HCC.

FTL is a ferritin light chain that forms ferritin with FTH to complete the storage function of iron. Due to its structural stability, FTL mainly exists in organs rich in iron storage and directly affects iron homeostasis (Li et al., 2015). Current studies on the function of FTL in HCC mainly focus on its role in iron death. It has been reported that FTL plays a role in the process of apoptosis (Fan et al., 2009), but more studies regard FTL as a factor related to iron metabolism and consider it to play a role in ferroptosis. Gsk-3β affects ferroptosis by antagonizing iron metabolites, including FTL, and disrupting iron homeostasis (Wang et al., 2021a). Transcriptional inhibition of FTL has also been reported to increase the sensitivity of cancer cells to ferroptosis in lung adenocarcinoma (Wang et al., 2021b). In this study, we found that the level of FTL expression was also associated with immunotherapy and molecular targeted therapy, including sorafenib and imatinib. In addition, FTL was highly expressed in HCC tumor tissue and served as a promising prognostic and diagnostic factor in HCC patients. Moreover, silencing FTL expression effectively suppressed HCC-cell proliferation and inhibited PCNA expression in HCC cells. FTL inhibition increased the levels of lipid peroxidation and ferric ion levels in HCC cells. This evidence indicates that FTL can be considered a critical ferroptosis regulator and a novel therapeutic target for HCC.

However, there are some limitations to our research. All RNA sequence data and clinical information in this study were obtained from public databases, such as the TCGA database, GEO database, and ICGC database. The predictive role of FTL in the response to immunotherapy and molecular targeted therapy in HCC patients needs to be validated in a clinical cohort, and a public database lacks a feasible cohort. More experiments, such as animal models and molecular biology experiments, are needed to explore the oncogenic effect of FTL and the potential regulatory mechanism in HCC.

DATA AVAILABILITY STATEMENT

The original contributions presented in the study are included in the article/**Supplementary Material**, further inquiries can be directed to the corresponding author.

AUTHOR CONTRIBUTIONS

SK: experiments conception and design, data collection and analysis, manuscript writing and editing. CW: data collection, analysis, and interpretation. ZS and SL: experiments conduct and data analysis. GW: manuscript writing and analysis tools contribution. All authors contributed to the article and approved the submitted version.

ACKNOWLEDGMENTS

The authors of the present work express their sincere gratitude for the freely available data information in the TCGA, ICGC, and GEO databases.

SUPPLEMENTARY MATERIAL

The Supplementary Material for this article can be found online at: https://www.frontiersin.org/articles/10.3389/fgene.2022.897683/full#supplementary-material.

REFERENCES

Amann, T., Bataille, F., Spruss, T., Mühlbauer, M., Gäbele, E., Schölmerich, J., et al. (2009). Activated Hepatic Stellate Cells Promote Tumorigenicity of Hepatocellular Carcinoma. *Cancer Sci.* 100 (4), 646–653. doi:10.1111/j.1349-7006.2009.01087.x

Arber, C. E., Li, A., Houlden, H., and Wray, S. (2016). Review: Insights into Molecular Mechanisms of Disease in Neurodegeneration with Brain Iron Accumulation: Unifying Theories. *Neuropathol. Appl. Neurobiol.* 42 (3), 220–241. doi:10.1111/nan.12242

Arlt, A., Sebens, S., Krebs, S., Geismann, C., Grossmann, M., Kruse, M.-L., et al. (2013). Inhibition of the Nrf2 Transcription Factor by the Alkaloid Trigonelline Renders Pancreatic Cancer Cells More Susceptible to Apoptosis through Decreased Proteasomal Gene Expression and Proteasome Activity. *Oncogene* 32 (40), 4825–4835. doi:10.1038/onc.2012.493

Ayuso, C., Rimola, J., Vilana, R., Burrel, M., Darnell, A., García-Criado, Á., et al. (2018). Diagnosis and Staging of Hepatocellular Carcinoma (HCC): Current Guidelines. *Eur. J. Radiol.* 101, 72–81. doi:10.1016/j.ejrad.2018.01.025

Chen, H. W., Wang, F. J., Li, J. Y., Lai, E. C., and Lau, W. Y. (2014). Hepatocellular Carcinoma Presenting with Obstructive Jaundice during Pregnancy. *Case Rep. Surg.* 2014, 502061. doi:10.1155/2014/502061

Chen, H., Zhou, X.-H., Li, J.-R., Zheng, T.-H., Yao, F.-B., Gao, B., et al. (2021). Neutrophils: Driving Inflammation during the Development of Hepatocellular Carcinoma. *Cancer Lett.* 522, 22–31. doi:10.1016/j.canlet.2021.09.011

Chen, P.-H., Wu, J., Ding, C.-K. C., Lin, C.-C., Pan, S., Bossa, N., et al. (2020). Kinome Screen of Ferroptosis Reveals a Novel Role of ATM in Regulating Iron Metabolism. *Cell Death Differ* 27 (3), 1008–1022. doi:10.1038/s41418-019-0393-7

Cozzi, A., Corsi, B., Levi, S., Santambrogio, P., Biasiotto, G., and Arosio, P. (2004). Analysis of the Biologic Functions of H- and L-Ferritins in HeLa Cells by Transfection with siRNAs and cDNAs: Evidence for a Proliferative Role of L-Ferritin. *Blood* 103 (6), 2377–2383. doi:10.1182/blood-2003-06-1842

Deng, T., Hu, B., Jin, C., Tong, Y., Zhao, J., Shi, Z., et al. (2021). A Novel Ferroptosis Phenotype-related Clinical-molecular Prognostic Signature for Hepatocellular Carcinoma. *J. Cel Mol Med* 25 (14), 6618–6633. doi:10.1111/jcmm.16666

Dietrich, P., Gaza, A., Wormser, L., Fritz, V., Hellerbrand, C., and Bosserhoff, A. K. (2019). Neuroblastoma RAS Viral Oncogene Homolog (NRAS) Is a Novel Prognostic Marker and Contributes to Sorafenib Resistance in Hepatocellular Carcinoma. *Neoplasia* 21 (3), 257–268. doi:10.1016/j.neo.2018.11.011

Ding, B., Fan, W., and Lou, W. (2020). hsa_circ_0001955 Enhances *In Vitro* Proliferation, Migration, and Invasion of HCC Cells through miR-145-5p/NRAS Axis. *Mol. Ther. - Nucleic Acids* 22, 445–455. doi:10.1016/j.omtn.2020.09.007

Du, X., and Zhang, Y. (2020). Integrated Analysis of Immunity- and Ferroptosis-Related Biomarker Signatures to Improve the Prognosis Prediction of Hepatocellular Carcinoma. *Front. Genet.* 11, 614888. doi:10.3389/fgene.2020.614888

Fan, Y., Yamada, T., Shimizu, T., Nanashima, N., Akita, M., Suto, K., et al. (2009). Ferritin Expression in Rat Hepatocytes and Kupffer Cells after lead Nitrate Treatment. *Toxicol. Pathol.* 37 (2), 209–217. doi:10.1177/0192623308328544

Ferlay, J., Soerjomataram, I., Dikshit, R., Eser, S., Mathers, C., Rebelo, M., et al. (2015). Cancer Incidence and Mortality Worldwide: Sources, Methods and Major Patterns in GLOBOCAN 2012. *Int. J. Cancer* 136 (5), E359–E386. doi:10.1002/ijc.29210

Forner, A., Reig, M., and Bruix, J. (2018). Hepatocellular Carcinoma. *The Lancet* 391 (10127), 1301–1314. doi:10.1016/s0140-6736(18)30010-2

Gao, R., Kalathur, R. K. R., Coto-Llerena, M., Ercan, C., Buechel, D., Shuang, S., et al. (2021). YAP/TAZ and ATF4 Drive Resistance to Sorafenib in Hepatocellular Carcinoma by Preventing Ferroptosis. *EMBO Mol. Med.* 13 (12), e14351. doi:10.15252/emmm.202114351

Gong, X.-L., and Qin, S.-K. (2016). Progress in Systemic Therapy of Advanced Hepatocellular Carcinoma. *Wjg* 22 (29), 6582–6594. doi:10.3748/wjg.v22.i29.6582

Hany, H., Shalaby, A., Al Kashef, W., Kandil, W., Shahin, R.-A., El-Alfy, H., et al. (2018). Evaluation of the Role of Notch1 Expression in Hepatic Carcinogenesis with Clinico-Pathological Correlation. *Pathology* 50 (7), 730–736. doi:10.1016/j.pathol.2018.08.007

Hassannia, B., Vandenabeele, P., and Vanden Berghe, T. (2019). Targeting Ferroptosis to Iron Out Cancer. *Cancer cell* 35 (6), 830–849. doi:10.1016/j.ccell.2019.04.002

He, Y., Fang, D., Liang, T., Pang, H., Nong, Y., Tang, L., et al. (2021). Atractylodin May Induce Ferroptosis of Human Hepatocellular Carcinoma Cells. *Ann. Transl Med.* 9 (20), 1535. doi:10.21037/atm-21-4386

Hirschhorn, T., and Stockwell, B. R. (2019). The Development of the Concept of Ferroptosis. *Free Radic. Biol. Med.* 133, 130–143. doi:10.1016/j.freeradbiomed.2018.09.043

Ikeda, M., Morizane, C., Ueno, M., Okusaka, T., Ishii, H., and Furuse, J. (2018). Chemotherapy for Hepatocellular Carcinoma: Current Status and Future Perspectives. *Jpn. J. Clin. Oncol.* 48 (2), 103–114. doi:10.1093/jjco/hyx180

Jadlowiec, C. C., and Taner, T. (2016). Liver Transplantation: Current Status and Challenges. *Wjg* 22 (18), 4438–4445. doi:10.3748/wjg.v22.i18.4438

Jiang, X., Stockwell, B. R., and Conrad, M. (2021). Ferroptosis: Mechanisms, Biology and Role in Disease. *Nat. Rev. Mol. Cel Biol* 22 (4), 266–282. doi:10.1038/s41580-020-00324-8

Leonardi, G. C., Candido, S., Cervello, M., Nicolosi, D., Raiti, F., Travali, S., et al. (2012). The Tumor Microenvironment in Hepatocellular Carcinoma (Review). *Int. J. Oncol.* 40 (6), 1733–1747. doi:10.3892/ijo.2012.1408

Li, W., Garringer, H. J., Goodwin, C. B., Richine, B., Acton, A., VanDuyn, N., et al. (2015). Systemic and Cerebral Iron Homeostasis in Ferritin Knock-Out Mice. *PloS one* 10 (1), e0117435. doi:10.1371/journal.pone.0117435

Liang, J.-y., Wang, D.-s., Lin, H.-c., Chen, X.-x., Yang, H., Zheng, Y., et al. (2020). A Novel Ferroptosis-Related Gene Signature for Overall Survival Prediction in Patients with Hepatocellular Carcinoma. *Int. J. Biol. Sci.* 16 (13), 2430–2441. doi:10.7150/ijbs.45050

Liu, J., Gao, L., Zhan, N., Xu, P., Yang, J. a., Yuan, F. e., et al. (2020). Hypoxia Induced Ferritin Light Chain (FTL) Promoted Epithelia Mesenchymal Transition and Chemoresistance of Glioma. *J. Exp. Clin. Cancer Res.* 39 (1), 137. doi:10.1186/s13046-020-01641-8

Liu, Y., Zhang, X., Zhang, J., Tan, J., Li, J., and Song, Z. (2020). Development and Validation of a Combined Ferroptosis and Immune Prognostic Classifier for Hepatocellular Carcinoma. *Front. Cel Dev. Biol.* 8, 596679. doi:10.3389/fcell.2020.596679

Llovet, J. M., Kelley, R. K., Villanueva, A., Singal, A. G., Pikarsky, E., Roayaie, S., et al. (2021). Hepatocellular Carcinoma. *Nat. Rev. Dis. Primers* 7 (1), 6. doi:10.1038/s41572-020-00240-3

Louandre, C., Marcq, I., Bouhlal, H., Lachaier, E., Godin, C., Saidak, Z., et al. (2015). The Retinoblastoma (Rb) Protein Regulates Ferroptosis Induced by Sorafenib in Human Hepatocellular Carcinoma Cells. *Cancer Lett.* 356 (2 Pt B), 971–977. doi:10.1016/j.canlet.2014.11.014

Monteran, L., and Erez, N. (2019). The Dark Side of Fibroblasts: Cancer-Associated Fibroblasts as Mediators of Immunosuppression in the Tumor Microenvironment. *Front. Immunol.* 10, 1835. doi:10.3389/fimmu.2019.01835

Nie, J., Lin, B., Zhou, M., Wu, L., and Zheng, T. (2018). Role of Ferroptosis in Hepatocellular Carcinoma. *J. Cancer Res. Clin. Oncol.* 144 (12), 2329–2337. doi:10.1007/s00432-018-2740-3

Ou, W., Mulik, R. S., Anwar, A., McDonald, J. G., He, X., and Corbin, I. R. (2017). Low-density Lipoprotein Docosahexaenoic Acid Nanoparticles Induce Ferroptotic Cell Death in Hepatocellular Carcinoma. *Free Radic. Biol. Med.* 112, 597–607. doi:10.1016/j.freeradbiomed.2017.09.002

Pansy, K., Uhl, B., Krstic, J., Szmyra, M., Fechter, K., Santiso, A., et al. (2021). Immune Regulatory Processes of the Tumor Microenvironment under Malignant Conditions. *Int. J. Mol. Sci.* 22 (24), 13311. doi:10.3390/ijms222413311

Piñeiro Fernández, J., Luddy, K. A., Harmon, C., and O'Farrelly, C. (2019). Hepatic Tumor Microenvironments and Effects on NK Cell Phenotype and Function. *Int. J. Mol. Sci.* 20 (17), 4131. doi:10.3390/ijms20174131

Rizvi, N. A., Hellmann, M. D., Snyder, A., Kvistborg, P., Makarov, V., Havel, J. J., et al. (2015). Mutational Landscape Determines Sensitivity to PD-1 Blockade in Non-small Cell Lung Cancer. *Science* 348 (6230), 124–128. doi:10.1126/science.aaa1348

Sayeed, A., Dalvano, B. E., Kaplan, D. E., Viswanathan, U., Kulp, J., Janneh, A. H., et al. (2020). Profiling the Circulating mRNA Transcriptome in Human Liver Disease. *Oncotarget* 11 (23), 2216–2232. doi:10.18632/oncotarget.27617

Sun, V. C.-Y., and Sarna, L. (2008). Symptom Management in Hepatocellular Carcinoma. *Clin. J. Oncol. Nurs.* 12 (5), 759–766. doi:10.1188/08.cjon.759-766

Sun, X., Niu, X., Chen, R., He, W., Chen, D., Kang, R., et al. (2016). Metallothionein-1G Facilitates Sorafenib Resistance through Inhibition of Ferroptosis. *Hepatology* 64 (2), 488–500. doi:10.1002/hep.28574

Sun, X., Ou, Z., Chen, R., Niu, X., Chen, D., Kang, R., et al. (2016). Activation of the P62-Keap1-NRF2 Pathway Protects against Ferroptosis in Hepatocellular Carcinoma Cells. *Hepatology* 63 (1), 173–184. doi:10.1002/hep.28251

Tang, B., Yan, R., Zhu, J., Cheng, S., Kong, C., Chen, W., et al. (2022). Integrative Analysis of the Molecular Mechanisms, Immunological Features and Immunotherapy Response of Ferroptosis Regulators across 33 Cancer Types. *Int. J. Biol. Sci.* 18 (1), 180–198. doi:10.7150/ijbs.64654

Tang, B., Zhu, J., Li, J., Fan, K., Gao, Y., Cheng, S., et al. (2020). The Ferroptosis and Iron-Metabolism Signature Robustly Predicts Clinical Diagnosis, Prognosis and Immune Microenvironment for Hepatocellular Carcinoma. *Cell Commun Signal* 18 (1), 174. doi:10.1186/s12964-020-00663-1

Tang, B., Zhu, J., Zhao, Z., Lu, C., Liu, S., Fang, S., et al. (2021). Diagnosis and Prognosis Models for Hepatocellular Carcinoma Patient's Management Based on Tumor Mutation burden. *J. Adv. Res.* 33, 153–165. doi:10.1016/j.jare.2021.01.018

Torre, L. A., Bray, F., Siegel, R. L., Ferlay, J., Lortet-Tieulent, J., and Jemal, A. (2015). Global Cancer Statistics, 2012. *CA Cancer J. Clin.* 65 (2), 87–108. doi:10.3322/caac.21262

Toyokuni, S. (2009). Role of Iron in Carcinogenesis: Cancer as a Ferrotoxic Disease. *Cancer Sci.* 100 (1), 9–16. doi:10.1111/j.1349-7006.2008.01001.x

Wang, K., Xu, X., Nie, Y., Dai, L., Wang, P., and Zhang, J. (2009). Identification of Tumor-Associated Antigens by Using SEREX in Hepatocellular Carcinoma. *Cancer Lett.* 281 (2), 144–150. doi:10.1016/j.canlet.2009.02.037

Wang, L., Ouyang, S., Li, B., Wu, H., and Wang, F. (2021). GSK-3β Manipulates Ferroptosis Sensitivity by Dominating Iron Homeostasis. *Cell Death Discov.* 7 (1), 334. doi:10.1038/s41420-021-00726-3

Wang, Y., Qiu, S., Wang, H., Cui, J., Tian, X., Miao, Y., et al. (2021). Transcriptional Repression of Ferritin Light Chain Increases Ferroptosis Sensitivity in Lung Adenocarcinoma. *Front. Cel Dev. Biol.* 9, 719187. doi:10.3389/fcell.2021.719187

Wculek, S. K., Cueto, F. J., Mujal, A. M., Melero, I., Krummel, M. F., and Sancho, D. (2020). Dendritic Cells in Cancer Immunology and Immunotherapy. *Nat. Rev. Immunol.* 20 (1), 7–24. doi:10.1038/s41577-019-0210-z

Wilkerson, M. D., and Hayes, D. N. (2010). ConsensusClusterPlus: a Class Discovery Tool with Confidence Assessments and Item Tracking. *Bioinformatics (Oxford, England)* 26 (12), 1572–1573. doi:10.1093/bioinformatics/btq170

Wu, Q., Zhou, L., Lv, D., Zhu, X., and Tang, H. (2019). Exosome-mediated Communication in the Tumor Microenvironment Contributes to Hepatocellular Carcinoma Development and Progression. *J. Hematol. Oncol.* 12 (1), 53. doi:10.1186/s13045-019-0739-0

Wu, T., Li, Y., Liu, B., Zhang, S., Wu, L., Zhu, X., et al. (2016). Expression of Ferritin Light Chain (FTL) Is Elevated in Glioblastoma, and FTL Silencing Inhibits Glioblastoma Cell Proliferation via the GADD45/JNK Pathway. *PloS one* 11 (2), e0149361. doi:10.1371/journal.pone.0149361

Xiong, S., Wang, R., Chen, Q., Luo, J., Wang, J., Zhao, Z., et al. (2018). Cancer-associated Fibroblasts Promote Stem Cell-like Properties of Hepatocellular Carcinoma Cells through IL-6/STAT3/Notch Signaling. *Am. J. Cancer Res.* 8 (2), 302–316. doi:10.3390/ijms20174131

Xu, Z., Peng, B., Liang, Q., Chen, X., Cai, Y., Zeng, S., et al. (2021). Construction of a Ferroptosis-Related Nine-lncRNA Signature for Predicting Prognosis and Immune Response in Hepatocellular Carcinoma. *Front. Immunol.* 12, 719175. doi:10.3389/fimmu.2021.719175

Zarrinpar, A., and Busuttil, R. W. (2013). Liver Transplantation: Past, Present and Future. *Nat. Rev. Gastroenterol. Hepatol.* 10 (7), 434–440. doi:10.1038/nrgastro.2013.88

Zhang, R., Gao, X., Zuo, J., Hu, B., Yang, J., Zhao, J., et al. (2020). STMN1 Upregulation Mediates Hepatocellular Carcinoma and Hepatic Stellate Cell Crosstalk to Aggravate Cancer by Triggering the MET Pathway. *Cancer Sci.* 111 (2), 406–417. doi:10.1111/cas.14262

Zhao, J., Yang, Z., Tu, M., Meng, W., Gao, H., Li, M. D., et al. (2021). Correlation between Prognostic Biomarker SLC1A5 and Immune Infiltrates in Various Types of Cancers Including Hepatocellular Carcinoma. *Front. Oncol.* 11, 608641. doi:10.3389/fonc.2021.608641

Zhao, Y., Li, M., Yao, X., Fei, Y., Lin, Z., Li, Z., et al. (2020). HCAR1/MCT1 Regulates Tumor Ferroptosis through the Lactate-Mediated AMPK-SCD1 Activity and its Therapeutic Implications. *Cel Rep.* 33 (10), 108487. doi:10.1016/j.celrep.2020.108487

Conflict of Interest: The authors declare that the research was conducted in the absence of any commercial or financial relationships that could be construed as a potential conflict of interest.

Publisher's Note: All claims expressed in this article are solely those of the authors and do not necessarily represent those of their affiliated organizations, or those of the publisher, the editors, and the reviewers. Any product that may be evaluated in this article, or claim that may be made by its manufacturer, is not guaranteed or endorsed by the publisher.

Advantages of publishing in Frontiers

OPEN ACCESS
Articles are free to read for greatest visibility and readership

FAST PUBLICATION
Around 90 days from submission to decision

HIGH QUALITY PEER-REVIEW
Rigorous, collaborative, and constructive peer-review

TRANSPARENT PEER-REVIEW
Editors and reviewers acknowledged by name on published articles

Frontiers
Avenue du Tribunal-Fédéral 34
1005 Lausanne | Switzerland

Visit us: www.frontiersin.org
Contact us: frontiersin.org/about/contact

REPRODUCIBILITY OF RESEARCH
Support open data and methods to enhance research reproducibility

DIGITAL PUBLISHING
Articles designed for optimal readership across devices

FOLLOW US
@frontiersin

IMPACT METRICS
Advanced article metrics track visibility across digital media

EXTENSIVE PROMOTION
Marketing and promotion of impactful research

LOOP RESEARCH NETWORK
Our network increases your article's readership